**EPA–600/9–78–004**
**CONF–770970**

Hi. 1976

252
4/4/78

Conf-770970--

# EPA/DOE Symposium on High Temperature High Pressure Particulate Control

MASTER

Sponsored By
950 5475
U.S. Department of Energy
Assistant Secretary for
Energy Technology
Fossil Energy Program

950 4030
U.S. Environmental Protection Agency
Office of Research and Development
Industrial Environmental Research Laboratory
Research Triangle Park, N.C.

**September 20–21, 1977**
**Washington, D.C.**

DISTRIBUTION OF THIS DOCUMENT IS UNLIMITED

EPA–600/9–78–004
CONF–770970
UC- 11

# EPA/DOE Symposium on High Temperature High Pressure Particulate Control

Sponsored By
U.S. Department of Energy
Assistant Secretary for
Energy Technology
Fossil Energy Program

U.S. Environmental Protection
Agency
Office of Research and Development
Industrial Environmental Research
Laboratory
Research Triangle Park, N.C.

EPA

**September 20–21, 1977**
**Washington, D.C.**

NOTICE
This report was prepared as an account of work sponsored by the United States Government. Neither the United States nor the United States Department of Energy, nor any of their employees, nor any of their contractors, subcontractors, or their employees, makes any warranty, express or implied, or assumes any legal liability or responsibility for the accuracy, completeness or usefulness of any information, apparatus, product or process disclosed, or represents that its use would not infringe privately owned rights.

DISTRIBUTION OF THIS DOCUMENT IS UNLIMITED

# INTRODUCTION

Advanced technology methods of using coal include pressurized fluidized bed combustion and coal gasification. These technologies have been under development for several years and have reached a level of development more advanced than the particle control technology required for its use. Therefore, a potential barrier to the utilization of advanced coal combustion technologies is the need for particulate control at high temperatures and pressures.

The development of a particle removal system capable of operating reliably at high temperatures and high pressures (HTHP), and able to meet the stringent cleanup requirements needed to assure acceptable turbine life is a formidable task. To accomplish this task will require high mass removal efficiency by particle control equipment which must operate in a severe environment. In addition, this particle control equipment must not be so costly as to destroy the economic advantages of the new coal combustion processes.

Development of high temperature and pressure cleanup devices in parallel with the coal conversion process represents an opportunity to integrate this technology into the process in a manner which can benefit the process economics and performance while minimizing damage to the environment. In addition, the research and development efforts needed to accomplish successful development of HTHP particle control devices will stimulate improvements in conventional particle control technology which may result in improvements in ambient air quality.

The "EPA/ERDA Symposium on High Temperature/Pressure Particulate Control" was held in Washington, D. C. September 20 and 21, 1977. A primary objective of the symposium was to promote an interchange of ideas among researchers on the HTHP problem. This proceeding is a compilation of papers presented at the symposium.

Sponsors of the symposium were: the Particulate Technology Branch of the U. S. Environmental Protection Agency (Research Triangle Park, North Carolina) and the Fossil Energy Division of the U. S. Energy Research and Development Administration (Washington, D. C.).

Aerotherm Division of Acurex Corporation (Mountain View, California) coordinated and hosted the meeting.

Dr. Dennis C. Drehmel from the EPA and Mr. Jack Seigel from ERDA deserve credit and my thanks for their help in organizing the meeting. I wish to thank each of the Authors as well for their efforts and cooperation which made the symposium and their proceedings a successful presentation of the current state of the art in high temperature and pressure particle control.

Mike Shackleton
Conference Coordinator
Aerotherm Division
Acurex Corporation

# TABLE OF CONTENTS

Page

Keynote Address: Dr. Philip C. White, Past Assistant Administrator For Fossil Energy, ERDA . . . . . . . . . . . . . . . . . . 1

A Review of the Symposium: Alan A. Smith, Babcock & Wilcox, Ltd., England . . . . . . . . . . . . . . . . . . . . . . . 7

## SESSION I: FUNDAMENTALS

"The Tolerance of Large Gas Turbines to 'Rocks', 'Dusts', and Chemical Corrodants," E. F. Sverdrup, D. H. Archer, M. Menguturk . . . 13

"Materials For Use in High Temperature/Pressure Hostile Environments," J. Hull . . . . . . . . . . . . . . . . . . . . . . . . . . 33

"High Temperature and Pressure Effects on Particle Collection Mechanisms," R. D. Parker, S. Calvert, D. Drehmel . . . . . . . . . . . 61

## SESSION II: FILTRATION

"Granular Bed Filter For Particle Collection At High Temperature and Pressure," S. Yung, R. D. Parker, R. G. Patterson, S. Calvert, D. C. Drehmel . . . . . . . . . . . . . . . . . . . . . . . . . . 89

"Evaluation of a Granular Bed Filter, For Particulate Control in Fluidized Bed Combustion," R. C. Hoke, M. W. Gregory . . . . . . . . . . 111

"Performance and Modeling of Moving Granular Bed Filters," G. L. Wade . . . . . . . . . . . . . . . . . . . . . . . . . . . . . 133

"Ceramic Fabric Filtration at High Temperatures and Pressures," M. Shackleton, J. Kennedy . . . . . . . . . . . . . . . . . . . . . 193

"High Temperature Fine Particle Control Using Ceramic Filters," D. C. Drehmel, D. F. Ciliberti . . . . . . . . . . . . . . . . . . . 235

"Problems of Gas Purification Occurring in the Use of New Technologies For Power Generation," E. Weber . . . . . . . . . . . . . . . . 249

# TABLE OF CONTENTS (Concluded)

Page

## SESSION III: OTHER COLLECTION DEVICES

"High Temperature, High Pressure Electrostatic Precipitation," P. Feldman, J. Bush, M. Robinson . . . . . . . . . . . . . . . . . . . . 281

Pulse-Jet Acoustic Dust Conditioning in High Temperature/Pressure Applications," D. S. Scott, W. M. Swift, G. J. Vogel . . . . . . . . . . 309

"The Application of Sonic Agglomeration for the Control of Particulate Emission," D. T. Shaw, J. Wegrzyn . . . . . . . . . . . . . . . . . 325

"Cyclocentrifuge Development For Particulate Control, Phase I: Feasibility Study," J. T. McCabe . . . . . . . . . . . . . . . . . . . . 355

"Fine Particle Collection Efficiency in the A P.T. Dry Scrubber," S. Calvert, R. G. Patterson, D. C. Drehmel . . . . . . . . . . . . . . . 399

"Hot Gas Clean-Up By Particle Entrainment in Coal Slag Based Glasses," L. R. McCreight, A. Gatti, H. W. Rauch, M. J. Noone . . . . . 415

"Molten Salt Scrubbing For Removal of Particles and Sulfur From Producer Gas," R. H. Moore, G. F. Schiefelbein, G. H. Stegen, D. G. Ham 429

## SESSION IV: PARTICLE SAMPLING AND MEASUREMENT

"Particulate Sizing in High-Temperature, High-Pressure Combustion Systems," H. W. Coleman . . . . . . . . . . . . . . . . . . . . . . . . 467

"Particulate Sampling at High-Temperature and High-Pressure – The Extractive Approach," W. Z. Masters . . . . . . . . . . . . . . . . . . . 495

"Particle Field Diagnostic Systems For High Temperature/Pressure Environments," J. D. Trolinger, W. D. Bachalo . . . . . . . . . . . . . 527

"On Line Particulate Analysis on a Fluidized-Bed Combustor," E. S. VanValkenburg, H. N. Frock . . . . . . . . . . . . . . . . . . . . 557

"Characterization of Suspended Flue Gas Particle Systems With On-Line Light Scattering Particle Analyzers," J. C. Montagna, G. W. Smith, F. G. Teats, G. J. Vogel, A. A. Jonke . . . . . . . . . . . . . . . . . 579

# KEYNOTE ADDRESS

By:

Dr. P. C. White
Assistant Adminstrator for Fossil Energy
Department of Energy
Washington D.C.  20545

SPEECH PREPARED FOR DELIVERY BY
DR. PHILIP C. WHITE
ASSISTANT ADMINISTRATOR FOR FOSSIL ENERGY
AT THE
SYMPOSIUM ON HIGH TEMPERATURE
HIGH PRESSURE PARTICULATE CONTROL
WASHINGTON, D. C.
SEPTEMBER 20, 1977

Welcome to this Symposium, which is being held to summarize ERDA and EPA-funded work in hot gas particulate cleanup. Past meetings convinced us that such an exchange would be worthwhile--because the implications of combined-cycle development on our nation's energy future are potentially so far-reaching. As we head into a time of energy shortages and the implied environmental problems, we especially need technologies that will provide clean, efficient energy.

The President, in his National Energy Plan, has outlined a course that will help us provide such energy, including the increased use of coal. While coal makes up 90 percent of conventional U.S. energy reserves, it supplies only 18 percent of the energy we use.

One of coal's most important energy uses is to generate electricity. Yet in recent years electric power generation from coal has declined. We want to reverse that trend. As you know, to save dwindling supplies of oil and gas, FEA, under the authority of the Energy Supply Environmental Coordination Act of 1974, ordered power plants to burn coal for steam generation. Along those lines, the NEP, through imposing taxes on the use of oil and natural gas, encourages industry and utilities to switch back to coal. Soon new industries and utilities will be prohibited from burning those two scarce fuels, except under exceptional circumstances. By 1990, nearly all utilities will be prohibited from burning gas.

While coal is our most abundant fossil resource, it is also our dirtiest, and its increased use presents environmental problems. To ensure that the new Department of Energy gives adequate weight to the environment, an Assistant Secretary for the Environment within the new Department will oversee environmental research and monitoring for Federally-funded energy technology development programs. In ERDA we have started Environmental Development Plans (EDPs) to coordinate the technological development of new energy technologies with related environmental research. The EDP is ERDA's means to ensure that in decision-making, the environment receives the same consideration as do economics and technology.

Of course, our role in Fossil Energy will be key to ensuring that coal is used in an environmentally acceptable way. No fossil energy technology will be commercialized unless it is environmentally acceptable.

This Symposium focuses on a technical problem of great importance and great difficulty--one that affects both energy production and environmental quality: the cleanup of gases from burning and converting coal.

If we can gasify coal and then pass hot off-gases directly into an advanced turbine to generate electricity, we can gain several percentage points in the efficiency of the power generation. This means we need less coal, less mining, and lower cost all along the operation. We can only charge those gases directly to the turbine however, if we can have a very high efficiency in the particulate removal of the gases coming from the gasifier.

Hot gas cleanup is also important to certain technologies in which parts of unburned or unconverted coal exit to the atmosphere with the gas. To have a more efficient and economical system, we must collect and recycle this coal or reinject it for more complete conversion or combustion.

In ERDA Fossil Energy we are researching five coal technologies for which hot gas particulate removal is especially important. These technologies are coal gasification for both low and high Btu gas, atmospheric and pressurized fluidized bed combustion (AFBC, PFBC) and advanced power systems.

The pressurized fluidized bed combustion and low Btu gasification technologies are those in which the hot combustion gas must be cleaned of particulates before entering the turbine.

In high Btu gasification and atmospheric fluidized bed combustion, the recycling or reinjection of portions of the coal exiting with the gas insures more complete combustion or conversion.

The advanced power systems program is researching the turbines themselves, both open and closed-cycle. The program addresses turbine design and material. If we are successful, the open-cycle turbine could be fired with a high-temperature, high-pressure coal-derived gas.

For all of those technologies, the objective is to clean the gas of particulates without lowering its temperature and pressure. By cooling the gas, there is at least a partial waste of energy that could be used in the turbine or in the next step in the process, resulting in lowered efficiencies and increased costs. For instance, low Btu gas can be cooled and cleaned using conventional devices, but this would not be economical or efficient if the gas is to be used in an advanced gas turbine.

Our research on gas turbines has reached a state where particulate control has gained the spotlight as a major impediment to combined cycle development.

To clean the hot gas of particulates without lowering its high temperature and pressure, we can focus our research on three general areas. First, we can determine the quality requirements of the turbine, that is, the degree of abrasion and corrosion the turbine can withstand, which tells us to what level we have to clean up the gas. Second, we can characterize the raw gas intended for use in the turbines in terms of its physical makeup--by this I mean the size distribution of the particles and the temperature and pressure of the gas, and its chemical makeup--what chemicals are present and in what form. Finally, we can zero in on collection devices to clean the raw gas to the level which the turbine requires. Here we are researching the various options for gas scrubbing, collection techniques and component materials. This Conference reflects ERDA's and EPA's interest in all three areas.

Research in these areas addresses a number of interrelated unknowns, making progress particularly challenging. Gas sampling and measurement equipment is as prone to erosion and corrosion as the turbine itself, making it difficult to sample or treat the gas to determine what is damaging the turbine. We need data on the performance of collection systems under the high temperature, high pressure conditions involved in advanced power systems. Usually the data are collected during experimental work performed on a bench-scale, or via computer modeling; thus, it is difficult to scale up results to the larger dimensions which we will encounter at pilot or commercial scale. Since problems involved in hot gas cleanup are often interrelated, the results can affect the direction of work on the entire energy system. That is why a symposium of this sort is particularly useful.

The advantages of overcoming the problems involved with high temperature, high pressure particulate control are many. Once developed, we could apply these controls to other processes, such as metallurgical ones, where heat recovery is not now economical because of particulate problems, and where we need expensive machinery to cool the gas to a temperature compatible with conventional gas cleanup devices. Hot gas cleanup also would improve the efficiency of technologies such as atmospheric fluidized bed combustion and high Btu gasification.

But especially in electricity production, the advanced gas turbine combined with a steam-powered generator will produce economic and environmentally clean energy. Open cycle gas turbines are now used as peaking load units in power plants, but are fired with natural gas or oil, both virtually particulate-free. The advanced gas turbine, coupled with advanced coal technologies that on their own are clean and efficient energy systems, will offer an improved conversion efficiency of up to 45-50 percent, a substantial gain (10-15 percent) over that of conventionally coal-fired utility boilers. This approach could provide mid- and baseload power in the future. Other technologies, such as magnetohydrodynamics, could exploit the results of advanced power systems' work related to the use of topping and bottoming cycles. If these advanced technologies are developed, the electricity needed in the coming decades could be produced at higher conversion efficiencies, lower costs, and with fewer adverse environmental impacts than those offered by today's conventional utility steam boilers.

## EPA AND ERDA PROJECTS

Complementing the ERDA-sponsored research on hot gas cleanup, EPA has funded extensive research on particulate control devices, focusing on electrostatic precipitators, scrubbers, and filters. EPA is continuing to evaluate techniques to enhance collection efficiencies at high temperatures, in particular, through charging and precharging of high resistivity dust.

EPA is working with ERDA on several environmental assessments and is participating in ERDA's environmental sampling and monitoring programs for both the fluidized bed combustion and low Btu gasification programs. EPA is represented on ERDA task forces and will review the environmental development plans for ERDA technologies. We will discuss many of these ERDA and EPA studies at the Symposium.

We are working together at ERDA and EPA to perfect hot gas cleanup techniques applicable to advanced power systems and other technologies. Our joint efforts will hasten the development of the advanced gas turbine as a major new method of producing electricity using coal as the energy source. Such advanced power systems will provide the clean, efficient, economical energy from coal on which our National Energy Plan is based.

As we strive to continue the availability of dependable, clean energy supplies, we have to find the answers to these problems. Coal is our most tangible and abundant energy resource. Finding ways to curb the potentially severe environmental impacts associated with its use are mandatory. Our work at ERDA and EPA on high temperature, high pressure particulate removal is a critical stage in our movement toward combined goals of more efficient energy use and a quality environment.

# A REVIEW OF THE SYMPOSIUM

By:

A. A. Smith
Babcock & Wilcox, Ltd.
England

## A REVIEW OF THE SYMPOSIUM

By

Alan A. Smith
Babcock & Wilcox Ltd., England

The subject of particulate control in a high pressure, high temperature environment has resulted in the presentation at this Symposium of many papers of a highly technical and scientific content. This was to be expected in the current atmosphere of appraisal of the utilisation of energy resources. Particulate control, or clean-up of combustion gases, is of particular significance in respect of the application of the new processes being developed for electrical power generation.

I believe it opportune to make this unrehearsed and unprepared statement from the point of view of a major contractor in the energy business.

I have come to this Symposium from my company, Babcock & Wilcox Ltd., of the UK, together with our Consultant, Dr. C. J. Stairmand, with the objective of making a necessary assessment of the state of the art in respect of particulate collection.

We in BW have a vested interest in this technology since we already have several contracts in North America in the field of atmospheric and pressurised fluidised combustion. Some of you may be aware of the work carried out in the UK by BW and our partners, the National Coal Board, and also by our licensor, Combustion Systems Ltd.

You may also be aware of the work currently being carried out by BW and our partners, Stal Laval of Sweden, for American Electric Power. Particulate collection and control is therefore, for us, very much a live and ongoing requirement.

Whilst this has been a very interesting Seminar and a great deal of know-how and experience has been made public, I must confess that it is disappointing to find that although considerable progress is being made, it will evidently be quite some time before the necessary hardware comes on to the market. That is, available to a main contractor at a firm price with performance guarantees, and on a commercial scale. By commercial scale I mean for power generation plants of say 200 MW capacity. I think we must accept that the next generation, say 1,000 MW plus are not likely to appear for another decade.

I think it was the Keynote speaker who told the story of the airline pilot who announced to his passengers that although lost, he was nevertheless 20 minutes early. I feel bound to question--are we lost and 20 minutes late?

On a constructive note may I suggest that, in addition to continuing the work on development of high temperature, high pressure collection equipment, we should perhaps be encouraging turbine manufacturers to develop a new breed of turbines.

Of course they would like the same clean gas from the coal based process that they get from combusting say distillate. This is what you are trying to give them.

Our studies have indicated that to give them this, we shall need to install huge complex (and currently unproven at the commercial scale) clean-up equipment costing many millions of dollars. I think this has been verified at this Symposium.

The turbine manufacturer could make a big contribution to getting this process off the ground, and thus allow us to utilise the low grade fuels which utility companies want to employ, by relaxing their standards. I appreciate and understand their problems. However, with changing load pattern on a commercial scale plant there will surely be periods anyway when they may have to accept a relatively dirty gas if only by virtue of the combustion process.

Is blasting nutshells through the turbine the only possible solution? We hear talk of possible self cleaning turbines. Well where are they? Is anybody doing anything about it?

Although the subject of particulate collection has many industrial applications, I believe the one of most current significance is that related to power generation, in particular applied to gas turbines.

This will still be the case with combined cycle plants where the bulk of the energy generation is achieved by producing steam.

Protection of the environment can always, as a last resort, be accomplished by conventional equipment--for example electrostatic precipitators or bag filters operating at conventional temperatures after the exhaust gases have been cooled through heat recovery systems.

It would appear then that there are two routes to be followed in realising the goal of how to burn low grade fuels and recover the energy in power generation via gas turbines. One is through the subject of this Symposium and the other through a redevelopment of the gas turbine. No doubt the final solution will be a compromise because each possibility imposes complex technical problems.

I have no doubt we will get there, the immediate problem is when.

# SESSION I:

# FUNDAMENTALS

DENNIS C. DREHMEL
CHAIRMAN

# THE TOLERANCE OF LARGE GAS TURBINES TO "ROCKS", "DUSTS," AND CHEMICAL CORRODANTS

By:

E. F. Sverdrup, D. H. Archer, M. Menguturk
Westinghouse Research & Development Center
Pittsburgh, PA 15235

# THE TOLERANCE OF LARGE GAS TURBINES TO "ROCKS", "DUSTS", AND CHEMICAL CORRODANTS

By:
E. F. Sverdrup, D. H. Archer, M. Menguturk
Westinghouse Research & Development Center
Pittsburgh, Pa. 15235

An order of magnitude estimate of the particle concentration that can be allowed in the gas flowing through large industrial gas turbines for combined-cycle electric utility service can be made. The estimate is based on theoretical models that predict the rates of arrival of submicron particles on the blade surfaces and assumptions about the quantity of material that will stick. The estimate is also based on calculations of the trajectories of micron sized particles and estimates of particle impact damage to turbine blading. Hard data, taken under conditions simulating turbine operation is needed to calibrate these models. Cleaning of the turbine expansion gas to 0.002 grains/scf with particles larger than six microns in diameter effectively removed is our best current guess as to the turbine expansion gas cleanliness required. Strict attention must also be given to controlling sodium compounds to about 50 parts per billion by volume in the expansion gas.

# SECTION 1

# INTRODUCTION

## BACKGROUND

Gas turbine generators used by electric utilities for meeting peak power demands have been fired with "clean" fuels - distillate fuel oil or natural gas. Erosion and deposit formation in these turbines has not been a problem. Hot corrosion has been controlled by limiting alkali metal concentrations in the fuel oil to between 0.25 and 0.5 ppm by weight. Formation of sodium sulfate melts which would rapidly corrode the blading has been prevented by this limitation. In those turbines burning oils having vanadium contents, hot corrosion is controlled with fuel additives such as magnesium oxide and silica. These additives react with the vanadium compounds to form solids and prevent aggressive vanadium based melts from forming on the blading.

The use of large gas turbines in combined cycle power plants fired with coal-derived fuels is being considered to provide for electric utilities' "intermediate-load" requirements. These combined-cycle plants offer the potential of higher cycle efficiencies at costs competetive with conventional steam plants with stack-gas cleaning to meet air quality standards. In coal fueled combined-cycle plants, the gas turbines expand a gas containing a new mix of aggressive chemicals and particles. Reliable and economic methods must be devised to achieve sufficient gas cleanliness, without degrading system performance to the extent that the combined-cycle plant loses its advantages over a conventional steam plant burning the coal directly.

### How Clean is Clean Enough?

We are concerned with three interacting tolerances: (1) to control corrosion of turbine parts, (2) to control the build-up of deposits in the flow path, and (3) to control erosion of the turbine parts by large particles. The gas cleaning system must control the concentrations of molecular sized chemical contaminants, sub-micron "dusts", and micron sized "rocks".

# SECTION 2

# CONTROL OF HOT CORROSION

## THE TOLERANCE FOR CHEMICAL CONTAMINANTS

Molten sodium sulfate must be prevented from remaining on the turbine blades for any appreciable length of time. These melts corrode turbine blading and act as glues to cement deposits. Chemical thermodynamics can be applied to establish the concentrations of gaseous sodium compounds which can be permitted above the blade surface. Figure 1 shows the reactions controlling the formation of sodium sulfate which melts at about 880°C (1620°F) and which can form on portions of the first and second stage blading of a modern turbine. Three processes are involved: (1) direct volatilization of sodium sulfate - this is not a very important process because of the sulfates' low volatility at blade temperatures, (2) reactions with water vapor and sulfur oxides to form volatile sodium hydroxide - a process important in oil and coal fired turbines, and (3) reactions with hydrogen chloride to form volatile sodium chloride - this reaction is important in turbines expanding gases derived from coal because of the appreciable chlorine contents of coal.

Figure 2 presents the calculated maximum sodium concentrations which can be permitted in the turbine expansion gas while preventing a liquid sodium sulfate deposit from remaining on the blading. The allowed concentration is a function of the chlorine and sulfur oxide concentrations in the gas. In an oil fired turbine the chlorine concentration in the expansion gas is negligible and this simple chemical equilibrium model predicts an allowable sodium concentration of about 50 parts per billion by volume in the expansion gas. (An oil fired turbine consuming about 16 pounds per second of fuel oil containing 0.5 ppm by weight of sodium and burning it with air will produce a turbine exhaust flow of about 760 lb/sec of combustion gases having a sodium concentration of about 80 parts per billion by volume.)

Although the primary concern of this conference is particulates, it is important to recognize that chemical contaminants which can form aggressive melts must be strictly controlled.

# SECTION 3

# CONTROL OF DEPOSITION

## TOLERANCE FOR SUB-MICRON PARTICLES

Among the many factors that affect the rate of arrival of sub-micron size particles at the turbine blade surface are the concentrations of these particles in the gas stream and the thickness and turbulence levels in the boundary layers which are present on the blading. These arrival rates have been calculated in two dimensional turbine flows where the main stream gas flow is highly turbulent and where there is both turning of the main stream and strong pressure gradients in the direction of flow. Three different mechanisms are controlling the rates of particle arrival: (1) molecular diffusion, (2) the changes in the intensity of the gases' turbulent fluctuations caused by the braking action of the blade surface on the fluid flow, and (3) the particle's size and inertia which control its response to the turbulent velocity fluctuations in the gas. The structure of the boundary layer gas flows is determined by the turbine's flowpath design and is calculated. The deposition program then calculates the arrival rates of the particles as a function of their size at the various locations through the turbine stage. By combining the calculated arrival rates with the concentrations of each size fraction of particles at the turbine inlet, the rate of deposit formation can be calculated provided one knows how much of what arrives sticks. Because we do not have either a theoretical model nor experimental data to predict deposit growth under conditions relevant to a coal fueled turbine to determine how much of the arriving particulate will stick, we can predict the rate of deposit growth and the consequent effects on turbine performance only by assuming how much of the arriving particles will stick on the surface.

If we assume that everything that arrives at the blade surface that is larger than one micron bounces off without removing surface material or deposition - and everything that is smaller than one micron sticks, and if we further assume that what sticks consolidates into a film having the particle density of 2.5 grams/cm$^3$, then Figure 3 presents the rates of deposit build up through the first stage of a large gas turbine for a particle concentration of 0.002 grains/scf entering the turbine having the particle size distribution shown in Figure 4. (This particle size distribution is similar to that measured after gas cleaning with fabric filters).

If everything smaller than one micron diameter arriving at the turbine blade is sticking, Figures 3 and 5 show that first stage stator passages constrict with a deposit growing 0.4 cm thick on both its pressure and suction surfaces in 1000 hours of operation. If only one tenth of what arrives sticks, it would take 10,000 hours for the same deposit thickness to develop.

How does the growth of this deposit effect power developed by the turbine? Preliminary calculations show that the effect of the changing blade profiles on the efficiency of the turbine stage are small, (assuming that the rapid arrival of material at the vane nose is mostly blown away) but the choked passage restricts the mass flow through the turbine. The power developed would be expected to drop off with time as shown in Figure 6. A five percent reduction in turbine stage power would be expected after 250 hours of turbine operation with everything sticking or after 2500 hours of turbine operation with only 10% sticking. Cleaning of the turbine would then be required.

It would appear that, depending on the actual sticking fraction, the concentrations of sub-micron particulate that can be permitted at the inlet to the turbine to control deposition lie in the range 0.002 to 0.02 grains/scf.

The amount of fine particulate that actually will stick depends on the gas chemistry, the choice of turbine inlet temperature, and the blade metal temperatures maintained by the turbine blade cooling system.

# SECTION 4

# CONTROL OF EROSION

## THE TOLERANCE TO MICRON SIZE PARTICLES

Just as it is possible to calculate the arrival rate of small particles on the turbine surfaces, a computer model is available to calculate the trajectories of the particles through a turbine stage and to determine the number, angle and velocity of impact of larger micron size particles whose motion is determined by the drag forces exerted by the gas flows and by the particles' inertia. Figure 7 shows the trajectories of six micron particles that are flowing through the first stage, midway between the inner and outer radius of the turbine flow path, in a large electric utility turbine. The figure shows that 18% of these six micron diameter particle impact on the pressure surface of the first stage turbine vane and all of them impact on the pressure surface of the first stage rotor blade. Figure 8 shows the calculated variation of angle and velocity of impact with position over the first stage vane surface. For each impact, the computer calculates the amount of metal removed from the blade considering both the angle and velocity of impact using the erosion damage prediction model of Figure 9 to make the estimate. Figure 10 shows the calculated metal recession rates as a function of position through the first stage vane and blade row. Again one can add up the damage expected from each particle size at the concentration expected to be present in the gases leaving a particle cleaning system.

Advantage can be taken of the ability of the computer model to permit us to mathematically vary the erosion damage response of the blade material from a very ductile to a very brittle material in order to see the sensitivity of the blading to the character of the blade. This has been done by calculating the response using the four assumed erosion damage characteristics of the blade material shown in Figure 11. If the gas being expanded through the turbine contains 0.002 grains/scf of particles with essentially no particles larger than 6 microns in diameter then the expected metal recession rates at the three critical locations - rotor blade nose - and rotor and stator trailing edges are shown in Figure 12 as a function of the "ductility" of the blade material. Figure 12 indicates that for the 0.002 grains/scf grain loading and the full range of "ductility", the greatest metal recession in 10,000 hrs. is on the order of 0.1 inch which is about the trailing edge thickness used in electric utility turbines.

These erosion predictions are based on estimates of peak erosion rates in the curves in Figure 11 for coal ash and sulfur sorbent particles impacting superalloy turbine materials under turbine conditions. Experimental erosion data for these materials and turbine conditions are necessary for more accurate erosion evaluations.

# CONCLUSIONS

- Extensive work has been done to understand how much particulate matter can safely be put through a turbine.

- Theoretical models to predict the arrival rates of submicron particles and the effect of a deposit layer on turbine performance have been developed.

- Models to predict the growth and removal of deposits are not available nor is experimental data taken under condition relevant to a coal fired combined cycle plant available to calibrate the deposition models.

- Erosion damage prediction models based on "guessed" data of the response of the materials to particle impact have been developed.

- Experimental data on the response of turbine materials to impact by micron size particles under appropriate turbine conditions is needed.

- An order of magnitude estimate of the gas cleanliness required to successfully operate a large industrial gas turbine in combined cycle service has come out of all this - in the gas flowing through the turbine we are looking for particulate concentrations within an order of magnitude of 0.002 grains/scf with the concentration of particles larger than 6 microns in diameter reduced to negligible levels.

- Careful attention must be given to maintaining sodium chloride and hydroxide concentration in the turbine gases in the tens of parts per billion by volume range to avoid corrosion and glueing of deposits.

Dwg. 6357A67

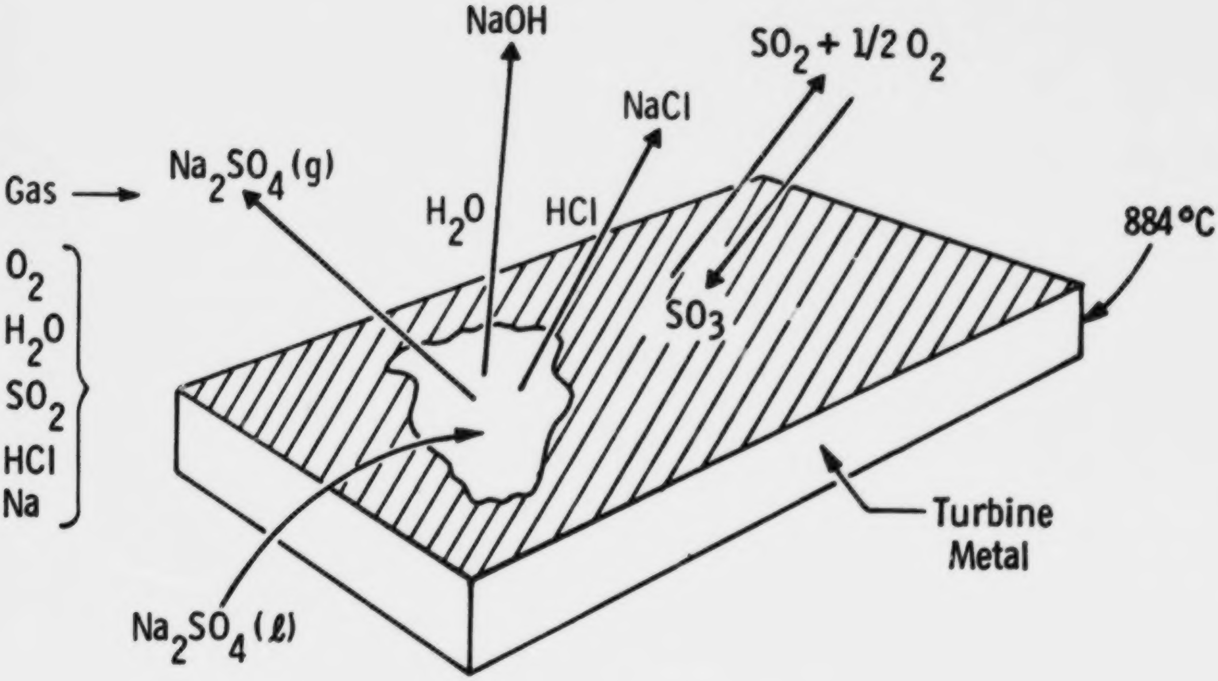
NaOH
$SO_2$ + 1/2 $O_2$
NaCl
Gas →
$Na_2SO_4$ (g)
$H_2O$
HCl
884 °C
$O_2$
$H_2O$
$SO_2$
HCl
Na
$SO_3$
Turbine Metal
$Na_2SO_4$ (ℓ)

Three Processes Remove Liquid Film:

(1) $Na_2SO_4 (\ell) \rightarrow Na_2SO_4 (g)$

(2) $Na_2SO_4 (\ell) + 2H_2O \rightarrow 2NaOH + SO_3 + H_2O$

(3) $Na_2SO_4 (\ell) + 2HCl \rightarrow 2NaCl + SO_3 + H_2O$

Fig. 1 —Theoretical turbine tolerance to alkali metals

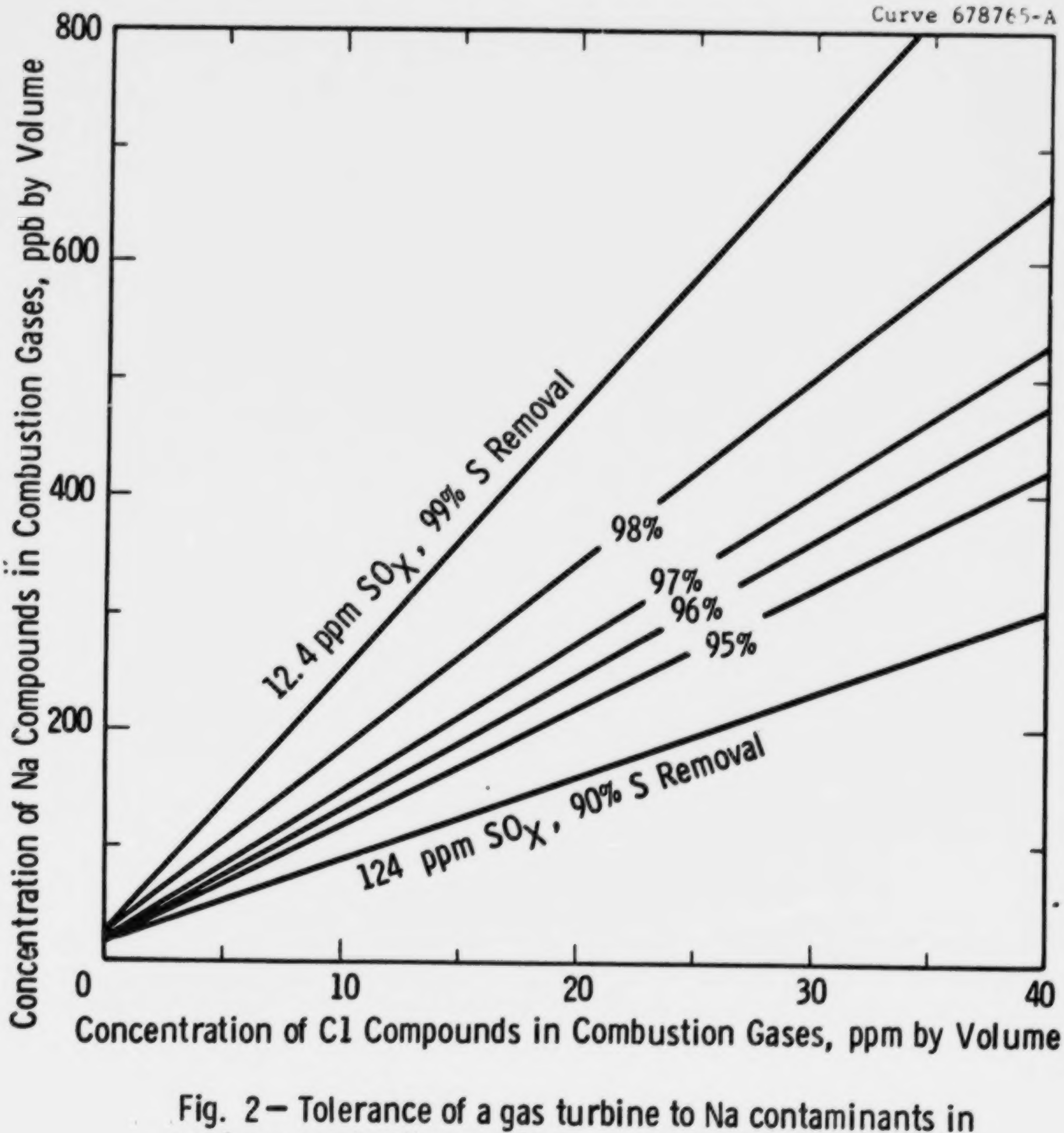

Fig. 2 — Tolerance of a gas turbine to Na contaminants in coal gas combustion products. The effects of Cl and $SO_X$ variations are indicated

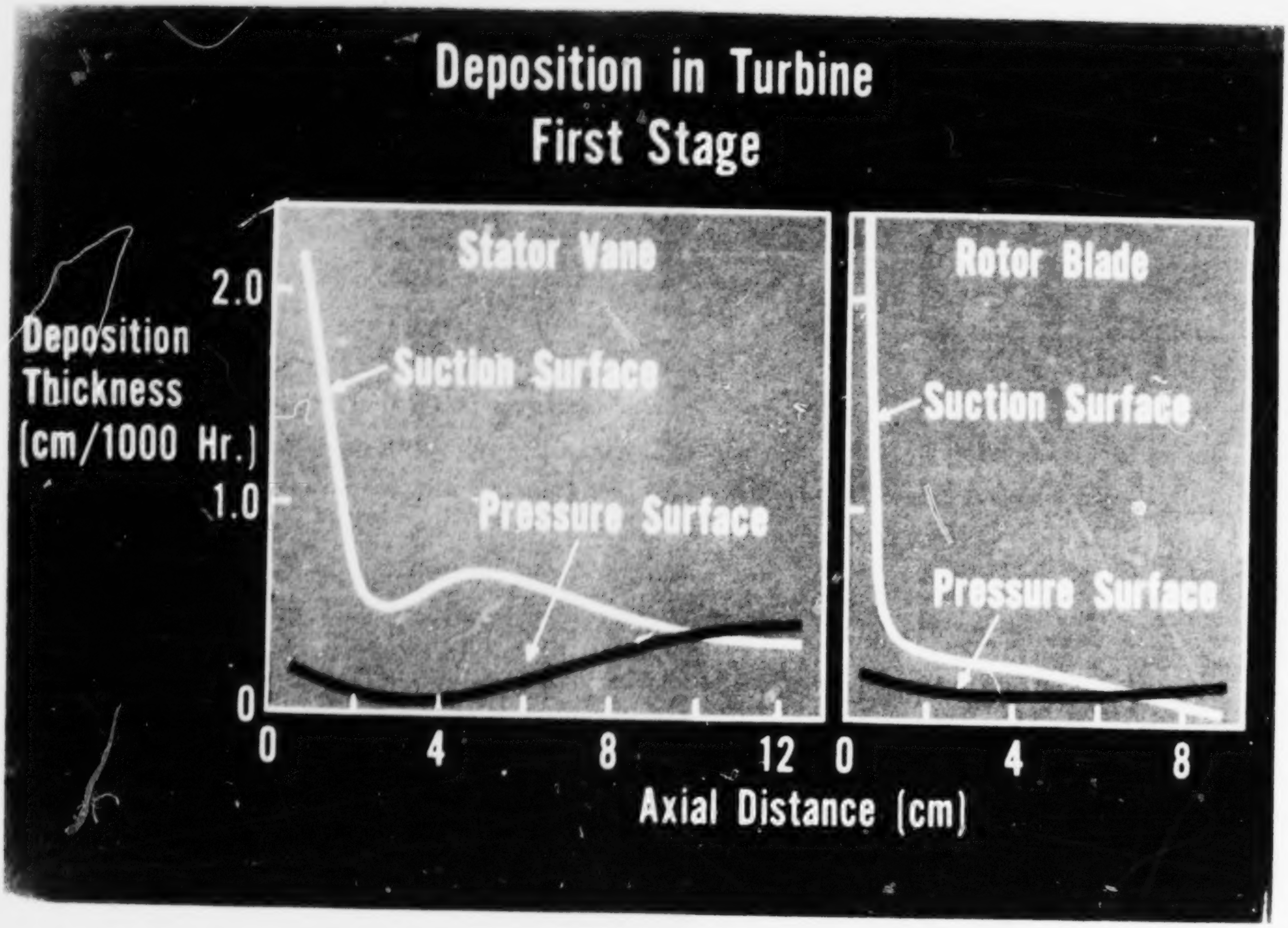

Fig. 3 – Deposition in first stage of a 60 - 70 MW turbine for an inlet particle concentration of 0. 002 gr/ scf - everything below 1 micron sticking

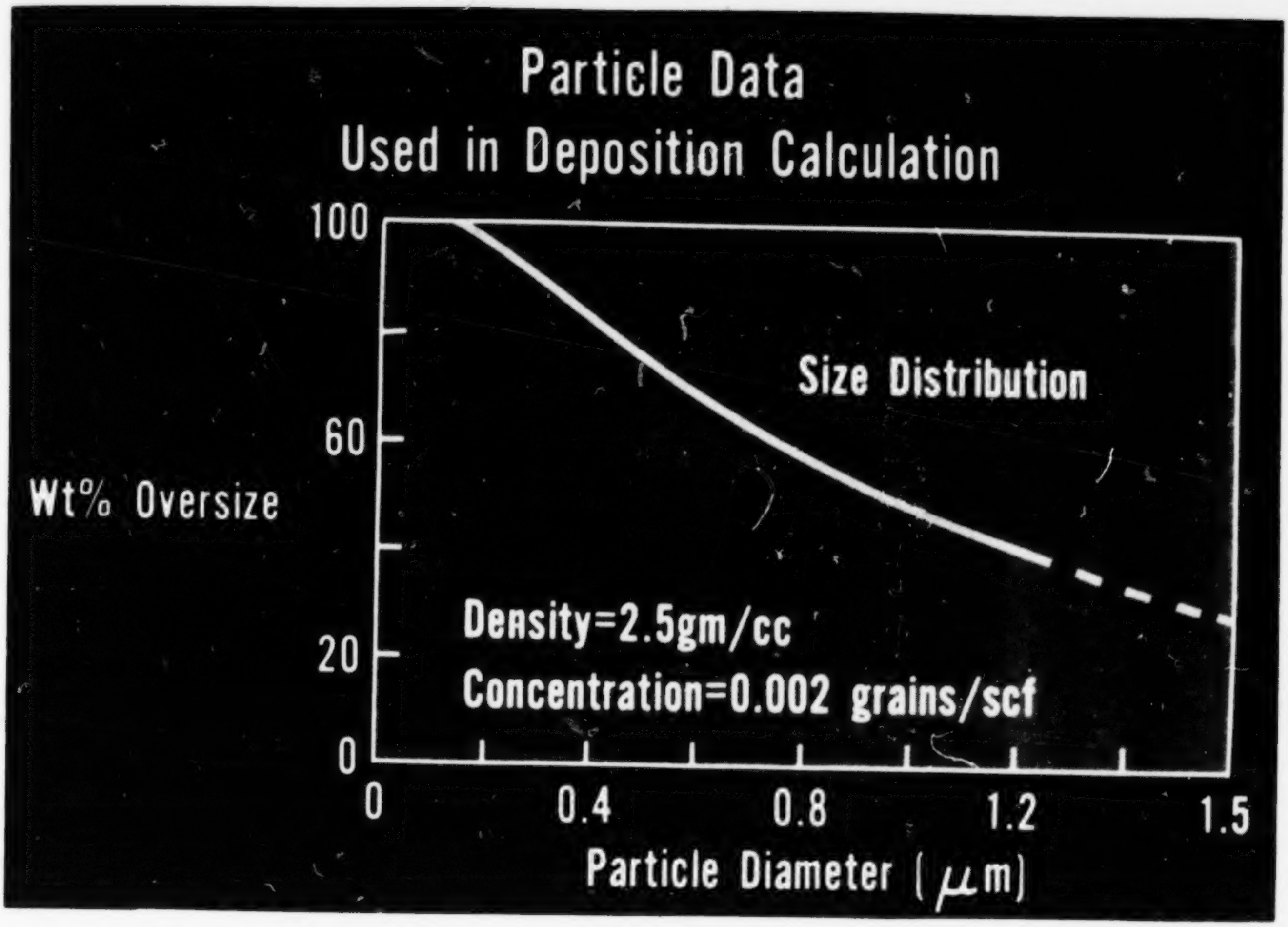

Fig. 4 — Particle size distribution used for deposition rate calculations

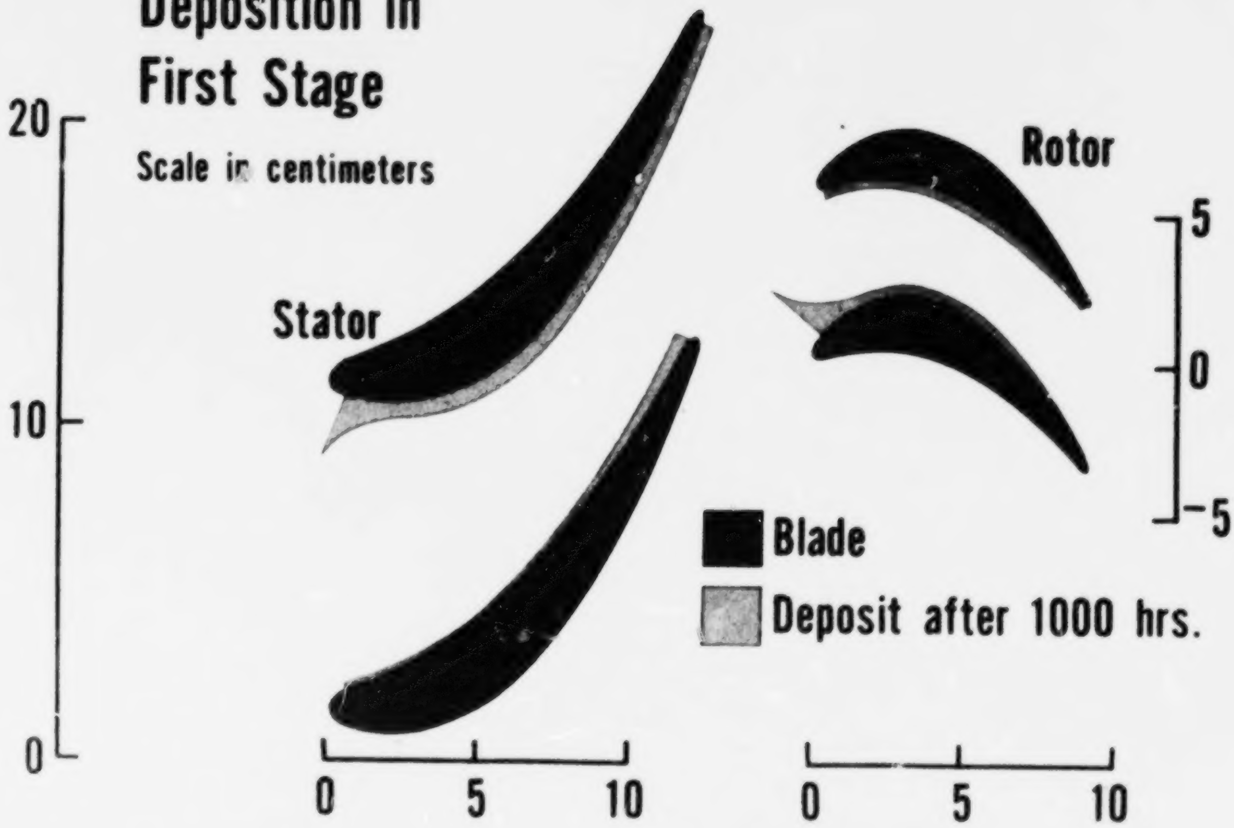
Deposition in First Stage
Scale in centimeters
20
10
0
Stator
Rotor
5
0
−5
Blade
Deposit after 1000 hrs.
0
5
10
0
5
10

Fig. 5 — Calculated deposit build- up after 1000 hours

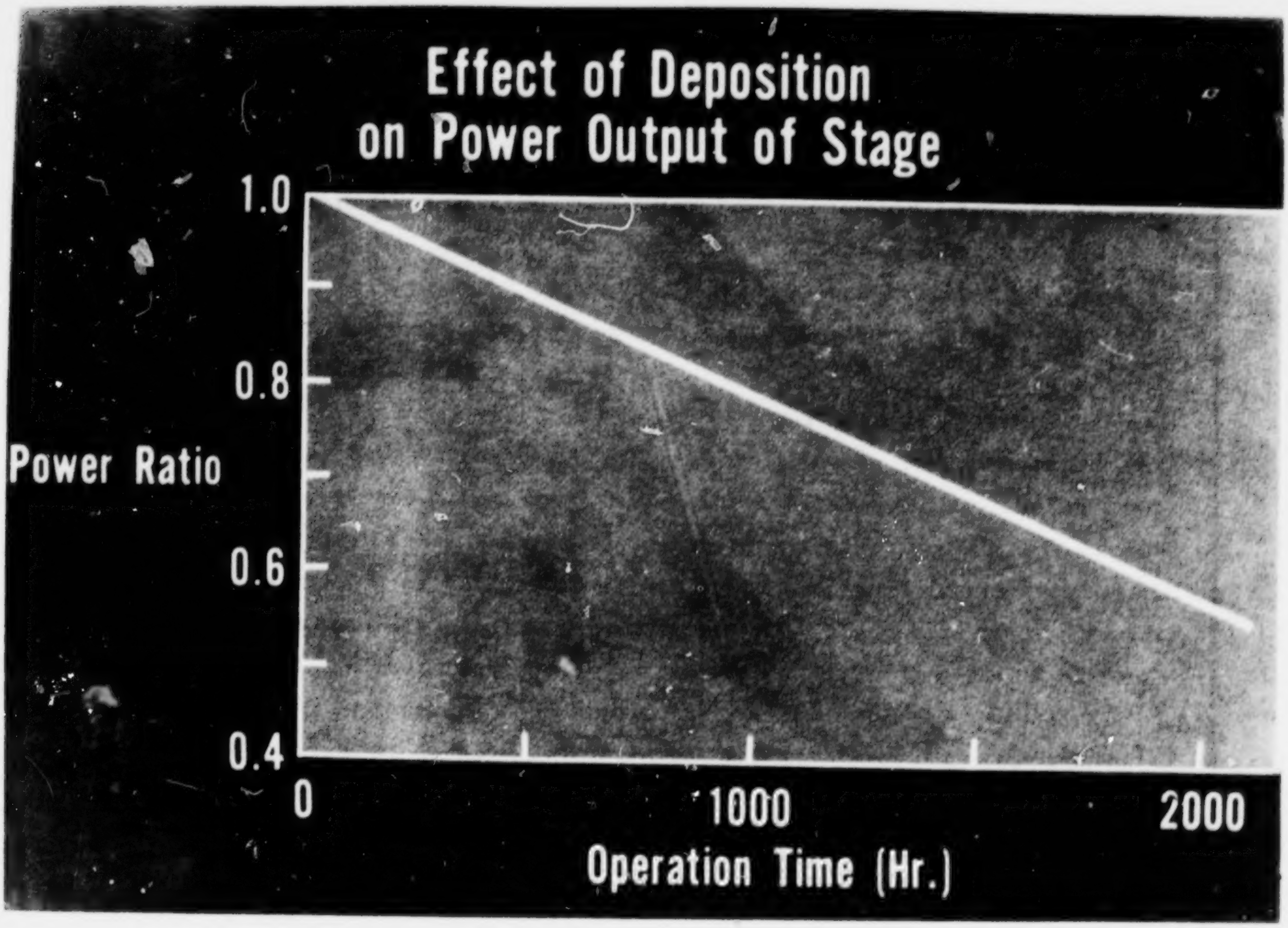

Fig. 6 — Effect of deposition on power output of the turbine stage

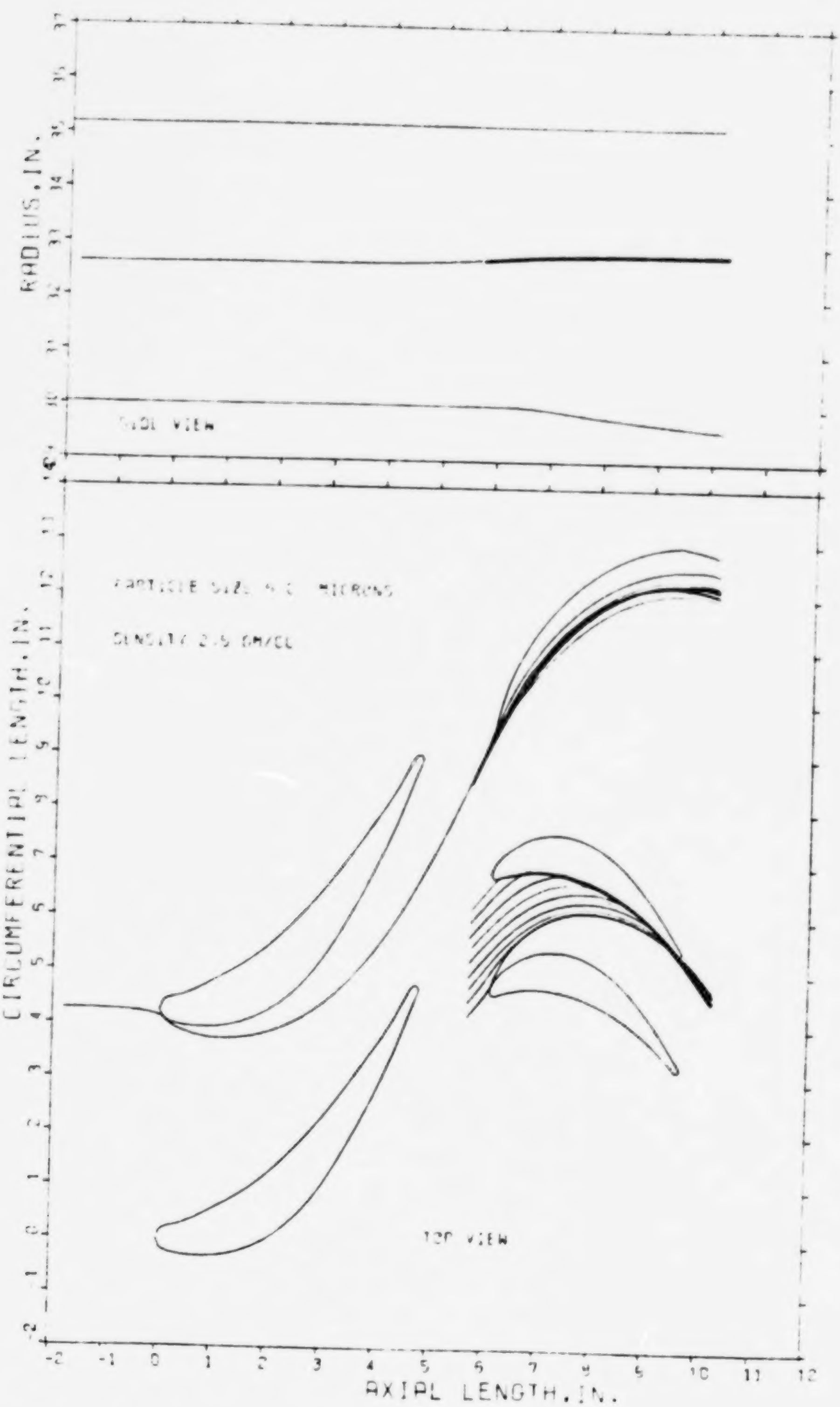

Fig. 7 — Trajectories of 6 micron particles through a turbine stage. (18% of 6 micron particles impact the first stage stator - 100% impact in the 1st stage rotor)

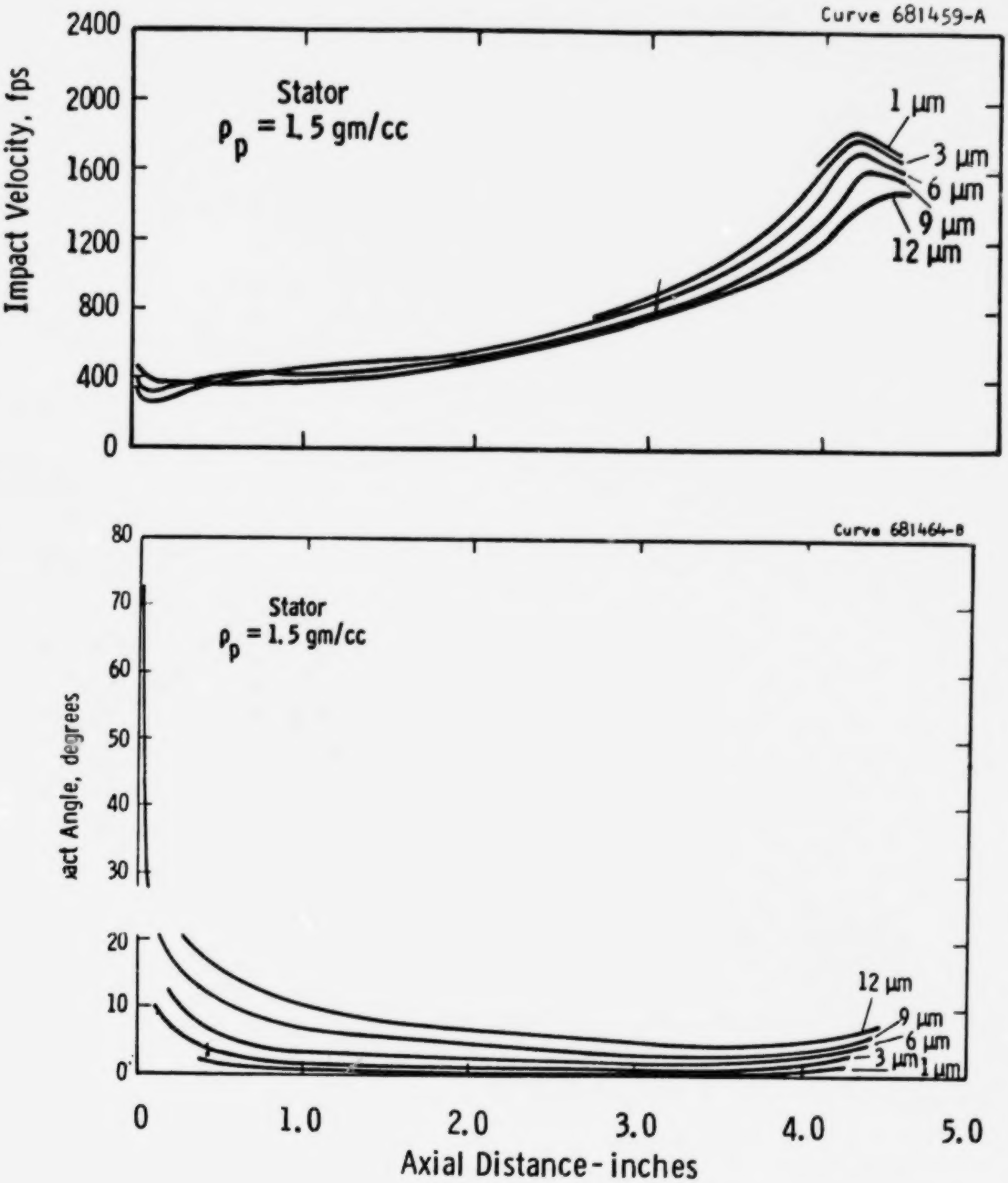

Fig. 8 — Particle impact velocities and impact angles as a function of position on the first stage stator vane of a 60 - 70 μω turbine

Curve 681611-A

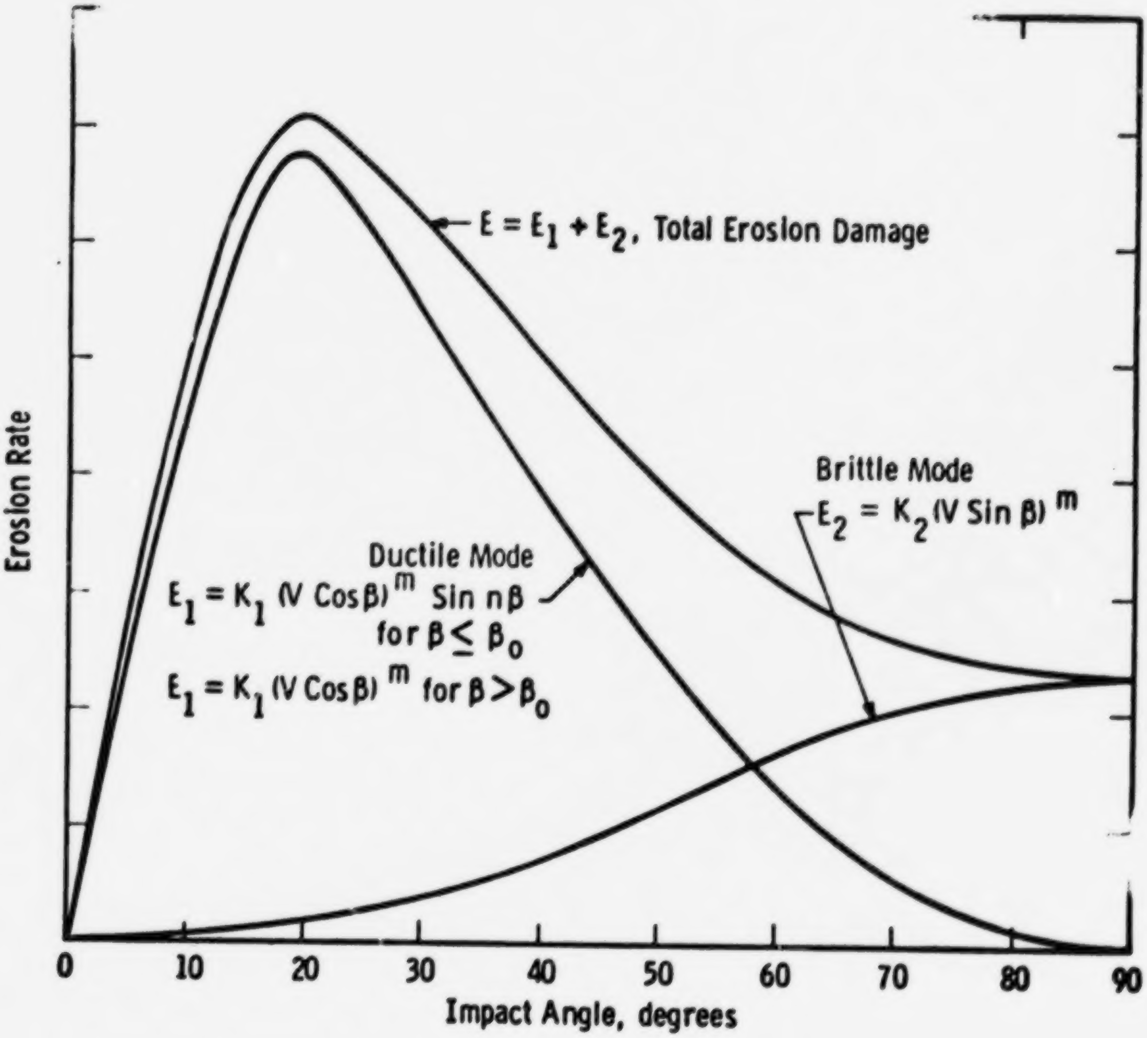

Fig. 9 — Erosion damage model

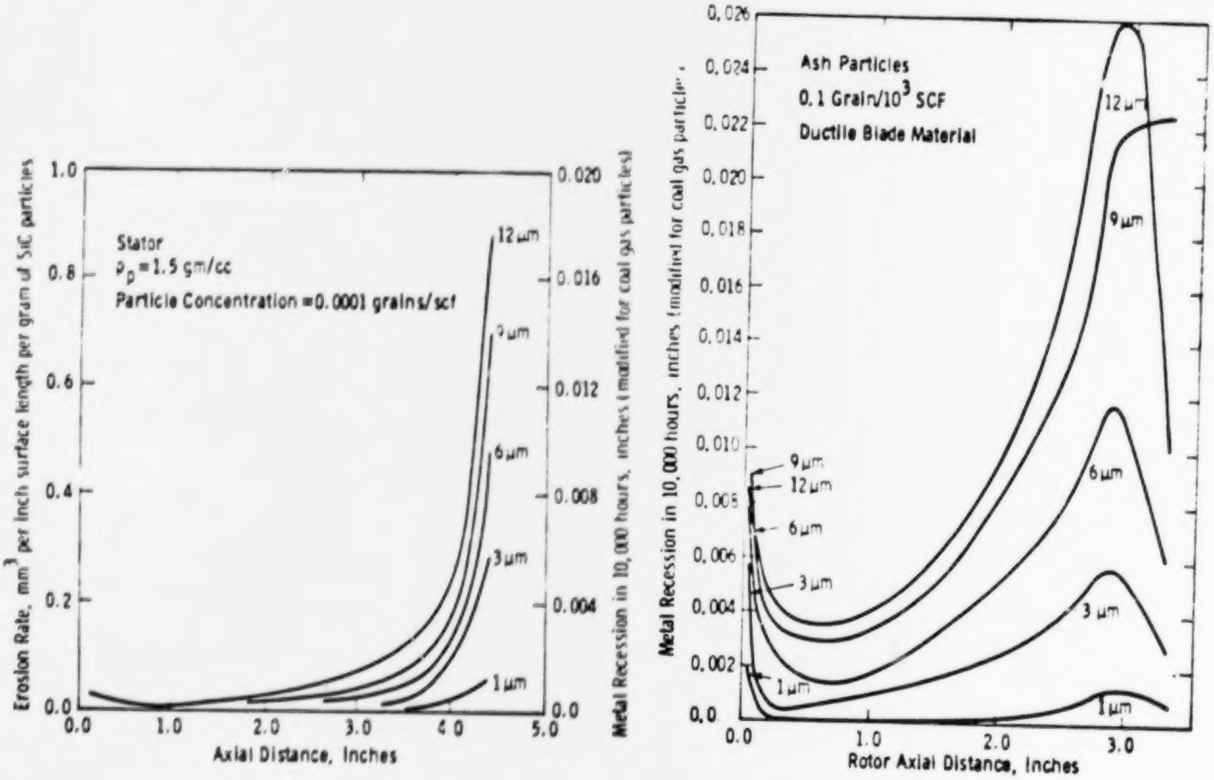

Erosion rate in stator as a function of axial position

Erosion rate in rotor as a function of axial position

Fig. 10 – Calculated erosion of 1st stage stator vane and rotor blade pressure surface - electric utility gas turbine

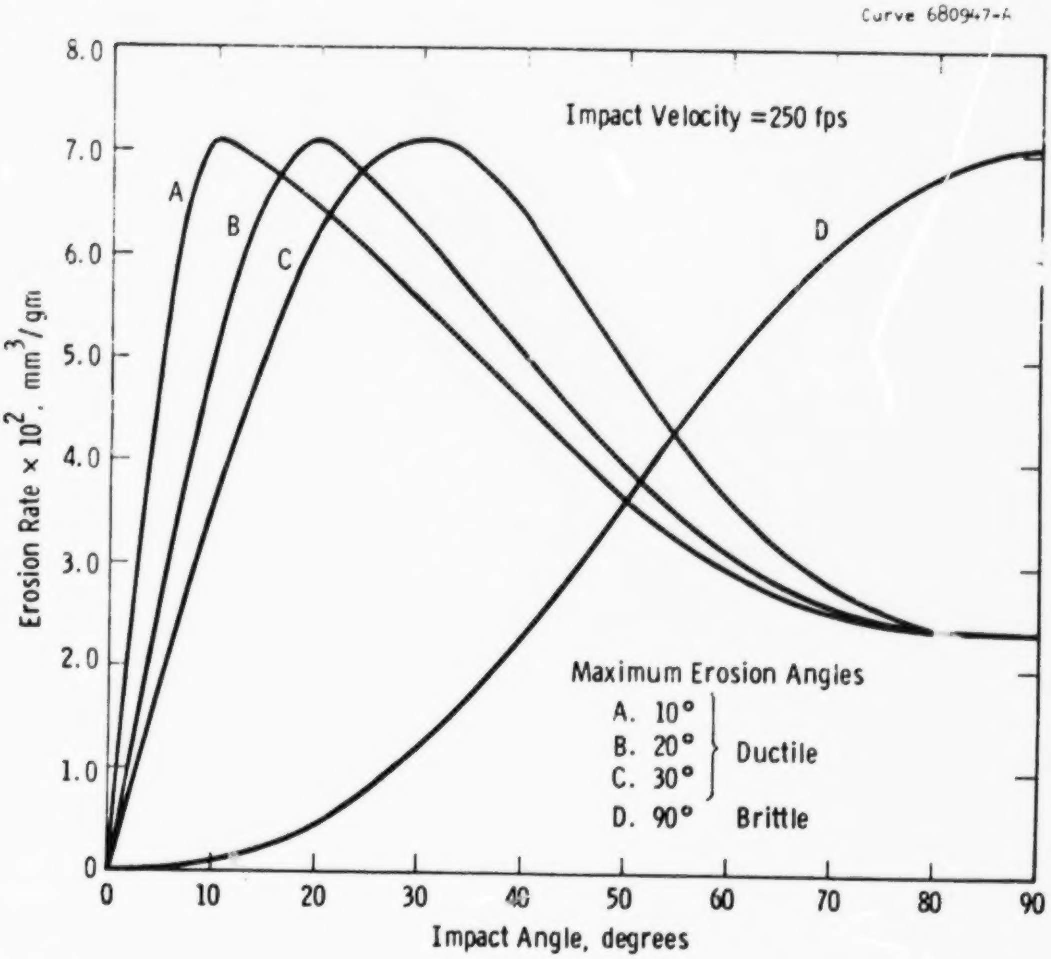

Fig. 11 – Erosion curves corresponding to four cases of blade material response

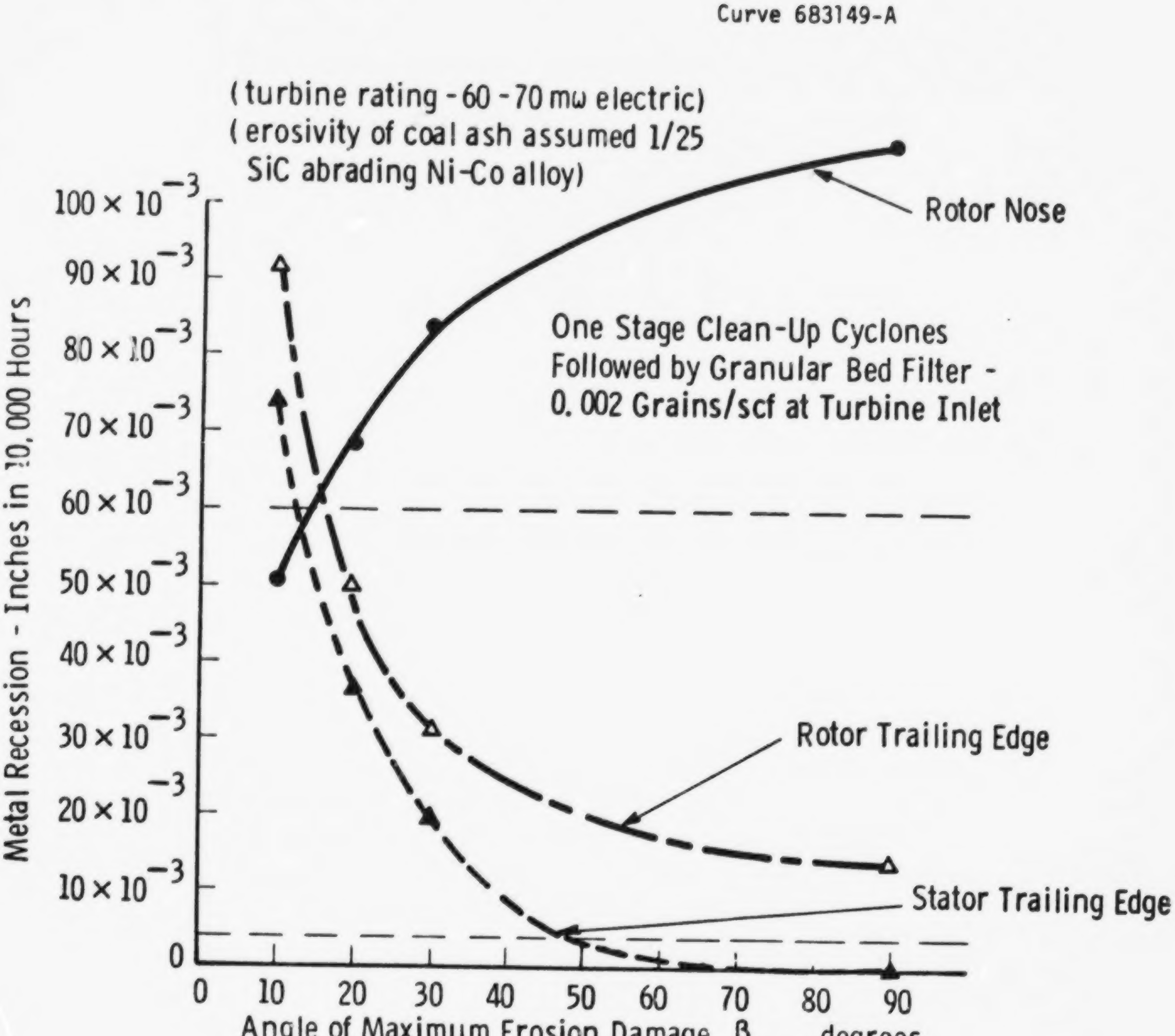

Fig. 12 — Sensitivity of gas turbine first-stage erosion to angle of maximum erosion damage

# PRESSURE AND HOSTILE ENVIRONMENTS

By:

J. Hull
Acurex Corporation/Aerotherm Division
Mountain View, CA 94042

# MATERIALS FOR USE IN HIGH TEMPERATURE/ PRESSURE HOSTILE ENVIRONMENTS

By:

Jacques Hull
Acurex Corporation/Aerotherm Division
Mountain View, California 94040

Particulate control equipment for coal conversion systems must withstand high temperatures (>1200°F), high pressures (>5 atm), and sulfidizing or carburizing atmospheres. In this paper, limitations of commercial materials used for particulate control equipment are summarized and causes for material deterioration are outlined. Data are presented on materials that resist deterioration, and possible trends in the development of improved materials are indicated.

# MATERIALS FOR USE IN HIGH TEMPERATURE/ PRESSURE HOSTILE ENVIRONMENTS

Coal conversion equipment requires materials that can withstand environments with particulates and gases containing carbon and sulfur at high temperatures (above 1200°F (650°C)) and high pressures (above 5 atm). While most commercially available high-temperature materials perform well at high temperatures in air, they may be subject to severe corrosion in carburizing or sulfidizing atmospheres.

Materials for coal conversion equipment must be either metallic or ceramic, since polymeric materials cannot survive temperatures above 800°F (427°C). Metallic materials are subject to compound formation, and can oxidize, carburize, and sulfidize. Because they are used primarily in air, alloys that resist oxygen at high temperatures do so by forming protective oxides. These oxides then act as barriers to further oxidation.

It is not surprising that these oxide barriers do not resist penetration by sulfur and carbon effectively at high temperatures. Until new alloys are specifically developed to resist these elements, the few alloys which have demonstrated some degree of resistance to corrosive attack in coal conversion environments will have to be used.

In contrast, ceramic materials are made up of compounds such as oxides, carbides, and sulfides. Since these compounds must dissociate and recombine in order to form new compounds, they tend to resist corrosive attack more successfully than metals. Ceramics also are more resistant to high-temperature attack because they are more refractory than metals (their melting or dissociation temperatures are significantly higher). But they do have some undesirable properties, such as poor thermal shock resistance.

Materials respond to high pressures somewhat differently. Pressure affects corrosive attack by altering the reactions (and the reaction rates) which occur at atmospheric pressure. Thus, while one reaction may control at room pressure, a different reaction may govern under high pressure, and the reaction products may be different. Pressure tends to slow down reaction rates in the solid state, and consequently, it can slow down corrosive attack. However, pressure can also slow down the formation of barriers which protect against corrosive attack. Metallic resistance to high-temperature and high-pressure corrosive attack can be seen in terms of two competing phenomena: the formation of protective barriers, and the simultaneous penetration of these barriers by hostile elements.

Ceramic materials behave somewhat similarly under corrosive attack. For instance, under the proper conditions, silicon carbide will react in air to form oxides of silicon. Under other conditions, silica will react with steam to form silicic acid. Consequently, the fact that the ceramics themselves can act as protective barriers does not protect them from corrosive attack.

In addition to the properties of the metals and ceramics, the forms that these materials are used in are important. While scrubbers, cyclones, and most other equipment for controlling particulates use metals and ceramics of more-or-less conventional dimensions, equipment such as electrostatic precipitators, fabric filters and granular bed filters will require that some of their components be of fine dimension. Thin metallic wire, ceramic filaments, or ceramic microspheres are required. This presents an additional problem since materials of fine size disintegrate more rapidly under corrosive attack than bulk materials. Consequently, it is even more necessary to obtain materials which are highly resistant to corrosive attack.

In the remainder of this paper, these problems will be discussed in detail. The corrosive attack of metallic materials will be described first. Because the presence of particulates also may result in erosive attack, the erosion resistance of both metals and ceramics will be considered, followed by a discussion of the corrosive attack of ceramic materials. Finally, materials of fine dimensions will be looked at in light of the more severe corrosive and erosive problems inherent in such materials.

## GASEOUS CORROSION OF METALLIC MATERIALS

Metals useful in high-temperature particulate control equipment include the iron-base, nickel-base and cobalt-base alloys. The iron-base alloys include both stainless steels and superalloys. Some examples are shown in Table I. While iron is the main constituent, chromium is an important alloying element present in significant quantity (~20 percent), and nickel generally is present. Chromium forms a tenacious, protective oxide barrier, and nickel adds significant high-temperature strength to the alloy.

Some nickel- and cobalt-base superalloys are listed in Table II. While nickel and cobalt generally are the predominant elements in the alloy classes listed, they are not always the major element present. For example, Inco-800 is an important nickel-base alloy not listed in Table II, consisting of 47 percent iron, 31 percent nickel, and 21 percent chromium. As in Table I, these superalloys contain a substantial amount of chromium and nickel.

The nickel in the alloys provides the necessary high-temperature strength, as illustrated in Figure 1.[1] This figure also shows that rupture strength increases with increasing nickel content in the alloy. While strength drops rapidly with increasing temperature, alloys containing more nickel have higher rupture strength at higher temperatures. Unlike failure at room temperature, delayed failure can occur at high temperatures under reduced loads. Materials often are selected on the basis of the time it takes them to rupture under stress at temperature. Design criteria generally include the creep rate (rate of change in dimensions) for the given stress and temperature conditions, since materials tend to creep at high temperatures.

Corrosive attack of a metal is highly dependent on the gaseous environment. Table III lists the type of gases generally present in coal conversion processes, and the typical amounts in which the gaseous components are present. Most of these gases can be present over a very wide range, and consequently, metals should be selected for the specific environments to which they will be exposed. In one typical environment (the laboratory gas used for screening tests at IITRI on the MPC/ERDA program[2]), a number of alloys have been tested at 10 atmospheres and 1800°F (982°C). This environment has an equilibrium composition (in volume percent) as follows: 32.5% $H_2O$, 31% $H_2$, 3% $CH_4$, 17% CO, 15% $CO_2$, 1% $NH_3$, 0.5% $H_2S$. If the temperature is lowered to 1500°F (815°C), the equilibrium composition shifts to 36.5% $H_2O$, 23% $H_2$, 9% $CH_4$, 11% CO, 19% $CO_2$, 1% $NH_3$, 0.5% $H_2S$. Thus, the reaction between the gas and metal is influenced not only by the temperature, but also by the change in the gas composition.

If sulfur is present in the environment, the melting temperature of the sulfides of the elements present in the alloy must be considered. These are listed in Table IV. It is evident that when nickel combines with sulfur at temperatures above 1193°F (645°C), the compound nickel sulfide will be in the form of a molten slag. This means that when sulfur penetrates the chromium oxide protective barrier and attacks the nickel, a molten slag will result at high temperature. The slag will flux away the surface material, removing the protective scale. This can result in catastrophic failure of the material. However, the sulfur first must combine with the nickel present. Since this is a diffusion-controlled phenomenon, the rate at which the combining occurs slows down at an exponential rate as the temperature is lowered. Consequently, this slagging phenomenon is only critical at very high temperature (over 1600°F for most alloys).

The formation of molten cobalt sulfide requires temperatures in excess of 1600°F (870°C); molten iron sulfide requires temperatures above 1800°F (982°C). Chromium sulfide remains solid to even higher temperatures. Sulfate formation in an oxidizing atmosphere (in contrast to sulfide formation in a reducing atmosphere), is not as severe a problem. The kinetics are not as favorable, and the respective melting temperatures are higher.

If the thermodynamic stability conditions are such that the metal oxide forms in preference to the sulfide, then sulfidation need not be feared. Figure 2 illustrates the influence of the gas composition at given temperature and pressure conditions on sulfide formation.[3] The IITRI gas is plotted for both 0.1 and 1.0% $H_2S$. In both cases, the points will be within the chromium oxide field of stability and will not form chromium sulfide. (This can be seen by extending the $CrS-Cr_2O_3$ line in Figure 2.) The 1.0% $H_2S$ point falls within the sulfide stability region of both the nickel and the iron, in preference to the oxide region. Consequently, these sulfides will form, subject to the kinetics of the reactions. The 0.1% $H_2S$ point falls on the boundary of the Fe-$Fe_xO_y$ fields and in the nickel field. This means that the nickel in the alloy will not combine with either sulfur or oxygen, and the iron may combine with oxygen. At somewhere between 0.1 and 1.0% $H_2S$ (approximately 0.3% $H_2S$ by interpolation), there will be enough sulfur present to form both iron and nickel sulfide. Consequently, the alloys are subject to sulfide damage if the $H_2S$ content of the gas is more than about 0.3% $H_2S$. Of course, if the CO, $CO_2$ and $H_2$ levels in the gas are changed (or the temperature or pressure changed), the sulfide formation conditions will also change.

Figure 3 illustrates the effect of changing the pressure and/or the gas composition on carburization.[4] The gas composition at 1 atmosphere and 1800°F (982°C) with a $CH_4$ level of 10% is 37% $H_2O$, 23% $H_2$, 17% CO, 12% $CO_2$, 1% $H_2S$. When the $CH_4$ content is increased to 30%, the composition changes to 29% $H_2O$, 18% $H_2$, 13% CO, 9% $CO_2$, 1% $H_2S$. As shown in Figure 3, as the $CH_4$ level is increased, the stability of the chromium oxide in equilibrium in the alloy in the presence of the gas, tends to disequilibriate towards the less desirable chrome carbide formation at atmospheric pressure and toward the even less desirable carbon deposition (metal dusting) condition at high pressure. If the $CH_4$ level is kept constant and the pressure increased, equilibrium tends to move toward the highly undesirable carbon deposition condition. This example illustrates the effect of pressure and gas composition in the formation of undesirable carburization.

Figure 4 illustrates the influence of chromium content on the corrosion rate in the IITRI gases.[5] Note that the oxidizing gas composition consists of 68% $N_2$, 1% $H_2$, 1% CO, 30% $CO_2$, and 0.1% $SO_2$. The reducing gas composition is as listed previously. The corrosion rate shown in Figure 4 is severe for less than 20 percent chromium, while more than 25 percent chromium significantly protects the alloy from corrosion. This strikingly illustrates the role of chromium oxide in forming a protective barrier which slows down the corrosion rate.

Pilot plant data are presented in Table V.[6] Tests A, B, and C occurred in the regenerator section of the gasifier at temperatures in excess of 1700°F (930°C) in the catalyzing presence of the calcium oxide from the dolomite. The results were rather erratic. For this type of gas, existing commercial alloys are on the "ragged edge" of corrosion resistance, and ready to corrode catastrophically. Aluminized alloys (in which an aluminum oxide coating is formed) provide an additional protective barrier which reduces the corrosion rate. Test D occurred at lower temperature in the off-gas condition in the gasifier. Here the corrosion rate is moderate to low for all eight alloys.

Alloys with superior performance in reducing atmospheres are listed in Table VI.[7] While the 0.5% $H_2S$ content is in the middle of the range anticipated for coal gas, the test temperature is relatively high. Alloys such as 310 stainless steel failed catastrophically at around 2000 hours. Subsequent testing to 5000 hours indicated that RA-333, Crutemp 25 and Thermalloy 63 WC deteriorated significantly. In-800, In-671, Haynes 188 and Stellite 6B continued to resist corrosion.

The following listing summarizes the available data on the corrosion resistance of alloys in sulfidizing atmospheres:

1. In the IITRI oxidizing atmosphere (0.1% $SO_2$), the 1000 hour, 10 atmosphere, 1850°F (1010°C) data indicate that the descending order of preference is 310 aluminized, 310, 800 aluminized and In-671.
2. In the IITRI reducing gas at 70 atmospheres and 1800°F (982°C), the data indicate the acceptable alloys to be:
    a. At 0.1% $H_2S$, 1000 hours:
    In-671, In-800, In-800 aluminized, Stellite 6B, Haynes 188, Hastelloy X, 310 Aluminized, Multimet N-155, Co-Cr-W#1, Al 29-4-2

    b. At 0.5% $H_2S$, 5000 hours:
    In-671, In-800, In-800 Aluminized, Stellite 6B, Haynes 188

    c. At 0.5% $H_2S$, 7000 hours:
    In-671, In-800

    d. At 0.5% $H_2S$, 10,000 hours:
    In-671

    e. At 1.0% $H_2S$, 1000 hours:
    800 Aluminized, Stellite 6B, Haynes 188

    f. At 1.5% $H_2S$, 1000 hours:
    Stellite 6B

3. In the $CO_2$ Acceptor Gasifier, in the off-gas location (trace $H_2S$) at 1600°F (870°C) for 15,000 hours:
   In-800

4. In the IITRI reducing gas at 70 atmospheres and 1500°F (815°C) for 1000 hours. (Only In-671 and the more common alloys are listed here. The corresponding alloys listed for 1800°F (982°C) will perform well at 1500°F.):

   a. At 1.0% $H_2S$:
      In-671, 446, 310, 800 Aluminized

   b. At 0.5% $H_2S$:
      In-671, 446, 310, 800 Aluminized, 310 Aluminized, In-800

   c. At 0.1% $H_2S$:
      In-671, 446, 310, 800 Aluminized, 310 Aluminized, In-800,
      In-793 [illegible]n-601, In-600, 316, 304, 302

## PARTICULATE EROSION OF METALS AND CERAMICS

Up to now we have considered the corrosive effect of gases on metallic materials available for particulate control. The erosive influence of particulates on both metals and ceramics is discussed below.

Within the range of conditions used, the effect of particulate on material wear is essentially proportional to the particulate loading. The influence of particle velocity on wear is approximately equal to the velocity to the 2.5 power for metals and to the 4.5 power for ceramics (see Table VII[8]). Consequently, the effect of particle velocity is greater for ceramics than for metals. The effect of particle size on erosive wear is essentially proportional to particle size, when particles are between 3 and 30 microns. When the particle size is below 0.1 micron, the particles flow with the gas stream. Intermediate sizes tend to deposit rather than impact, and may cause slagging corrosion.

The effect of the angle of impact is shown in Table VIII. When the impact is perpendicular to the surface, the erosive effect on ceramics is moderate. With a glancing angle of around 20°, the erosive effect on ceramics becomes very slight. Not so with metals. Glancing angles of around 20° cause severe erosion, while impacts perpendicular to the surface result in significantly less erosion (although such erosion is much more severe than the erosion in ceramics). Consequently, metallic parts should be designed for perpendicular impact conditions, and should be coated with ceramic whenever low-angle impacts are anticipated.

Erosion resistance appears to be associated with the Young's modulus, and is high for high-modulus materials. Hardening a metal by heat treatment or cold working does not change its erosion resistance. As shown in Table IX, cemented tungsten carbides are highly erosion resistant (though not as erosion resistant as compacted diamond). Alumina ceramics are less resistant, but still are superior to silicon carbide. Among the metals, the cobalt-base alloys are the most erosion resistant.

## GASEOUS CORROSION OF CERAMIC MATERIALS

As noted in Table X, ceramic materials are weak in terms of tension and are subject to cracking under thermal cycling. Ceramics are subject to attack by steam in the temperature range from 1000 to 1700°F (540 to 930°C), where silica is leached out to form silicic acid.[9] The higher the pressure, the more severe is this effect. When the temperature exceeds 1700°F (930°C), ceramics are subject to hydrogen attack, leading to formation of the monoxide. This effect is less severe with increasing pressure. Carbon monoxide attacks iron impurities in ceramics, dissociates, and results in carbon deposition.

High-alumina ceramics have been found to be weakened by steam, while 50-percent alumina ceramics are not affected. High-density ceramics are preferable to low-density ceramics, since the latter abrade more readily. It has been found that the bond in calcium-bonded ceramics does not hold up well in the coal gas environment, while phosphate-bonded ceramics seem to have bonds which do not deteriorate in coal gas. Self-bonded ceramics are the most resistant to the severe condition of slag erosion. Silicon carbide bonded ceramics have been found to be subject to oxidation of the bond.

## MATERIALS FOR HIGH-TEMPERATURE FILTRATION

The materials for high-temperature filtration must be fine-sized, whether in the form of metallic wire or porous foil, as ceramic cloth or felt, or as fine granular aggregates such as sand or ceramic microspheres. Corrosive attack will rapidly disintegrate these finely-sized materials and they will lose their structural integrity very rapidly.

This problem is particularly severe with metallic materials, whether in the form of continuous wire, felted wire, or porous metallic foil. As shown in Table XI, metallic wire must be very fine if it is to be useful for filtration. However, at temperatures on the order of 1500°F (815°C), such wire will disintegrate in less than 1 month. Porous foil is subject to both rapid pore enlargement (making it an ineffective filter) and pore clogging from corrosion products. But coarse wire can be used economically--both in electrostatic precipitators and as a supportive wire mesh for ceramic felts which otherwise would tend to separate.

Ceramic felts include Saffil alumina (produced by ICI), which consists of 3-micron staple filaments 1 to 2 inches long. This is available as mats, blankets or paper of moderate cost. Zirconia felt (produced by Zircar Corp.) is available with 5-micron filaments--both continuous or staple--with a significantly higher cost than the Saffil alumina. Low-cost felts, generally used for insulation purposes, are readily available. These include Kaowool (Babcock and Wilcox), Cerafelt and Fiberchrome (J. Manville), and Fiberfrax (Carborundum). They are essentially 50-percent silica-50-percent alumina staple filaments, approximately 3 microns in diameter. Fiberfrax is available as blankets, papers, and moderately high-cost staple-cloth reinforced with nichrome wire or glass filaments. The Fiberchrome is chromized for better abrasion resistance.

Ceramic cloth woven from continuous filaments can also be obtained. Leached-out E glass consists almost entirely of silica, and is available woven at moderate cost as Refrasil (Hitco) or Sil Temp (Haveg). The filaments are 9 microns in diameter, but of low strength. Refrasil is also available chromized, which should have superior abrasion resistance. High-strength silica is available in the form of Astroquartz cloth (J. P. Stevens), with filaments 6 microns in diameter, but it is a high cost material. Finally, cloth is produced from continuous filaments of AB-312 (3M Co.), which consist of alumina-boria-silica. These are coarse, high-strength, high-modulus filaments, 11 microns in diameter. The cloth also can be obtained with a chromized finish.

These filtration materials are currently under evaluation, and conclusions as to their effectiveness cannot as yet be drawn.

## REFERENCES

1. *Metals Handbook*, Vol. 1, ASM, Metals Park, Ohio, 1961, p. 482.
2. A. O. Schaefer, "A Program To Discover Materials Suitable For Service Under Hostile Conditions Obtained In Equipment For the Gasification of Coal And Other Solid Fuels," Metal Properties Council Program At IITRI, ERDA Annual Report FE-1784-24, January 1, 1976 To December 31, 1976, p. 1 - 4.
3. *Ibid.*, ERDA Report FE-1784-21, Supplement To Quarterly Report July 1, 1976 To September 30, 1976, p. 22.
4. I. G. Wright, "Correlation Of The High-Temperature Corrosion Behavior Of Structural Alloys In Coal Conversion Environments With The Components Of The Alloys And Of The Corrosive Environments," Battelle, Columbus, Ohio, ERDA First Quarterly Report, September 3, 1976, p. 11.
5. *Ibid.*, Ref. 2, Based On Data In ERDA Annual Report FE-1784-12, January 1, 1975 To December 31, 1975, p. 108.
6. *Ibid.*, Ref. 2, Based On Data In ERDA Annual Report FE-1784-24, Janu 1976 To December 31, 1976, p. 2 - 17, And In ERDA Quarterly Report FE-1784-27, January 1, 1977 To March 31, 1977, p. 2 - 7.
7. *Ibid.*, Ref. 2, Based On Data In ERDA Quarterly Report FE-1784-30, April 1, 1977 To June 30, 1977, p. 1 - 18.
8. Jack W. Clark, " Conversion To Power – Gas Turbines," Westinghouse R&D Center, And A. W. Ruff, "High Temperature Erosion in Oxidizing and Reducing Atmospheres," NBS, Papers Presented At ASM Materials/Design Conference on Materials for Coal Conversion Systems Design, April 26 - 27, 1976, Pittsburgh, Pa.
9. M. S. Crowley, *Amer. Ceramic Soc. Bull.*, 46, No. 7., 1967, and 49, No. 5, 1970.

TABLE I. IRON BASED METALS FOR SERVICE ABOVE 650°C (1200°F)

| Alloy | Composition, Percent By Weight | | | | |
|---|---|---|---|---|---|
| | Fe | Ni | Co | Cr | Other |
| Stainless: | | | | | |
| 446 | 75 | | | 24 | |
| 304 | 70 | 9 | | 19 | |
| 316 | 65 | 14 | | 17 | |
| 310 | 52 | 20 | | 25 | |
| Iron Base: | | | | | |
| Al-16-5-Y | 78 | | | 16 | 5 Al |
| Al-29-4-4 | 63 | 4 | | 29 | 4 Mo |
| Armco 22-13-5 | 57 | 13 | | 22 | 5 Mn |
| Crutemp 25 | 47 | 25 | | 25 | 2 Mn |

TABLE II. SUPERALLOYS FOR SERVICE ABOVE 650°C (1200°F)

| Alloy | Composition, Percent By Weight Fe | Ni | Co | Cr | Other |
|---|---|---|---|---|---|
| Nickel Alloys: | | | | | |
| In-600 | 7 | 76 | | 16 | |
| Inconel-625 | 3 | 62 | | 22 | 9 Mo |
| In-671 | | 49 | | 50 | |
| Hastelloy X | 19 | 45 | 3 | 22 | 9 Mo |
| Cobalt Alloys: | | | | | |
| Stellite 6B | 2 | 2 | 56 | 29 | 7 W |
| Haynes 188 | 1 | 23 | 36 | 23 | 15 W |
| Multimet N155 | 29 | 20 | 20 | 22 | 4 W |
| Thermalloy 63WC | 18 | 35 | 15 | 26 | 5 W |

TABLE III. ENVIRONMENTAL GASES IN COAL CONVERSION PROCESSES

| Gas | Typical Range Volume Percent |
|---|---|
| $H_2O$ | 0-50 |
| $H_2$ | 10-50 |
| $CH_4$ | 0-75 |
| CO | 5-70 |
| $CO_2$ | 0-30 |
| $N_2$ | 0-70 |
| $C_xH_y$ | 0-2 |
| $NH_3$ | 0-1 |
| $H_2S$ or $SO_2$ | 0-1 |

Also Present: Flyash and Char Particulates

TABLE IV. MELTING TEMPERATURES FOR METAL SULFIDES

| Compound | Melt Temperature, °F |
|---|---|
| Nickel Sulfide | 1193 |
| Cobalt Sulfide | 1611 |
| Iron Sulfide | 1810 |

TABLE V. PILOT PLANT CORROSION TESTS

Consol-$CO_2$ Acceptor Environment

| | Loss of Sound Metal in Mils Per Year | | | |
|---|---|---|---|---|
| Alloy | Test A 1700°F 800 Hrs | Test B >1700°F 1600 Hrs | Test C >1700°F 1127 Hrs | Test D >1500°F 2390 Hrs |
| 21-6-9 | 78 | 199 | -- | 34 |
| 22-13-5 | 85 | > 1000 | 32 | 26 |
| In-800 | 218 | > 1000 | 145 | 14 |
| 310 | 64 | 412 | 38 | 2 |
| In-793 | 149 | 317 | 177 | 16 |
| Hastelloy X | 438 | > 1000 | -- | 8 |
| 310 Aluminized | 65 | 80 | 92 | 30 |
| In-800 Aluminized | 65 | 79 | 121 | 31 |

Gas: 70 $N_2$-27$CO_2$-3CO-Trace $H_2S$ Except For Test D:
$48H_2$-$23H_2O$-$12CH_4$-8.5CO-$6CO_2$-$2.5N_2$

TABLE VI. ALLOYS OF LOW WEIGHT CHANGE

Less Than 10 $mg/cm^2$ in 3000 Hours at
1800°F - 1000 psi - 0.5% $H_2S$

(Corrosion Rates of <20 mils per year)

In-800
In-671
In-800 Aluminized
RA-333
Haynes 188
Hastelloy X
Crutemp 25
Stellite 6B
Thermalloy 63WC

TABLE VII. INFLUENCE OF PARTICLE PARAMETERS ON EROSION

| Particle | Effect on Wear |
|---|---|
| Loading | ~ Proportional |
| Velocity | ~ 2.5 Power For Metals<br>~ 4.5 Power For Ceramics |
| Size, Microns | |
| >3 | Impact Damage ~ Proportional to Size |
| 0.3-1 | Particles Deposit, Cause Slagging Corrosion |
| <0.1 | Particles Remain in Gas Stream |

TABLE VIII. INFLUENCE OF IMPACT ANGLE ON EROSION

| Impact Angle | Metallic Erosion* | Ceramic Erosion |
|---|---|---|
| Low -20° | High | Low |
| High -90° | Lower | Moderate |

*To Reduce Metallic Erosion, Coat with Ceramic

TABLE IX. EROSION RESISTANT MATERIALS*

Listed in Descending Order

- Cemented Carbides - K701 and K703
- Ceramics - Alumina
- Cobalt Alloys - Stellite 6B

*Erosion Resistance Increases With Intrinsic Hardness

TABLE X. PROBLEM AREAS WITH CERAMICS

| Problem | Effect |
|---|---|
| Tensile Stressing | Mechanical Failure |
| Thermal Cycling | Cracking Leading to Hot Spots |
| Attack by Steam | Leaching Out of Silica |
| Attack by $H_2$ | Less Severe Than Steam |
| Attack by CO | Less Severe, Attacks Iron Impurities |
| Attack by $CO_2$ | Less Severe Yet |
| Attack by Alkali Vapors | Least Severe |

## TABLE XI. METALS FOR FILTRATION ABOVE 650°C (1200°F)

- Metallic Wire Cloth or Felt
  - Sub-Mil Size Required for Effective Filtration
  - Corrosion Resistant Lifetime Measured in Days
  - Coarse Wire (>20 mils dia.) Can Be Used As Supportive Wire Mesh for Ceramic Felts
- Porous Metals
  - Subject to Rapid Clogging by Sticky Particulates
  - Pores Rapidly Enlarged by Corrosion Render Filtration Ineffective

S-059b

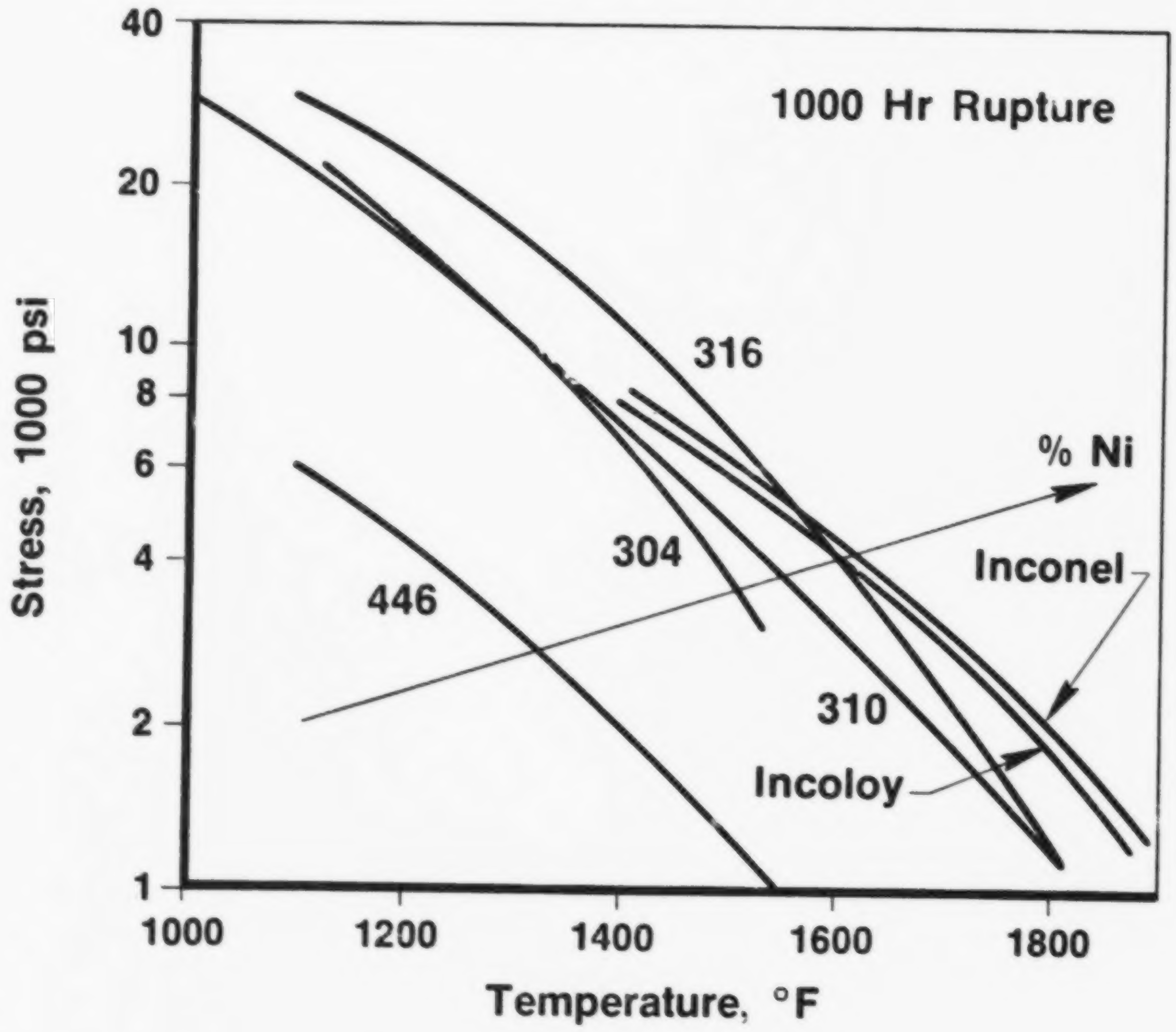

Figure 1. Rupture stress for high temperature alloys.

S-062b

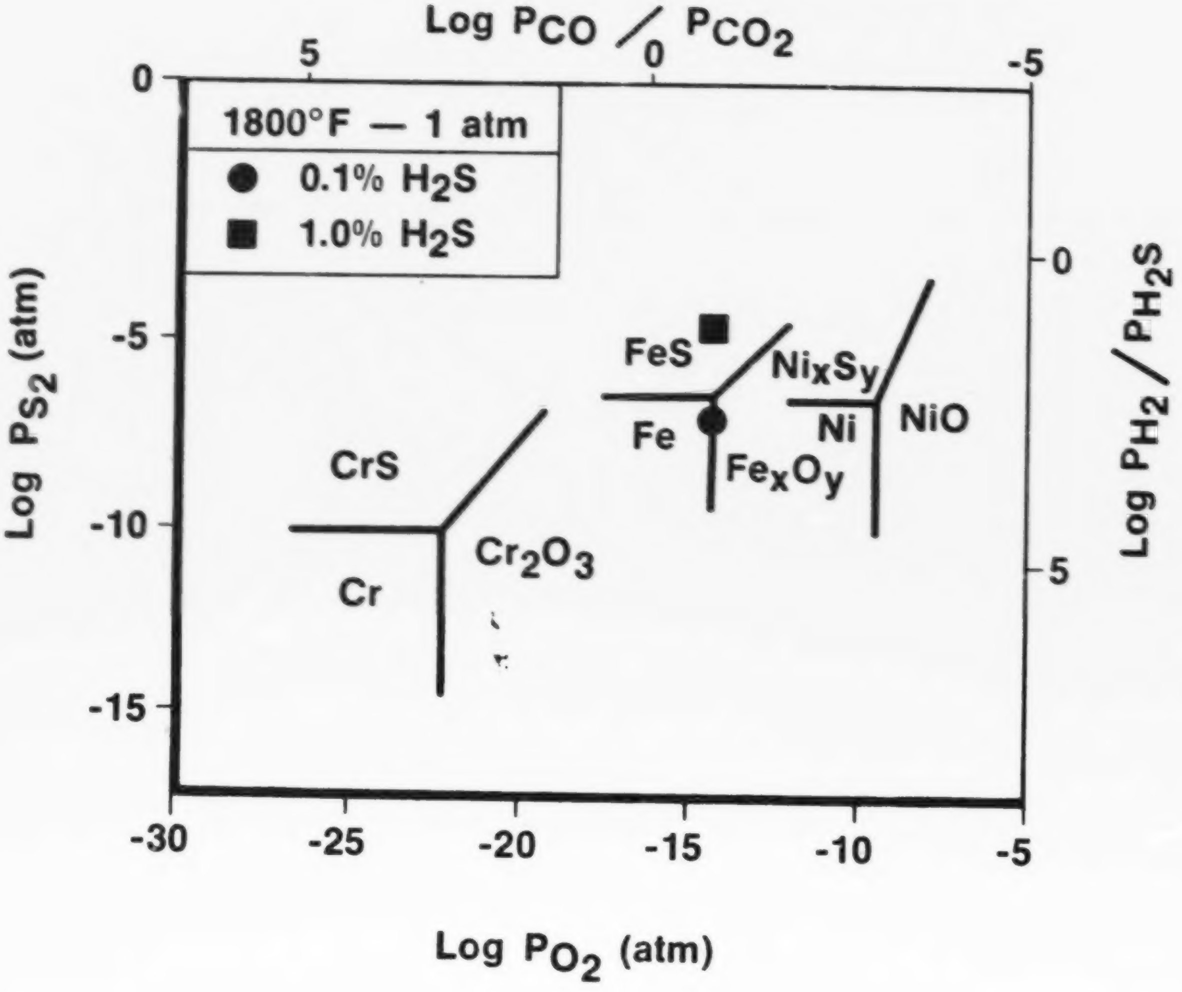

Figure 2. Thermodynamic stability diagram for metal-0-S.

S-063b

| 1800°F | | |
|---|---|---|
| Atm | $CH_4$ | |
| | 10% | 30% |
| 1 | ● | ■ |
| 102 | ○ | □ |

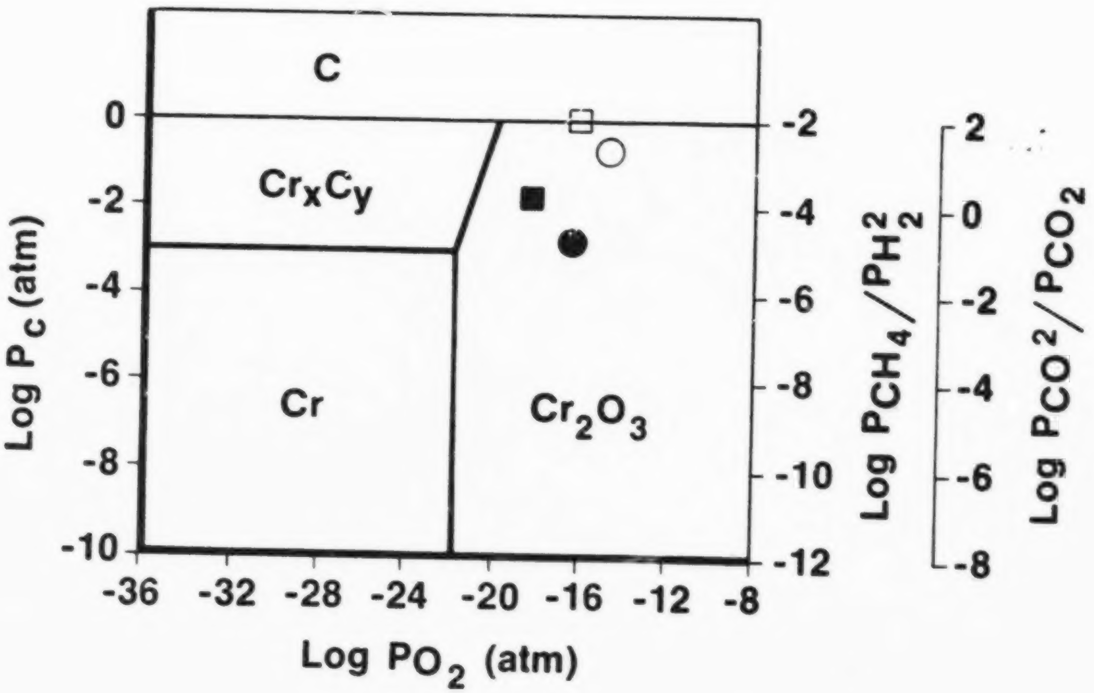

Figure 3. Thermodynamic stability diagram for Cr-O-C.

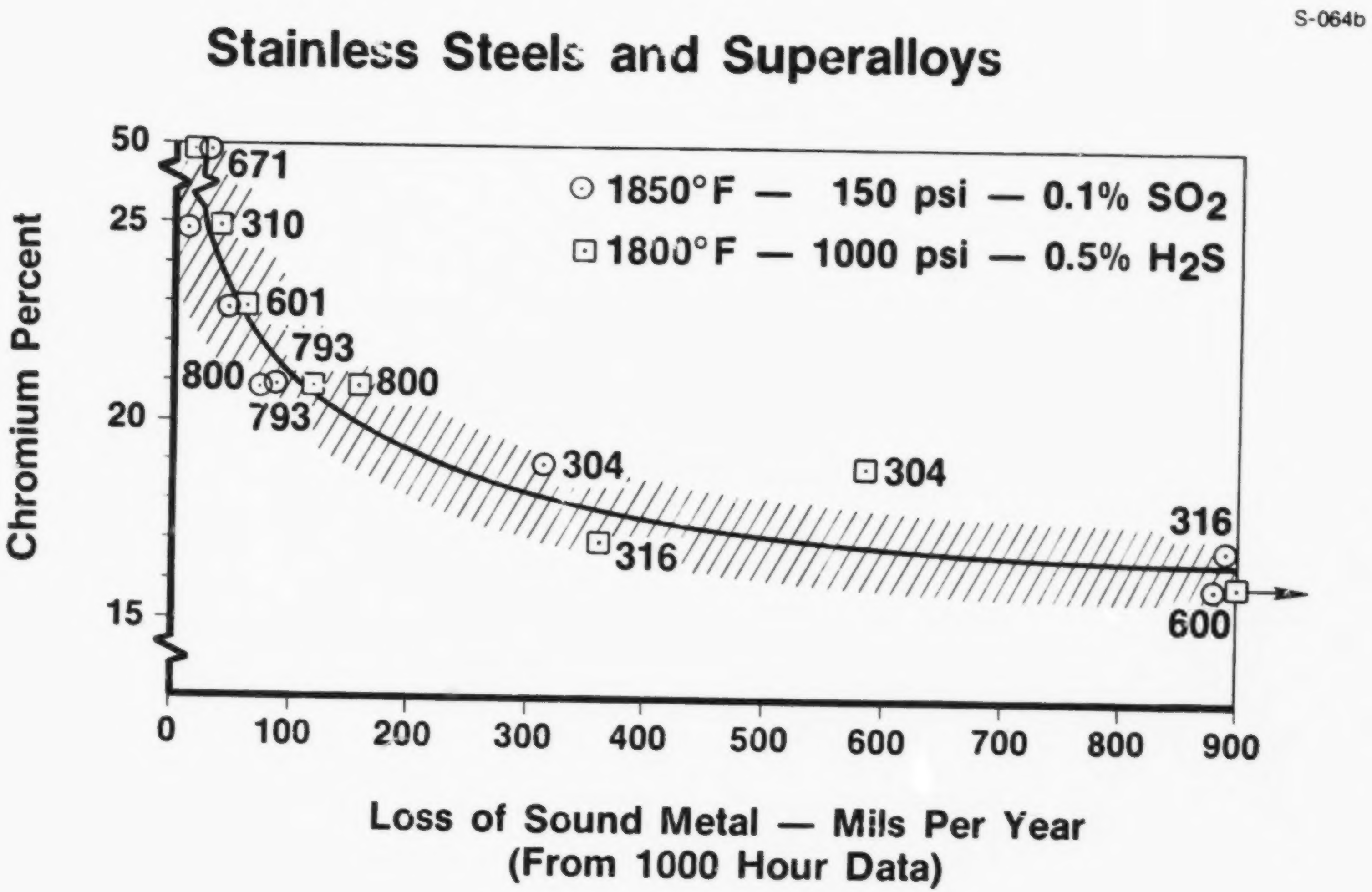

Figure 4. Influence of chromium content on corrosion rate.

# HIGH TEMPERATURE AND PRESSURE EFFECTS ON PARTICLE COLLECTION MECHANISMS

By:

R. D. Parker, S. Calvert
Air Pollution Technology, Inc.
San Diego, CA 92117

D. C. Drehmel
Environmental Protection Agency
Industrial Environmental Research Laboratory-RTP
Research Triangle Park, NC 27711

# HIGH TEMPERATURE AND PRESSURE EFFECTS ON PARTICLE COLLECTION MECHANISMS

By:

Richard D. Parker and Seymour Calvert
Air Pollution Technology, Inc.
4901 Morena Boulevard, Suite 402
San Diego, CA 92117

Dennis C. Drehmel
Particulate Technology Branch
Industrial Environmental Research Laboratory
U.S. Environmental Protection Agency
Research Triangle Park, NC 27711

## ABSTRACT

High temperatures and pressures affect the physical mechanisms by which particles are removed from gas streams. This paper examines the theoretical basis for predicting high temperature and pressure effects on particle collection mechanisms. In general particles larger than a few tenths of a micrometer in diameter appear to be more difficult to collect at high temperature and pressure than at standard conditions. Experimental data are needed to confirm these predictions. An EPA-sponsored project to obtain experimental data is discussed and the test facility is described.

# HIGH TEMPERATURE AND PRESSURE EFFECTS
# ON PARTICLE COLLECTION MECHANISMS

## INTRODUCTION

When designing, troubleshooting, or evaluating the performance of particulate control equipment it is important to have a firm understanding of the physical mechanisms by which the particles are removed from the gas stream. This is especially true when the control device is to be used at high temperatures and pressures (HTP) where current design models are unproven. In order to provide a rational basis for design and scale up, a sound theoretical understanding of the HTP effects on particle collection mechanisms is essential.

We have conducted a thorough examination of the literature concerned with HTP effects on particle collection (Calvert and Parker, 1977). Although HTP particle collection has been of interest for over 30 years no fundamental evaluation of the theory has been attempted. In general, conventional models for particle collection (valid at low temperatures and pressures) have been extrapolated to predict performance in HTP situations. Very few performance data are available to evaluate these models at HTP conditions, especially as a function of particle size.

This paper presents a review and evaluation of the theory normally used to describe particle collection mechanisms, and a discussion of the EPA-sponsored experimental program currently under way at A.P.T., Inc.

## THEORY

Particle collection devices usually can be characterized by a deposition velocity, $u_d$, which is related to the particle collection efficiency, $\eta$, and the penetration, Pt, as follows:

$$Pt = 1 - \eta = \exp\left\{\frac{-u_d\ A_d}{Q_G}\right\} \qquad (1)$$

where $A_d$ = deposition area, $cm^2$

$Q_G$ = volumetric flow rate, $cm^3/s$

Particles are kept suspended in a gas stream by the viscous force (drag) of the gas which resists forces tending to precipitate particles. The deposition velocity for any collection mechanism depends on the balance between the driving force (precipitating force) and the resistance force of the gas.

The major difference between the collection of particles at normal conditions and at high temperature and pressure is in the fluid resistance force. The fluid resistance force is generally approximated by Stokes' law modified to allow for non-continuum slip flow effects:

$$F_r = \frac{3\pi \mu_G d_p u_o}{C'} \qquad (2)$$

where $F_r$ = fluid resistance force, dynes

$\mu_G$ = fluid dynamic viscosity, g/cm-s

$d_p$ = particle diameter, cm

$u_o$ = relative velocity between the particle and the gas, cm/s

$C'$ = Cunningham slip correction factor, dimensionless

The temperature and pressure dependence of Equation 2 is contained in the terms $\mu_G$ and $C'$. The viscosity of a gas increases with increasing temperature. At extreme pressures, viscosity also increases with pressure. This effect is not significant at pressures below about 20 atm. Adequate theory and experimental data for predicting viscosities at high temperature and pressure are available in the literature.

The Cunningham slip correction factor may be calculated as:

$$C' = 1 + \frac{2\lambda}{d_p} \left| 1.257 + 0.40 \exp\left(-1.1\, d_p/2\lambda\right) \right| \qquad (3)$$

where $\lambda$ = mean free path of gas molecules, cm

The Cunningham slip correction factor is a function of temperature, pressure, and particle diameter. It becomes important for small particles, high temperatures, and low pressures.

Equation 3 is an empirical expression based on Millikan's oil drop experiments (conducted at room temperature and reduced pressure). The constants are dependent on the momentum transfer (and hence accommodation coefficient) between the gas molecules and the particle and may not be accurate at extreme temperatures. Experimental data are needed to resolve this uncertainty.

The particle deposition velocity for most collection mechanisms of interest is inversely proportional to the fluid resistance force, and therefore proportional to the ratio $C'/\mu_G$. The effects of high temperature and pressure on this ratio, plotted as a function of particle diameter, are illustrated in Figure 1. At atmospheric pressure, the ratio decreases with increasing temperature for particles larger than about 0.4 μm. At 15 atm pressure, the ratio decreases with temperature for all particles larger than 0.1 μm. Therefore, the particle deposition velocity will generally be smaller at high temperature and pressure than at normal conditions.

## Inertial Impaction

One of the most important mechanisms for the collection of particles larger than a few tenths of a micrometer in diameter is inertial impaction. Inertial impaction takes advantage of the difference in mass between the particles and gas molecules by impinging them on a target. The relative effect of inertial impaction for different particles and flow conditions may be characterized by the inertial impaction parameter, $K_p$, defined as:

$$K_p = \frac{C' \rho_p d_p^2 u_o}{9 \mu_G d_c} \tag{4}$$

where $\rho_p$ = particle density, g/cm³

$d_c$ = characteristic diameter for collector, cm

The inertial impaction parameter is equivalent to the ratio of the particle stopping distance, $x_s$, to $d_c/2$. The particle stopping distance is that distance the particle would travel before coming to rest if injected into a still gas at a velocity, $u_o$, when only the fluid resistance force acts on the particle. By considering the particle stopping distance divided by $u_o$, the particle's relative inertia can be characterized by a relaxation time, $\tau$, defined as:

$$\tau = \frac{x_s}{u_o} = \frac{K_p \, d_c}{2 \, u_o} = \frac{C' \, \rho_p \, d_p^2}{18 \, \mu_G} \qquad (5)$$

From Equation 5 it can be seen that the effects of high temperature and pressure on the particle relaxation time come in through the ratio $C'/\mu_G$. Therefore Figure 1 can be used to illustrate the effects of high temperature and pressure on the particle relaxation time. A longer relaxation time (larger $C'/\mu_G$) implies that the particle can more easily be removed from the gas by inertial impaction. For large particles, therefore, inertial impaction decreases with increasing temperature and pressure.

For small particles (less than about 0.3 μm) at high temperature and atmospheric pressure, Figure 1 indicates that inertial impaction begins to improve with temperature. However, high pressure tends to nullify this beneficial effect of high temperature.

## Brownian Diffusion

Small particles can undergo significant Brownian motion resulting from the random bombardment of the particle by gas molecules. The rate of diffusion is characterized by the particle diffusivity, defined as:

$$D = \frac{C' \, k \, T}{3 \pi \, \mu_G \, d_p} \qquad (6)$$

where $D$ = particle diffusivity, $cm^2/s$
$k$ = Boltzman's constant, erg/°K
$T$ = absolute temperature, °K

Figure 2 shows the effects of temperature and pressure on particle diffusivity. Smaller particles undergo higher rates of diffusion. High temperature increases the diffusivity for all particle sizes. High pressure decreases the beneficial effect of high temperature because of its effect on the mean free path in $C'$.

## Electrical Migration

The migration of a particle in an electric potential field is proportional to the field strength, the particle charge, and the fluid resistance force.

Electrical migration is generally characterized by a deposition velocity which may be approximated as:

$$u_e = \frac{C' \; q_p \; E}{3 \pi \; \mu_G \; d_p} \, (10^7) \tag{7}$$

where $u_e$ = deposition velocity, cm/s

$q_p$ = particle charge, C

$E$ = electric field strength, V/cm

For a given field strength and particle charge, the effects of temperature and pressure are contained in the ratio $C'/\mu_G$ and are illustrated in Figure 1. The particle charge and electric field strength, however, are also complicated functions of temperature and pressure.

Gravitational Settling and Centrifugal Separation

Using Equation 2 to describe the fluid resistance force, the gravitational settling velocity and the deposition velocity of a particle in a centrifugal force field may be approximated as:

$$u_s = \frac{1}{18} \; \frac{C' \; d_p^2 \; (\rho_p - \rho_G) g}{\mu_G} \tag{8}$$

$$u_c = \frac{1}{18} \; \frac{C' \; d_p^2 \; (\rho_p - \rho_G) u_t^2}{\mu_G} \tag{9}$$

where $u_s$ = gravitational settling velocity, cm/s

$u_c$ = centrifugal force deposition velocity, cm/s

$g$ = acceleration of gravity, cm/s$^2$

$u_t$ = tangential particle velocity at radius $R$, cm/s

$R$ = radial position of particle, cm

$\rho_G$ = density of the gas, g/cm$^3$

In general, even at relatively high pressures (~50 atm), the gas density is much smaller than the particle density and may be neglected in Equations 8 and 9. Therefore the temperature and pressure dependence of Equations 8 and 9 is contained in the ratio $C'/\mu_G$ and is illustrated in Figure 1.

## Particle Agglomeration

One way to improve the collection efficiency for fine particles is to cause the fine particles to agglomerate into larger aggregates which can be collected more easily.

Particles undergoing random Brownian motion will tend to agglomerate over a period of time. The rate of agglomeration is generally considered to be proportional to the square of the particle number concentration. That is:

$$\frac{d\, N_p}{dt} = -K_o\, N_p^2 \qquad (10)$$

where $N_p$ = particle number concentration, $cm^{-3}$

$K_o$ = proportionality constant or agglomeration coefficient, $cm^3/s$

Using Equation 2 for the gas resistance force, Fuchs (1964) presents the following equation for the agglomeration coefficient of a particle undergoing Brownian motion in a still gas, assuming particles stick together upon touching:

$$K_o = 4\, \pi\, D\, d_p = \frac{4}{3}\, \frac{C'\, k\, T}{\mu_G} \qquad (11)$$

The agglomeration coefficient is shown as a function of temperature, pressure, and particle diameter in Figure 3. The agglomeration of particles increases with temperature and decreases with pressure. The net effect of high temperature and high pressure (20°C, 1 atm to 1,100°C, 15 atm) is to increase the rate of agglomeration for a 1 μm diameter particle by a factor of 1.5 ($K_o$ increases from $3.5 \times 10^{-10}$ $cm^3/s$ to $5.3 \times 10^{-10}$ $cm^3/s$). For a 0.1 μm diameter particle, the rate of agglomeration remains relatively constant ($K_o = 8.5 \times 10^{-10}$ $cm^3/s$). Therefore it appears that at high pressure and high temperature the rate of agglomeration increases for particles larger than 0.1 μm. At high temperature and atmospheric pressure, the rate of agglomeration of fine particles should increase more substantially.

Particles may also agglomerate as a result of turbulence, particle charge, and sonic disturbances. These agglomeration mechanisms were examined theoretically by Calvert and Parker (1977) and did not appear to offer any improvement at high temperature and pressure. Sonic agglomeration appeared to increase with temperature but this was countered by a substantial decrease at high pressures.

## EXPERIMENTAL PROGRAM

### Test Facility

An experimental program to study fundamental particle collection mechanisms at high temperature and pressure is under way at A.P.T., Inc. under EPA sponsorship. The experiments will investigate the collection mechanisms of inertial impaction, Brownian diffusion, and electrical migration at temperatures up to 1,100°C and pressures up to 15 atm. Particles in the general size range of 0.5 to 10 µm will be considered.

A special high temperature and pressure test facility has been designed and constructed. This facility is illustrated in Figure 4. All the high temperature and pressure components are located inside a steel safety barricade. Tests are controlled remotely at the control panel.

High pressure gas is supplied by a manifold of nitrogen gas cylinders. The gas then passes through a high pressure redispersion fly ash dust generator and a cyclone precutter. The dust generator is a batch type high pressure blender. Steady output concentration and size distribution can be maintained for approximately 2 to 4 hours.

The gas and particles are heated in two stages. The first stage uses high temperature heating tapes which can raise the gas temperature to 750°C. The second stage uses resistance heated tube furnaces to increase the gas temperature to a maximum of 1,100°C. Stainless steel type 316, Inconel 600, or Hastelloy X are used for high pressure piping and flanges depending on the maximum temperature anticipated at specific locations.

The high temperature and pressure gas passes through one of three specially designed test sections and is then cooled and returned to the control panel before being vented. The test sections are designed to isolate specific particle collection mechanisms for study at the high temperature and pressure conditions. Specific test sections are discussed in more detail later.

Isokinetic samples are taken at the inlet and outlet of the test section. The samples are collected on sintered metal filters which can be used at temperatures up to 1,100°C in the nitrogen environment. There is a provision for adding dilution flow before the filters so that low temperature filters can also be used.

The filter samples are removed after each test and are analyzed using an electronic particle counter (Coulter Counter Model TA-II) to determine the mass and size distribution of the fly ash collected on each filter. Also the sample probes are washed after each test and analyzed to determine the amount and size of particles deposited in each probe.

One potential problem using the electronic particle counter is that particles which may have been agglomerates in the test gas stream will be analyzed as single particles. To investigate this problem we have run parallel size distributions using a cascade impactor and a filter (analyzed with the electronic counter). The results were in very close agreement. Also we have used an optical microscope to observe particles collected on a glass slide. There appeared to be very few agglomerates. The dilution line enables us to use cascade impactors at low temperature for comparison with the data we obtain from the sintered metal filters. Also we will examine samples using the microscope as a further check on our analysis.

### Inertial Impaction Tests

The inertial impaction test section is illustrated in Figure 5. It is essentially a single stage impactor placed between two flanges. Five separate jet plates are available so that we can look at cut diameters (diameter corresponding to 50% particle collection) ranging from 0.5 μm to 10 μm.

Particles are collected on a ceramic fiber substrate which is used to minimize particle bounce at the impaction plate. The substrate will be removed and analyzed after each test in order to complete the mass balance of particles and to check the efficiency determined from the inlet and outlet samples. We have calibrated this impactor under controlled conditions in the laboratory using monodisperse particles impacting on a greased plate and on the fiber substrates. The agreement between greased and fiber substrates was good.

The data obtained from analysis of the inlet and outlet samples will be used to determine an experimental penetration curve as shown in Figure 6. The penetration curve will be used to determine an experimental cut diameter,

$d_{cx}$. Experiments will be run at temperatures ranging from 100°C to 1,100°C and pressures from 1 to 15 atm.

Conventional impaction theory will be used to predict a cut diameter, $d_{cp}$, based on the impactor calibration. The predicted cut diameter will be determined from the following equation:

$$d_{cp} = \left( \frac{9\ \mu_G\ d_h\ K_{p_{50}}}{\rho_p\ C'\ u_h} \right)^{\frac{1}{2}} \tag{12}$$

where $K_{p_{50}}$ = calibrated value for $K_p$ at 50% collection efficiency

$d_h$ = jet diameter, cm

$u_h$ = jet velocity, cm/s

The particle density will be determined by comparing the calibrated cut diameter with the cut diameter measured using fly ash at standard temperature and pressure.

By comparing the experimental and predicted cut diameters at various temperatures and pressures we will be able to evaluate the theory as a function of temperature and pressure. The viscosity of nitrogen gas has been determined at temperatures up to 1,200°C (Saxena, 1971). Therefore any discrepancies between the experimental and predicted cut diameters at high temperatures can be related to the slip correction factor in Stokes' law (Equations 2 and 3).

## Brownian Diffusion Tests

The diffusion test section is illustrated in Figure 7. It is basically a screen-type diffusion battery held inside high temperature and pressure pipe. The screens are 120 mesh and made of 316 stainless steel. There will be 50 to 100 screens in the test section.

Particle penetration through the screens will be measured as a function of particle size using the electronic counter for particles down to 0.3 μm diameter. Cascade impactors will also be used to measure particles as small as 0.1 μm. The penetrations will be measured at temperatures ranging from 100°C to 1,100°C and pressures from 1 to 15 atm.

Predictions of penetrations for various temperature and pressure conditions are shown in Figure 8. The predictions were based on the theory presented by Patterson and Calvert (1977). That is:

$$Pt = \exp\left\{-6.0\ S\ N_{Pe}^{-0.67}\right\} \tag{13}$$

where $S$ = geometric solidity factor, dimensionless

$N_{Pe}$ = Peclet number = $u_G d_w/D$, dimensionless

$u_G$ = superficial gas velocity, cm/s

$d_w$ = wire diameter of screen, cm

This theory will be confirmed by experimental penetrations at ambient conditions and then used to predict experimental particle diffusivities from penetrations obtained at HTP conditions. The experimental particle diffusivities thus obtained will be compared with theoretical predictions.

## Electrical Migration Tests

The electrical migration test section is illustrated in Figure 9. It is basically a laminar flow, concentric cylinder electrical precipitator. Particles will be charged to saturation using a corona charging section at the outlet of the dust generator (before heating). The particle charge collected will be measured using an electrometer. The size distribution collected will be measured using the electronic counter. From the size distribution and total charge collected we will estimate the charge per particle. These data will then enable us to predict a deposition velocity using the expression:

$$u_e = \left(\frac{C'\ q_p\ V}{3\ \pi\ \mu_G\ d_p\ r_o}\right)10^7 \tag{14}$$

where $V$ = applied voltage, V

$r_o$ = radius of outer electrode, cm

The particle penetration through the electrical migration test section will be measured by taking inlet and outlet samples and analyzing them for particle mass and size distribution. Experimental migration velocities will be determined from the basic equation for a laminar flow electrical precipitator:

$$u_e = \frac{\eta \, Q_G}{\pi \, D_c \, L} \qquad (15)$$

where $D_c$ = diameter of outer electrode, cm

$L$ = length of cylindrical electrodes, cm

The particle saturation charge can be predicted theoretically (White, 1963). Using a charging field strength of 6 kV/cm, particle charges have been predicted and used to estimate the collection efficiency of our test section at various temperatures and pressures. The results are shown in Figure 10. A field strength of 1 kV/cm was assumed for the precipitator with an actual flow rate of 472 $cm^3/s$ (1 ACFM).

The comparison between experimental and predicted migration velocities will enable us to evaluate the conventional theory and determine its suitability for use in design models for high temperature electrical precipitation.

## CONCLUSIONS

From theoretical considerations it appears that the collection of particles larger than a few tenths of a micron in diameter will be more difficult at high temperature and pressure than at standard conditions. This is largely a consequence of the stronger drag force exerted on particles in high temperature and pressure gas streams.

The theoretical predictions presented in this paper are based on extrapolation of current aerosol theory to high temperature and pressure conditions. Satisfactory theory and experimental data exist for predicting the gas properties at these conditions. However, the available data are insufficient to validate theoretical predictions for particle motion.

To obtain the necessary data, experimental measurements of the fluid resistance force, particle diffusivity and electrical deposition velocity at high temperature and pressure are being made. This experimental research program is scheduled for completion in May of next year.

## ACKNOWLEDGEMENT

This work is supported by the U.S. Environmental Protection Agency.

REFERENCES

1. Calvert, S. and R.D. Parker, "Effects of temperature and pressure on particle collection mechanisms: theoretical review," A.P.T., Inc., EPA-600/7-77-002, NTIS PB-264-203, January 1977.

2. Fuchs, N.A., The Mechanics of Aerosols. Pergamon Press, New York, 1964.

3. Saxena, S.C. Transport properties of Gases and Gaseous Mixtures at High Temperatures. High Temp. Sci. 3:168, 1971.

4. Patterson, R.G. and S. Calvert. Screen Diffusion Battery for Monitoring Submicron Aerosols in Stack Gases. Presented at AIHA Conference, New Orleans, Louisiana, May 24, 1977.

5. White, H.J. Industrial Electrostatic Precipitation. Addison-Wesley Publication Company, Reading, Massachusetts, 1963.

## LIST OF SYMBOLS

$A_d$ = deposition area, $cm^2$

$C'$ = slip correction factor, dimensionless

$D$ = particle diffusivity, $cm^2/s$

$d_c$ = outer electrode diameter, cm

$D_c$ = collector diameter, cm

$d_h$ = jet diameter, cm

$d_p$ = particle diameter, cm

$d_w$ = wire diameter, cm

$E$ = electric field strength, V/cm

$F_r$ = drag force, dynes

$g$ = gravitational acceleration, $cm/s^2$

$k$ = Boltzman's constant, erg/°K

$K_o$ = agglomeration coefficient, $cm^3/s$

$K_p$ = inertial impaction parameter, dimensionless

$K_{p50}$ = $K_p$ at 50% collection efficiency, dimensionless

$L$ = length of electrode, cm

$N_p$ = particle number concentration, $cm^{-3}$

$N_{Pe}$ = Peclet number, dimensionless

$Pt$ = penetration, dimensionless

$Q_G$ = volumetric flow rate, $cm^3/s$

$q_p$ = particle charge, C

$R$ = radial position of particle, cm

$r_o$ = radius of outer electrode, cm

$S$ = solidity factor, dimensionless

$T$ = absolute temperature, °K

$t$ = time, s

$u_c$ = centrifugal force deposition velocity, cm/s

$u_d$ = deposition velocity, cm/s

$u_e$ = electrical migration deposition velocity, cm/s

$u_G$ = superficial gas velocity, cm/s

$u_h$ = jet velocity, cm/s

$u_o$ = relative velocity between particle and gas, cm/s

$u_s$ = gravitational settling velocity, cm/s

$u_t$ = tangential velocity of gas, cm/s

$V$ = applied voltage, V

$x_s$ = stopping distance, cm

$\eta$ = collection efficiency, dimensionless

$\lambda$ = mean free path, cm

$\mu$ = gas viscosity, g/cm-s

$\rho_G$ = gas density, g/cm$^3$

$\rho_p$ = particle density, g/cm$^3$

$\tau$ = relaxation time, s

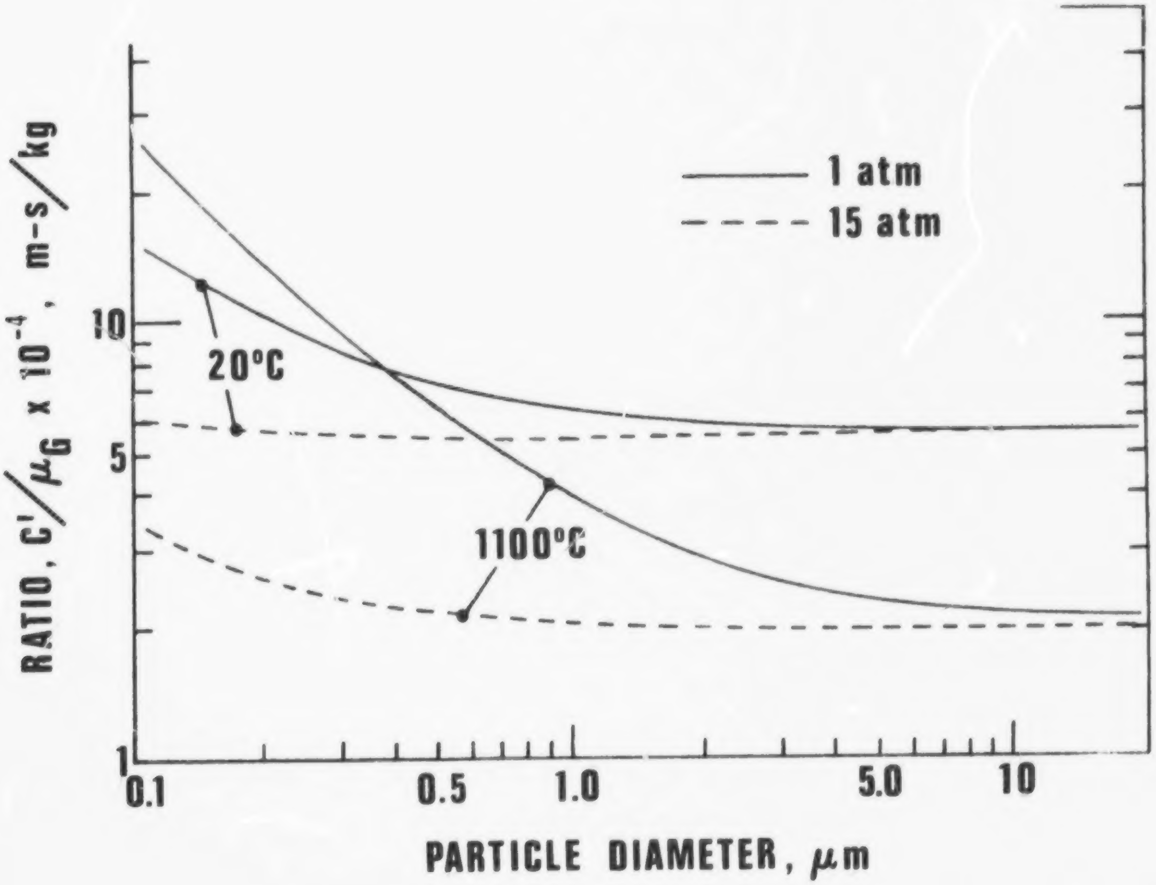

Figure 1. The effect of HTP on the ratio $C'/\mu_G$ .

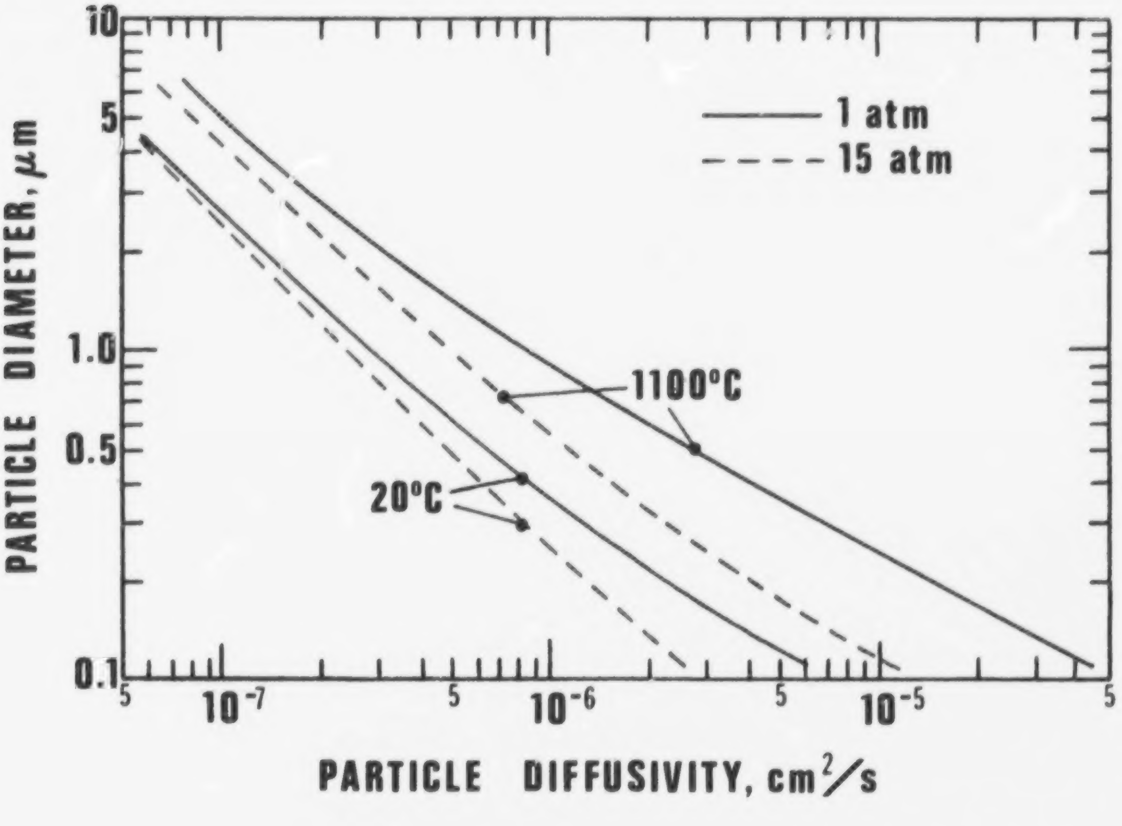

Figure 2. The effect of HTP on particle diffusivity.

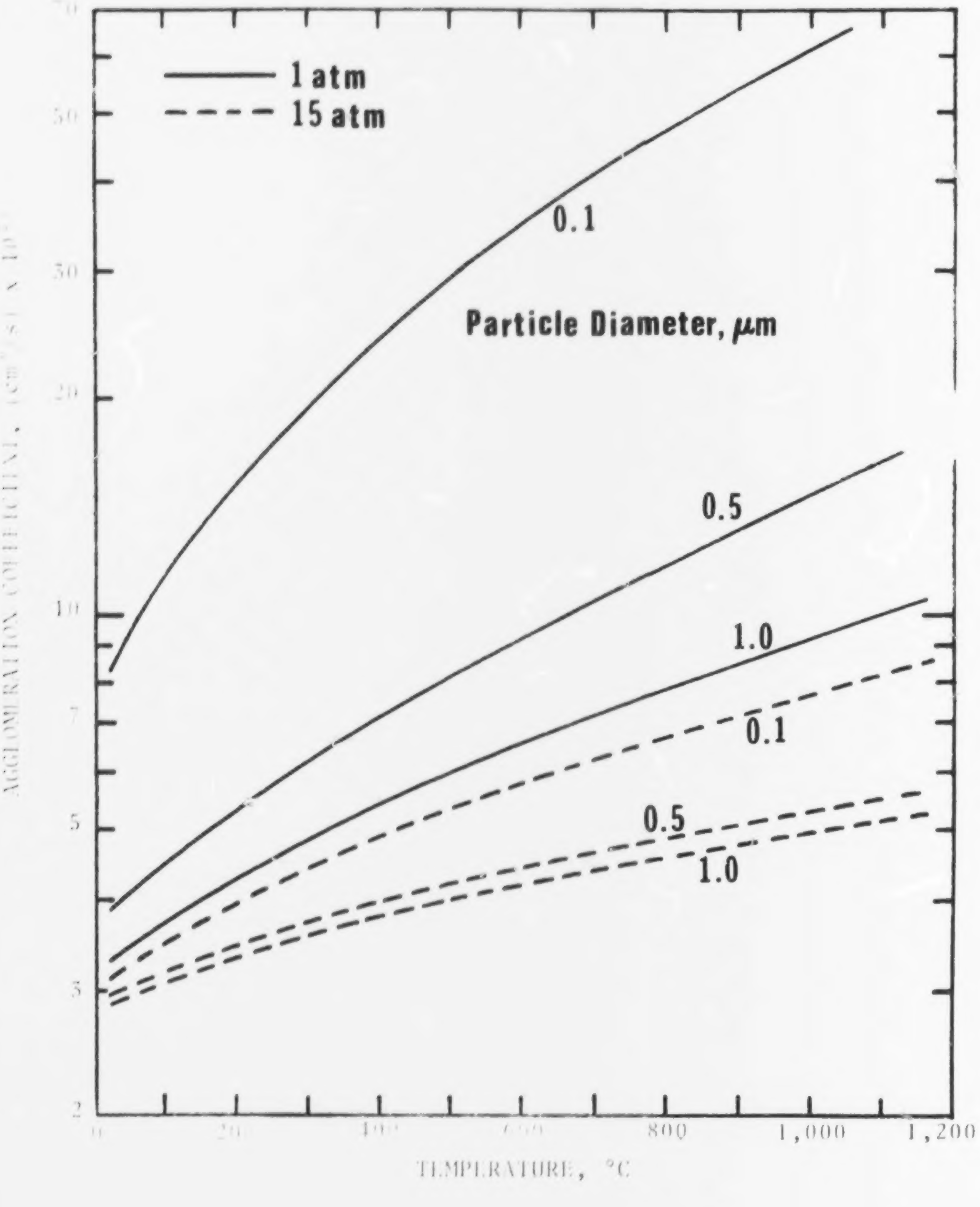

Figure 3. The effect of HTP on Brownian agglomeration.

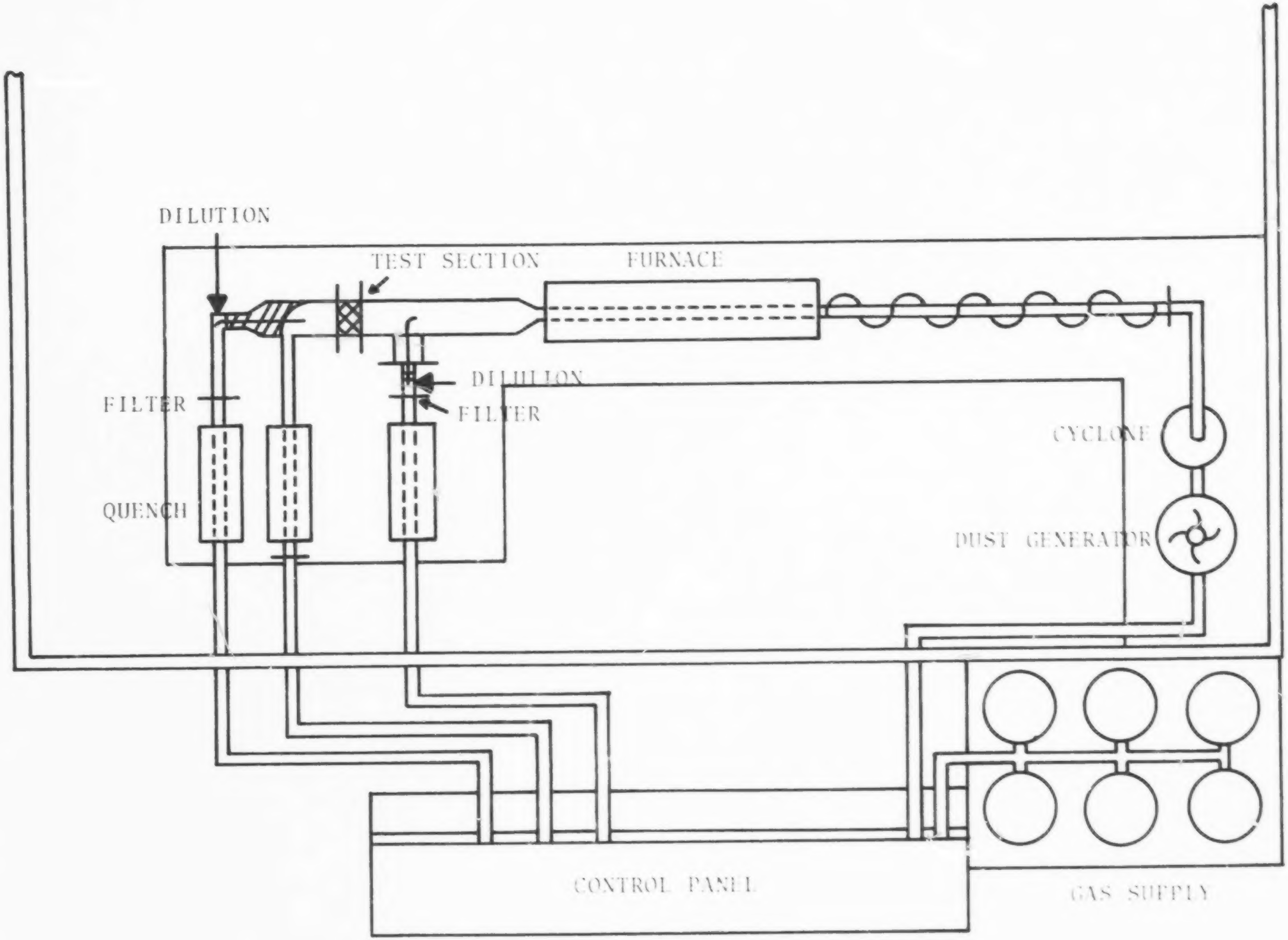
DILUTION
TEST SECTION
FURNACE
DILUTION
FILTER
FILTER
QUENCH
CYCLONE
DUST GENERATOR
CONTROL PANEL
GAS SUPPLY

Figure 4. Test facility.

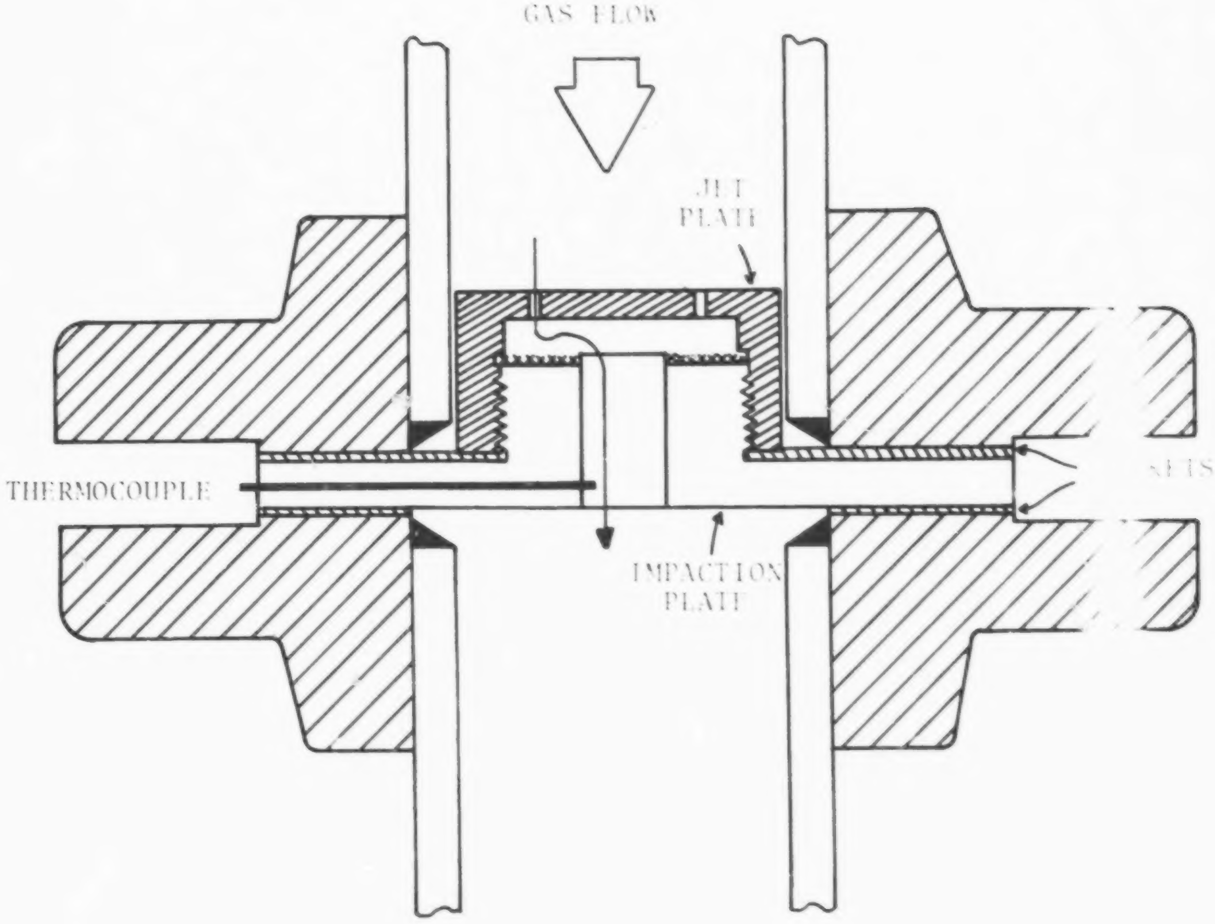
GAS FLOW
JET PLATE
THERMOCOUPLE
JETS
IMPACTION PLATE

Figure 5. Impaction test section.

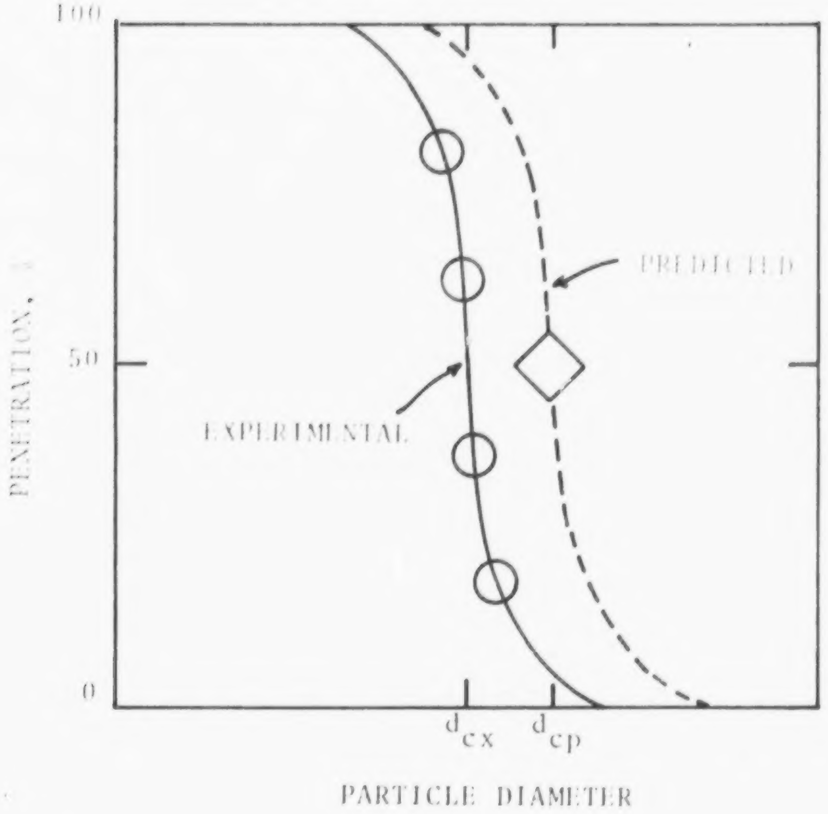

Figure 6. Comparison of Experimental and Predicted Cut Diameters.

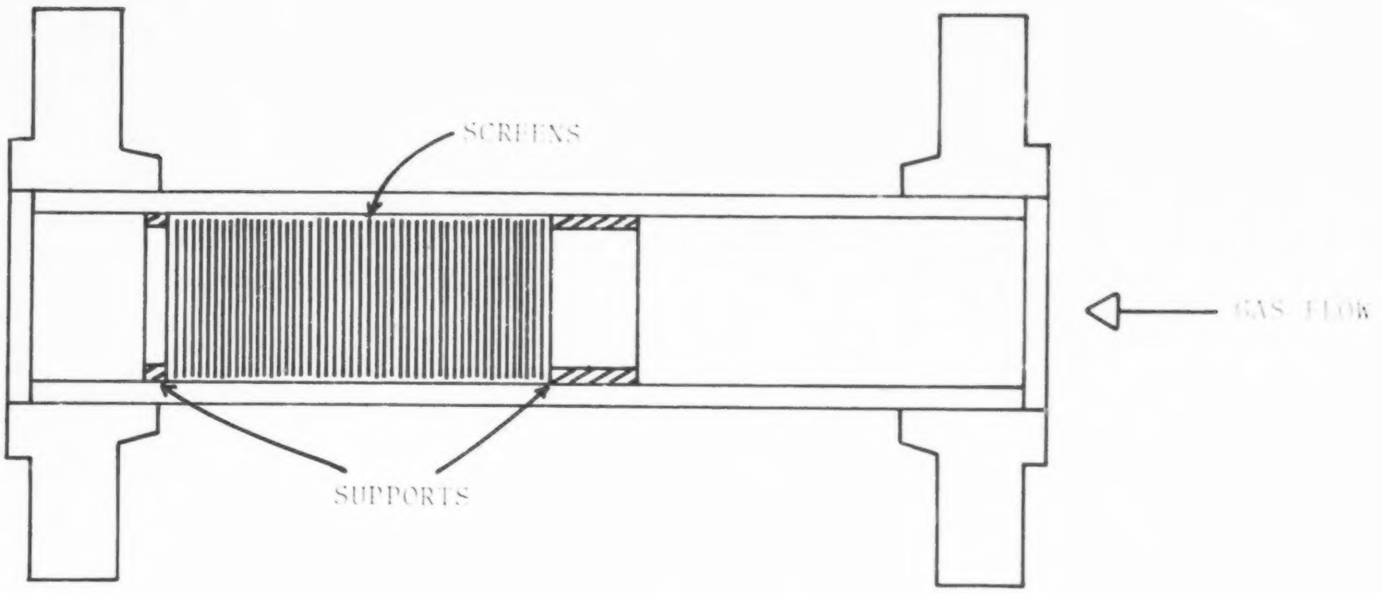
SCREENS
GAS FLOW
SUPPORTS

Figure 7. Diffusion test section.

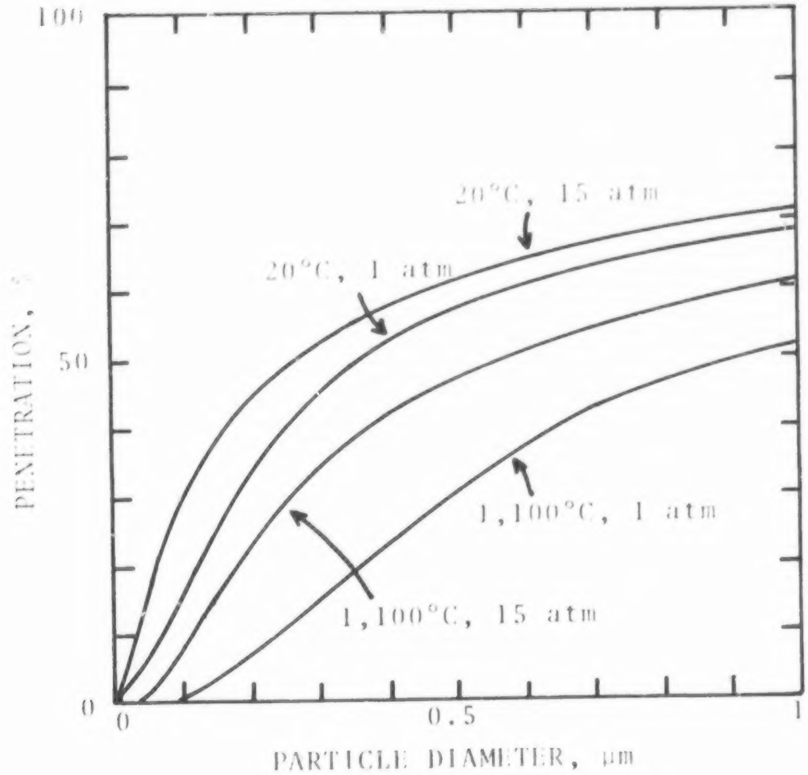

Figure 8. Predicted penetrations for diffusion test section.

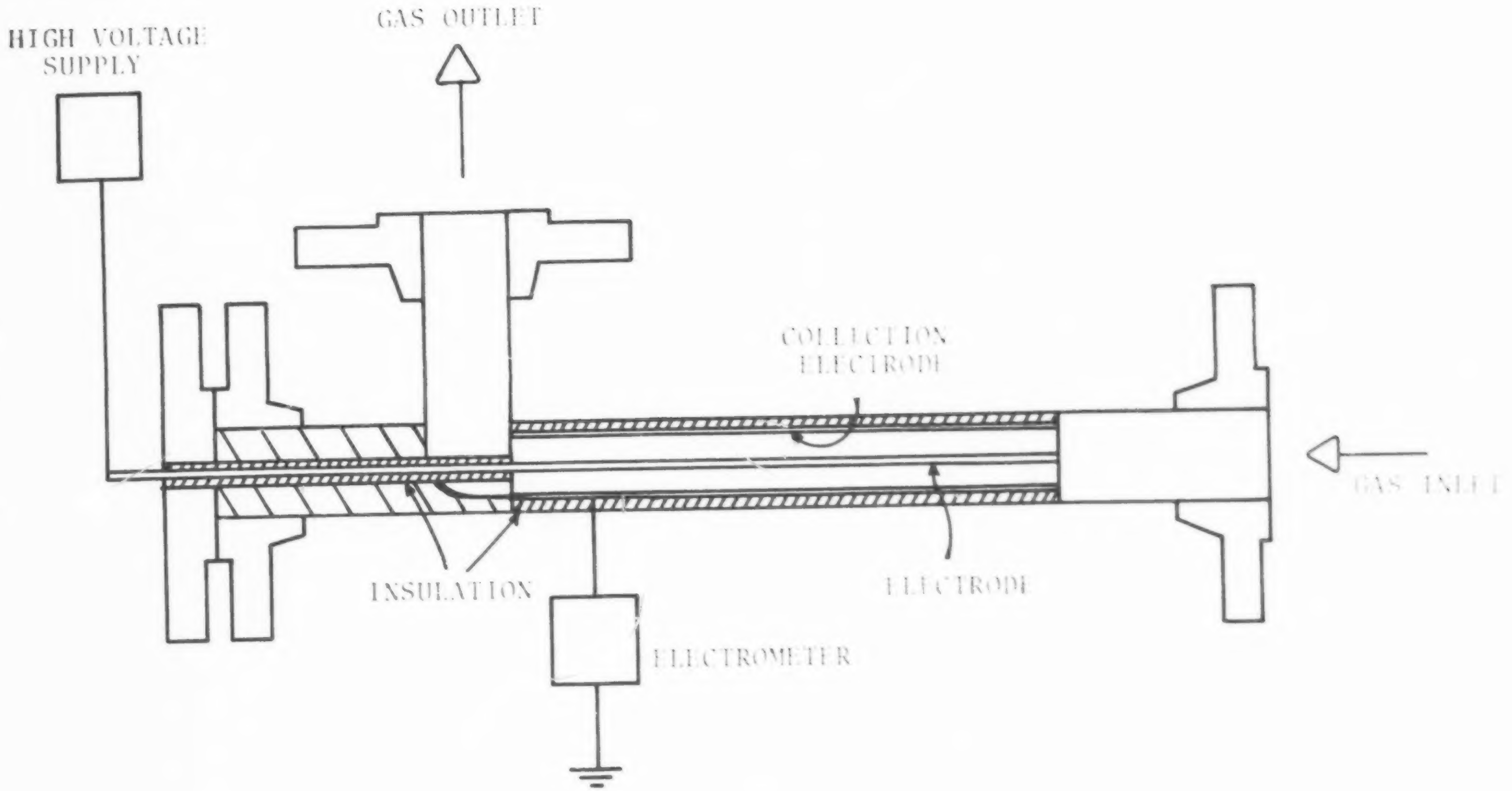
HIGH VOLTAGE SUPPLY
GAS OUTLET
COLLECTION ELECTRODE
GAS INLET
INSULATION
ELECTRODE
ELECTROMETER

Figure 9. Electrical migration test section.

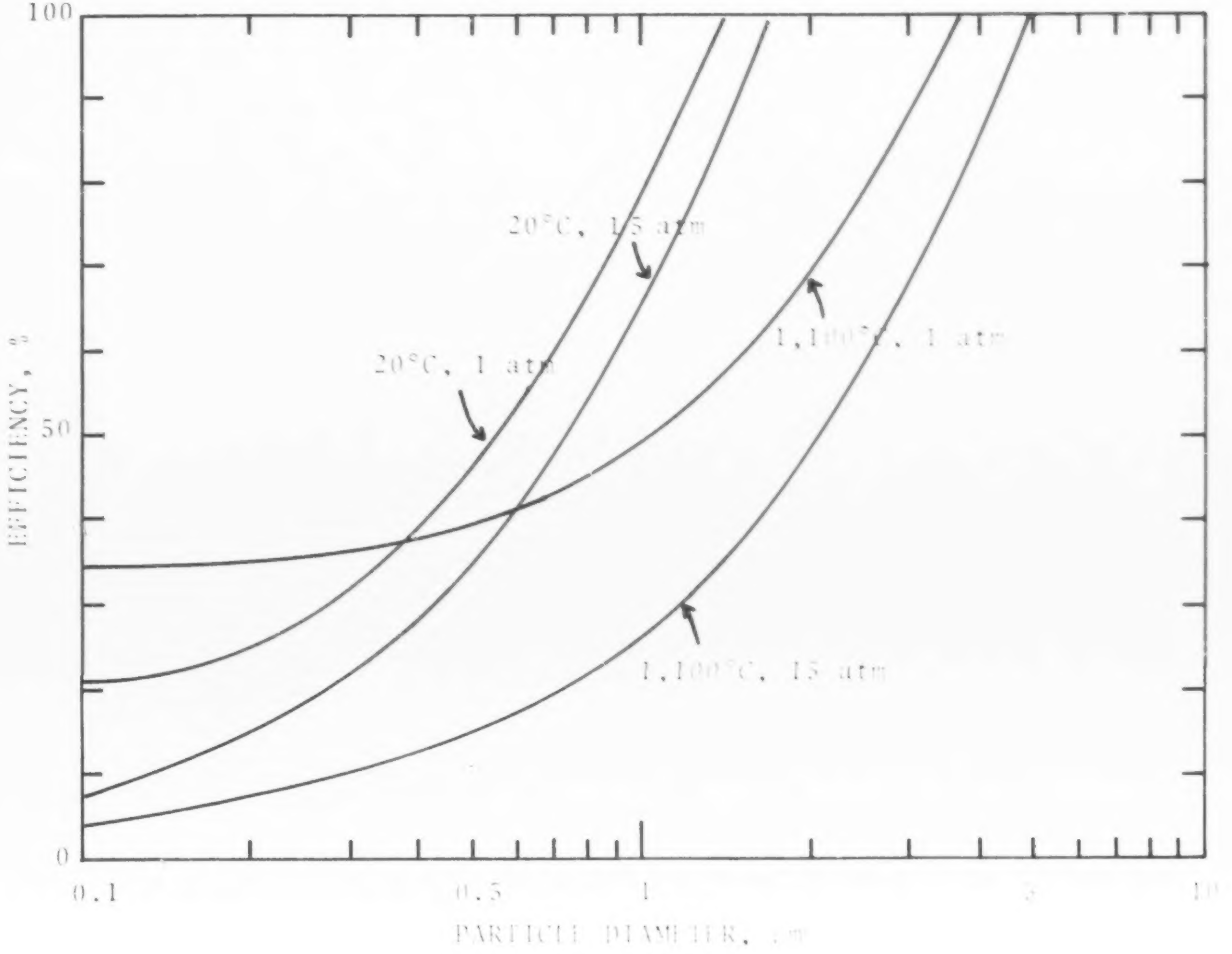

Figure 10. Predicted efficiencies for electrical migration test section.

# SESSION II:

# FILTRATION

JACK SIEGEL
CHAIRMAN

# GRANULAR BED FILTER FOR PARTICLE COLLECTION AT HIGH TEMPERATURE AND PRESSURE

By:

S. Yung, R. D. Parker, R. G. Patterson, S. Calvert
Air Pollution Technology, Inc.
San Diego, CA 92117

D. C. Drehmel
Environmental Protection Agency
Industrial Environmental Research Laboratory-RTP
Research Triangle Park, NC 27711

# GRANULAR BED FILTER FOR PARTICLE COLLECTION
# AT HIGH TEMPERATURE AND PRESSURE

By

Mr. Shui-Chow Yung
Dr. Richard D. Parker
Dr. Ronald G. Patterson
Dr. Seymour Calvert

Air Pollution Technology, Inc.
4901 Morena Blvd., Suite 402
San Diego, California 92117

Dr. Dennis C. Drehmel
Particulate Technology Branch
Utilities and Industrial Power Division
Industrial Environmental Research Laboratory
U.S. Environmental Protection Agency
Research Triangle Park, NC 27711

This paper presents an evaluation of particulate control using granular bed filters. Data and design models for collection efficiency and pressure drop are presented. This information was obtained from the literature, available performance data, and in-house experiments.

The experimental program considered particles in the 0.1 - 5 μm size range. The penetration of monodisperse aerosols through the granular bed is determined with an optical particle counter.

The effect of filter cake on performance is discussed. Applications for particulate removal from high temperature and pressure gas streams are emphasized.

# GRANULAR BED FILTER FOR PARTICLE COLLECTION AT HIGH TEMPERATURE AND PRESSURE

## INTRODUCTION

High temperature and pressure gas streams are encountered in the development of advanced energy processes such as coal gasification and fluidized bed combustion. It is often economically desirable to utilize this gas stream directly by passing it through a gas turbine. To prevent the erosion and corrosion of turbine blades and heat exchanger tubes, it is necessary to remove the particulates before utilization.

There are a number of particulate removal systems under development that are capable of operating at high gas temperature and pressure. The granular bed filter is one of these systems. "Granular bed filter" is a general term describing any filtration system including a bed of discrete granules, or particles, as the filtration medium. By selecting the proper bed material, granular bed filters offer the possibility of simultaneous removal of particulate and gaseous pollutants. One example suggested by Squires and Graff (1971) is the use of half-calcined dolomite for the simultaneous removal of fly ash and sulfur dioxide.

## LITERATURE SURVEY

### Types of Granular Bed Filters

A granular bed filter is defined as any filtration system including a stationary or slowly moving bed of separate, relatively close-packed granules or particles as the filter medium. In order to prevent the particulate matter from plugging the interstices between granules and causing excessive pressure drop, the device needs some means for either periodic or continuous removal of the collected particles from the collecting surfaces. This definition then excludes continuously fluidized or dispersed beds where the granular particles are kept in motion by the gas being treated. It does include fixed bed or closely packed moving bed systems.

With respect to the cleaning method, granular bed filters may be classified as continuously moving, intermittently moving, or fixed bed filters.

The continuously moving bed filter is usually arranged in a cross-flow configuration. The bed is a vertical layer of granular material held in place by louvered walls. The gas passes horizontally through the granular layer while the granules and collected dust continuously move downward and are removed from the bottom. The dust and granules are separated by vibration. The cleaned granules are then returned to the overhead hopper and the panel by a granule circulation system.

The Dorfan Impingo Filter, the Consolidation Coal Company filter, and the Combusition Power Company's "Dry Scrubber" are continuously moving bed filters. The "Dry Scrubber" is the only one that is presently marketed.

In the late 1950's, Squires modified the continuous moving bed design to obtain a fixed bed device with an intermittent movement of granular solids. The bed is stationary during filtration. The accumulated filter cake and the surface layer of granules are ejected from the panel by a sharp backwash pulse and are immediately replaced by downward moving fresh granules from the overhead hoppers. This design still requires a granule recirculation system.

As opposed to the continuous and intermittent moving beds, fixed bed granular filters require no granule circulation. Collected particles in the bed are removed either mechanically or pneumatically. There are three fixed-bed devices. The "Lurgi-MB-Filter" and the "Rex-Gravel Bed Filter" clean the bed mechanically. The "Ducon Granular Bed Filter" uses a reversed gas flow to clean the bed.

The "Lurgi-MB-Filter", which was discontinued in 1969, uses a shaking mechanism to clean the bed. The "Rex-Gravel Bed Filter" is a revised version of the Lurgi. It uses a rake-shaped double-arm stirring device to loosen the filter cake and a backwash of clean air to blow the dust out of the bed.

In the Ducon design, the bed is cleaned by blowback air which is sufficient to momentarily fluidize the bed. This blowback gas flexes the bed and expels deposited dusts.

## Particle Collection Mechanisms

The primary mechanisms for particulate collection in a bed of granular solids are:

1. Inertial impaction.
2. Flow-line interception.
3. Diffusional collection.
4. Gravity settling.

In finely packed beds operated at low gas velocities, gravity settling and diffusional deposition will predominate. The collection efficiency will be expected to decrease as the gas velocity increases. Coarsely packed beds operating at higher velocities (but still below fluidizing velocities) provide separation mainly by inertial deposition and interception. Increased velocity will be expected to increase the collection efficiency, if the gas velocity is not high enough to re-entrain collected material.

Interception is the mechanism whereby particles are collected on surfaces by gas convection. Collection by this mechanism is negligible for a clean granular bed. However, during a filtration cycle, particles will deposit in the interstices of the bed to form an internal cake and on the surface to form a surface cake. As the cake builds up the bed porosity and flow channels decrease and interception becomes an important collection mechanism. When the flow channels are too small to allow particles to pass, collection is ensured, being referred to as complete interception or sieving.

The operation of granular bed filters is similar to that of fabric filters even though granular bed filters have larger pore sizes and thicknesses. Payatakes (1977) classified the filtration cycle into four different successive stages.

1. When the filter is new, particles deposit directly on the granule surfaces. This is referred to as clean bed filtration. The collection

efficiency for this stage of filtration depends primarily upon the granule size and the depth of the bed.

2. Particles deposit not only directly on granules but also and preferentially on already deposited particles forming particle dendrites.

3. The dendrites grow to the extent that they intermesh with their neighbors, forming a particulate coating around each granule which is non-uniform in thickness.

4. If the granules of the bed are sufficiently small, particle coatings of neighboring granules will bridge the gap to form an internal cake. Lee (1975) called the internal cake a rooting cake, since it is the foundation which supports the formation of a surface cake. Once a surface cake is formed, filtration efficiency no longer depends on the depth of the granular bed but rather on the thickness and structure of the surface cake. Cake filtration results in a much higher efficiency than the original granular bed. This is because particle collection by sieving becomes a more important collection mechanism.

## Mathematical Models -- Clean Granular Bed

### Particle Collection --

Currently several mathematical models are available for predicting particle collection in a granular bed (Table 1). All models are for the prediction of particle collection by clean beds; i.e., stage 1 filtration. Stage 1 filtration may be very brief compared to the total filtration cycle.

Stage 2 filtration has been observed experimentally by several researchers. Billings and Wilder (1970) summarized the studies by various investigators concerned with the cake formation process during the initial stage of filtration. They concluded that aerosol deposition occurs primarily on previously deposited particles.

Based on this observed dendrite-like growth, Payatakes and Tien (1976) proposed a model describing the dendrite growth over the entire filtration period. This model was expanded and revised by Payatakes (1977).

Payatakes and Tien's model described the rate of dendrite growth, but did not explain the reason for dendrite formation. In a recent paper, Wang et al. (1977) proposed the shadow-effect concept for dendrite growth.

They hypothesized that once a particle is deposited, it creates a shadow area around itself on the collector surface, within which no subsequent particle deposition may take place.

The creation of shadow areas by deposited particles has two consequences. Since there will be no deposition within any shadow area, it means that particle collection takes place at a discrete position along a collection surface. The deposited dust cannot be in the form of a smooth coating. The second consequence arises from the fact that with the creation of a shadow area, subsequent approaching particles which would have deposited within the shadow area had there been no deposition now attached themselves to the deposited particle.

Currently there is no theory available for stage 3 and stage 4 filtration.

Pressure Drop --

Ergun (1952) proposed the following equations to describe the pressure drop for flow through packed beds:

$$-\Delta p = \frac{f\, z\, u_G^2\, (1-\varepsilon)\, \rho_G}{d_c\, \varepsilon^3} \tag{1}$$

$$f = \frac{150}{N_{Re}} + 1.75 \tag{2}$$

$$\text{and} \quad N_{Re} = \frac{d_c\, u_G\, \rho_G}{\mu_G\, (1-\varepsilon)} \tag{3}$$

Mathematical Model -- Filter Cake Filtration

Particle Collection --

There are only a few qualitative studies on filter cake filtration. No quantitative study has been reported. Miyamoto and Bohn (1975) studied the effect of particulate load on collection efficiency of granular bed filters. Particulate load is defined as the weight of particles collected per unit bed area. They found that collection efficiency increased with increasing particulate load. Deeper beds had higher initial collection efficiencies but had little influence on collection efficiency at higher particulate load. This was because collection occurs primarily in the surface cake rather than the filter medium itself at higher particulate load.

Leith et al. (1976) and Leith and First (1977) studied high velocity cake filtration of fabric filters. Three mechanisms were described by them by which particles can pass through a fabric filter or a granular bed:

1. Straight through penetration.
2. Seepage or bleeding penetration.
3. Pinhole plug penetration.

In straight through penetration, particles pass through the filter without stopping; i.e., they are not collected by the filter. Once a particle lands on or in the filter, it does not necessarily remain at its point of initial impact. As the dust deposit builds up, the dust may work its way through from the dirty to the clean side of the filter. Gas flowing through the bed produces a drag force on the particle deposits which may move particles through the bed. Penetration of this sort is called seepage or bleeding. The pinhole plug mechanism postulates that a plug of deposited particles dislodges from the dust deposit and moves out of it, leaving behind a pinhole.

They found significant trends in the dust penetration mechanisms. Straight through penetration is important after a cleaning cycle but rapidly diminishes in importance after a filter cleaning cycle. The seepage mechanism is relatively constant during the entire filtration cycle. The pinhole plug mechanism rapidly rises in importance after cleaning, passes through a maximum, and then declines as the dust deposit becomes thicker and pressure drop through the deposit increases.

### Pressure Drop --

In granular bed filters, the flow resistance should change little as long as the large pores are open, but will increase when the large pores are closed by surface cake. The rate at which the pressure drop increases depends on whether the filter cake compacts during formation. For laminar flow and no cake compaction effect, the pressure drop across the filter cake is:

$$-\Delta p = \frac{150\ \mu_G\ C_{pi}\ u_G^2\ (1-\varepsilon)\ t}{d_c^2\ \varepsilon^3\ \rho_p} \qquad (4)$$

This equation predicts, that at constant inlet conditions, the pressure drop across the surface cake varies linearly with time as long as the porosity of the filter cake remains constant. Leith et al. (1976) have studied the compaction of filter cake. They found that compaction did occur for fly ash. They also found that the Carman Kozeny equation yields excellent results for dusts which are compressed to a specified porosity provided the particles are isometric. They gave the following equation for the increase in pressure drop.

$$t\left(\frac{C_{pi}\ u_G}{k}\right) = \varepsilon_i{}^2\left[e^{-a(\Delta p)}\right]\ -2\varepsilon_i\ e^{-a(\Delta p)}\ -2\ \left[1-\varepsilon_i\ e^{-a(\Delta p)}\right]$$

$$\ell n\left[1-\varepsilon_i\ e^{-a(\Delta p)}\right]\ -\left[1-\varepsilon_i\ e^{-a(\Delta p)}\right]\ \left[\frac{2\varepsilon_i-\varepsilon_i{}^2\ +\ 2(1-\varepsilon_i)\ \ell n\ (1-\varepsilon_i)}{1-\varepsilon_i}\right] \qquad (5)$$

## EXPERIMENTS

For a granular bed filter to be of any practical use the filter should be operated at high gas flow rates. For superficial gas velocities greater than 10 cm/s, inertial impaction is the principal particle collection mechanism. The theoretical prediction equations listed in Table I were compared with experimental data reported by McCain (1976), Knettig and Beeckmans (1974), Paretsky et al. (1971), Gebhart et al. (1973), Thomas and Yoder (1956), and Lemezis (1976). These comparisons revealed that none of the equations listed in Table I can adequately predict the inertial collection in a granular bed over a wide range of variables.

To obtain further information on the mechanism of particle collection by impaction and generate additional clean bed performance data, the experimental apparatus shown in Figure 1 was constructed. Filtered room air was used for the study and all flow rates were monitored with rotameters. Monodisperse polystyrene latex aerosol was generated using a Collison atomizer. The aerosol mist from the generator mixed with a stream of dilution air and passed through a dryer to vaporize the water. Static charges were removed by passing the aerosol through a charge neutralizing section. The charge neutralizing section consisted of a Krypton-85 charge neutralizer.

Following the neutralizing section, the aerosol (further diluted with filtered room air) flowed into the granular bed test section. Gas flow through the granular bed was controlled with the bypass vent.

The granular bed test section was made of 15 cm (6 in.) I.D. glass pipe and the filter was a bed packed with iron shot. The aerosol concentrations before and after the bed were measured with an optical counter (Climet model CI-201). Pressure drop was monitored with calibrated gauges.

Figure 2 shows experimental data on particle penetration for a 1.1 μm diameter polystyrene latex aerosol. The bed granule was SAE-170 iron shot with a mass median diameter of 620 μm. The bed porosity determined by weighing was 0.39. As can be seen, deeper beds give higher collection efficiency.

Figure 3 shows the effect of granule diameter on collection efficiency. Higher collection efficiency (or lower penetration) is obtained with smaller granular diameter.

Figure 4 shows the data obtained on Agsco No. 2 quartz granules. The granule diameter is -30+50 mesh. This granular material was obtained from Exxon Research & Engineering Company. Two different aerosols were tested, collection improved with increased particle size indicating that inertial impaction is important.

Table II is a list of pressure drops and collection efficiencies of 1.1 μm diameter latex at a superficial gas velocity of 50 cm/s. It reveals that less pressure drop is required for particle collection with smaller-granule bed material and shallower beds.

For a granular bed with a bed depth of 3.2 cm and operated at a superficial gas velocity of 50 cm/s, the collection efficiencies for 1.1 μm diameter particles are 22% and 53%, respectively, for 620 μm and 490 μm diameter iron shot. The pressure drop increases from 10 cm W.C. for 620 μm diameter granules to 21 cm W.C. for 490 μm granules. The increase is 110%. However, by using the finer grade of granules, the increase in efficiency is 140%.

Table II is a list of pressure drops for various beds whose collection efficiencies are 50% for 1.1 μm diameter particles. As can be seen the pressure drops for shallow beds are less than for deep beds.

For a shallow bed to have the same collection efficiency as a deep bed, it has to run at a high superficial gas velocity. Therefore, the gas flow capacity of a shallow bed is higher than that of a deep bed. However, there is a limit on the gas velocity at which the bed can be safely operated without causing particle re-entrainment.

Figure 5 shows the pressure drop data along with predictions by Ergun's equation (1). As can be seen, the predicted and the experimentally determined pressure drops are in excellent agreement. Thus, Ergun's equation can be used to predict the pressure drop across a clean (i.e., no filter cake) granular bed.

## CONCLUSION

Most of the granular bed filter installations reported in the literature are for the control of emissions from clinker coolers in cement plants. The size of particulates from these sources is quite large. Therefore, granular bed filters have no trouble in meeting the efficiency requirements.

Performance data for removing fine particles with granular bed filters are lacking for industrial applications. Data obtained on laboratory scale granular bed filters demonstrate that they have the ability to remove fine particles if small granules are used.

Operating experience at high temperature and pressure is limited. Mechanical problems (handling and cleaning) could be much more severe at high temperature and pressure.

# REFERENCES

Billings, C.E. and J. Wilder. Handbook of Fabric Filter Technology, Vol 1. EPA-APTD-0690, NTIS No. PB 200-648, December 1970.

Böhm, L. and S. Jordan. On Filtration of Sodium Oxide Aerosols by Multilayer Sand Bed Filters. J. of Aerosol Science, 7: 311-318 (1976).

Ergun, S. Fluid Flow Through Packed Columns. Chemical Eng. Progress, 48: 89-94 (1952).

Gebhart, J. et al. Filtration Properties of Glass Bead Media for Aerosol Particles in the 0.1.2 μm Size Range. J. of Aerosol Science, 4: 355-371 (1973).

Jackson, S. and S. Calvert. Entrained Particle Collection in Packed Beds. AIChE Journal, 12: 1075-1078 (1966).

Knettig, P. and J.M. Beeckmans. Capture of Monodispersed Aerosol Particles in a Fixed and in a Fluidized Bed. Canadian J. of Chemical Eng. 52: 703-706 (1974).

Lee, K.C. Filtration of Redispersed Power-Station Fly Ash by a Panel Bed Filter with Puffback. Ph.D. Dissertation. The City University of New York (1975).

Leith, D. et al. High Velocity, High Efficiency Aerosol Filtration. EPA-600/2-76-020, NTIS No. PB 249-457 (1976).

Leith, D. and M. First. Performance of a Pulse-Jet Filter at High Filtration Velocity, I. Particle Collection. J. of APCA, 27: 534-539 (1977).

Lemezis, S. Advanced Coal Gasification System for Electric Power Generation, Research and Development Report No. 81, Interim Report No. 3. Prepared by Westinghouse Electric Corporation for U.S. Energy Research & Development Admin. 1975.

McCain, J.D. Evaluation of Rexnord Gravel Bed Filter. EPA 600/2-76-164, NTIS No. PB 255-095, June 1976.

Miyamoto, S. and H. Bohn. Filtration of Airborne Particulates by Gravel Filters: I. Initial Collection Efficiency of a Gravel Layer. J. of APCA, 20: 1051-1054 (1974).

Miyamoto, S. and H. Bohn. Filtration of Airborne Particulates by Gravel Filters: II. Collection Efficiency and Pressure Drop in Filtering Fume. J. of APCA, 25: 40-43 (1975).

Paretsky, L. et al. Panel Bed Filters for Simultaneous Removal of Fly Ash and Sulfur Dioxide: II. Filtration of Diluted Aerosol by Sand Beds. J. of APCA, 21: 204-209 (1971).

## REFERENCES (continued)

Payatakes, A.C. and C. Tien. Particle Deposition in Fibrous Media with Dendrite-Like Pattern: A Preliminary Model. J. of Aerosol Science, I: 85-100 (1976).

Payatakes, A.C. Model of Transient Aerosol Particle Deposition in Fibrous Media with Dendrite Pattern. AIChE Journal, 23: 197 (1977).

Squires, A.M. and R.A. Graff. Panel Bed Filters for Simultaneous Removal of Fly Ash and Sulfur Dioxide: III. Reaction of Sulfur Dioxide with Half-Calcined Dolomite. J. of APCA, 21: 272-276 (1971).

Thomas, J.W. and R.E. Yoder. Aerosol Penetration Through a Lead Shot Column, A Method of Particle Size Evaluation. AMA Archives Ind. Health, 13: 550 (1956).

Wang, C.S. et al. New Concepts of Particle Deposition from Suspensions Flowing Past a Collector. Paper 18b, presented at the AIChE 83rd. National Meeting, Houston, Texas, March 20-24, 1977.

## LIST OF SYMBOLS

$a$ = empirical constant, $cm^2$/dyne

$C_{pi}$ = inlet particle concentration, g/$cm^3$

$C_1$ = empirical constant

$D_p$ = particle diffusivity, $cm^2$/s

$d_c$ = single collector diameter, cm

$d_p$ = particle diameter, cm

$f$ = friction factor, dimensionless

$f'$ = ratio of collector diameter to initial capillary diameter, dimensionless

$g$ = gravitational acceleration, cm/$s^2$

$K_d$ = D'Arcy permeability, $cm^2$

$K_p$ = inertial impaction parameter, dimensionless

$k$ = Boltzman's constant = 1.38 x $10^{-16}$ erg/°K

Pt = particle penetration, percent or fraction

$R_c$ = collector radius, cm

$T$ = absolute temperature, °K

$t$ = time since last cleaning, s

$u_G$ = superficial gas velocity, cm/s

$u_{Gi}$ = interstitial gas velocity, cm/s

$Z$ = bed depth, cm

### GREEK

$\varepsilon$ = bed porosity, fraction

$\varepsilon_i$ = initial bed porosity, fraction

$\mu_G$ = gas viscosity, poise

$\eta$ = total single collector efficiency, dimensionless

$\rho_G$ = gas density, g/$cm^3$

$\rho_p$ = particle density, g/$cm^3$

$\Delta p$ = pressure drop, dyne/$cm^2$

### DIMENSIONLESS NUMBERS

$N_{Re}$ = Reynolds number

$N_{Pe}$ = Peclet number

$N_{Nu}$ = Nusselt number

Table I. AVAILABLE EQUATIONS FOR THE PREDICTION OF PARTICLE COLLECTION IN A GRANULAR BED

| INVESTIGATOR | EQUATION | NOTES |
|---|---|---|
| Jackson and Calvert (1966) | $Pt(d_p) = \exp\left[-C_1 \frac{Z}{d_c} K_p\right]$ | Impaction only. |
| Paretsky et al. (1971) | $Pt(d_p) = \exp\left[-\frac{3}{2}\left(\frac{1-\varepsilon}{\varepsilon}\right)\frac{Z}{d_c}\eta\right]$ | "η" is the total single granule collection efficiency based on Happel's free surface model. |
| Miyamoto and Bohn (1974) | $Pt(d_p) = \exp\left[-\frac{6(1-\varepsilon)Z}{d_c}\left(\frac{N_{Nu}}{N_{Pe}}\right)\right]$ | Collection by diffusion only. |
| Gebhart et al. (1973) | $Pt(d_p) = \exp\left[-6.39 \frac{D_p^{2/3} Z}{u_{Gi}^{2/3} R_c^{2/3}}\right]$ | Collection by diffusion only. |
| Böhm and Jordan (1976) | $Pt(d_p) = \exp\left[-\left(\frac{2}{3}\frac{k T \varepsilon f'}{d_p u_G} + \frac{d_p^2 g \rho_p \varepsilon d_c}{36 u_G} + \frac{d_p^2 \rho_p u_g}{18 \varepsilon}\right)\frac{4 f' Z}{u_G d_c^2}\right]$ | Collection by diffusion, gravity settling, and impaction. |

TABLE II. PRESSURE DROP AND COLLECTION EFFICIENCY FOR 1.1 μm DIAMETER PARTICLES AT A SUPERFICIAL GAS VELOCITY of 50 cm/s.

| Granule Diameter (μm) | Bed Depth = 3.2 cm | | Bed Depth = 6.2 cm | | Bed Depth = 9.2 cm | | Bed Depth = 12.2 cm | |
|---|---|---|---|---|---|---|---|---|
| | % Coll. | ΔP (cm W.C.) | % Coll. | ΔP (cm W.C.) | % Coll. | ΔP (cm W.C.) | % Coll. | ΔP (cm W.C.) |
| 490 | 53 | 21 | 83 | 38 | 93 | -- | -- | -- |
| 620 | 22 | 10 | 38 | 20 | 55 | 28 | 68 | 37 |
| 790 | 12 | 5.4 | 30 | 12 | 44 | 18 | 55 | 23 |
| 860 | 10 | 6 | 19 | 12 | 27 | 28 | 38 | 23 |

Table III. PRESSURE DROP FOR 50% COLLECTION OF 1.1 μm DIAMETER PARTICLES.

| Granule Diameter (μm) | Pressure Drop (cm W.C.) | | | |
|---|---|---|---|---|
| | Bed Depth 3.2 cm | Bed Depth 6.2 cm | Bed Depth 9.2 cm | Bed Depth 12.2 cm |
| 490 | 19 | -- | -- | -- |
| 620 | 17 | 24 | 26 | 22 |
| 730 | 16 | 23 | -- | 25 |
| 790 | 15 | 20.5 | 22 | 21 |
| 860 | 15 | 23 | 28 | 30 |

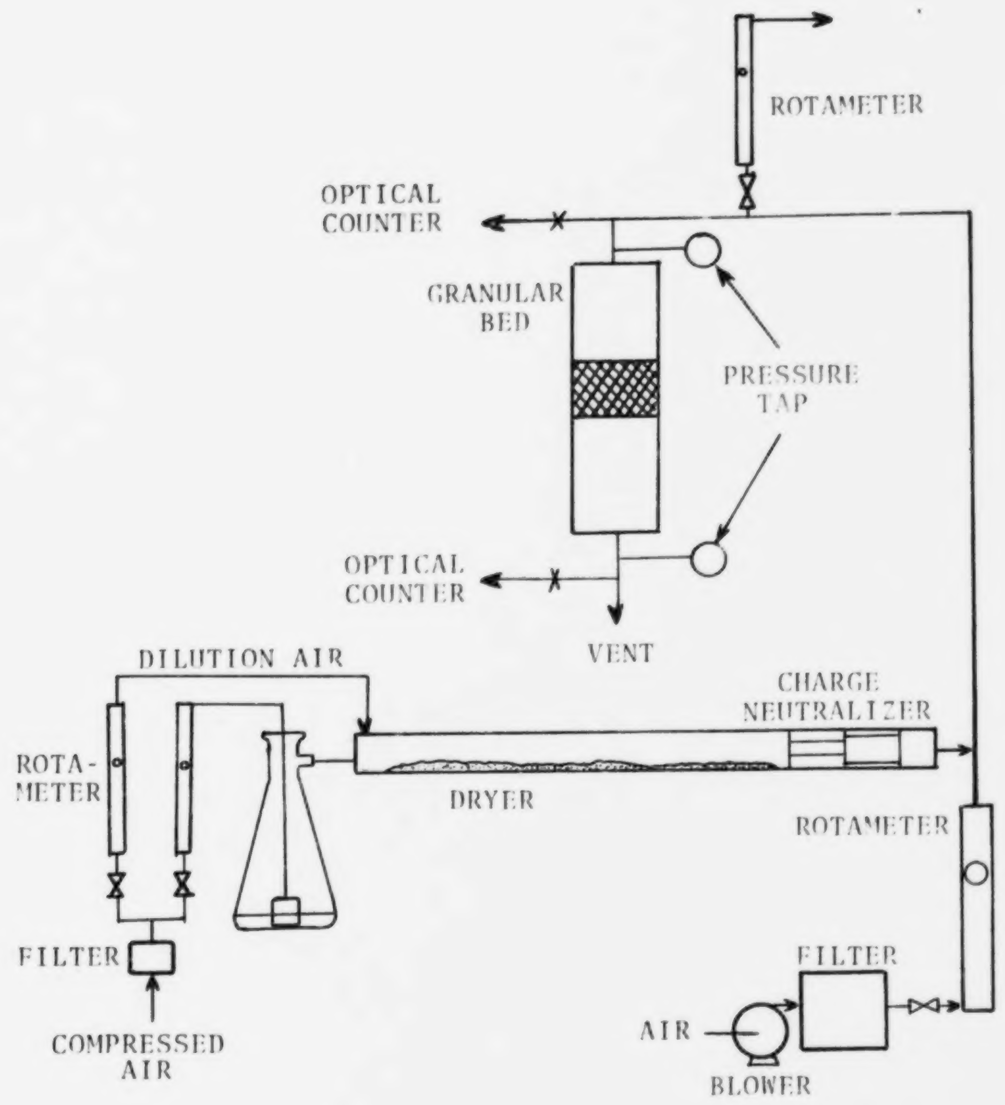
ROTAMETER
OPTICAL COUNTER
GRANULAR BED
PRESSURE TAP
OPTICAL COUNTER
VENT
DILUTION AIR
CHARGE NEUTRALIZER
ROTA-METER
DRYER
ROTAMETER
FILTER
FILTER
COMPRESSED AIR
AIR
BLOWER

Figure 1. Schematic diagram of the experimental apparatus.

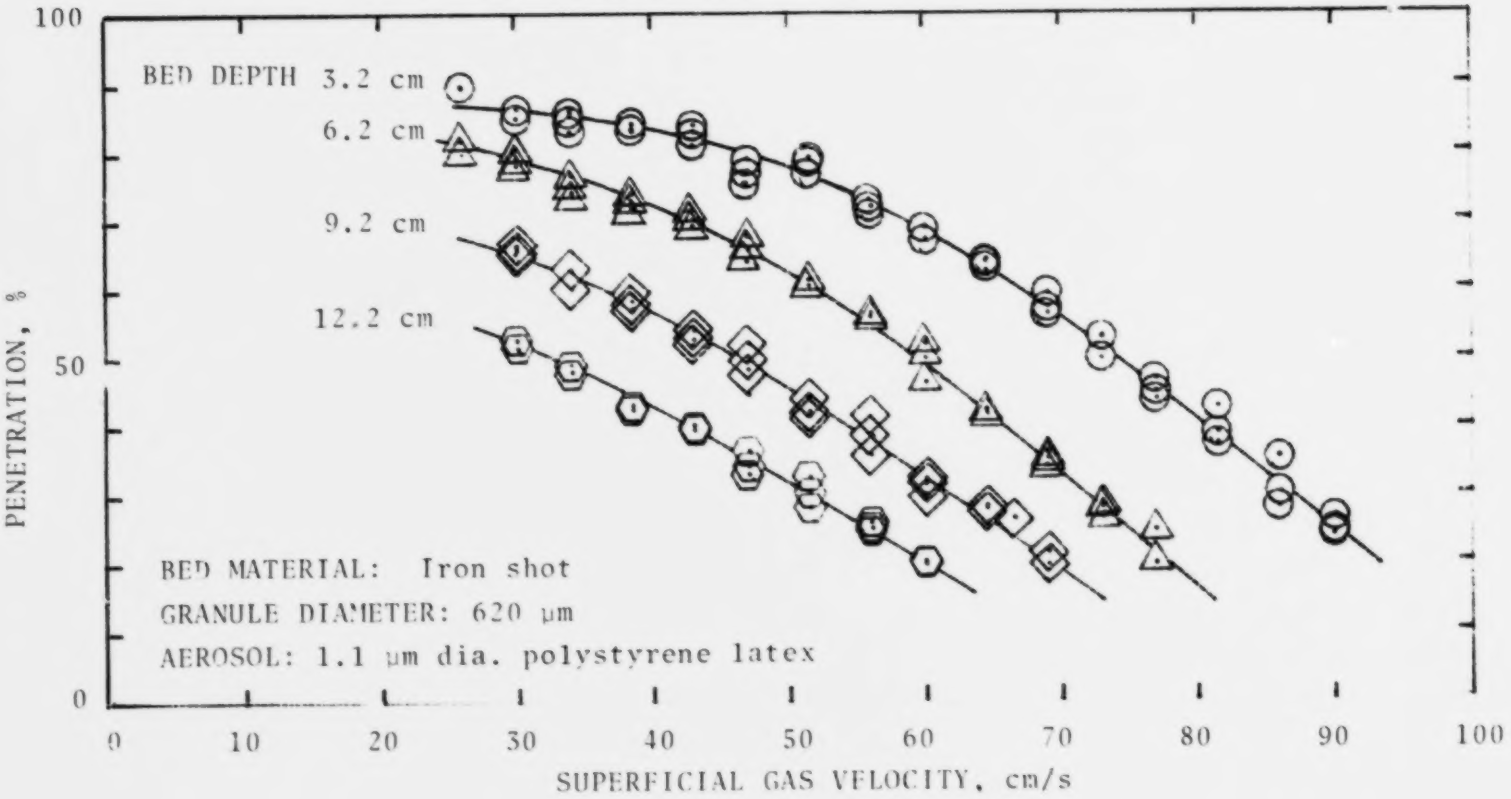

Figure 2. Experimental particle penetration of granular bed filter.

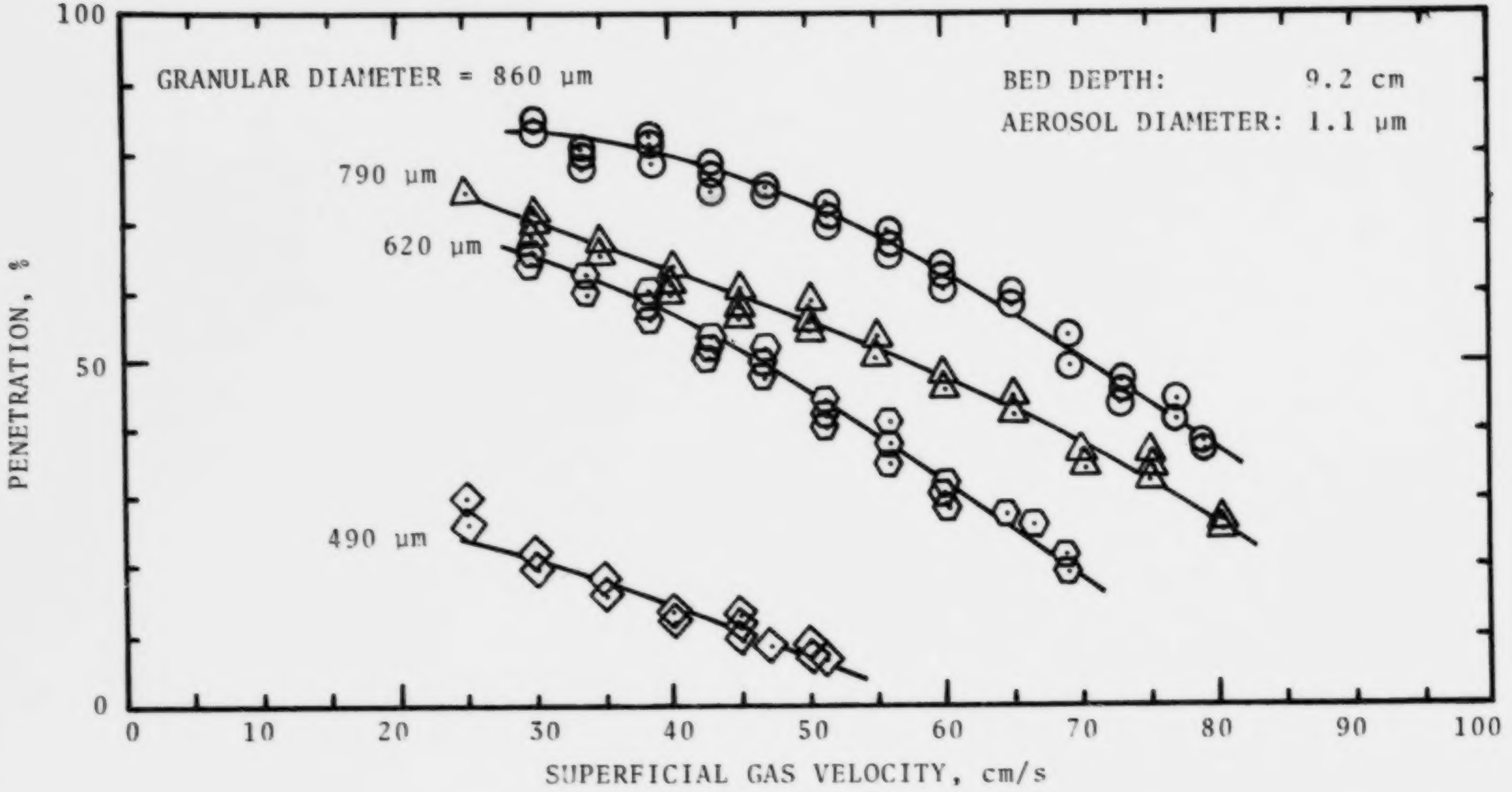

Figure 3. Experimental particle penetration of granular bed filters.

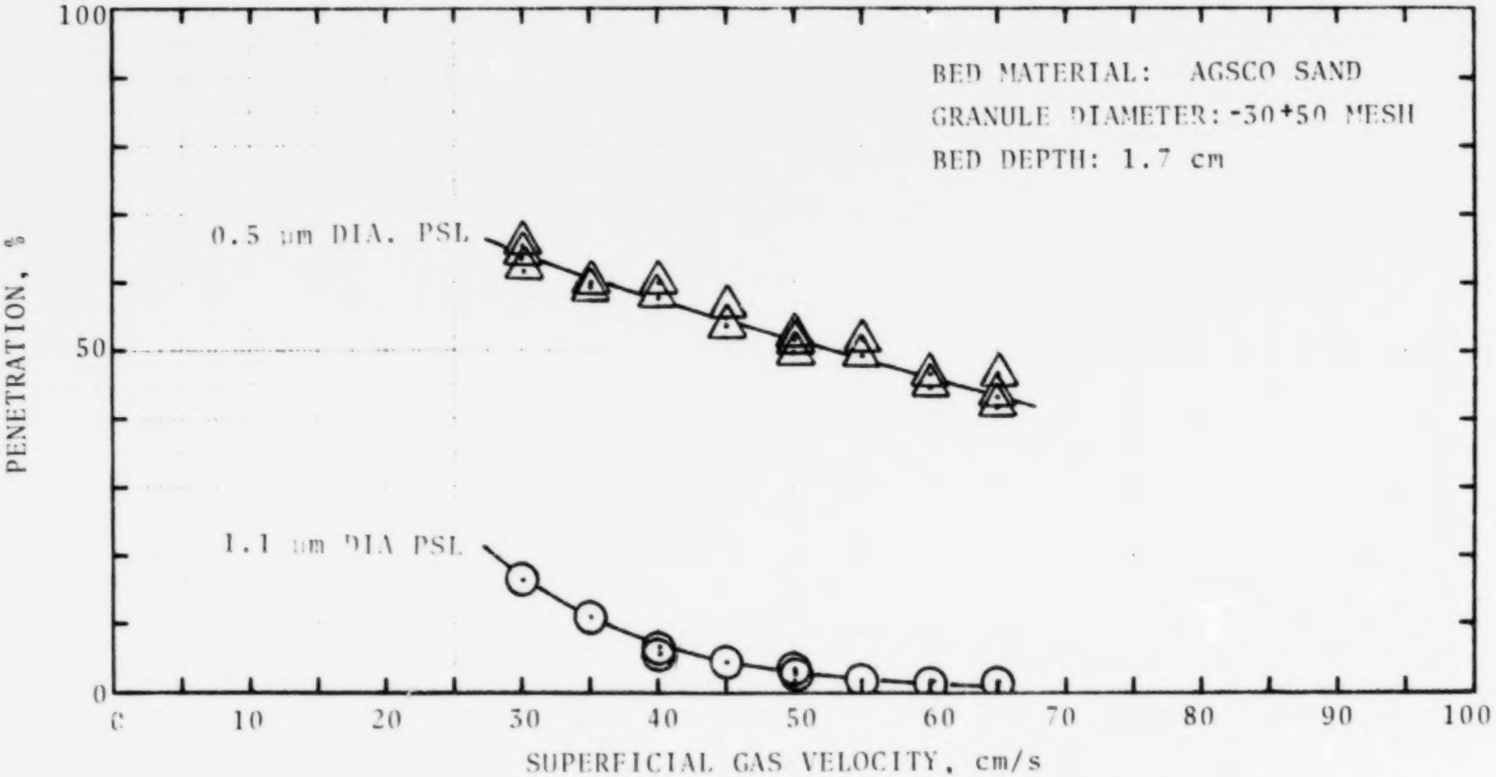

Figure 4. Experimental particle penetration of granular bed filter.

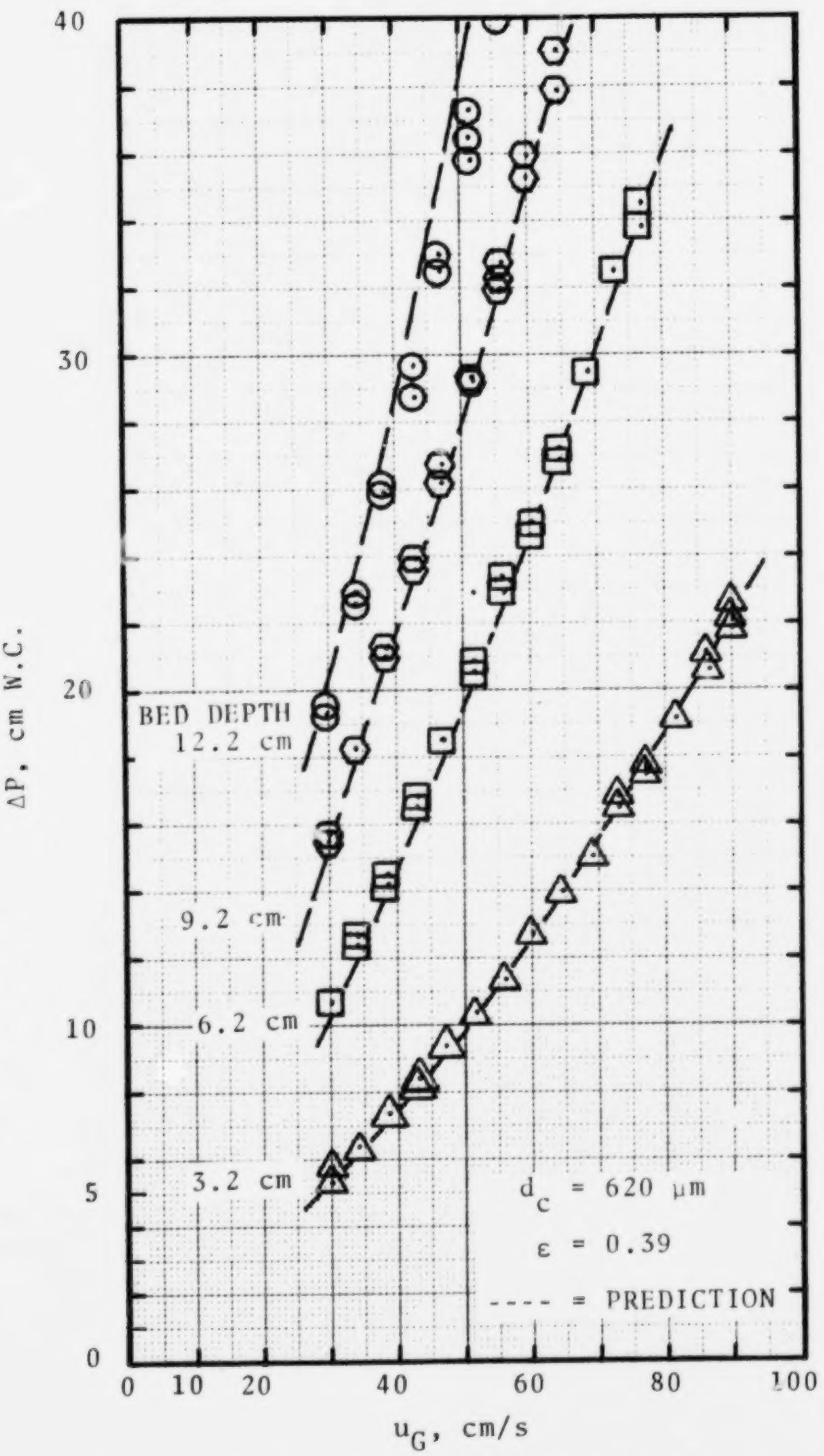

Figure 5. Experimental and predicted pressure drops across granular bed consisting of iron shot.

CE

# EVALUATION OF A GRANULAR BED FILTER FOR PARTICULATE CONTROL IN FLUIDIZED BED COMBUSTION

By:

R. C. Hoke, M. W. Gregory
Exxon Research and Engineering Company
Linden, NJ  07036

# EVALUATION OF A GRANULAR BED FILTER FOR PARTICULATE CONTROL IN FLUIDIZED BED COMBUSTION

By:

R. C. Hoke, M. W. Gregory
Exxon Research and Engineering Company
Linden, New Jersey 07036

A program is underway to evaluate the use of a granular bed filter to reduce emissions of particulates in the flue gas from pressurized fluidized bed coal combustion. Since the filtered flue gas is to be expanded through a gas turbine, the emissions should be at a level satisfying both the turbine and environmental requirements.

A granular bed filter of the Ducon Company design was installed on the EPA/Exxon pressurized FBC Miniplant unit and tested.' Initial tests were terminated due to plugging of inlet screens by the particulates. The filter system was modified and further tests were more successful. A 24 hour run was completed and in this and other tests, the ability of the system to remove and collect particulates and maintain low pressure drops was demonstrated. However, the filter outlet particulate concentration is still slightly above the upper limit of the tentative target range set by gas turbine requirements. The concentration also appears to increase with time. Screens used to retain the filter media during the filter cleaning cycle plug very readily and cannot be used. Retention of the filter media in the beds therefore, requires close control of the operation during the filter cleaning cycle. The filter system has been vulnerable to upsets and it has not been possible to take corrective action to offset the effects of the upsets.

The current program is aimed at resolving these problems. Tests are now underway using dense filter media with no retaining screens and employing various filter cleaning cycle conditions. The objective of these studies is to increase the filtration efficiency further and to prevent the drop in efficiency with time. If current tests are successful, extended testing of the system will begin, coupled with a gas turbine materials test program. Environmental assessment tests will also be made.

# EVALUATION OF A GRANULAR BED FILTER FOR PARTICULATE CONTROL IN FLUIDIZED BED COMBUSTION

## INTRODUCTION

The successful development of the pressurized fluidized bed coal combustion process is dependent on the ability of particulate control devices to remove particulates from the hot combustor flue gas to very low levels. This must be done to assure that the expansion of the flue gas through a gas turbine does not cause damage to the turbine by erosion, corrosion, or deposition of solids on the turbine blades. Current estimates of the allowable particulate concentration in the flue gas entering the turbine range from 45 to 1 mg/m$^3$ (0.02 to 0.0004 grains/SCF)(2). To-meet these estimated requirements, the flue gas leaving a pressurized combustor must first be precleaned in a two stage cyclone and then sent to a third stage high efficiency device for final cleaning. The efficiency of the third stage device must be in the range of 95 to 99.7% to be within the currently estimated particulate loading target range.

In addition to the gas turbine inlet requirements, the U.S. Environmental Protection Agency has imposed limits on the emission of particulates from coal fired installations of 0.1 lb/MBTU coal fired. This translates to a particulate concentration in the flue gas of about 115 mg/m$^3$ (0.05 gr/SCF), somewhat higher than the limit set by turbine requirements. Therefore, at the present time, removal efficiencies are dictated by the turbine requirements. However, the environmental standards are currently being reviewed and may be tightened in the future, especially with regard to the emission of particulates less than 2 microns in size. This is the size which is more difficult to remove and also causes the least amount of damage to the gas turbines. Therefore, environmental considerations may indeed limit the allowable particulate emission levels in the future.

The present particulate removal program at Exxon Research and Engineering Co., which is sponsored by the U.S. Environmental Protection Agency, will test two particulate removal devices. The first device is a granular bed filter of a design developed by the Ducon Company. The choice of the second device will most likely be from one of those discussed at this conference.

The Ducon-type granular bed filter consists in a number of small beds packed with suitable granular filter media such as alumina, quartz, etc. A stack of the filter beds form a single filter element. A number of filter elements can be used depending on the volume of gas to be filtered. A photograph of a filter element purchased from the Ducon Company for this program is shown in Figure 1. The photograph is a closeup which shows five individual filter beds of the total twelve which form this particular element. Dirty gas passes through the screen sections down into the filter beds immediately below the screen sections. Clean gas from the beds is collected in a manifold in the interior of the element and then passes to the clean gas outlet system. As the filtration step proceeds, the pressure drop across the element increases and eventually the element must be cleaned by the reverse flow of clean gas. This "blow back" occurs by flowing clean gas in reverse direction through the outlet gas manifold, up through each filter bed and out through the screens. The function of the screens is to retain the filter media during the blow back step, keeping it inside the filter beds, while allowing the fine particulates removed from the filter media by the blow back gas to pass through. The fine particulate then settles outside the filter elements and is collected at the bottom of the vessel containing the filter elements.

This type of granular bed filter was chosen to be tested in the EPA/Exxon Miniplant since it was felt to possess certain advantages over other high temperature particulate removal systems. In the first place, development of granular bed filters as a class was believed to be further along than the development of other high temperature particulate removal systems. Of the granular bed filters under development, the Ducon filter had been previously tested at relatively high temperatures and pressures and showed some promise in meeting the high particulate removal efficiencies required by the gas turbines(3). The Ducon design also had the desirable feature of retaining the granular filter media in the filter vessel during the cleaning step. In all other high pressure granular bed filters, the filter media is removed, cleaned externally and recycled back to the filter vessel.

The objectives of the granular bed filter test program at Exxon Research were to measure the outlet loading from the granular bed filter, determine if the removal efficiency was maintained with use, measure operational stability of the filter e.g., can low pressure drop across the filter be maintained, does the filter plug, is the amount of blow back gas needed to maintain steady operation within reason, etc. and finally, to measure the long term life of the filter hardware. The primary operating parameters were the filtered gas flow rate, usually measured as the gas velocity entering each filter bed, the blow back gas flow rate, the duration and the frequency of the blow back step, and the type of filter media used i.e., particle size, shape, density.

## DESCRIPTION OF EQUIPMENT

The granular bed filter was installed in a pressure vessel tied into the flue gas exit system from the EPA/Exxon Miniplant pressurized fluidized bed combustion unit. The Miniplant has been described in detail in a previous report(1). Briefly, it consists of a combustor, 33 cm (13 in) inside diameter and 10 m (32 ft) high, capable of operating at pressures up to 1000 kPa (10 atm abs), temperatures up to 980°C (1800°F), superficial gas velocities up to 3 m/s (10 ft/sec) with coal feed rates up to 200 kg/hr (450 lbs/hr). The maximum flue gas rate is about 34Sm$^3$/min (1200 SCFM) but a typical flue gas rate is 18Sm$^3$/min (650 SCFM). A photograph of the Miniplant is given in Figure 2.

The pressure vessel housing the filter elements consists of a refractory lined vessel approximately 2.4 m (8 ft) in diameter by 3.4 m (11 ft) high. Figure 3 is a photograph. Access to the interior can be made through a 70 cm (27 in) manhole. The vessel can hold up to four filter elements installed through four flanges at the top of the vessel as shown in Figure 4. Each filter element is contained within a shroud in the inside of the pressure vessel. Inlet gas is piped to each shroud, passing through a measuring orifice which determines the flow rate to each filter element. This is shown in Figure 5. Clean gas exits from each shroud through openings at the top (Figure 5) and fills the interior of the pressure shell. Blow back air enters each filter element through the top flanges of the pressure vessel (Figure 4) and flows in reverse direction through each filter element. Particulates removed from the filter element during blow back impinge on the inside surface of the shroud, fall to the bottom and are collected in lock hoppers. The blow back gas leaving a filter element flows in reverse direction through the inlet gas system into the filter elements which are in the filtration step.

A natural gas preheat burner was installed to heat the interior of the pressure vessel to a temperature above the dew point of the combustor flue gas before starting a filtration test. The burner fires into the vessel through a side port for an 8 to 12 hour period prior to the start of a run. The filter vessel is at atmospheric pressure during this period. The burner was installed after initial operation of the filter resulted in condensation of moisture on the filter elements and inside the pressure vessel during heat up with flue gas from the coal combustor. Condensation in the presence of flue gas particulates caused plugging of the filter and particulate removal lines.

A number of filter element designs and blow back methods were tested during the filter shakedown tests. Each design and the results of the tests are described in the following Section.

## RESULTS

### GBF MODEL 1

Initially, three filter elements were purchased from the Ducon Company. Figure 6 is a photograph of one of the elements and the shroud in which it is contained when placed in the pressure vessel. Each element was 20 cm (8 in) in diameter by 1.8 m (6 ft) long and contained twelve beds. The inlet screen size was 50 mesh. The nominal flow capacity of each element was 8.5s $m^3$/min (300 SCFM). One of the Ducon elements was designed to be blown back by short pulses of high pressure air. The pulse duration was approximately 0.5s. This blow back method was not tested. The other two Ducon elements were blown back with a larger volume of air for longer durations. The intent was to fluidize the filter beds rather than shocking them with a short pulse of high pressure air. The volume of blow back air was sufficient to fluidize the filter media. The duration was designed to be less than 10s. Blow back was accomplished by isolating one end of a filter element by a blow back nozzle and seal plate and blowing back with air at a pressure slightly higher than filtration pressure.

After installation of the filters, shakedown began with ambient temperature testing of the system.

The objectives of these preliminary tests were to (1) check combustor pressure control with the filter on line, (2) pressure test the system, (3) check the alignment of the blow back nozzles, (4) check out the operation of the blow back flow system, and (5) measure the distribution of flow to each one of the filter elements. A number of mechanical problems were discovered (leaks, misalignments, etc.) and had to be corrected before further testing could be resumed.

A number of high temperature runs were then attempted but the pressure drops across the filter were extremely high and all attempts at blow back were unsuccessful. Inspection of the filter elements after each of these runs showed that a hard filter cake had formed on the inlet retaining screens. This is shown in Figure 7. The filter medium was usually particulate free indicating very little penetration through the screens. It was originally thought that the plugging occurred during startup when moisture was present. The preheat burner was later installed and a run was made to re-evaluate the Ducon filter. The same screen plugging problems occurred and the original Ducon filter was deemed to be unacceptable for our application.

GBF MODEL 2

A fourth filter element designed by Exxon was also fabricated and tested. The Exxon filter element consisted of ten beds instead of twelve and was designed to permit easy diassembly and removal of the 50 mesh retaining screens. The blow back method was also different. The Exxon filter element used a "positive blow back" technique. It was equipped with shut off valves to allow it to be completely isolated from the feed and product streams during blow back. The element was then depressurized and blown back with a larger volume of low pressure air.

Runs using the Exxon designed filter also proved unsuccessful. Some screen plugging was in evidence but it was the inability to seal the blow back nozzles which caused the most problems. Evaluation of the Exxon filter was discontinued at this point.

## GBF MODEL 3

Discussions with the Ducon Company led to the design and fabrication of the third filter system. Ducon indicated that they had encountered the same screen plugging problem with flyash and bypassed it by removing the screens and designing the individual beds with more freeboard to prevent entrainment of the filter media during blow back. It was also recommended that a fluidizing grid be used at the bottom of the beds to assure good distribution of the blow back air. The use of an ejector to replace the sometimes troublesome plunger type blow back nozzles was also suggested. Filter elements incorporating these suggestions were fabricated and shakedown continued using two of these elements each of which contained five filter beds. A photograph of one of these modified filter beds is shown in Figure 8. Figure 9 is a photograph of an element.

Dirty gas enters the bed through the opening below the top flange and passes downward through the filter bed and out into the clean gas outlet tube in the center of the element. During blow back, the blow back air passes up through the fluidizing grids supporting each bed, fluidizes the beds and blows the fine particulates out through the inlet slot. A 18 cm (7 in) freeboard above the filter beds acts as a disengaging section for the filter media and prevents its entrainment through the outlet slot.

Operability of the modified filter system has been demonstrated. The end of the initial shakedown phase was signified by the successful completion of a 24 hour demonstration run. This run was preceded by a number of shorter duration runs used to establish suitable operating conditions for the demonstration run. The successful use of an ejector was also demonstrated during one of these runs. These runs were successful in that filtration, ability to blow back, ability to maintain low pressure drops and collection of particulates after blow back were demonstrated. Collection efficiencies of about 90% were measured based on outlet particulate concentrations of about 70 mg/m$^3$ (0.03 gr/SCF) although efforts to optimize filter performance were not completed. Stable operation for up to 24 hours was also demonstrated with no significant increase in baseline pressure drop across the filter. Blow back was usually required every 10-20 minutes during which time the filter pressure drop had increased by 2 psi above its baseline value. A range of blow back conditions were used to restore the baseline pressure drop. Blow back durations ranged between 2 and 30 seconds and superficial velocity between 0.5 and 2.5 ft/sec. Filtration velocities generally ranged between 60 and 80 ft/min. Filter media consisting of 300 to 600 micron quartz particles and alumina particles greater than 840 microns were tested. The quantity of blow back air used ranged from 1 to 5% of the filtered gas rate.

## PROBLEM AREAS

A number of problem areas were defined during the shakedown portion of our program. Demonstrated particulate outlet concentrations are still higher than those required to meet the turbine requirements, although the lowest levels measured to date are only slightly above the upper limit of the tentative target range. Changes in filter media size could be expected to improve collection efficiency. However, at times, the filtration efficiency was very poor and the outlet particulate concentrations were as high as 700 to 1200 mg/m$^3$ (0.3 to 0.5 gr/SCF). It was also observed that the efficiency appeared to decrease with time in some of the longer runs, dropping from 90% initially to about 50% later in the run. Loss of filter media during blow back was another reoccurring problem during shakedown. Further attempts were made to use retaining screens on the GBF-3 model but failed because of plugging. Figure 10 is a photograph of a 50 mesh screen plugged during a test. Additional tests made with 10 mesh screens also resulted in significant screen plugging. Since inlet retaining screens are susceptible to plugging, a denser filter media will probably have to be used or better control of the blow back air supply established to minimize these losses. A significant buildup or particulates in the filter beds was also observed amounting to about 30% of the weight of the filter media. A possible steady long term increase in filter pressure drop may result because of this. However, no significant increase in filter pressure drop was noted during any of the shakedown runs.

It was also observed that the particulates were not only building up in the beds, but were uniformly mixed with the filter media. It is possible that the buildup and mixing of particulates in the bed could be responsible for the increase in the particulate concentration in the outlet gas with time. The formation of a hard filter cake on the filter media surface resulting in rat holding and decreased efficiency could possibly be another problem area. This was noted during one of the shakedown runs in which kerosene was burned for a prolonged period of time.

Another potential problem with the current design is its vulnerability to upsets. If upsets occur, such as bed plugging or loss of filter media, the operating problems caused by such upsets usually require shutdown of the system. It is usually not possible to take corrective action which restores good operation. Another problem which may be unique to the Miniplant was the interaction of the granular bed filter with the rest of the FBC system during the blow back cycle. An increase in system pressure was noted during blow back resulting in problems with the coal feed system which is controlled by the differential pressure between the coal feed vessel and combustor. This required modifications to the coal feed control system to minimize the effects.

## CURRENT PROGRAM

In the current program it is planned to conduct additional tests or further modify the filter system to minimize some of the problem areas uncovered during the shakedown runs. Since plugging of the inlet retaining screens was a serious problem, testing will be done to determine whether filter media losses during blow back can be reduced to an acceptable level by examining the relation between entraining velocity particle size and density. Filter media of different densities will be tested and acceptable blow back conditions will be established. During these tests the effect of blow back velocity and duration on blow back efficiency will be determined. Ways to increase filtration efficiency will be studied by evaluating the effect of filter media particle size, bed depth, and filtration velocity. The apparent problem of efficiency decline with time will also be studied further.

After a practical set of operating conditions has been determined, several extended runs will be attempted to evaluate long term performance at these conditions. These runs will allow a better evaluation of the mechanical and material performance. Extended runs are also planned using the granular bed filter aimed at determining erosion and corrosion effects on gas turbine samples located downstream of the filter. This work will be done as part of a separate program sponsored by ERDA. Further EPA sponsored studies will consist in testing another particulate control device and measuring the concentration of trace emissions from a fluidized bed combustion system using a high efficiency particulate removal system.

## ACKNOWLEDGEMENT

This work is being carried out by Exxon Research and Engineering Company under contract to the U.S. Environmental Protection Agency, Industrial Environmental Research Laboratory. The Contract Number is 68-02-1312. The EPA project officer is D. B. Henschel.

## REFERENCE

1. Hoke, R. C., et al, "Studies of the Pressurized Fluidized-Bed Coal Combustion Process," EPA-600/7-76-011, September 1976.
2. Keairns, D. L., et al, "Fluidized Bed Combustion Process Evaluation," EPA-650/2-75-027-C, September 1975
3. AIChE Symposium Series No. 137 Vol. 70 pp. 388-396 (1974).

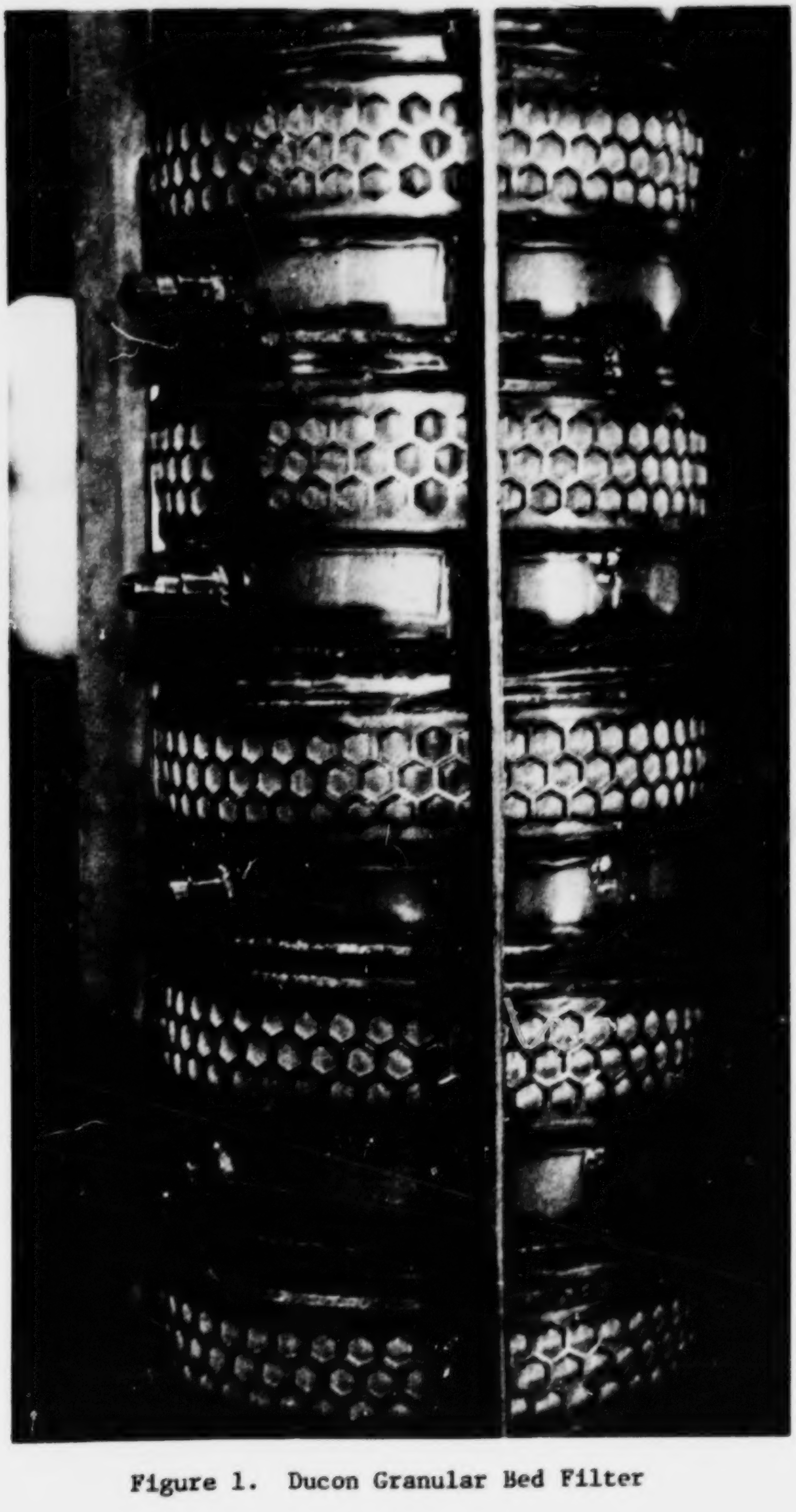

Figure 1. Ducon Granular Bed Filter

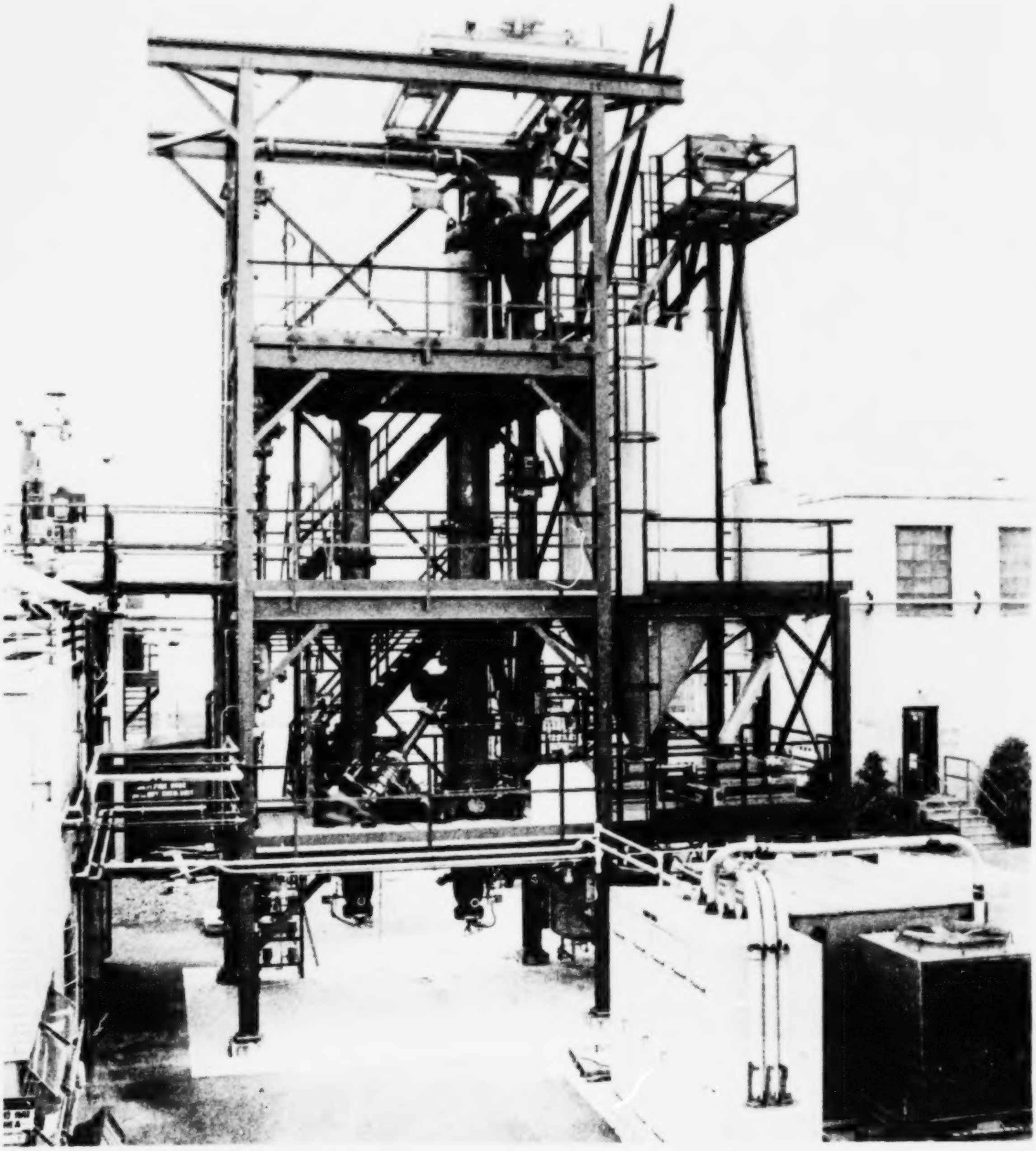

Figure 2. EPA/Exxon Pressured Fluidized Combustion Miniplant

Figure 3. Filter Pressure Vessel Side View

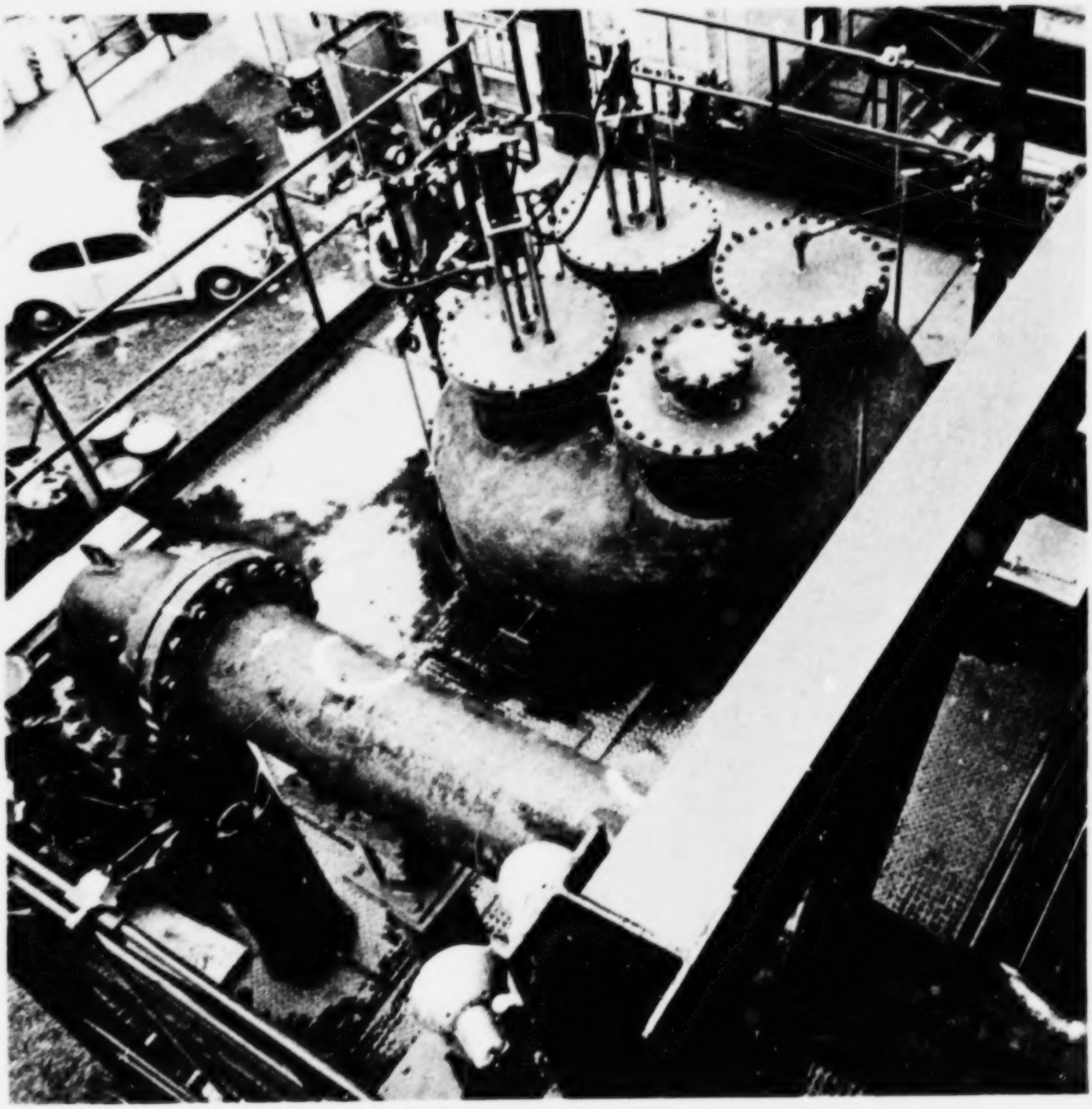

Figure 4. Filter Pressure Vessel Top View

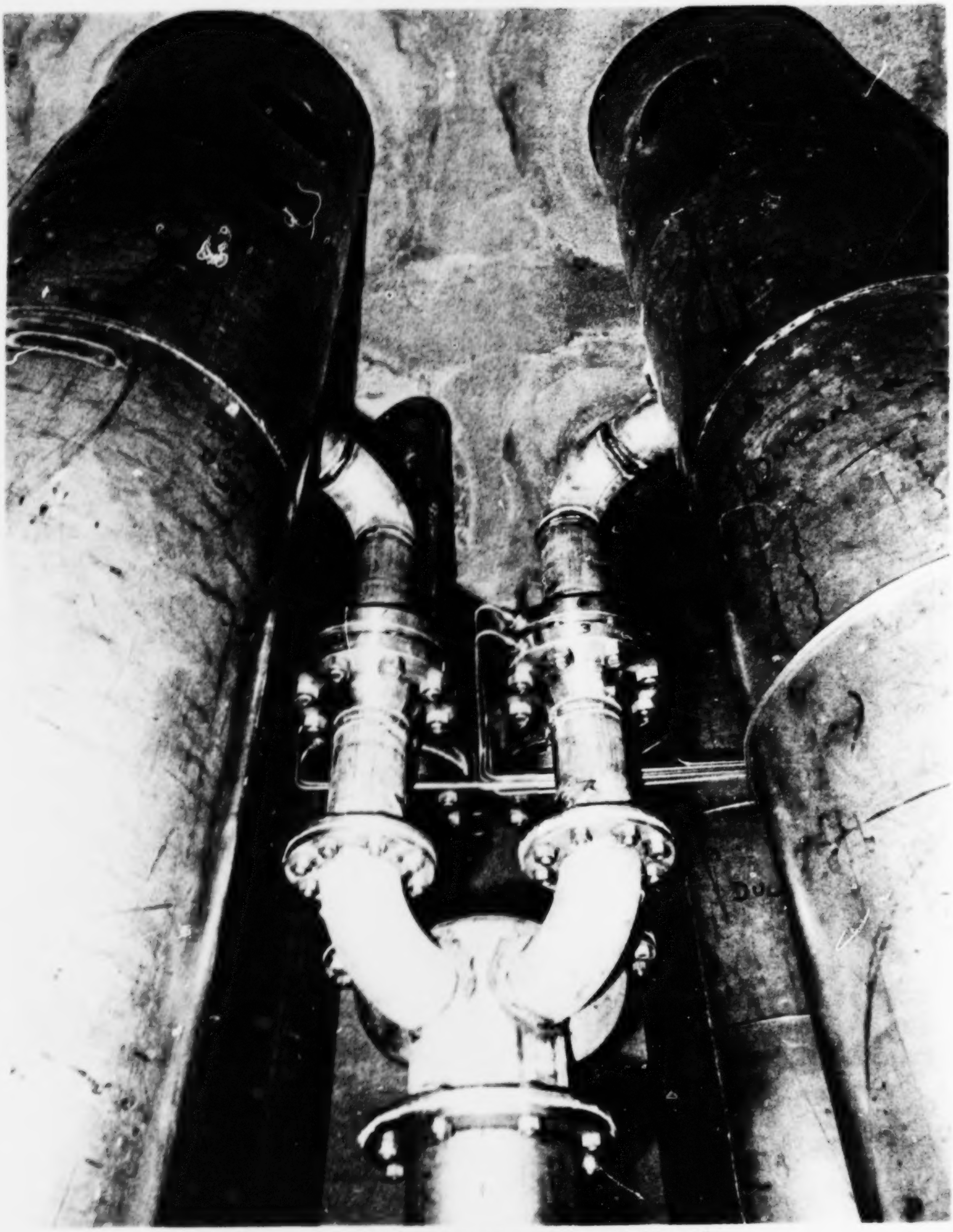

Figure 5. Filter Pressure Vessel Interior

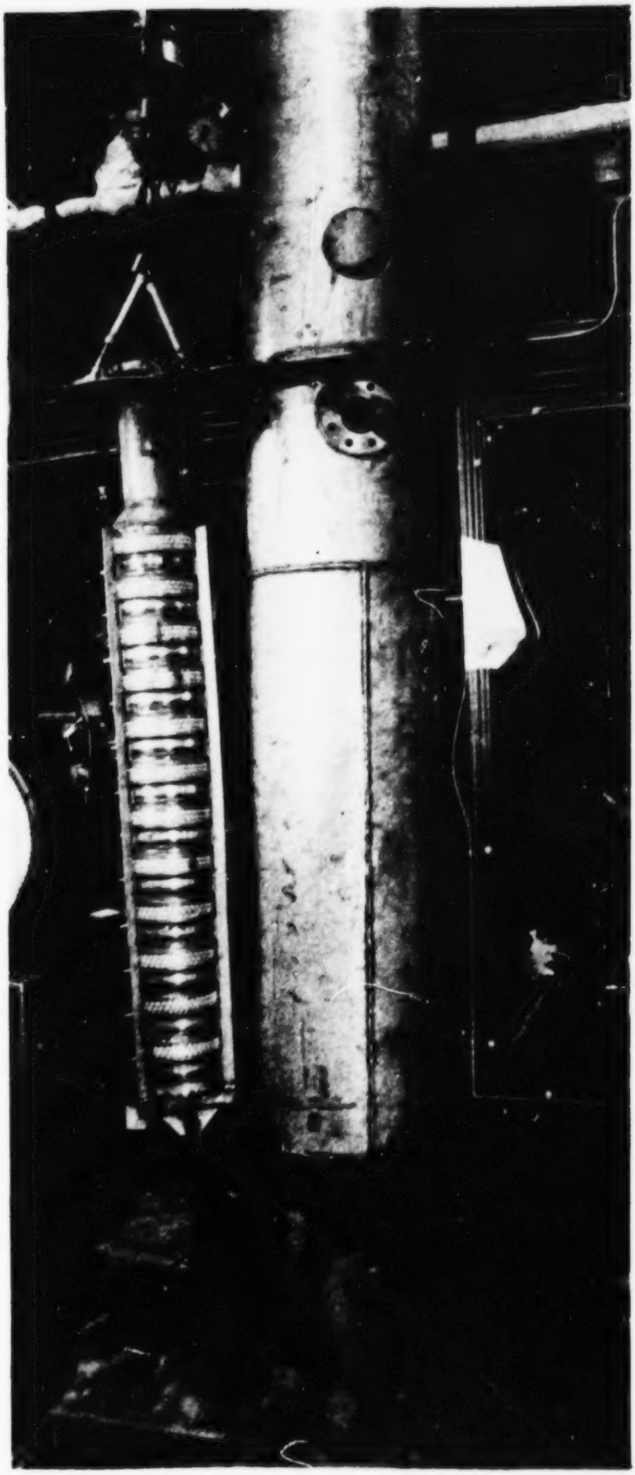

Figure 6. Ducon Granular Bed Filter and Shroud

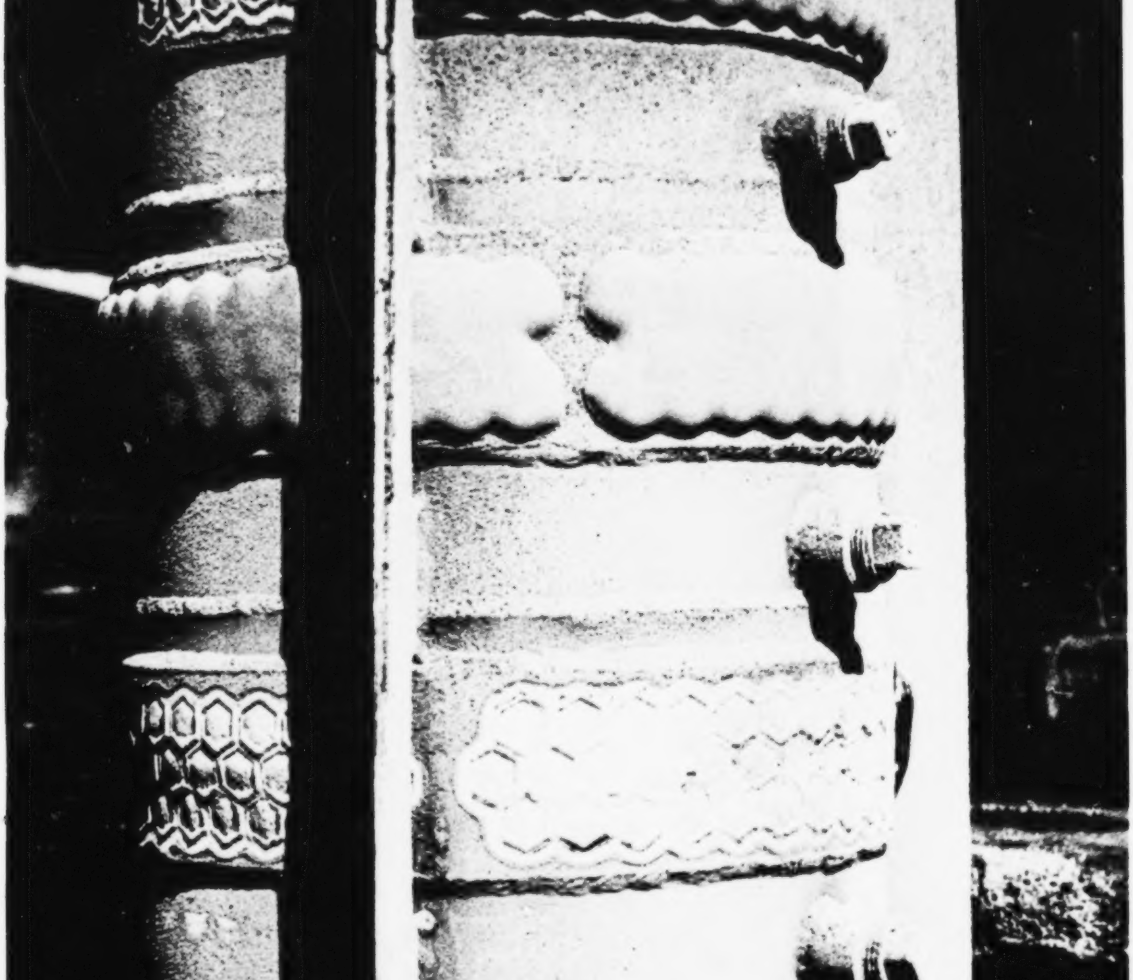

Figure 7. Filter with Plugged Inlet Retaining Screens

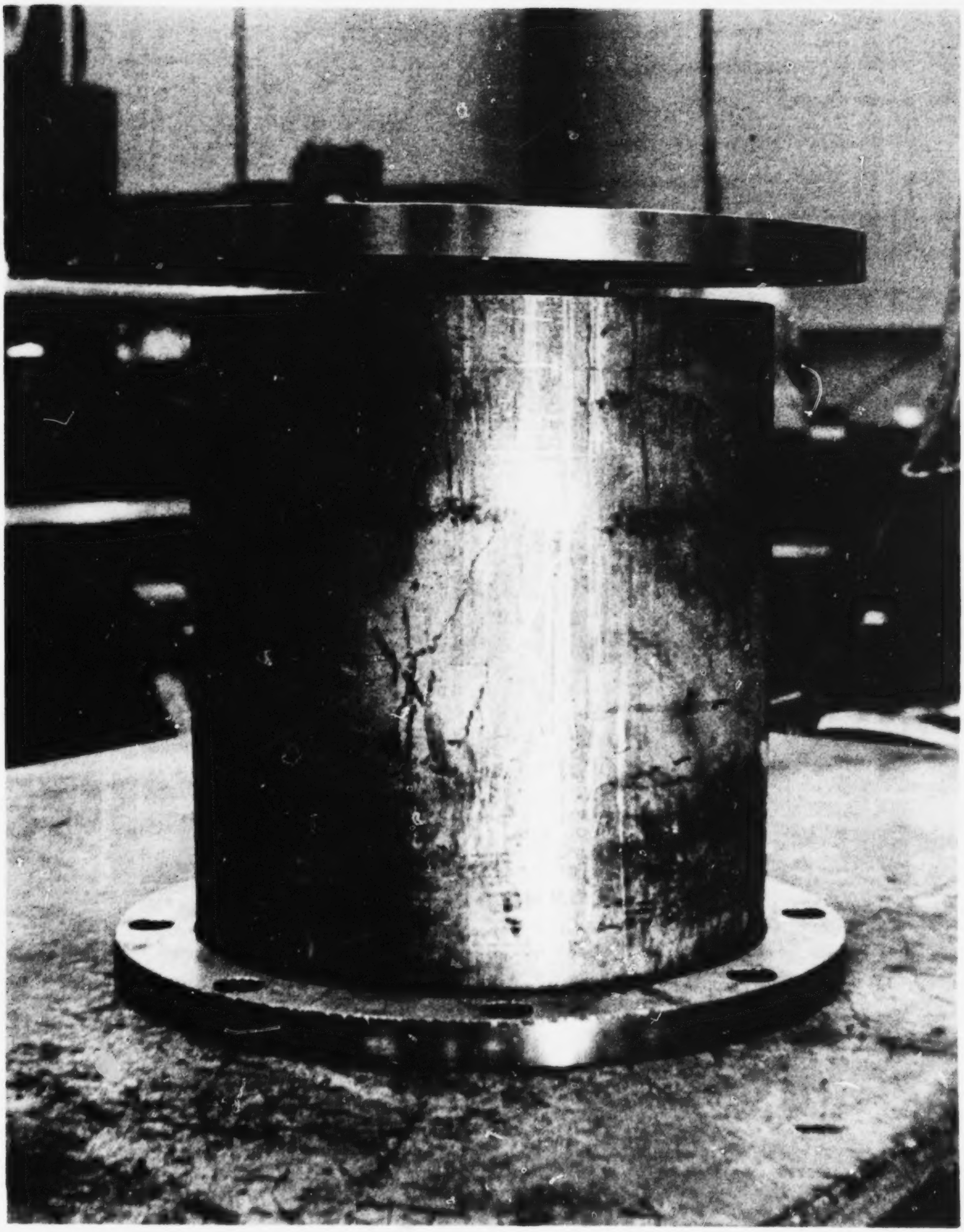

Figure 8. Modified Filter Bed

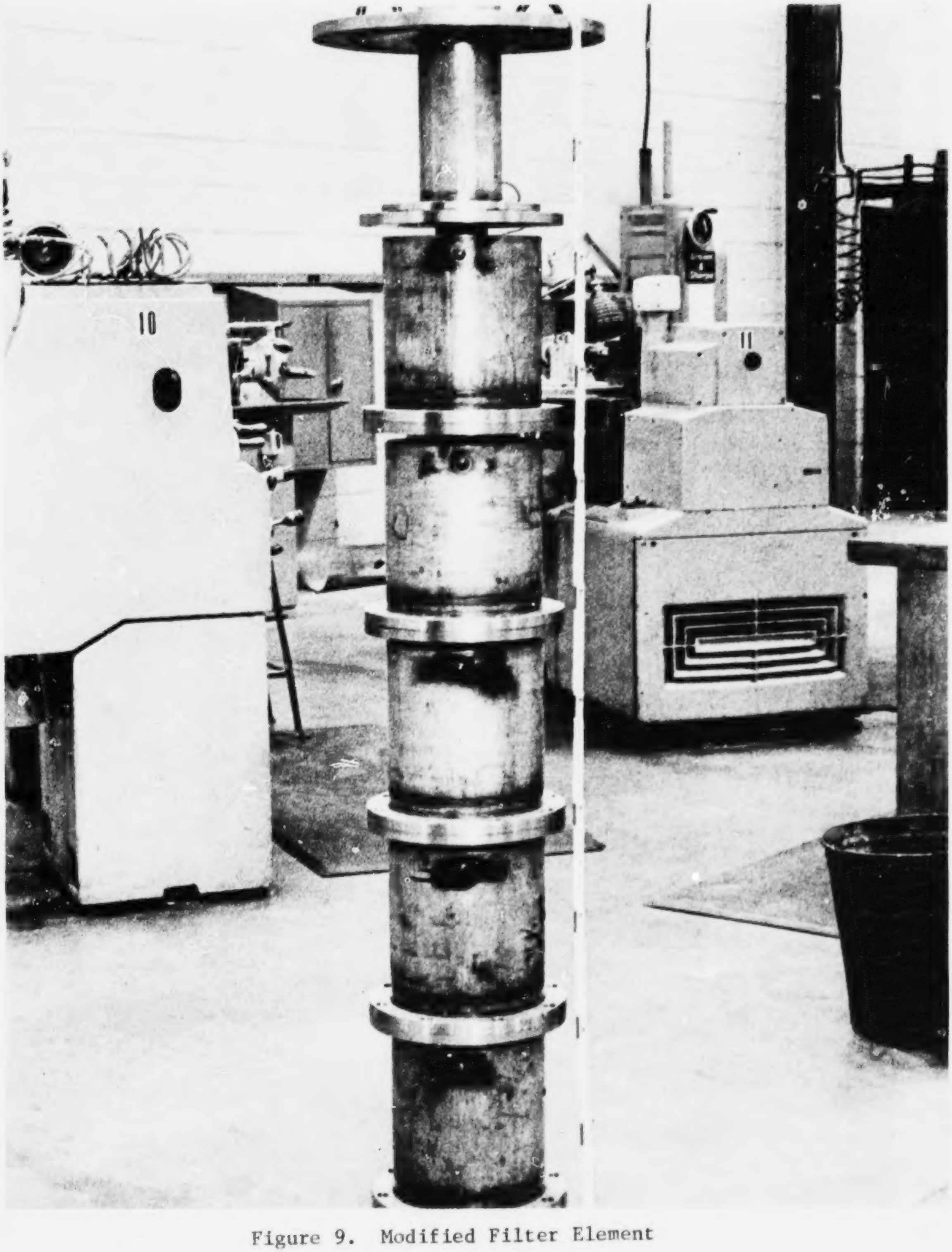

Figure 9. Modified Filter Element

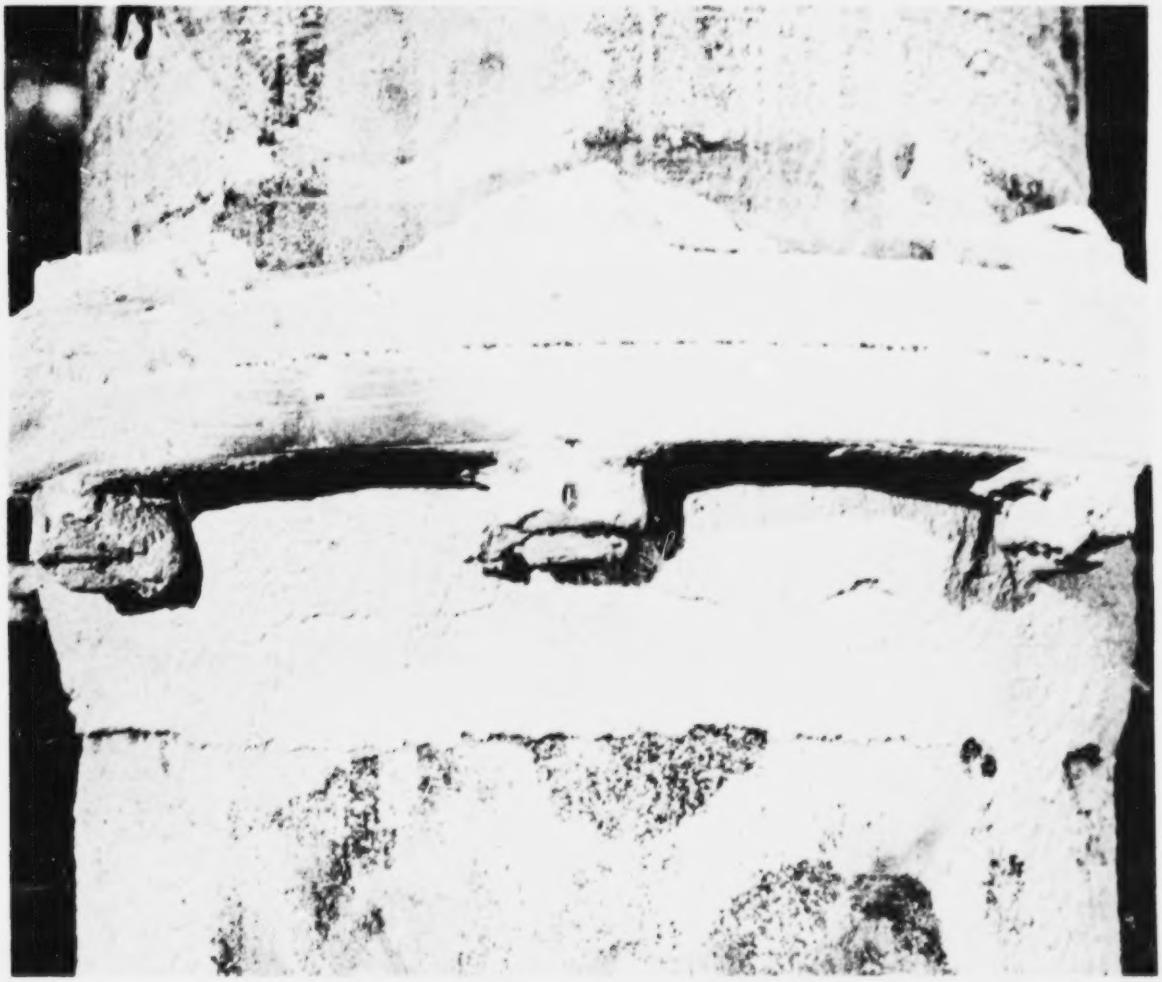

Figure 10. Filter with Plugged Inlet Retaining Screen

# PERFORMANCE AND MODELING OF MOVING GRANULAR BED FILTERS

By:

G. L. Wade
Combustion Power Company, Inc.
Menlo Park, CA 94025

# PERFORMANCE AND MODELING OF
MOVING GRANULAR-BED FILTERS

By:

Gordon L. Wade

Combustion Power Company, Inc.

Menlo Park, California 94025

## ABSTRACT

An ongoing experimental and theoretical effort sponsored by ERDA on moving granular-bed filters is decribed. Test apparatus includes a flexible cold-flow facility featuring a 3500-cfm filter where a parametric test program is in progress. The test facility is described along with the completed and planned variations in operating conditions and configuration geometry.

Initial data on measured collection efficiency and pressure drop are presented; regression analysis indicates that reasonable operating conditions may be specified for which total efficiency in excess of 95 percent is readily attainable.

A parallel mathematical-modeling effort is discussed, and key features of the resulting computer simulation program are identified.

# SECTION 1

# INTRODUCTION

## BACKGROUND

Many energy-producing processes based on fossil fuel include a stringent requirement for separation of particulate materials from hot pressurized gas streams. Protection of such downstream equipment as combustors, turbines, and heat exchangers is normally the dominant motivation, although compliance with emission standards may also pose similar performance requirements. Existing separation equipment such as cyclones and electrostatic precipitators, though still evolving in performance and operating costs, are generally held to have distinct limitations. This is particularly the case in the environment produced by combustion or gasification of high-sulfur coal.

A promising device for this application is the moving granular-bed filter (GBF) now in development under ERDA Contract EF-77-C-01-2579 at Combustion Power Company. Shown conceptually in Figure 1, a GBF features a downward-moving bed of packed granules (media) through which the dirty gas passes in a cross-flow pattern. Experience has shown that the process efficiently transfers particulate from the gas stream to the solids stream, where several possibilities for subsequent separation are available to permit circulation and re-use of the media.

Commercial versions of the concept, restricted to temperatures below about 800 F and to pressures near atmospheric, have been marketed by Combustion Power Company for the past four years. These devices, known as Dry Scrubbers, have been supplied for numerous stack-cleaning applications on existing plants.

## CURRENT PROGRAM

The current contract includes an intensive program to determine the physical principles upon which GBF's operate, and to provide a quantitative verification of these principles by controlled testing of a sizable unit (up to 3500 cfm) under cold-flow conditions.

The scope of the cold-flow program includes (1) theoretical analysis, in which the theories and mechanisms of the interaction of particle-laden gas and granular media are studied and mathematically expressed for computer simulation; (2) design and construction of the cold-flow model for parametric testing and correlation with the math model; (3) installation of a particle-injection and sampling facility to enable controlled dust injection, particle sampling, and analysis; and (4) carrying out of a parametric test matrix.

The primary objective is to generate information on the cold-flow model for future application, correlation, performance prediction, and implementation on a next-generation GBF hot-flow model.

At the time of this writing, the five-month parametric testing effort is in progress, along with analysis of the experimental data and operation of the computer simulator. Accordingly, the present paper should be regarded as a status report containing presentations of early data. Continued analysis, acquisition of new data, and forthcoming computer results are expected to modify and improve understanding of the subject material.

# SECTION 2

# APPARATUS FOR COLD-FLOW TESTS

## GBF SCHEMATIC

The GBF and its media circulation loop are shown in Figure 2. Pneumatic lift is employed to transport media exiting the GBF a vertical distance of 36 ft, after which it is disengaged to begin another pass of the filter. The pneumatic-transport process also serves as a first stage of media-particulate separation. Second and third stages of media cleaning occur in the counter-flow "rattler" and fluidized-bed sections atop the GBF. Separated particulate is thus concentrated in a relatively small air stream directed to a conventional baghouse. The fluidized bed also serves as a convenient media reservoir. Media flow rates are controlled by modulation of ejector air admitted near the base of the lift pipe. Glass sections in upper and lower seal legs and in the disengagement vessel permit visual monitoring of media flows at those points.

Many design features of the cold-flow unit look ahead to the high-temperature, high-pressure environment of subsequent program phases. Thus, for example, pneumatic processes were selected for media cleaning and transport instead of vibrating feeder-screeners and bucket conveyors (such as used in commercial scrubbers) since the latter combination is not suited to high-temperature applications.

The GBF is housed in a 3/16-inch-thick 304 stainless-steel vessel that is 15.5 ft long and 5 ft in diameter. The vessel is sized to accommodate any one of three outer panels to form bed depths of 3.8, 7.6, or 15.2 in, based on a fixed inner-panel diameter of 15.4 in. Height of the slotted section of the inner panel is nominally 53 in, to give an approach area of 17.5 sq ft for air flow. Rubber boots on top of each panel provide a flexible gas seal that has minimal effect on panel load measurements.

The inner panel for 2-mm media (nominal granule size) contains 1/8-in x 1-in slots (Figure 3). This slot configuration promotes media spillage for front-face cleaning during operation. The louvers in all outer panels are based on positive retention of 0.8-mm media.

All panels are suspended from above by load cells mounted on the vessel cover. Figure 4 shows details of load-cell orientation along with the relative location of 12 pressure sensors adapted to the measurement of normal pressures developed by the flowing media. Analysis of these measurements is expected to improve the understanding of loads imparted to GBF structures by this unique configuration and process.

## DUST INJECTION

Early in the GBF Cold-Flow Program, it was recognized that many factors which are independent of granular-bed filter design, operation, and performance would nevertheless have a major impact on the successful conduct and completion of the program. These vital factors include:

- Selection of artificial dust(s) with properties in the same range as typical combustion particulate but compatible with special test requirements such as flowability, non-toxicity, and economy.
- Reliable, consistent dust feed over a range of 1 to 100 lb/hr.
- Injection of dust against the positive pressure upstream of the GBF.
- Uniform and repeatable deagglomeration and dispersion of dust in the inlet duct.
- Selection and/or development of equipment and techniques for sampling particulate concentration and size distribution.
- Efficient laboratory analysis of samples including automated data reduction.

* Development of procedures for efficient subcontractor sampling.

Since these functions are not necessarily dependent upon the availability of an operating GBF, it was possible to initiate this task during the fabrication and erection of the filter, thereby providing lead time to address and resolve inevitable problems associated with hardware development.

It was deemed most economical to install the plumbing upstream of the filter for injection "calibration" as well as for its ultimate GBF service. Techniques and operating procedures developed during the calibration phase would thus not require "translation" to a new system since all equipment selected, modified, and calibrated for this task would naturally be applicable to GBF testing without further alteration in design or operation.

Figure 5 illustrates the facility constructed for use in the GBF Cold-Flow Program. An existing Sutorbilt positive-displacement blower capable of continuous operation at about 5 psig and 4000 scfm supplies air to the GBF and auxiliary systems, including dust-injection air, media-circulation air, and fluid-bed air (but excluding instrumentation air). This air is branched ahead of the dust-injection station; the portion of flow which passes through the main venturi is controlled by a pneumatically-actuated 8-in. butterfly valve. An "Annubar" integrating pitot-static flow-sensing element is located in the main flow branch to provide both flow indication and a signal for the main air-flow control system.

The purpose of the dual-venturi dust-injection system is threefold:

1. It provides a means of feeding dust into the main air line (which is typically at a gage pressure between 2 IW and 50 IW) without special rotary airlocks or similar non-continuous feeding devices.
2. It deagglomerates the dust from its compacted storage condition to stable particles near the intrinsic crystal size of the dust.
3. It removes very large foreign material or particles of dust which failed to deagglomerate.

Dust injection is accomplished in an air stream that passes through a venturi with an inlet-to-throat ratio of six. A $\frac{1}{2}$-in coupling forms a "tee" with the throat. To this coupling is threaded a hopper into which dust is introduced by a variable-speed vibrator feeder. Dust so introduced is subjected to high velocity in the venturi throat, which deagglomerates most of the compacted material. The venturi also produces a depression in static pressure of about 70 IW (maximum) below atmospheric, sufficient to prevent backflow from the injection system during minor downstream upsets.

From the feed venturi, the air/dust mixture flows into an 8-inch-diameter cyclone having a 4-in outlet and three 1-in x 16-in x $\frac{1}{4}$-in baffles in the annulus. This component serves both to further the deagglomeration process and to remove any remaining large particles. Fallout from the cyclone is captured in a sealed -- and periodically emptied -- container at the bottom of the conical section.

The main venturi (inlet-to-throat area ratio of four) produces a depression to help overcome losses in the feed venturi and cyclone, as well as a high-velocity region in which to disperse the air/dust mixture before its deceleration into the main duct. Downstream from the main venturi are two sample stations, each consisting of two 3-in threaded couplings at $90^{\circ}$. Each station is located in accordance with EPA recommendations (8 diameters downstream and 2 diameters upstream from the nearest disturbances).

Desirable properties of candidate dusts for the GBF Cold-Flow Program include:

- Flowability (for feeding purposes) and ease of dispersion.
- Narrow size distribution.
- Particle sizes between 0.5 μm and 50 μm.
- Specific gravity between 1 and 3.
- Non-toxicity.
- Availability and economy.

A number of commercially available dusts of suitable size were considered, including hydrated alumina, magnesium oxide, kaolin clay, zinc, zinc oxide, and carbon.

Kaolin clay was eliminated on the basis of in-house experience with feeding problems. The zinc materials were much heavier than typical flyash, so that data obtained with them would be of limited practical utility. Carbon was thought to represent an unacceptable housekeeping problem.

Actual dust-injection tests were carried out on hydrated alumina (Alcoa Hydral 710, Alcoa C-333, and Reynolds RH-730) and magnesium oxide (Basic Chemical Magox 90 and 98-HR). All materials behaved reasonably well during feeding, although the larger particle sizes (C-333 and Magox 90) required less attention. The size range of magnesium oxide was quite wide. Magox 98-HR and Hydral 710 had similar median particle sizes, but the next grade of magnesia (Magox 90) had a median particle size approximately twice that of C-333. As a result of a number of trials, it was found that Hydral 710 and C-333 consistently yielded median sizes of about 3 μm and 20-30 μm, respectively. These results, along with considerations of availability (shelf stock in Moraga, California), cost (19¢ to 26¢ per pound, depending upon grade and quantity), and safety (the normal use of these grades is as the polishing compound in toothpaste), led to a decision to use these two materials as the basic dusts for all tests. Table I lists typical properties. In order to synthesize different mean particle sizes, the materials are used as follows:

- Small Particle Size: Hydral 710 (<5 μm median).
- Nominal Particle Size: Mixture of Hydral 710 and C-333 in the proportion 2 lb H-710 to 1 lb C-333 (5-10 μm median).
- Large Paricle Size: C-333 (>15 μm).

PARTICLE SAMPLING

A number of manufacturers have developed continuous quantitative and semi-quantitative particle monitors in recent years, but it was thought best in this program to rely on methods that already have wide acceptance. This meant that we would deal with discrete samples, would measure total loading by conventional EPA filtration techniques, and would determine size distribution by one of several impaction methods. Total loading was thus measured with an EPA Method-5 sampling train (without impingers, since preliminary runs showed no need for them). CPC's measurements of size distribution were made with an Andersen 2000 Mark III impaction classifier. Size distribution was measured only at the central axis of the air line, but experience showed that good total-loading measurements were possible only with a six-point traverse of both a horizontal and a vertical diameter.

To establish the consistency and accuracy of our sampling operations, we engaged as subcontractors a sampling team from Air Pollution Technology (APT) of San Diego. The APT team also used the EPA Method-5 train for total loading, but a University of Washington impactor for determining size distribution.

There are three ways available to us for assessing the accuracy and reproducibility of total-loading measurements. We can compare simultaneous EPA-5 measurements; we can compare the sampling results with a material balance on dust and air flow; and we can compare with results obtained by summing up the several sizes measured by impingers. Statistical comparisons using the latter two approaches are shown in Figure 6. Least-squares curve fits of straight lines through the origin demonstrate quite good agreement. Any particular sample, of course, represents the time period when it was taken while the material balance provides an average for the complete run. A special document giving additional details of the calibration task, sampling procedures, and data-processing techniques has been published.

Also employed (and shown in Figure 5) is an on-line opacity meter directly across the GBF outlet stream. This unit, a Lear-Seigler Model PM7A, proved valuable in subsequent GBF operations. A stabilized reading from the semi-quantitative output signal provided one indication (of several) that steady-state operating conditions had been achieved in the filter, so that meaningful particle sampling could begin. The highly responsive signal also was a prime indicator of transient upset conditions.

## DATA ACQUISITION

Aside from particulate sampling upstream and downstream of the GBF, the bulk of operational measurements were logged by a data acquisition system (DAS) based on a Tektronix Model 4051 computer (desk-top class).

The DAS 4051 unit, with its internal magnetic-tape cartridge, CRT screen and 32 K bytes of memory, is shown adjacent to the control console in Figure 7. An extended BASIC language gives easy access to the 4051 with its high-resolution CRT (1024 x 780 addressable points).

A special feature of the 4051 used in the DAS application is the general-purpose interface bus (GPIB) available for plugged connections to an extensive family of programmable instruments. The four external devices shown in Figure 8, for example, can be plugged to the GPIB to give a highly flexible and powerful DAS operating under full control of 4051 software.

Programmed (and therefore adjustable in real time) signals from the timing generator are processed by the 4051 into convenient elapsed-time scales for test purposes. The programmable scanner and variable-gain voltmeter are commanded by the 4051 to read and submit measurements of 40 instrumentation channels at adjustable periodic intervals. These are transformed by the 4051 into larger sets of performance parameters in engineering units; the latter are logged on tape cartridges for post-test processing and display. A separate Tektronix 4051 with hard-copy unit is available for that function.

Software for the DAS 4051 accomplishes many auxiliary functions in addition to the primary sampling/transformation/logging process outlined above.

Most of these utilize the programmable memory and graphical-display capabilities of the 4051. A periodically refreshed schematic diagram annotated with latest measurements is generated on the CRT, for example, to provide quantitative status for test conductors and observers at a glance (Figure 9 shows the format).

Another feature of the developed software involves storage in memory of the most recent 51 time-slices of data from 19 selectable channels. Between sampling/logging episodes, one or more of these channels may be selected at will for graphical display. Simple statistical summaries of the selected channel are calculated and presented along with the plotted data. The intent is to provide observers with self-consistent trend indicators in a quasi-real-time environment. One important use of such displays is to permit a determination that steady-state conditions have been achieved.

# SECTION 3

# PARAMETRIC TEST PROGRAM

## SCOPE OF THE PROBLEM

From an academic point of view, the precise description of GBF performance is an exceedingly complex subject involving many dimensions. The diagram of Figure 10 is intended to convey some appreciation of this point and to facilitate an orderly discussion of the subject.

The purpose of a given GBF design is to remove particulate matter from a dirty gas characterized by the six somewhat generalized quantities identified on the left of Figure 10. One set of parameters (among many possible alternatives) for characterizing the clean gas thus produced is shown on the right of the diagram. Primary interest naturally centers on quantification of the particulate parameters. The incremental losses suffered by the gas stream are nearly as important, however, since these represent penalties that must be suffered if a GBF is to be incorporated in a process. Chief among those listed (for most applications) is pressure loss. Relief of intolerable pressure drop, of course, provides the original motivation for keeping the granular bed in motion.

Size and shape of granules is a key factor in any model of granular filtration, but moving the bed adds several other factors. The media flowrate, in fact, is the parameter ordinarily used for control purposes; an increase acts to reduce pressure drop, but with some degradation in collection efficiency. The practical necessity of circulating media introduces a potential modification of collection performance owing to imperfect cleaning of the media, as does the implementation of necessary pressure gradients around a solids transport loop.

For purposes of design synthesis, geometrical parameters that define the filter must also be regarded as independent factors in any functional performance model.

At elevated temperatures, the issue of heat transfer within the GBF and the associated impact of non-isothermal conditions on performance must be addressed. If media and gas inadvertently (or intentionally) enter at different temperatures, resultant spatial distributions of temperature will likely produce a detectable variation in GBF behavior.

The purpose of the foregoing comments is to indicate that the principal "dependent" performance parameters of a hot, pressurized GBF may be influenced by as many as 15 "independent" factors. In fact, the reader will have little difficulty suggesting other candidate factors for addition to those shown in Figure 10 (gas properties such as molecular weight, for example).

For purposes of the present ERDA cold-flow program, the list of parameters to be varied experiementally was trimmed to the following seven:

1. Gas flow
2. Media flow
3. Particulate loading
4. Particulate size distribution
5. Media size
6. Element height
7. Element depth

Following satisfactory completion of this effort, and assuming indications of promising performance over some region of the "independent factor space", the general plan will be to proceed into a hot-testing program where three more factors are added:

1. Gas temperature
2. Media temperature

3. "Real" particulate properties as generated by combustion of coal in a fluidized bed at near-atmospheric pressure.

Assuming positive results, a final stage of development would add the factor of elevated pressure to those already studied.

## PLANNED TEST MATRIX

The number of tests required to fully explore a seven-dimensional space in any statistically satisfying way when each factor has three or four levels of interest is exceedingly large. Furthermore, the disparity between any such ideal number and a realizable number is magnified when each test is necessarily time-consuming and expensive. And unfortunately, GBF testing falls into this category. First, primary interest is limited to "steady-state" performance -- that typically dictates a 1-4 hour dwell time at given operating conditions before useful data can be recorded. During this period, the entire inventory of media must be exchanged at least once as equilibrium concentration profiles of captured dust are established within the bed. Once steady-state conditions are approached, sampling of particulate concentrations can begin. That, too, consumes a significant amount of time, particularly at the GBF outlet, where low loadings translate into extended time intervals if measurable quantities of particulate are to be extracted.

Time and funding constraints applied to the considerations above dictated an appreciable compromise in test planning. It was found that the number of separate test points that could be scheduled on a two-shift basis with allowance for configuration changes, inspections, replications, and contingency reruns was just over 100.

Ranges of interest in the independent factors together with the number of discrete levels in each are presented in Table II.

Test organization was facilitated by partitioning into 9 groups or subexperiments and selection of "nominals" for the last four factors to serve as a basis for single-factor excursions (see Table II). Nominal values for the geometric factors were derived from overall scale considerations, available air supplies, and previous experience regarding element depth/height ratio. A plentiful stock of 2-mm Arlcite (a highly spherical, high-alumina ceramic manufactured as a grinding product) and successful prior experience led to the choice of nominal media.

The entire set of planned factor combinations is presented in Table III. The first sub-experiment, a survey of variations in the first three independent factors (readily altered without apparatus changes), has been completed with nominal values for the other factors. Factor combinations for the 25 tests were purposely selected to be an approximate subset of an applicable "double-latin-squares" design (for 3 factors, each with 4 levels, a full set calls for 32 combinations).

The short series involving intermittent movement of media constitutes a side experiment to study possible performance advantages of a mode of operation featuring variations on this approach.

Two variations in the size distribution of injected particulate were addressed in the next two sub-experiments of 12 tests each. There followed three sub-experiments dealing with factor-of-two changes in bed geometry. In the final two sub-experiments, significant changes in media size will be made. The larger size, like the nominal, consists of nearly spherical high-alumina material; use of the thin bed for this series instead of the nominal was dictated by limited supplies of the media. Gopher sand, a relatively pure silica sand of high sphericity, was selected as a small media for the final sub-experiment.

# SECTION 4

# PRELIMINARY RESULTS

As previously stated, the test program and related data reduction and analyses are in progress at the time of this presentation. Accordingly, the results and discussion contained in this section are necessarily preliminary in nature.

## PARTICLE SAMPLINGS

Certain general results in this area have already been discussed; others are documented in Reference 1. Satisfactory sampling equipment and procedures for the application were developed (by both CPC and APT) and are also described in the reference. Reasonable agreement between the data produced by the two teams is demonstrated. Since the subcontractor effort is continuing, additional comparative data will be generated and reported.

Tests by both CPC and APT teams indicate that both of the dusts used in the program are bimodally distributed. This characteristic produces an S-shape in a cumulative-distribution plot such as that displayed in Figure 11 (the "S" is here truncated by the inability of the impactor to characterize the largest particulate any more precisely than "larger than 19.2 microns"). The fitted regression line is used only to facilitate quick comparisons of samples; the distribution is clearly not log-normal. The term "median diameter" thus has only a relative meaning, and very little of the material may actually have sizes near to it.

The display in Figure 11 is typical output from a Tektronix 4051 program written to process CPC measurements made with the Anderson impactor. The ordinate used is the "aerodynamic diameter" of the particles. Note that compensation is made for the degree of isokinetic sampling during the collection period.

## FLOW SURVEY, LARGE PARTICULATE, AND SMALL PARTICULATE

Tests in these three sub-experiments were recently completed and will be discussed here as one group. Pending further detailed study, this recombination into a simple 4-factor experiment appears to be partly justified by difficulties in test-to-test control of the size distribution of the particulate, particularly in the earliest tests.

A typical display generated by the DAS is shown (reduced size) in the several traces of Figure 12. Inspection of the traces leads to a number of observations.

- The plugged-together DAS and Tektronix 4051 software make a highly satisfactory unit.
- The control system for GBF airflow works well, maintaining essentially constant levels after the momentary shutdown near ET = 30 min.
- Media circulation rate is likewise well controlled by the scheme illustrated earlier (Figure 5).
- The initiation of dust injection at ET = 50 min is readily observed in the opacity signal, and in the positive response of GBF pressure drop to the event.
- A 7-minute interruption in dust feed centered around ET = 140 min produced an immediate reaction in opacity of the GBF outlet air stream. This response, corroborated by visual observations of the exhaust, illustrates the value of the opacity meter and the fact that GBF collection (or penetration) mechanisms have a short-term component as well as a long-term one assocaited with equilibrium distributions within the bed.

- GBF pressure drop also responds to the disturbance, and follows with a transient quite similar to its earlier approach to steady state.
- The temperature traces remind us that the cold-flow facility is in reality a "warm-flow" configuration where some heat exchange between warm air (heat of compression) and cooler media (see fluid-bed trace) occurs.
- Load cells supporting the inner panel show a distinct (and similar) response to the early air-flow disturbance; response to the dust-flow interruption is much less distinct. Differing magnitudes and long-term trends among the three traces have not yet been explained; the apparent indication of imbalanced lateral loading with long-term drift will be studied.

Post-test disassemblies and inspections proved to be less of a problem than originally supposed. Figure 13 shows one such operation in progress. The bed side of the suspended inner panel is in view (white dust accounts for the appearance) along with the downstream surface of the outer panel. Note the relatively long smooth section of bed annulus above and below the active cross-flow region.

No plugging or deposit problems were encountered with the slotted inner panel. Some dust deposits on the bed side of the cone section at the base of the inner panel have been noted but are not yet known to present potential problems.

Selected steady-state data from 45 tests is given in Table IV. To aid in characterizing the mass of data for diverse combinations of the independent factors (i.e., the first four columns), note the following mean values for the last three columns:

| | |
|---|---|
| GBF pressure drop | 6.95 IW |
| Overall collection efficiency | 0.917 |
| Outlet loading | 0.039 gr/sdcf |

Additional insight is afforded by the histograms for efficiency and outlet loading, shown in Figure 14. Here, for example, the two low-efficiency cases (C1634R and C1671) are highlighted. Reference to Table IV shows that both of these tests feature low air velocity, relatively high media flowrate, and low inlet loading, a combination expected to yield low efficiency. It should be remembered that the test program is specifically designed to impartially explore neighborhoods of suspected low performance as well as those of anticipated high performance.

A first step in multiple-regression work on the data base of Table IV has been performed, using the form:

$$\text{Eff T} = 1 - \text{EXP}\,\{C_1 + C_2(\text{VELOC}) + C_3(\text{MEDIA}) + C_4(\text{L in}) + C_5(\text{d in})\}. \quad (1)$$

where the symbols are those of Table IV. Results of a Tektronix least-squares solution give a correlation coefficient of 0.775 (reasonable for first attempt) with the coefficients:

$C_1$ = -1.400
$C_2$ = -0.005540
$C_3$ = 0.1793
$C_4$ = -0.9434
$C_5$ = -0.02201

Scans of the regression function with respect to each independent factor are shown in Figure 15 along with residuals (points are entered as characters to aid in identification with test numbers). All of the indicated trends are reasonable and in accord with expectations.

- Efficiency improves with increased air velocity. No downward curvature is evident at higher velocities to suggest any pronounced reentrainment, bouncing, etc.
- Efficiency increases as media rate decreases. This can be explained by the increased concentration of captured particulate residing in the bed, which itself becomes a collector of other particulate. The

slightly higher bed void fraction existing for high media flow may also produce some reduction in efficiency.

* Efficiency increases as inlet loading increases. This trend is a corollary to the one just noted. The apparent strength of the trend is also very encouraging since it tends to reduce the requirements for cyclone collectors upstream of the GBF.
* Efficiency improves as the mean diameter of injected particles increases. This is to be expected, of course. The surprise is that the trend is not more emphatic than it is. The data (and theory) bearing on this relationship will receive special attention.

It is interesting to note that the regression line indicates that total efficiencies in excess of 0.95 are readily attainable with reasonable operating conditions and with the "nominal" geometry factors used. In view of the relatively thin absolute depth of the bed, that is encouraging. The penalty in pressure drop must be fully assessed, of course, to obtain a more complete picture.

THICK BED

This sub-experiment was completed on 2 September 1977. A preliminary set of steady-state data is given in Table V. The general improvement in efficiency [illegible] reduction in outlet loading) produced by doubling the bed depth can be seen in mean values. The average outlet loading is lower by a factor of 2.8 than that achieved with the 7.6-inch-thick bed under similar conditions. On the other hand, the increase in average pressure drop is less than 50 percent.

Preliminary regression attempts (with mean size of particulate excluded as an independent factor) yielded trends in collection efficiency with respect to inlet loading and media rate similar to those discussed above. The first trend obtained with respect to air flow, however, was opposite to that expected, albeit with a very small indicated slope. Realistically, the result probably constitutes a non-indication; further data analysis will be needed.

## INTERMITTENT MEDIA FLOW

Addition of timer circuitry to the lift-pipe controls permitted this set of exploratory tests to be run in an automated fashion. There were no special surprises in this departure from normal continuous operation. Periodicity is clearly shown in the three DAS traces of Figure 16. The opacity trace is distinctly in phase with the programmed waveform in media flow - more penetration of particulate when media is flowing than when it is not. (The apparent level change in the opacity signal from that recorded in Figure 12 should be ignored - it was later found that a stalled purge pump in the instrument had allowed lenses to become dirty.) One way to view an objective of these tests is that one wishes to discover if the opacity waveform develops a downward bias for some on-off pattern in media flowrate. If such an indication of improved collection efficiency can be found, one may be willing to pay the implementation penalties. A direct penalty is the systematic ripple in GBF pressure drop so produced since process design must consider the peaks instead of the mean. Observe the predictable phasing of the near-triangular ripple - the downward ramp is initiated with media flow, the upward ramp at flow cessation. Another direct penalty is the need to provide high capacity in the media lift pipe, again to accomodate peaks instead of means.

Normal sampling operations were conducted for these four tests; total loading by EPA methods is incorporated in the columns of Table VI. Also tabulated is a calculated total efficiency based on the regression cited for the data of Table IV and the measured values of the four independent factors. The purpose of the calculation is to display an efficiency value for a hypothetical test with all factors identical to the test in question but without the intermittent media flow. The measured efficiency can then be compared with the fitted value as one means of assessing whether the on-off pattern produced an improvement. Interestingly, all four tests exhibit a mild improvement from expected performance of their continuous counterparts (increments in last column ranging from 0.8 to 4.1 percentage points). Such enhancements are judged to be marginally significant rather than dramatic, but they may justify deeper investigation in the future.

With regard to an optimum waveform for on-off media flow, the data are inconclusive. If the concept is to be pursued, it now seems clear that long-duration tests featuring sequential bursts of several different waveforms would be the most promising experimental approach. Measured response of the opacity and pressure-drop waveforms would be the basis for comparison. Such an approach eliminates particle sampling from the procedure, a very cumbersome and error-prone operation in an environment featuring periodic changes in dust concentration.

# SECTION 5

# MATHEMATICAL MODELING

The purpose of theoretical investigations in the present program is to develop and implement a computerized model of GBF performance. If successful, such an analytical tool will have a number of potential applications and benefits including those listed below.

- The understanding of physical principles and mechanisms contributing to observed filter performance will be enhanced. Just as importantly, those mechanisms that have negligible influence may be identified.
- Interaction between the model results and an ongoing experimental program can build confidence and improve accuracy in the former, and provide useful direction to the latter.
- Empirical correlation efforts for a set of experimental data can be guided in the choice of promising forms, etc. by reference to available computer solutions.
- The model can be extended to predict performance for new designs, conditions, and applications.
- The model can be used to search for optimal operating conditions, and to define sensitivities.

In addition to the preceding motivations, the transitional justification for simulators -- to generate solutions that simultaneously satisfy a large number of interacting relationships in a consistent, accurate, and repeatable manner -- applies with special force to the GBF situation.

A detailed presentation of model equations, program listings, and the like is beyond the scope of this paper (a special document addressing the subject will be published later in the contract). In this section, however, the effort and approach will be outlined.

## COMPONENTS OF THE MATH MODEL

An assumption of axisymmetry makes this a two-dimensional problem, in which the "control volume" concept illustrated in Figure 17 is used. An array of contiguous ring elements defined by the sequence 1234 in Figure 17 is assembled to simulate the global volume denoted ABCD. Height of the global volume, H, exceeds the panel height (53 in) by an arbitrary amount to account for end effects. Both cross sections are defined by rectangular areas in a diametral plane of the GBF.

A two-dimensional adaptation of the Ergun correlation equation (Reference 2) for gas flow through a packed bed of granules is solved. The standard form for pressure drop, consisting of additive viscous and kinetic terms (respectively linear and quadratic with regard to local superficial velocity), is modified to account for the axisymmetric variation of gas velocity with radius. It is also re-expressed in terms of weight flowrates to permit convenient application of continuity relationships.

The gas-flow model itself is a comlex problem of some interest, even in the restricted case of a bed of uniform granules and fixed void fraction throughout. General closed-form solutions for the two-dimensional problem are not available since the problem is decidely nonlinear by virtue of the kinetic term. (In the present application, the contributions of the two terms to total pressure drop are approximately equal.) In this so-called "clean-bed" case, the sensitive terms in the coefficients dealing with bed void fraction ($\varepsilon$) and granule sphericity ($\phi$) may be treated as fixed constants.

In the GBF application, added complexity comes from the fact that, in general, each control volume features a unique void fraction and a unique sphericity for its resident granules depending on the local concentration of captured particulate. Such a non-uniform distribution of "resistance" to gas flow produces a related distortion of the clean-bed profiles for gas flow.

Relationships used to calculate the parameter modifications are:

$$\phi = \phi_o \ \mathrm{Max} \left\{ 0.5, \ \frac{1}{1 + \frac{1}{4} \frac{\rho_c}{\rho_p} \frac{d_c}{d_p} C_s} \right\} \qquad (2)$$

and

$$\varepsilon = \varepsilon_o - \frac{\rho_{bc}}{\rho_{bp}} Cs \qquad (3)$$

where: $\rho_{bc}$ = bulk density of the media

$\rho_{bp}$ = bulk density of the particulate

$C_s$ = ash concentration in weight of particulate per weight of media

$\varepsilon_o$ = void fraction of clean media

$d_c$ = diameter of the granule

$d_p$ = diameter of the particulate

$\rho_p$ = density of the ash particulate

$\rho_c$ = density of the media granule

$\phi_o$ = sphericity of the clean granule

A unique feature of the GBF model, however, is the set of expressions used to describe transfer of particulate from a gas-borne state to a media-borne (i.e., "captured") state. Neglecting electrostatic and thermophoric effects, individual granules capture particles by at least four mechanisms:

1) Inertial impaction
2) Interception
3) Diffusion
4) Sedimentation

From literature surveys and inputs of program consultants, candidate expressions for collection by each of the four mechanisms have been obtained. The expressions are held to apply for an intrinsic collection stage that consists of a layer of granules oriented normal to the gas flow. Along the direction of gas flow, the layer is thought to consist of a single granule. Efficiency for each control volume is obtained by cascading (i.e., staging) a relatively small number of layers.

Indications to date are that the impaction mechanism dominates the others, particularly for larger particles, since it is proportional to at least the second power of $d_p$. It is also at least proportional to local gas flow. Since each of the contributions to collection by a single layer is much smaller than unity, the net efficiency for the layer is taken as the sum of the contributions.

One of the least understood phenomina is re-entrainment of captured particulate within the moving-bed environment. It may develop that empirical reductions in one or more of the collection mechanisms will suffice to match experimental findings. Conversely, a separate re-entrainment form may need to be developed in order to adequately discount the collection mechanisms over a wider range of conditions.

All of the preceding pertains to a bed of clean granules. The present approach to describing the enhanced collection efficiency observed for a dirty (i.e., loaded) bed is to apply the ratio $\Delta P/\Delta P_o$ to the values obtained above.

Flow of captured particulate is modeled by reference to a concept of "state variables" wherein the array of particulate concentrations in each control volume seek equilibria based on continuity restrictions applied to inflow-outflow balances. Thus concentrations are increased by the net efficiency of removal from entering gas streams (both radial and axial) plus inflows of already captured particulate, and decreased by outflows of captured particulate. Concentration of outflowing captured particulate is presumed to be identical to the existing concentration of resident particulate in the control volume.

At the present time, the distribution of media flows through the bed is treated as a prescribed invariant. Uniformly distributed downward flow is one limiting assumption but variations and radial profiles may be specified to simulate spillage at the front face.

All of the preceding aspects of computer modeling are complicated by a desire to account simultaneously for more than one size of particulate. Though straightforward in principle, this added dimension adds appreciably to the programming difficulty as well as to the cost of production runs.

## COMPUTER-PROGRAM PROFILE

A diagram giving some of the nomenclature as applied to a control volume in the interior of the global volume is included as Figure 18. Observe that 32 individual flows are treated: 4 gas flows, 4 granular-media flows, and 24 particulate flows. The larger number of partiuclate flows comes from the presumed necessity to subdivide the particulate into at least three classes by size. This is in recognition of the different collection efficiencies applicable to different-sized particles. Further, it is necessary to distinguish between gas-borne particulate and media-borne particulate, since this is the essence of the collection process in a moving GBF.

The choice of the resident weights of caught particulate (each size class) as "state variables" for each control volume (CV) is natural since that permits use of the capacitive form of particulate-continuity relations as a convenient basis for time-domain integration to a convergent equilibrium solution. Inherent in this mechanization is the assumption that media-borne particulate flow from a CV has the same particulate/media concentration as the resident weights (i.e., perfect mixing within each CV).

### Fixed and Initial Conditions

The array of CV cross sections forms a rectangular pattern that is subdivided into an arbitrary number of equal-volume rings arranged in columns (along the axis) and rows (along the radius).

The top surfaces of the top row and the bottom surfaces of the bottom row have boundary conditions of zero flow in the radial direction. This is the portion of the GBF above and below the slotted or louvered panels included in the model to account for "end effects".

Distributions of media and media flow are specified and presumed to remain unchanged; allowances are made for the possibility of variable packing density over the field, and for simulation of spillage at the inner (front) panel. General non-zero inflows of media-borne particulate can be specified to simulate imperfect cleanup of circulated granules. Initial values for the array of captured particulate in each CV are specified. The initial value for GBF pressure-drop, a state variable, is specified.

### Gas-Flow Model

A two-dimensional implementation of the Ergun flow equation is solved. Uniform bed properties are assumed within each CV, but differing from CV to CV as a function of the distribution of resident particulate. Because of the nonlinear kinetic term, iteration is generally required at every time step.

The effective void fraction for each CV is calculated as a function of resident particulate. The effective sphericity for granules in each CV is calculated as a function of resident particulate.

The radial and axial components of gas flow are calculated along with the pressure profile in an iterative scheme accelerated by a multi-dimensional form of the Newton-Raphson method. These distributions coincide with the current value of GBF pressure drop.

### Particulate-Collection Model

Individual efficiency parameters for removal of particulate from radial and axial gas streams are calculated. It is recognized that each CV consists of a number of instrinsic collection stages in series. There are individual numbers for the radial and axial directions based on the ratio of CV dimensions to granule diameter. Terms for each instrinsic stage include impaction, interception, and re-entrainment effects as modified by local void fraction. Separate collection-efficiency parameters are calculated for each size of particulate.

### Gas-Borne Particulate-Flow Model

Flows at the inlet panel are based on loading factors applied to the radial gas-flow distribution found above. The flow network of gas-borne particulate is evaluated in an inlet-to-outlet marching process that proceeds by columns. Efficiency parameters are applied at the inlet edge of each CV (conceptually) for the removal of particulate from the gas streams. Multiple outgoing streams from any CV have identical particulate/gas concentrations (i.e., perfect mixing).

### Media-Borne Particulate-Flow Model

This distribution depends on the fixed media-flow distribution and the existing particulate/media concentration profile by hypothesis, so the calculation is straightforward.

### Equilibrium-Solution Display

When all convergence criteria are satisfied, the program branches to a display section that includes the following:

Overall GBF collection efficiency, total and by particulate size.
GBF pressure drop.
Particulate/media concentrations at media outlet and throughout the GBF.
Gas-flow profiles through the GBF.
Numerous secondary outputs.

# REFERENCES

1. Combustion Power Company, Inc. Particle Sampling Facility Operation. Report No. FE-2579-10 under ERDA Contract No. EF-77-C-01-2579. Menlo Park, California, 1977.

2. Ergun, S. Fluid Flow Through Packed Columns, In: Chemical Engineering Progress, Vol. 48, No. 2, 1952.

## TABLE I

## TYPICAL PROPERTIES OF ALCOA HYDRATED ALUMINA USED IN GBF COLD-FLOW TESTS

| Grades | Hydral 710 | C-333 |
|---|---|---|
| Typical Properties | | |
| $Al_2O_3$ .................... % | 64.7 | 65.0 |
| $SiO_2$ .................... % | 0.04 | 0.01 |
| $Fe_2O_3$ .................... % | 0.01 | 0.004 |
| $Na_2O$ (total) ............. % | 0.45 | 0.15 |
| Bulk density, loose ....$lb/ft^3$ | 8-14 | 44.0 |
| Bulk density, packed ...$lb/ft^3$ | 16-28 | 77.0 |
| Specific gravity ............ | 2.40 | 2.42 |
| On 325 mesh ................ % | 0.04 | 1.0 |
| Specific surface area ... $m^2/g$ | 6-8 | ② |
| Particle distribution, cumulative ① | | |
| % less than 2 microns ...... | 100.0 | 2 |
| % less than 1 micron ....... | 85.0 | 2 |
| % less than 0.5 microns ... | 28.0 | 2 |
| Median Particle Size..microns | 0.7 | 6.5-9.5 |

1 As determined by electron microscope on a weight basis.

2 Not available from manufacturer.

## TABLE II

## RANGE SUMMARY FOR INDEPENDENT FACTORS

| Independent Factor | | Range | No. of Levels | Nominal Value |
|---|---|---|---|---|
| Description | Selected Form | | | |
| Air flow | Approach Velocity | 40-160 fpm | 4 | ---- |
| Media Flow | lb/granules/lb air | 0.4-1.6 | 4 | ---- |
| Particulate loading | gr/sdcf | 0.25-2 gr/sdcf | 4 | ---- |
| Particulate size distribution | mean diameter per Andersen | 3-15 microns | 3 | 7 microns |
| Media size | granular diameter per sieve analysis | 0.8-3.5 mm | 3 | 2 mm |
| Element height | panel dimension | 26.5-53 in | 2 | 53 in |
| Element depth | bed differential radius | 3.8-15.2 in | 3 | 7.6 in |

## TABLE III

## PLANNED ERDA COLD FLOW TESTS

Page 1 of 2

| | Operating Conditions | | | Particulate | Media | Filter | | |
|---|---|---|---|---|---|---|---|---|
| Test No. | Approach Velocity (fpm) | Media Circulation Rate (#media/#air) | Loading (gr/sdcf) | Nominal Size (μm) | Size (mm) | Bed Thickness (inches) | Panel Height (inches) | Comments |
| FLOW SURVEY | | | | | | | | |
| C1610 | 40 | 1.2 | 1.0 | 7 | 2 | 7.6 | 53 | |
| C1611 | 80 | 0.8 | 2.0 | 7 | 2 | 7.6 | 53 | |
| C1612 | 40 | 0.8 | 0.5 | 7 | 2 | 7.6 | 53 | |
| C1613 | 120 | 0.8 | 2.0 | 7 | 2 | 7.6 | 53 | |
| C1614 | 120 | 1.6 | 2.0 | 7 | 2 | 7.6 | 53 | |
| C1615 | 160 | 1.6 | 2.0 | 7 | 2 | 7.6 | 53 | |
| C1616 | 80 | 1.2 | 1.0 | 7 | 2 | 7.6 | 53 | |
| C1617 | 160 | 0.4 | 1.0 | 7 | 2 | 7.6 | 53 | |
| C1618 | 80 | 0.4 | 0.5 | 7 | 2 | 7.6 | 53 | |
| C1619 | 120 | 0.4 | 0.25 | 7 | 2 | 7.6 | 53 | |
| C1620 | 40 | 0.4 | 0.4 | 7 | 2 | 7.6 | 53 | |
| C1621 | 160 | 1.2 | 0.25 | 7 | 2 | 7.6 | 53 | |
| C1622 | 40 | 1.2 | 0.25 | 7 | 2 | 7.6 | 53 | |
| C1623 | 80 | 1.6 | 2.0 | 7 | 2 | 7.6 | 53 | |
| C1624 | 40 | 1.6 | 0.5 | 7 | 2 | 7.6 | 53 | |
| C1625 | 120 | 1.2 | 2.0 | 7 | 2 | 7.6 | 53 | |
| C1626 | 120 | 0.8 | 1.0 | 7 | 2 | 7.6 | 53 | |
| C1627 | 160 | 1.2 | 2.0 | 7 | 2 | 7.6 | 53 | |
| C1628 | 80 | 1.6 | 1.0 | 7 | 2 | 7.6 | 53 | |
| C1629 | 160 | 0.4 | 1.0 | 7 | 2 | 7.6 | 53 | |
| C1630 | 80 | 0.4 | 0.5 | 7 | 2 | 7.6 | 53 | |
| C1631 | 120 | 0.4 | 0.25 | 7 | 2 | 7.6 | 53 | |
| C1632 | 40 | 0.4 | 2.0 | 7 | 2 | 7.6 | 53 | |
| C1633 | 160 | 1.6 | 0.25 | 7 | 2 | 7.6 | 53 | |
| C1634 | 40 | 1.6 | 0.25 | 7 | 2 | 7.6 | 53 | |
| INTERMITTENT MEDIA MOVEMENT | | | | | | | | Min. between media movement |
| C1635 | 80 | 1.0 | 1.0 | 7 | 2 | 7.6 | 53 | 3 |
| C1636 | 80 | 1.0 | 1.0 | 7 | 2 | 7.6 | 53 | 6 |
| C1637 | 80 | 1.0 | 1.0 | 7 | 2 | 7.6 | 53 | 9 |
| C1638 | 80 | 1.0 | 1.0 | 7 | 2 | 7.6 | 53 | 12 |
| LARGE PARTICULATE | | | | | | | | |
| C1640 | 160 | 1.6 | 0.5 | 15 | 2 | 7.6 | 53 | |
| C1641 | 120 | 1.6 | 0.25 | 15 | 2 | 7.6 | 53 | |
| C1642 | 120 | 0.4 | 2.0 | 15 | 2 | 7.6 | 53 | |
| C1643 | 40 | 0.4 | 0.25 | 15 | 2 | 7.6 | 53 | |
| C1644 | 160 | 0.4 | 1.0 | 15 | 2 | 7.6 | 53 | |
| C1645 | 80 | 0.8 | 2.0 | 15 | 2 | 7.6 | 53 | |
| C1646 | 80 | 1.2 | 0.25 | 15 | 2 | 7.6 | 53 | |
| C1647 | 40 | 1.2 | 0.5 | 15 | 2 | 7.6 | 53 | |
| C1648 | 80 | 1.6 | 1.0 | 15 | 2 | 7.6 | 53 | |
| C1649 | 40 | 1.6 | 2.0 | 15 | 2 | 7.6 | 53 | |
| C1650 | 80 | 0.4 | 0.5 | 15 | 2 | 7.6 | 53 | |
| C1651 | 40 | 0.8 | 1.0 | 15 | 2 | 7.6 | 53 | |
| SMALL PARTICULATE | | | | | | | | |
| C1660 | 120 | 1.6 | 1.0 | 3 | 2 | 7.6 | 53 | |
| C1661 | 120 | 0.4 | 2.0 | 3 | 2 | 7.6 | 53 | |
| C1662 | 120 | 1.2 | 0.25 | 3 | 2 | 7.6 | 53 | |
| C1663 | 120 | 0.8 | 1.0 | 3 | 2 | 7.6 | 53 | |
| C1664 | 160 | 1.2 | 1.0 | 3 | 2 | 7.6 | 53 | |
| C1665 | 80 | 1.2 | 1.0 | 3 | 2 | 7.6 | 53 | |
| C1666 | 160 | 0.8 | 0.25 | 3 | 2 | 7.6 | 53 | |
| C1667 | 80 | 0.8 | 0.5 | 3 | 2 | 7.6 | 53 | |
| C1668 | 80 | 0.4 | 0.25 | 3 | 2 | 7.6 | 53 | |
| C1669 | 40 | 0.8 | 2.0 | 3 | 2 | 7.6 | 53 | |
| C1670 | 80 | 1.6 | 0.25 | 3 | 2 | 7.6 | 53 | |
| C1671 | 40 | 1.2 | 0.25 | 3 | 2 | 7.6 | 53 | |

## TABLE III

## PLANNED ERDA COLD FLOW TESTS

Page 2 of 2

| | Operating Conditions | | | Particulate | Media | Filter | | |
|---|---|---|---|---|---|---|---|---|
| Test No. | Approach Velocity (fpm) | Media Circulation Rate (#media/#air) | Loading (gr/sdcf) | Nominal Size (µm) | Size (mm) | Bed Thickness (inches) | Panel Height (inches) | Comments |
| REDUCED HEIGHT | | | | | | | | |
| C1680 | 120 | 1.2 | 1.0 | 7 | 2 | 7.6 | 26.5 | Blank bottom 1/2 of both panels |
| C1681 | 160 | 1.6 | 1.0 | 7 | 2 | 7.6 | 26.5 | " |
| C1682 | 80 | 1.6 | 2.0 | 7 | 2 | 7.6 | 26.5 | " |
| C1683 | 80 | 0.4 | 1.0 | 7 | 2 | 7.6 | 26.5 | " |
| C1684 | 40 | 1.2 | 2.0 | 7 | 2 | 7.6 | 26.5 | " |
| C1685 | 80 | 0.8 | 0.5 | 7 | 2 | 7.6 | 26.5 | " |
| C1686 | 160 | 0.8 | 0.25 | 7 | 2 | 7.6 | 26.5 | " |
| C1687 | 80 | 1.2 | 0.25 | 7 | 2 | 7.6 | 26.5 | " |
| C1688 | 40 | 0.4 | 0.5 | 7 | 2 | 7.6 | 26.5 | " |
| THICK BED | | | | | | | | |
| C1690 | 120 | 0.8 | 0.5 | 7 | 2 | 15.2 | 53 | |
| C1691 | 160 | 0.8 | 1.0 | 7 | 2 | 15.2 | 53 | |
| C1692 | 80 | 0.8 | 2.0 | 7 | 2 | 15.2 | 53 | |
| C1693 | 80 | 0.4 | 1.0 | 7 | 2 | 15.2 | 53 | |
| C1694 | 40 | 1.2 | 2.0 | 7 | 2 | 15.2 | 53 | |
| C1695 | 80 | 1.6 | 0.5 | 7 | 2 | 15.2 | 53 | |
| C1696 | 160 | 0.4 | 0.25 | 7 | 2 | 15.2 | 53 | |
| C1697 | 80 | 1.2 | 0.25 | 7 | 2 | 15.2 | 53 | |
| C1698 | 40 | 0.4 | 0.5 | 7 | 2 | 15.2 | 53 | |
| THIN BED | | | | | | | | |
| C16100 | 120 | 1.2 | 0.25 | 7 | 2 | 3.8 | 53 | |
| C16101 | 160 | 1.2 | 0.5 | 7 | 2 | 3.8 | 53 | |
| C16102 | 80 | 0.4 | 1.0 | 7 | 2 | 3.8 | 53 | |
| C16103 | 160 | 0.8 | 0.25 | 7 | 2 | 3.8 | 53 | |
| C16104 | 40 | 0.8 | 2.0 | 7 | 2 | 3.8 | 53 | |
| C16105 | 80 | 0.8 | 0.5 | 7 | 2 | 3.8 | 53 | |
| C16106 | 40 | 1.2 | 1.0 | 7 | 2 | 3.8 | 53 | |
| C16107 | 80 | 1.6 | 0.25 | 7 | 2 | 3.8 | 53 | |
| C16108 | 40 | 1.6 | 0.5 | 7 | 2 | 3.8 | 53 | |
| LARGE MEDIA | | | | | | | | |
| C16110 | 160 | 0.4 | 0.25 | 7 | 3.5 | 3.8 | 53 | |
| C16111 | 40 | 1.6 | 1.0 | 7 | 3.5 | 3.8 | 53 | |
| C16112 | 120 | 0.8 | 0.5 | 7 | 3.5 | 3.8 | 53 | |
| C16113 | 120 | 0.4 | 1.0 | 7 | 3.5 | 3.8 | 53 | |
| C16114 | 160 | 0.8 | 1.0 | 7 | 3.5 | 3.8 | 53 | |
| C16115 | 80 | 0.8 | 2.0 | 7 | 3.5 | 3.8 | 53 | |
| C16116 | 160 | 1.2 | 0.25 | 7 | 3.5 | 3.8 | 53 | |
| C16117 | 80 | 1.6 | 0.5 | 7 | 3.5 | 3.8 | 53 | |
| C16118 | 80 | 1.2 | 1.0 | 7 | 3.5 | 3.8 | 53 | |
| C16119 | 40 | 0.4 | 2.0 | 7 | 3.5 | 3.8 | 53 | |
| C16120 | 80 | 0.4 | 0.25 | 7 | 3.5 | 3.8 | 53 | |
| C16121 | 40 | 1.2 | 0.5 | 7 | 3.5 | 3.8 | 53 | |
| SMALL MEDIA | | | | | | | | |
| C16130 | 120 | 1.2 | 2.0 | 7 | 0.8 | 7.6 | 53 | |
| C16131 | 40 | 1.6 | 0.25 | 7 | 0.8 | 7.6 | 53 | |
| C16132 | 80 | 0.4 | 0.5 | 7 | 0.8 | 7.6 | 53 | |
| C16133 | 120 | 0.4 | 0.25 | 7 | 0.8 | 7.6 | 53 | |
| C16134 | 160 | 0.8 | 0.5 | 7 | 0.8 | 7.6 | 53 | |
| C16135 | 80 | 0.8 | 1.0 | 7 | 0.8 | 7.6 | 53 | |
| C16136 | 160 | 1.6 | 1.0 | 7 | 0.8 | 7.6 | 53 | |
| C16137 | 80 | 1.6 | 2.0 | 7 | 0.8 | 7.6 | 53 | |
| C16138 | 40 | 0.8 | 2.0 | 7 | 0.8 | 7.6 | 53 | |
| C16139 | 160 | 1.2 | 0.5 | 7 | 0.8 | 7.6 | 53 | |
| C16140 | 40 | 0.4 | 0.5 | 7 | 0.8 | 7.6 | 53 | |
| C16141 | 80 | 1.2 | 0.25 | 7 | 0.8 | 7.6 | 53 | |

# TABLE IV

## SELECTED STEADY-STATE DATA

Note: See Table III for Test Configurations

| TEST | VELOC | MEDIA | L in | d in | Del P | Eff T | L out |
|---|---|---|---|---|---|---|---|
| C1611 | 74.0 | 0.869 | 2.255 | 2.87 | 4.25 | 0.964 | 0.081 |
| C1613R | 119.1 | 0.734 | 0.597 | 9.75 | 9.06 | 0.950 | 0.030 |
| C1614 | 119.3 | 1.367 | 1.103 | 8.27 | 11.22 | 0.937 | 0.070 |
| C1615 | 156.9 | 1.436 | 0.769 | 10.94 | 14.35 | 0.948 | 0.040 |
| C1616RB | 80.0 | 1.128 | 0.538 | 4.45 | 6.04 | 0.890 | 0.059 |
| C1617 | 158.3 | 0.368 | 0.536 | 8.27 | 10.83 | 0.970 | 0.016 |
| C1619 | 149.5 | 0.442 | 0.129 | 27.97 | 8.33 | 0.907 | 0.012 |
| C1620 | 72.6 | 0.240 | 0.150 | 4.22 | 1.99 | 0.860 | 0.021 |
| C1623 | 83.0 | 1.098 | 0.929 | 35.92 | 5.70 | 0.971 | 0.027 |
| C1624 | 61.6 | 0.196 | 0.325 | 3.09 | 8.05 | 0.849 | 0.049 |
| C1625 | 120.0 | 1.572 | 1.859 | 5.34 | 9.09 | 0.971 | 0.054 |
| C1626 | 119.7 | 0.848 | 0.810 | 2.36 | 5.24 | 0.917 | 0.067 |
| C1627 | 157.6 | 1.149 | 1.020 | 5.72 | 8.78 | 0.920 | 0.082 |
| C1628 | 84.9 | 1.684 | 0.589 | 1.95 | 3.81 | 0.951 | 0.029 |
| C1630 | 93.4 | 0.289 | 0.164 | 44.04 | 4.68 | 0.902 | 0.016 |
| C1631 | 119.9 | 0.503 | 0.320 | 3.05 | 3.03 | 0.863 | 0.044 |
| C1632 | 61.0 | 0.655 | 1.618 | 1.58 | 17.35 | 0.958 | 0.068 |
| C1633 | 155.9 | 1.340 | 0.253 | 2.31 | 12.21 | 0.881 | 0.030 |
| C1634P | 70.4 | 1.082 | 0.190 | 1.87 | 4.62 | 0.702 | 0.055 |
| C1640 | 162.5 | 1.451 | 0.607 | 28.01 | 9.50 | 0.960 | 0.024 |
| C1641 | 120.0 | 1.371 | 0.213 | 29.29 | 7.29 | 0.930 | 0.015 |
| C1642 | 119.2 | 0.509 | 1.552 | 23.61 | 3.49 | 0.976 | 0.038 |
| C1643 | 69.6 | 0.523 | 0.142 | 50.37 | 3.64 | 0.944 | 0.008 |
| C1644P | 162.3 | 0.303 | 0.655 | 1.68 | 7.85 | 0.980 | 0.013 |
| C1645P | 80.9 | 0.724 | 0.927 | 35.65 | 2.80 | 0.988 | 0.011 |
| C1646 | 78.8 | 1.591 | 0.183 | 39.05 | 5.39 | 0.967 | 0.006 |
| C1647 | 65.7 | 1.253 | 0.411 | 35.65 | 4.09 | 0.973 | 0.011 |
| C1648P | 79.9 | 1.473 | 0.617 | 38.45 | 1.99 | 0.950 | 0.031 |
| C1649 | 63.9 | 1.580 | 1.051 | 43.91 | 1.65 | 0.921 | 0.083 |
| C1650 | 86.5 | 0.505 | 0.320 | 31.28 | 2.82 | 0.954 | 0.042 |
| C1651 | 57.8 | 0.685 | 0.653 | 35.93 | 7.08 | 0.940 | 0.039 |
| C1660 | 119.4 | 1.528 | 0.514 | 1.74 | 4.74 | 0.887 | 0.058 |
| C1661 | 120.3 | 0.622 | 1.232 | 6.12 | 14.91 | 0.976 | 0.029 |
| C1662 | 120.0 | 1.090 | 0.370 | 1.97 | 5.17 | 0.908 | 0.034 |
| [illegible] | 118.1 | 0.781 | 0.449 | 1.70 | 5.83 | 0.906 | 0.042 |
| C1664 | 159.9 | 1.052 | 0.470 | 2.97 | 7.33 | 0.915 | 0.040 |
| C1665 | 80.0 | 1.103 | 1.439 | 4.04 | 8.80 | 0.962 | 0.055 |
| C1666 | 160.6 | 0.613 | 0.140 | 1.97 | 6.36 | 0.893 | 0.015 |
| C1667R | 79.2 | 0.750 | 0.614 | 1.91 | 6.85 | 0.902 | 0.060 |
| C1667RA | 80.1 | 1.083 | 0.271 | 1.96 | 6.67 | 0.815 | 0.050 |
| C1667RB | 80.1 | 0.358 | 0.592 | 1.22 | 8.79 | 0.943 | 0.034 |
| C1668 | 80.5 | 0.466 | 0.199 | 2.09 | 3.86 | 0.829 | 0.034 |
| C1669 | 60.9 | 0.719 | 1.582 | 4.05 | 11.28 | 0.976 | 0.038 |
| C1670R | 82.0 | 1.428 | 0.126 | 1.79 | 6.02 | 0.941 | 0.020 |
| C1671 | 59.3 | 1.082 | 0.250 | 1.51 | 4.07 | 0.712 | 0.072 |

Legend

| | |
|---|---|
| Veloc.. | Air approach velocity, fpm |
| Medi | Media flowrate, lb/media/lb air |
| L in | Inlet loading, gr/sdcf |
| d in: | Median diameter of inlet dust, microns |
| Del P: | GBF pressure drop, IW |
| Eff T: | Overall collection efficiency |
| L out: | Outlet loading, gr/sdcf |

## TABLE V

### SELECTED STEADY STATE DATA FOR THICK BED SUBEXPERIMENT

Note: See Table III for Test Configurations

| : TEST | VELOC | MEDIA | L in | d in | Del P | Eff T | L out |
|---|---|---|---|---|---|---|---|
| :C1690 | 120.3 | 0.763 | 0.102 | 5.50 | 4.03 | 0.863 | 0.014 |
| :C1691 | 157.1 | 0.739 | 0.922 | 3.25 | 23.09 | 0.989 | 0.010 |
| :C1691A | 81.5 | 0.719 | 0.499 | 3.40 | 5.18 | 0.966 | 0.017 |
| :C1691B | 121.5 | 0.711 | 0.377 | 2.68 | 15.52 | 0.979 | 0.008 |
| :C1692 | 82.2 | 0.672 | 0.796 | 2.25 | 19.01 | 0.994 | 0.005 |
| :C1693 | 81.5 | 0.341 | 0.372 | 1.81 | 14.81 | 0.995 | 0.002 |
| :C1694 | 42.5 | 1.001 | 0.756 | 1.84 | 3.69 | 0.962 | 0.029 |
| :C1695 | 79.9 | 1.544 | 0.370 | 1.69 | 2.85 | 0.935 | 0.024 |
| :C1696 | 161.2 | 0.347 | 0.221 | 1.62 | 12.51 | 0.973 | 0.006 |
| :C1698 | 42.5 | 1.428 | 0.554 | 1.54 | 1.99 | 0.948 | 0.029 |
| | | | | Mean values: | 10.27 | 0.960 | 0.014 |

Legend

| | |
|---|---|
| Veloc: | Air approach velocity, fpm |
| Media: | Media flowrate, lb/media/lb air |
| L in: | Inlet loading, gr/sdcf |
| d in: | Median diameter of inlet dust, microns |
| Del P: | GBF pressure drop, IW |
| Eff T: | Overall collection efficiency |
| L out: | Outlet loading, gr/sdcf |

## COLLECTION EFFICIENCY FOR INTERMITTENT FLOW OF MEDIA

Note: See Table III for Test Configuration

| Test | Veloc. | Media | L In | D In | Tot. Eff. | Fitted Eff. | Inc. Eff. |
|---|---|---|---|---|---|---|---|
| 1635R | 80.20 | 0.663 | 0.572 | 6.32 | 0.951 | 0.910 | 0.041 |
| 1636R | 79.00 | 0.827 | 1.239 | 12.27 | 0.964 | 0.956 | 0.008 |
| 1637 | 80.50 | 0.74 | 0.344 | 2.90 | 0.892 | 0.878 | 0.014 |
| 1638R | 79.36 | 0.747 | 0.655 | 4.31 | 0.940 | 0.912 | 0.028 |

Legend

Veloc: Air approach velocity, fpm
Media: Media flowrate, lb media/lb air
L in: Inlet loading, gr/sdcf
d in: Median diameter of inlet dust, microns
Eff T: Overall collection efficiency
Fitted Eff: Result of substituting values of independent factors into regression function generated for continuous-flow data of Table IV
Inc. Eff: (Tot Eff) - (Fitted Eff)

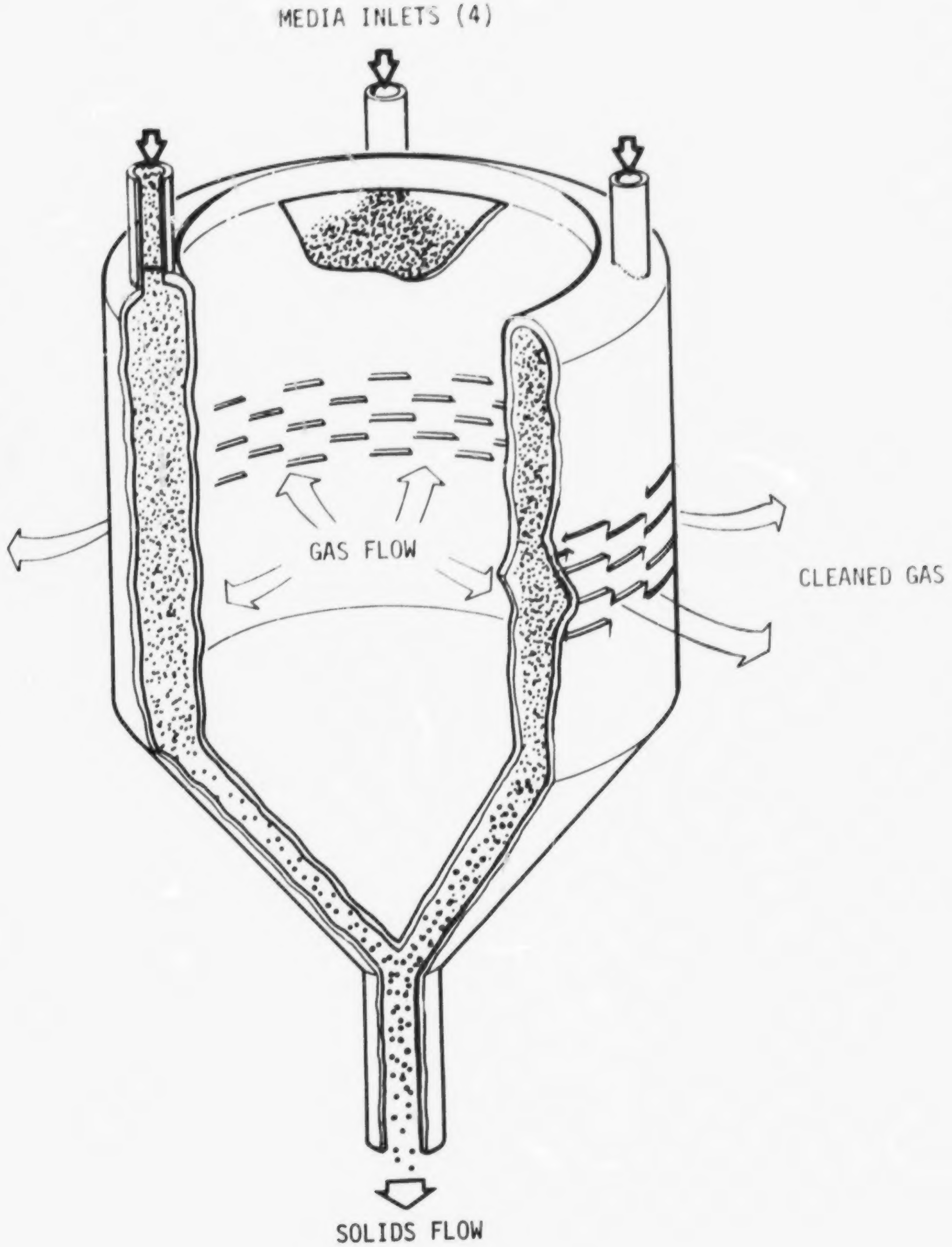
MEDIA INLETS (4)
GAS FLOW
CLEANED GAS
SOLIDS FLOW

Figure 1 GBF concept.

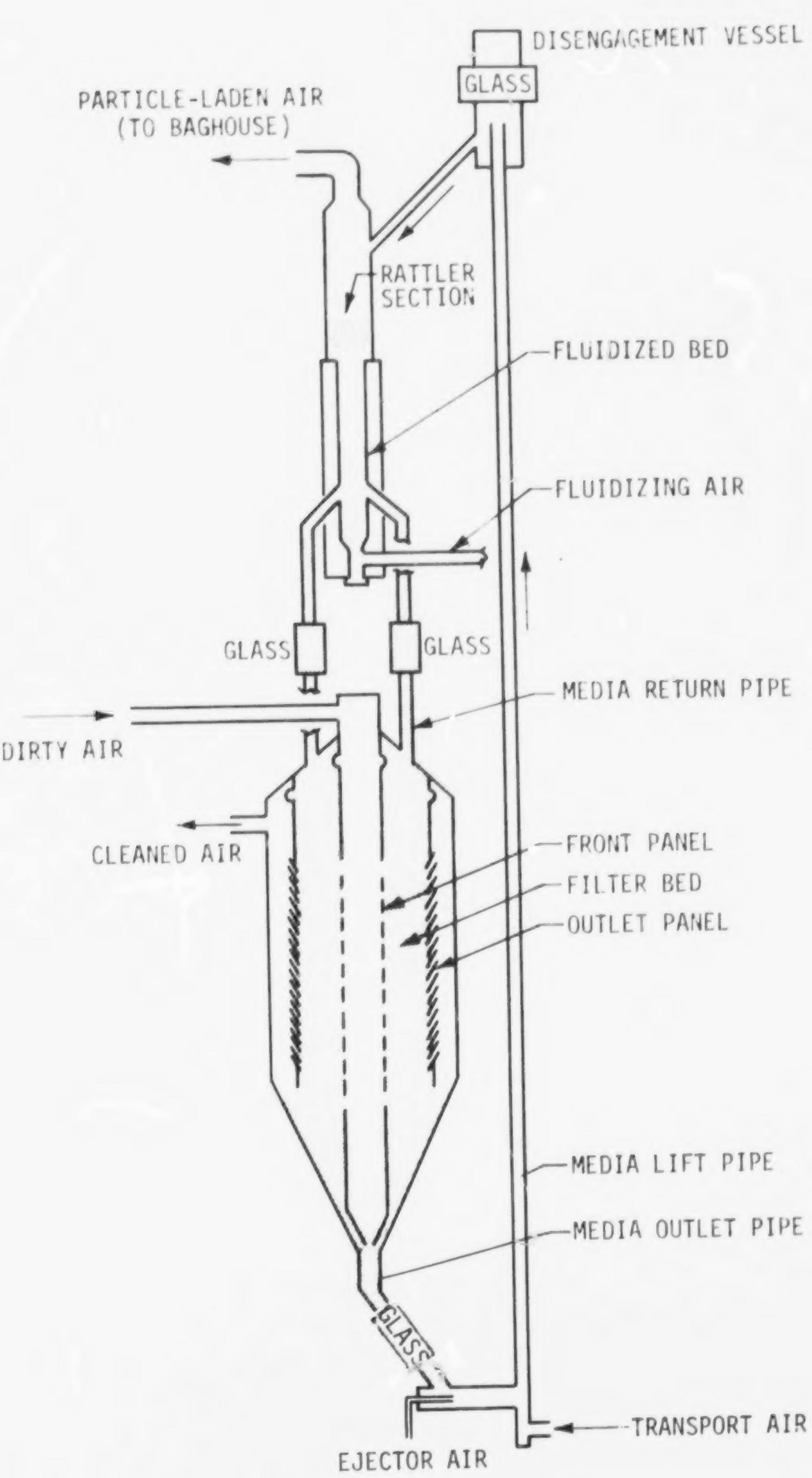
DISENGAGEMENT VESSEL
GLASS
PARTICLE-LADEN AIR (TO BAGHOUSE)
RATTLER SECTION
FLUIDIZED BED
FLUIDIZING AIR
GLASS
GLASS
MEDIA RETURN PIPE
DIRTY AIR
CLEANED AIR
FRONT PANEL
FILTER BED
OUTLET PANEL
MEDIA LIFT PIPE
MEDIA OUTLET PIPE
GLASS
TRANSPORT AIR
EJECTOR AIR

Figure 2 GBF media loop.

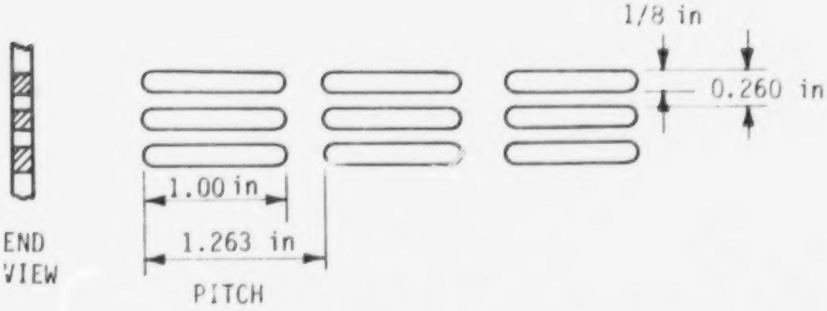
1/8 in
0.260 in
1.00 in
1.263 in
PITCH
END VIEW

(a) Slot Pattern for Inner Panel with 2mm Media

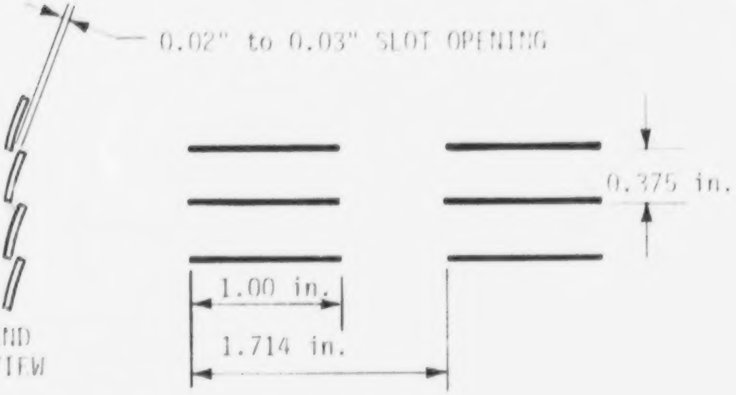
0.02" to 0.03" SLOT OPENING
0.375 in.
1.00 in.
1.714 in.
END VIEW

(b) Louver Pattern for Outer Panel

Figure 3 Typical panel slot and louver patterns.

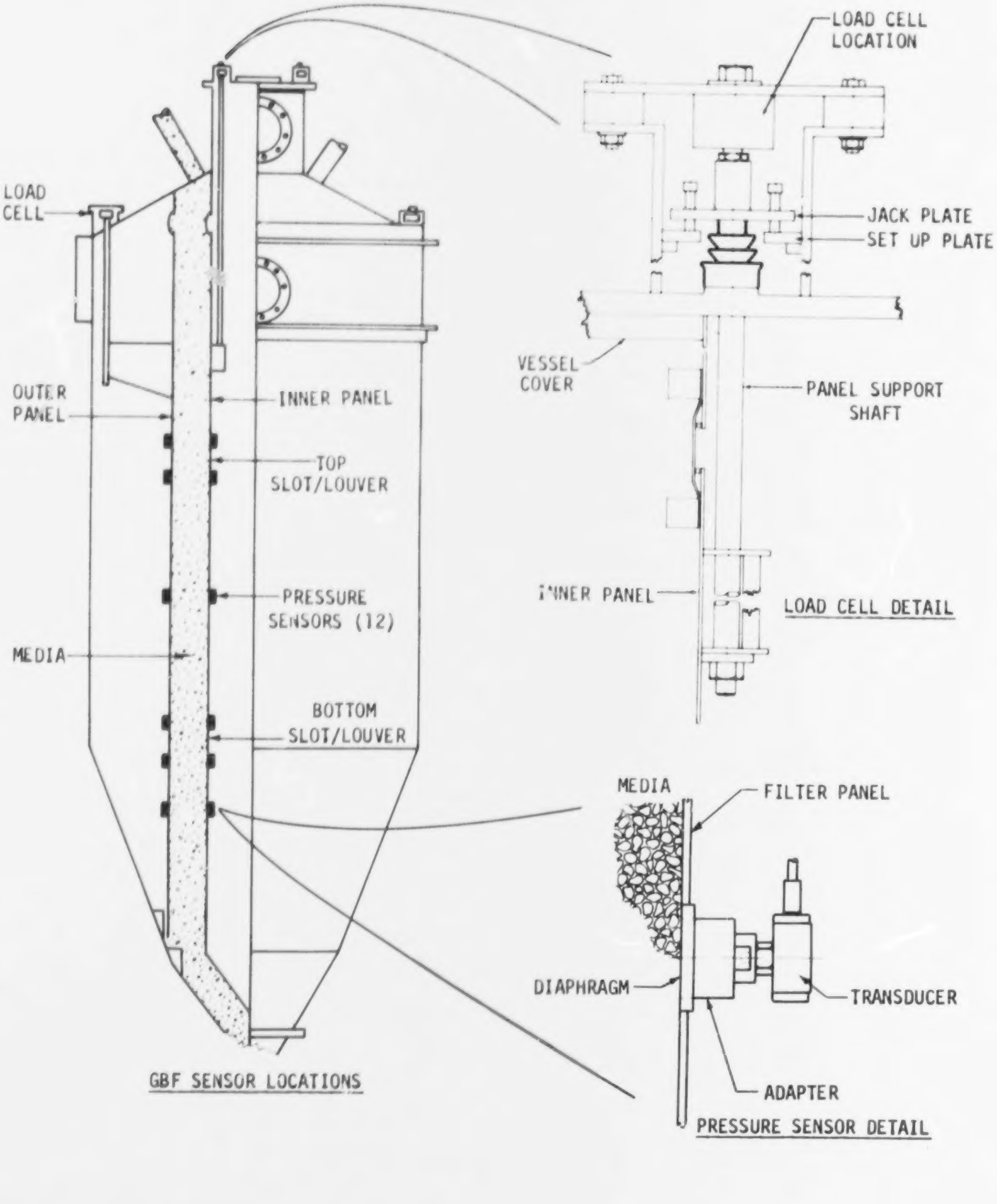

LOAD CELL LOCATION
JACK PLATE
SET UP PLATE
VESSEL COVER
PANEL SUPPORT SHAFT
INNER PANEL
LOAD CELL DETAIL
LOAD CELL
OUTER PANEL
INNER PANEL
TOP SLOT/LOUVER
PRESSURE SENSORS (12)
MEDIA
BOTTOM SLOT/LOUVER
GBF SENSOR LOCATIONS
MEDIA
FILTER PANEL
DIAPHRAGM
TRANSDUCER
ADAPTER
PRESSURE SENSOR DETAIL

Figure 4  Load cells & media pressure sensors.

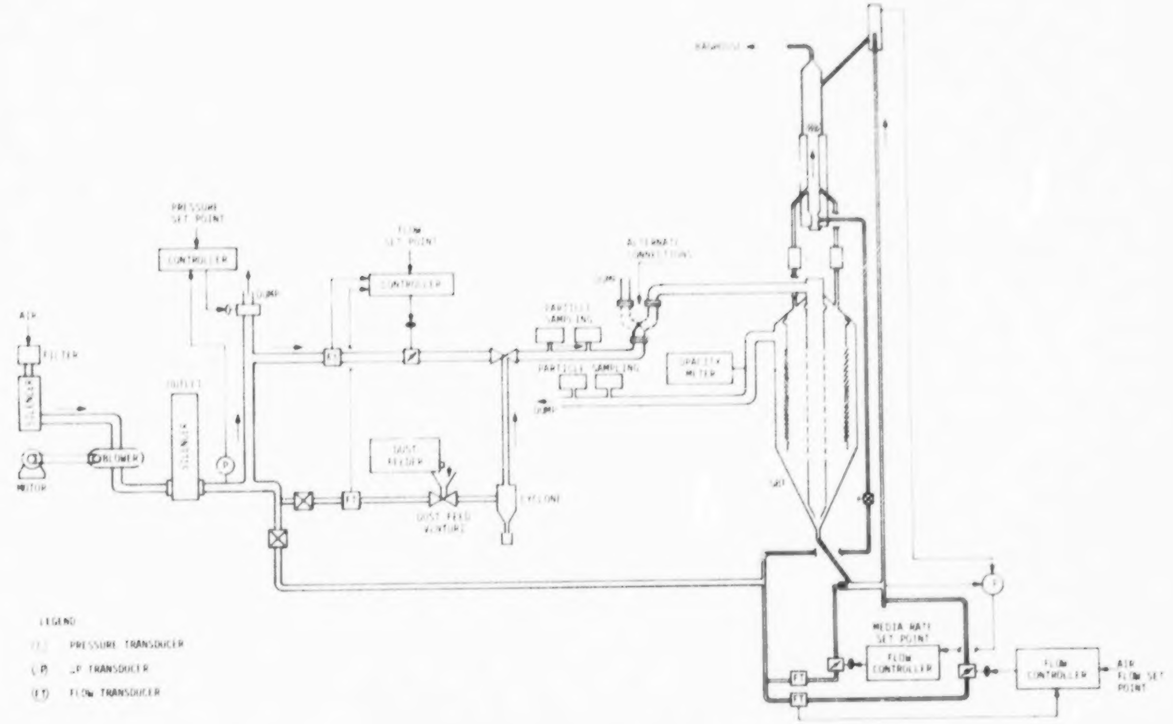
BAGHOUSE
PRESSURE SET POINT
CONTROLLER
DUMP
FLOW SET POINT
CONTROLLER
ALTERNATE CONNECTIONS
DUMP
AIR
FILTER
SILENCER
PARTICLE SAMPLING
PARTICLE SAMPLING
OPACITY METER
OUTLET
SILENCER
FT
P
DUMP
MOTOR
BLOWER
DUST FEEDER
FT
DUST FEED VENTURI
CYCLONE
GBF
LEGEND
(P) PRESSURE TRANSDUCER
(ΔP) ΔP TRANSDUCER
(FT) FLOW TRANSDUCER
MEDIA RATE SET POINT
FLOW CONTROLLER
FT
FT
FLOW CONTROLLER
AIR FLOW SET POINT

Figure 5 GBF cold-flow program facility.

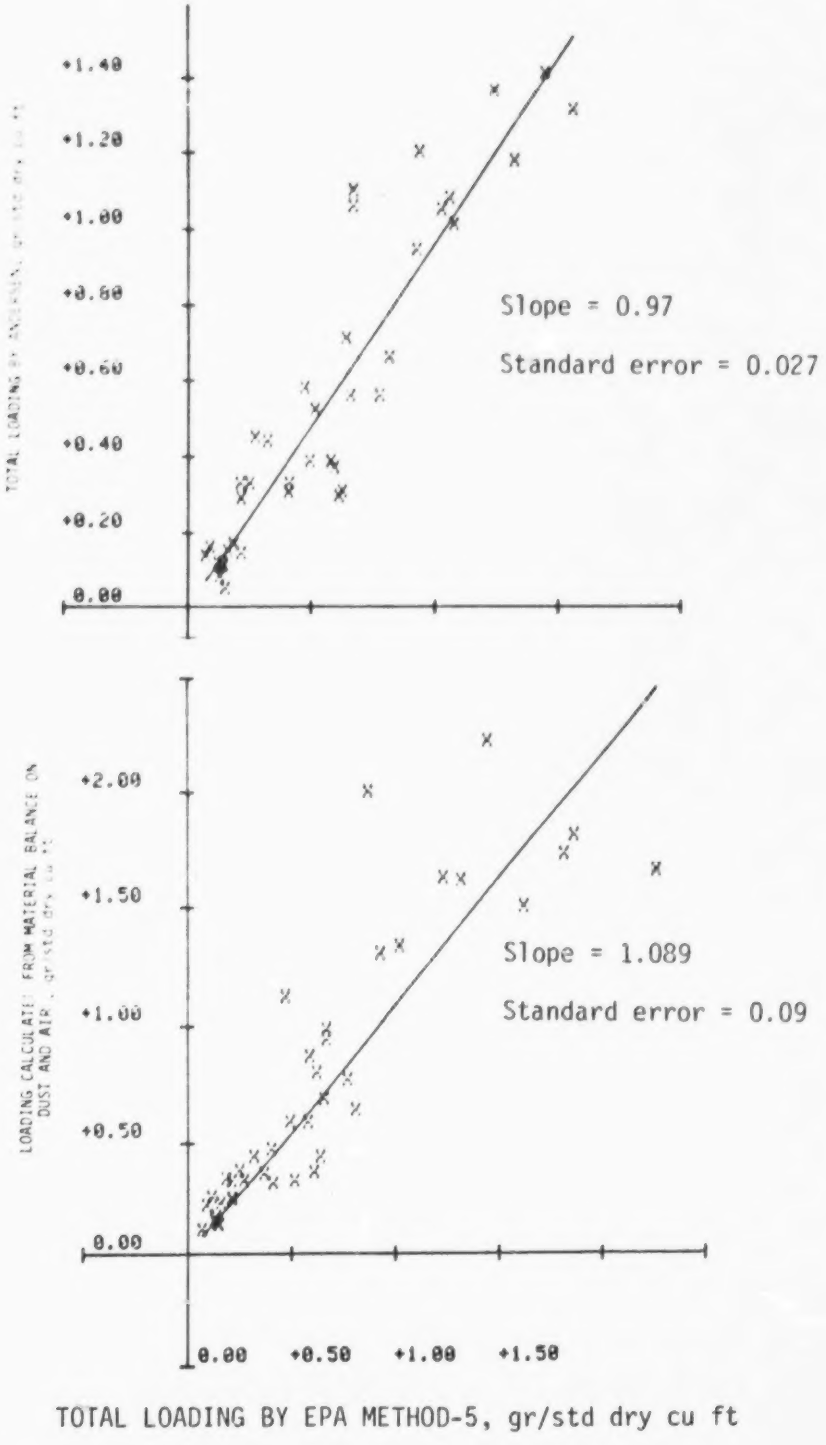

Figure 6 Comparison of EPA method-5 measurements with other measurements.

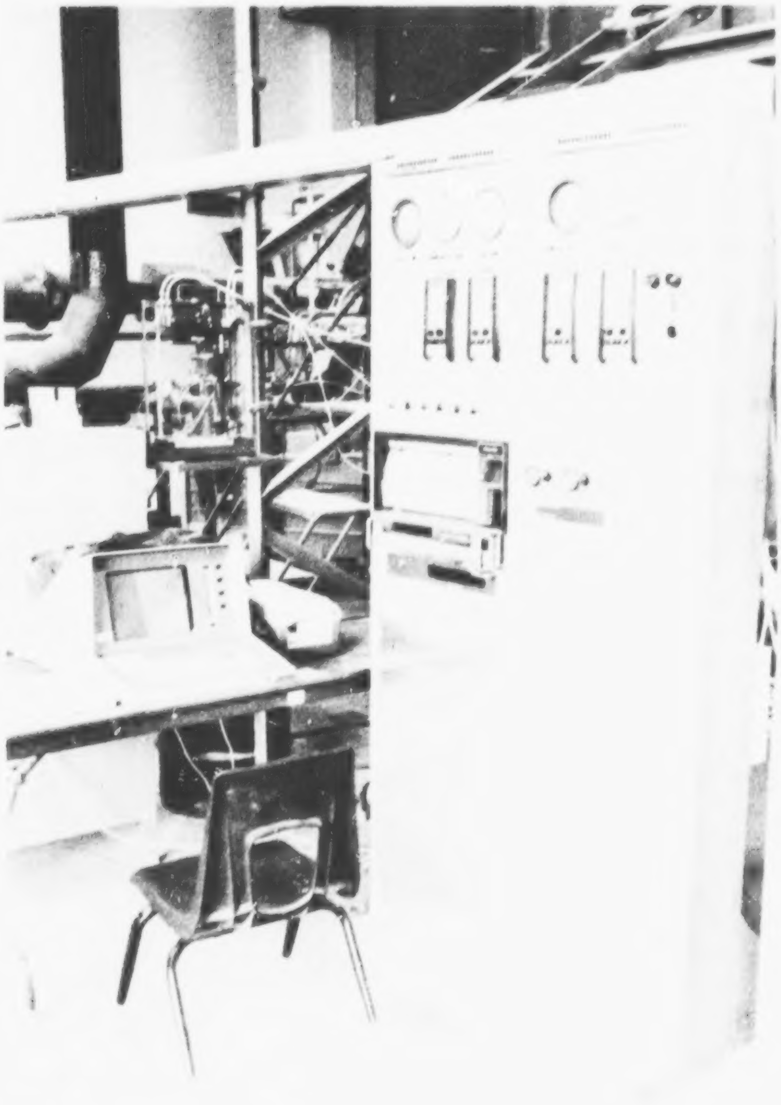

Figure 7 GBF data acquisition system & control console.

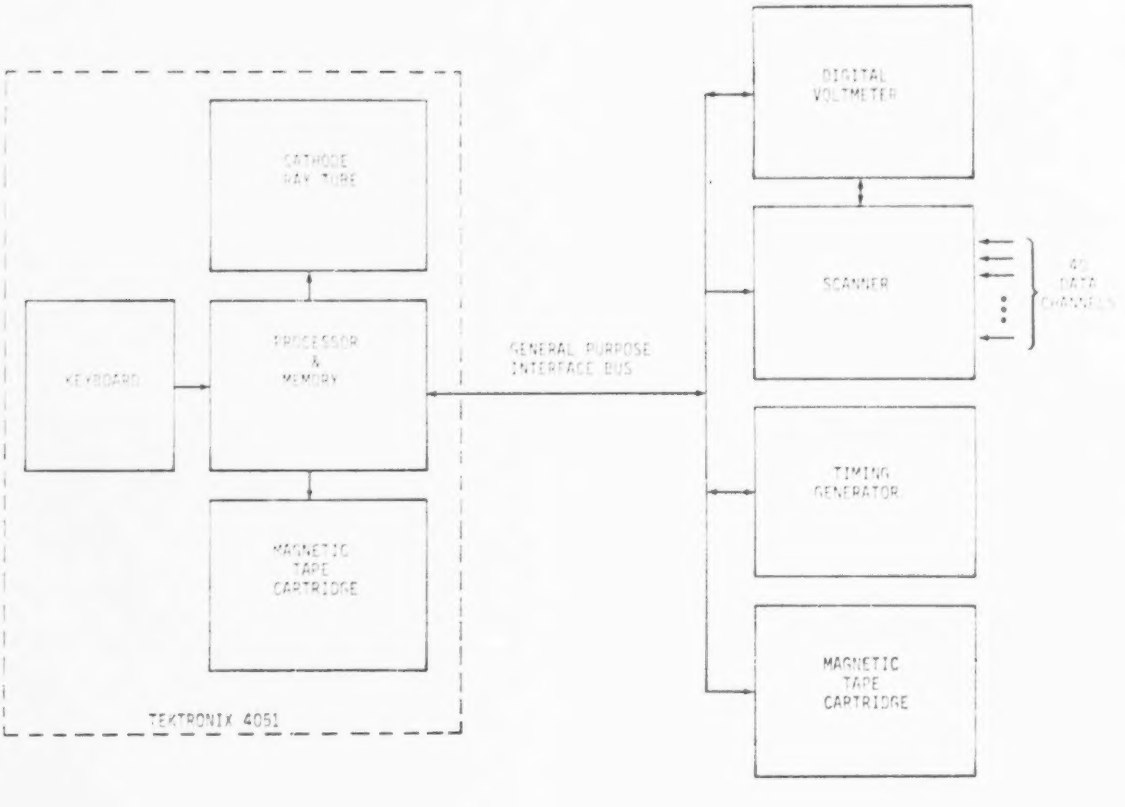
CATHODE RAY TUBE
KEYBOARD
PROCESSOR & MEMORY
MAGNETIC TAPE CARTRIDGE
TEKTRONIX 4051
GENERAL PURPOSE INTERFACE BUS
DIGITAL VOLTMETER
SCANNER
40 DATA CHANNELS
TIMING GENERATOR
MAGNETIC TAPE CARTRIDGE

Figure 8 Programmable data-acquisition system configuration.

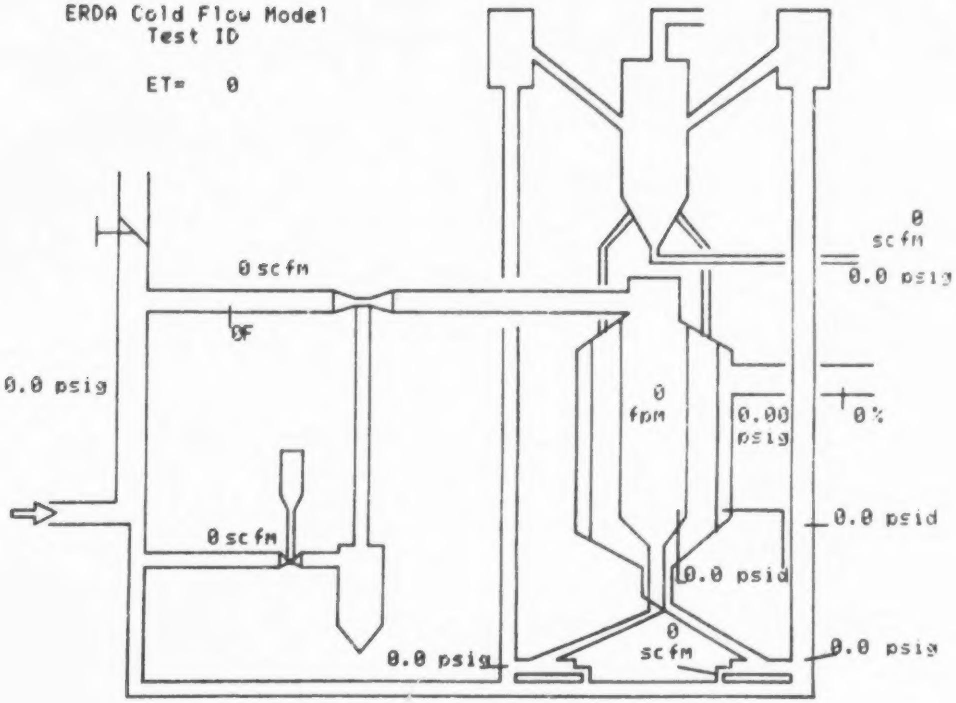
ERDA Cold Flow Model
Test ID
ET= 0
0 scfm
0F
0.0 psig
0 scfm
0 fpm
0.00 psig
0 scfm
0.0 psig
0%
0.0 psid
0.0 psid
0 scfm
0.0 psig
0.0 psig

Figure 9 Data acquisition system CRT display.

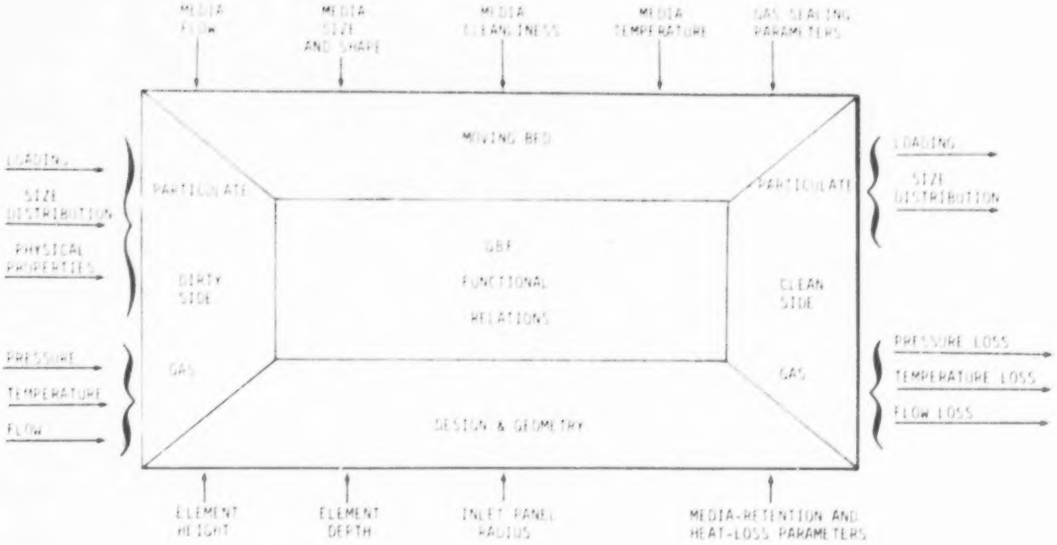
MEDIA FLOW
MEDIA SIZE AND SHAPE
MEDIA CLEANLINESS
MEDIA TEMPERATURE
GAS SEALING PARAMETERS
MOVING BED
LOADING
SIZE DISTRIBUTION
PHYSICAL PROPERTIES
PARTICULATE
DIRTY SIDE
GAS
PRESSURE
TEMPERATURE
FLOW
GBF
FUNCTIONAL
RELATIONS
PARTICULATE
CLEAN SIDE
GAS
LOADING
SIZE DISTRIBUTION
PRESSURE LOSS
TEMPERATURE LOSS
FLOW LOSS
DESIGN & GEOMETRY
ELEMENT HEIGHT
ELEMENT DEPTH
INLET PANEL RADIUS
MEDIA-RETENTION AND HEAT-LOSS PARAMETERS

Figure [illegible] Diagram of GBF performance dependencies.

```
** ERDA COLD-FLOW ANDERSEN IMPACTOR DATA **
TEST DATE:07/27/77          TEST STARTING TIME:          TEST ID:C164Z_
```

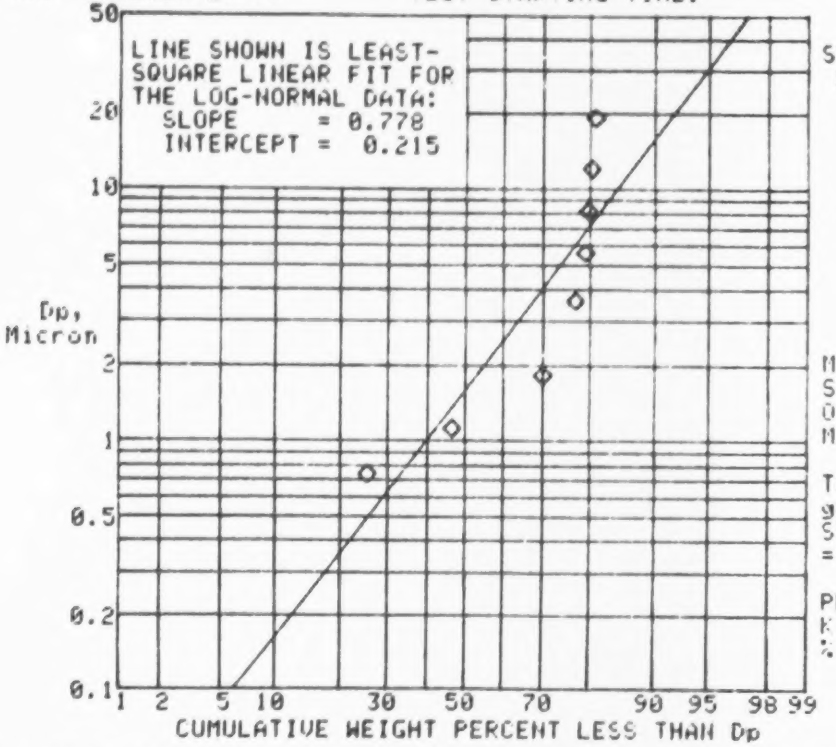

```
LINE SHOWN IS LEAST-
SQUARE LINEAR FIT FOR
THE LOG-NORMAL DATA:
  SLOPE      = 0.778
  INTERCEPT  =  0.215

                        CUMUL.
STAGE      Dp,          WT %
 NO.     Micron          <Dp

  B       19.2          81.05
  C       12.0          80.39
  D       8.16          79.74
  E       5.57          79.08
  F       3.59          77.12
  G       1.81          69.93
  H       1.12          46.41
  I       0.74          25.49

MEDIAN PARTICULATE
SIZE FROM INTERCEPT
OF THE FIT.
Micron =  1.641

TOTAL LOADING.
gr/sdcf = 0.023 (
STANDARD CONDITIONS
=70 F. 1 atm )

PERCENT OF ISO-
KINETIC SAMPLING.
% = 151

NOTE: Dp=CALCULATED 50% EFFECTIVE CUTOFF DIAMETER OF PARTICULATES WITH
        AN ASSUMED DENSITY OF 1 g/cc ( DUST = ALCOA C-333 )
```

Figure 11 Andersen impactor data.

Figure 12 Typical DAS record.

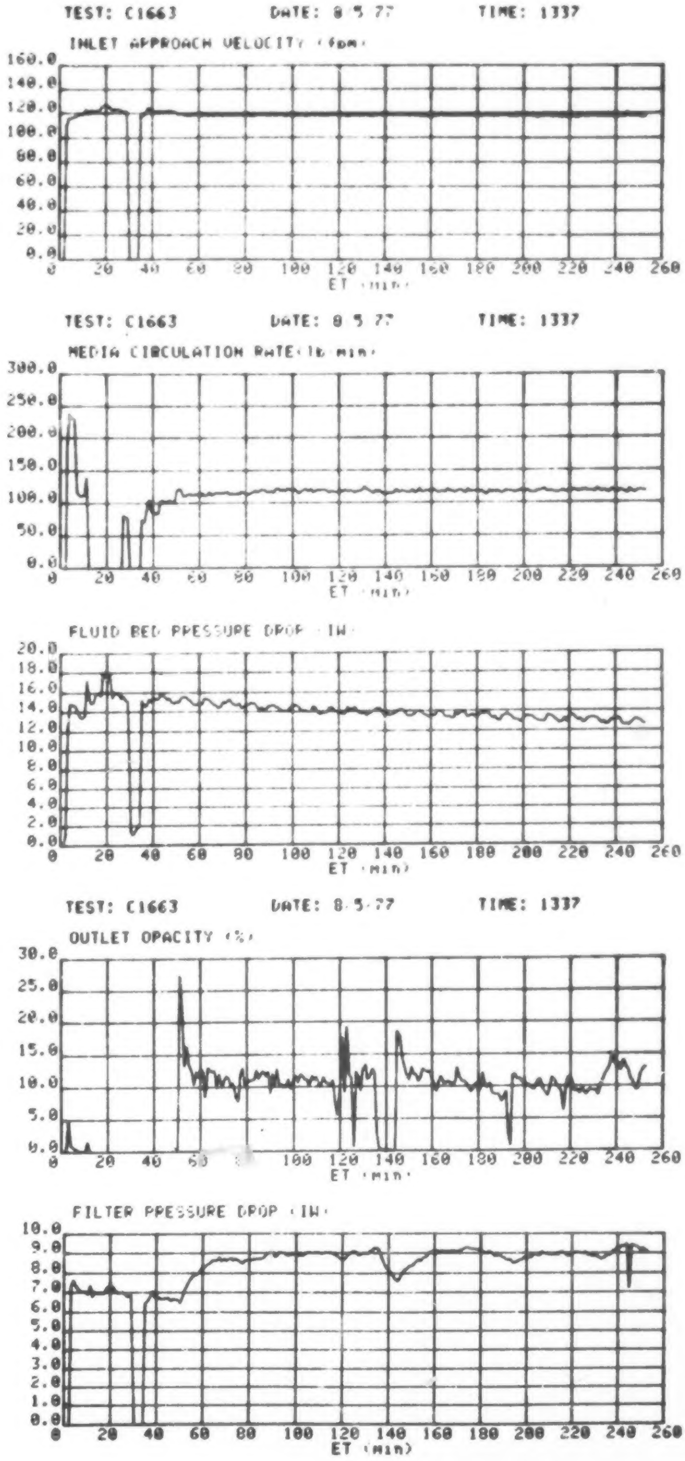

Figure 12, continued.

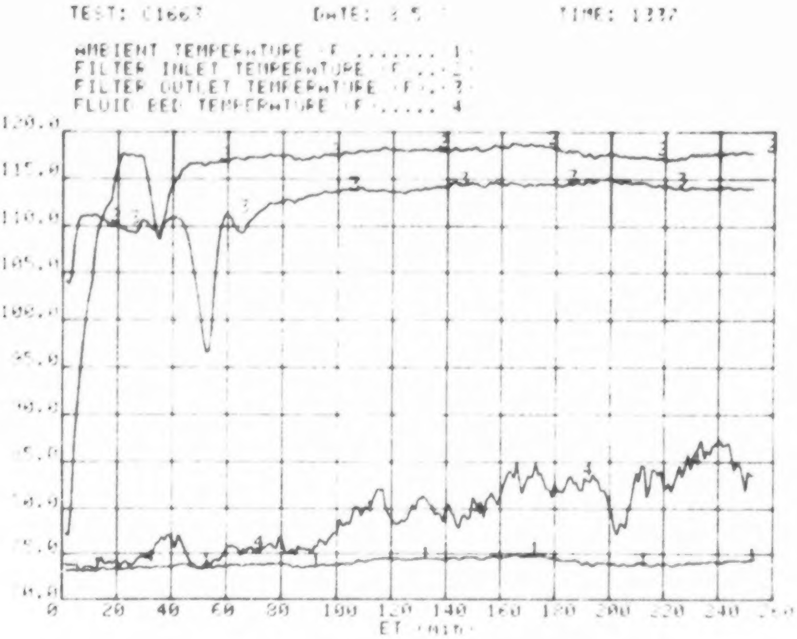

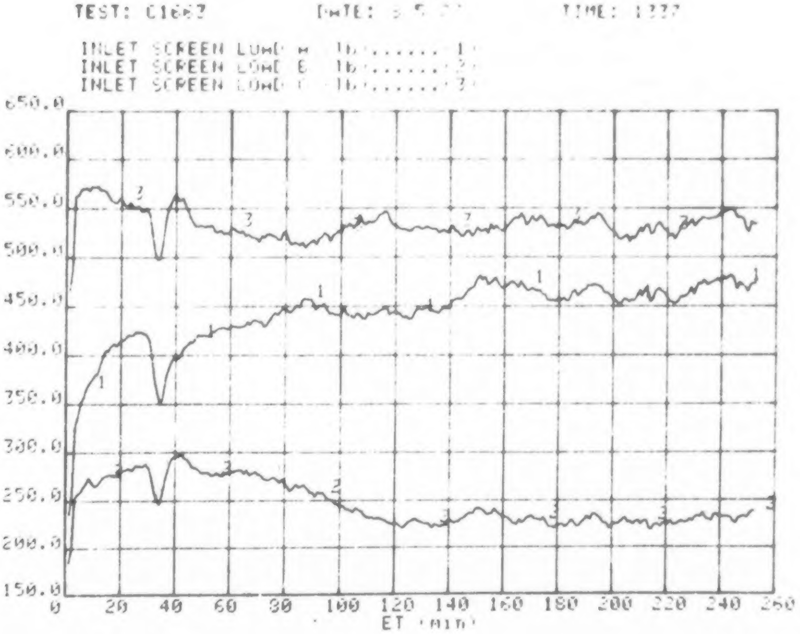

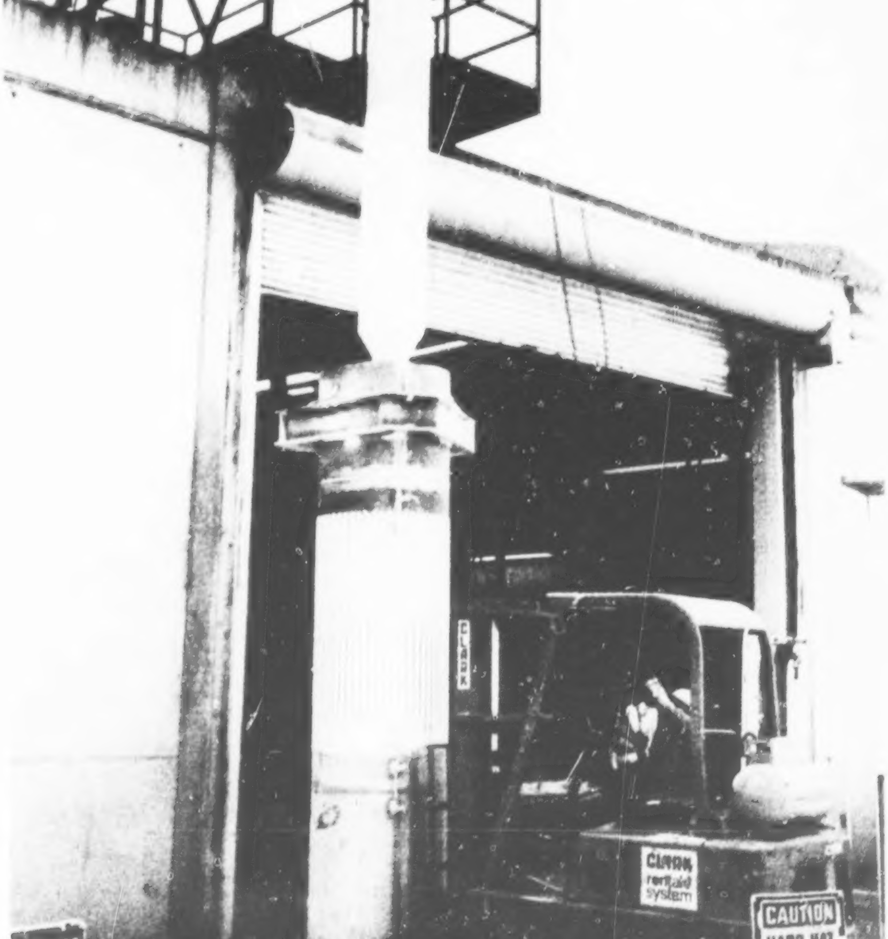
CLARK
CLARK
rentaid
system
CAUTION
HARD HAT
AREA
TION
OTECTION
IRED

Figure 13 Post-test disassembly of GBF.

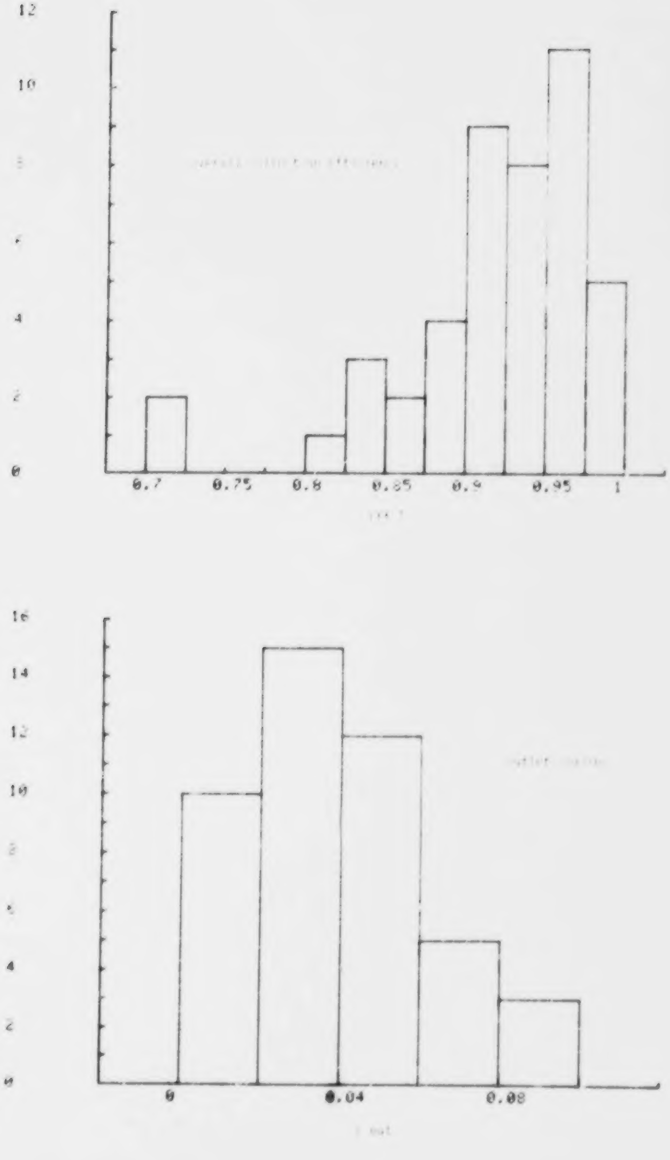

Figure 14 Histograms for final two columns of Table IV.

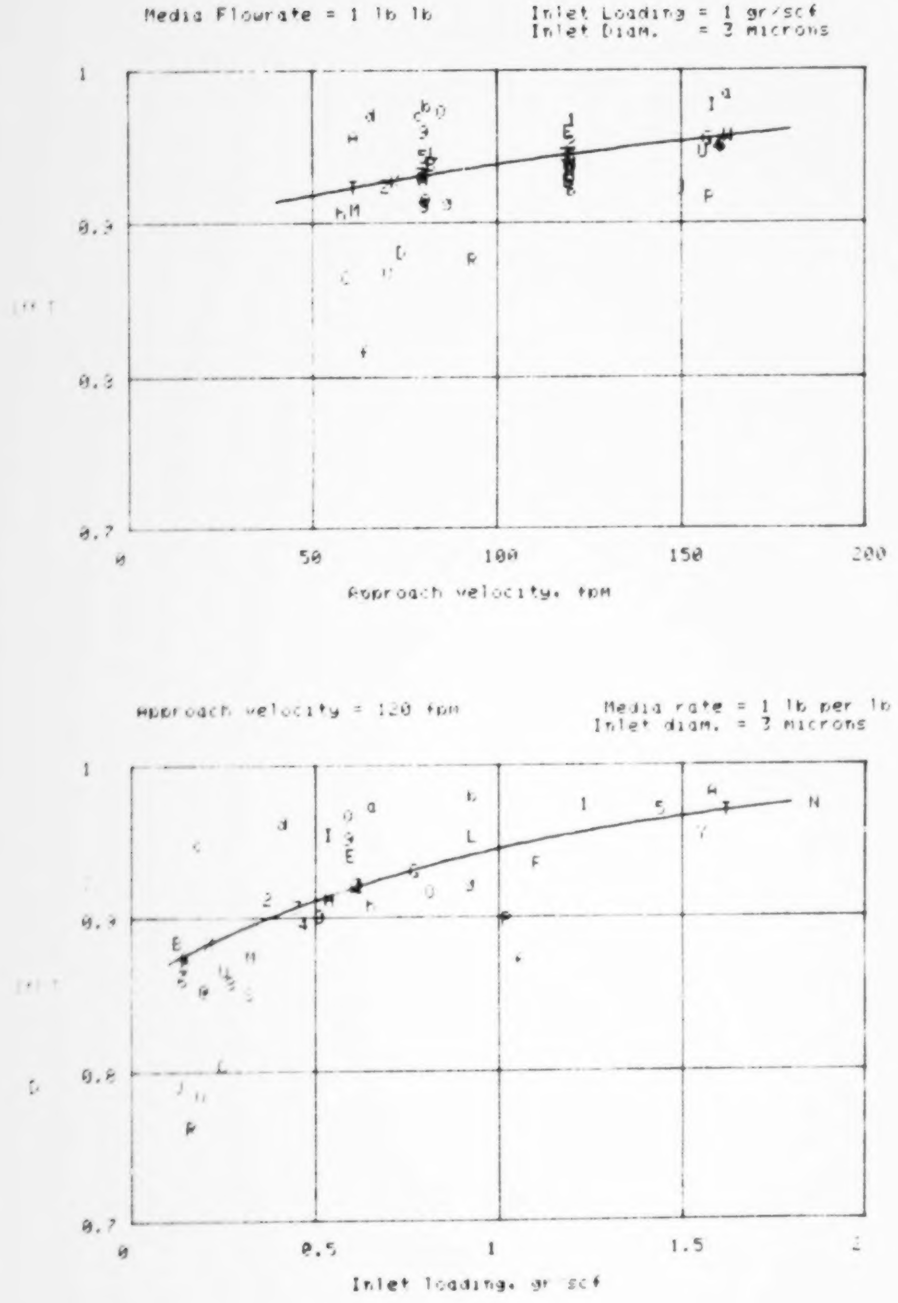

Figure 15 Regression for GBF total efficiency
Typical DAS record

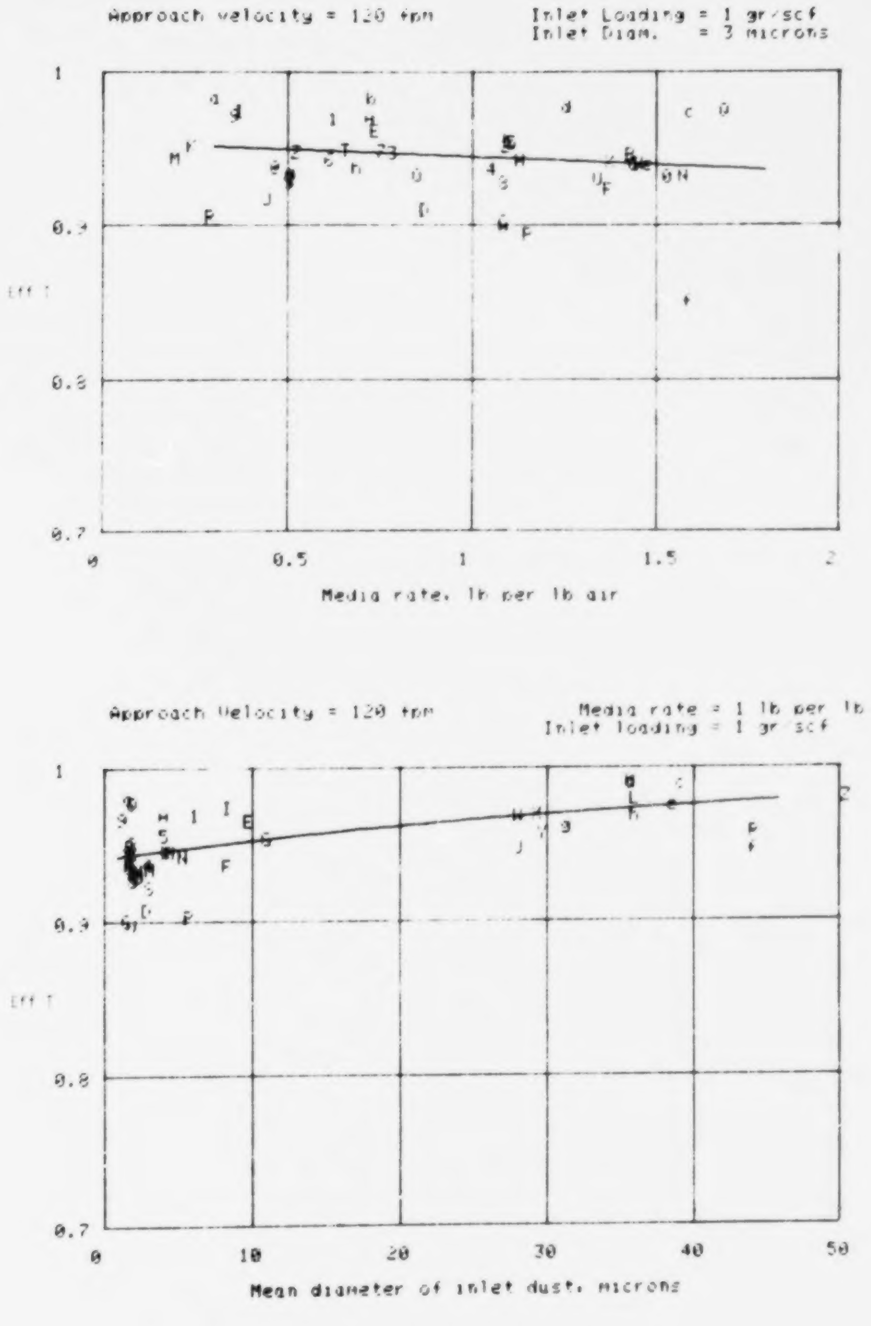

Figure 15, continued.

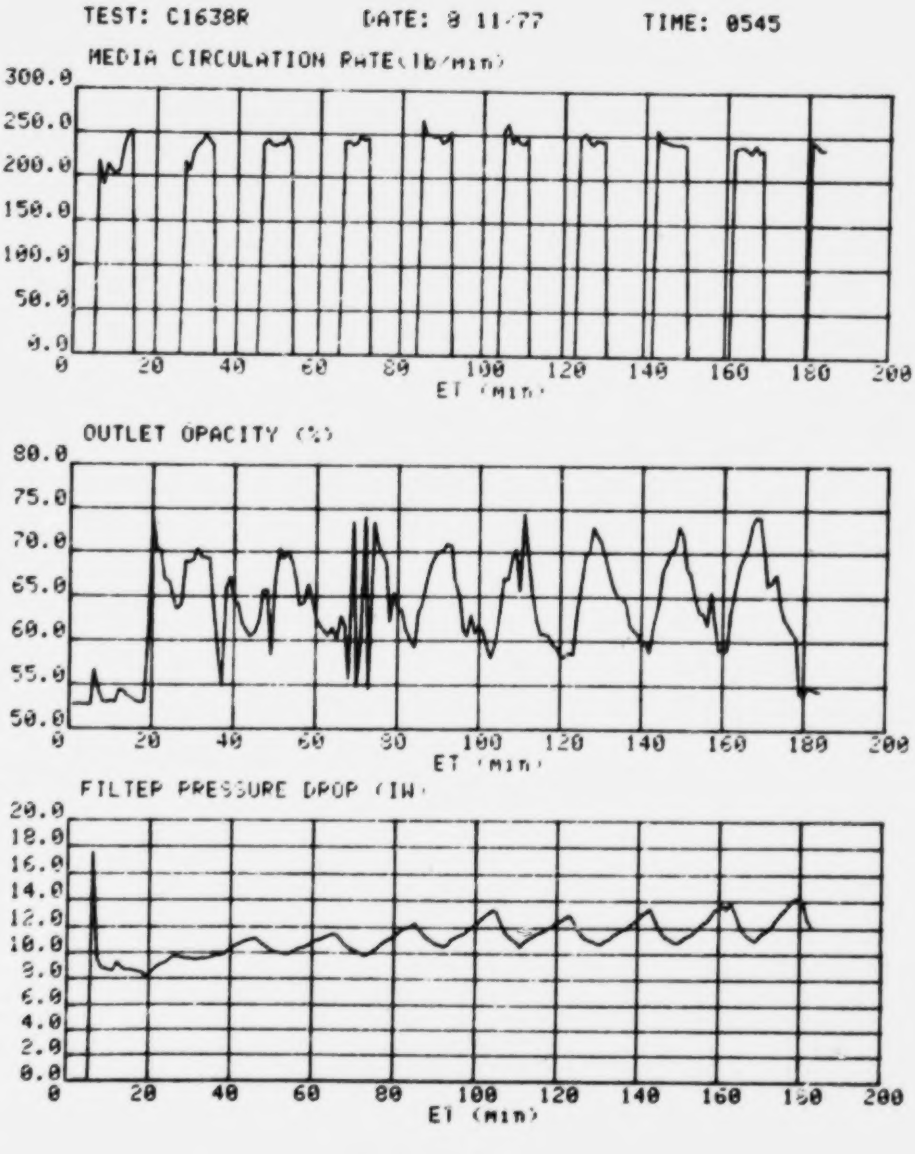

Figure 16 Typical DAS record for intermittent media flow.

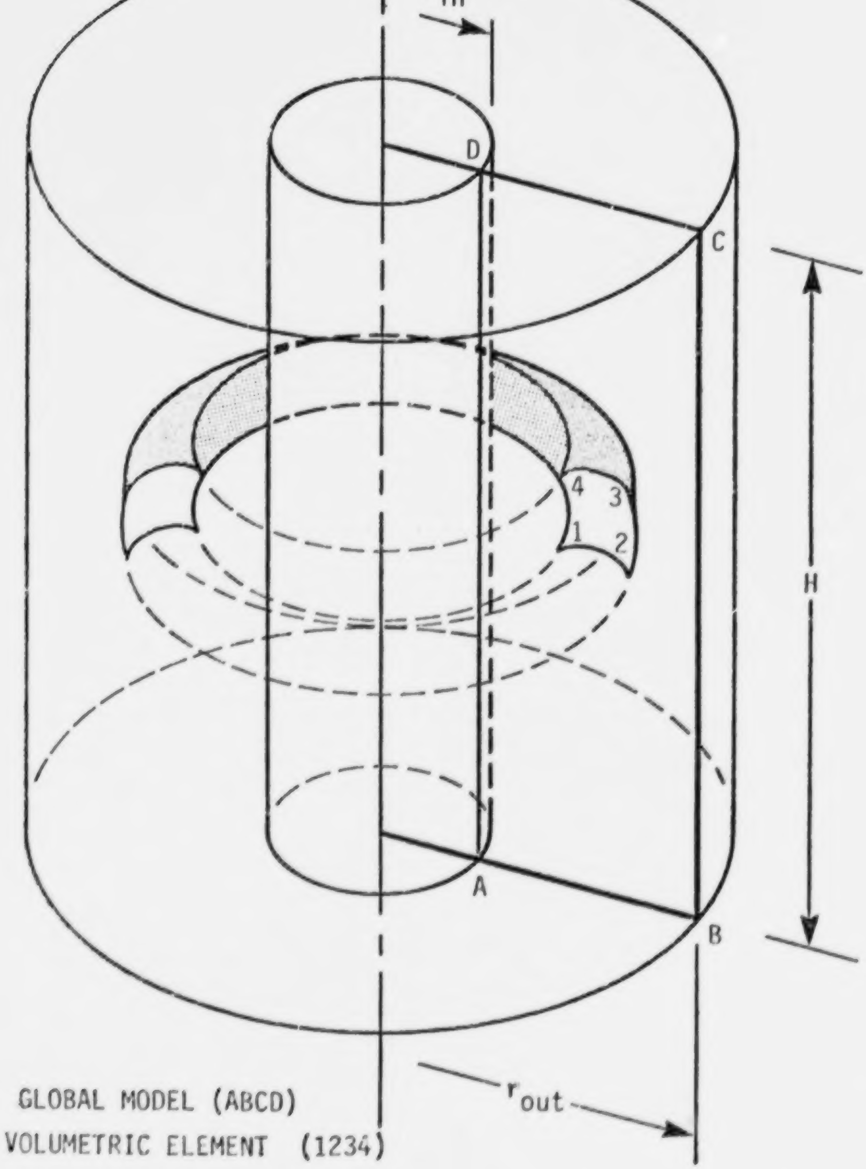
r_in
D
C
4
3
1
2
H
A
B
r_out
GLOBAL MODEL (ABCD)
VOLUMETRIC ELEMENT (1234)

Figure 17 Control volumes.

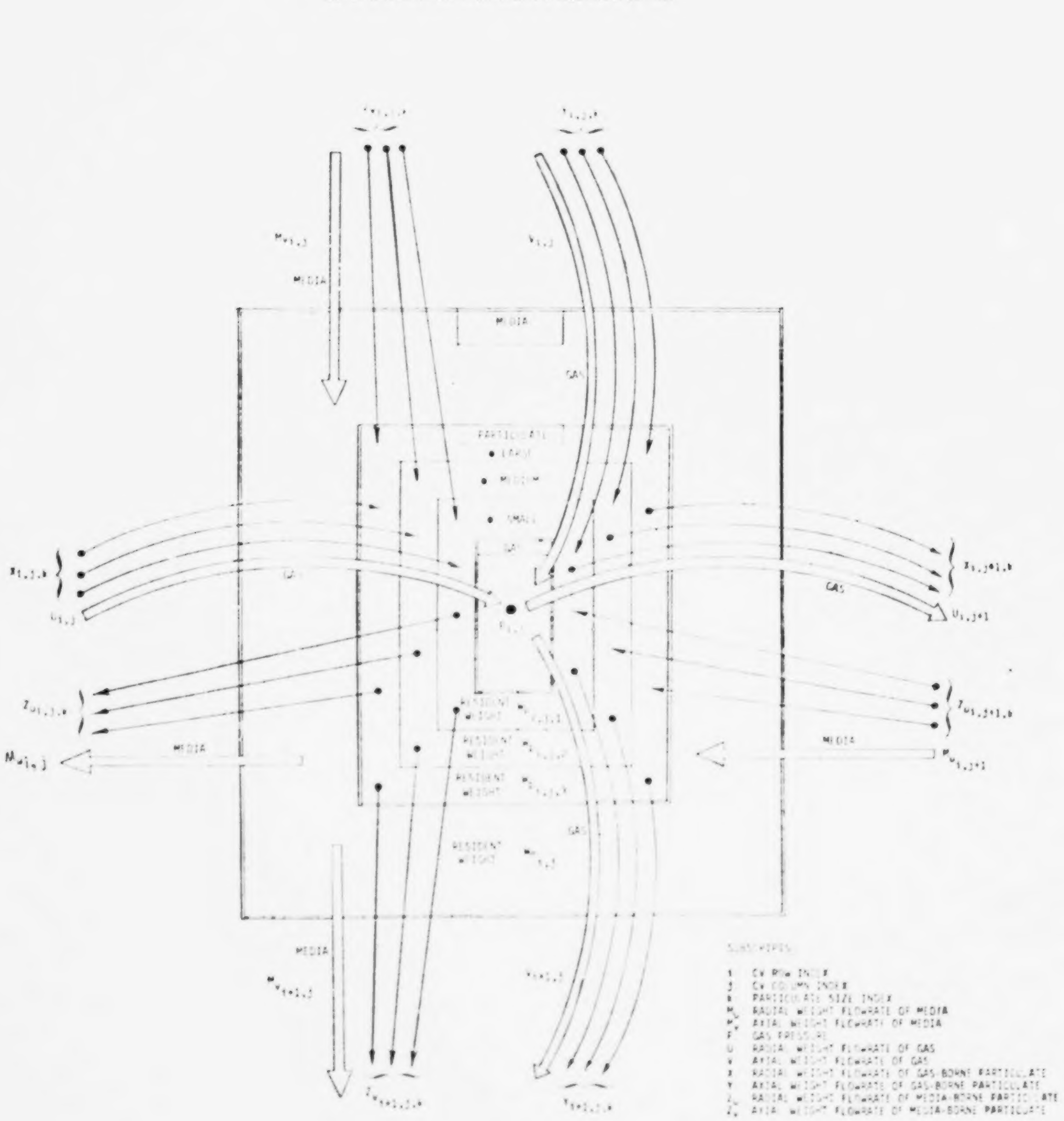
INTERIOR CONTROL VOLUME (TOTAL VOLUME = V)
ONE OF A RECTANGULAR ARRAY HAVING N ROWS AND M COLUMNS
MEDIA
GAS
PARTICULATE
LARGE
MEDIUM
SMALL
RESIDENT WEIGHT
SUBSCRIPTS
i CV ROW INDEX
j CV COLUMN INDEX
k PARTICULATE SIZE INDEX
$M_u$ RADIAL WEIGHT FLOWRATE OF MEDIA
$M_v$ AXIAL WEIGHT FLOWRATE OF MEDIA
P GAS PRESSURE
U RADIAL WEIGHT FLOWRATE OF GAS
V AXIAL WEIGHT FLOWRATE OF GAS
X RADIAL WEIGHT FLOWRATE OF GAS-BORNE PARTICULATE
Y AXIAL WEIGHT FLOWRATE OF GAS-BORNE PARTICULATE
$Z_u$ RADIAL WEIGHT FLOWRATE OF MEDIA-BORNE PARTICULATE
$Z_v$ AXIAL WEIGHT FLOWRATE OF MEDIA-BORNE PARTICULATE

Figure 18 Nomenclature for computer model of GBF performance.

# CERAMIC FABRIC FILTRATION AT HIGH TEMPERATURES AND PRESSURES

By:

M. Shackleton, J. Kennedy
Acurex Corporation/Aerotherm Division
Mountain View, CA 94042

# CERAMIC FABRIC FILTRATION AT HIGH TEMPERATURES AND PRESSURES

By:

Michael Shackleton and Jeffrey Kennedy
Acurex Corporation/Aerotherm Division
Mountain View, California 94042

Barrier filtration using ceramic fiber filters offers a promising solution to the problem of controlling particles in the high-temperature, high-pressure environment. Industrial experience has proven this technique is capable of high efficiency particle control, including fine particles, in near ambient temperatures and pressures. Examining those particle removal mechanisms which apply to barrier filtration indicates that a small decrease in efficiency should be expected at high temperatures and pressures.

This is primarily caused by a reduction in the effectiveness of the mechanism of inertial impaction. This reduction can be compensated for in the design of the filter medium and in the design of the filter system. Ceramic fibers are available which have smaller diameters (3 μm) than conventional fibers used for filters (10 to 20 μm). Analysis indicates that using these fine diameter fibers should make it possible to use filter media having weights less than or, at most, equal to conventional media.

This paper reports on work being performed under EPA Contract 68-02-2169 to demonstrate the feasibility of high-temperature, high-pressure particle control by filtration. A description of the high-temperature and pressure media test facility is presented along with test results to date.

# CERAMIC FABRIC FILTRATION AT HIGH TEMPERATURES AND PRESSURES

## INTRODUCTION

Many advanced technology processes currently being developed require removing particles from high-temperature and pressure gas streams. An objective of developing these processes is to increase coal use by making it economically efficient and environmentally safe. These processes, such as pressurized fluidized-bed coal combustion, involve expanding the high-temperature and pressure gases across a turbine to generate power to produce electricity. Such applications require removing particulate flyash from the gas streams before expansion across the turbine. Techniques to accomplish the required particle control have not yet been demonstrated.

Under normal environmental conditions, barrier filtration is an effective method of achieving the required level of particle control. However, at high temperature (815°C) and pressure (10 atm), barrier filtration and other conventional particle control methods are limited by materials capable of surviving in the environment and by effects of changes in gas properties.

Under EPA Contract 68-02-2169, Aerotherm is investigating the suitability of commercially-available ceramic fiber filters for high-temperature filtration. This work is sponsored by the Particulate Technology Branch of the Industrial Environmental Research Laboratory at Research Triangle Park, North Carolina.

Major goals of this program are to:

- Design and build a filter media test facility capable of operating at 815°C and 10 atm pressure
- Test available ceramic fiber forms (woven cloths, felted mats) to determine if any can survive mechanical displacements and accelerations likely to be encountered in online cleaning of high-temperature filter applications

- Develop preliminary performance data for those configurations which appear most promising for high-temperature filter applications
- Make recommendations based on the experience and data collected

## TEST PLAN

To provide the data needed to justify further development of high-temperature, high-pressure barrier filtration equipment, Aerotherm has outlined the following test plan:

- Obtain and classify ceramic media candidates. A survey of available ceramic filters and materials has been made. The materials available are generally made for insulation applications, and those that are not rigid structures can be catagorized into three groups: (1) Woven fabrics, produced by several companies are made from yarns produced from a continuous length of ceramic fibers. They are available in various weaves, are flexible, and exhibit good strength relative to other ceramic fibrous structures. (2) Ceramic papers are available which are constructed from short fibers generally held together with binders. These structures are characterized by a relatively higher packing density of fibers and poor mechanical strength compared to other ceramic fibrous structures. (3) Ceramic felts consisting of relatively long fibers are available. These materials are relatively porous mats held together by randomly intermixing the fibers. They are flexible and exhibit reasonably good strength.
- Mechanical Screening Tests — In the first phase of the test program, the various candidate filter media are subjected to "filter cleaning loads" to determine their relative strength. These tests are being performed on samples shaped into tubular bags. The tests are performed at an air-to-cloth ration of 5 to 1 (2.54 cm/sec) at high temperature and pressure in the presence of flyash. Samples are initially subjected to reverse flow cleaning cycles, but the primary test is pulse-cycling. While maintaining forward flow, the sample is shook using 5 to 10 pulses per minute from a reservoir pressure

of 1100 kPa (160 psig), with a duration of 100 ms. The relative strength of each sample is determined by the number of cycles it withstands. If several thousand cycles are required to cause failure, then it is probable that the filter would last a long time, provided the cleaning technique is perfected.

- Parameter Variation Tests — Filter performance data are being developed from these tests. Those samples which withstand filter cleaning loads will be given longer tests to investigate their operating limits in a filtration application. Flyash will be metered into the gas stream at a controlled rate, while monitoring pressure drop of the filter. Reverse flow and/or pulse cleaning will be used to maintain a reasonable stabilized pressure drop. Pressure drop and efficiency will be determined as a function of air-to-cloth ratio, cleaning method and energy level, time and dust-loading. These tests will provide a basis for selecting near-optimum operating conditions for each sample tested.
- Life Tests — Our tests may identify media samples and operating limits which appear capable of meeting the proposed requirements for high-temperature and pressure barrier filtration. If so, extended tests will be given to attempt to determine their long-term performance. This work is scheduled for completion in August 1978. Preliminary results from the mechanical screening tests are included in this report.

## Theory

Barrier filtration with available ceramic fibers is likely to be a good technique for particle control at high temperature and pressure. To illustrate why this is true, a short review and discussion of barrier filtration theory is helpful.

Figure 1 is taken from a report titled "Effects of Temperature and Pressure on Particle Collection Mechanisms: Theoretical Review" by Seymour Calvert and Richard Parker (EPA-600/7-77-002), January 1977. This figure shows a calculated fractional efficiency curve for a fiber bed. Minimum efficiency is indicated for a particle size of about 0.5 μm. The dip in the curve occurs because of the interaction of the three collection mechanisms which apply to barrier filtration. These mechanisms are direct interception, diffusion, and inertial impaction. For particle size less than about 0.5 μm, collection by diffusion is increased, improving the efficiency of the filter bed. For particle size larger than about 0.5 μm, collection by inertial impaction is improved, increasing the collection efficiency of the filter bed. It should be remembered that this curve applies only to initial performance of a clean fiber bed. That is, it does not include the increased collection efficiency that results from the filtration of the accumulating dust cake. Note also that the No. 3 curve indicates that the inertial impaction parameter for high-temperature and pressure conditions should show a small decrease in performance. To understand the magnitude of this effect we can compare the performance of standard filter media when tested with Dioctylphthalate smoke (D.O.P.) to its performance when tested after a stabilized dust cake has been developed. A D.O.P. smoke penetration test is a standard test to measure the efficiency of high performance filters such as those used to filter "Clean Room" air or to collect biological contaminants. This test measures how efficiently a filter removes a 0.3 μm diameter D.O.P. smoke particle. Woven or felt filter media of the type commonly used for industrial filters will collect only 10 or 20 percent of 0.3 μm D.O.P. smoke. Yet, after developing a dust cake, these same filter media will collect submicrometer particulate at an efficiency of greater than 90 percent. Thus, compared to the changes in performance which take place in a filter media during the conditioning process, the changes predicted as a result of high-temperature operation are small.

Available ceramic fibers offer unique advantages for filtration, since many of these fibers have finer diameters than conventional filter fibers. Conventional fibers are usually 10 or 20 μm in diameter, while ceramic fibers are available with average diameters of only 3.0 μm.

Collection efficiency can be improved simply by making a filter bed thicker, thus increasing the basis weight of the filter (its weight per unit area). However, to achieve high collection efficiency in this way can lead to high operating pressure drops. Collection efficiency can also be increased by reducing the fiber diameter, which can result in decreased basis weight and filter bed thickness. The importance of fiber diameter is illustrated in the following equations which describe the three primary particle collection mechanisms applicable to barrier filtration.

$$\text{Interception parameter } K_I = \frac{d_p}{d_f}$$

$$\text{Impaction parameter } K_p = \frac{C'\rho_p d_p{}^2 U_g}{9\mu_g d_f}$$

$$\text{Diffusion parameter } K_d = \frac{C'kT}{3\pi\mu_g d_p U_g d_f}$$

These equations describe the collection mechanisms, but are not collection efficiency equations. However, when expressed as above, an increase in any of the mechanism parameters ($K_I$, $K_p$, $K_d$) will result in an increase in efficiency.

The interception parameter is not a function of temperature and pressure, but it is a function of fiber diameter. Changing from a 20-μm fiber to a 3.0-μm fiber will increase the interception parameter by a factor of 6.67 times.

The impaction parameter is a function of temperature and pressure, essentially through changes in the gas viscosity (μg). For air, increasing temperature from 20 to 815°C increases viscosity by about 2.5 times. This reduces the impaction parameter by a factor of 1/2.5 or 0.4. But, the change in fiber diameter from 20 μm to 3.0 μm increases the impaction parameter by 6.57 times. The net effect of the two changes is to increase the impaction parameter by 2.7 times.

The diffusion parameter is a function of temperature and pressure through changes in the ratio of (C'T/μg). When operating at 815°C and 10 atm pressure, this ratio tends to remain unchanged or to increase slightly. But, the diffusion parameter is also a function of fiber diameter and a change in fiber diameter from 20 μm to 3.0 μm will increase the diffusion parameter by 6.67 times.

From the above discussion it is evident that if we make a filter using 3.0-μm diameter ceramic fiber (which is commercially available), it is reasonable to expect that even at high temperature and pressure this filter will have high collection efficiency without excessive filter bed thicknesses or basis weights. Using the method developed by Torgeson, it is possible to calculate collection efficiency for a given particle size and fiber bed parameters. This calculation was performed for a 0.5-μm diameter particle with a density of 1.5 g/cm$^3$ (as measured at the Exxon Miniplant), for gas temperature of 815$^{\circ}$C, and pressure of 10 atm. A fiber bed composed of alumina fibers with 3.0-μm diameter and fiber density of 2.8 g/cm$^3$ was assumed. Results of this analysis for two filtration velocities and two solidities ($\alpha$ - the volume fraction of the fiber bed which is solid) are plotted in Figure 2. This analysis indicates that a 3.0-μm diameter ceramic fiber filter bed with a basis weight of 500 to 600 g/m$^2$ will collect submicrometer particulate with an initial (clean) efficiency of about 90 percent at high temperature and pressure. Recall that a typical industrial filter media (20-μm fibers) would collect such particles at only 20 percent efficiency for the same basis weight. Another way to look at this is to note that to achieve collection efficiency comparable to commercial industrial media will require a ceramic fiber filter media with weights only one-tenth that of the commercial media. Another interesting feature of the analysis is that efficiency decreases for increasing velocity. However, by adding fibers, the given efficiency can be maintained as velocity is increased. The quantity of additional fiber required is relatively small, especially if only 20-percent initial efficiency is adequate for a 0.5-μm particle.

Most commercially-available ceramic fiber structures are produced for insulation applications. Consequently, these materials are generally characterized by an open fibrous structure. That is, they have low solidity, with perhaps only 2 percent of the volume occupied by fibers ($\alpha = 0.02$), A solidity of $\alpha = 0.10$ is more typical of a structure designed for filtration. Figure 3 shows the effect on fiber bed thickness for changes in solidity and air-to-cloth ratio. For solidity typical of insulation materials ($\alpha = 0.02$), a fiber bed about 1 cm thick should achieve high initial collection efficiency of submicrometer particulate, while a more compressed media with $\alpha = 0.10$

would achieve this efficiency with a bed thickness of only 2 mm. If efficiency typical of industrial filters is adequate, very thin layers of the 3.0-μm diameter fibers will suffice. Note also that filter media thickness is not a strong function of air-to-cloth ratio, indicating that high filtration velocity should be possible. Of course, higher filtration velocity will result in increased pressure drop, but this may be acceptable in a PFBC application.

## Ceramic Media Performance at Ambient Conditions

To test the performance predicted analytically for ceramic fiber media, several ceramic media samples were tested for D.O.P. penetration at two air flow velocities. The resulting data are plotted in Figure 4. This data shows that the paper media had the highest efficiency, felts in general had intermediate efficiency, and the woven materials had the lowest efficiency. More importantly, it shows that many of the samples collect D.O.P. smoke at higher efficiency than standard industrial-grade filters which usually perform at less than 20-percent efficiency in a D.O.P. test. Also, several of the woven samples perform as well as industrial filters (these specific media are identified in the appendix). In order to compare these results with the calculated performance shown in Figure 2, the D.O.P. data for several paper and felt samples are plotted in Figure 5 using the same scale as Figure 2. Woven samples were not included in the curve because the analysis assumes a random orientation or bed of fiber. Figure 5 clearly shows that many of the fine fiber ceramic media collect fine particles at high efficiency with low basis weight. Two of the paper media performed nearly as predicted from the high-temperature, high-pressure analysis. The vertical line through the data points represents the extremes measured for the two velocities tested. The performance line is drawn through the average of these two data points. All of the media, except Fiberchrome type 800, are claimed to have 3.0-μm average fiber diameter. Fiberchrome type 800 is claimed to have a 3.5-μm average fiber diameter. The performance for the blanket samples was less than predicted. This may be explained by variations in actual fiber diameter and the potentially nonuniform fiber distribution in the relatively open mat and blanket materials. However, all of these materials have higher collection efficiency for 0.3-μm D.O.P particles than an equal weight per unit area of most standard filter media in industrial applications.

## Summary Barrier Filtration Theory

We have examined those particle collection mechanisms that apply to barrier filtration. Our particle collection efficiency predictions indicate that barrier filtration at high temperature and pressure should be possible. Furthermore, if we take advantage of the small diameter fibers currently available in ceramic materials it should be possible to produce acceptable filtration efficiency using thin, lightweight fiber structures. There is no theoretical reason why these filters cannot operate at high air-to-cloth ratio for particle collection. Room temperature tests of ceramic fiber media using 0.3-μm D.O.P smoke tend to confirm these theories. Thus, we can conclude that ceramic fiber filter media should be able to remove particles from high-temperature and pressure gas streams.

The major unanswered question is, can these media be cleaned adequately to maintain an acceptable pressure drop? Fundamental to that question is, can these media, or specially-designed media, survive the stresses they will be subjected to in operation and cleaning cycles in a high-temperature and pressure application? Aerotherm is attempting to answer these questions. As a first step in this effort we have designed and built the high-temperature and pressure filter media test rig described below.

## Ceramic Media Test Facility

The Hot filtration Testing Facility (shown in Figure 6) is capable of subjecting 46-cm (18-inch) by 9.5-cm (3-3/4-inch) diameter test filters to an 815$^{\circ}$C, 10-atmosphere environment with air-to-cloth ratios from 0.5 to 5 cm/sec (1 to 10 ft/min). During high-dust loadings, bags tested in the facility can be either reverse-flow or pulse-jet cleaned. There are three test chambers so that three bags can be tested simultaneously, though only one chamber is presently in use.

The filter media test chamber (Figure 7) is a 244-cm (8 foot) by 30.4-cm (1 foot) diameter length of pipe with inlet and outlet tubes welded into the blind flanges on the top and bottom. The inside of the chamber is lined with 5 cm (2 inches) of castable refractory which surrounds a 10-kilowatt, 230-volt electrical resistance heater used to compensate for refractory and external piping heat losses. Clean, high-temperature, high-pressure air enters the chamber through the bottom, where it is passed through a dust pot.

The dust pot, an inverted conical container filled with flyash, funnels the dust into the clean air entering the chamber, and then recaptures the dust after it is filtered. Except for losses through the bag, the dust pot is self-recharging and ideal for tests not requiring precise and controllable dust loadings. The diameter of the dust pot is about 6.3 cm (2-1/2 inches), opening up to the full 20.3 cm (8 inches) of the inner wall.

The 46-cm (18-inch) long test bag is above the dust pot. The bag-shaped filter is mounted around a 9.2-cm (3-5/8-inch) diameter support cage screen which prevents the bag from collapsing during outside-in filtering. The test bags are open at both ends, requiring clamping at the top around the venturi and at the bottom around a sealing plate attached to the cage. The filtered air passes through the venturi, into the pulse-jet plenum and exits the chamber through the outlet tube.

Once the filtered air leaves the test chamber, it is cooled with a forced air, finned-tube heat exchanger. It is then directed through a commercial, low-temperature, high-efficiency, tube-type filter (Figure 8). This filter can be inspected periodically to determine the test bag's filtering effectiveness. Downstream of the low-temperature filter, the high-pressure air is bled through a sonic-flow metering orifice, through a noise suppressor, and vented to the atmosphere.

Gas temperatures are measured using thermocouples located at selected points within the facility. The air temperature measurements are taken at the test chamber inlet, above and below the test bag, at the low temperature filter, and at the orifice meter. These temperatures are displayed in the control room and stored on a 24-channel strip chart recorder. Pressure measurements using diaphragm pressure transducers are taken above and below the bag, at the orifice and in the pulse-jet reservoir. This information is also displayed and recorded in the control room.

There are two methods available for cleaning the test bag during operation: pulse-jet and reverse-flow. The pulse-jet method cleans the bags using quick blasts of high-pressure air, introduced at the clean side of the bag. Pulse pressure can be regulated from 1033 kPa (150 psi) to 1723 kPa (250 psi). Fast-acting solenoid valves provide 100 msec pulses at a nominal 6 to 7 pulses per minute. Pulse-jet cleaning does not interrupt forward flow filtering.

Reverse-flow cleaning is a milder cleaning technique, which requires interrupting forward flow. The first step of the reverse-flow cleaning sequence is to shut off the main flow and bleed the test chamber down to a lower pressure. Next, the downstream outlet valve is shut and the main flow redirected in through the outlet tubes at the top of the chamber. The inside-out flow across the filter blows the dust off the bag. This process stops when the chamber is once again pressurized. Reverse-flow effectiveness can be varied by adjusting either the bleed-down pressure or the rate of repressurization. To prevent dust from entering the inlet lines during reverse flow, a small regulated amount of the main flow is introduced into the chamber through the inlet tubes while repressurizing.

Both cleaning operations can be controlled manually or automatically at the control room. A digital time sequencer, in combination with a solid-state logic sequencer, can be programmed to provide automatic cleaning. The following parameters are adjustable: pulse frequency and duration, or reverse-flow frequency, bleed-down duration, and repressurization rate. The number of cleaning cycles in a given time can be either predetermined, or dependent on the pressure drop buildup across the bag. Automatic shutdown in the event of bag failure or overtemperatures allows for optional, unattended operation of the facility.

Before entering the test chambers, the high-pressure air is heated to 815°C (1500°F). This is accomplished by passing the air through 0.95 cm (3/8-inch) holes in a 152-cm (5-ft) long by 15-cm (6-inch) diameter stainless steel block with a wall temperature in excess of 870°C (1600°F). The block is heated using a 50-kW induction coil and power supply operating at 30 kHz.

Additional capabilities are presently being added to the Hot Filtration Test Facility: a revolving disk, high-pressure dust feeder and a steam injection system. The dust feeder introduces flyash to the main air upstream of the block heater at a controlled rate. It is enclosed in a pressurized vessel with a dust hopper filling a small groove in a rotating disk. The pressurized air enters the vessel below the disk and exits, carrying the dust out through a small tube directly above the dust-filled groove. The feedrate is adjustable by varying either the disk rotation speed or the groove cross sectional area.

A 1033-kPa (150-psi) steam generator injects steam into the air stream, subjecting the test filter media to 30-percent steam in addition to the high temperature and pressure.

## High-Temperature and Pressure Test Data

This paper reports on work being done under EPA Contract 68-02-2169, scheduled for completion in August 1978. Consequently, at the time of this writing only limited data is available from our high-temperature/pressure test facility. The data that are available for reporting here have been obtained during shakedown tests of the test rig, and should be viewed as preliminary data. That is, no strong conclusions are warranted by the high-temperature/pressure data available to date.

## Mechanical Screening Test Data

As stated previously, the available ceramic fiber structures can be generally classed into three groups: woven, paper, and felt. During the preliminary testing, all three types of media were subjected to survey tests. The objective of the mechanical screening tests was to subject the media to typical filter-cleaning loads in the high-temperature and pressure environment and determine which media can survive these loads. All the tests reported here have been operated at an air-to-cloth ratio of 2.54 cm/sec (5 ft/min).

## Woven Media Tests

Three woven media have been tested. Results of these tests are summarized in Table I. These tests were performed early in the program before we had fully proved the 815°C capability of the heater. Since these tests are fairly qualitative, the following photographs and discussion are offered to augment the data in Table I.

The AB 312 media test was stopped because of excessive dust penetration through the relatively large pores around the yarn filaments of the cloth. This media clearly showed a clean separation of the dust cake from the media surface (Figure 9 illustrates this effect, which has been seen on other tests as well). This apparent cleanability will be studied in greater detail to determine its reliability, and whether it can be used to enhance cleaning.

An Irish refrasil bag was tested with pulse cleaning after surviving 195 reverse-flow cycles. This media developed holes during the pulse testing. Examination after 3,100 pulse cycles revealed the condition shown in Figures 10 and 11. In general, the holes were located near the center of the openings formed by the support cage. They appear to be a result of bending and shock at the maximum points of media acceleration during cleaning. This effect could possibly be controlled by making the support cage openings smaller. Note that Table I shows an 1100-m/sec pulse duration. This occurred because of an error in setting the pulse duration and was not discovered until after the test. This could also have caused the media failure. In addition, it should be noted that pulse cleaning is probably not required for woven media since the less rigorous reverse-flow cleaning can remove the dust cake.

Figure 12 shows a seam failure which occurred on the first pulse and illustrates the force of the pulse. This particular test element had been installed several times, and therefore had been handled more than normal. Failure can be caused by excess handling and sharply bending the fiber.

### Paper Media Tests

One test of paper media has been performed. Results of this test are summarized in Table II. No failures were evident after a short reverse-flow test; however, the media did not survive pulse testing. A bias-cut wire screen supported this media on both surfaces. The bias-cut allowed the tubular shape of the element to stretch, contributing to its failure. A straight-cut screen would provide better support for paper media. Figures 13 and 14 show the bias-cut screen, and several tears in the media.

### Felt Media Tests

Test results for felt media are summarized in Table III. In the first test no damage was evident as a result of reverse-flow testing. After about 5,000 cycles of pulse testing, the pressure-drop monitor indicated a problem. Visual examination revealed that the lower band clamp had slid upward, allowing a leak under the filter element. The lower end of the media was reclamped, and the tests continued. The lateral seam for this media was accomplished by rolling a flat sheet of media into a cylinder and overlapping the ends. This tube shape was supported inside and out by a wire screen. After a total of 9,405 pulse cycles, visual examination revealed that the seam had separated by sliding apart. This separation probably started when the band clamp moved earlier in the test. The flexible bias-cut support screen also contributed to this problem. Figures 15 and 16 show the element and a close-up of the seam separation. The whiteness shown in Figure 16 indicates a good separation of the dust cake from the media surface. Cleaning in this region was accomplished by tapping the screen several times with a pencil!

For the second test, a screen with a fine diameter wire with more strands per unit length was used to support the media. While this screen was also cut on the bias, it provided a stiffer support for the media. Extra care was taken to ensure that the clamps were tight. This media operated for 7,450 pulse cycles with no apparent damage. The test was stopped because of a failure of the test rig heater element. Figure 17 is a photo of the element after the test.

## Present Program Data Objectives

It should be emphasized that the data presented here is preliminary data. The test program is continuing and will provide information outlined below over the next year.

- Mechanical screening tests will continue to develop information on media durability.
- Filter performance at high temperature and pressure will be measured. Efficiency and pressure drop will be measured as a function of air-to-cloth ratio, time, dust loading and cleaning techniques, and energy. These tests will be performed for various media and media support techniques. The objective of these tests will be assess both filtration performance and durability.
- This data will be evaluated to provide a basis for preliminary cost estimates for a high-temperature-pressure ceramic fabric barrier filter system.

## Conclusions

While much remains to be done, the following tentative conclusions summarize the current state of development for ceramic fiber barrier filtration:

- Barrier filtration using ceramic fiber filter media offers a promising approach to high-temperature, high-pressure particle control. Based on room ambient tests, some of the available ceramic materials appear to have good filtration properties.
- Innovative cleaning and media support techniques can be designed which are compatible with the special properties of ceramic media. Demonstrating these techniques is the major task to be accomplished.
- Theory indicates that high air-to-cloth ratio operation may be possible for a HTHP filter system. To accomplish operation at high air-to-cloth ratio will require special cleaning techniques. This is a desirable objective because smaller less expensive control equipment may result.

## REFERENCES

1. Calvert, Seymour, Parker, Richard, "Effects of Temperature and Pressure on Particle Collection Mechanisms: Theoretical Review," EPA-600/7-77-002, January 1977.

## LIST OF SYMBOLS

$d_p$ = Particle diameter

$d_f$ = Fiber diameter

C' = Cunningham correction factor

$\rho_p$ = Particle density

$U_g$ = Gas velocity at media face (flow/area)

$\mu_g$ = Gas viscosity

k = Boltzmann constant

T = Absolute temperature

# APPENDIX A

Following is a list of media samples tested for D.O.P. penetration. The list contains descriptive information taken from advertising literature for each material as well. In examining these data, the reader should remember that in general these materials were not produced for filtration applications. Based on this information none of the materials can be recommended or rejected. Additional information will be required before the judgment can be made. The available information does indicate that at least some of the materials will probably offer good filtration performance.

## DOP Test Results, High Temperature Filter Media

| | Sample Identification | % Efficient @ 5.3 cm/sec Face Velocity | % Efficient @ 16.6 cm/sec Face Velocity |
|---|---|---|---|
| 1. | Fiberfrax Cloth with wire<br>L144TT | 2% | 48% |
| 2. | Fiberfrax Paper<br>970J 09-306-007 | 84% | 82% |
| 3. | Zircar Zirconia Felt<br>Type ZYF-100 | 43% | 62% |
| 4. | ICI Saffil Alumina AL4 Paper | 69% | 75% |
| 5. | ICI Saffil Alumina HT Mat LD | 30% | 56% |
| 6. | Kaowool ¼ thick 6 lb Density | 70% | 76% |
| 7. | Carburundum<br>Fiberfax Dura Blanket | 90% | 90% |
| 8. | Johns Mansville (8lb/$ft^3$)<br>Fiberchrome ½ in. thk type 800 | 38% | 70% |
| 9. | J. P. Stevens and Company<br>Astro Quartz Style 581/38-4<br>Finish 9073 Lot 30701 | 0% | 0% |
| 10. | Hitco Type C100-96<br>Roll No. 96-6293 | 16% | 27% |
| 11. | Hitco Type C100-48<br>oll No. 48-5597 | 11% | 10% |
| 12. | J. P. Stevens Style 570/38<br>Finish 9073 Lot 30601 | 10% | 10% |
| 13. | 3M Company AB 312<br>Basket Weave Style 22B | 0% | 0% |
| 14. | 3M Company AB 312<br>Twill Weave Style 22T | 0% | 1% |
| 15. | UC 100 Hitco Type - 48 | 14% | 4% |
| 16. | Zircar Zirconia Cloth<br>Type ZYW-30A | 28% | 35% |
| 17. | FMI Astroquartz (Custom Weave) | 4% | 6% |

Note: Sample size 100 square cm. The lower face velocity tests were run at 32 SLPM. This conforms with the military specification for high efficiency media and represents a face velocity of 10.5 ft/min. The high face velocity tests were run at 100 SLPM (standard liters/min).

## Media Samples — Description

| | | |
|---|---|---|
| Fiberfrax Cloth | | No organic binder (removed), $2300^{\circ}$F service temperature |
| | L-126TT grade: | 1/8" thick, twill weave, 21 pcf, 32 oz/sq. yd. |
| | L-144TT grade: | 1/10" thick, twill weave, 28 pcf, 34 oz/sq. yd., has nichrome wire insert, strong to $2000^{\circ}$F |
| Fiberfrax Paper | | 52% $Al_2O_3$, 48% $SiO_2$, $2300^{\circ}$F service temperature, up to 1" long, 2-3 microns (mean) fibers, 2.53 gm/cc density |
| | 970-AH grade: | 1/32" thick, no binder, 12 pcf, 4.5 oz/sq. yd. |
| | 970-J grade: | 1/8" thick, has up to 5% binder, 10 pcf, 15 oz/sq. yd. |
| Zircar Zirconia | Felt ZYF-100: | 19 oz/sq. yd., 0.1" thick, 15 pcf, 96% voids, 600 scfm/ft$^2$ at 0.5 psi, 5.8 gm/cc density, 4.5 μm fibers, no binders. Breaking strength 1.6 pounds/in. width |
| Saffil Alumina (ICl) | | Fiber density 3.4 gm/cm$^3$, $3000^{\circ}$F service temperature, 3 micron fibers, 1-2" long, 1.5 cm$^2$/gm surface area, 95% $Al_2O_3$ – 5% $SiO_2$ |
| | Mat | 4 pcf, ½ in. thick, 2.4 oz/sq. yd., no binder |
| | Paper | 12 pcf, 0.04 in. thick, 6 oz/sq. yd., has binder |
| Kaowool (Babcock & Wilcox) | | 47% alumina — 53% silica, good to $2600^{\circ}$F, 2.8 micron fibers, 2 in. long and up to 4 in. long. Has no binder. 2.6 g/cc density, 6 pcf, ¼, ½, and 1" thick, 18, 36, 72 oz/sq. yd. |
| Fiberfrax (Carborundum) | | |
| | Durablanket | 48% $Al_2O_3$, 52% $SiO_2$, $2300^{\circ}$F service temperature, long fibers, 2-3 micron (mean) fiber diameter, density 2.62 gm/cc. No binder, 6 pcf, ¼ in., 18 oz/sq. yd. |
| Fiberchrome (J. Manville) | Felt | 41% alumina, 55% silica, 4% $Cr_2O_3$. good to $2700^{\circ}$F. 3.5 micron fibers, 8 pcf, ½ in. thick, 48 oz/sq. yd. |

Media Samples — Description (Continued)

| | | |
|---|---|---|
| Astroquarts<br>J. P. Stevens) | Cloth (with binder) | |
| | Style 570: | 5 Harness Satin 300-2/8, 27 mils thick, 19.5 oz/sq. yd., 38 x 24 thread count/inch, 325 (warp) and 300 (fill) pounds/inch width breaking strength. Pure Silica (99.9%), 2000°F service temperature. Filament diameter ~ 6 microns) |
| | Style 581: | 8 Harness Satin 300-2/2, 11 mils thick, 8.4 oz/sq. yd., 57 x 54 thread count/inch, 175 (warp) and 170 (fill) pounds/inch width breaking strength. Pure Silica (99.9%). Good to 2000°F continuous service. ~ 6 micron filaments |
| | Custom Weave:<br>FMI Astroquartz | Crow foot Satin 300-2/2 (warp), 4/2 (fill) 54 (warp) x 36 (fill) threadcount per inch, ~ 12 mils thick, ~ 11 oz/sq. yd. Pure Silica (99.9%), good to 2000°F service. |
| Refrasil<br>(Hiteco) | (Fibers 8 to 10 microns diameter) | |
| | Irish (Chromized)<br>C 1554-48: | 8 Harness Satin, 26 mils thick, 19.2 oz/sq. yd., 53 x 40 thread count per inch, 96 (warp) and 62 (fill) pounds/inch breaking strength. Consists of almost pure Silica with 1 to 3% Chrome Oxide. Continuous use to 2300°F. |
| Refrasil | Heat Cleaned (Preshrunk) | |
| | C 100-48: | 8 Harness Satin, 26 mils thick, 18.6 oz/sq. yd., 52 x 39 thread count per inch, 86 (warp) and 61 (fill) pounds/inch breaking strength. Consists of almost pure Silica (99%+). Good to 2300°F. |
| | C 100-96: | 12 Harness Satin, 50 mils thick, 37.1 oz/sq. yd., 50 x 39 thread count per inch, 130 (warp) and 65 (fill) pounds per inch breaking strength. Essentially pure (99%+) Silica. Good to 2300°F |

## Media Samples — Description (Concluded)

| | | |
|---|---|---|
| Refrasil (continued) | | |
| | UC 100-48: | 8 Harness Satin, 26 mils thick, 18 oz/sq. yd., 46 x 36 thread count per inch, 80 (warp) and 60 (fill) pounds per inch breaking strength, good to 2300°F.<br>99%+ Silica |
| AB-312<br>(3M Co.) | Heat Cleaned. Alumina-Boria-Silica, 390 filament strand, 11 micron diameter filaments, 250,000 psi tensile strength, $22 \times 10^6$ psi modulus, 2300°F service temperature, 2.5 gm/cc density | |
| | Style 22B: | 50-1/0, 32 x 38 thread count/inch, 9.3 oz/sq. yd, 12 mils thick basket weave. |
| | Style 22T: | 50-1/0, 32 x 25 thread count/inch, 7.6 oz/sq. yd., 10 mils thick, twill weave |
| Zircar Cloth<br>(Zircar Corp) | ZYW 30A: | 20 oz/sq. yd., 0.030 in. thick, 5 Harness Satin, 63 pcf, 83% porosity, 5.7 gm/cc density, 5 micron continuous filaments. Breaking strength 4 pounds/in. width BET surface area 1 $m^2$/gm, 92% $Zr_2O_3$ - 8% $Y_2O_3$. Good to 3300°F, 2-ply x 480 filament yarn, 45 x 34 threads/in. |

TABLE I. WOVEN MATERIALS TEST RESULTS

| | Temperature | Cleaning | Cycles | Time | Failed |
|---|---|---|---|---|---|
| 3M Company AB 312 Twill Weave | 538°C | Reverse Flow | 153 | 8.5 hr | No |
| Irish Refrasil Silica/Chrome Satin | 538°C | Reverse Flow | 195 | 13 hr | No |
| | 538°C | Pulse 1400 kPa (200 psi) 100 mS | 3100 | 7 hr | Yes, holes |
| Irish Refrasil Silica/Chrome Satin | 538°C | Reverse Flow | 100+ | 15 hr | No |
| | 815°C | Pulse 1100 kPa (160 psi) 1100 mS | 1 | -- | Seam |

TABLE II. PAPER MATERIALS TEST RESULTS

| | Temperature | Cleaning | Cycles | Time | Failed |
|---|---|---|---|---|---|
| ICI<br>Saffil Alumina | 815°C | Reverse Flow | 21 | 1 hr | No |
| | | Pulse 1100 kPa<br>(160 psi)<br>100 mS | 496 | 9 hr | Yes |

TABLE III. FELT MATERIALS TEST RESULTS

| | Temperature | Cleaning | Cycles | Time | Failed |
|---|---|---|---|---|---|
| ICI<br>Saffil Alumina | $815^{\circ}C$ | Reverse Flow | 75 | 3 hr | No |
| | $815^{\circ}C$ | Pulse 1100 kPa<br>(160 psi)<br>100 mS | 9405 | 49 hr | Yes, seam |
| ICI<br>Saffil Alumina | $815^{\circ}C$ | Pulse 1100 kPa<br>(160 psi)<br>100 mS | 7450 | 38 hr | No |

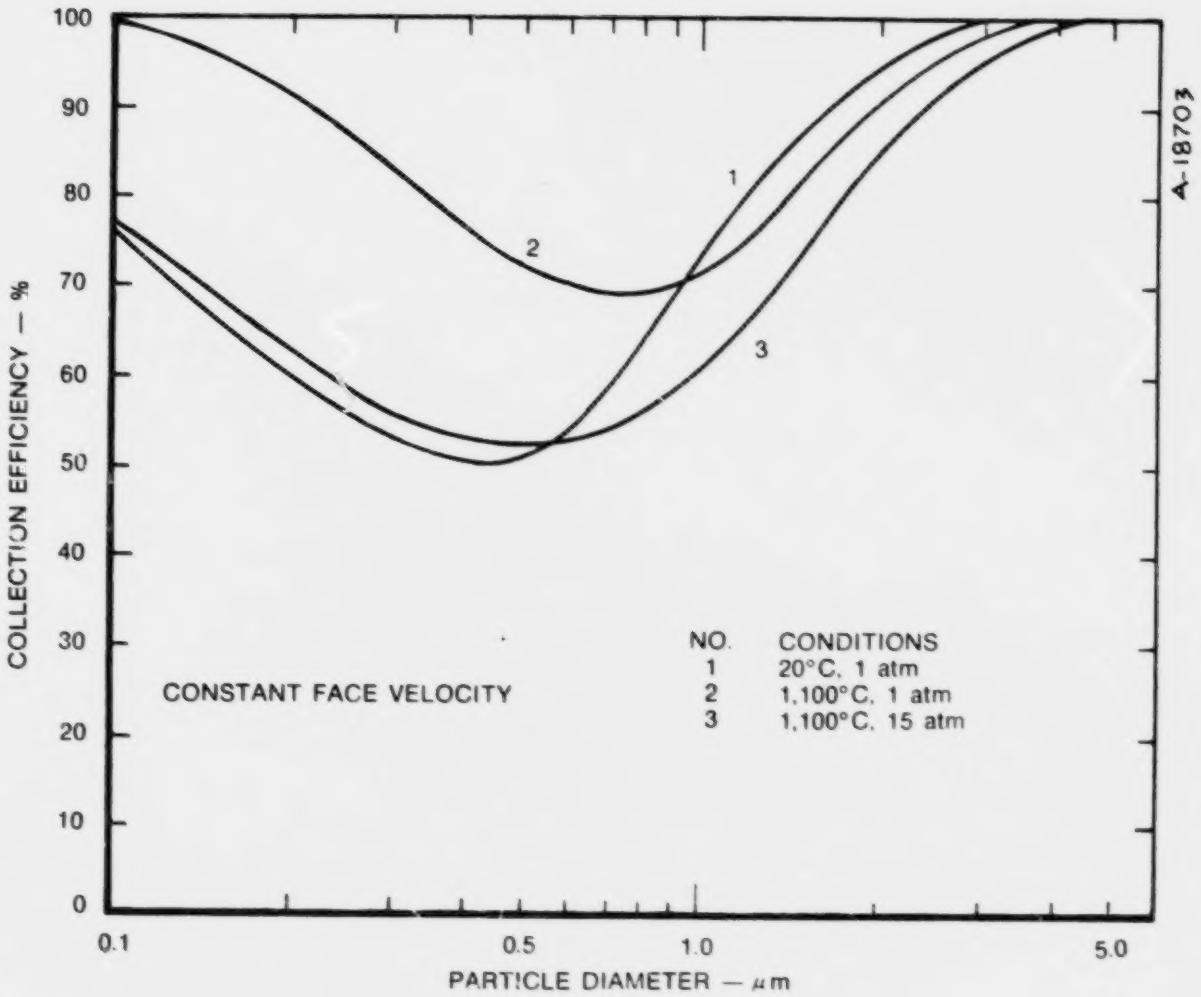

Figure 1. The effects of high temperature and pressure on the collection efficiency of a fiber bed.

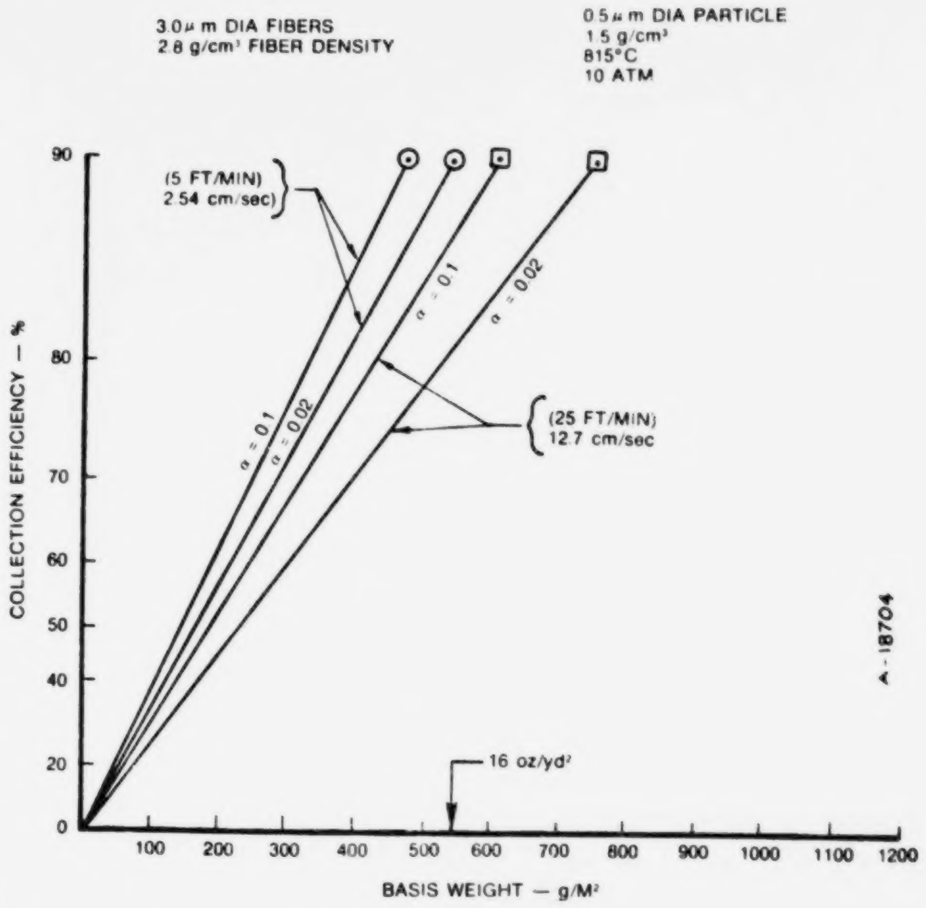

Figure 2. Calculated performance 3.0 µm alumina fiber bed.

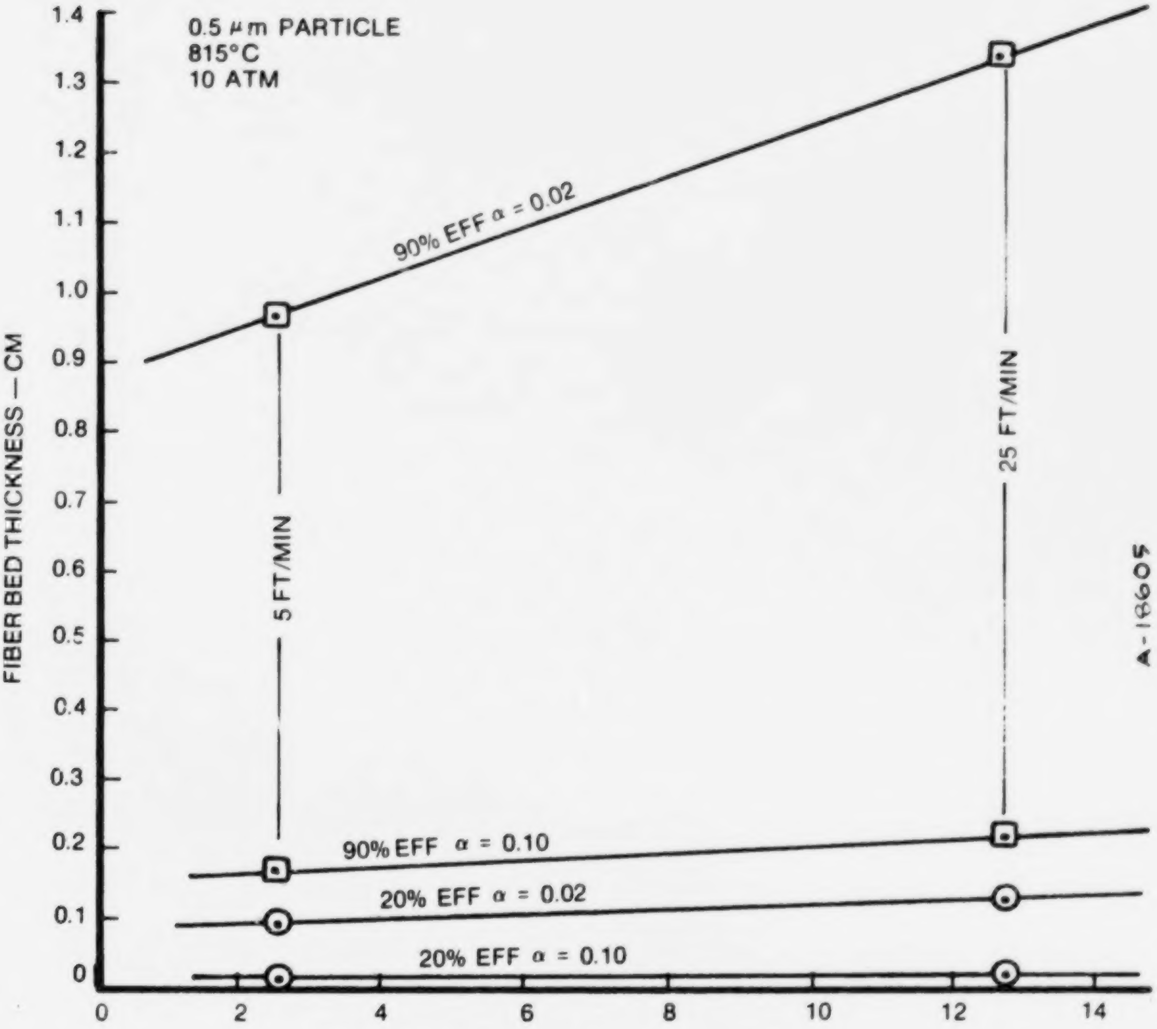

Figure 3. Fiber bed thickness.

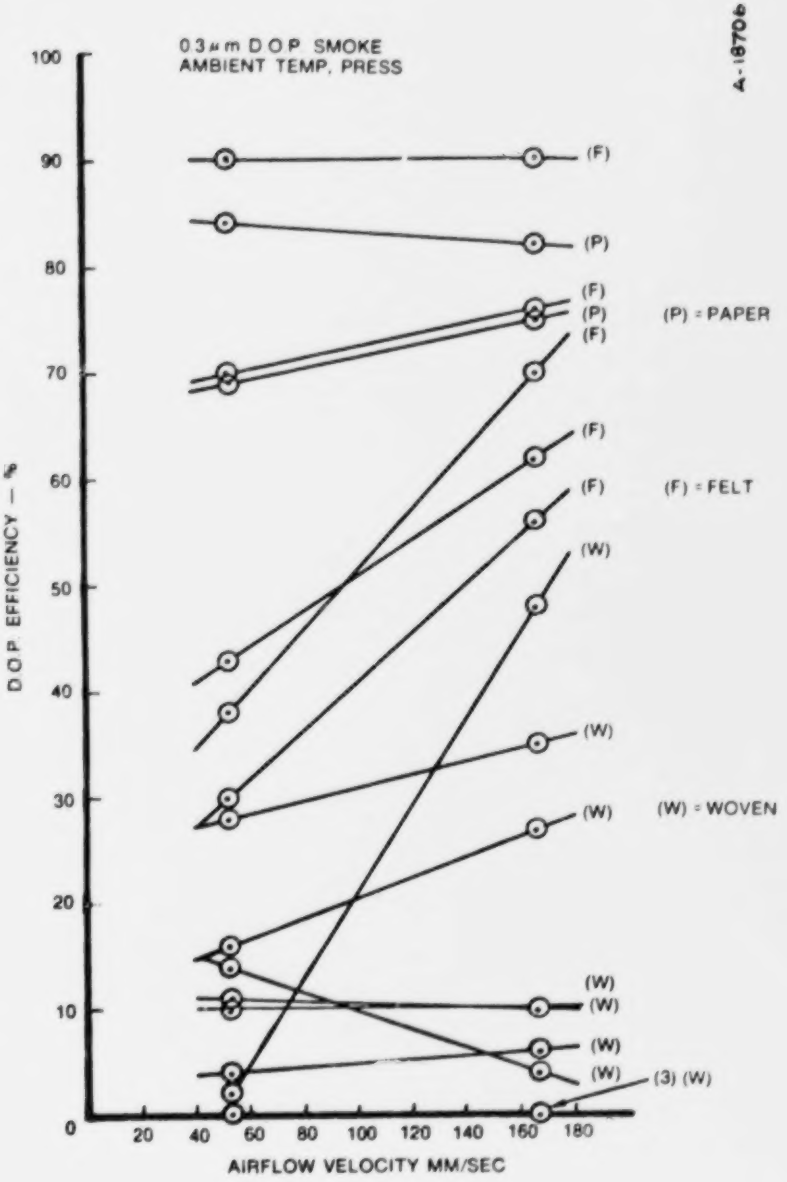

Figure 4. D.O.P. efficiency test data.

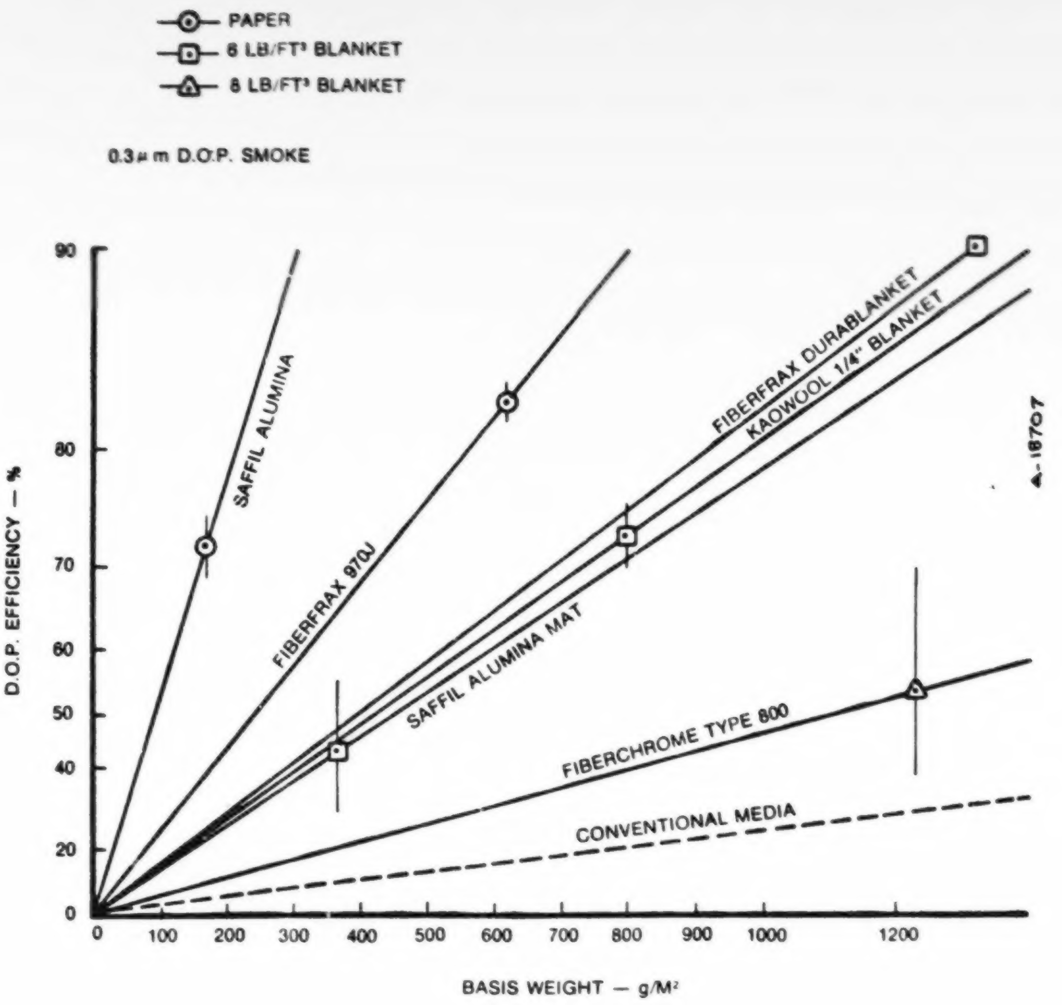

Figure 5. DOP efficiency test data.

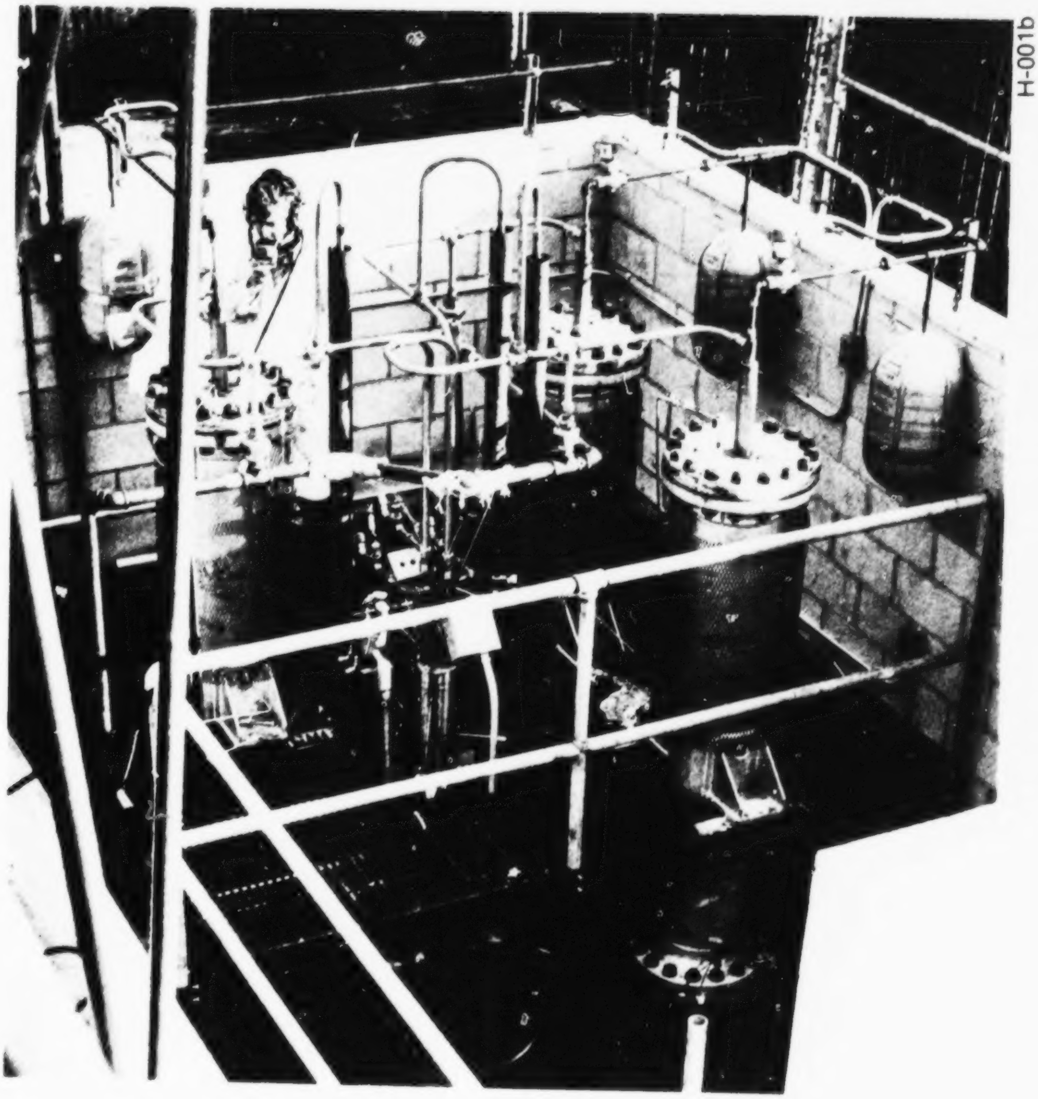

Figure 6. Hot filtration facility.

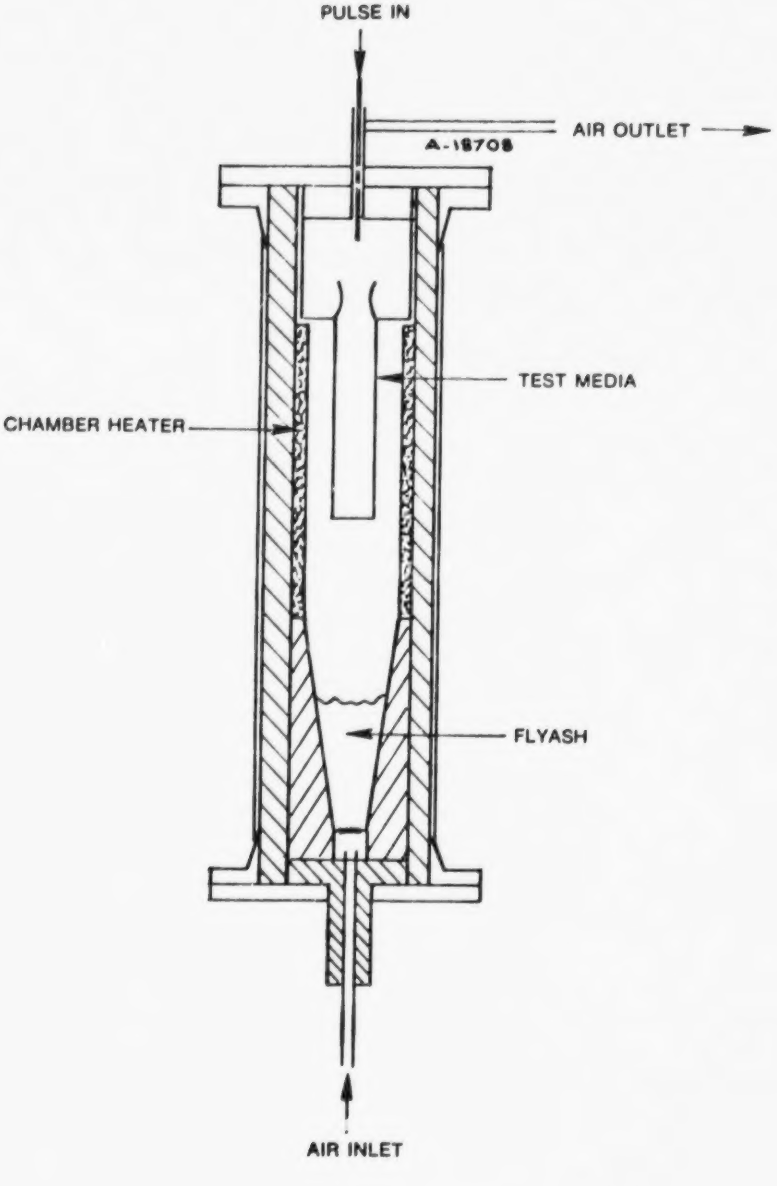
PULSE IN
AIR OUTLET
A-18708
TEST MEDIA
CHAMBER HEATER
FLYASH
AIR INLET

Figure 7. Test chamber cross section.

AEROTHERM FACILITY MODIFIED AIR SYSTEM

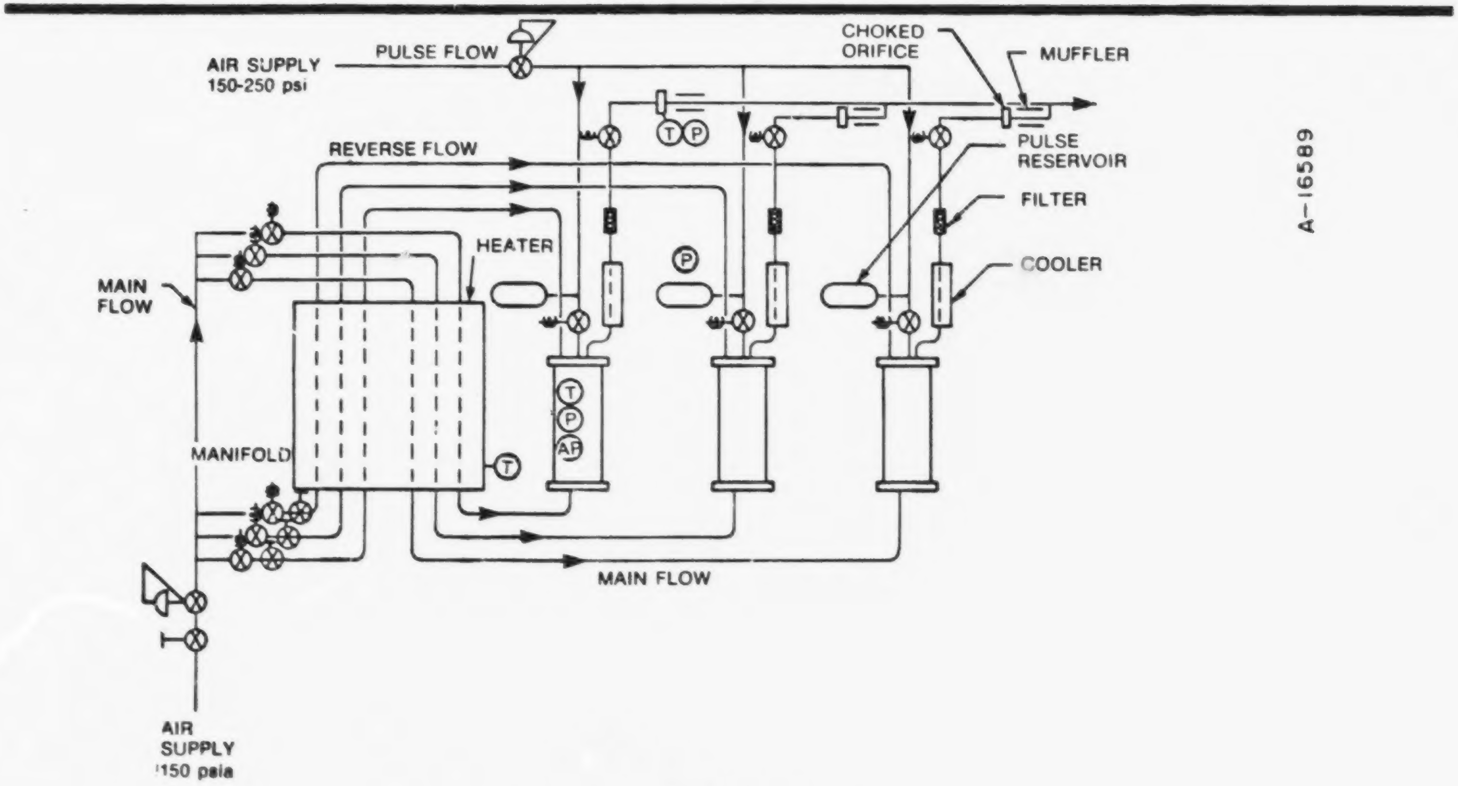
AIR SUPPLY 150-250 psi
PULSE FLOW
CHOKED ORIFICE
MUFFLER
REVERSE FLOW
PULSE RESERVOIR
FILTER
HEATER
COOLER
MAIN FLOW
MANIFOLD
MAIN FLOW
AIR SUPPLY '150 psia
T
P
AP
A-16589

Figure 8. HTHP media test facility schematic.

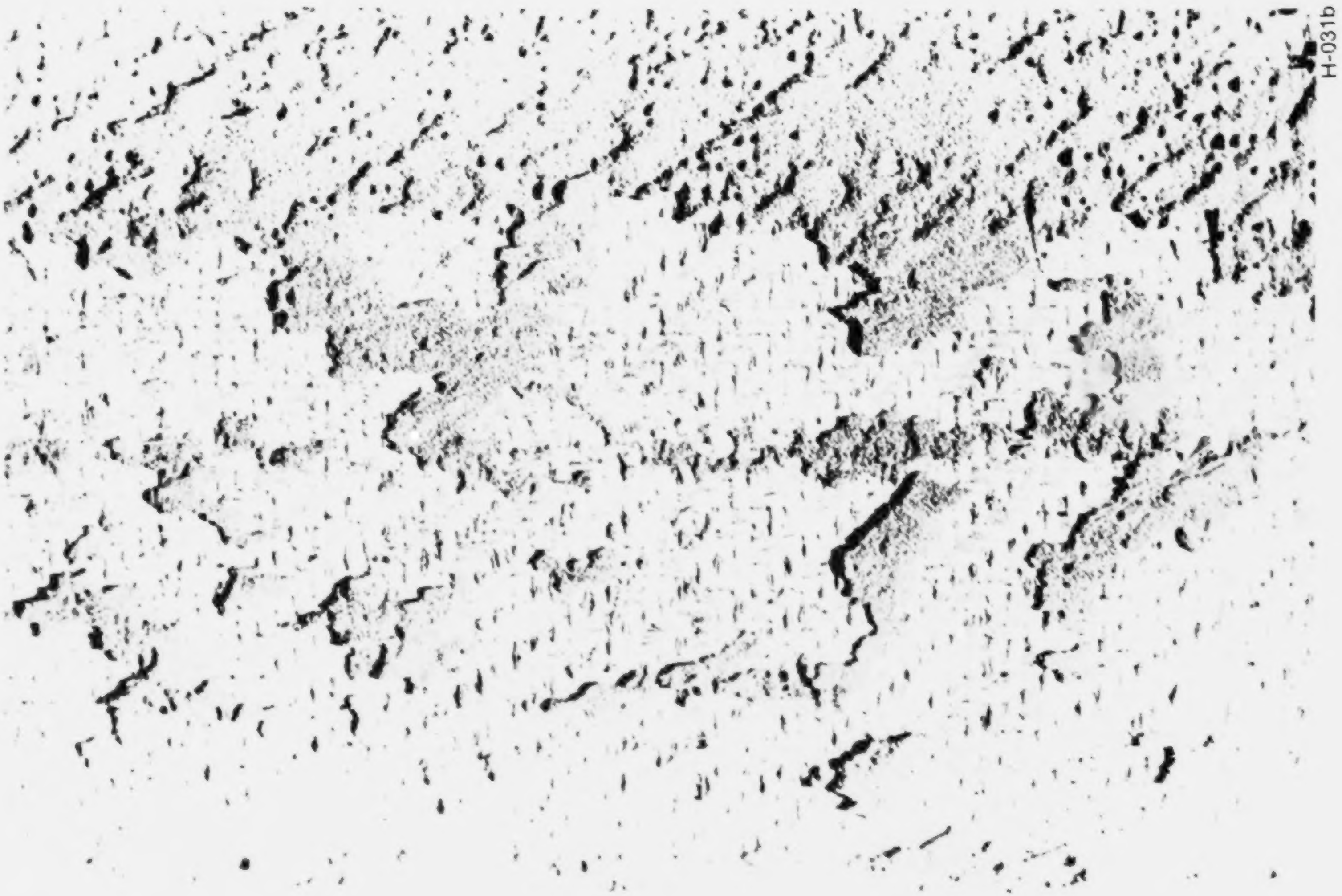

Figure 9. Post-test dust cake — Test B103 3M-AB312 twill weave.

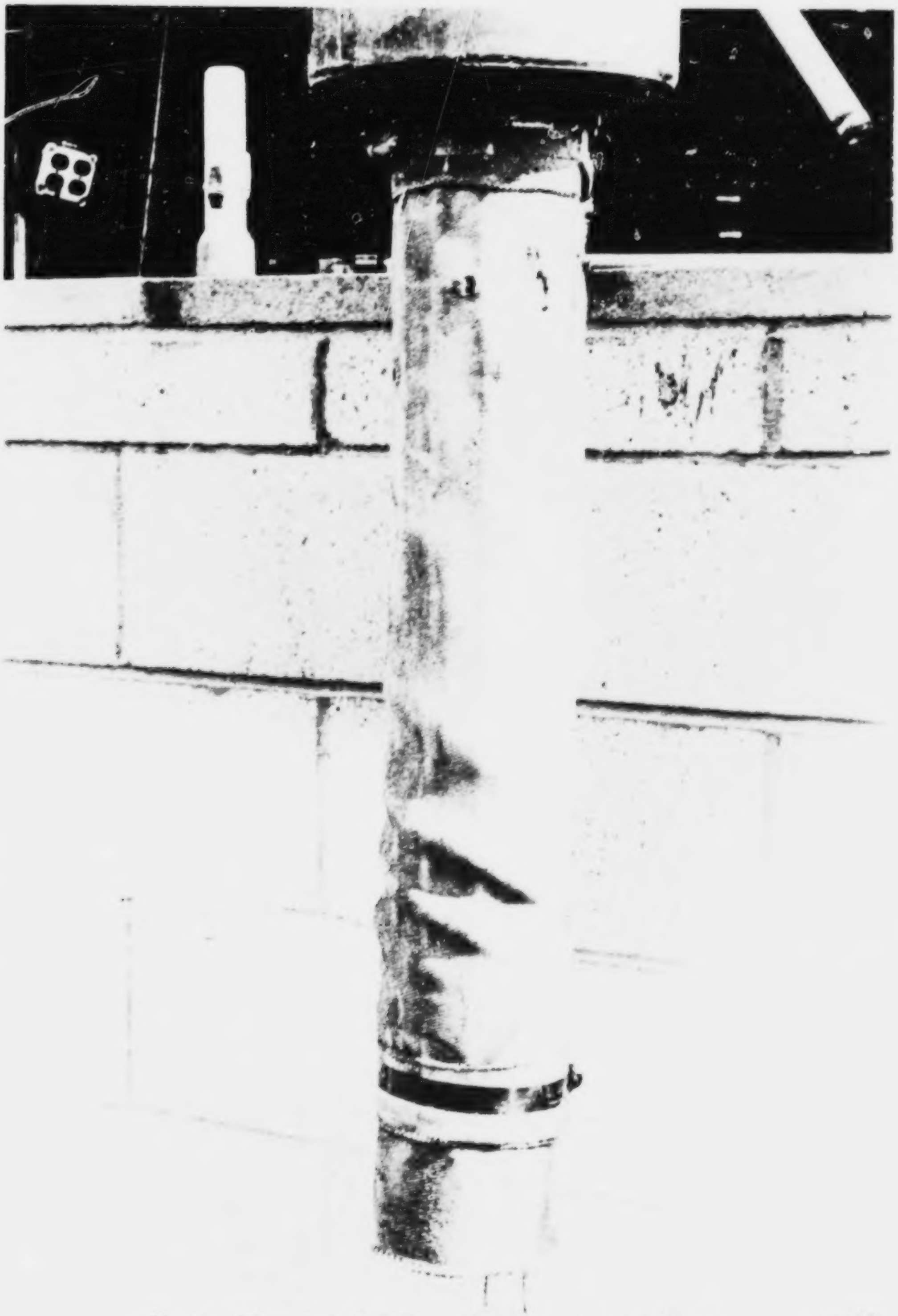

Figure 10. Irish Refrasil pulse test failure. H-029b

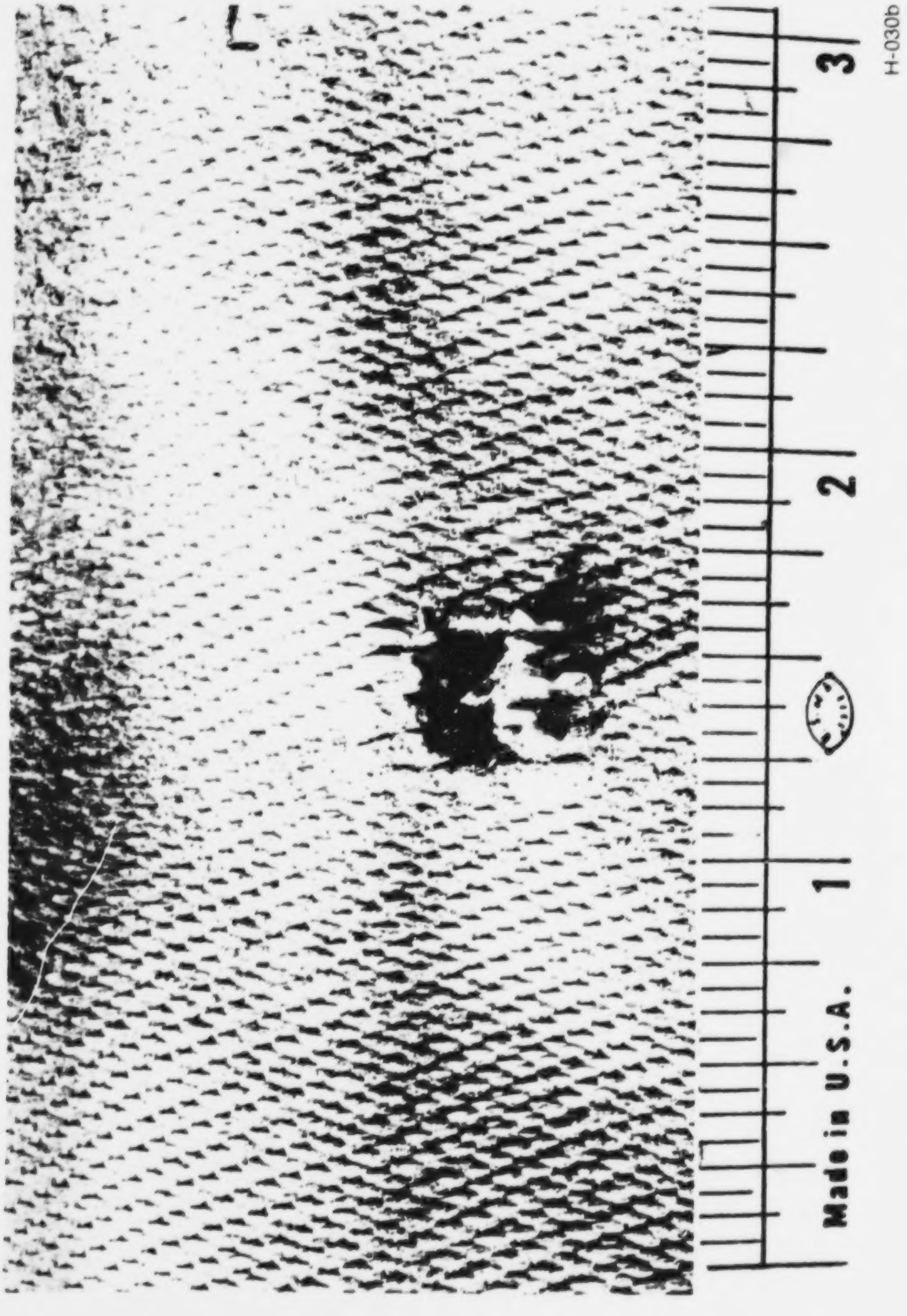
H-030b
3
2
1
Made in U.S.A.

Figure 11. Irish Refrasil pulse test failure.

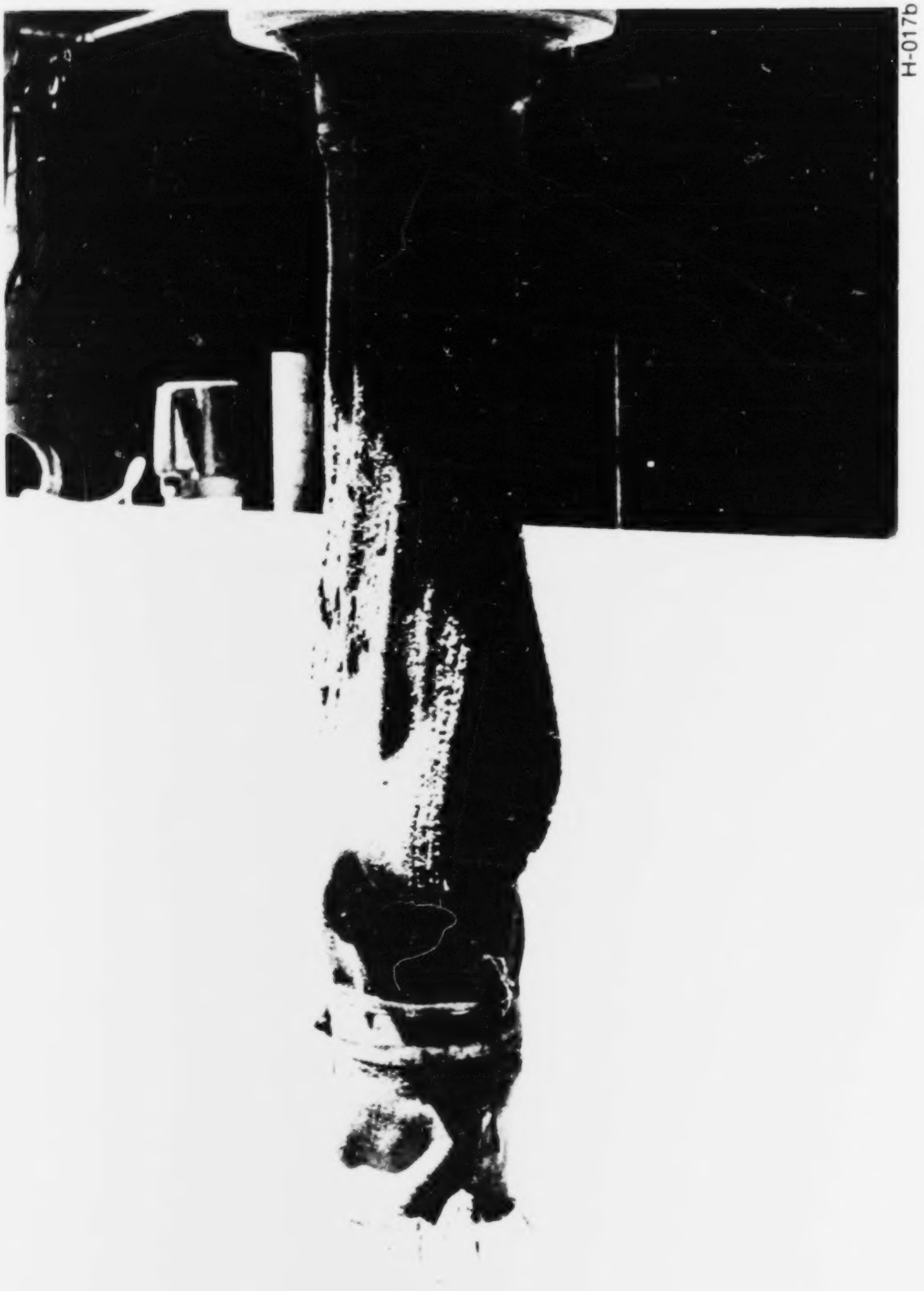

Figure 12. Refrasil media seam failure.

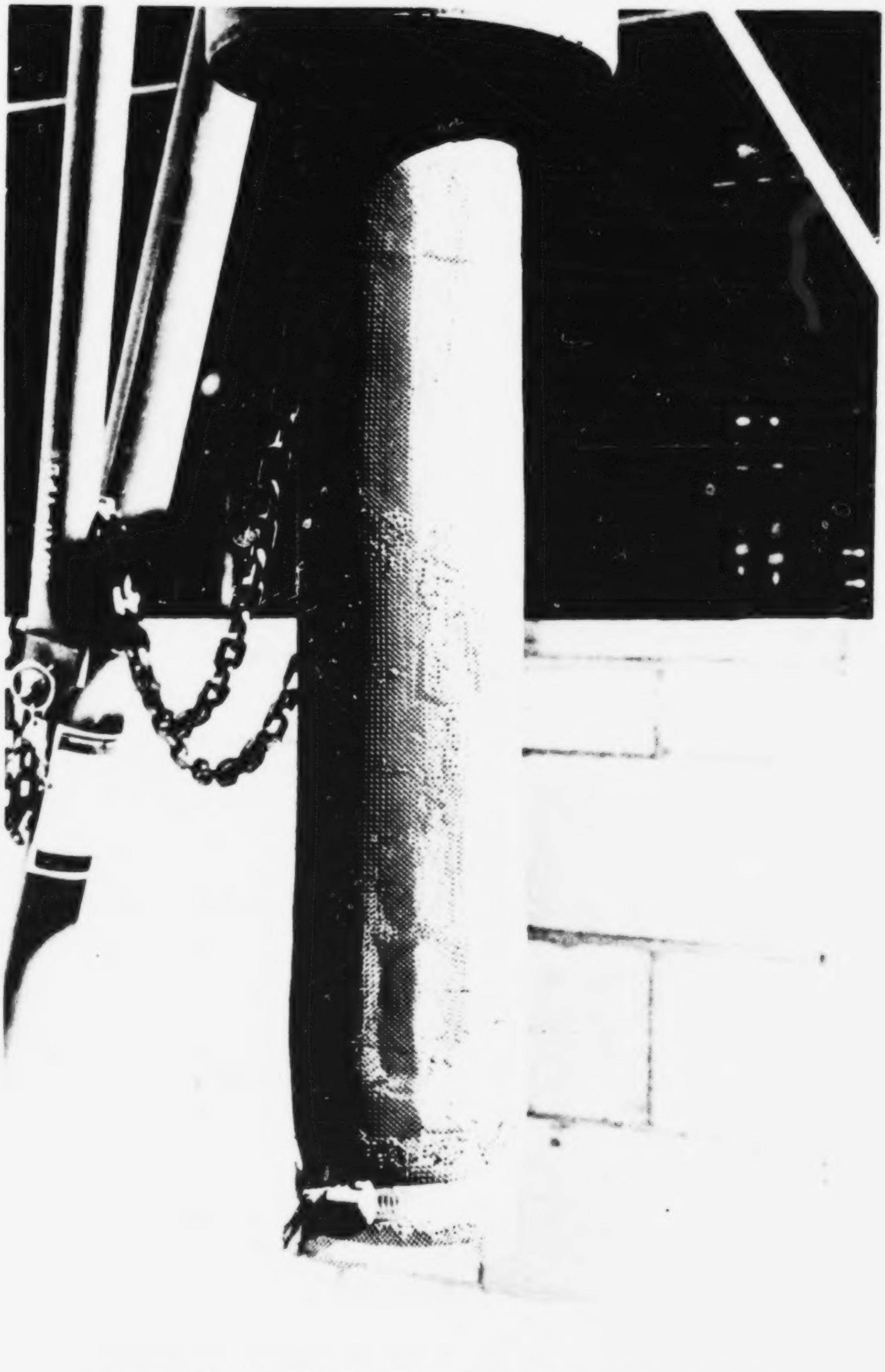

Figure 13. Saffil alumina paper after pulse testing.

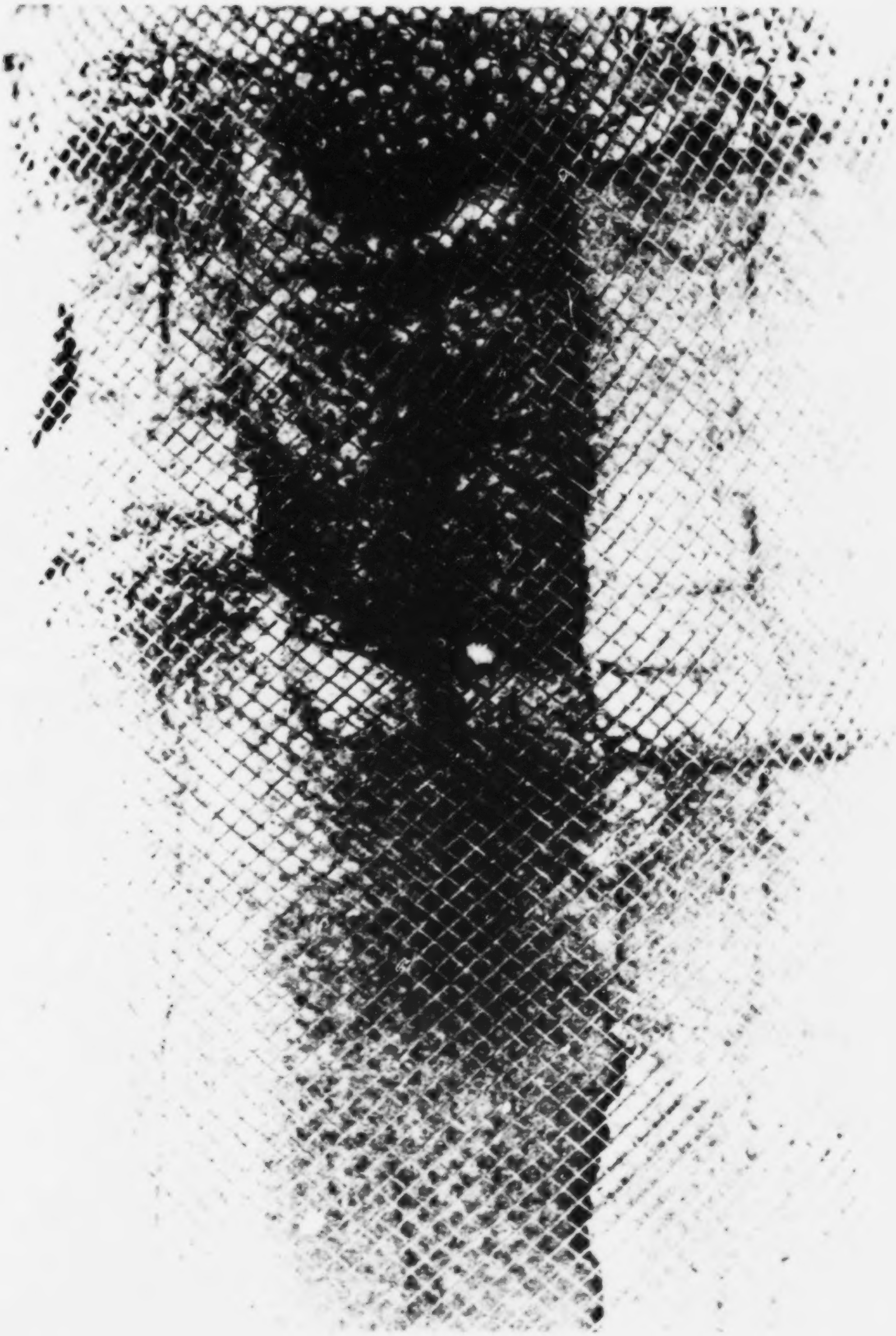

Figure 14. Saffil alumina paper after pulse testing.

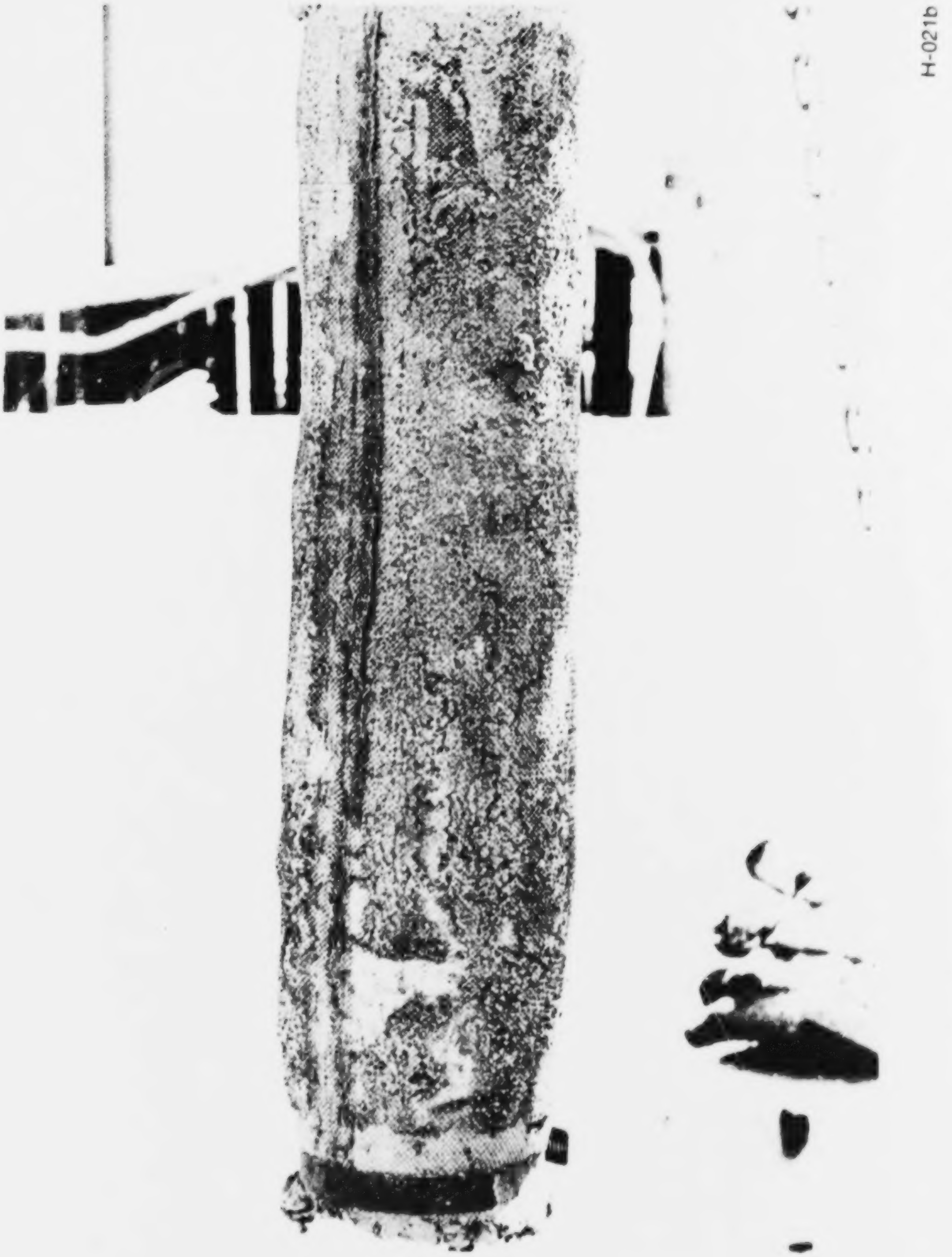

Figure 15. Saffil alumina felt bag post-test.

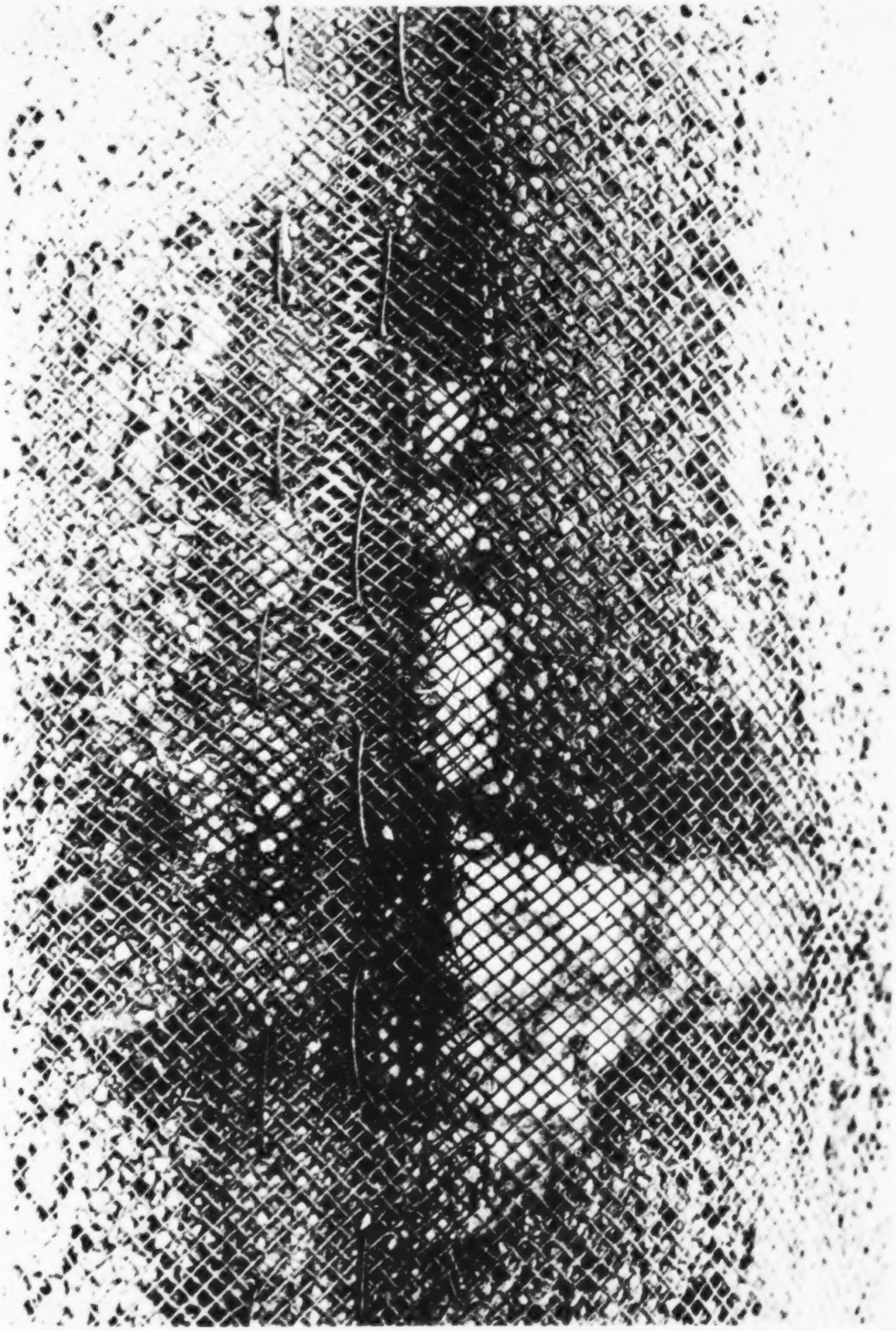

Figure 16. Separated seam.

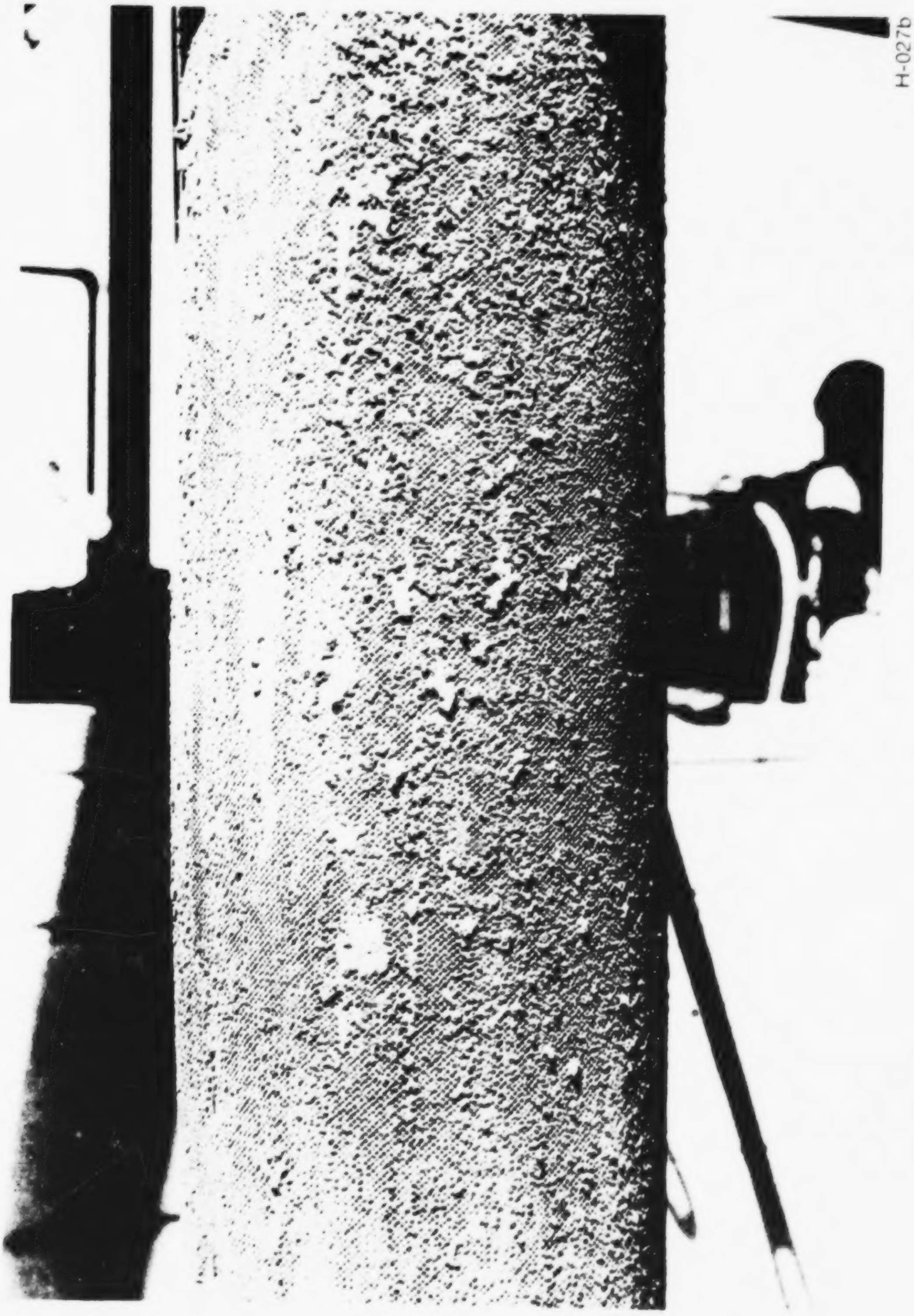

Figure 17. Saffil alumina blanket after pulse tests.

# HIGH TEMPERATURE FINE PARTICLE CONTROL USING CERAMIC FILTERS

By:

D. C. Drehmel
Environmental Protection Agency
Industrial Environmental Research Laboratory
Research Triangle Park, NC 27711

D. F. Ciliberti
Westinghouse Electric Corporation
Pittsburgh, PA 15235

## Introduction

During the next two decades, the use of coal for the generation of electrical energy in the United States will triple. New coal-fired power plants will be built whose total capacity will almost equal that of plants currently installed. There is a real need for a lower cost, higher efficiency, less polluting means of generating power from coal. Gasification coupled with combined gas and steam turbine generation is one promising technique. But if coal gasification with combined cycle generation is to be completely successful, a system of cleaning and burning hot fuel gases is needed to meet emission standards on particulates, and to protect high temperature turbine blading.

Consequently, the objective of this work was to establish the technical and economic feasibility of using a porous ceramic filter for fine particle control in advanced power systems.

## Theory

Experimental information is available in the literature on various filtration devices which have similar operating characteristics to the ceramic filter.

The most appropriate information is on membrane (e.g. "Millipore") filters which have controlled pore sizes in the sub micron range. For example, Fitzgerald(1) and Detweiler found complete retention of particles greater than 0.1 μm diameter on Millipore filters with 0.85 μm pores. Minimum collection was found with particles approximately 0.02 μm diameter and this minimum varied with the superficial gas velocity. (78% at 10 cm/sec., 20% at 40 cm/sec.).

Porous metal filters have been used extensively for particle collection from high temperature gases. Complete retention down to 1 μ is reported, and good efficiency for sub micron particles is implied.(2)

Fabric filters rely on an accumulated filter cake to provide high efficiency dust collection. This will also occur with the ceramic membrane filters. Consequently collection efficiencies with the ceramic membrane should be at least as high as for fabric filters operating under similar conditions. 95 to 99% collection of sub micron particles has been reported in fabric filter installation.

Particles which penetrate the filter cake may also penetrate into the ceramic pore structure. If a pore size of 1 μm is assumed, all particles greater than 1 μ will be collected, however, there will be a significant possibility that smaller particles will be collected within the pores, or alternatively, will penetrate the filter.

A simplified method of calculating Brownian deposition suggested by Kaufmann(3) has been used to examine this situation. This assumes that in deposition from laminar flow, all particles moving along stream lines located a distance x from a collector surface would be deposited on the collector, if x was equal to the mean Brownian displacement in the x direction, i.e.:

$$x = \sqrt{\frac{4Dt}{\pi}}$$

(D is Brownian diffusivity and t is time of flow past the collector).

This is modified for collection in a cylindrical pore by allowing for the possibility of collection in both the x and y directions. As a consequence "x" becomes

$$x = \sqrt{\frac{8Dt}{\pi}}$$

Complete collection is achieved when:

$$x = \sqrt{\frac{8Dt}{\pi}} \geq \frac{d - dp}{2}$$

where d is the pore diameter and
dp is the particle diameter.

For a ceramic filter with 1 μm pores, and a thickness of 250 μm, complete collection is estimated at gas velocities up to approximately 30 cm/sec. (Table I).

It should be stressed, however, that not all sub micron particles will enter the pores, and it is not reasonable to assume that all particles which meet the pore wall will be captured by it. So while the estimate implies high efficiency collection it cannot be used in a quantitative sense.

Table I. Collection by Brownian diffusion in pores.

| | | Gas Velocity in Pore | | | |
|---|---|---|---|---|---|
| | | 6 cm/sec | | 30 cm/sec | |
| dp μm | D $cm^2$/sec | $\sqrt{\frac{8Dt}{\pi}}$ μm | $\frac{d - dp}{2}$ μm | $\sqrt{\frac{8\,Dt}{\pi}}$ μm | $\frac{d - dp}{2}$ μm |
| 0.7 | $1.9 \times 10^{-7}$ | 0.44 | 0.15 | 0.20 | 0.15 |
| 0.5 | $2.8 \times 10^{-7}$ | 0.53 | 0.25 | 0.24 | 0.25 |
| 0.3 | $5.0 \times 10^{-7}$ | 0.66 | 0.35 | 0.30 | 0.35 |
| 0.1 | $2.7 \times 10^{-6}$ | 1.48 | 0.40 | 0.66 | 0.40 |

If particles are deposited in the pores, as suggested above, they must subsequently be removed in the clean up cycle if a useful filter life is to be achieved. A reverse flow of gas equivalent to the initial forward flow is unlikely to dislodge such particles and a high velocity surge may be required.

Pall(2) suggests that a low flow for clean up is preferred, such that the accumulated cake is removed from the filter surface, but a protective population of particles is left clustered at each pore opening. These particles prevent penetration of other particles into the pore.

## Experimental Methods

Several ceramic materials in many configurations were screened as possible high temperature filters. One of the most promising materials tested was a ceramic cross flow monolith produced by 3M Company under the tradename of ThermaComb. This material is composed of alternate layers of corrugations separated by thin filtering barriers. This type of configuration affords a large amount of filter surface in a very small volume.

Bench side experiments were conducted in the high temperature ceramic test facility shown in Figure 1. Part of this facility included a test jig for the ThermaComb material which is shown in Figure 2. Provisions were made to blow back from the clean side and also down the channels on the dirty side so that various cleaning schemes could be investigated. A schematic of the testing loop is shown along with the sequence to be used for the cleaning cycle in Figure 3. A sequencer was designed to automatically step the system through the cleaning cycle so that the operation of the system after start up was automatic. A 17.8 cm diameter by 38 cm deep tubular furnace was used to heat the filter. An additional furnace was added to preheat the dust laden air.

The size distribution of the test dust (limestone) was determined using cascade impactors. The typical mass median diameter was 1.4 μm and the geometric deivation was 3.0. Some difficulty in maintaining constant feed rate was experienced but dust loadings were maintained at levels from 2 $gm/m^3$ to 7 $gm/m^3$.

## Results

Typical results for the 3M ThermaComb filtering the limestone test dust are shown in Figures 4 and 5. Figure 4 shows the effect of varying the initial pressure of a 0.6 sec pulse. The 69 kPa initial pressure dropped to a steady pressure of 34.5 kPa for the remainder of the .6 sec pulse and the 34.5 kPa pulse dropped somewhat below 10 kPa. Figure 5 shows the result of a similar set of runs except that the pulse time was increased to 5 sec. from 0.6 sec. It can be seen from these data that the length of the pulse does not have much effect on the cleaning results. In both runs the collection efficiency was very high (99.6 to 100%) at a linear velocity of 0.41 m/min (1.33 ft/min.). Using the 103.4 kPa pressure pulse for cleaning it was possible to return to a stable pressure drop across the filter in spite of the relatively high dust loadings which in these two runs were 2.6 and 3.75 $gm/m^3$.

## Discussion of Results

The behavior of the ceramic filter is remarkably similar to that of fabric filters, with a short transient of rapid increase in pressure drop followed by a steady, linear increase in $\Delta P$ with time. The data is consistent with filteration theory as indicated by the following analysis. The total pressure drop is considered to consist of a contribution due to the media $\Delta P_m$, and due to the accumulated cake, $\Delta P_c$.

$$\Delta P_{tot} = \Delta P_m + \Delta P_c$$

For given gas properties, the pressure drop across a filter media, $\Delta P_m$, is proportional to the face velocity, U and filter thickness, $L_m$. The pressure drop across the cake is similarly proportional to the face velocity and cake thickness $L_c$. If a constant dust concentration, C, is assumed, the cake thickness is proportional to the product of the measured variables, UCt, where t is time. The total pressure drop for a given gas, temperature and filter is given by:

$$\Delta P_{tot} = K'U + KU^2tc,$$

where K' and K are constants for a given filter and incompressible cake. The linear dependence of $\Delta P_{tot}$ on time is substantiated by the steady part of the $\Delta P_{tot}$ vs. t curves. Confirmation of the assumed form of dependence of the variables U and C can be achieved by plotting the slope of the $\Delta P_{tot}$ vs. t curves, normalized by division by $U^2$ vs. C. This plot should yield a straight line with a slope equal to K which is a property of the filter cake and gas viscosity only. Figure 6 presents this data and indicates that the assumed form of $\Delta P_c$ is confirmed by all the data.

Two further observations of major importance can be made concerning the initial steady pressure drop.

(1) The magnitude of the initial steady pressure drop is not prohibitively high.

(2) The initial steady pressure drop remained constant with the adopted cleaning technique.

## Conclusions

Tests using the 3M ThermaComb as a filtering media were conducted at temperatures from ambient to 970°K. Filtering efficiency was found to be close to 100% even though the test dust had a mass median diameter of 1.4 μm and a significant fraction of sub micron material. Cleanability of the media was verified in experiments evaluating the effect of cleaning pulse intensity and duration. It was determined that the ceramic filter behaved similarly to fabric filters in that the pressure drop could be attributed to a residual pressure drop and that across an incompressible cake.

References

1. J. Fitzgerald and C. Detweiler, Arch. Ind. Health 15, 3, (1957).

2. D. B. Pall, Ind. Eng. Chem., 45, 1197 (1953).

3. A. Kaufmann, Z. Ver Deutsch Ing. 80, 593, (1936).

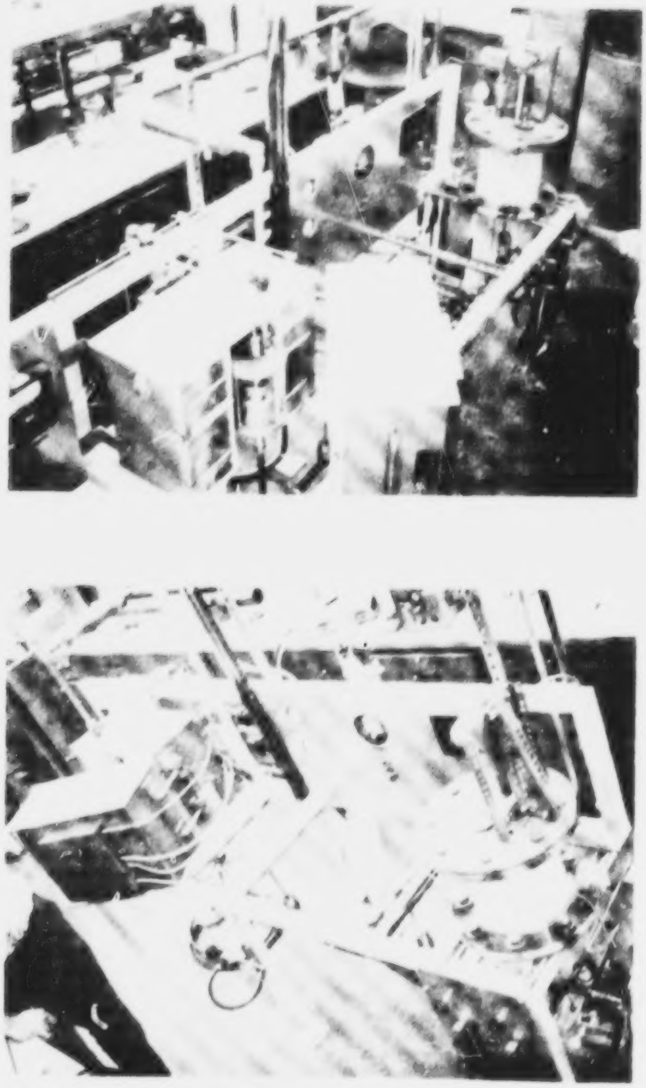

Fig. 1 — High temperature ceramic test facility

CS-667[illegible]

D. Ciliberti
m.m. - k.b. 8/12/76

Dwg. 1684B44

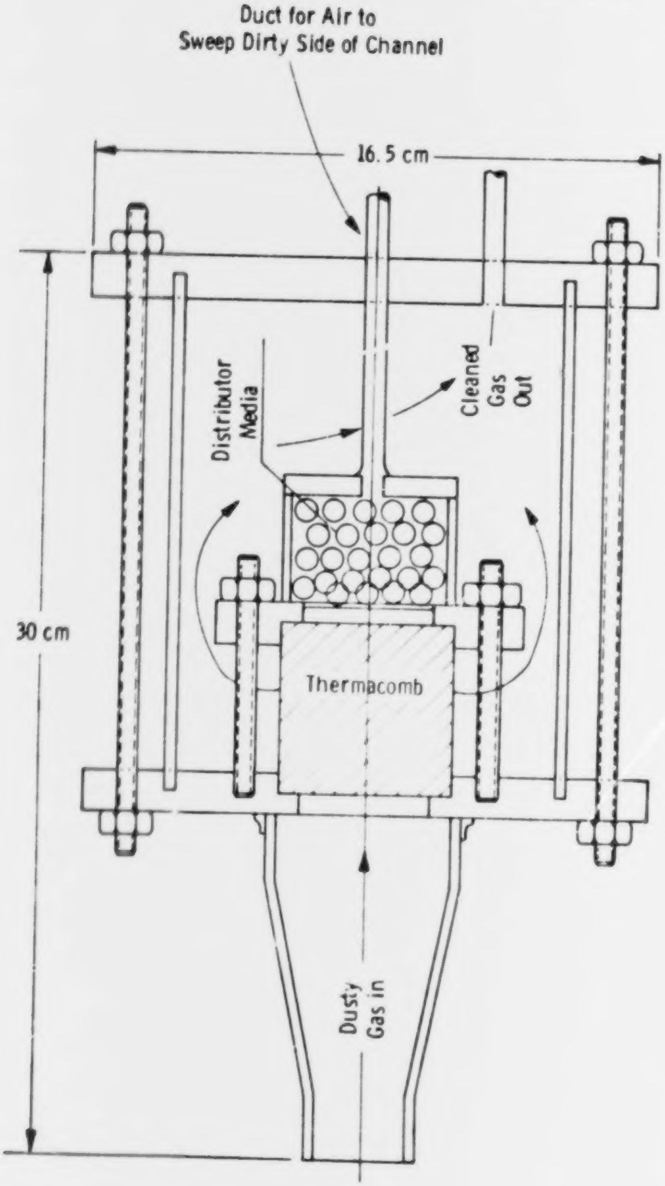
Duct for Air to Sweep Dirty Side of Channel
16.5 cm
Distributor Media
Cleaned Gas Out
30 cm
Thermacomb
Dusty Gas in

Fig. 2—Hot thermacomb test jig

Dwg. 1684B44

Dwg. 6387A60

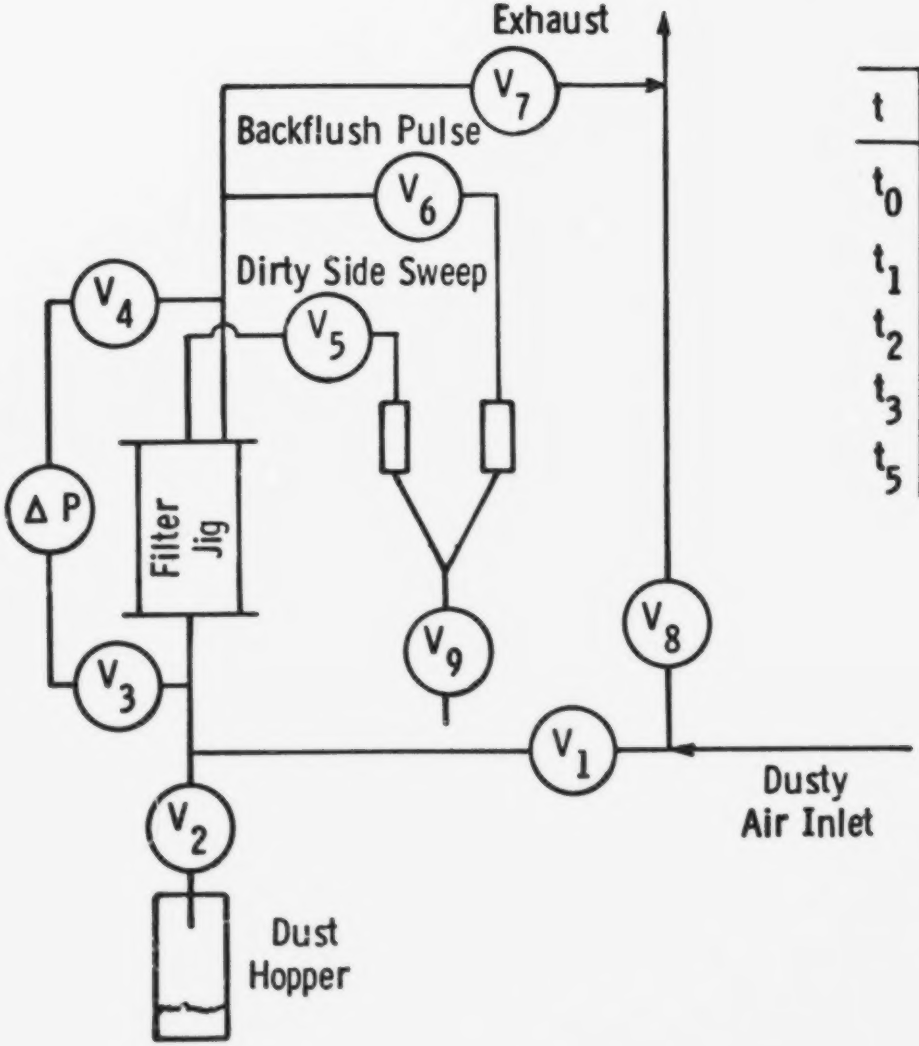
Exhaust
V7
Backflush Pulse
V6
Dirty Side Sweep
V4
V5
ΔP
Filter Jig
V9
V8
V3
V1
V2
Dusty Air Inlet
Dust Hopper

Cleaning Sequence
0 – Open
C – Closed

| t | $V_1$ | $V_2$ | $V_3$ | $V_4$ | $V_5$ | $V_6$ | $V_7$ | $V_8$ | $V_9$ |
|---|---|---|---|---|---|---|---|---|---|
| $t_0$ | 0 | C | 0 | 0 | C | C | 0 | C | C |
| $t_1$ | C | 0 | C | C | C | C | C | 0 | C |
| $t_2$ | C | 0 | C | C | 0 | 0 | C | 0 | C |
| $t_3$ | C | 0 | C | C | C | C | C | 0 | 0 |
| $t_5$ | 0 | C | 0 | 0 | C | C | 0 | C | C |

Fig. 3— Flow schematic and cleaning sequence for low flow-high temperature system

D. Ciliberti
l.t. - k.b. 8/12/76

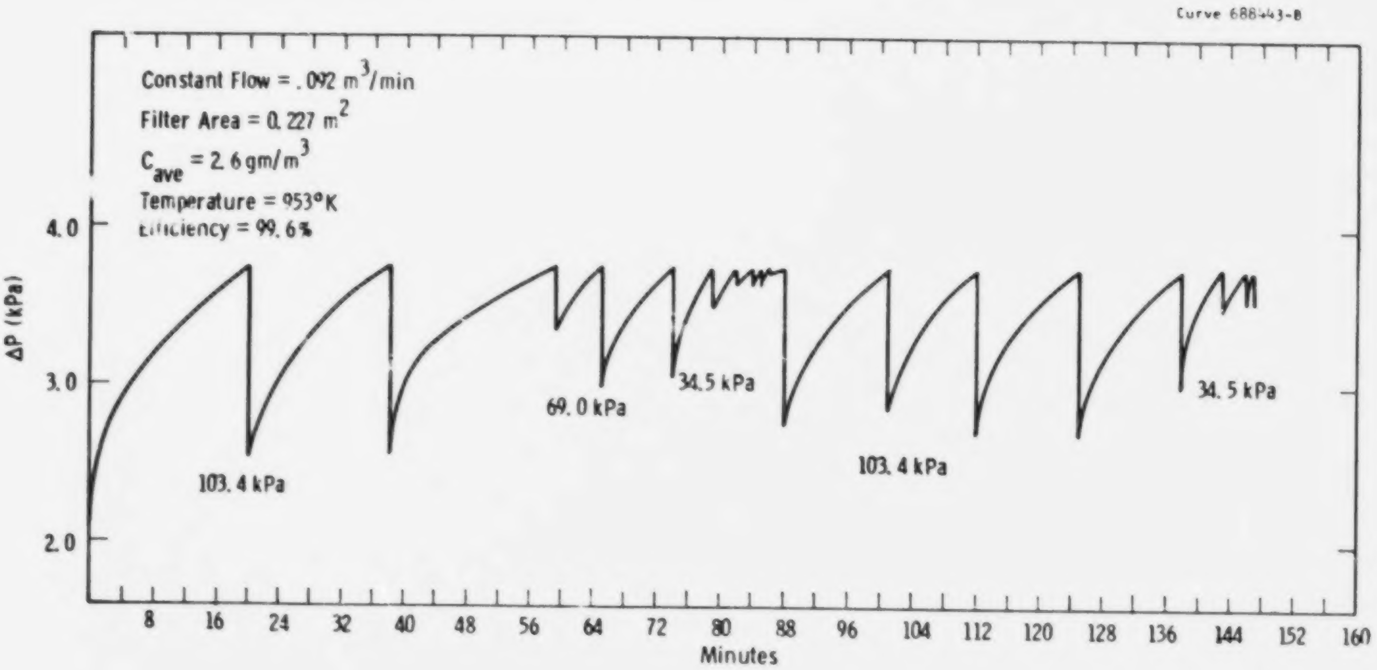

Fig. 4— Hot thermacomb test

J. H. Meyer
I. t. - r. m. 1-13-77

Curve 688443-B

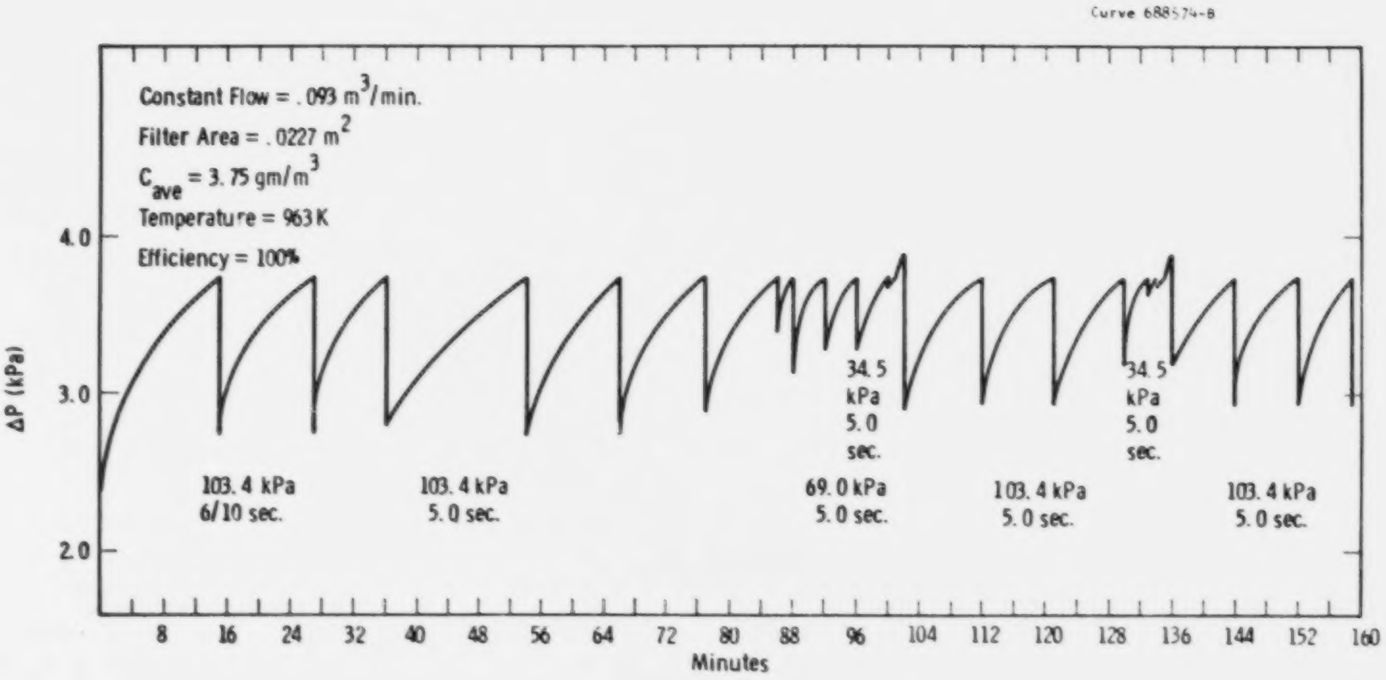

Fig. 5 – Hot thermacomb test

J. H. Meyer
I. t. - k. b. 1/19/76
Ⓐ

Curve 688574-B

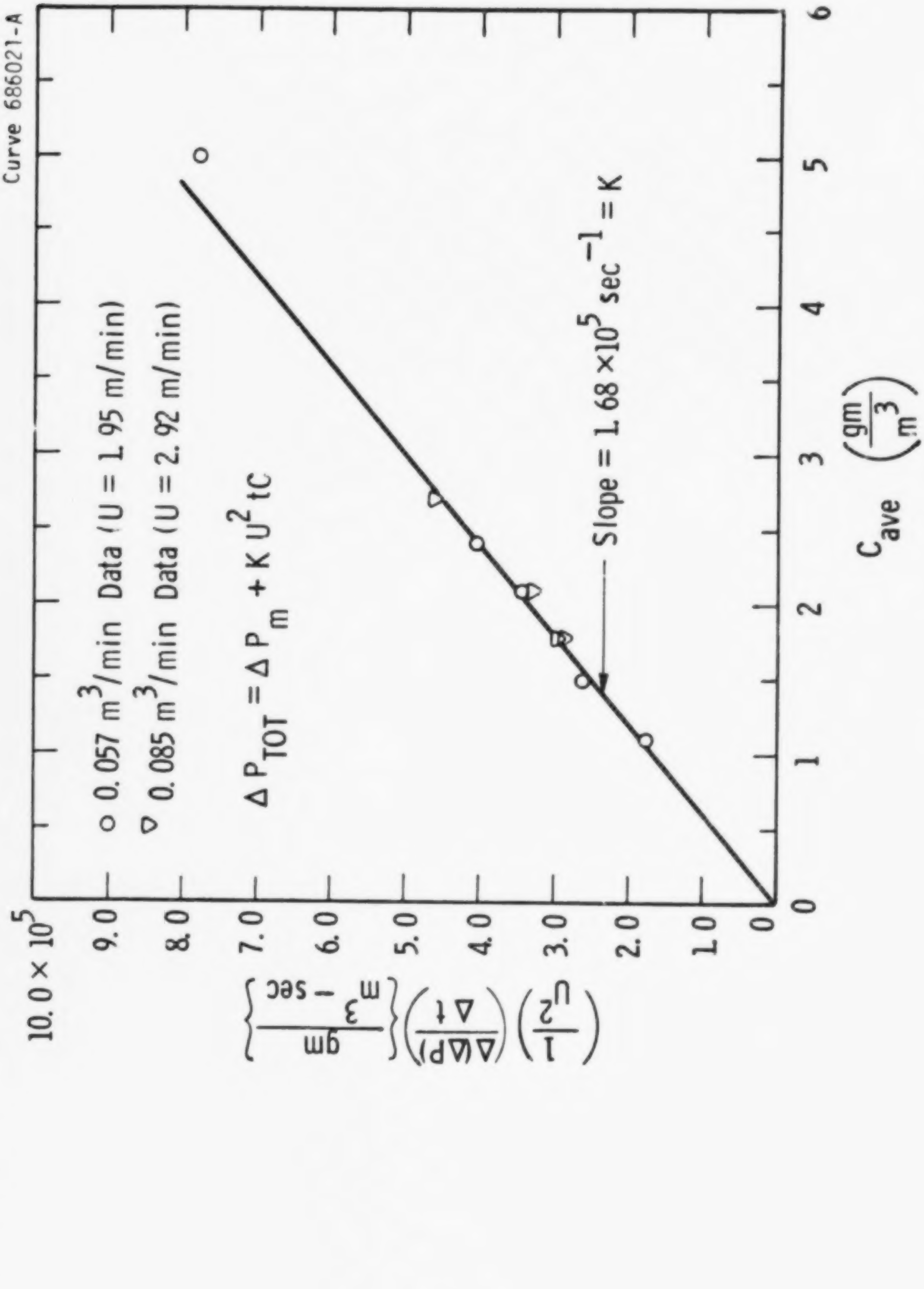

Fig. 6— Determination of filter cake constant

D. Ciliberti
l.t. - r.m. 7-13-76

Curve 686021-A

# PROBLEMS OF GAS PURIFICATION OCCURRING IN THE USE OF NEW TECHNOLOGIES FOR POWER GENERATION

By:

E. Weber
University Essen
West Germany

BLANK PAGE

## Problems of Gas Purification Occurring in the Use of New Technologies for Power Generation

In the Federal Republic of Germany there are some conceptions for new coal conversion technologies based on the assumption that the development of conventional steam power plants has in principle attained perfection. The optimum efficiences which are usually between 36 and 37 % will decrease somewhat by the employment of waste gas desulfurization plants due to their requirement for additional energy.

Among the new technologies expected to increase considerably the efficiency of power plants are the combined gas steam turbine processes preceded by a suitable coal conversion system. For the latter there are coming into consideration

- Fluid bed combustion
- Fixed bed gasification
- Partial dust gasification
- Fluid bed gasification.

As an example figure 1 shows the application of the combined gas steam turbine process behind a fluid bed combustion. The crushed coal is passed to a pressure tank and burned in a fluid bed. It is a precondition for the application of a gas turbine that the west gases formed in the tank are dedusted and desulfurized to a large extent before passing to the turbine. To avoid a decreasing efficiency of the process the gas purification is required to cause minimum losses of heat and pressure.

Nearly the same problems arise in the case of the so-called fixed bed gasification ( Figure 2 ). The coal is gasificated by the use of air. The formed lean gas has a temperature of about 600 °C and pressures up to 2o bars. Before the combustion in the vessel the gas is partially expanded and the resulting energy is utilized by a gas turbine.

This and the reaction of the gases in the vessel are only practicable when the lean gas has been already dedusted to a far extent and when the hydrogen sulfide and sulfur dioxide contents of the gas have been reduced - if possible at operating temperatures and pressures. At present a pilot plant with a throughput of 60 tons coal per hour, equivalent to a power output of 170 MW, is tested at Lünen by the STEAG using five LURGI fixed bed gasifiers. Among others, however, a sufficient solution is missing for the problems of gas purification at operating temperatures and pressures.

Similar problems with respect to the necessary gas cleaning system for high temperatures and pressures occur also in the case of the partial dust gasification and the fluid bed gasification. These processes are not discussed explicitly in this paper.

It can be summarized that the gas purification represents an important element of the coal conversion processes. The gas purification has apart from the necessary desulfurization to fulfill the following conditions:

1) Precipitation of the solid components down to dust contents of less than 5 mg/m$^3$ at S.T.P.

2) Dust separation at gas temperatures up to 1000 °C and pressures up to 40 bars.

Low dust contents in the purified gas are the precondition for a successful gas turbine process whereas the dust separation at the high gas temperatures and pressures is necessary to avoid efficiency losses when applicating a steam turbine process. It may be noticed that an energy sparing high temperature and high pressure purification is of major interest not only for power plants but even for other branches of industry e.g. in the case of remelting processes and refuse and sludge burning.
It shall be discussed whether a dust separation under extreme conditions is possible with known dust separators or whether new seperating systems have to be developed. To illustrate the situation figure 3 shows a survey of well known dust separation systems and their efficiency. The gas purification systems are divided into four groups:

Gravity and momentum separators
Fabric filters
Electrostatic precipitators
Wet scrubbers

Without further discussion of the separation effects of each single apparatus it can be stated that the obtainable efficiency is different for each separator system. Gravity and momentum separators depending on the mass of the solid particles usually attain a poor or average dust separation. Fabric filters and electrostatic precipitators however reach high degrees of separation. In principle this aim can also be achieved by the use of suitable wet scrubbers.

In the last row of figure 3 there are the maximum values of the gas temperatures and pressures that have been realized for each dust separator system till today. It can be seen that only gravity and momentum separators can be applicated at high temperatures whereas there is an upper limit for fabric filters and electrostatic precipitators at about 350 °C. The corresponding value for wet scrubbers is at about 100 °C. According to the laws of physics the gas pressures can have any magnitude for all dust seperator systems, except the electrostatic precipitators. For the latter it seems possible to increase the gas pressure comparable although that has not been consistently proved. Industrial plants have been built for pressures up to 3 bars.

It can be summarized that the only wellknown system applicable without complications at high temperatures and pressures are the gravity and momentum separators. Due to their mode of action even the best gravity and momentum separators do not reach low dust contents in the purified gas. Furthermore their efficiency is decreasing at high gas temperatures according to the increasing viscosity of the gas. This is illustrated in figure 4 for several pressure drops. The ratio of the collectable particle diameter at 20 °C to that of higher temperature is plotted as a function of the gas temperature up to 1000 °C. Due to these conditions it can not be expected that gravity and momentum force separators will fulfill the demands for a sufficient gas purity at high temperatures. At extreme conditions these separators can therefore only be applicated as pre-stage systems.

Very low dust contents in the perified gas can be achieved, however, by the use of fabric filters. The fibrous materials applicated on an industrial scale are till today suitable only for gas temperatures up to about 350 °C.

In principle the gas purification is also possible at high temperatures using fibrous materials which resist gas temperatures of more than 1000 °C ( Table 5 ). This fibrous materials can be divided into:

1. mineral fibres
2. graphite fibres
3. metallic fibres

According to the obtainable minimum fibre thickness all mentioned fibrous materials should be applicable for a high-grade gas purification. It is difficult, however, to process fleeces, fabrics, and felts of mineral fibres, for these materials are frequently brittle or fragile. Moreover graphite and metallic fibres are extremely expensive caused by the manufacturing processes. At present there are several investigations in the FRG concerned with new technologies for the manufacturing and processing of fibres with the aim of using these materials for gas cleaning. Besides this it is necessary to study the possibilities of cleaning and the durability of the filter materials. With financial support of the Ministery for Research and Technology the prototype of a high temperature fabric filter is under construction as shown in figure 6. Two parallel filters consisting of fleeces, fabrics, or mat weaves are used to study the properties of several materials with respect to:

1. Efficiency of dust separation
2. Durability
3. Cleaning

To generate a dust-laden waste gas a pulverized coal firing is used which can be fed additionally with oil in order to obtain higher temperatures. Each filter has an effective area of about 2 $m^2$. The filters allow to test all kinds of cleaning procedures. Preliminary experiments especially with respect to new cleaning procedures seem to offer successful results. According to these fine-woven fabric filters should be applicable at low cost for the high temperature gas purification. Detailed informations about the experiments and their results shall be reported in the near future.

In contrast to fabric filters, packed bed separators of adequate material can always be used at nearly all temperatures and pressures. At acceptable pressure drops packed bed separators achieve low dust contents in the purified gas only in special cases. In addition it may be difficult to clean the packed beds [illegible] that this separator can not solve [illegible]

Like fabric filters electrostatic precipitators belong to the most effective gas cleaning devices. Their mode of function is largely determined by physical and chemical factors. On an industrial scale these precipitators are realized hitherto to gas temperatures of 350 °C and to gas pressures of 3 bars. At present it is the aim of a research project supported by the Ministery for Research and Technology to investigate the feasibility and the operating conditions of electrostatic precipitators at high temperatures and pressures. It shall be examined if they can be successfully applied with respect to the dust concentration of the purified gas.

Some aspects of this problem have been studied already by a number of investigators ( 1, 2, 3, 4 ), but up to now the subject has not been treated comprehensively.

Figure 7 shows a laboratory plant which operates as a tube precipitator with variable diameters allowing temperatures up to 1000 °C and pressures of 30 bars. The air or gas with the dispersed dust is hold in a closed circuit.

Apart from construction problems, the application of electrostatic precipitators at high pressures and high temperatures is only of interest, if the physical effects of precipitation are not disadvantageously affected. As a consequence the migration velocity, defined by DEUTSCH, would become to small.
The main factors are:

1. The current-voltage characteristics, that is the correlation between corona current and applied voltage,

2. the corona starting voltage,

3. the maximal permissible voltage, that is the sparkover voltage,

4. the electrical resistivity of the dust.

The operation of an electrostatic precipitator requires a considerable difference between the corona starting voltage and the sparkover voltage. Experimental investigations have to clarify, to what extent these quantities are influenced by pressure and temperature. The results of previous investigations on the corona starting voltage and the sparkover voltage are shown in figure 7. The voltages are outlined as functions of the gas temperatures for two pressures. Accordingly the operating range of an electrostatic precipitator decreases with increasing temperature and constant pressure. This can be explained above all by the increase of the ion mobility. For instance the diagram shows that at a pressure of 1 bar and temperatures of 800 °C the difference between the sparkover voltage and the corona starting voltage does not guarantee the operation of an electrostatic precipitator. But this is possible at a pressure of 4 bars and identical temperature. In figure 8 one can see the pressure dependence of the operating range at temperatures of 300 °C and 800 °C. From this figure as well as from figure 7 one has to deduce, according to theoretical considerations, that an electro static precipitator at high temperatures can be realized only, if the pressures are raised.

From very simplified assumptions like axial electric field, simple flow conditions, spherical particles, and the validity of STOKE's law, a theoretical migration velocity can be deduced. It is at least qualitatively correlated with the effective migration velocity. The shortened derivation is shown in Figure 9. It appears that the theoretical migration velocity depends on the product of the charging and collecting field intensities.

At constant electrical field intensity the theoretical migration velocity is inversely proportional to the gas viscosity, which in its turn depends mainly on the gas temperature. Proceeding from a linear relationship between the mean field intensity and the pressure as well as the temperature of the gas, individual values of theoretical migration velocity can be calculated. Figure 10 shows the variation of the theoretical migration velocity in air with temperature and pressure. The ordinate is the ratio of the actual theoretical migration velocity to that at 100 °C and 1 bar. It can be seen that the theoretical migration velocity decreases with rising temperatures and increases with increasing pressure. The unfavorable influence of high temperatures can be therefore balanced by rising the pressure.

Another influence on the characteristics of electrostatic precipitators is due to the already mentioned resistivity of the dust. This electrical quantity, dimensioned Ω cm, is significant for the adherence of the dust to the collecting electrodes. It is in general accepted that dust resistivities of more than $10^{11}\Omega$ cm or less than $10^{4}\Omega$ cm are disadvantageously according to the diminished adherence of the dust. Theoretical understanding and present experience suggest that electrical resistivities may become to low at high gas temperatures. This, however, has not been confirmed for converter dust by the experimental investigations of SCHÜTZ and WINKEL. Therefore it is necessary to study more detailed dust resitivities at extremely high pressures and temperatures.

Based on today's knowledge the effectiveness of electrostatic precipitators at high gas pressures and temperatures can be summarized as follows:
Probably the current voltage characteristics should allow at least a suitable precipitation if in addition to high temperatures also high pressures are at hand. It must be seen wether this view will be confirmed and how the electrical resistivity of the dust will behave at these extreme conditions. Besides of the mentioned physical effects the industrical realization of the electrostatic precipitator at high pressures and high temperatures is opposed by severe constructive and technical problems.
After all the present investigation has to show if it is possible to design an electrostatic precipitator having a sufficient effectiveness as well as reasonable cost.

In contrast to the three already mentioned separation systems, wet scrubbers allow the simultaneous precipitation of both solid particles and gaseous constituents. This combination of two separation processes in a single unit enables a low cost gas purification as compared to the use of a two stage system for the separation of gaseous and solid constituents. It is a severe disadvantage, however, of all known wet scrubbing systems using water as a washing medium that the gas is cooled considerably before or during the separation process. Wet scrubbers although offering several advantages with respect to other separation systems cannot be employed if the gas shall be kept at a constant high temperature level to avoid energy losses.

To overcome these difficulties it should be possible to use a suitable washing medium instead of water or aqueous solutions. Evidently the choice of the washing liquid is most important.

Substances for the separation of gaseous and solid pollutants at high gas temperatures have to fulfill the following conditions:

1. The substances have to be in the liquid state at temperatures of about 500 °C. They should be sprayable and must have a low surface tension.

2. The vapour pressure of the melt should be negligible at least for temperatures up to 800 °C.

3. There should be formed no toxic or harmful compounds.

4. The melt has to be either loss-free reprocessable or convertable into products that can be led to disposal.

5. The cost for the used melt should be acceptable.

Due to these restricting preconditions orientating studies have shown that a number of inorganic substances can be used for a suitable melt. In contrast to other investigated metals that are toxic, high melting, or very expensive the metallic tin has a very low vapour pressure and can be well applicated as a washing liquid.

Due to their low oxidative stability metal melts are only handable in the case of gases with low oxygen content which are present in coal gasification processes. The possibility of separating gaseous constituents by liquid metals is restricted. So they are mainly appropriate to the separation of solids at high gas temperatures and pressures. Laboratory experiments have pointed out that metals are well sprayable and that their ability to remove dust is comparable to that of water. Qualitative experiments concerning the separation showed that the adhesive forces at the surface of the tin are sufficiently strong to enable the sticking of dust. Owing to the difference of densities the solid particles penetrated into the bulk liquid get very fast to the surface. Due to their high density the tin droplets dispersed in the gas can be separated easily and with high efficiency using gravity and momentum forces. Orientating measurements have shown up that the separation of solid particles from the tin melt can by carried out without losses of metal. This is a necessary precondition due to the high costs of the material.

In contrast to metal melts it is possible to use inorganic salt melts as well in an oxidizing as in a reducing atmosphere. Besides solids a large number of gaseous constituents like hydrogen chloride, nitrogen oxides, sulfur oxides and hydrogen sulfide can be separated. Depending on the gas to be cleaned and on the gaseous and solid pollutants, compounds of sodium, potassium, and calcium can be applicated some of which have low melting points and behave at high temperatures like water of room temperature. The vapour pressures of the mixtures are sufficiently low even at high gas temperatures, especially when the gaseous and solid constituents are reacting with the melt.

It is noteworthy that alkaline carbonate and hydroxide melts can bind a great number of oxidic materials by solving or chemical reaction. Laboratory experiments with alkali hydroxides have pointed out that silica can react with the melt nearly up to the stoichiometric ratio without affecting the wanted physical properties of the melt. This result is important in as much as silica is a main constituent of the fly ash of coal power plants. Experiments have shown that fly ash is completely soluble in alkaline melts. Particles of coal and soot, however, remain undissolved and may be separated from the melt by mechanic methods.

According to experimental results the use of nickel is recommended as a material for a laboratory plant because of the great corrosivity of the alkaline melts. On an industrial scale it may be possible to use cast iron.

For the investigated salt melts the dust separation is in principle comparable to the conventional wet scrubbing process. The alkaline melts show special features due to their chemical reactivity. The melts can precipitate as well chemical reactive dust particles as nonreactive substances like coal particles.

In principle it is possible to reprocess the salts formed by reaction with the gaseous components. Usually this is not necessary because the cost of the melt material are sufficiently low. Commonly disposal problems are not to be expected for the waste materials. For instance the waste materials yielded by the purification of gases from power plants can be converted into a nearly water-insoluble substance, at least by addition of fly ash and by heating up to temperatures of more than 800 °C. The disposal of the resulting waste products causes cost between 2 and 4 dollars per ton. These cost are comparable low with respect to the employed materials and to other waste substances.
Investigations in this field are supported by the Ministry of the Interior and by the [illegible].

Preliminary studies have already been finished. At present a laboratory plant for a gas flow rate of 300 $m^3/h$ as shown in figure 13 is under construction. The gas flow is led in a closed circuit. The scrubbing system is connected to a separate liquid reprocessing circuit. Gas temperatures of more than 600 °C can be maintained. It is possible to use various gas compositions and to apply as well metal and salt melts for dust precipitation and the absorption of gaseous constituents. The plant operates [illegible] because the physical conditions for a separation are not changed considerably at high pressures. It must be seen if and to what extent the results of the preliminary investigations will be confirmed.

Summarizing it can be stated:

The optimum use of new coal conversion technologies for power generation requires the development of suitable gas purification systems at high temperatures and high pressures. It has been shown that in principle scrubbing processes are suitable. The separation of solids should be also feasible with electrostatic precipitators and fabric filters while gravity and momentum separators are not of interest because of their low efficiency. It can be expected that in about two or three years the first gas purification system operating at high temperatures and pressures will be employed on a technical scale.

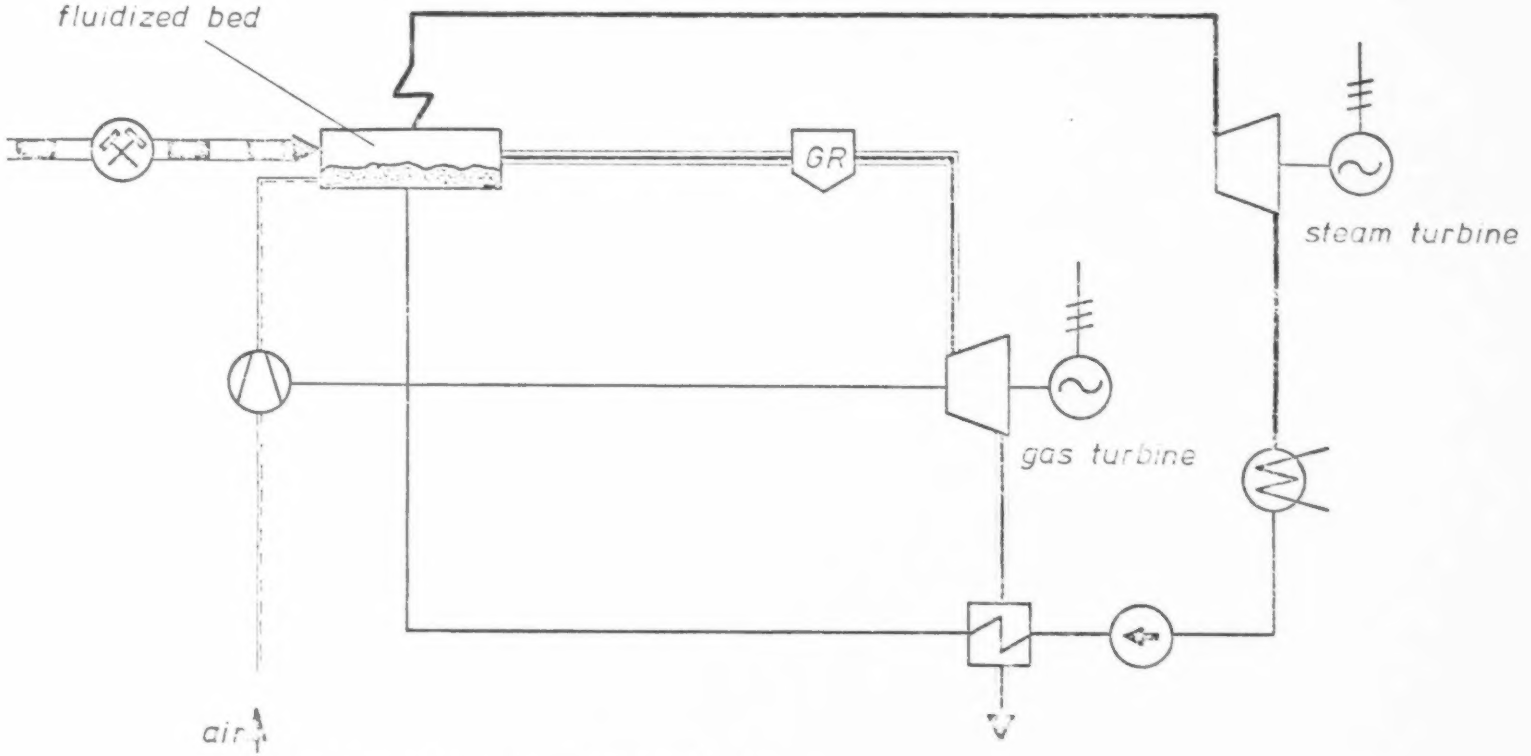
fluidized bed
GR
steam turbine
gas turbine
air

gas flow rate: $V \approx 15\,m_n^3/kg$ coal
pressure: $p = 4{,}5/10$ bar
temperature: $\vartheta \approx 860\,°C$
dust concentration $c_{St}$ up to $20\,g/m_n^3$

| | | |
|---|---|---|
| Mechanische<br>Verfahrenstechnik<br>Universität Essen | Fluidized Bed Furnace(schematic)with Loaded Vessel | UA<br>1 |

gas flow rate: $V = 2{,}5$ [illegible] / kg coal
pressure: $p = 20$ bar
temperature: $\vartheta = 600$ °C
dust concentration: $c_{St} = 3\text{-}8\ g/m^3_n$

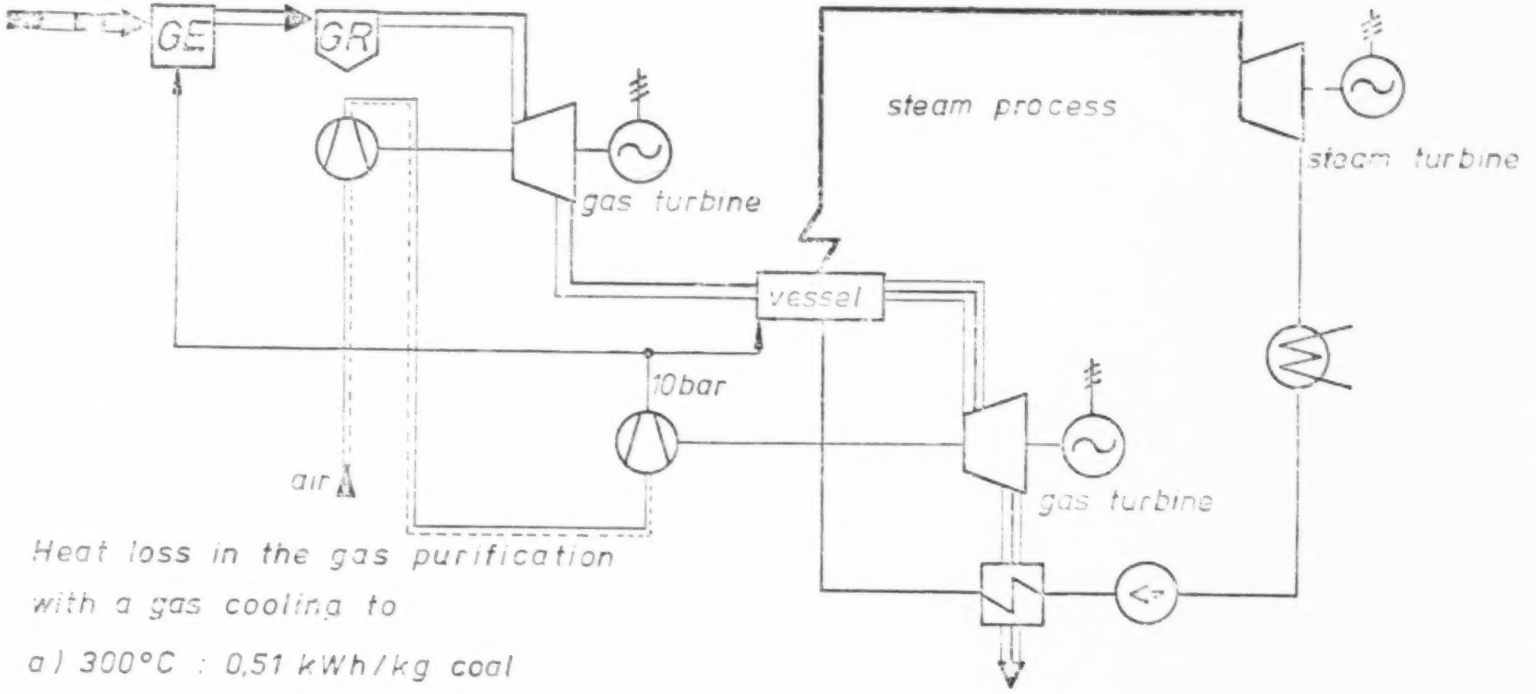
GE
GR
gas turbine
vessel
10bar
air
steam process
steam turbine
gas turbine

Heat loss in the gas purification
with a gas cooling to

a) 300°C : 0,51 kWh / kg coal
b) 100°C : 0,79 kWh / kg coal

Mechanische
Verfahrenstechnik
Universität Essen

# Fixed Bed Gasification (schematic) with Loaded Vessel

UA
2

| characterization | gravity and momentum separators | porous layer dust collectors | electrostatic precipitartors | wet scrubbers |
|---|---|---|---|---|
| dust separation by | mass forces (gravitational force, inertial force, centrifugal force,) | filtration with porous media | electrostatic forces | linkage of the dust to the scrubbing liquid |
| fundamental constructions | inertial dust collector, centrifugal force dust collector (cyclone) | cloth filter collector, packed tower collector, candle filter | dry electrostatic precipitator, wet electrostatic precipitator | statical and rotary scrubbers |
| effectiveness | moderate to medium | medium to very high | medium to very high | medium to very high |
| hitherto designed for a maximal:<br>gas temperatur of (°C<br>gas pressure of (bar | cir. 1000<br>cir. 20 | cir. 350<br>cir. 1-2 | cir. 350<br>cir. 3 | 50 - 100<br>cir. 5 |

Classification of Dust Collectors

UA
3

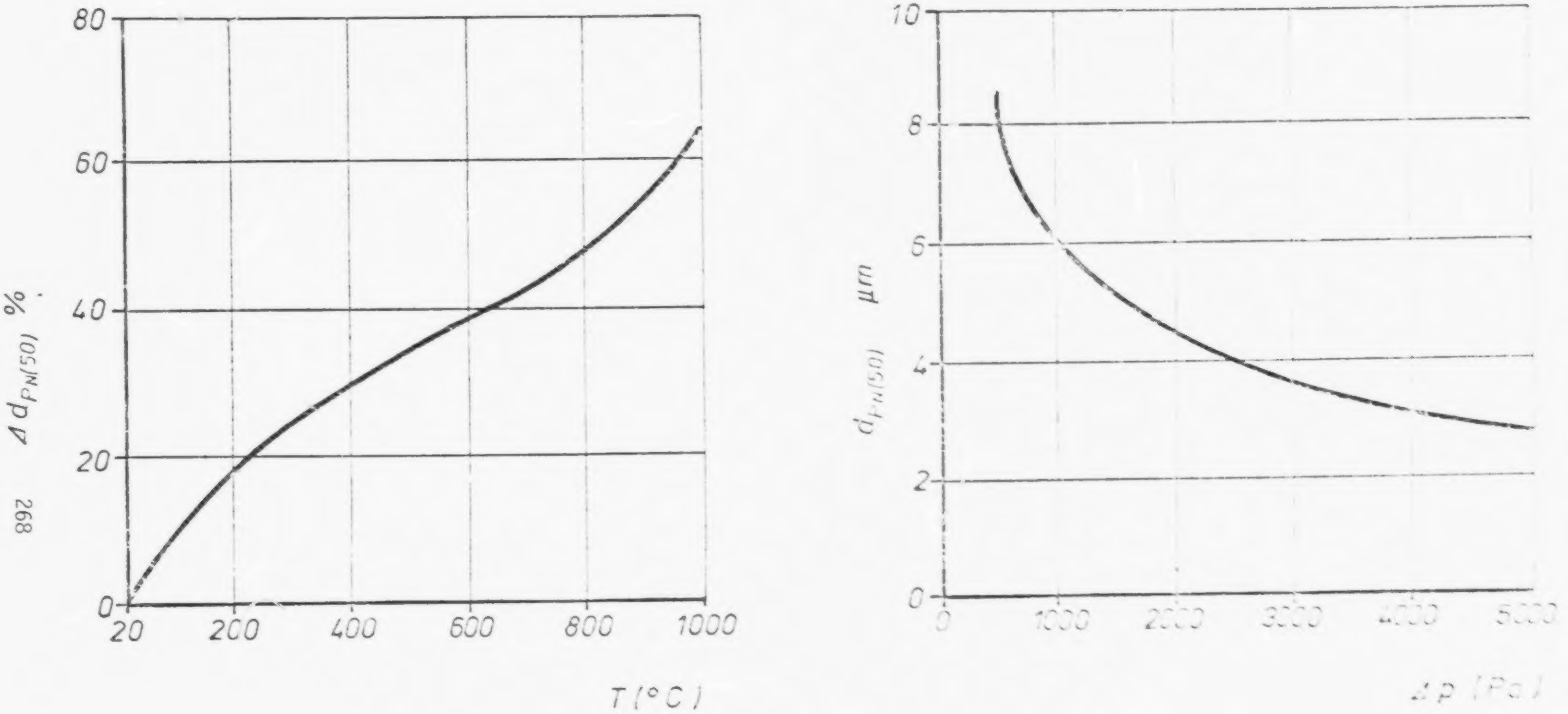

$d_{P_N(50)}$ relating to 20°C

| Mechanische<br>Verfahrenstechnik<br>Universität Essen | Collectable Particle' Diameter of Cyclones with Respect to Pressure and Temperature | UA<br>4 |
|---|---|---|

| material | temperature-resisting up to ( °C ) | manufactured into | lowest diameter of the fibres (µm) | chief constituents |
|---|---|---|---|---|
| glass | 550 | fabric<br>fleece | 2 - 5 | $SiO_2$ $Al_2O_3$<br>$CaO$<br>$B_2O_3$ |
| chrysotile-asbestos | 550 | fabric<br>fleece | 2 - 10 | $Mg_6[(OH)_8Si_4O_{10}]$ |
| amphibolite-asbestos | 800 | fabric<br>fleece | 2 - 10 | Ca, Na, K, Mg, Fe, Al, Mn, Ti, Si, F |
| quartz | 1200 | fabric<br>fleece | 2 - 5 | $SiO_2$ |
| basalt | 1000 | fabric<br>fleece | 10 - 20 | $SiO_2, Al_2O_3, CaO, MgO, FeO$ |
| ceramics | 1200 | fleece | 4 - 20 | $SiO_2, Al_2O_3$ |
| slag | 700 | fleece | 5 - 20 | $SiO_2, Al_2O_3, CaO, MgO$ |
| rock | 700 | fleece | 15 - 30 | $SiO_2, Al_2O_3, CaO, MgO$ |
| graphite<br>oxidizing atmosphere<br>reducing atmosphere | <br>400<br>>2000 | felt | 8 - 15 | C |
| metal | 700 | fleece<br>fabric<br>felt | 4 - 10 | C, Cr, Ni, Cu, Mo, Fe |

[illegible]ische
[illegible]technik
Universität Essen

Fibrous Materials for the High Temperature Filtration

UA
5

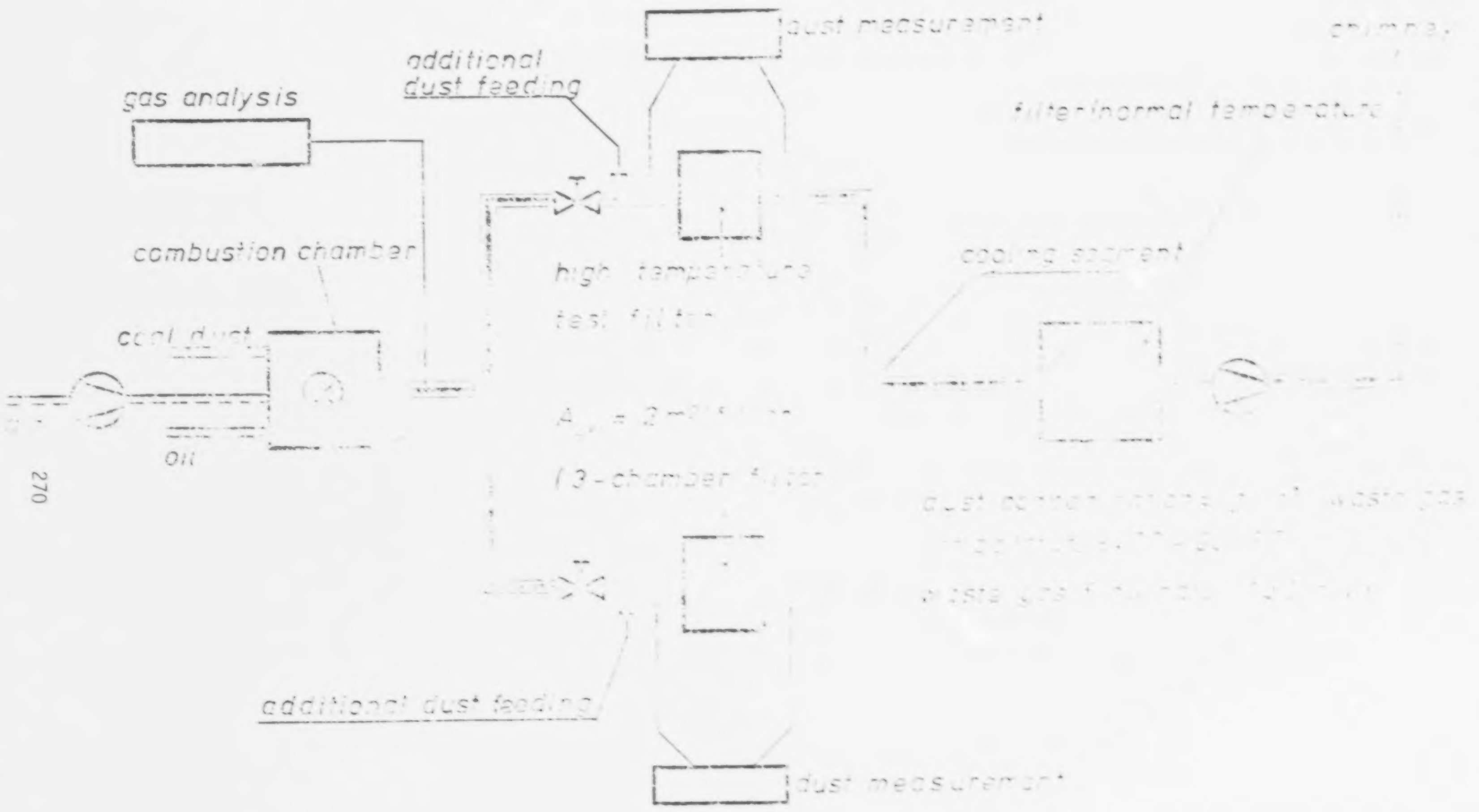
dust measurement
chimney
additional dust feeding
gas analysis
filter/normal temperature
combustion chamber
cooling segment
coal dust
oil
high temperature
test filter
A = 2 m²
(3-chamber filter
dust concentration of waste gas
waste gas
additional dust feeding
dust measurement

Experimental Arrangement for Fabric Dedusting at High Temperatures

UA

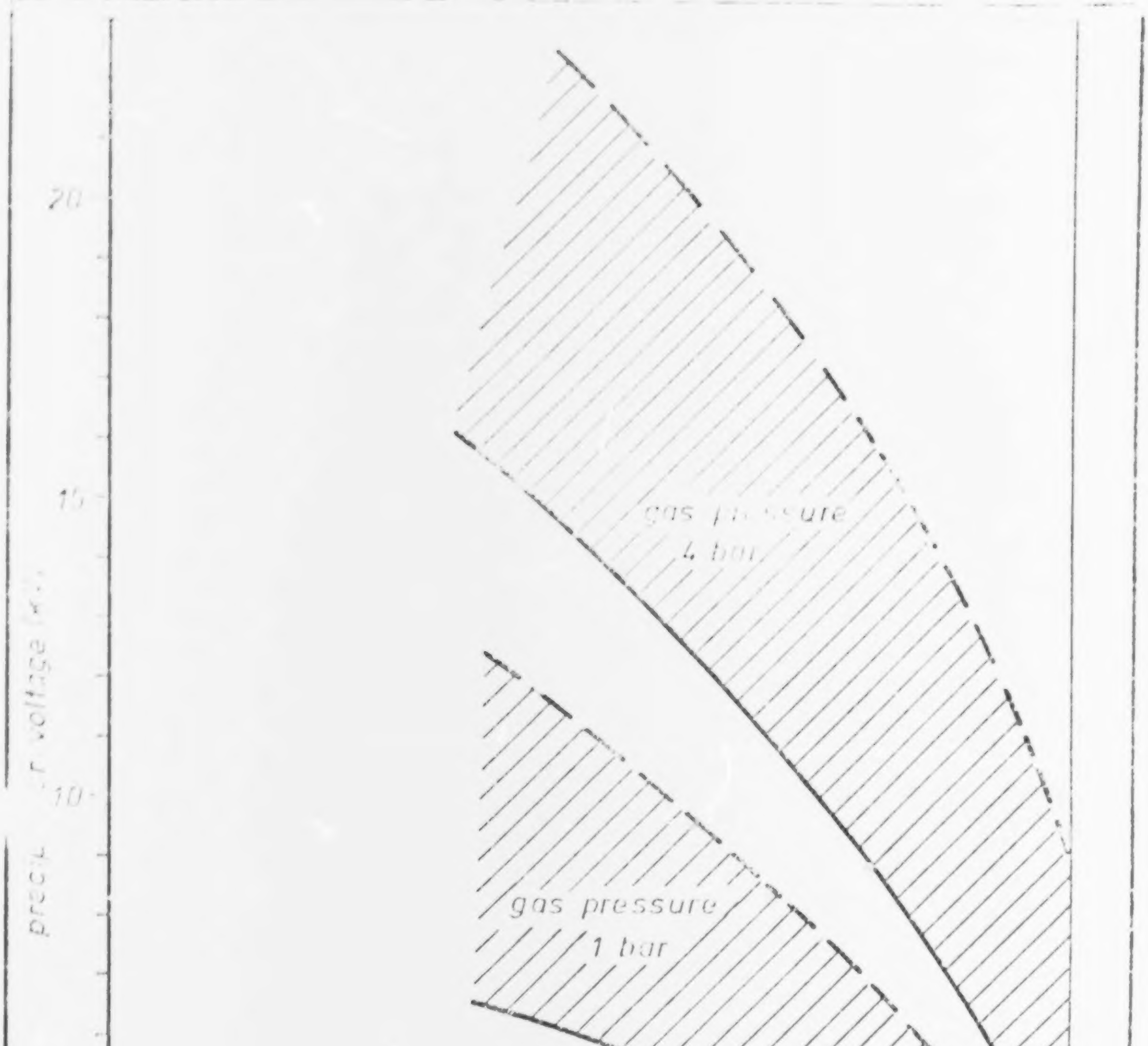

| | | |
|---|---|---|
| Mechanische Verfahrenstechnik Universität Essen | Operating Ranges of an Electrostatic Precipitator versus Gas Temperature | UA 7 |

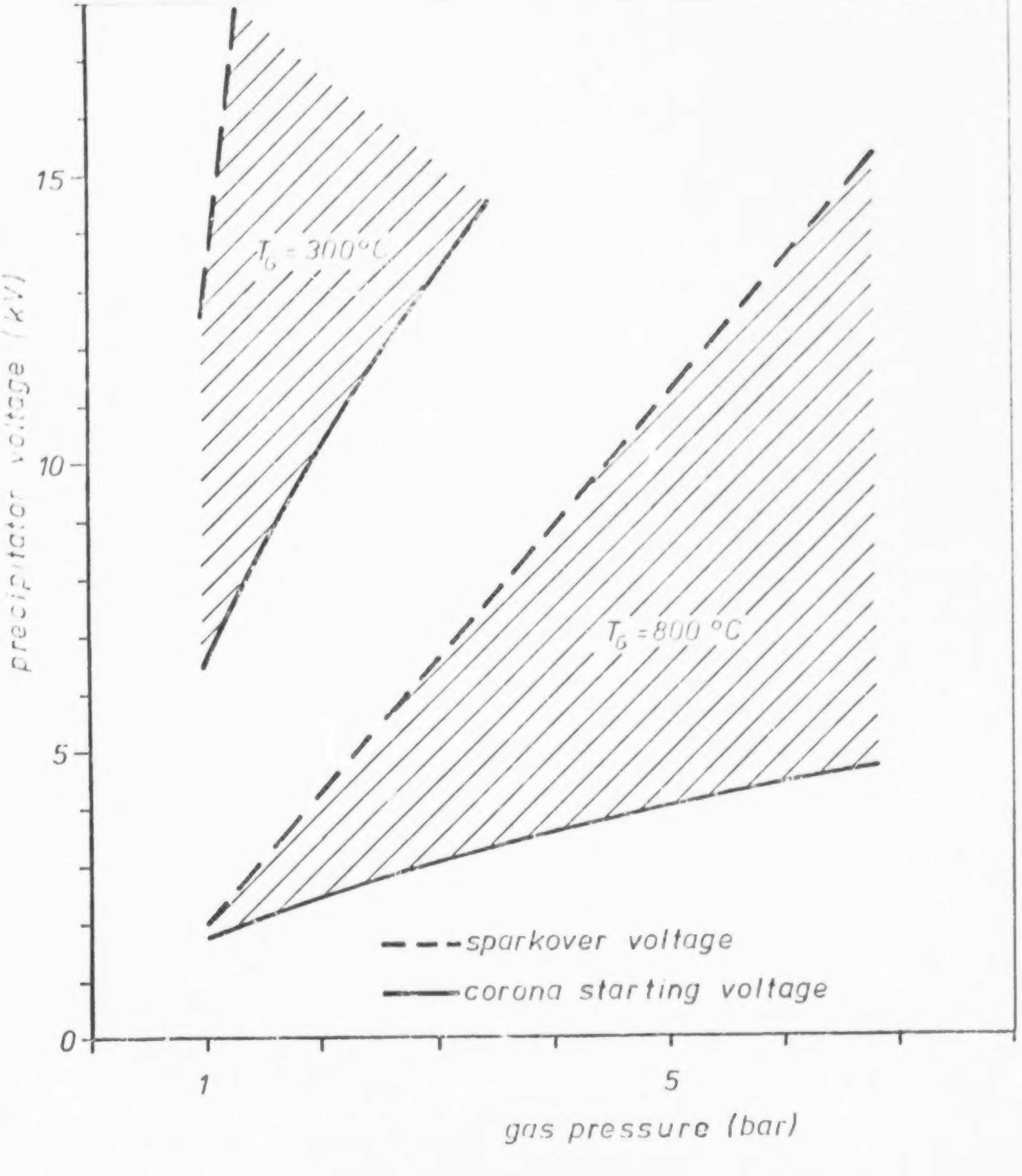

| | | |
|---|---|---|
| Mechanische<br>Verfahrenstechnik<br>Universität Essen | Operating Ranges of an Electrostatic<br>Precipitator versus Gas Pressure | UA<br>8 |

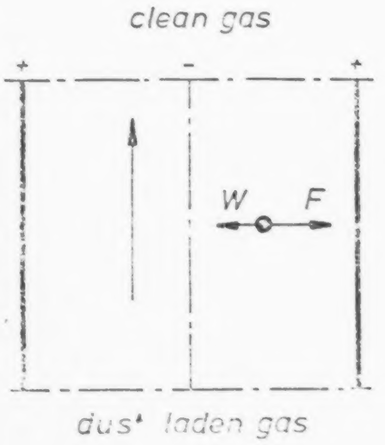

$$\boxed{m_p \cdot \frac{dw_{th}}{dt} = F - W} \quad \text{Equation of Motion} \qquad (1)$$

$$F = q \cdot E_p \qquad (2)$$

$$W = 6 \cdot \pi \cdot \eta_G \cdot r_p \cdot w_{th} \quad (\text{for } Re < 0.1) \qquad (3)$$

$$w_{th} = \frac{q \cdot E_p}{6 \cdot \pi \cdot \eta_G \cdot r_p} \qquad (4)$$

$$q = n_s \cdot e = 3 \cdot E_0 \cdot r_p^2 \qquad (5)$$

$$E_0 \cdot E_p \sim U^2 \qquad (6)$$

$$\boxed{w_{th} \sim \frac{U^2 \cdot r_p}{2 \cdot \pi \cdot \eta_G}} \qquad (7)$$

$q$ particle charge
$E_0$ charging-field intensity
$\eta_G$ gas viscosity
$r_p$ particle radius
$n_s$ number of particle charges
$e$ electronic charge
$E_p$ collecting-field intensity
$w_{th}$ migration velocity (theoretical)
$m_p$ mass of particle
$U$ precipitator voltage

| Mechanische Verfahrenstechnik Universität Essen | Theoretical Migration Velocity of Electrostatic Precipitators | UA 9 |
|---|---|---|

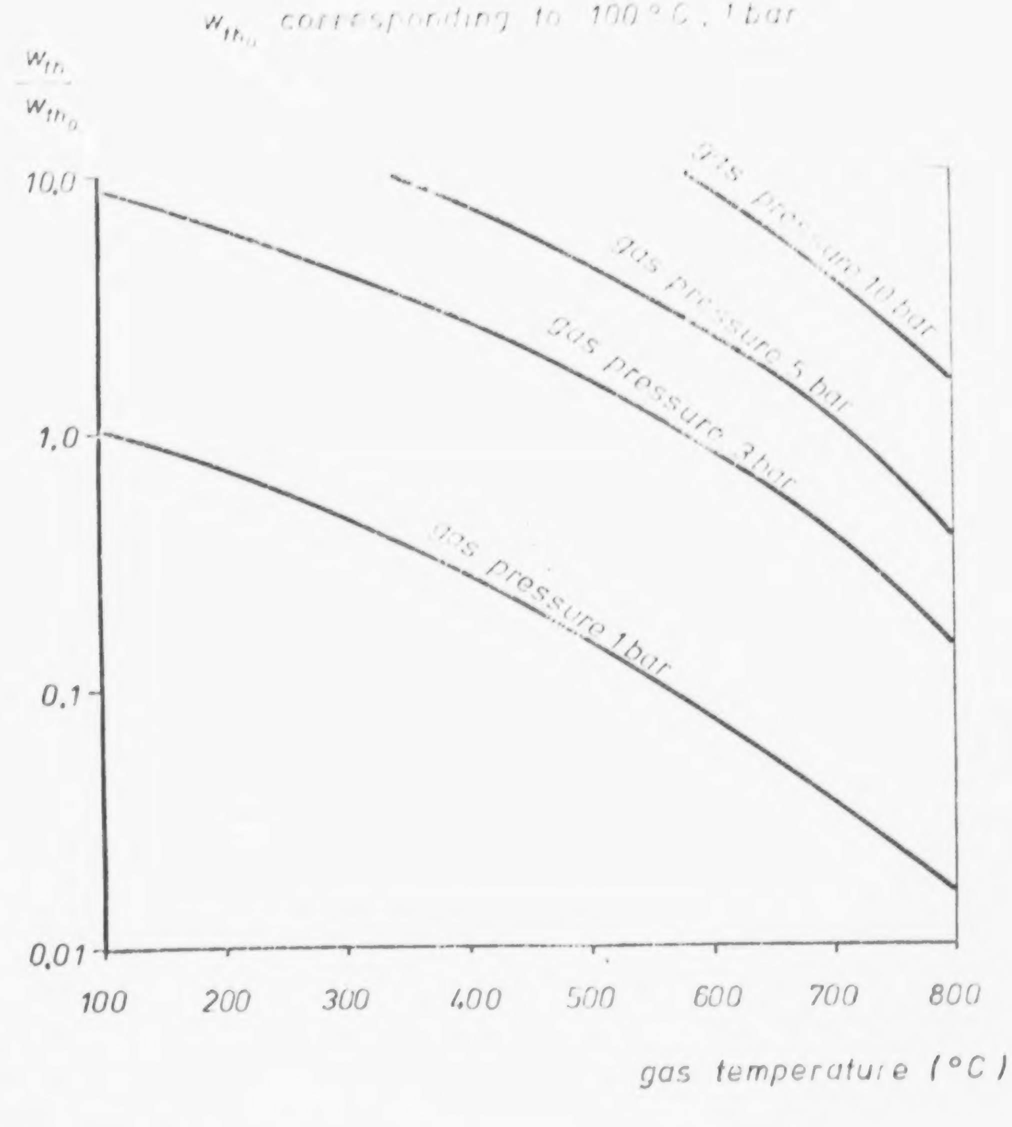

| | | |
|---|---|---|
| Mechanische<br>Verfahrenstechnik<br>Universität Ess | Theoretical Migration Velocity as a Function of Gas Temperature and Gas Temperature | UA<br>10 |

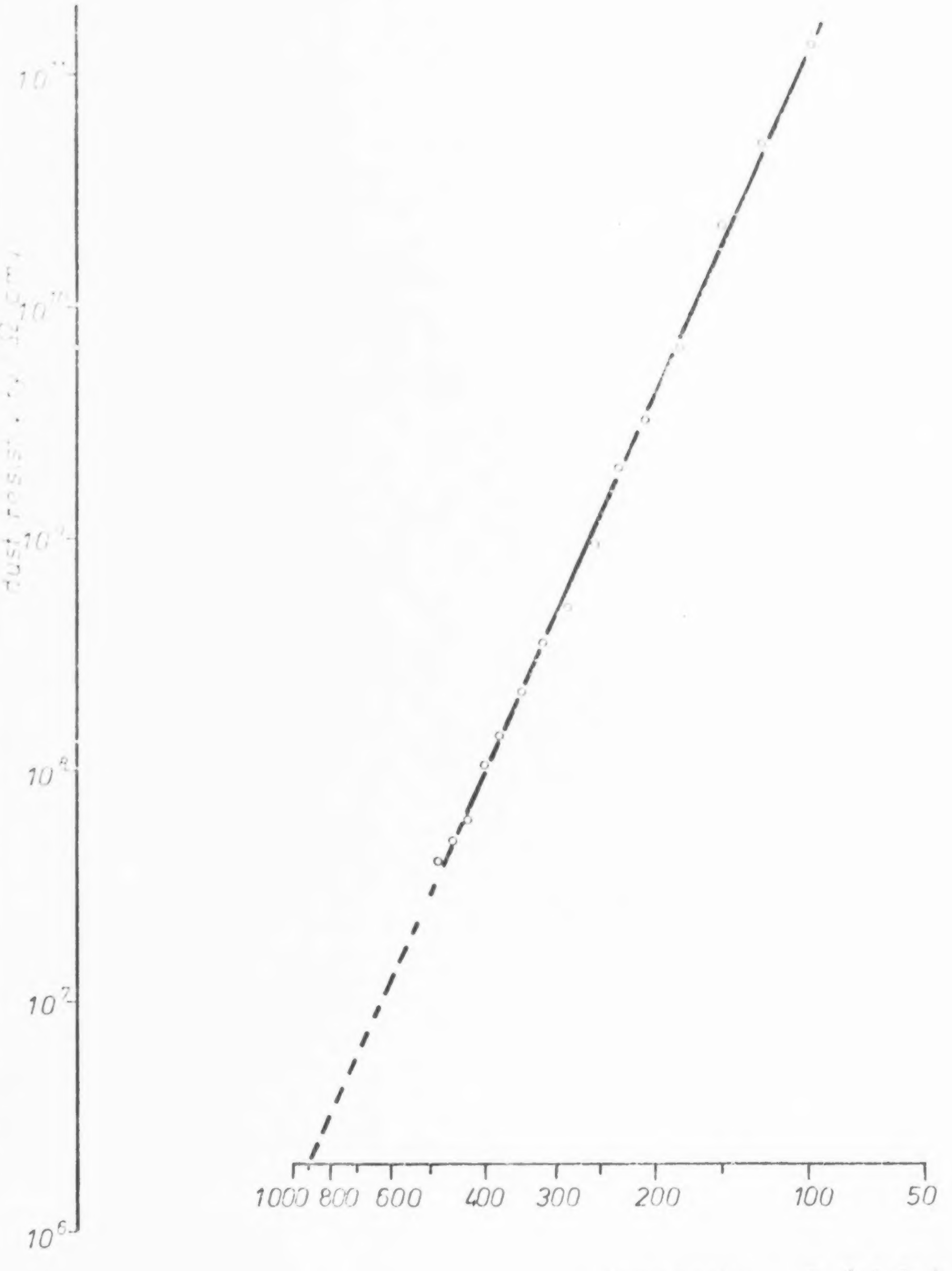

Mechanische Verfahrenstechnik Universität Essen

**Resistivity of Converter Dust (from Winkel und Schütz)**

UA 11

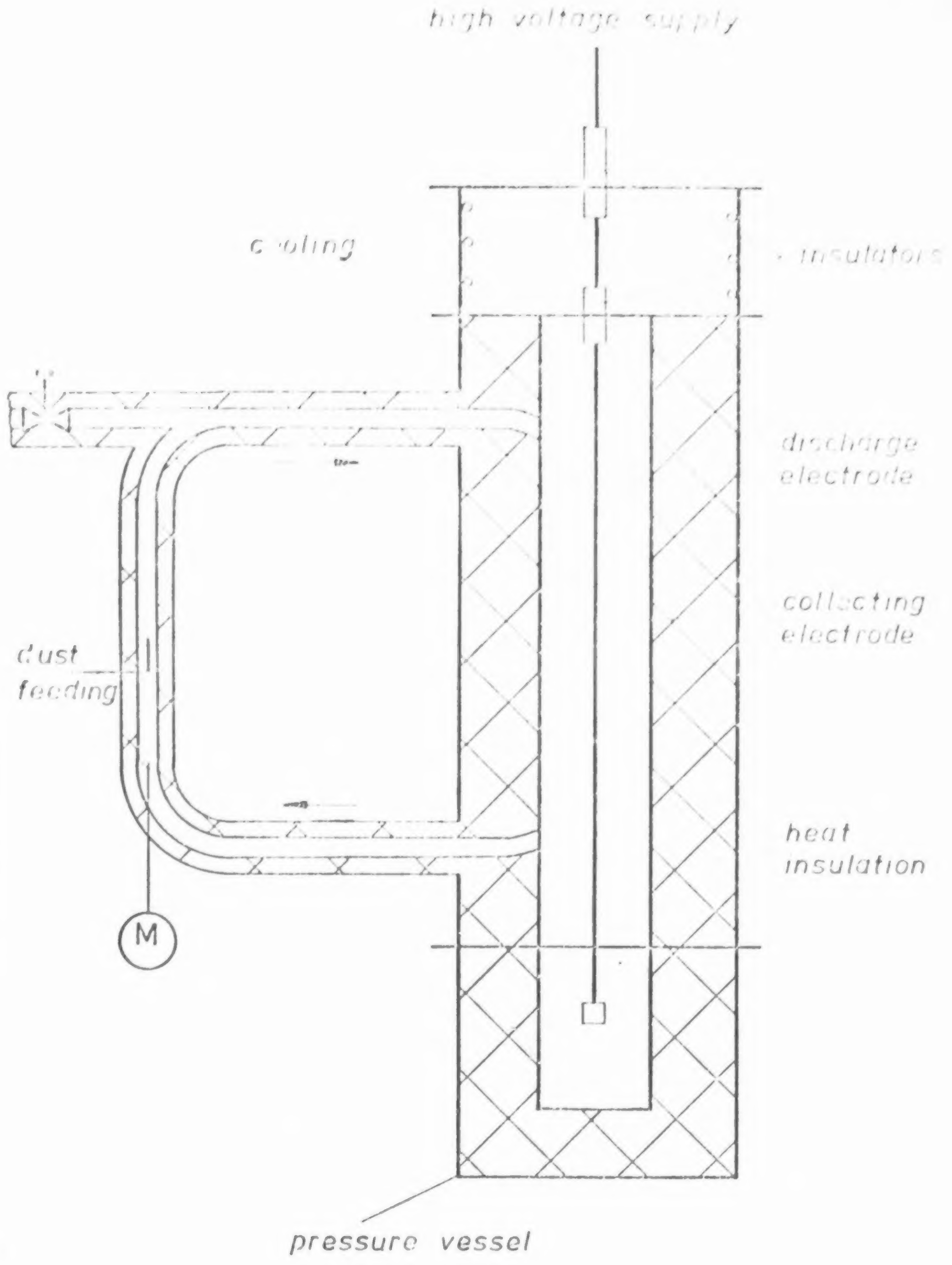
high voltage supply
cooling
insulators
discharge electrode
collecting electrode
dust feeding
heat insulation
M
pressure vessel

| | | |
|---|---|---|
| Mechanische Verfahrenstechnik Universität Essen | High Pressure and High Temperature Electrostatic Precipitator | UA 12 |

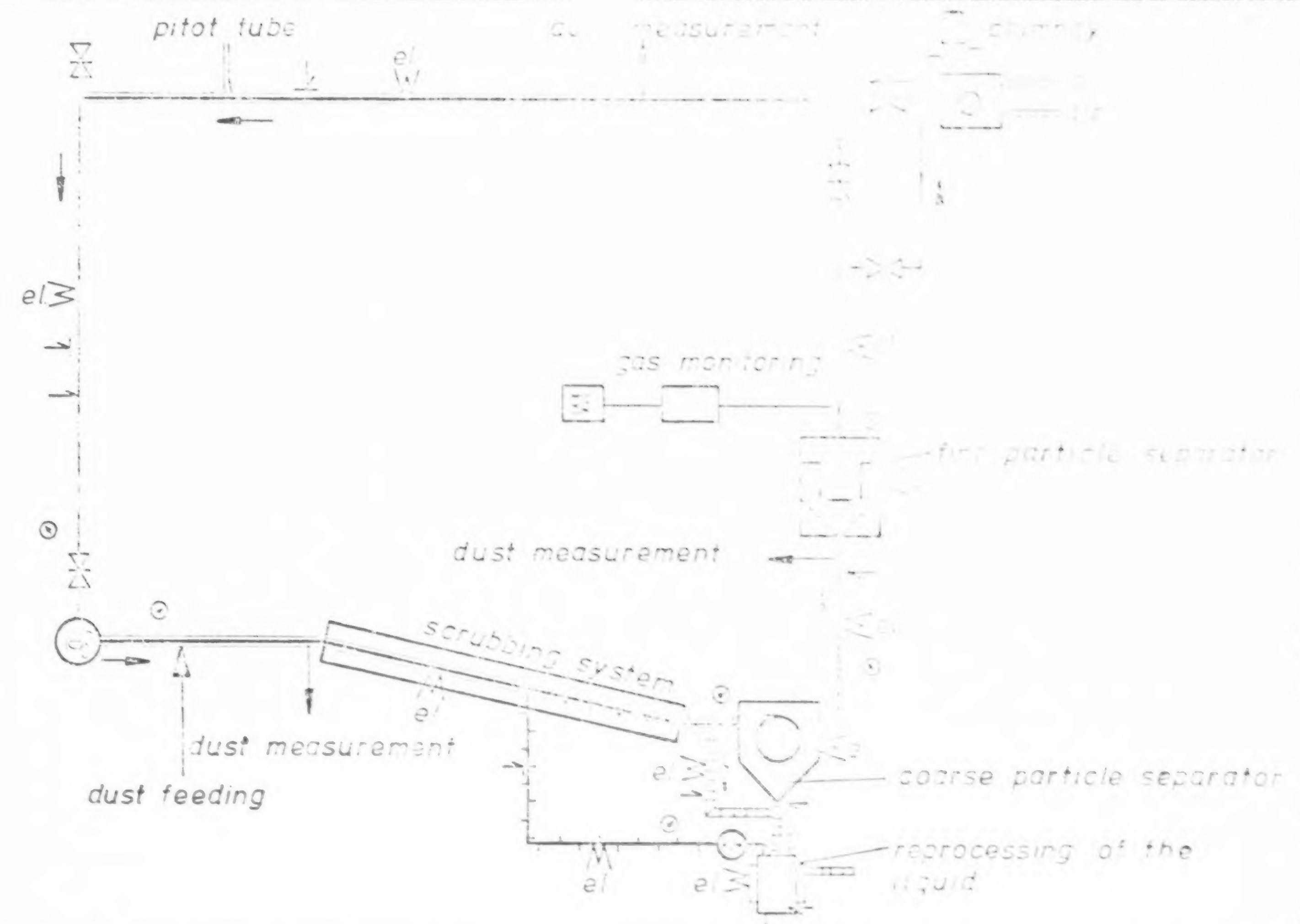
pitot tube
measurement
chimney
el
el
gas monitoring
fine particle separator
dust measurement
scrubbing system
el
dust measurement
dust feeding
el
coarse particle separator
reprocessing of the liquid
el
el

| Mechanische<br>Verfahrenstechnik<br>Universität Essen | Scheme of the High Temperature Scrubbing System | UA<br>13 |
|---|---|---|

# SESSION III:

# OTHER COLLECTION DEVICES

JIM ABBOTT
CHAIRMAN

# HIGH TEMPERATURE, HIGH PRESSURE ELECTROSTATIC PRECIPITATION

By:

P. F. Feldman, J. Bush, M. Robinson
Research-Cottrell, Inc.
Bound Brook, NJ  08805

# HIGH TEMPERATURE, HIGH PRESSURE ELECTROSTATIC PRECIPITATION

By:

Paul Feldman
John Bush
Myron Robinson
Research-Cottrell, Inc.
Bound Brook, New Jersey 08805

## ABSTRACT

This paper presents results of work conducted by Research-Cottrell under EPA Contract 68-02-2104. The purpose of the work completed to date was to demonstrate the ability to generate stable corona at temperatures to 2000°F and pressures to 500 psig, thus establishing the feasibility of electrostatic precipitation as a means of particulate removal from the effluent of fluidized bed combustors or coal gasifiers at high temperature and pressure. The work was quite successful in demonstrating stable corona generation and in defining ranges of temperature and pressure over which the stable discharge can be maintained.

Gases investigated were air, flue gas, and simulated (noncombustible) fuel gas in coaxial wire-pipe electrodes. Pipe diameter was fixed at 3 inches; wire diameter varied from 0.062 to 0.125 inches. Results are reported for both polarities in terms of current-voltage characteristics, corona onset and sparkover voltages, and critical gas densities above which sparkover alone, without antecedent corona, occurs.

# SUMMARY

The objective of this project was to demonstrate the technical feasibility of electrostatic precipitation at temperatures to 2000°F and pressures to 500 psig. By technical feasibility is meant the ability to generate stable corona over the range of temperature and pressure indicated. This was accomplished in a laboratory scale tubular precipitator in no-flow, particle-free operation. This method of operation was chosen because it allowed a well-controlled, economical evaluation of the electrical characteristics of the system over the total range of the variables. A second phase program is needed to carry the work further into evaluation of particulate collection characteristics.

The primary variables studied were temperature, pressure, gas composition, discharge polarity, and discharge electrode geometry. Data were taken in the form of current-voltage curves to define ranges of the variables over which electrostatic precipitation is feasible.

The work was very successful in that stable corona was demonstrated over the entire range of temperature and pressure of interest to the emerging fluidized-bed combustion and coal gasification applications. Furthermore, this work indicates that conditions for electrostatic precipitation actually become more favorable as temperature and pressure increase.

# FUNDAMENTALS OF HIGH TEMPERATURE/PRESSURE PRECIPITATION

The electrostatic precipitator appears to be unique among conventional particulate collectors such as fabric filters, cyclones, and scrubbers, in that elevated gas pressure offers the promise of increased collecting efficiency. Such improvement results from the potentially higher sparkover voltages, and hence greater electric field strength and particle-migration velocities, attainable at high pressures[1]. The advantage holds for precipitation at high temperature, as long as the condition occurs in combination with adequate pressure.

There is a fundamental problem encountered in designing a precipitator for a given high temperature/pressure service. This is our incomplete knowledge of i) the range of variables (pressure, temperature, electrode geometry, gas composition, polarity) over which a stable corona discharge can be maintained, and ii) the current-voltage characteristics in that range. In particular, there exists for the positive discharge a critical pressure above which sparkover alone, without antecedent corona, prevails. When the discharge polarity is negative, the critical phenomenon is not so precisely defined, and a postcritical discharge (often unstable) may be found at pressures extending beyond the critical value.

Two opposing effects are responsible for the phenomenon of the critical pressure. First, shorter mean-free paths at elevated pressures impede ionization by collision and so tend to raise the sparkover level. Second, the denser packing of gas molecules renders photoionization more likely and reduces ion diffusion.

Thus, pressure facilitates streamer propogation from the anode across the gap and, at the critical pressure, sparkover results.

The likely explanation of the relatively low value attained by the positive sparkover voltage and its concomitant lower critical density is as follows: Intense ionization of the gas is produced in the high-field region in the vicinity of the discharge wire which attracts and removes the highly mobile electrons. The heavy positive ions are repelled from the wire and move slowly toward the collecting electrodes. However, on the far side of the ion cloud (away from the wire), the field, suffering from positive-ion space-charge distortion, is increased, and with it, the rate of ionization. Conditions are now favorable for the growth of a positive streamer to develop toward the cathode. On the other hand, when the wire is negative, the positive space charge surrounding it in the corona sheath tends to shield the wire from the anode. This action reduces the field on the anode side and so a higher voltage is needed to promote a spark.

Thermal ionization is another effect which must be considered in high temperature precipitation. At normal temperatures ionization is governed by i) electronic and molecular collision processes in the presence of an electric field and ii) photon absorption. At very high temperatures an additional mechansim enters the picture: thermal ionization. This introduces the following new possibilities.

i) Electron-ion production by collision of the gas molecules with each other. Such ionization may occur even in the absence of ionized particles and a high-intensity electric field. It is the high-temperature condition that provides velocities and kinetic energies high enough to cause ionization.

ii) Photoionization resulting from thermal emission of the hot gas. When a high-temperature gas flows through a precipitator, it will emit quanta in accord with the laws of black-body radition.

The electrode surface and the walls of the pressure vessel will reflect most of this radiation. Thus, photons capable of ionizing are always availabe when the temperature is high enough. Calculation, however, shows that this condition is probably not met under present circumstances.

iii) Ionization by collision with high-energy electrons that have been generated by the above two processes.

Apprehensions arise for precipitation at very high temperaatures because significant thermal-ionization rates may lead to catastrophic currents at reduced voltages. Earlier predictions that this condition might occur at a temperature of about 1500°F[2] have been shown experimentally to be untenable[3]. Revised work[4] now suggests that whereas thermal effects may become noticeable below 1500°F, practical high-temperature precipitation may be limited only by temperatures exceeding 2000-2400°F. The lower limit of this range would apply to gases containing a component of low ionization potential, say potassium, in quantities as low as one atom in $10^4$. Potassium is singled out because of the alkali metals (all of which have characteristically low ionization potentials), it is the most common. Hence, the probability of its appearance in industrial gases is not remote.

## EXPERIMENTAL APPARATUS

Figure 1 shows the configuration of the test precipitator used in this program. It is a wire-pipe design enclosed in a pressure vessel. The pressure vessel was designed for pressures to 500 psig and was assembled in three sections, each serving a specific purpose. The top section contains the feedthrough bushing for applying high voltage to the discharge electrode and a pressure relief line to protect from over pressurization. The bottom section has a side access opening for adjustments and observations, a bottom support insulator to center the discharge electrode, and the gas inlet. The center section of the vessel holds the precipitator tube surrounded by a three-zone heater used to reach the desired operating temperature. A layer of Kaowool insulation separates the heater and the pressure vessel wall.

The collection tube electrode is a 7.26 cm internal diameter, Inconel 601 tube, sectioned into three electrically isolated pieces. This arrangement provides a center section with precisely known area and uniform field for corona current measurements. The endpieces are flared in order to prevent sparkover at premature voltage levels. The discharge wire is also of Inconel 601.

The precipitator was powered by a power supply capable of 400 kV and 60 milliamps. Gas was charged to the precipitator from compressed gas cylinders to obtain the desired gas compositions. Moisture was adjusted to desired levels by passing the gas through a humidifier at controlled temperature.

# TEST CONDITIONS

The experimental test plan was designed to establish ranges of stable corona generation as a function of temperature, pressure, gas composition, discharge polarity and discharge electrode geometry. Table I shows the ranges of these variables studied. Temperature was varied in 500°F intervals from 500°F to 2000°F for all gas compositions, and, with air, ambient temperature data were also taken.

Pressure was varied in 50 psi intervals from ambient to 500 psig. In moving from one test condition of pressure to a new condition, at constant temperature, gas was always released from the vessel to maintain constant composition and thermal stability. At each pressure level, results for both negative and positive polarity were obtained.

Data were taken in the environments of three different gas compositions: air, combustion gas and substitute fuel gas. A substitute gas mixture was used in place of actual fuel gas because of laboratory safety requirements. This mixture was similar to actual fuel gas except helium was substituted for hydrogen and carbon dioxide for carbon monoxide. The resultant mixture was similar to fuel gas in important physical properties including thermal conductivity and ionic mobility. The fuel and combustion gas mixture used are shown in Table II.

Data were taken for three discharge electrode sizes as shown in Table I with air. For the combustion gas and and substitute fuel gas mixtures, only the 2.34 mm wire was used.

The primary data taken were current-voltage curves for each of the experimental conditions. The current-voltage curves were obtained on an X-Y recorder by recording the curves for both increasing and decreasing voltage levels and repeating each trace. Sparking voltage was determined as the final voltage attained after being held at sparking for two minutes. Corona starting voltages were determined by (1) observation of voltage at which corona pips disappeared on the oscilliscope with decreasing applied voltage and (2) extrapolation of the current-voltage curves to zero.

# RESULTS

The raw experimental data, consisting of curves of linear current density (mA/m) vs impressed voltage (kV) are reproduced in Figures 2 through 5 for air, Figure 6 for simulated combustion gas and Figure 7 for substitute (i.e., noncombustible) fuel gas. Corona-starting and sparkover voltages, derived from these curves and independent measurements, are shown as functions of relative gas density, $\delta$*, in Figures 8 to 10 for air, Figure 11 for combustion gas, and Figure 12 for substitute fuel gas.

The first and most important objective is to examine the data for the purpose of establishing temperature or pressure limits to a stable corona discharge. Such limits may be caused by: i) excessive currents at low voltages resulting from thermal ionization (where "excessive" and "low" are taken from the point of view of practical precipitator operation) and ii) the disappearance of (stable) corona due to the manifestation of the critical pressure.

Examination of the data shows that catastrophic high-temperature currents are not observed in this study under any conditions. This significant point is evident over the full range of experimental pressures and temperatures and both polarities.

It might be expected that runaway currents at low voltages are most likely to occur at the lowest gas densities. However, for the negative corona at $\delta$ less than about unity, the reverse is generally true, i.e., the presparkover currents are much less than at higher densities. For positive polarity, the low-δ presparkover currents are mixed: in most cases they are not lower than at higher δ. Still considering the positive discharge, the data show that combustion gas and fuel gas to a lesser extent, but not air, reveal a tendency to sparkover without corona at the lowest densities. But, in any event, a problem of high gas conductivity associated with low densities does not arise.

---

*The relative gas density $\delta$ is taken with respect to atmospheric pressure and room temperature ($294^{\circ}$K)

On the basis of earlier critical-pressure studies[1,5] it might be supposed, at least at lower temperatures, that the critical-pressure phenomenon would set an upper-pressure limit to the positive current-voltage curves and the associated voltage-density curves -- upon converting density to pressure -- that the positive critical pressure increases with temperature. This comes about because the greater molecular diffusivity prevailing at the higher temperatures more effectively suppresses the sparkover streamer before it completely bridges the interelectrode space[6]. The effect described has not hitherto been demonstrated over so wide a span of temperatures.

The negative critical pressure, as already explained, is expected to be higher than the positive, all other conditions being held fixed. Indeed, by comparison of families of curves for each polarity, it is clear that the negative critical pressure always exceeds the positive. It is further apparent that the negative critical pressure, like the positive, increases with temperature. In other words, the higher the temperature, the greater the range of pressures for stable negative corona.

Comparison of the sparkover-voltage vs gas-density data of Figures 8-10 reveals a tendency for the positive sparkover voltage to exceed the negative at temperatures of 533 K and higher and for low air densities (δ less than about 1 or 2). The data are not unequivical on this score in each case, but the trend seems clear, particularly when supported by experimental results of earlier workers. The significantly higher negative than positive currents prevailing at a given voltage at the higher temperatures are, however, unmistakable.

Somewhat higher negative than positive currents that may be observed at the lower temperatures are, in part, to be attributed to the significant free-electron component of the current present for relatively long mean free paths (low $\delta$) and narrow interelectrode spacing.

Again, it may be generally (though not invariably) seen from Figures 8-10 that, above an air density of 1 or 2, the negative sparkover voltage is higher than the positive. Since increased density reduces the mean free paths and mobilities of the charge carriers, enhanced electron attachment and increased negative-ion space-charge density might be expected to lead to higher negative sparkover voltages. That is, high pressure in combination with high temperature restores, in a sense, the low-temperature situation.

In the case of substitute fuel gas (Figure 12) the positive sparkover voltage exceeds the negative, over the full temperature range shown, up to a density of 6 or 7. For combustion gas (Figure 11) the transition occurs at about a density of 4 for temperatures of, or greater than, 1089 K.

As temperature and pressure are increased together, for all of the experimental situations, it is clear from the data that precipitation is possible at significantly higher voltages than at normal conditions. This is a most important fact when assessing the viability of electrostatic precipitation for high temperature, high pressure particulate removal applications, especially in comparison to other collection devices. The reason for this is that the rate of particle collection in a precipitator is roughly proportional to the square of the electric field strength in the precipitator. The field strength in turn increases with applied voltage. The net effect of an increase in operating voltage is therefore a proportionally larger increase in particle collection efficiency, or a decrease in precipitator size. Thus precipitation becomes more efficient as temperature and pressure increase together.

Other particle collection devices such as filters of various types, cyclones, etc. do not benefit from increasing temperature and pressure. In fact, performance deteriorates in these devices because of increasing gas viscosity and decreasing molecular mean free path. The higher voltage effect in electrostatic precipitation greatly overrides these adverse effects.

## CONCLUSIONS

Following are the major conclusions derived from this work:

1. There are no temperature or pressure limitations to electrostatic precipitation over the range studied.

2. Precipitation becomes more efficient with increasing temperature and pressure. This is in direct contrast to the trend of other particle collection devices.

3. Critical pressure increases with temperature.

4. Negative critical pressure is higher than positive.

5. Negative currents are higher than positive in most cases.

# REFERENCES

1. Robinson, M., "Electrostatic Precipitation" in Air Pollution Control, W. Strauss, ed., Vol. 1, Wiley-Interscience, New York, 1971, pp. 227-335

2. Cooperman, P., "Spontaneous Ionization of Gases at High Temperature, "Conference Paper 63-173, Amer. Inst. Elec. Engrs., 1963.

3. Brown, R. F. and Walker, A. B., "Feasibility Demonstration of Electrostatic Precipitation at 1700°F" J. Air Pollution Control Assoc. 21, 617-620 (1971).

4. Cooperman, P., "Spontaneous Ionization of Gases at High Temperature," Paper ES-MON-6, Inst. Electron. Engrs., 1971.

5. Robinson, M., "Critical Pressures of the Positive Corona Between Concentric Cylinders in Air," J. Appl. Phys. 40, 5107-5112 (1969).

6. Howell, A. H., "Breakdown Studies in Compressed Gases," Trans. Am. Inst. Elec. Engrs., 58, 193-204 (1939).

## TABLE I. TEST VARIABLES

| | |
|---|---|
| Temperature: | Ambient to 2000°F |
| Pressure: | Atmospheric to 500 psig |
| Discharge Electrode Diameter: | 1.58 mm, 2.34 mm, 3.18 mm |
| Discharge Polarity: | +, - |
| Gas Composition: | Air, Combustion Gas, Substitute Fuel Gas |

## TABLE II. GAS COMPOSITION

(Volume %)

| Component | Substitute Fuel Gas | Combustion Gas |
|---|---|---|
| $CO_2$ | 23.0 | 9.2 |
| He | 18.5 | -- |
| $O_2$ | -- | 2.8 |
| $N_2$ | 53.5 | 83.0 |
| $H_2O$ | 5.0 | 5.0 |

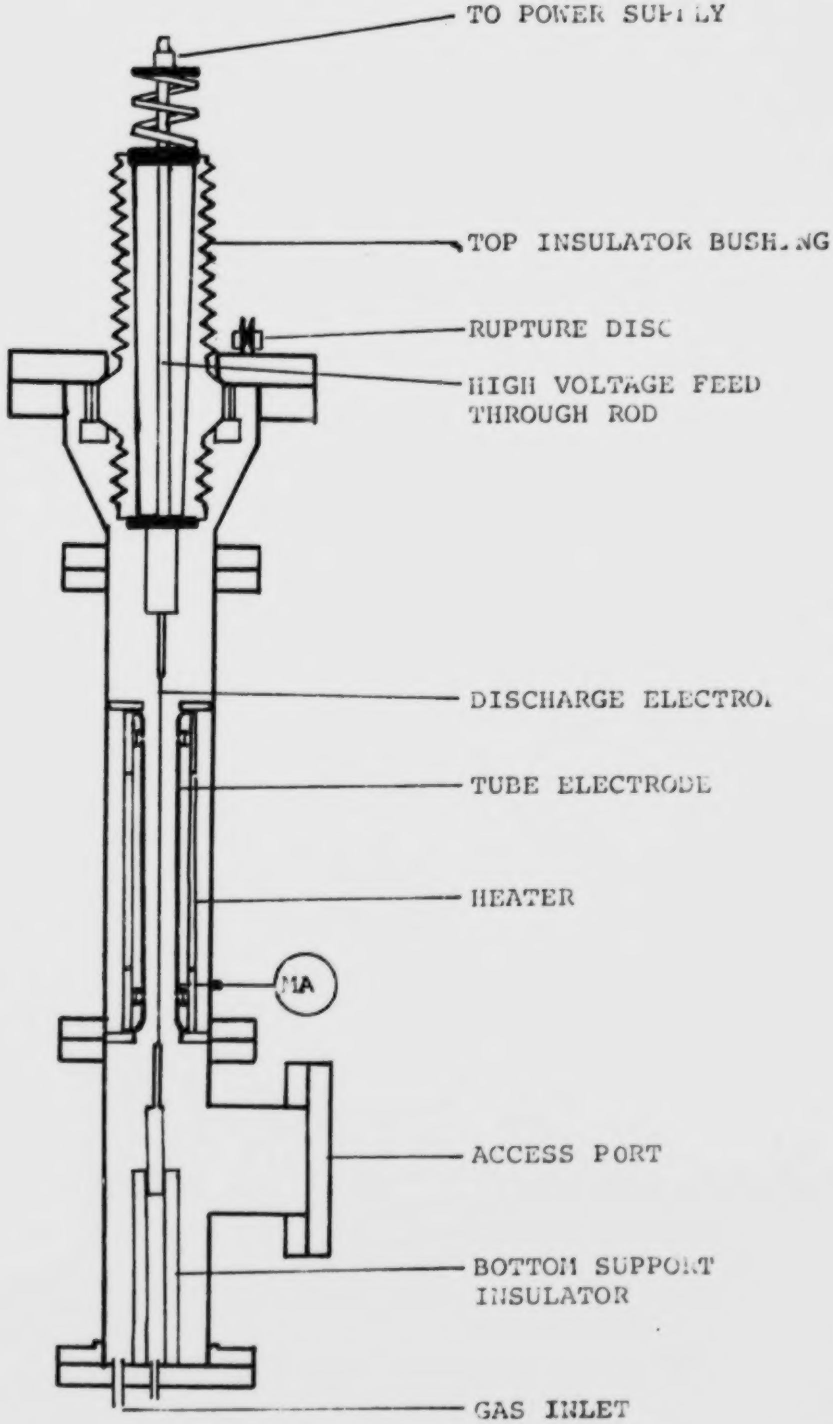
TO POWER SUPPLY
TOP INSULATOR BUSHING
RUPTURE DISC
HIGH VOLTAGE FEED THROUGH ROD
DISCHARGE ELECTRO
TUBE ELECTRODE
HEATER
MA
ACCESS PORT
BOTTOM SUPPORT INSULATOR
GAS INLET

TEST PRECIPITATOR

Figure 1. Laboratory Precipitator and Pressure Vessel for Test Program

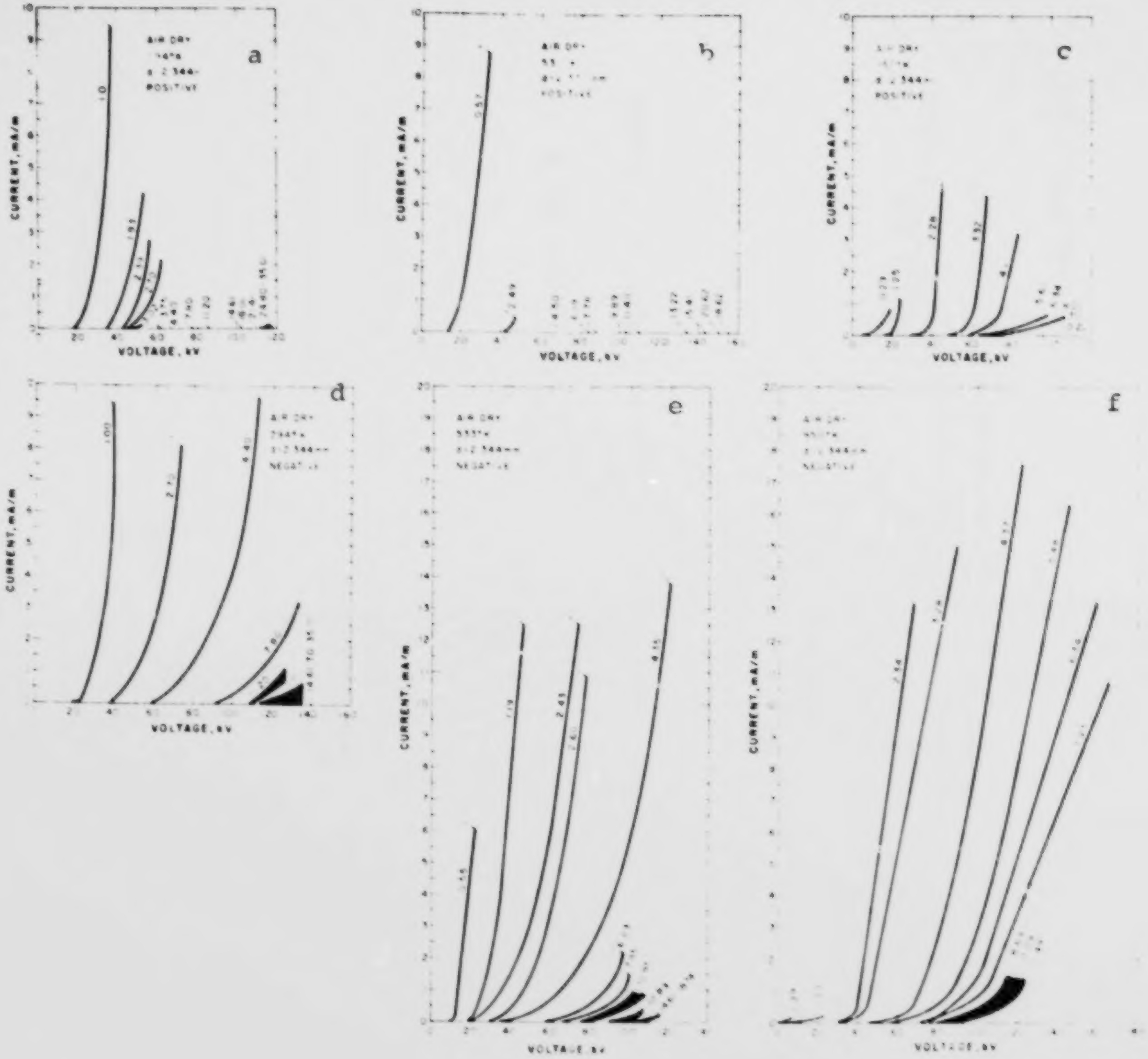

Figure 2. Current-Voltage Curves Taken in Dry Air at Temperatures of 294 K, 533 K, and 950 K for a 2.344 mm Wire Electrode.

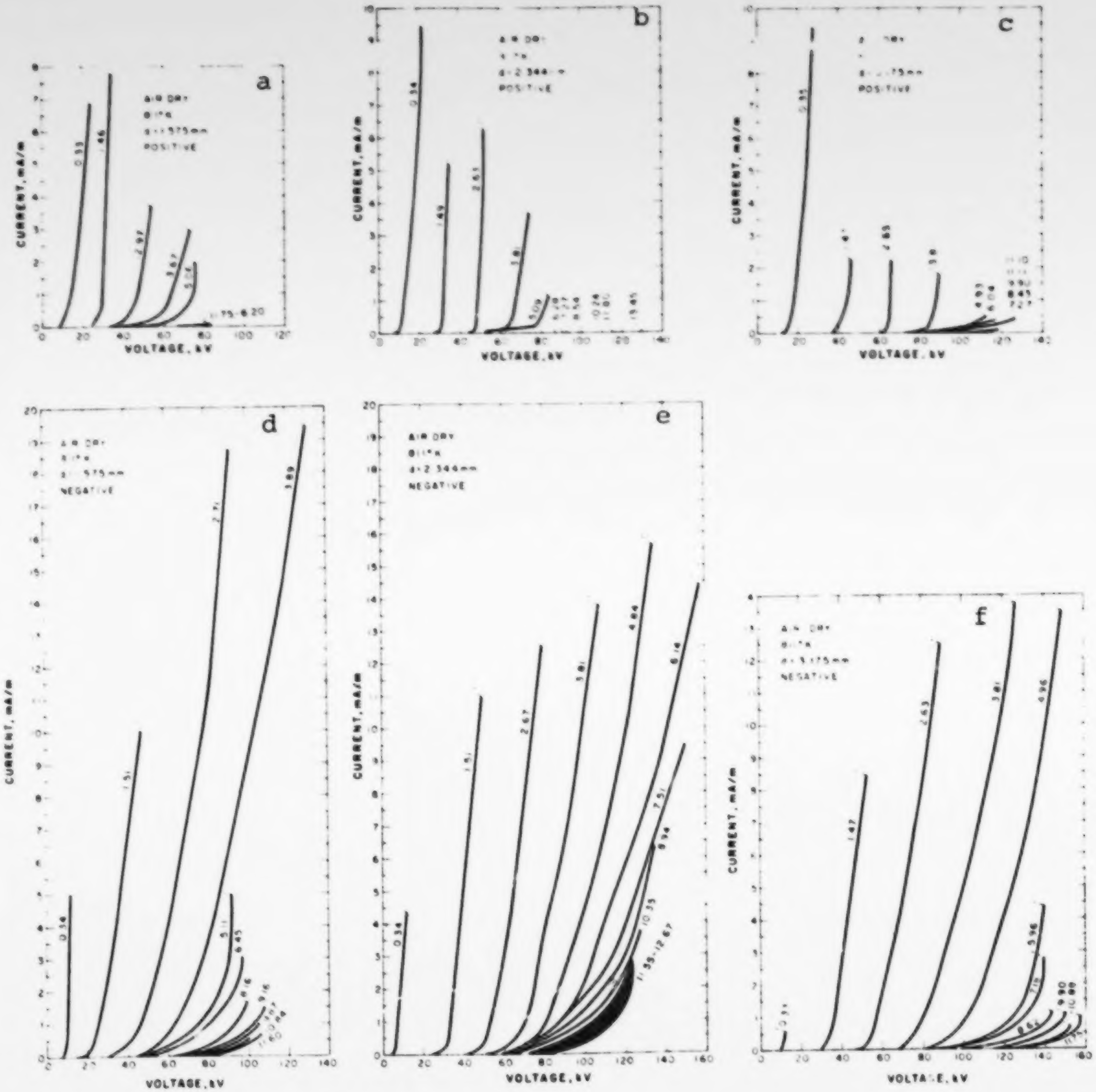

Figure 3. Current-Voltage Curves Taken in Air at a Temperature of 811 K for Wire Electrodes of 1.575mm, 2.344mm, and 3.17 mm.

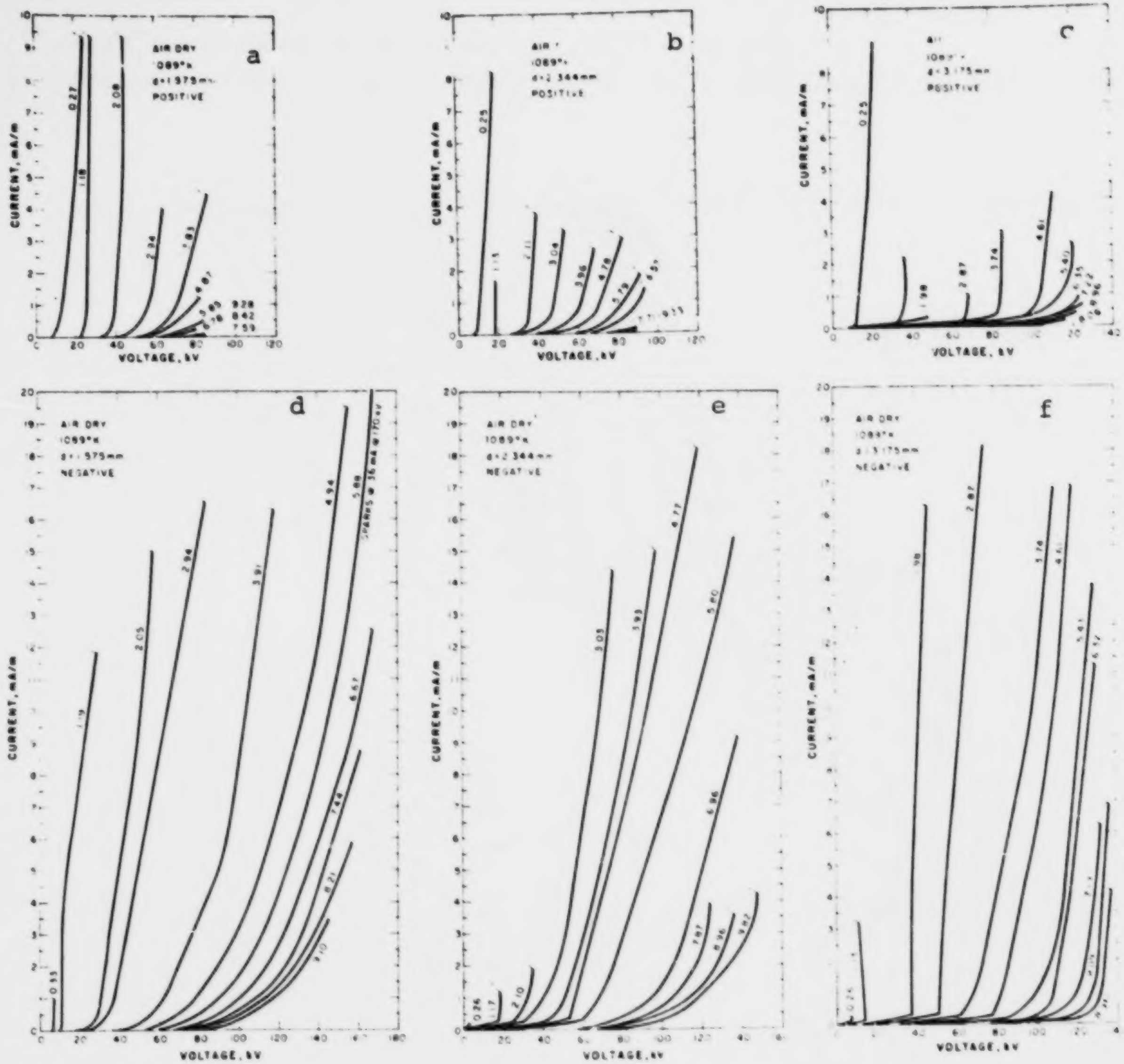

Figure 4. Current-Voltage Curves Taken in Air at a Temperature of 1089 K for Wire Electrodes of 1..75m 2 44 , d .175mm.

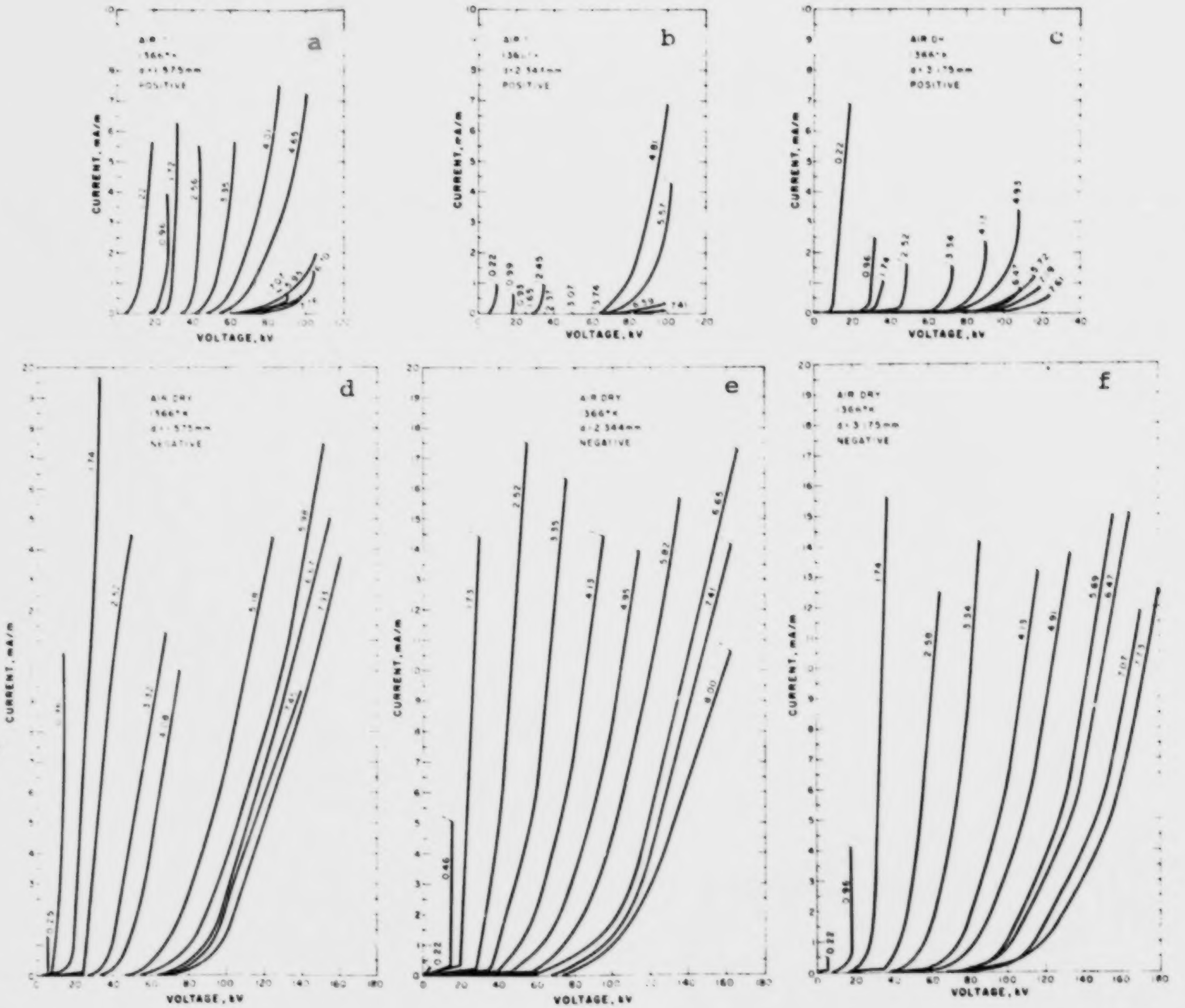

Figure 5. Current-Voltage Curves Taken in Air at a Temperature of 1366 K for Wire Electrodes of 1.575mm, 2.344mm, and 3.175mm.

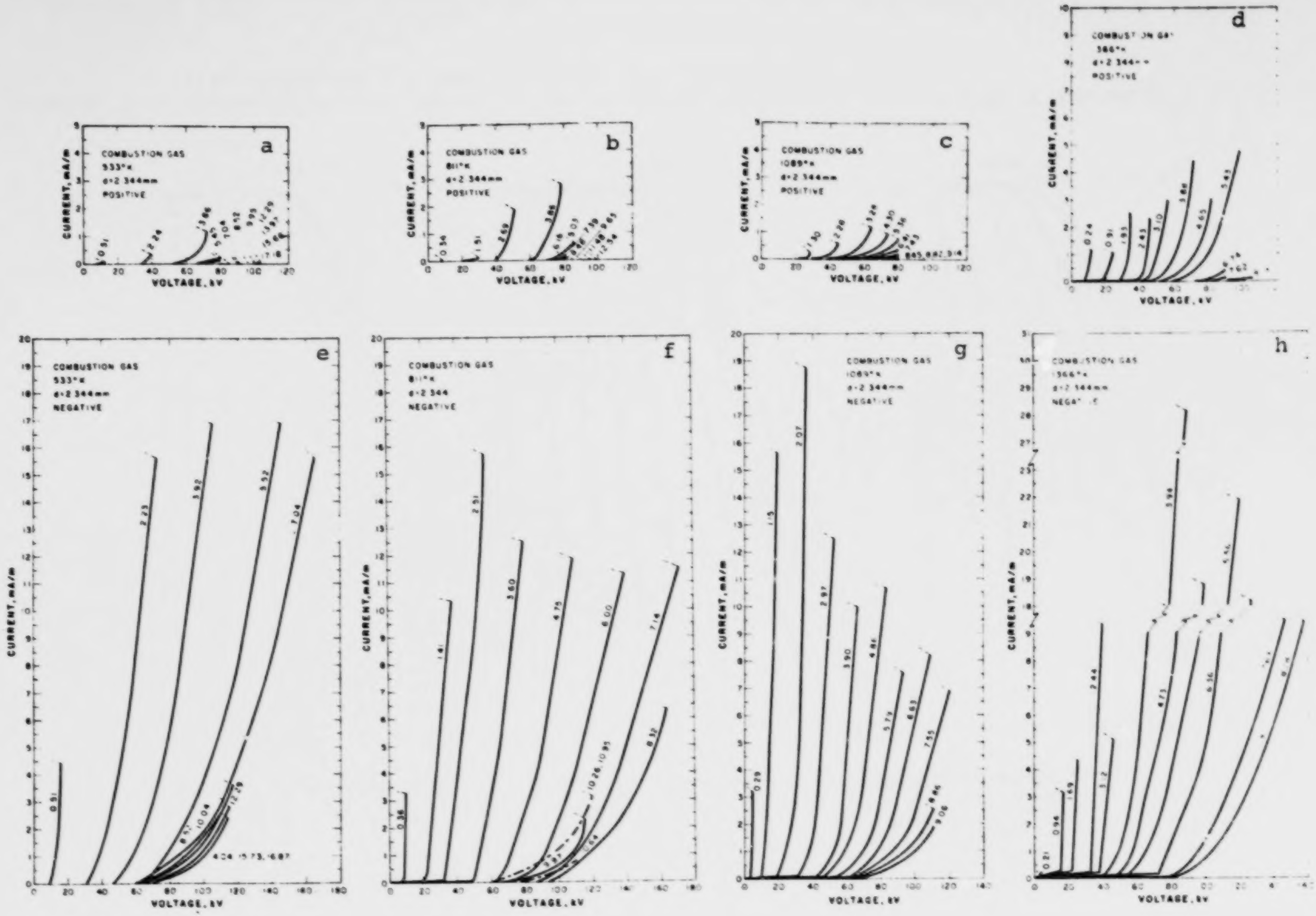

Figure 6. Current-Voltage Curves Taken in a Simulated Combustion Gas Mixture for Temperatures of 533 K, 811 K, 1089 K, and 1366 K Using a 2.344mm Wire Electrode.

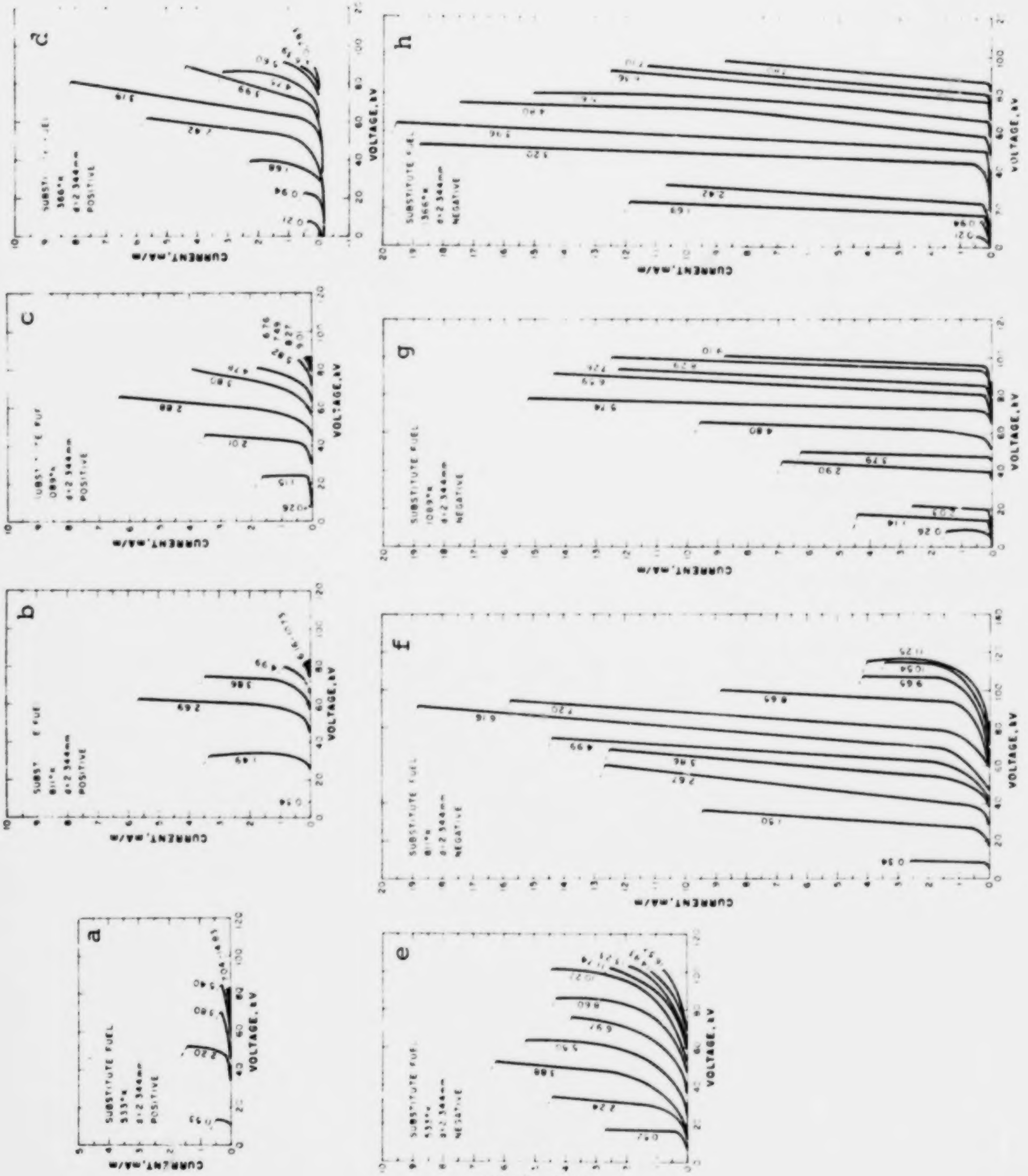

Figure 7. Current-Voltage Curves Taken With a Substitute Fuel Gas Mixture at Temperatures of 533 K, 811 K, and 1366 K for a 2.344mm Wire Electrode

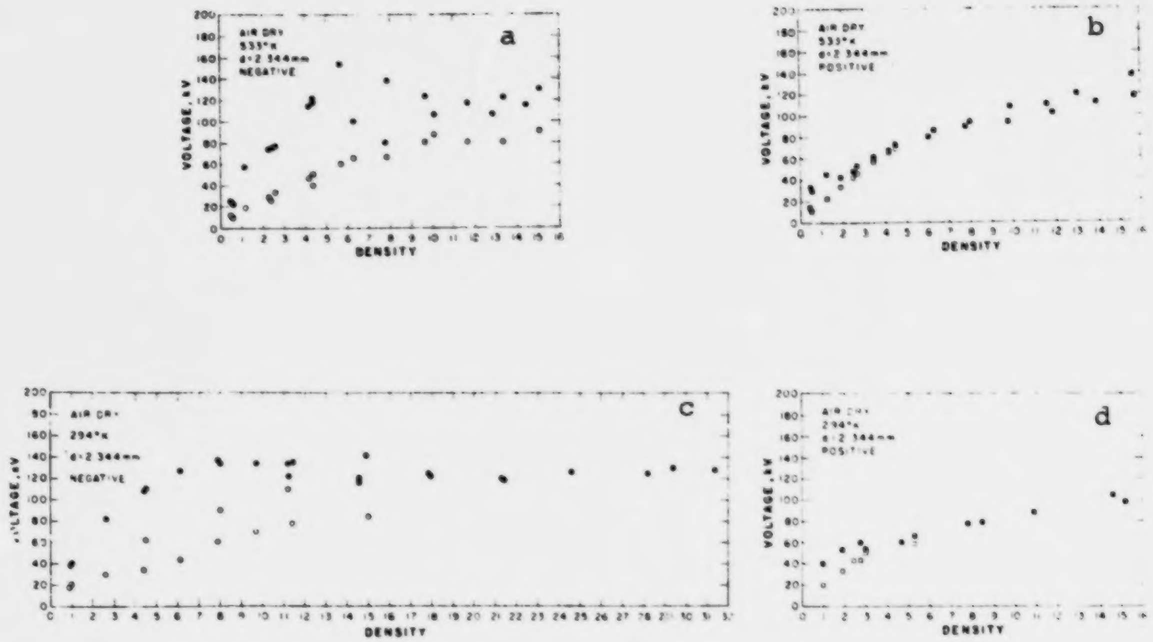

Figure 8. Sparking and Corona Starting Voltage in Air as a Function of Relative Air Density at 294 K and 533 K.

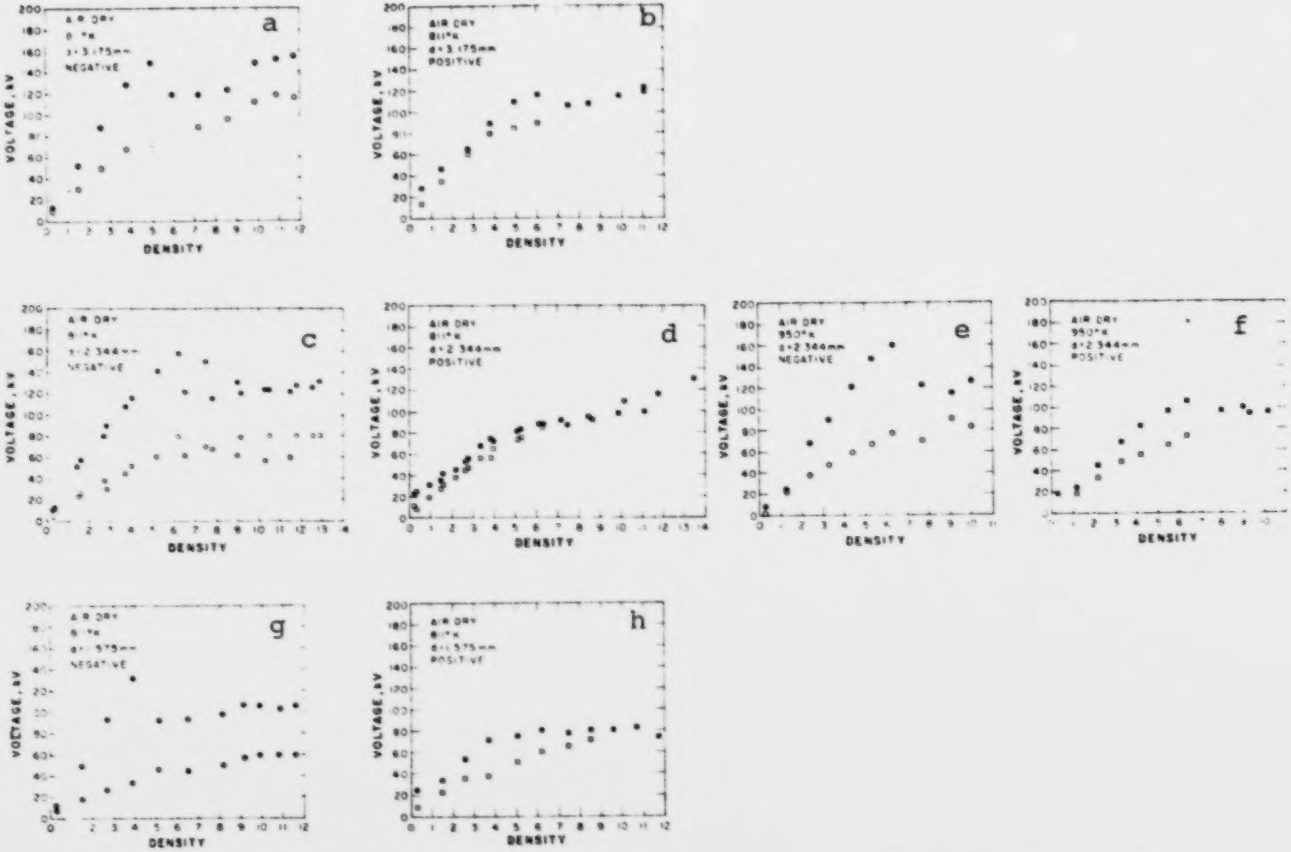

Figure 9. Sparking and Corona Starting Voltages in Air as a Function of the Relative Air Density at 811 K and 950 K for Wire Electrodes of 3.175mm, 2.344mm, and 1.575mm.

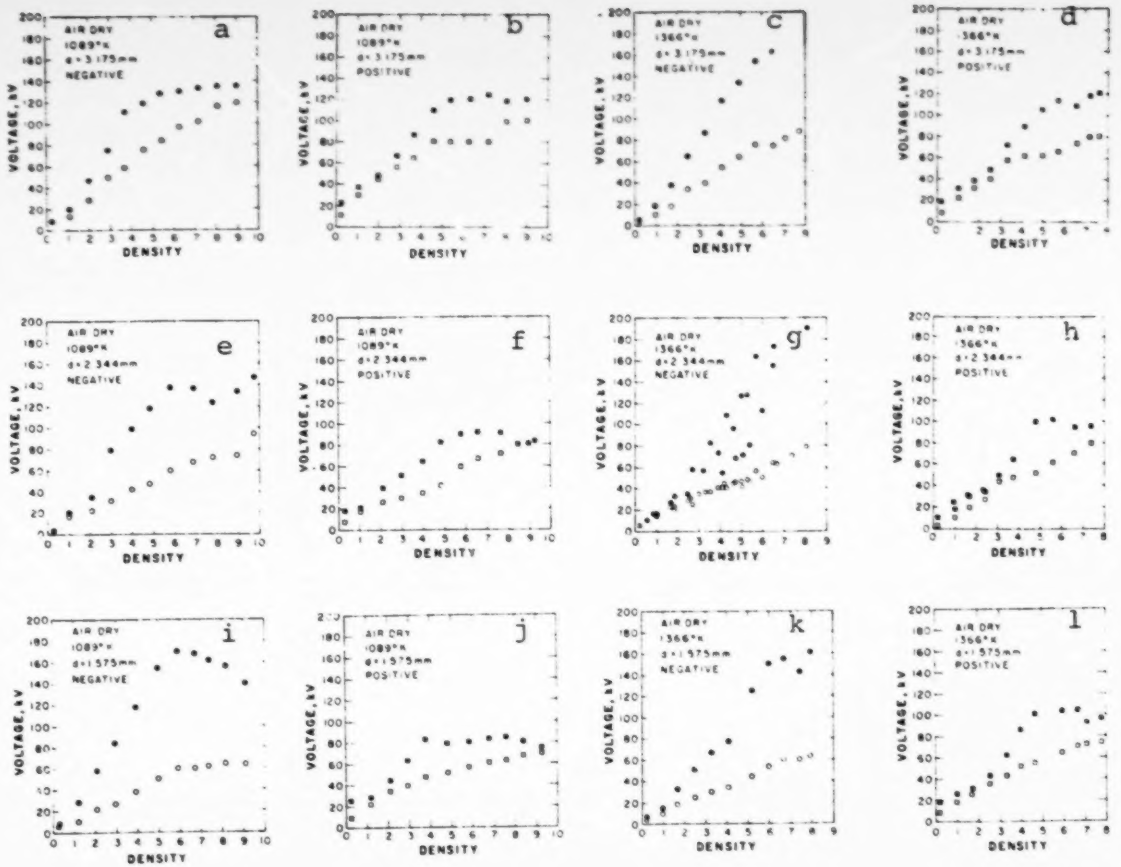

Figure 10. Sparking and Corona Starting Voltages in Air as a Function of Relative Air Density at 1089 K and 1366 K and for Wire Electrodes of 3.175 mm, 2.344mm, and 1.575mm.

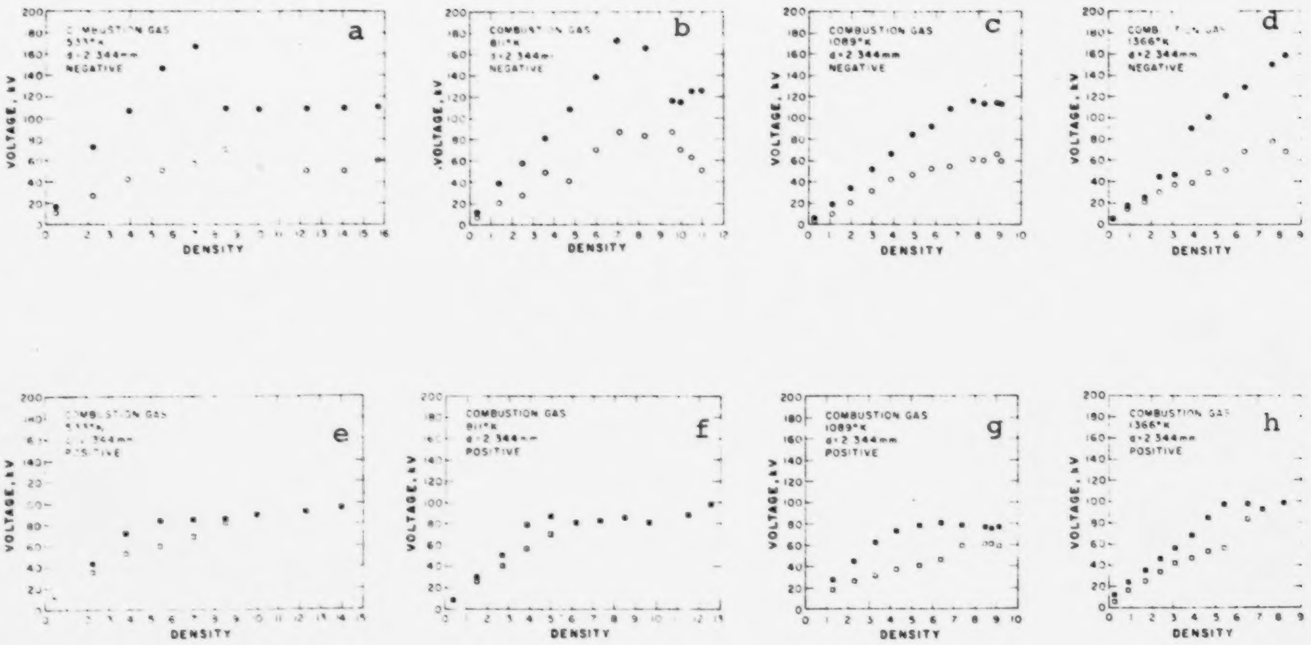

Figure 11. Sparking and Corona Starting Voltages for a Simulated Combustion Gas Mixture as a Function of Relative Gas Density at 533 K, 811 K, 1089 K, and 1366 K for a 2.344mm Wire Electrode.

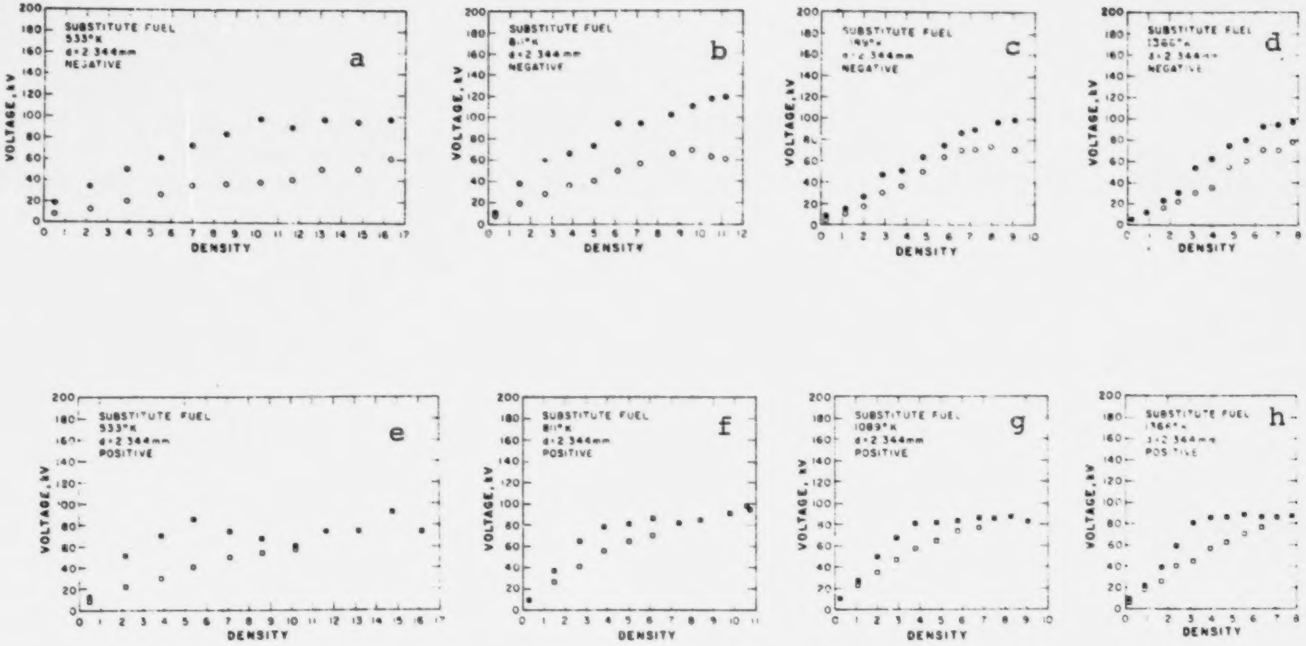

Figure **12.** Sparking and Corona Starting Voltages in a Substitute Fuel Gas Mixture as a Function of Relative Gas Density at 533 K, 811 K, 1089 K, and 1366 K for a 2.344mm Wire Electrode.

CE

# PULSE-JET ACOUSTIC DUST CONDITIONING IN HIGH TEMPERATURE/PRESSURE APPLICATIONS

By:

D. S. Scott
University of Toronto
Toronto, Canada M5S 1A4

W. M. Swift, G. J. Vogel
Argonne National Laboratory
Argonne, IL 60439

# PULSE-JET ACOUSTIC DUST CONDITIONING IN HIGH TEMPERATURE/PRESSURE APPLICATIONS

By:

David S. Scott*, William M. Swift†, G. John Vogel†
*University of Toronto, Toronto, Canada, M5S 1A4
†Argonne National Laboratory, Argonne, Illinois, 60439

## ABSTRACT

The results of a completed investigation of pulse-jet acoustic dust conditioning (PJ-ADC) at conventional gas cleaning temperatures and pressures are reviewed with emphasis on how these performance characteristics might reasonably be extrapolated to high temperature/pressure operation. These arguments indicate that PJ-ADC at high pressure/temperatures might be more effective than at more conventional conditions. On this basis, a planned experimental program to evaluate PJ-ADC upstream of high efficiency cyclones in the pressurized fluidized-bed combusion (PFBC) process development unit (PDU) at the Argonne National Laboratory, is described. Two promising features of PJ-ADC in this application are: (i) the heat of PJ combustion contributes to the PFBC heat, and (ii) the PJ should operate more effectively at elevated pressures.

# PULSE-JET ACOUSTIC DUST CONDITIONING
# IN HIGH TEMPERATURE/PRESSURE APPLICATIONS

## SECTION 1

## INTRODUCTION

Acoustic conditioning of fine-particle aerosols is a process by which the mean size of the particle is increased and their number density decreased through exposure to finite-amplitude acoustic fields. This change in the particulate size distribution is important — for it can allow an increase in the collection efficiency of a downstream dust collector and/or a reduction in the overall particulate-gas separation cost because, with few exceptions, collecting devices retain higher mass fractions as the particulate size is increased. The increased coagulation rate which achieves this rapid change in the size distribution is the result of manyfold increase in the particle-particle collision frequency — which in turn results from dynamic acousto-aerosol interactions (and perhaps to some extent through intermediate processes such as acoustically enhanced turbulence). Experimental evidence, and straightforward physical arguments, indicate that the process can be particularly effective on high dust load fine particle aerosols.

Although the principle of acoustic dust conditioning (ADC) has been known for some time and has been shown to be technically effective, the process has enjoyed little industrial application. This absence of industrial application has been the consequence — primarily — of economic limitations. The first of these is high operating costs due to high specific power requirements, and the second is high capital costs.

Scott (1975) reviewed studies performed at the Ontario Research Foundation and the University of Toronto which examined a new approach to ADC — in which the following two complementary principles were explored.

(i) Firstly, the conventional standing sinusoidal acoustic field, used in most earlier ADC studies was dropped in favour of progressive saw-tooth fields. This change in acoustic configuration allowed major simplifications in the agglomeration chamber yielding both capital and operating cost savings.

(ii) Secondly, the normal techniques of sound generation — such as sirens and mechanically activated pistons — were discarded in favour of a resonant pulse-jet acoustic source. This not only allowed a direct conversion of fuel to sound and the use of a simple no-moving-part device, but also readily produced high intensity progressive saw-tooth acoustic fields.

In summary, the practical results of this program showed that significant — 0(10) — advances can likely be achieved by this new process in all three areas of (a) capital, (b) maintenance, and (c) operating costs. At the same time, the mean particle size was increased 5-7 fold.

The more important aspects of Scott (1975) results for the research plan described in this paper were that (i) mean particle size increases of 0(6) appears to be fairly readily achieved, (ii) the process requires a low level of technical sophistication and (iii) it is possible to make approximate cost evaluations relating to the process should it be proven technically feasible. By these criteria, it appeared reasonable to examine the feasibility of using Pulse Jet Acoustic Dust Conditioning (PJ-ADC) in the high pressure/temperature application of pressurized fluidized-bed combusion. (PFBC).

## SECTION 2

## BASIC APPROACH OF PLANNED RESEARCH/DEVELOPMENT

Development of PFBC for use in thermal power generating stations is being carried out at several laboratories. The process involves coal combustion in a fluidized-bed of $CaSO_3$. The lime solids react with the combustion released sulphur oxides to form $CaSO_4$ which remains in the bed as particulate matter. Thus, compared with conventional combustion processes, the aerosol effluent contains a lower level of $SO_2$ — but the particulate mass loading can be much greater (due to entrainment of calcium particulate along with the ash particulate). In a sense, the gaseous pollution problem is reduced at the expense of increased particulate loading.

In the PFBC configuration being examined by Argonne National Laboratory (as well as at several other laboratories), the combustion process is pressurized to approximately 10 atmospheres with the intention that the off-gases be expanded through gas turbines. But hot, particulate laden, gases cannot pass through gas turbines without massive destruction to the turbine blades resulting in unacceptably short lifetimes. And so we have particulate-gas separation requirements at high temperatures and pressures which are critical not only for environmental but also process requirements.

At the temperatures $0(1150^{o}K)$ and pressures 0(10 atm.) which are anticipated, most conventional particulate removal techniques are unsuitable. Separation by cyclones seems to be one of the few systems that can operate under these conditions. Unfortunately, the performance characteristics of current cyclones do not appear sufficient to meet the gas cleanliness standards set by turbine manufacturers — although there remains some uncertainty regarding what these standards should be. Nevertheless, it appears likely that the ultimate criteria may require that there be no more than $3x10^{-3}g/m^{3}$ of particulate matter above 2 μm diameter.

Results of the PFBC program at ANL indicate that the mass loading and size distribution of the particulate matter exiting from a two stage high efficiency cyclone should not be far from that which would be acceptable as turbine inlet conditions. Moreover, a fairly straightforward evaluation indicates that if the mean particle size of particulate matter entering the cyclone was increased by perhaps less than a factor of 5, the performance of the cyclone would be improved such that the effluent *would* meet turbine inlet criteria. For these reasons it is our current plan to initiate a research program to investigate the effects of using ADC in this application.

The program at ANL will evaluate the effectiveness of pulse-jet ADC in a bench scale fluidized-bed combustor.

There are several promising aspects of this approach. Firstly, the heat of combustion from the pulse-jet simply adds to the overall process heat. Thus the power requirements will, in principle, be zero — although the cost per heating unit for pulse-jet fuel may be expected to be somewhat higher than that of coal. Secondly, because the pulse-jet will run at higher power levels due to the elevated pressures it should, in principle, be a more effective sound generator than if it were running at ambient conditions — the result of both charge density effects and more efficient combustion.

Conceivably, there might be deleterious ADC effects. For instance, very fine submicron particles might be agglomerated into a size range below that which would be effectively removed by the cyclone, but within a range which could do damage to turbines. Evaluations of the mass loading ratio in the very fine particle spectrum indicate that this should not be a problem — but it will clearly be an aspect which shall be monitored during the experimental program.

Turning to the experimental program itself, one of the main difficulties of process evaluation shall be "scaling". A pulse-jet is a device which cannot be scaled up or down without changing the acoustic characteristic — for a pulse-jet is a quarter wavelength device. Ultimately, it is expected that single pulse-jets will generate sufficient sound to treat between 5,000 to 10,000 cfm. But the current test plant at ANL yields approximately 81 scfm, or on the order of 20 acfm.

In response to these scaling demands, the pulse-jet will exhaust into a resonant-manifold. The manifold shall be capable of splitting the acoustic energy into a "waste" stream and two "process streams". Two process streams are required in order to examine the effects of ADC on both the primary cyclone and secondary cyclone performance. Pulse-jet products of combustion will be exhausted primarily through the "waste" stream duct (vent). By means of the resonant-manifold a large total acoustic power output can be reduced to match the amount of particulate-laden gas being treated. At the same time, this approach will allow the acoustic field to be varied in intensity from approximately 165 db downwards, in order to parametrically evaluate sound intensity requirements. By exhausting the pulse-jet into a resonant-manifold, and then drawing off the acoustic power as required for the much smaller scale dust treatment streams, we expect to eliminate both the scaling difficulties as well as allow a greater degree of parametric flexibility than would be the case were we to exhaust the pulse-jet directly into the particulate-laden gas.

## SECTION 3

## SOME EXPERIMENTAL DETAILS

Although our experimental program is very much in the formulation stage, it is possible to make additional comments regarding the experimental capability we are developing.

## PULSE-JET (PJ) SOUND GENERATION

A range of literature has been reviewed on pulse-jet operation. From this, we conclude that the power generated by a pulse-jet is essentially linearly related to pulse-jet rating — that is, its ability to consume fuel. On this basis, it is clear that our expectations that the pulse-jet operate more effectively at higher pressures should be fulfilled. Several pulse-jet configurations will be tried. And it is expected that fundamental operating frequencies between 250-300 Hz should be achievable. From private communication with pulse-jet researchers, it appears that units designed to operate at frequencies much above this range tend to be temperamental. Aerodynamically valed (i.e. no moving part) pulse-jets using propane as the fuel are now under development for our research program.

## RESONANT MANIFOLD SYSTEM (RMS)

As we noted earlier, it is intended to exhaust the pulse-jet into a resonant manifold which shall act as a sound source from which acoustic energy can be drawn for aerosol treatment. A schematic illustration of the RMS is given in Fig. 1. The manifold will be designed as a "length resonator". In this configuration, the flat plate ends of the chamber will act as velocity nodes for standing waves set up within the RMS. It is from the flat end walls that the acoustic field shall be drawn for ADC processing. Fig. 1 shows two process sound ducts existing from the same end plate that contains the pulse jet. Two ducts are intended so that the aerosol entering both the primary and secondary cyclones may be treated.

It should be noted that all dimensions involving the acoustic wave length, are to be adjustable. This flexibility is required since it is impossible to predict in advance — except within a fairly broad range — the frequencies and wave lengths which will be generated.

## PRESSURE CONTROL

One of the unique requirements of this research is that of providing sound at elevated pressures — specifically between 1 and 10 atmospheres. This requires that the entire PJ-RMS be capable of operating over this pressure range. And this includes the pulse-jet fuel and air manifolds.

To meet these requirements, the design as currently envisaged incorporates a pressure differential measuring unit between the PDU and RMS which in turn will operate a valve controlling the rate of exhaust from the vent shown in Fig. 1. This control will be critical to the entire experiment. And it is expected that a very small $\Delta \rho$ between the RMS and PDU will be maintained — with the pressure in the RMS being the higher.

Fail-safe valves for PDU/RMS isolation in the event of a disruptive loss of pressure in either, will be installed in the process sound ducts. These valves will also serve as isolation valves while the PDU and RMS are brought up to operating conditions.

ACOUSTIC TREATMENT SECTION (ATS)

One of the advantages in examining PJ-ADC by means of this intermediate RMS, is that alternate acoustic treatment sections will be particularly straightforward to install. We intend to use a simple "two flange" procedure, whereby we interchange various ATS configurations quickly, and with little cost, in order to cover several alternatives. A schematic illustration of one "two flange" ATS configuration is shown in Fig. 2. The spiral is an intentional design which — from previous research — we believe might be effective. This conclusion comes from both experimental findings and the impression that interactions between finite amplitude acoustic fields and basic flow induced turbulence can enhance the coagulation process. The spiral configuration will cause additional circulation phenomena. But the use of grids and other turbulence generators might also be examined.

## SECTION 4

## CONCLUDING REMARKS

It is our view that earlier work on PJ-ADC has shown that modifications to the mean size of the particulate matter in a dusty gas stream can be accomplished to a degree and at a cost, that would be very attractive if such could be achieved in the high pressure/temperature off-gases associated with fluidized-bed combustion processes. Since there is no presently identifiable reason why these basic results should not be possible to reproduce at high pressures and temperatures — indeed the high pressure/temperature environment seems likely to enhance the success of the process — it appears reasonable to examine the feasibility of PJ-ADC in this application.

But, the transformation from the operation of PJ-ADC at approximately atmospheric conditions to these higher pressures, involves certain non-trivial advances to current technology. For this reason, what we learn regarding these supportive aspects of the experimental program may be of as much interest as will our success or failure at illustrating the feasibility of PJ-ADC under these conditions.

# REFERENCES

1 Scott, D.S., "A New Approach to the Acoustic Conditioning of Industrial Aerosol Emissions", *J. Sound and Vibration*, Vol. 43, no. 4, pps. 607-619, 1975.

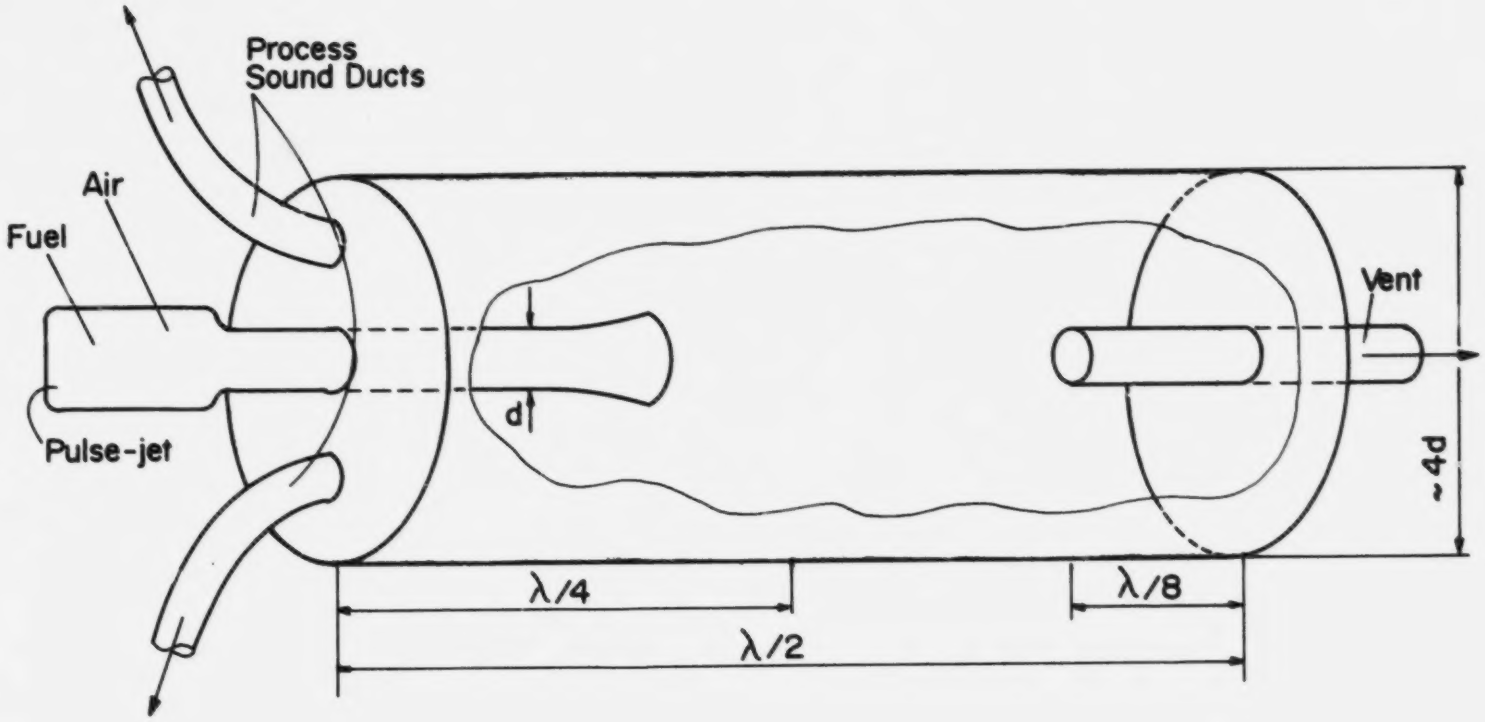
Process
Sound Ducts
Air
Fuel
Pulse-jet
d
Vent
~4d
$\lambda/4$
$\lambda/8$
$\lambda/2$

FIG. 1: SCHEMATIC OF RESONANT MANIFOLD SYSTEM

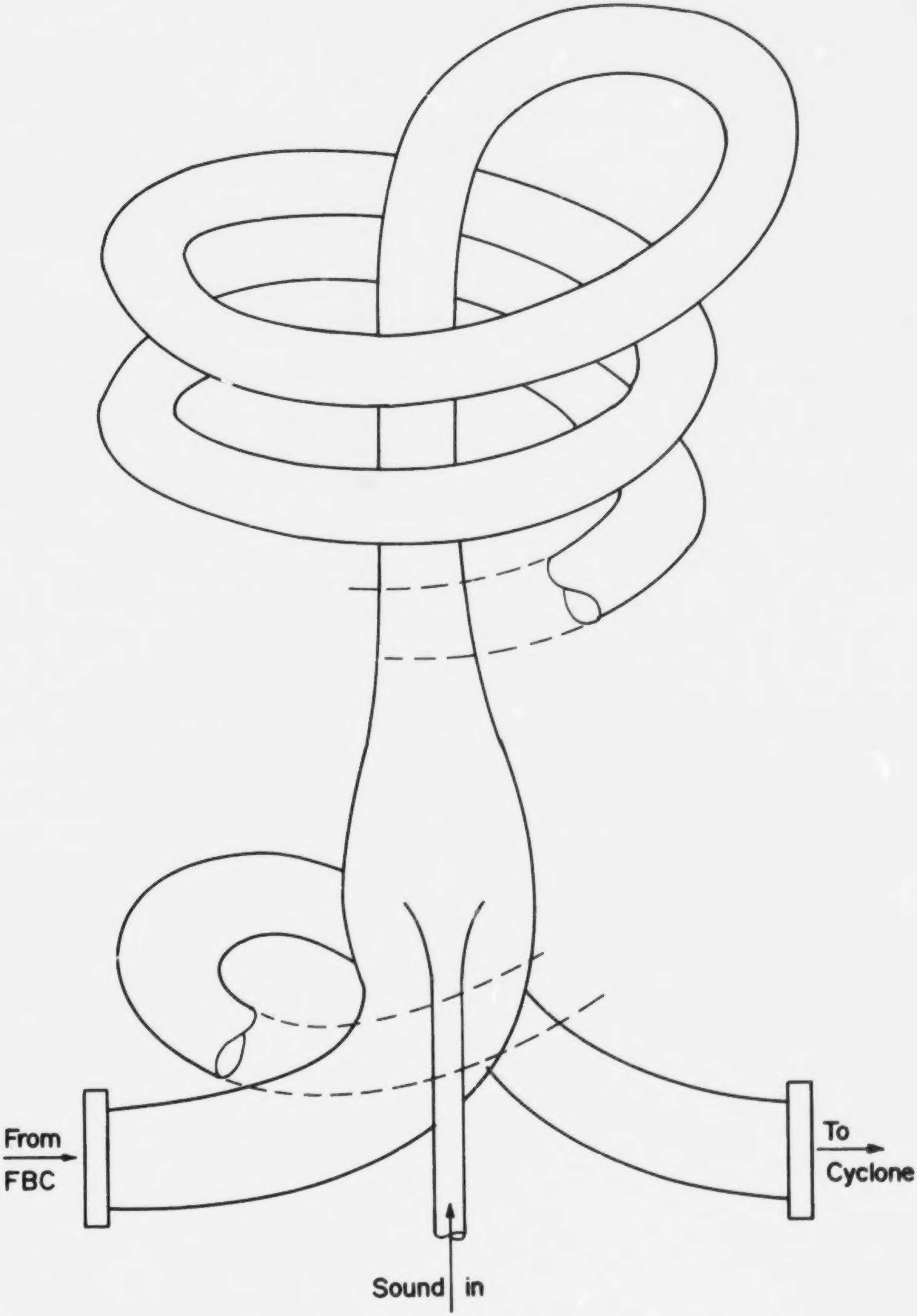
From
FBC
To
Cyclone
Sound in

FIG. 2: FLANGE TO FLANGE ACOUSTIC TREATMENT SECTION

CC

# THE APPLICATION OF SONIC AGGLOMERATION FOR THE CONTROL OF PARTICULATE EMISSION

By:

D. T. Shaw, J. Wegrzyn
State University of New York at Buffalo
Buffalo, NY 14226

# ABSTRACT

The feasibility of using acoustic agglomeration for particulate emission control in industry is evaluated. The dependence of the agglomeration time, which determines the agglomerator size, on various parameters - such as the mass loading, particle geometric mean diameter and standard deviation, acoustic frequency and intensity - is analyzed. Two agglomeration mechanisms are included: the inertial capture and the hydrodynamic collision. Based on the estimated agglomerator size and the specific energy consumption, possible applications of the acoustic agglomerator in industry is discussed, with special emphasis on the possible use of such a device in an environment in which the combined effects of high-pressure, temperature and chemical corrosion make it difficult to use the conventional devices.

## Introduction

Sonic agglomeration has been a rather controversial subject ever since the first experiment by Patterson and Cawood in 1931 [1] who discovered that aerosol particles are quickly agglomerated in a standing-wave sound tube. Shortly afterward independent acoustic agglomeration experiments were carried out by Brandt, Freund, and Hiedemann [2] in Germany, Andrade and his co-workers in Great Britain [3] and St. Clair at the U.S. Bureau of Mines [4]. Their results generated great enthusiasms for acoustic agglomeration and eventually the large scale industrial testing of its effectiveness. During the second World War, serious efforts were made by the U.S. Navy and Army to use acoustic dissipation of fogs for the improvement of visibility for landing at airports and on aircraft carriers. Although the field testings gave a positive result in calm weather, this technique was proved to be ineffective under moderately high-wind conditions and the project was abandoned [5]. During the post war years several commercial models of high power sirens with an acoustic efficiency of the order of 40-60% were available and this spurred a widespread interest in the application of sound waves for the control of particulate emissions from power plants, steel mills, and other process and chemical industries [6-11]. The work in this period was summarized by Mednikov [12] and more recently by Shirokova [13]. However, the results of the industrial-type acoustic agglomeration testings were invariably discouraging, mostly due to the high power consumption for the sound generation. This greatly reduce any interest among the researchers in the United States and after 1953 the acoustic agglomeration work was almost completely stopped in this country.

Recently, there has been a renewed interest in acoustic agglomeration as related to energy-environmental research. In order to reduce our national dependence on foreign oil imports numerous new programs have been established by the Department of Energy to seek answers to problems associated with how to generate electricity with high-sulfur coal, to improve central power plant efficiency and above all, to accomplish these with a minimum environmental degradation. These new programs lead to new engineering problems such as dust removal in a coal-gasification plant, solid-seed extractions from a MHD generator, and so forth. These new problems create a critical need for a nonconventional particulate-emission control device which can operate effectively in a combined high temperature, pressure and corrosive environment.

As an example, acoustic agglomerators are considered to be one of the primary candidates for the removal of dust particles before the combustion gas enters the gas turbine in a pressurized fluidized-bed boiler power plant. Several concepts of the fluidized in-bed combustors have been considered for power plant applications. Among these the ideas of using a pressurized, fluidized bed combustor in a combined gas-turbine and steam-turbine cycle is particularly attractive. Steam for operating a turbine is raised by both the steam tubes immersed in the fluidized bed and by the heat convertor boiler of the gas turbine. The heat of combustion is removed from the bed to run directly to the gas-turbine. Typically such a fluidized bed uses crushed coal of about 1/4" diameter. Most of the fly-ash particles are rather large, say 100 μm; however, some smaller particles are also produced which must be removed from the flue gas to avoid the attack of gas-turbine blades by such corrosive particulates as sodium salts.

Cyclones are used to effectively remove large particles. For particles in the range of 2-20 μm diameter nonconventional devices are suitable for this application. Filters are difficult to use because of the high temperature, corrosive environment and because of the inherent high-pressure drop across the filters. The electrostatic precipitator is not applicable because under the high pressure (10-20 Atm in the fluidized-bed boiler) it is difficult to produce the corona discharge without generating excessive electric arcs. The use of an acoustic agglomerator, operating either in standing-wave or traveling-wave mode, appears very attractive.

## Evaluation of Sonics for the Control of Particulate Emissions

Under the sponsorship of the Environmental Protection Agency, a report on the application of acoustic agglomeration for fine particle control, was published by Hegarty and Shannon of the Midwest Research Institute [16]. While the report represents a good review of the work done during the 1950's it contains some questionable assumption in its evaluation of the system. Specifically, the effectiveness of an acoustic agglomerator is evaluated on the basis of the agglomeration tiem $t_o$, which according to Mednikov [12] can be written as

$$t_o = \frac{3}{K_a} \ln\left[\left(\frac{\rho_p}{\rho_{po}}\right)^{1/3} \frac{a}{a_o}\right] \tag{1}$$

where,

a is the particle radius, $\rho_p$ is the particle density. The subscript o represents the conditions at time $t = 0$, $K_a$ is the agglomeration constant which will be shown later to be directly proportional to the square root of the acoustic intensity Ω. In reference [16], however, $K_a$ is assumed to be equal to $\Omega^{1/2}$; that is

$$K_a = F(d_g, d_c, \sigma_g, m, f)\ \Omega^{1/2} \quad \text{and } F = 1 \tag{2}$$

where F is a complex function of the geometric mean diameter of the particle $d_g$, the particle diameter to be controlled $d_c$, the geometric standard deviation $\sigma_g$, the mass concentration m, and the acoustic frequency f. In reference [16] the value of F is assumed to be 1 at all times. The justification of the assumption is not available in the report.

The objective of the present paper is to carry out a more realistic evaluation based on the theoretical model and the experimental data obtained recently in our laboratory.[15,17-20] To do this, we write

$$K_a = \alpha\pi\ (a_1 + a_2)^2\ \varepsilon(\chi,\xi)\ \mu_{12} U_g\ n_1 \tag{3}$$

where $\alpha$ is the refill factor, $\varepsilon$ is the particle collection efficiency, $n_1$ is the concentration of large particles, $\mu_{12}$ is the relative entrainment given by

$$\mu_{12} = \omega(\tau_1 - \tau_2)(1 + \omega^2\tau_1^2)^{-\frac{1}{2}}(1 + \omega^2\tau_2^2)^{-\frac{1}{2}} \tag{4}$$

where $\omega$ is the angular frequency $\omega = 2\pi f$. $\tau$ is the particle relaxation time defined by

$$\tau = \frac{2}{9}\ \frac{\rho_p}{C\eta}\ a^2 \tag{5}$$

where C is the Cunningham correction factor, $\eta$ is the dynamic viscosity and $U_g$ in Eq.(3) is the amplitude of the particle oscillating velocity

$$U_g = (2\Omega/c\ \rho_g)^{1/2} \tag{6}$$

where, c is the sound speed in air and $\rho_g$ is the gas density. It is clear from Eq.(3) and Eq.(6) that $K_a$ is proportional to $\Omega^{1/2}$ as shown in Eq.(2).

The derivations of the analytical expressions for $\varepsilon$ are given in reference [17] for both the case of inertial capture and that of hydrodynamic collisions and are not repeated here, only the results are given.

For hydrodynamic interaction we have

$$\varepsilon = a_1^{-2}\left\{1 + l - \left[(l^6 + p_1^6)^{-1/6} - ((1-l)^{1.5} + p_2^{1.5})^{-2/3}\right]\right.$$
$$\left.\left[\frac{1.587}{a_e} + \frac{32.73}{a_e^2} + \frac{344}{a_e^2(20/a_e)^{1.56}} \exp\left(-\frac{a_e-10}{15}\right)\sin\left(\frac{a_e-10}{63}\right)\right]\right\} \tag{7}$$

where $\tau_1$ is the large particle relaxation time. $a_e$ is the effective radius of an acoustic equivalent particle whose gravitional settling velocity is the same as the average flow around velocity of the large particle of radius $a_1$[17]

$$a_e = (2\mu_g/\tau_1 g)^{1/3}(\Omega/\rho_g)^{1/6}a_1$$

For inertial capture, we have

$$\varepsilon = \frac{K_e^2}{(K_e + 0.25)^2} \tag{8}$$

where $K_e = \dfrac{\tau_e^2 g}{a_e}$ .

Using Eqs. (3) to (8), computer calculations have been carried out on the variation of the particle size distribution function as a function of time under various acoustic conditions. These theoretical results are then compared with the experimental data based on the combined use of the electromagnetic speakers for low-frequency sound and the aerodynamic siren in our laboratory for the high-frequency sound [18,19]. The good agreements between the theory and our experimental data give us reasonable confidence on the validity of our theoretical model, More specifically, the hydrodynamic interaction and the inertial capture as represented by Eqs. (7) and (8) respectively, can be considered as the principal mechanisms responsible for the enhanced agglomeration rate under an acoustic field. Other secondary mechanisms, such as the parakinetic interaction, attractional interaction and drift are considered to be primarily responsible for refilling of the controlled volume every time after the particles are swept clean during each oscillating cycle. Experimental data show that at high intensities ( > 150 db) the refill processes are very effective. Thus the refill factor $\alpha$ in Eq.(3) is assumed to have a value of 1 in the present paper. Depending on the magnitude of the interception number I (= $a_2/a_1$), the present model determines the acoustic agglomeration constant in two regions: (1) the hydrodynamic collision region(I $\simeq$ 1) and (2) the inertial capture region (I <<1).

In the following sections we will attempt to make some predictions concerning the agglomeration rate and the dwell time based on this model. These results will then be used to compare with the results obtained in ref. [16].

### Determination of the Half-Life Decay Time

Consider now a polydisperse aerosol. We define a half-life decay time $t_{1/2}$ as the time when the aerosol concentration reduces to half of its original value. Using the rate equation

$$\frac{dN(a_2)}{dt} = -K_a N(a_2) \tag{9}$$

we have by integration:

$$\frac{N(a_2)}{N_o(a_2)} = \frac{1}{2} = \exp(-\tilde{K}_a t_{1/2}) \tag{10}$$

or

$$t_{1/2} = \ln 2/K_a \tag{11}$$

where $N(a_2) = \int_o^{a_2} n(a)\,da$ is the particle number concentration with radius less than $a_2$, $N_o(a_2)$ is the value of $N(a_2)$at $t = t_o$ and $\tilde{K}_a$ is the effective acoustic agglomeration constant for a log-normally distributed aerosol. According to Eq.(4) we can write

$$\tilde{K}_a = \int_{a_2}^{\infty} K_a n(a_1)\,da_1 \tag{12}$$

where $a_1$ and $a_2$ are the radii for large and small particles, respectively. Using Eq.(3) we have

$$\tilde{K}_a = U_g \int_{a_2}^{\infty} \mu_{12}(a_1,a_2)\,\varepsilon\,(a_1,a_2)a_1^2 n(a_1)\,da_1 \tag{13}$$

$n(a_1)$ is assumed to be a log-normal distribution function which is justified both from our measurements and from direct measurements of the combustion products from a boiler [21]. Based on Eqs. (11) and (13), the variation of the half-life decay time $t_{1/2}$ can be calculated once the particle mass loading ($\mu g/cm^3$), the geometric standard deviation $\sigma_g$, the geometric mean diameter $d_g$ ($\mu m$), the acoustic intensity $\Omega$ (Watt/$cm^2$) and acoustic frequency f are given.

Figure 1 shows some theoretical predictions based on this model. Here, the fraction of the fine particles ($d_2$=2μm) remained airborne after the acoustic field (f = 1 KHz) is turned on at t = 0. The geometric mean diameter of the particles, weighed with respect to number concentration, is fixed at 0.15 μm. The size distribution function is assumed to be log-normal with the total number concentration N and the geometric standard deviation $\sigma_g$ as variables. The initial values of N and $\sigma_g$ are $1.2 \times 10^5 cm^{-3}$ and 3.45 respectively (curves 1,2 and 3). As shown, the $t_{1/2}$ for curve 1 ($\Omega = 0.01\ W/cm^2$), curve 2 ($\Omega = 0.1 W/cm^2$) and curve 3 ($\Omega = 1 W/cm^2$) are respectively 95, 30 and 9.5 sec. This is consistent with the theoretical model as expressed in Eq.(2) which is an analytical relation for inertial capture of particles based on Eq.(8).

The effect of reducing the standard deviation value $\sigma_g$ is demonstrated by curve 4. Here $\sigma_g$ is reduced from 3.45 (for curves 1, 2 and 3) to 1.6. Such a relatively monodisperse aerosol has a very small value of acoustic agglomeration constant $\tilde{K}_a$ and thus a very large value of $t_{1/2}$ (Eq.11). The agglomeration becomes ineffective because the number of large particles (which act as the collecting centers of small particles) are drastically reduced when $\sigma_g$ is decreased.

The fact that the number of available large particles has a dominant effect on agglomeration rate suggests that for practical applications, it may be advantageous to introduce some sort of spray system in the agglomeration chamber. The mean size of the spray droplets should be large in comparison with the fine-particle size to be controlled, but should be kept small enough so that the droplets remain airborne for a relatively long period of time. Also the spray liquid must be chemically inert so that no additional air-pollution problem is introduced.

The effect of increasing particle concentration is demonstrated by curves 5 and 6 of Fig. 1. For example, for the case when the initial conditions are those shown in the figure, and $\Omega = 0.1 W/cm^2$, an increase of concentration by a factor of 5 reduces the value of $t_{1/2}$ from 30 sec (curve 2) to 6 sec (curve 6). In fact, it can be seen from Eqs.(11) and (13) that

$$\tilde{K}_a \sim \frac{1}{N_1} \qquad (14)$$

where $N_1$ is the total number of large-collecting particles.

For convenience, it is useful to define a critical diameter below which particles can be considered oscillating together with the carrier gas. Typically, this is specified as the radius at which $\mu_p = 0.8$. From Eq.(2) we have

$$\frac{d_2^2 \rho_p f}{\eta} \simeq 2.2 \quad \text{or} \quad d_2^2 f \simeq 4.10^{-4} cm^2/sec = 40\ \mu m^2 KHz \qquad (15)$$

For $d_2 = 2 \mu m, f = 10$ KHz. Thus, if an acoustic field of 10 KHz is applied to an aerosol, particles with diameter less than 2 μm would oscillate with nearly full amplitude ($\mu_p \geq 0.8$) while particles with diameter larger than

2 microns are virtually stationary ($\mu_p \simeq 0$). Such differential motion of the oscillating particles leads to particle agglomeration.

Using this critical frequency, Fig. 2 shows the variation of $t_{1/2}$ for an aerosol ($d_g$ = 1 μm, N = $10^6 cm^{-3}$, and $\Omega$ = 1 W/$cm^2$) with respect to the standard deviation $\sigma_g$ for the removal of particles with diameters less than 2 μm, 4 μm and 10 μm. For each curve the acoustic frequency is set at the value determined by the critical relation (Eq.15). It is seen here that the larger the mean particle size to be removed, the higher the values of $t_{1/2}$ Furthermore, the advantage of a high value of σ is obvious. This, together with the fact that $\bar{K}_a$ is inversely proportion to number concentration (Eq.14), makes it attractive to use the acoustic agglomerator as a preconditioner, i.e., use it upstream ahead of a conventional device such as a cyclone or an electrostatic precipitator for the best effect.

In most of the practical cases, it is common to use the mass concentration m(in μg/$cm^3$ or g/$m^3$), and not the number concentration, to indicate the amount of particulate emission. Thus, instead of keeping number concentration N constant, m is maintained constant in Fig. 3. Here $t_{1/2}$ reduces initially as $\sigma_g$ increases, reaches a minimum, and eventually increase rapidly. This increase is due to the fact that a fixed mass concentration, the total number of particles reduces as $\sigma_g$ increases, leads to a reduction in $K_a$ as shown in Eq.(14).

Figure 4 shows the same calculations but is presented with $t_{1/2}$ vs. the mass concentration for various values of $\sigma_g$ for fine-particle control ($d_2$ = 2 μm). For a given value of the mass concentration, the optimum value of $\sigma_g$ is again shown. The drastic reduction in the required agglomeration time $t_{1/2}$ for increasing value of the mass concentratin suggests again that the device should be used as a preconditioner.

## Comparative Energy Requirements of the Acoustic Agglomerator and Other Conventional Control Systems

It is useful to compare the specific energy requirement for the operation of an acoustic agglomerator to other devices for the control of particulate emissions. The procedure used is similar to that used in reference [16] which is based on Mednikov's work [12]. The specific energy requirement for acoustic agglomeration is given by

$$E = \frac{\Omega\ t_o}{0.36\ \varepsilon_s\ \varepsilon_c\ \varepsilon_{uf} H} \tag{16}$$

where E is the specific energy in Kw-hr/1000 $m^3$, $\Omega$ is the sound intensity in W/$cm^2$, $t_o$ is the agglomeration time in sec, $\varepsilon_s$ is the acoustic efficiency of the sound source, $\varepsilon_c$ is the overall efficiency of the compressor for the sound source and $\varepsilon_{uf}$ is the utilization factor of the agglomeration chamber. H is the height of the agglomeration chamber and can be estimated by requiring that the aerosols spend an average time $t_o$ in the agglomerator. Thus we have

$$H = 21.2\ t_o/D^2 \tag{17}$$

where D is the diameter of the agglomerator. Substituting Eq.(17) in Eq. (16), we have

$$E = \frac{0.13\ \Omega\ D^2}{\varepsilon_s\ \varepsilon_c\ \ \varepsilon_{uf}} \tag{18}$$

Equation (18) which was used in reference [16] for the evaluation of the acoustic agglomerators, is also used here. However, instead of using Eqs. (1) and (2), $t_o$ is estimated based on the values shown in Figs. 2 and 4.

Following reference [16] we assume that $\varepsilon_s = 0.5$, $\varepsilon_c = 0.65$ and $\varepsilon_{uf} = 0.7$.

The first two rows in Table 1 are the result of the present estimation of the specific energy requirements and the size for acoustic agglomerators under traveling-wave conditions. $t_o$ (in column V) is estimated from $t_{1/2}$ (in column IV) by assuming a 99% removal, i.e.,

$$t_{1/100} = \ln 100/\tilde{K}_a \tag{19}$$

By comparing Eq.(19) with Eq.(11), we have

$$t_o = t_{1/100} = 6.63\ t_{1/2} \tag{20}$$

where $t_{1/100}$ is the agglomeration time for the reduction of the particle concentration to 1% of its original value.

It should be noted that in all calculations in Table 1 the aerosol size distribution function is assumed to be constant, i.e., it is lognormally distributed with $d_g = 1\ \mu m$ and $\sigma_g = 2.0$. Consequently, $t_{1/2}$ is inversely proportional to the mass loading, m according to Eq.(14). The particles to be controlled have diameters less than 2 μm ($d_2 = 2\ \mu m$). For other values of $d_2$ similar tables may be constructed. These particular values of $d_2$ (2μm) are picked because it is a reasonable value for applications in the pressurized fluidized-bed boilers, coal gasification plants and MHD solid-seed separators.

It should be noted that the value of $\tilde{K}_a$ (column VI), as determined by Eq.(13), is not equal to $\Omega^{1/2}$ as was assumed in reference [16]. In fact, $\tilde{K}_a$ increases rapidly as the mass loading increases.

Another interesting point is that the value of E is independent of $t_o$ as shown in Eq.(18). An increase in the effectiveness of acoustic agglomeration leads only to a more compact agglomerator (the value of H reduces). At 160 db and when the mass loading is low ($m < 0.5$ g/m$^3$), the length of the agglomeration chamber is more than 15 m even if a larger chamber diameter is used ( D = 4m) However, at higher mass loadings, the values of H become more reasonable; again indicating the advantage of using acoustic agglomerators as preconditioners under traveling-wave conditions. When $\Omega$ is decreased to 150 db, E is reduced by a factor of 10 and the value of H increases by a factor of about 3. But for most industrial applications, the mass loading is less than 2 g/m$^3$, and the value of H is considered to be unacceptably high.

### Standing-wave Acoustic Agglomerators

In a recent paper, the acoustic agglomeration of aerosol particles have been reported under standing-wave conditions [20]. The half-life decay time, as determined by Eq.(11), has been measured for acoustic frequencies ranging from 640 Hz to 1.7 KHz under both the stationary condition and the flow-through condition. For the stationary system Fig. 5 shows the variation of $t_{1/2}$ as a function of the acoustic intensity at three frequencies. For agglomeration under the standing-wave condition, it is found that acoustic turbulence plays a critical role in the agglomeration process. At low intensities, a small flow velocity which reduces the degree of acoustic turbulence in the agglomeration chamber,thus decreases the effectiveness of the system. But, when the acoustic intensity at the node-points is larger than 175 db (corresponding to open air intensity of about 140 db) the turbulent eddy velocities of the particles lie in the range between 70 to 110 cm/sec. Thus according to our experimental data, the acoustic agglomeration rate would not be reduced significantly by the flow velocity as long as the flow velocity is less than the particle eddy velocity.

In Table 1 two open-air intensities are used: 140 and 150 db. By extrapolating the present data, we obtain the values of $t_{1/2}$ as shown in the table. It is seen that a general reduction of the agglomeration time $t_o$ is obtained by changing from a traveling-wave system to a standing-wave system. For a given intensity, the specific energy consumption is the same for either a traveling-wave or a standing-wave system, the improvement in the required agglomerating time would reduce the agglomerator length H. The compactness of the agglomerator is of critical importance since very long chambers are undesirable from the standpoint of increasing acoustic attenutation losses in the chamber.

## DISCUSSIONS AND CONCLUSIONS

In order to evaluate acoustic agglomeration for particulate-emission control we have estimated the specific energy consumption and the size of the agglomerator as shown in Table 1. The calculations have been made for a set of conditions similar to those used in reference [16] for easy comparison of the results. Specifically, it is assumed that:

- Gas flow rate = 1000 $m^3$/min
- $\varepsilon_c = 0.65$, $\varepsilon_s = 0.5$ and $\varepsilon_{uf} = 0.7$
- Cylindrical chamber with diameter = 2 and 4 m.

The major differences between our model and the Mednikov model used in reference [16] are as follows:

(1) The only parameter in Mednikov's model is the growth ratio $d_f/d_i$ (final diameter/initial diameter) which is varied in reference [16] between 2 and 20. For practical application $d_f/d_i$ seldon exceeds the value of 10. All estimates made in the present paper assume $d_f/d_i = 2$; i.e., $d_f = 2$ μm, $d_i = 1$ μm.

(2) The agglomeration time for a given intensity depends only on $d_f/d_i$ in reference [16]. Our model shows it is a function of $d_f/d_i$ the geometric standard deviation $\sigma_g$, the mass loading m and the acoustic frequency f. Assuming the optimum values of the acoustic frequency and the aerosol standard deviation are used, the agglomeration time $t_0$ then depends only on the mass loading for fixed values of $d_f/d_i$ and the acoustic intensity as shown in Table 1.

(3) For a specific value of acoustic intensity, $K_a$ is constant in reference [16] according to Eq.(2). For traveling-wave and at $\Omega = 160$ db. $K = 1\ \text{sec}^{-1}$ when $m \simeq 1.6\ \text{g/m}^3$. Since this is not an unreasonable number for mass loading, the major conclusions on the specific energy consumption and the size of reference [16] are in the same order of magnitude as those reached in the present paper.

(4) Thus for traveling-wave, the use of Eq.(2) is close to the optimum performance of an acoustic agglomerator for moderate growth ($d_f/d_i = 2$), medium mass loading ( $m \simeq 1.6\ \text{g/m}^3$ ) and high intensity ($\Omega = 160$ db). However, the estimates of reference [16] are overly conservative when the mass loading

is higher than 1.6 $g/m^3$.

It is interesting to compare the estimates for the traveling-wave system to those of the standing-wave system. At 150 db, when the system is changing from a traveling-wave to a standing-wave, the agglomeration time is increased by a factor 3 to 4. At 150 db open-air intensity,the node-point intensity is measured at 180 db. It is interesting to note that for standing-wave, the agglomeration mechanisms are no longer those for the traveling-wave systems in which the inertial capture and the hydrodynamic interaction are the dominant mechanisms. As shown in Eq. ( 2 ) for traveling-wave, $K_a$ increases in proportion to $\Omega^{1/2}$. This relationship is obviously not valid when switching from traveling-wave to standing-wave in which turbulence plays a critical part in particle agglomeration.

Typical energy requirements for conventional systems are given in reference [16] as follows:

- Cyclones - 0.5 to 5 hp/1000 cfm
- Fabric filters - 2 to 3 hp/1000 cfm
- Electrostatic Precipitators - 1 to 1.5 hp/1000 cfm
- Venturi Scrubbers - 10 to 20 hp/1000 cfm

Based on Table 1 the energy consumption for standing-wave acoustic agglomerators is estimated to be in the range between 0.5 and 2 hp/1000 cfm, which is about the same as those for the cyclone, the fabric filter and the electrostatic precipitators and is less than that for the venturi scrubbers.

In conclusion, it is important to point out that caution must be exercized in the use of the results in Table 1. First, the estimates are made on specific assumptions such as $d_f/d_i=2$ and the standard deviation of the aerosol size distribution function is optimum. The latter assumption implies that the aerosol is properly conditioned for maximum acoustic effectiveness. Secondly, the results have been tested only in the low-intensity region (less than 150 db for traveling-wave and an open-air intensity less than 130 db for standing-wave). While there are reasons to believe that the extrapolation should be at least semi-quantitatively correct, experimental verifications of the findings at high intensities are urgently needed for the further development of the acoustic agglomerators. Finally, as was done both in reference [16] and in Table 1 in the present paper, the agglomeration time $t_o$ estimated for each case, is determined on the assumption that $K_a$ remains constant with respect to time. This, however, is not the case. During the early phase of acoustic agglomeration, $\tilde{K}_a$ is high because of the high mass loading. As soon as acoustic precipitation starts, $\tilde{K}_a$ decreases accordingly. Thus the actual agglomeration time required for 99% removal is higher than those estimated in Table 1.

The last point- i.e., the advantage of high mass loadings on accoustic agglomeration- makes it attractive to use acoustic agglomeration in a hybrid system. For example, in the pressurized fluidized-bed boiler, the standing-wave acoustic agglomerator can be followed by a high-pressure cyclone which removes the relatively large residual particles from the acoustic agglomerator.

The application of acoustic agglomeration for the removal of corrosive particles at high temperatures and pressures has attracted great interest in recent years partially because of the limitations encountered with various conventional devices under these unconventional environments. At high pressures the gas medium density increases and thus the particle velocity in the acoustic field decreases. Thus reduction in particle velocities would lead to a lower acoustic agglomeration rate. Therefore, to compensate for these effects, the acoustic intensity must be increased at high pressures. Acoustic agglomeration of aerosols has been reported by Mednikov in the early 1960's at pressures as high as 50 atm [12].

The effects of an increasing temperature on acoustic agglomeration is less certain. Mednikov [12] stated that the only effect of the temperature is to increase the viscosity which also leads to a decrease in the particle oscillating velocity, thus it is expected that the acoustic agglomeration rate would decrease as the temperature increases. But Belenkii, Timoshenko and Fedorak [22] recently have reported an increase in acoustic agglomeration rate as the temperature is increased. No explanation has been given for the increase.

Given the uncertainties of the effects of temperature and pressure on acoustic agglomeration, the important fact is that there does not exist any fundamental reason for the acoustic agglomerators not to perform effectively at high temperatures and pressures. To compensate for the effects of high temperature and pressure the standing-wave agglomerator may have to increase its open-air intensity from the 150 db in Table 1 to 160 db. Questions concerning the economic competitiveness of such an increase in the specific energy consumption cannot be fully answered until more experimental data are obtained in this area.

## References

1. H.S. Patterson and W. Cawood, "Phenomena in a Sounding Tube," Nature, 127, 667 (1931).
2. O. Brandt and E. Hidemann,"The Aggregation of Suspended Particles in Gases by Sonic and Supersonic Waves," Trans.Faraday Soc. 32 (184):1101-1110 (1936).
3. E.N. da C. Andrade, "The Coagulation of Smoke by Supersonic Vibrations," Trans.Faraday Soc. 32 (184) 30-35 (1936).
4. H.W. St.Clair, "Agglomeration of Smoke, Fog, or Dust Particles by Sonic Waves," Ind. & Eng. Chem., 41, 2434 (1949).
5. D. Sinclair, "Coagulation by Sonic and Supersonic Vibrations," Handbook of Aerosols, Washington, D.C 1950.
6. J. Krebs and R.C. Binder, "Use of Ultrasonic Coagulation with a Cyclone Separator," Combustion, 23, 12, 45 (1952).
7. H.W. Danser and E.P. Neumann, "Industrial Sonic Agglomeration of Collection Systems," Ind.& Eng.Chem., 41, 2439 (1949).
8. E.P. Neumann and J.L. Norton, "Application of Sonic Energy to Commercial Aerosol Collection Problems," Chem.Eng.Progr., Symposium- Sec.1, 47 (1):4-10 (1951).
9. C.R. Soderberg, Jr.,"Industrial Applications of Sonic Energy," Iron Steel Engr. 29, (2): 87-94 (1952).
10. M. Nord, "Sonic Precipitation of Smoke, Fumes and Dust Particles," Chem. Engr., pp. 116-119, October 1950.
11. C.A. Stokes and J.E. Vivian, "Application of Sonic Energy in the Process Industries," Chem.Engr.Prog.Symp. Series 1, 47 (1): 11-21 (1951).
12. E.P. Mednikov, Acoustic Coagulation and Precipitation of Aerosols, Translated from Russian by C.V. Larrick, Consultants Bureau, New York 1965.

13. N.L. Shirokova, "Aerosol Coagulation," *Physical Principles of Ultrasonic Technology Vol. 2*, ed. L.D. Rozenberg, Trans. from Russian by J.S. Wood, Plenum Press, New York 1970, p 4 7-541.

14. A.A. Jonke, W.M. Swift and G.J. Vogel, "Fluidized-Bed Combustion Development and Status," *Trans.ASME*, *258*, 159 (1975).

15. D.T. Shaw and J. Wegrzyn, "New Applications of Acoustic Agglomerators in Particulate Emission Control," *Research Workshop on Novel Concepts, Methods and Advanced Technology in Particulate-Gas Separation*, Univ. of Notre Dame, April 1977.

16. R. Hegarty and L.J. Shannon, "Evaluation of Sonics for Fine Particle Control," Report 600/2-76-001 EPA, Washington, D.C. January 1976.

17. D.T. Shaw and N. Rajendran, "Application of Acoustic Agglomerators for Emergency Use In LMFBR Plants," submitted for publication to *Nuclear Science and Engineering*, November 1977.

18. D.T. Shaw and K.W. Tu, "Acoustic Particle Agglomeration Due to Hydrodynamic Interaction Between Monodisperse Aerosols," submitted for publication to the *Journal of Aerosol Science*, November 1977.

19. D.T. Shaw, S. Patel and N. Rajendran, "The Removal of Airborn Dust Particles in an Acoustic Field Under Traveling Wave Conditions," submitted to the *Journal of the Acoustic Society of America,* November 1977.

20. N. Rajendran, J. Wegrzyn and D.T. Shaw, "Acoustic Precipitation of Aerosol under Standing-Wave Condition," submitted to the *Journal of Aerosol Science*, November 1977.

21. L.J. Shannon, P.G. Gorman and M. Reichel, "Particulate Pollutant System Study," Vol. III - Fine Particle Emission, Midwest Research Institute, August 1971, PB-203-521.

22. V.A. Belenkii,V.I. Timoshenko and T. Ya.Fedorak, "Choosing the Optimum Conditions for the Acoustic Coagulation of Aerosols," *Soviet Phys-Acoustics*, *19*, 2, 181 (1973).

TABLE 1 Estimated Specific Energy Requirements E and the Agglomeration Time $t_o$

($d_g$ = 1 µm, $d_2$ = 2 µm, $\sigma_g$ = 2.0, $\varepsilon_c$ = 0.65, $\varepsilon_s$ = 0.5 and $\varepsilon_{uf}$ = 0.7)

| I | II | III | IV | V | VI | VII | VIII | IX | X | |
|---|---|---|---|---|---|---|---|---|---|---|
| | | | | | | | | | E | |
| | $\Omega$ [w/cm$^2$] | m[g/m$^3$] | $t_{1/2}$[sec] | $t_o$[sec] | $\tilde{K}_a$[sec$^{-1}$] | D[m] | H[m] | U [m/sec] | $\frac{\text{KWhr}}{1000\ \text{M}^3}$ | $\frac{\text{hp}}{1000\ \text{CFM}}$ |
| TRAVELING-WAVE | 160 | 0.125 | 9.0 | 59.7 | 0.077 | 2 | 316 | 5.3 | 2.3 | 5.2 |
| | | | | | | 4 | 79 | 1.3 | 9.1 | 21 |
| | | 0.62 | 1.8 | 11.9 | 0.385 | 2 | 63 | 5.3 | 2.3 | 5.2 |
| | | | | | | 4 | 16 | 1.3 | 9.1 | 21 |
| | | 5.0 | 0.225 | 1.49 | 3.08 | 2 | 8 | 5.3 | 2.3 | 5.2 |
| | | | | | | 4 | 2 | 1.3 | 9.1 | 21 |
| | | 10.0 | 0.113 | 0.75 | 6.152 | 2 | 4 | 5.3 | 2.3 | 5.2 |
| | | | | | | 4 | 1 | 1.3 | 9.1 | 21 |
| | 150 | 0.125 | 28.4 | 188.3 | 0.024 | 2 | 998 | 5.3 | 0.23 | 0.5 |
| | | | | | | 4 | 247 | 1.3 | 0.91 | 2.1 |
| | | 0.62 | 5.7 | 37.8 | 0.122 | 2 | 200 | 5.3 | 0.23 | 0.5 |
| | | | | | | 4 | 50 | 1.3 | 0.91 | 2.1 |
| | | 5.0 | 0.711 | 4.7 | 0.976 | 2 | 25 | 5.3 | 0.23 | 0.5 |
| | | | | | | 4 | 6 | 1.3 | 0.91 | 2.1 |
| | | 10.0 | 0.36 | 2.3 | 1.925 | 2 | 12 | 5.3 | 0.23 | 0.5 |
| | | | | | | 4 | 3 | 1.3 | 0.91 | 2.1 |

TABLE I, Estimated Specific Energy Requirements E and the Agglomeration Time $t_o$

**Cont.** ($d_g$ = 1 μm, $d_2$ = 2 μm, $\sigma_g$ = 2.0, $\varepsilon_c$ = 0.65, $\varepsilon_s$ = 0.5 and $\varepsilon_{uf}$ = 0.7)

| I | II | III | IV | V | VI | VII | VIII | IX | X | |
|---|---|---|---|---|---|---|---|---|---|---|
| | $[w/cm^2]$ | $m[g/m^3]$ | $t_{1/2}$[sec] | $t_o$[sec] | $K_a[sec^{-1}]$ | D[m] | L[m] | U[m/sec] | E | |
| | | | | | | | | | $\frac{KWhr}{1000\ M^3}$ | $\frac{hp}{1000\ CFM}$ |
| STANDING-WAVE | 150 | 0.125 | 7.68 | 50.9 | 0.09 | 2 | 269 | 5.3 | 0.23 | 0.5 |
| | | | | | | 4 | 67 | 1.3 | 0.91 | 2.1 |
| | | 1.6 | 0.6 | 3.98 | 1.16 | 2 | 21 | 5.3 | 0.23 | 0.5 |
| | | | | | | 4 | 5 | 1.3 | 0.91 | 2.1 |
| | | 5 | 0.19 | 1.26 | 3.46 | 2 | 6.6 | 5.3 | 0.23 | 0.5 |
| | | | | | | 4 | 1.6 | 1.3 | 0.91 | 2.1 |
| | | 10 | 0.08 | 0.53 | 8.66 | 2 | 2.3 | 5.3 | 0.23 | 0.5 |
| | | | | | | 4 | 0.7 | 1.3 | 0.91 | 2.1 |
| | 140 | 0.125 | 23.0 | 152 | 0.03 | 2 | 805 | 5.3 | 0.023 | 0.05 |
| | | | | | | 4 | 201 | 1.3 | 0.091 | 0.2 |
| | | 1.6 | 1.8 | 11.9 | 0.38 | 2 | 63 | 5.3 | 0.023 | 0.05 |
| | | | | | | 4 | 16 | 1.3 | 0.091 | 0.2 |
| | | 5.0 | 0.576 | 3.8 | 1.21 | 2 | 20 | 5.3 | 0.023 | 0.05 |
| | | | | | | 4 | 5 | 1.3 | 0.091 | 0.2 |
| | | 10 | 0.288 | 1.9 | 2.41 | 2 | 10 | 5.3 | 0.023 | 0.05 |
| | | | | | | 4 | 3 | 1.3 | 0.091 | 0.2 |

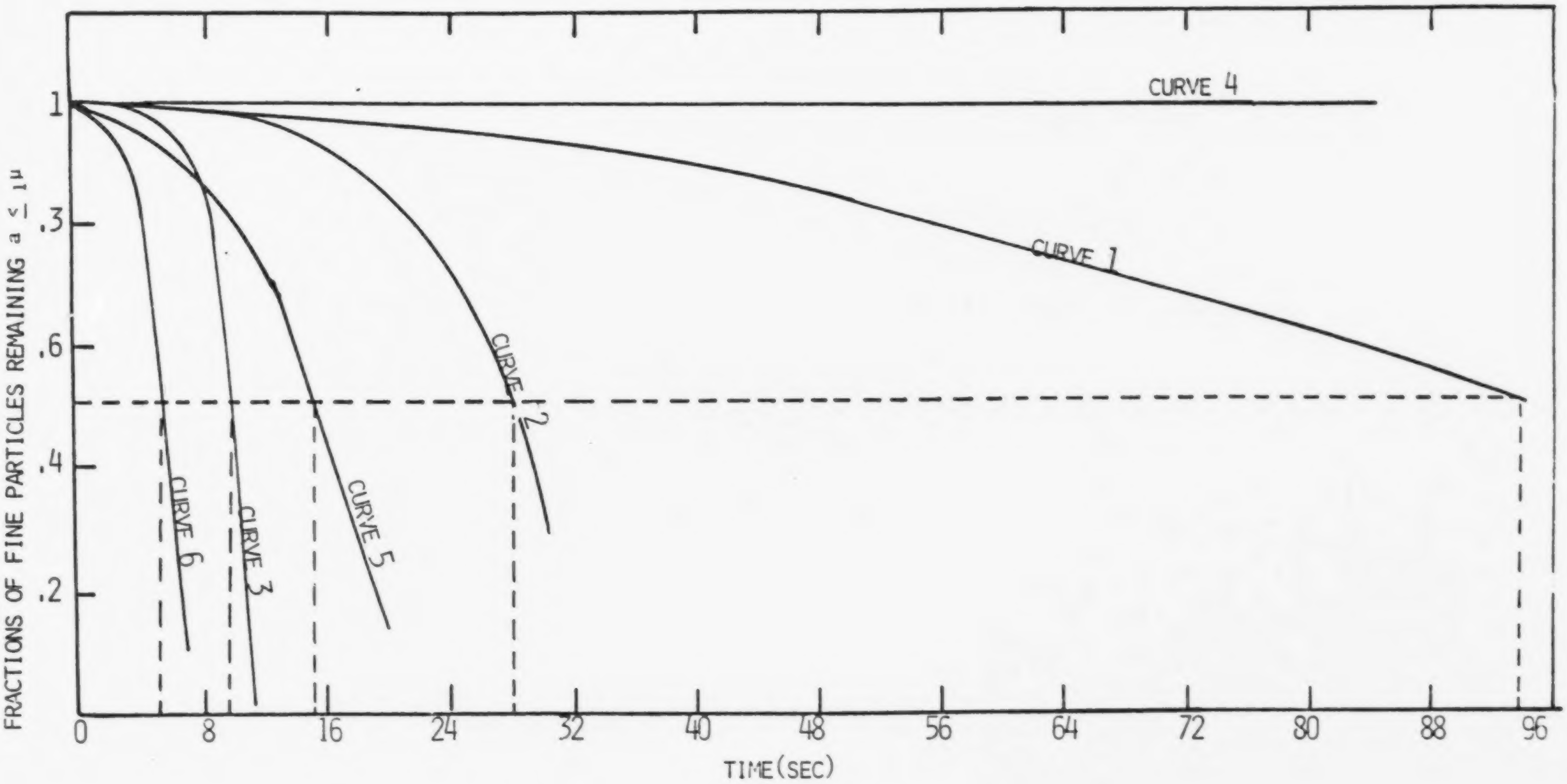

FIG. 1 - Fraction of fine particles (radius a $\leq$ 1.0 μm) remaining airborne as a function of time.

Curve 1, Curve 2, Curve 3: $N = 1.2 \times 10^5 cm^{-3}$, $d_g = 0.15$ μm, $\sigma_g = 3.45$, f = 1 KHz, $\Omega = 0.01 W/cm^2$ / $\Omega = 0.1 W/cm^2$ / $\Omega = 1.0 W/cm^2$

Curve 4 " " $\sigma_g = 1.6$ " $\Omega = 1.0$ and $0.1 W/cm^2$

Curve 5 $N = 6 \times 10^5 cm^{-3}$ " $\sigma_g = 3.45$ " $\Omega = 0.01 W/cm^2$

Curve 6 " " " " "

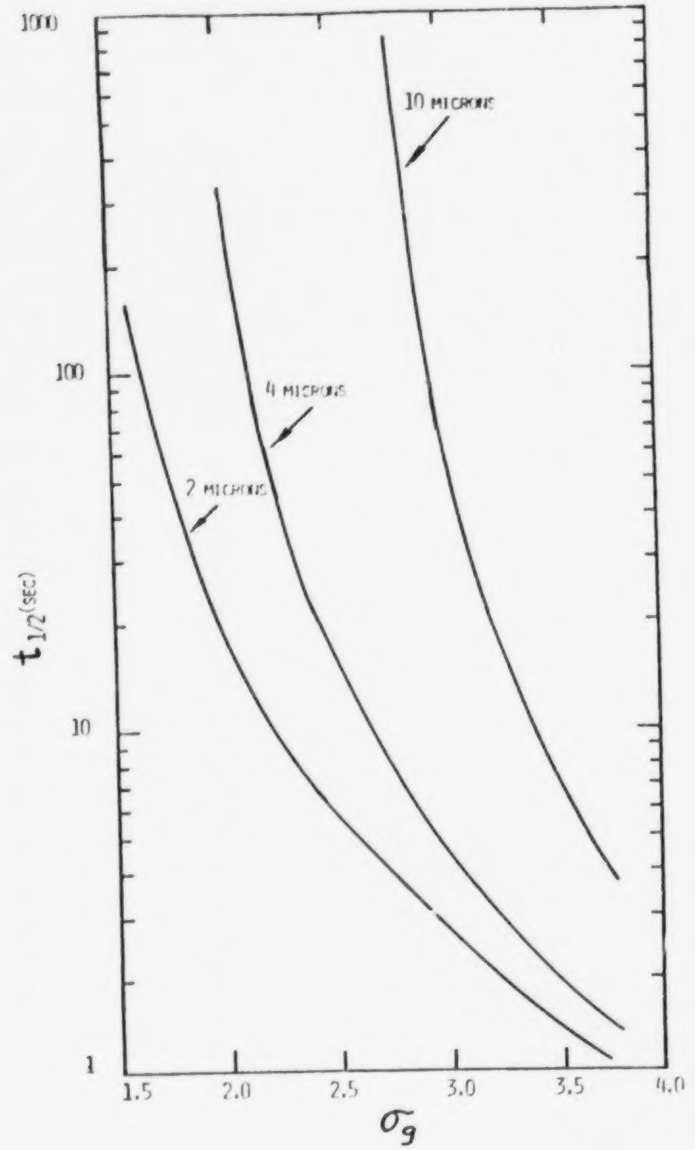

FIG. 2 The half-life decay time $t_{1/2}$ vs. the standard deviation $\sigma_g$ for three critical diameters ($d_c$ = 2 μm, 4 μm, 10 μm), number concentration N = $10^6 cm^{-3}$, geometric mean diameter $d_g$ = 1.0 μm, Ω = 1 W/$cm^2$, critical frequency as determined by Eq. 52 is used for all three values of $d_c$.

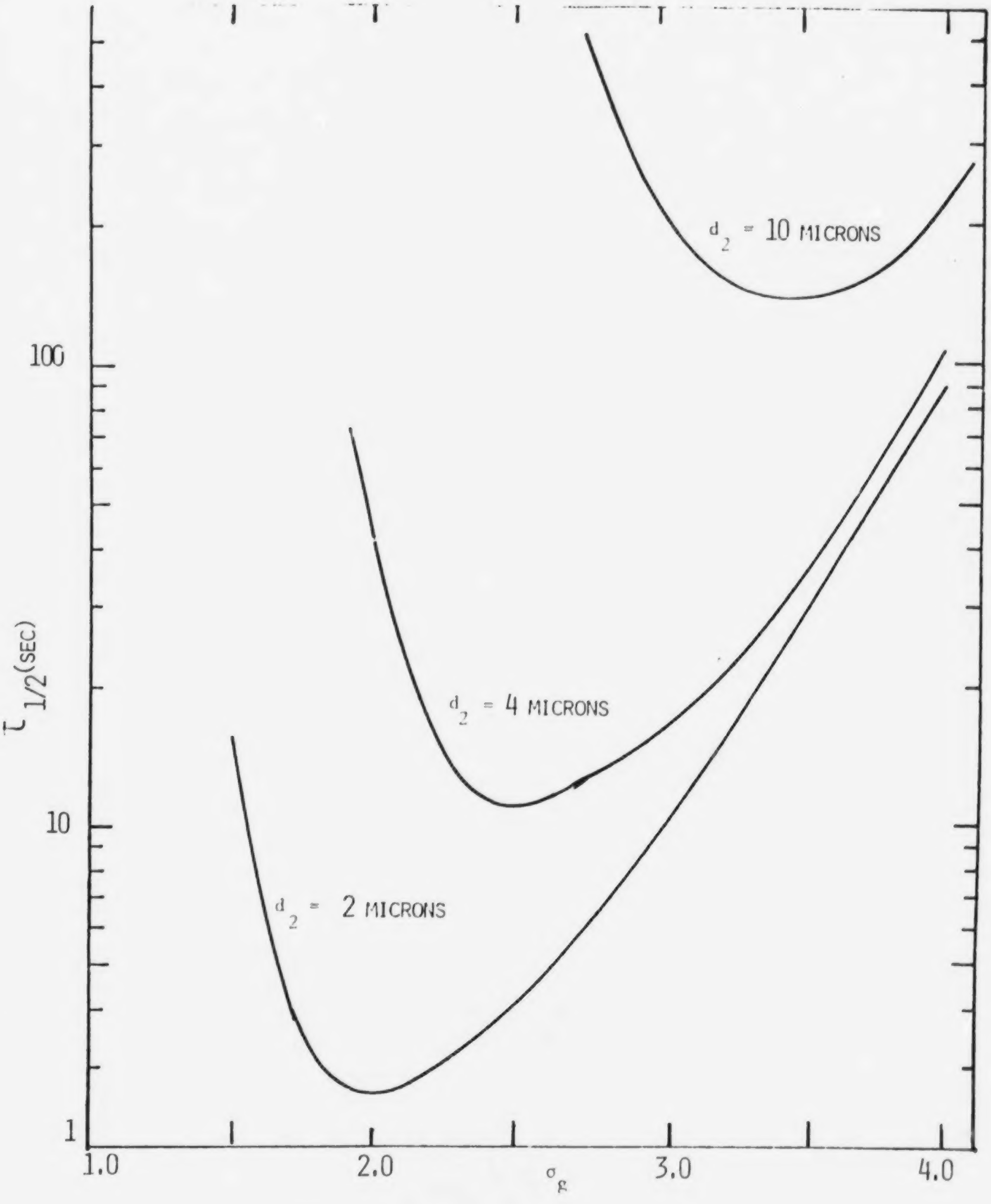

FIG. 3 - Half-life decay time $t_{1/2}$ vs. the standard deviation $\sigma_g$ for a fixed mass concentration ($M = 0.62\ \mu g/cm^3$), $d_2$ = 2 µm, 4 µm, 10 µm. $\Omega = 1\ W/cm^2$, $d_g = 1.0\ \mu m$, critical frequency determined by Eq. 52 is used for all three curves.

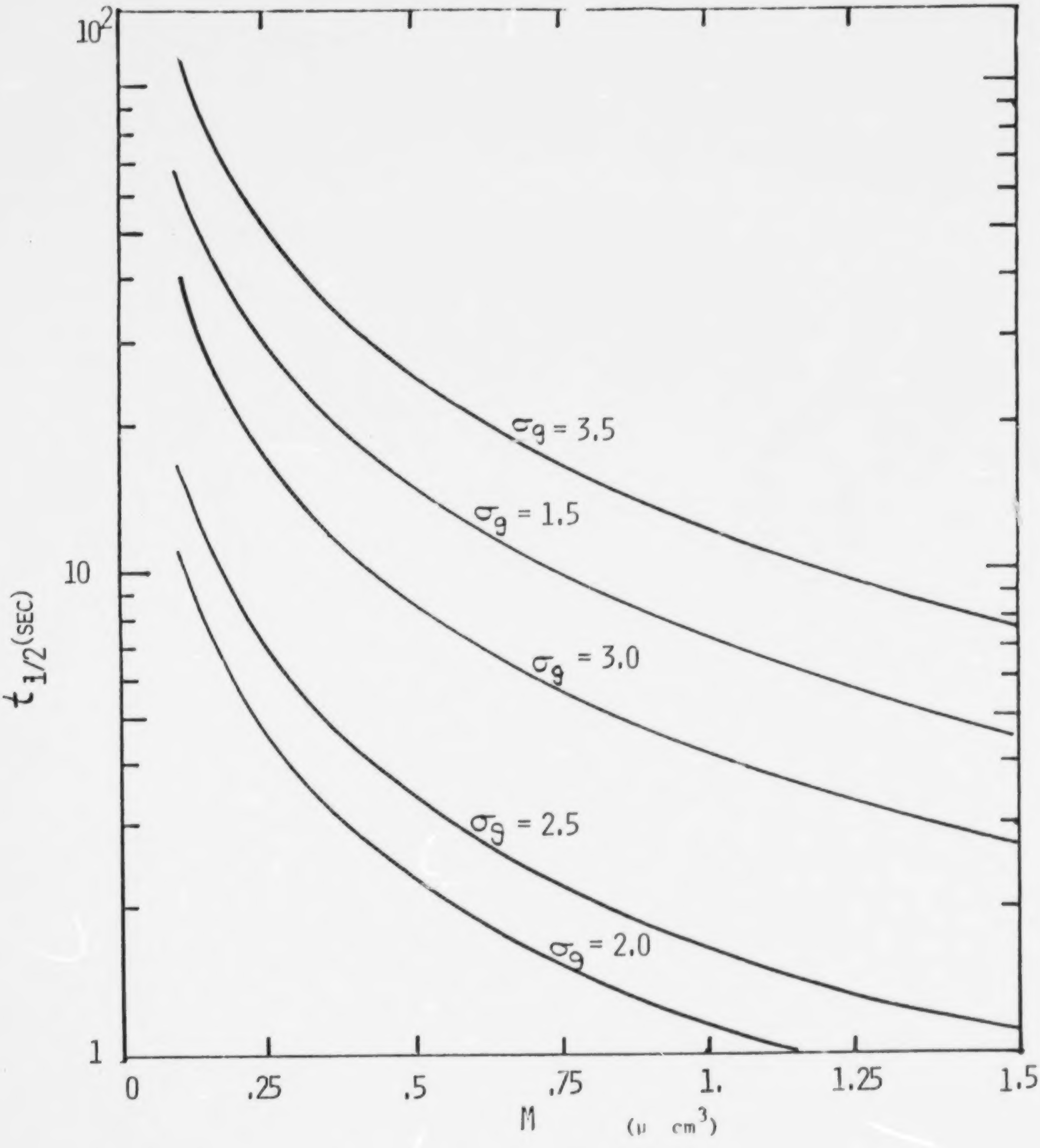

FIG. 4 - Half-life decay time $t_{1/2}$ vs. mass concentration M for five values of the standard deviation ($\sigma_g$ = 1.5, 2.0, 2.5, 3.0, 3.5), $d_2$ = 2 μm, Ω = 1 W/cm$^2$, $d_g$ = 1.0 μm, critical radius determined by Eq.52 is used.

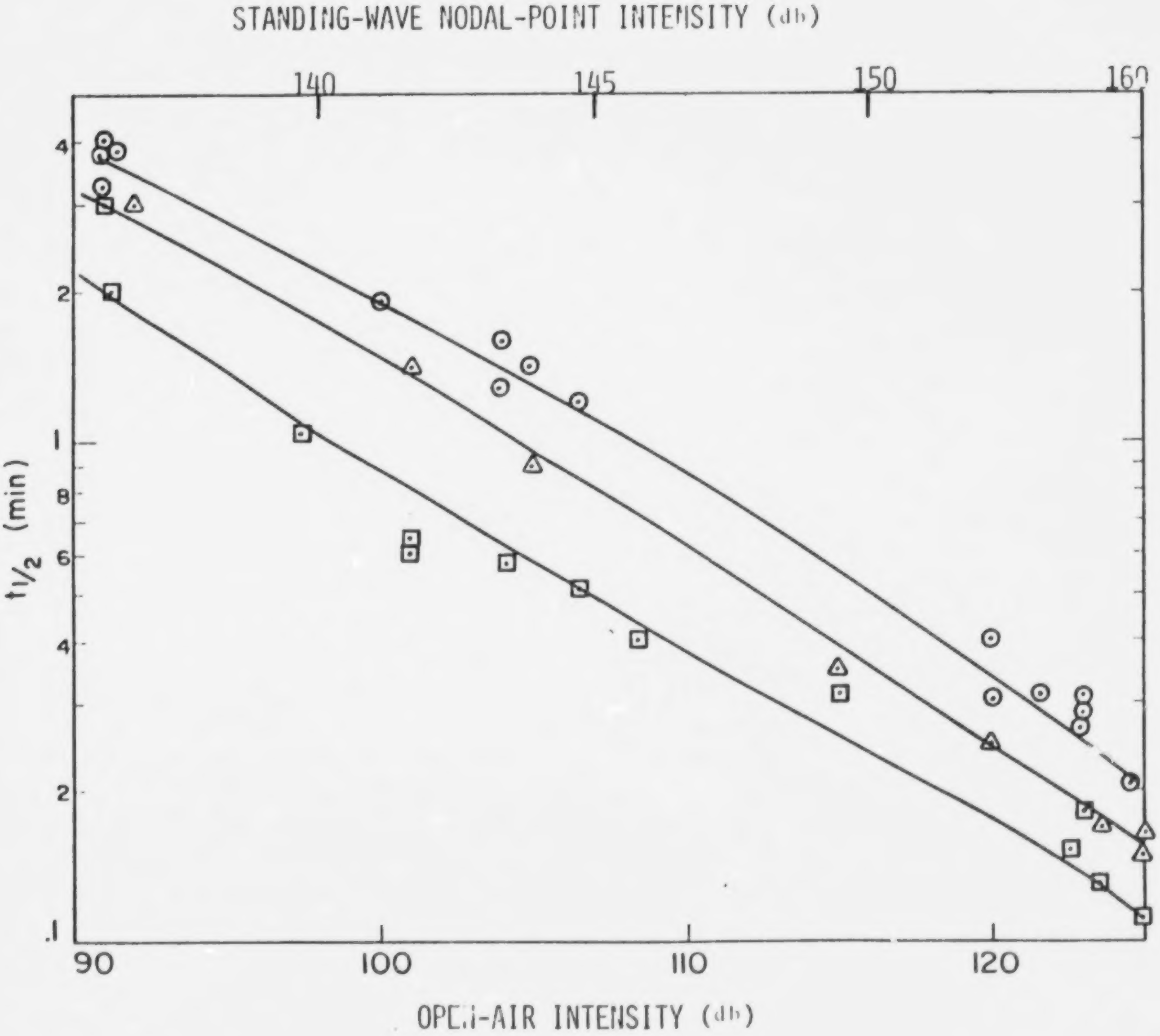

**Fig. 5** Half-life decay time vs. intensity for three frequencies in vertical position with driver at the bottom.
□- 640 Hz, △- 850 Hz, ○-1070 Hz

CE

# CYCLOCENTRIFUGE DEVELOPMENT FOR PARTICULATE, PHASE I: FEASIBILITY STUDY

By:

J. T. McCabe
Mechanical Technology Incorporated
Latham, NY 12110

BLANK PAGE

# ABSTRACT

Gas cleanup was determined to be an area in which the special characteristics of a modified centrifuge offered technical and economic advantages over existing approaches. A new concept, called a Cyclocentrifuge, was evolved during an analytical study in which the desirable characteristics of a cyclone and a centrifuge were combined in a compact design capable of separating fine particulate matter from hot pressurized gas at large flow rates on a continuous basis. A design example is given which shows the Cyclocentrifuge to be capable of achieving a purity of 1 ppm of solids with a nominal maximum particle diameter of one micron when processing 125,000 scfm of low Btu fuel from a coal gasifier.

## 1. INTRODUCTION

Existing techniques for removing fine particulate matter from coal conversion gases are not considered sufficiently effective or efficient for meeting many current and projected application demands. The fundamental question addressed in this study was to determine if gas centrifuges technology could provide the bases for technical or economic improvements in the fields of gas particulate cleanup and other related processes. The initial study of the general application of gas centrifuge technology quickly focused on the special field of particulate control, which is the subject of this paper. This field is important because it bears directly upon the efficiency with which the overall coal conversion process can be carried out, and the efficiency of the conversion process will determine the extent to which the vast coal reserves that are available will be exploited.

Cleanup of gasifier-produced low-Btu fuel for direct firing in the gas turbine of power generating system was selected as a representative study application because failure to remove fine particulate matter from the fuel gas can cause severe and expensive erosion and corrosion. In addition to cyclones, there are presently three approaches to resolving the gas cleanup problem for this application: Filters, electrostatic precipitators, and scrubbers. Filters require large surface areas. Carry-over of filter material is often equally as bad, or worse, than by-passing the original contaminant. Filters must also be taken off-line to be purged, and clogging is a problem because it is difficult to remove fine particles and tar from a high efficiency bed.

Electrostatic precipitators are bulky and must be contained in large pressure vessels. They must be shut down to be cleaned, they consume considerable electrical power, they are inefficient when the gas is hot, they are ineffective with certain types of gas and process upsets can result in carry-over and sometimes fires.

Liquid scrubbing systems are effective in removing fine particulates; however, corrosion remains a problem, and the quantity of energy lost in the gas due to cooling during the scrubbing process is very significant. In addition, disposal of the blow-down water and the need for sludge ponds present the added expense of resolving the accompanying pollution control problem.

A unique and viable alternative to existing methods for gas cleanup was evolved during the study called a Cyclocentrifuge. The principal difference between the Cyclocentrifuge and a simple cyclone is the magnitude and method of generating the swirl velocity. Cyclones are limited in the magnitude of the swirl velocity because, as the swirl velocity is increased beyond about 100 feet per second, secondary effects, such as the strength of eddies shed from the expanding inlet nozzle jet, eventually become equivalent in strength to the vortex core. This results in mixing rather than separation. The swirl velocity limit for the Cyclocentrifuge is expected to be six to seven times greater than a cyclone because the gas is accelerated gradually by a cascade of swirl augmentation blades that are designed to minimize the generation of mixing eddies.

Feasibility for the Cyclocentrifuge is established by presenting a design example which includes design analyses, conceptual drawings, and cost data for a Cyclocentrifuge based on delivering 125,000 scfm of high-purity, low-Btu gas at 250 psi and 1000°F.

The application chosen for this study was typical of those used in a combined-cycle electrical power system based on the gasification of coal. The arrangement is shown schematically in Figure 1, where the key gas cleanup element is a Cyclocentrifuge. This schematic arrangement is similar to that given in Reference 1, which presents the economic analysis of a combined cycle. The economic data in Reference 1 was also used as a Baseline for the purposes of this study. The major differences between Figure 1 and the system analyzed in Reference 1 is that a steam generator has been inserted in the gasifier to limit the gas stream temperature entering the Cyclocentrifuge and thereby obtain satisfactory long-term rupture and creep properties in the centrifuge shell. It may be feasible to operate at a higher gas stream temperature by using the externally cooled bearing lubricant or process gas to control the centrifuge shell temperature; however, shell cooling schemes were not considered in this study.

## 2. PERFORMANCE GOALS

Reference 2 indicates that turbine blade erosion will be avoided if the fuel gas contains less than 30 ppm of solids by weight, and the maximum equivalent spherical particle diameter is less than 10 microns. There is no equivalent specification for limiting the number and size of solid particles that contain corrosion or deposit-causing contaminants. The most troublesome trace contaminants are sodium, potassium, lead, vanadium, calcium, and sulfur (References 2, 3, and 4), and the most corrosive compounds are sodium sulfate and vanadium pentoxide which form during the combustion process and damage the hot gas path components. However, in addition to appearing as solids, some of the contaminants can be in the gaseous or liquid state. In order to establish design goals for the Cyclocentrifuge so that gas cleanup also includes the elimination fine solids containing corrosion and deposit producing elements, the following assumptions are made:

- All of the corrosion and deposit-causing contaminants are contained in solid particles that have the weight density of ash.
- The gas purity requirement for corrosion and deposit protection of hot turbine blades is the sum of the allowable trace metal contaminants.

The second assumption leads to a total purity requirement that depends on the air/fuel ratio and limits the present cases to approximately 1 ppm of solids by weight according to recient G.E. gas turbine specifications. Reference 5 shows typical probability curves, which assume that all particles are less wher the maximum particle size measurable was limited to 80 microns, for particle size ranges, and calculations contained in Reference 12 show that the theoretical cut for the Cyclocentrifuge must be approximately 1 micron to achieve a purity of 1 ppm.

Based on Reference 1, Figure 1, and the above discussion, the design requirements were taken as follows:

- Volume flow from coal gasifier: 125,260 scfm
- Inlet pressure: 250 psi
- Inlet temperature: 1000°F
- Purity: 1 ppm total solids by weight
- Nominal particle size (cut): 1 micron

## 3. GENERAL ARRANGEMENT OF THE CYCLOCENTRIFUGE

Figure 2 shows that the general arrangement of the Cyclocentrifuge consists of two major components: a rotating assembly called the "centrifuge" and a stationary assembly called the "cyclone". The cyclone is both a pressure vessel and a containment vessel for the rotating centrifuge.

Particulate matter is separated outside of the centrifuge shell. The high centrifugal field, which is the basis for separation, is generated by the cyclone swirl velocity caused by the tangentially located inlet duct and, primarily, by the energy imparted to the gas by the swirl augmentation blade arrangement that is fixed to the centrifuge.

The rotating gas forms a vortex which originates in the dust collecting vessel below the cyclone cone. At the bottom of the conical section, the layer of gas at the cyclone wall is subjected to an intense centrifugal field because the angular velocity of the gas increases as the radius decreases in accordance with the law of conservation of angular momentum. The gas layer at the wall, which contains the centrifuged particulate matter, is bled-off into the collection vessel to complete the separation; the remainder of gas feeds the rising vortex core with clean gas. Re-entrainment is prevented by diffusing the bleed gas in the expanding cross-section of the dust collected vessel where the particulate matter settles to the bottom of the vessels. In leaving the collection vessel, the particles are again fluidized and carried through a duct to the suspensions pump.

The centrifuge drive power is extracted from the process gas in the form of a pressure drop across the built in reaction turbine. Figure 3 shows the rotating assembly, which contains the following design features:

- The swirl augmentation blades are arranged to gradually accelerate the gas to achieve the centrifugal force field necessary to separate fine particulate matter without exceeding the maximum throughput velocity for conventional cyclone design.

- The exit vanes are zero-lift structural support struts that carry the weight of the rotating assembly.

- The upper bearing rotates; the lower bearing is stationary.
- The drive turbine is located at the centrifuge entrance.
- The structural stiffness-to-weight ratio is maximized to place the first critical speed 25 percent above the operating speed.

Figure 4 shows the upper bearing and shaft assembly. The important features are:

- Both the journal and thrust bearings are externally pressurized hyrostatic bearings. The bearings are essentially optimized with respect to stiffness and consist of a number of deep pockets surrounded by "lands", all of which are vented to the return line.
- Pressure for forcing the lubricant through the return lines is provided by the process gas.
- The weight of the centrifuge assembly is carried by the upper surface of the thrust bearing; the lower surface of the thrust bearer provides the additional stiffness necessary to control the axial critical frequency.
- The stator guide vanes are canted to direct the flow towards the exit duct.
- A gas blow-back seal, shown in View A, overcomes the outside-to-inside pressure gradient and prevents dirty gas from mixing with clean gas.
- Dust protection for the bearings is provided by a cover surrounding the upper shaft support and by the labyrinth seal at the top of the bearing. Pressure seals are not required.
- The upper support blades, which are also exit vanes, are twisted to a zero-lift configuration.

Figure 5 shows the lower bearing and shaft assembly. The important features are:

- The journal bearing is similar to the upper journal bearing.
- Bearing lubricant is supplied and returned through passages in the lower bearing support struts. Dust protection is provided by the labyrinth seal. A pressure seal is not required.
- Power to drive the centrifuge at 5500 rpm comes from a turbine. The turbine extracts energy from the cyclone swirl component; however, the primary source of energy is the process gas.
- The lower bearing support struts are twisted clockwise to an average zero-life angle for the downward flow outside the centrifuge and then twisted counter-clockwise for the upward flow entering the centrifuge drive turbine. Transition occurs at the lower bearing support ring.
- The outboard struts are attached to the support ring in a "semi-bicycle-spoke" arrangement to accomodate differential expansion of the struts (see Section AA, Figure 2).
- By virtue of the relative moment stiffness between the strut assembly and the journal bearing, the strut assembly forms an elastic gimbal to accommodate angular misalignment of the lower bearing.
- The lower bearing and mounting assembly is designed to align to the upper assembly in order to accommodate slow, thermally induced dimensional changes in the mounting members or support points.

Figure 6 shows the lubrication schematic which is typical in design for most similar applications.

## 4. AERODYNAMIC DESIGN

The Aerodynamic analyses were performed iteratively with stress and rotor dynamic studies to insure that stress limits were not exceeded and that the first critical speed was at least 25 percent higher than the design speed. The final compromise in this process was to reduce the operating speed from 5370 rpm to 5500 rpm. This change of 4 percent, which was made to satisfy rotor dynamic considerations, is not reflected in the subsequent sections because the effect is too insignificant from an aerodynamic view-point to warrant another iteration.

### A. Principal Dimensions

After consideration of flow areas and structural stiffness requirements, the centrifuge OD was set at 26 inches.

The centrifuge design speed was determined on the basis of preliminary design sketches and a maximum allowable stress of 80,000 psi. This stress limitation is based on the material In 718 at 1000°F. The design speed was set at 5730 rpm, which is equivalent to a centrifuge surface speed of 650 ft/sec.

Based on Reference 6, the throughput velocity between the cyclone and centrifuge was taken as 24 ft/sec and the required inside diameter of the cylindrical section of the cyclone was calculated to be 57 inches.

The axial length of the Cyclocentrifuge was determined by calculating the axial distance traveled by a 1 micron particle in its spiral path from the wall of the centrifuge to the wall of the cyclone.

In keeping with Reference 6, the axial length of the cyclindrical section below the centrifuge inlet was taken equal to one diameter, and the length of the conical section as 2.5 diameters.

The required distance from the top of the inlet duct to the bottom of the centrifuge was determined from preliminary design of the inlet duct and swirl augmentation blade section to be 80 in.

The overall Cyclocentrifuge height also includes the distance from the top of the inlet duct to the top of the vessel head, plus the length of the particulate discharge flange, plus the height of the particulate collection vessel. These lengths are taken as 20 inches, 6 inches, and 6'-4 1/4", respectively, making the overall length of the Cyclocentrifuge vessel was 30'-11 1/2".

## B. Separation Efficiency

There is a critical size of particle of given density for which the centrifugal and drag force exactly balance so that the particle moves neither outward nor inward. All particles larger than the critical size will be collected; all smaller will escape. The critical particle size is called the theoretical cut. The theoretical cut for the Cyclocentrifuge was determined in accordance with Reference 7, and is calculated to be 1.08 microns for the present case.

Figure 7 shows the predicted grade efficiency for the Cyclocentrifuge and for a conventional, high efficiency cyclone. This curve anticipates the following:

- Compared to an ordinary cyclone, more particles larger than the Cyclocentrifuge cut size will be prevented from entering the exit duct because:
    - The distance from the inlet duct to the centrifuge entrance is greater than the equivalent distance in a cyclone.
    - The cycloncentrifuge "exit duct" is the spinning centrifuge which will reject particles that bounce off the cyclone wall.
    - The re-entrainment potential is reduced because the outward "g" field is larger than a cyclone.
- Compared to a cyclone, more particles smaller than the cut size will be separated because collisions with larger particles will increase and smaller size aggregates of fine particles will be removed by the increased centrifuged field.

## C. Swirl Augmentation Blades

The swirl augmentation blades are designed with a constant cross-section and no individual camber. The blades are arranged in cascade such that the effective camber of the cascade is 70 degrees, as shown in Figure 8, the required gas deflection of 88 degrees is accomplished using 11 blade rows occupying an axial length of 45 inches. There are 16 individual blades spaced uniformly in each of the 11 rows.

Figure 9 shows the velocity triangles which are the bases for the blade design. The tangential velocity at the hub is seen to be 650.6 ft/sec, while the axial component is 24.08 ft/sec and the entering gas velocity, due to cyclone swirl, is 150 ft/sec. At the blade tip, the tangential velocity is seen to be 850.8 ft/sec with the axial and entering velocity components being identical to hub section conditions. The lower velocity triangle sketch in Figure 9 shows that the swirl velocity of the gas is increased uniformly through the 11 rows of blades, without changing the axial velocity.

### D. Centriguge Drive Turbine

The centrifuge is rotated by a high-reaction axial turbine driven by energy extracted from the process gas. The exit gas velocity vector is purely axial and so that the gas passing through the centrifuge will not tend to centrifuge particles, and solids buildup on the inside wall of the centrifuge will be minimized.

The whirl component from the cyclone vortex is used as an energy source for the turbine, and inlet nozzle guide vanes are not used. The remainder of the drive power is produced by a pressure drop in the process gas across the rotor blades.

The power required to be delivered by the turbine can be approximated by

$$P = W_a U \, (\Delta U_\theta)$$

where $W_a$ is the gas mass flow through the annular area, $A_a$, based on the centrifuge diameter and the diameter at the tip of the swirl augmentation blades.

$U$ is the gas tangential velocity at the centrifuge OD = 650.9 ft/sec from Figure 9.

$\Delta U_\theta$ is the increase in tangentail velocity due to the swirl augmentation blades = 500.6 ft/sec from Figure 9.

Using the above data, the required horsepower is approximately 500.

Figure 10 shows the blade cross-sections at the root, mid-cord, and tip, and the pressure drop across the turbine is calculated to be 6.1 psi.

The turbine inlet whirl distribution is obtained from the assumption $U^2R$ = constant as suggested in Reference 6. Figure 10 incicates that most of the turbine work output is produced in the hub to mid-cord region where the prevailing whirl velocity is of significant magnitude. Thus, the blades are straight near the tip and highly twisted at the hub. The blade solidity for the cascade is based on avoiding choking everywhere and on a Zweifel coefficient of approximately 1.1 at the hub. The incidence is taken as zero at the design point, and the deviation angle is based on the recommendation given by Horlock in Reference 9.

## E. Total Pressure Drop

The total pressure drop through the Cyclocentrifuge $\Delta p$ is

$$\Delta p = \Delta p_t + \Delta p_c$$

where $\Delta p_t$ = drop across the drive turbine = 6.1 psi

In accordance with the calculation procedure given in Reference 7,

$$\Delta p_c = 8.5 \text{ psi}$$

therefore,

$$\Delta p = 14.6 \text{ psi}$$

## F. Static Pressure Distribution

Figure 11 gives the static pressure at selected points in the Cyclocentrifuge. The basis for this estimate is References 6 and 7 and the calculation for the pressure drop across the turbine.

### G. Particle Buildup

Even though the absolute velocity of the gas entering the centrifuge is purely axial, the potential for particle build-up on the inside wall of the centrifuge still exists. Accumulation depends on particle size distribution, radial velocity, velocity in the boundary layer, and the rate of particle arrival relative to departure.

Preliminary calculations based on particle concentration derived from spectral measurements presented in Reference 10 and frictional velocity estimates suggested in Reference 11 indicate, particle buildup should not occur to any significant degree.

## 5. SIGNIFICANT STRESSES AND DEFLECTIONS

Nickel-chromium alloy In 718 was selected for all rotational parts because of its long-life properties at temperatures up to about 1200°F and because it can be cast and welded. Based creep data, a design temperature of 1000°F was selected and the maximum stress was set at 80,000 psi. Figure 12 shows the maximum stress and deflections at and between the swirl augmentation blades, which are considered acceptable.

## 6. ROTOR DYNAMICS ANALYSES

### A. Rotor Model

Figure 13 shows a schematic of the Cyclocentrifuge rotor assembly and a tabulation of the engineering data used in mathematical modeling for dynamic analyses.

The design stiffness of each of the journal bearings is $1.0 \times 10^6$ lb/in., and including the bearing mounting stiffness, the total support stiffness at each bearing station is $0.857 \times 10^6$ lb/in.

### B. Critical Speeds

The first two undamped lateral critical speeds are plotted in Figure 14 versus the stiffness of the upper journal bearing, which, for the present case, is the same as the lower journal bearing. At the design stiffness of $1 \times 10^6$ lb/in., the first two critical speeds are 6,936 and 11,244 rpm, thus, the first critical is 26 percent above the operating speed. The modes shape for the first critical speeds is shown in Figure 15.

### C. Unbalance Response

The degree of expected residual unbalance as calculated by 4 W/N, gives 0.726 oz-in. of unbalance for the present rotor. This balance specification is often used by the U.S. Navy for rotors of the present size where the unbalance is given in inch-ounces and W = weight of rotating assembly, lb; N = rotor speed, rpm. The response is tabulated for an unbalance of 1.0 oz-in. at Stations 4 and 29. The amplitude of response at the bearings is plotted versus speed in Figure 16, and is seen to be acceptable because the expected residual unbalance can degrade by an order of magnitude before the bearing eccentricity ratio exceeds 25 percent.

### D. Damped Lateral Critical Frequencies and Stability

Damping coefficients of 320 lb sec/in. were calculated for each journal bearings and the first two damped critical frequencies were determined to occur at speed of 7053 and 10,933 rpm. Thus, the lowest damped critical speed is about 28 percent above the operating speed.

Figure 17 gives the mode shape and stability corresponding to the first natural frequency. The stability is determined from the system log decrement which indicates if a disturbance to the rotor will grow or decay in amplitude. The threshold of stability is designated by a zero log decrement. If the log decrement is positive, a disturbance will decay and the system is stable; if the log decrement is negative, the opposite is true. In the present case, all natural frequencies are well within the stable region.

## BEARING DESIGN

Hydrostatic oil bearings were selected because they will provide long life without replacement.

### A. Journal Bearings

The upper and lower journal bearings are identical and their geometry is shown in Figure 18. Table 1 gives the design summary for the journal bearing.

Since the rotor is mounted vertically, the only load on the journal bearing will be due to rotor unbalance. The touch-down load can be estimated with reasonable accuracy by assuming the stiffness is constant and the eccentricity

## TABLE I

## DESIGN SUMMARY FOR JOURNAL BEARINGS

Hydrostatic Journal Bearing with Two Rows of Pads Separated by a Circumferential Groove.

| | | |
|---|---|---|
| Length | | = 3.000" |
| Diameter | | = 5.000" |
| Radial Clearance | | = 0.0025" |
| Land Widths | Axial | = 0.300" |
| | Circumferential | = 0.300" |
| Drain Grooves | Axial | = 0.200" x .25" deep |
| | Circumferertial | = 0.400" x .25" deep |
| Number of Circumferential Rows of Pads | | = 2 |
| Number of Pads per Row | | = 5 |
| Number of Pockets per Pad | | = 1 |
| Depth of Pocket | | = 0.15" |
| Number of Restrictors per Pocket | | = 1 |
| Restrictor Dimension | Length | = 0.30" |
| | Diameter, $d_o$ | = 0.020" |
| Pressure | Supply, $p_s$ | = 600 psia |
| | Pocket, $p_r$ | = 369 psia |
| | Ambient, $p_a$ | = 250 psia |
| Total Lubricant Flow | | = 8.74 gpm |
| Journal Speed | | = 5500 rpm |
| Radial Stiffness | Theoretical | = 1,360,000 lb/in. |
| | Used in Design Cal. | = 1,000,000 lb/in. |
| Power Loss | Couette | = 2.40 hp |
| | Pumping | = 1.79 hp |
| | Total | = 4.19 hp |

ratio at touch-down is 0.75. Using these assumptions, the touch-down load is estimated to be 1875 lb per bearing or a total radial load of 3750 lb. The estimated maximum radial load capacity is a factor of 3.78 times greater than the weight of the rotor, which should be satisfactory for reasonable contingencies.

## B. Thrust Bearing Design

The thrust bearing is designed to support the centrifuge weight on a hydrostatic film. Figure 19 shows the geometry of the double-acting thrust bearing and Table 2 summarizes the design. Figure 20 gives the load capacity, stiffness, flow, and power loss as functions of axial displacement. Figure 20 shows the design has ample load capacity and stiffness and that the rigid body axial critical speed is 7201 rpm which is safely above the operating speed.

## C. Lubricant Properties and Flow Requirements

Lubricant properties used in the bearing analyses are listed below. These properties are obtainable from fluorinated oils such as Krytox 143.

| | Temperature | |
|---|---|---|
| Property | 100°F | 400°F |
| Viscosity $\mu$, lb sec/in.$^2$ | $8.56 \times 10^{-5}$ | $9.0 \times 10^{-7}$ |
| Density $\rho$, lb/in.$^3$ | $6.76 \times 10^{-2}$ | $5.76 \times 10^{-2}$ |
| Heat Capacity $C_p$, BTU/lb °F | 0.238 | 0.290 |
| Thermal Conductivity K Btu/(sec in. °F) | $1.16 \times 10^{-6}$ | $1.16 \times 10^{-6}$ |

Flow requirements for the bearings are:

| | | |
|---|---|---|
| Upper Journal Bearing | | 8.74 gpm |
| Lower Journal Bearing | | 8.74 gpm |
| Thrust Bearing | | 8.80 gpm |
| | Total | 26.28 gpm |

## TABLE 2

## DESIGN SUMMARY FOR THRUST BEARING

Double-Acting Thrust Bearing with 20 Pads/Side

OD = 7.200"
ID = 6.475"
Drain Grooves: Width x Depth = 0.10" x 0.10"
Land Widths: Circumferential = 0.10"
Land Widths: Radial = 0.10"
Pocket Depth = 0.05"
Supply Orifices: Length = 0.45"
Supply Orifices: Diameter ← = 0.0160 (Loaded Side)
= 0.0135 (Unloaded Side)
Total Clearance (Both Sides) = 0.0050"
Design Weight (Load) = 991 lb
Design Eccentricity (From Centered Position) = 0.000835"
Design Stiffness = 1,460,000 lb/in.
Design Speed = 575.96 Rad/Sec = 5500 RPM
Pressure:
- Supply = 600 psia
- Ambient = 250 psia

| | Loaded Side | Unloaded Side | Total |
|---|---|---|---|
| Flow (GPM) | 5.21 | 3.59 | 8.80 |
| Power Loss, HP: | | | |
| • Couette | 1.73 | 0.86 | 2.59 |
| • Pumping | 1.06 | 0.73 | 1.79 |
| • Total | 2.79 | 1.59 | 4.38 |
| Temperature Rise °F | 5.90 | 4.84 | 5.47 |

### D. Temperature Distribution Around Bearing Assemblies

Heat flow rates, heat transfer coefficients, and selected temperatures in the upper and lower bearing areas are shown sketched in Figures 21 and 22, respectively. The temperature levels are considered acceptable for satisfactory bearing performance except for the metal area surrounding the journal bearing, which will require insulation to avoid condinsation of tar.

## 8. ECONOMIC ANALYSIS SUMMARY

The economic viability of the Cyclocentrifuge can be assumed to be determined by its effect on the production cost of electricity in a typical combined steam and gas turbine plant burning low Btu gas from coal. For purposes of this analysis, the production cost was calculated on the same basis as that used in ERDA Report 76-49, "Economic Analysis of Westinghouse Low Btu Gasification - Combined Cycle Power Generating System Producing 134.1 Megawatts", prepared by U.S. Department of the Interior, Bureau of Mines for the Energy Research and Development Administration, March 1976.

The production cost, as calculated in ERDA 76-49, includes the cost of coal, dolomite, water, spent oxidizer disposal, labor and supervision, plant maintenance including supervision and materials, payroll overhead, operating supplies, administration and general overhead, and capital charges at 17 percent of total capital investment.

With the Cyclocentrifuge concept as presently developed, the temperature of the low Btu gas must be reduced to about 1000°F from the Baseline temperature of 1546°F. This requires a higher gas flow for the same gas turbine firing temperature and corresponding output (i.e., constant gas turbine air flow). The higher gas flow requires a 5.5 percent increase in coal to the gasifier.

To provide the lower gas temperature, additional steam generating surface must be provided in the gasifier, with a resulting increase in low pressure steam generated. This steam, over and above that required by the gasification process, can be expanded in the steam turbine and will produce additional electrical output of about 4.4 Megawatts. The net effect is to reduce the cycle efficiency a little over 2 percent.

At the same time, the Cyclocentrifuge is estimated to have only 15 psi pressure drop through it, which is less than the 30 psi of the cyclone and sand bed filters used in the Baseline cycle. This reduction in pressure drop reduces the work required of the booster compressor to maintain the same pressure at the gas turbine control valve by about 450 kw, or 0.34 percent gain in net output. This gain in output was neglected in estimating the production cost as offsetting other losses that might not have been properly calculated or accounted for.

In order to calculate the capital cost of the complete installation and the corresponding capital charges to be included in the production cost of electricity, an estimate was made of the cost of the Cyclocentrifuge based primarily on the weight of the complete assembly. This estimated installed cost of $93,573 was substituted in the capital cost estimate for the $86,000 allowed in the Baseline system for the cyclone and sand bed filters.

Allowance was also made for the increase in the steam turbine-generator and condenser cost, due to the increased rating, the increase in coal preparation, dolmite preparation, and gasification cost due to the increased coal flow. The total capital cost increased from $40,915,400 to $41,654,980 and the corresponding capital charges from $6,955,600 to $7,081,47.

With the increase in plant output, the net effect is to reduce the production cost of electricity, with coal at $11.00 per ton, from $.01592 per kw hr to $.01581 per kw hr, a cost improvement of .7 percent. Considering the effect of reduced pressure drop in the gas clean-up system, this is probably realistic.

Table 3 summarizes the comparison between the baseline system and the modified system.

## TABLE 3

Economic Summary of Comparison Between Baseline System and Cyclocentrifugal

| Item | Baseline System | Modified System | Percent Increase |
|---|---|---|---|
| Gas temperature to gas turbine, °F | 1546 | 1000 | -35.3 |
| Output, Mw | 134.1 | 138.5 | 3.3 |
| Coal fired tph | 49.6 | 49.5 | 5.5 |
| Steam produced in gasifier lb/hr | 42,000 | 51,926 | 23.6 |
| Pressure drop across cleaning equipment, psi | 30 | 15 | -50.0 |
| Gas cleanup, equipment cost, $1,000 | 86.0 | 93.6 | 8.8 |
| Cycle efficiency, % | 37.40 | 36.65 | -2.0 |
| Capital cost, $1,000,000 | 40.92 | 41.6 | 1.7 |
| Capital charges, $1,000,000 | 6.96 | 7.08 | 1.7 |
| Output cost per kw hr | 0.01592 | 0.01581 | -0.7 |

## 9. SUMMARY AND CONCLUSIONS

The mechanical arrangement of the Cyclocentrifuge developed during this study is shown in Figure 1. It has may intrinsic advantages, some of which are unique to the concept. These advantages, listed below. implicitly define areas in which the concept can be employed to aid in improving the effectiveness and efficiency of coal conversion.

- Fine particulate matter can be separated from a gas stream. Separation of sub-micron particles is possible.

- High gas purity can be attained. One pound of solids per million pounds of gas is feasible (1 ppm total solids).

- Hot gas can be treated without special heat transfer design. A nominal gas stream temperature of 1000°F is practical. With special heat transfer schemes, higher temperatures are possible.

- Pressurized gas can be treated. The centrifuge assembly is pressure-balanced because it is located inside a modified conventional cyclone.

- The design concept does not accumulate particulate matter. Continuous operation is practical.

- Electrical input power is not required. The rotating assembly is efficiently turbine-driven by the process gas.

- The design is compact and does not require intricate piping or controls.

- There are a minimum of interface problems.

- The design does not create new secondary pollution problems.

- First cost and operating costs should be equal to or less than present alternate cleanup approaches.

## 10. ACKNOWLEDGEMENTS

This work was performed under Contract No. E(49-18)-2428 for the Fossil Energy Research and Technology Division of ERDA by the Mechanical Equipment Section of the MTI Engineering Department. The ERDA Program Manager was Mr. W. Fedarko. Mrs. A. O. White, L. Folsom, A. Tuzinkiewicz, S. Park, A. Artiles, and P. McGee made significant contributions to this project in behalf of MTI.

## 8. REFERENCES

1. Process Evaluation Office, ERDA at Morgantown, W. Va., "Economic Analysis of Westinghouse Low-Btu Gasification Combined-Cycle Power Generating System Producing 134.1 Megowatts, ERDA Report 76-49.

2. Foster, A. D.; Von E. Doering, H.; Hickey, J. W., "Gas Turbine Fuel", General Electric Gas Turbine Reference Library, Document GER-2222H with Supplement "Specifications for Gas Turbine Fuel, Gases", GEI-41040C; "Liquid Fuels Specification", GEI-41047E.

3. White, A. O., "20 Years Experience Burning Heavy Fuels in Heavy Duty Gas Turbines", ASME publication 73-GT-22.

4. Buckland, B. O., "The Effect of Treated High-Vanadium Fuel on Gas Turbine Load, Efficiency and Life", ASME publication 58-GTP-17.

5. Weth, G.; Farmer, W. M., "In-Sites Laser Measurements in Coal Processing Systems", View-Graph presentation at ERDA, Washington, 9 Novermber 1976; From Spectron Development Laboratories, Inc. SDL Report 77-6801.

6. Stairmand, C. J., "The Design and Performance of Cyclone Separators", Trans. Instr. Chem. Engr., Vol. 29, 1951 (Great Britain).

7. Stairmand, C. J., "Pressure Drop in Cyclone Separators", Engineering, October 21, 1949.

8. Zweifel, )., "The Spacing of Turbomachine Blading, Especially with Large Angular Deflection", Brown Boveri Rev. 32, December 1945.

9. Harlock, J. H., "Axial Flow Turbines", Butterworths, 1966.

10. In Situ Laser Measurements in Coal Processing Systems, Spectron Development Laboratories, Inc., Report No. 77-6801, Nov. 9, 1976.

11. Howarth, L., ed., Modern Developments in Fluid Dynamics - High Speed Flow, Vol. I, Aeronautical Research Council.

12. McCabe, J. T., "Centrifuges for Coal Conversion and Related Processes, Phase I: Feasiblility Study", Final Report MTI 77TR34 Mechanical Technology Incorporated to ERDA, contact E(49-18)-2428, March 1977.

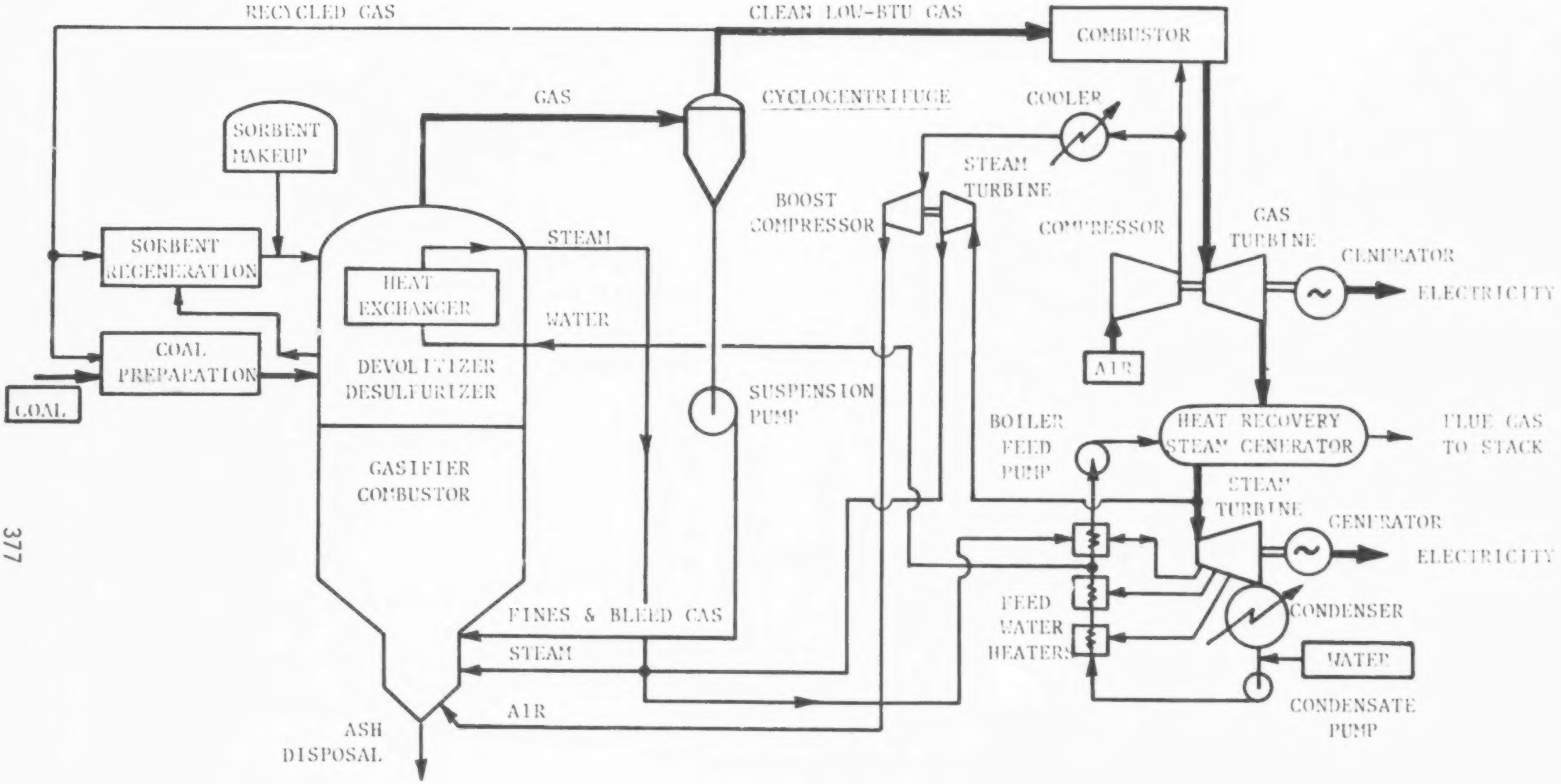
RECYCLED GAS
CLEAN LOW-BTU GAS
COMBUSTOR
GAS
CYCLOCENTRIFUGE
COOLER
SORBENT MAKEUP
STEAM TURBINE
BOOST COMPRESSOR
COMPRESSOR
GAS TURBINE
GENERATOR
ELECTRICITY
SORBENT REGENERATION
STEAM
HEAT EXCHANGER
WATER
COAL PREPARATION
DEVOLATIZER DESULFURIZER
AIR
COAL
SUSPENSION PUMP
BOILER FEED PUMP
HEAT RECOVERY STEAM GENERATOR
FLUE GAS TO STACK
GASIFIER COMBUSTOR
STEAM TURBINE
GENERATOR
ELECTRICITY
FEED WATER HEATERS
CONDENSER
FINES & BLEED GAS
STEAM
WATER
AIR
CONDENSATE PUMP
ASH DISPOSAL

Fig. 1 Low-Btu Process Schematic for Combined Cycle Electricity Generation using Cyclocentrifuge for Gas Cleanup

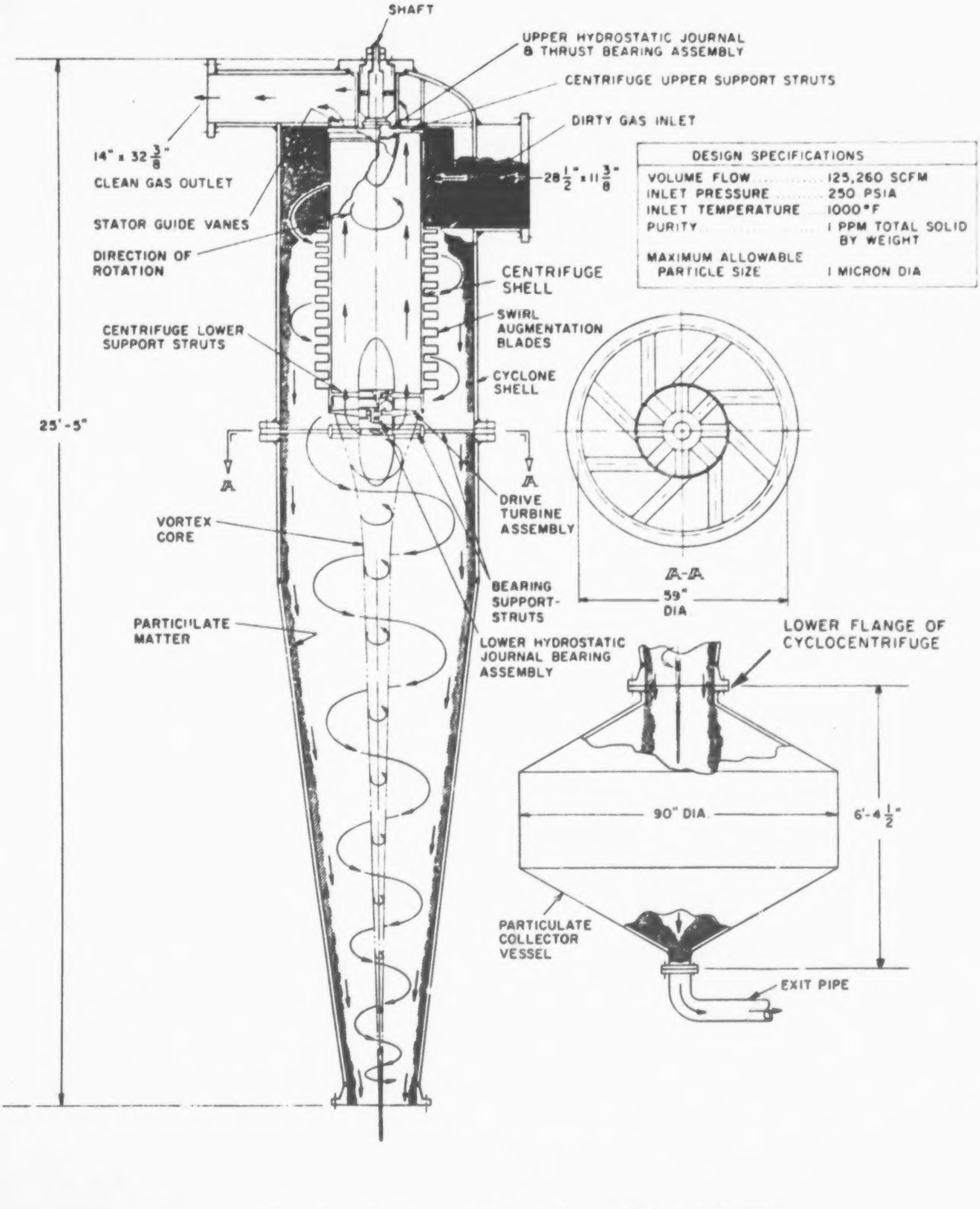
SHAFT
UPPER HYDROSTATIC JOURNAL & THRUST BEARING ASSEMBLY
CENTRIFUGE UPPER SUPPORT STRUTS
DIRTY GAS INLET
14" x 32 3/8"
CLEAN GAS OUTLET
28 1/2" x 11 3/8"
DESIGN SPECIFICATIONS
VOLUME FLOW ........ 125,260 SCFM
INLET PRESSURE ........ 250 PSIA
INLET TEMPERATURE .... 1000°F
PURITY ........ 1 PPM TOTAL SOLID BY WEIGHT
MAXIMUM ALLOWABLE PARTICLE SIZE ..... 1 MICRON DIA
STATOR GUIDE VANES
DIRECTION OF ROTATION
CENTRIFUGE SHELL
SWIRL AUGMENTATION BLADES
CENTRIFUGE LOWER SUPPORT STRUTS
CYCLONE SHELL
25'-5"
A
A
DRIVE TURBINE ASSEMBLY
VORTEX CORE
BEARING SUPPORT-STRUTS
A-A
59" DIA
PARTICULATE MATTER
LOWER HYDROSTATIC JOURNAL BEARING ASSEMBLY
LOWER FLANGE OF CYCLOCENTRIFUGE
90" DIA.
6'-4 1/2"
PARTICULATE COLLECTOR VESSEL
EXIT PIPE

Fig. 2 Cyclocentrifuge, General Arrangement

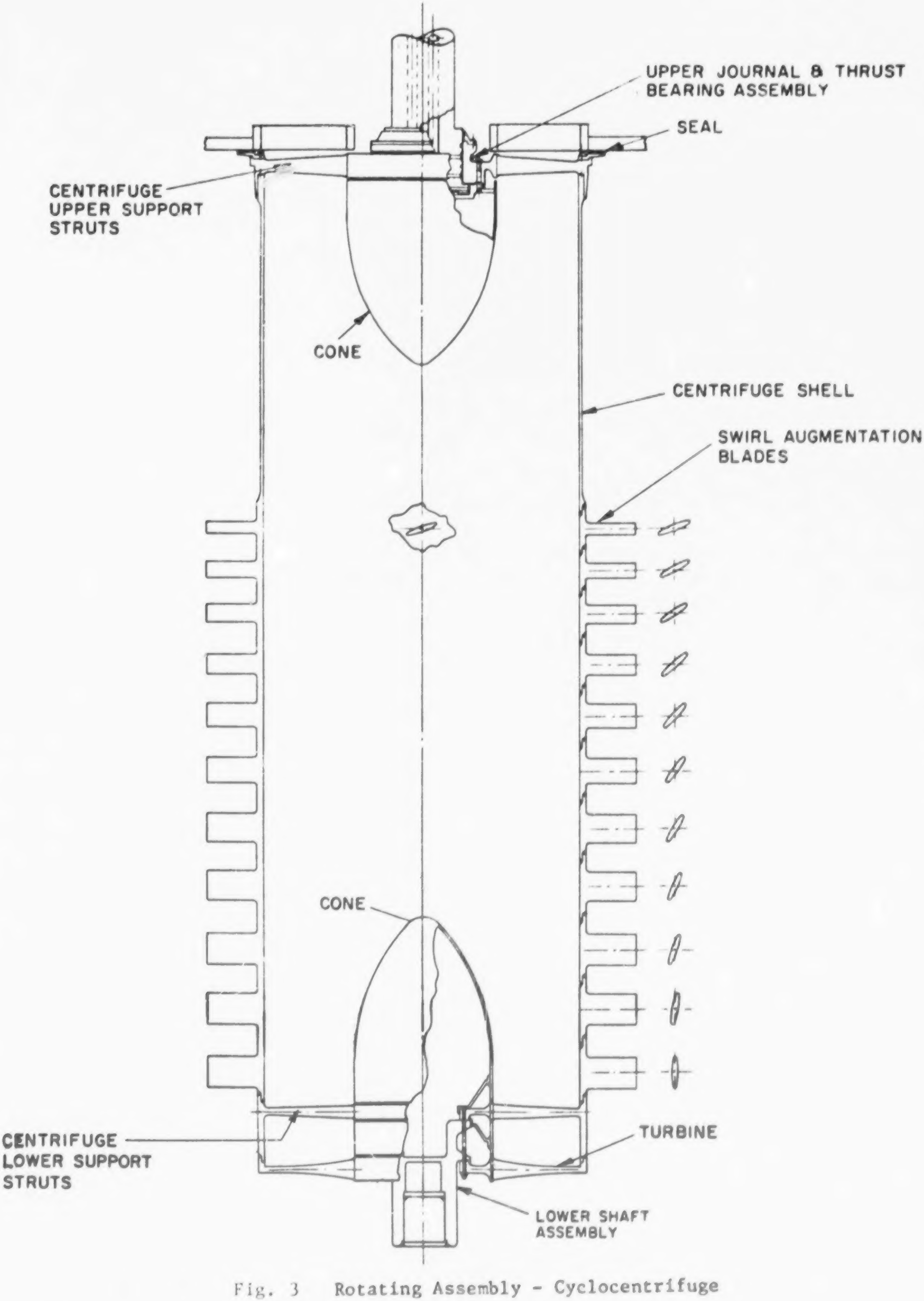
UPPER JOURNAL & THRUST BEARING ASSEMBLY
SEAL
CENTRIFUGE UPPER SUPPORT STRUTS
CONE
CENTRIFUGE SHELL
SWIRL AUGMENTATION BLADES
CONE
CENTRIFUGE LOWER SUPPORT STRUTS
TURBINE
LOWER SHAFT ASSEMBLY

Fig. 3 Rotating Assembly - Cyclocentrifuge

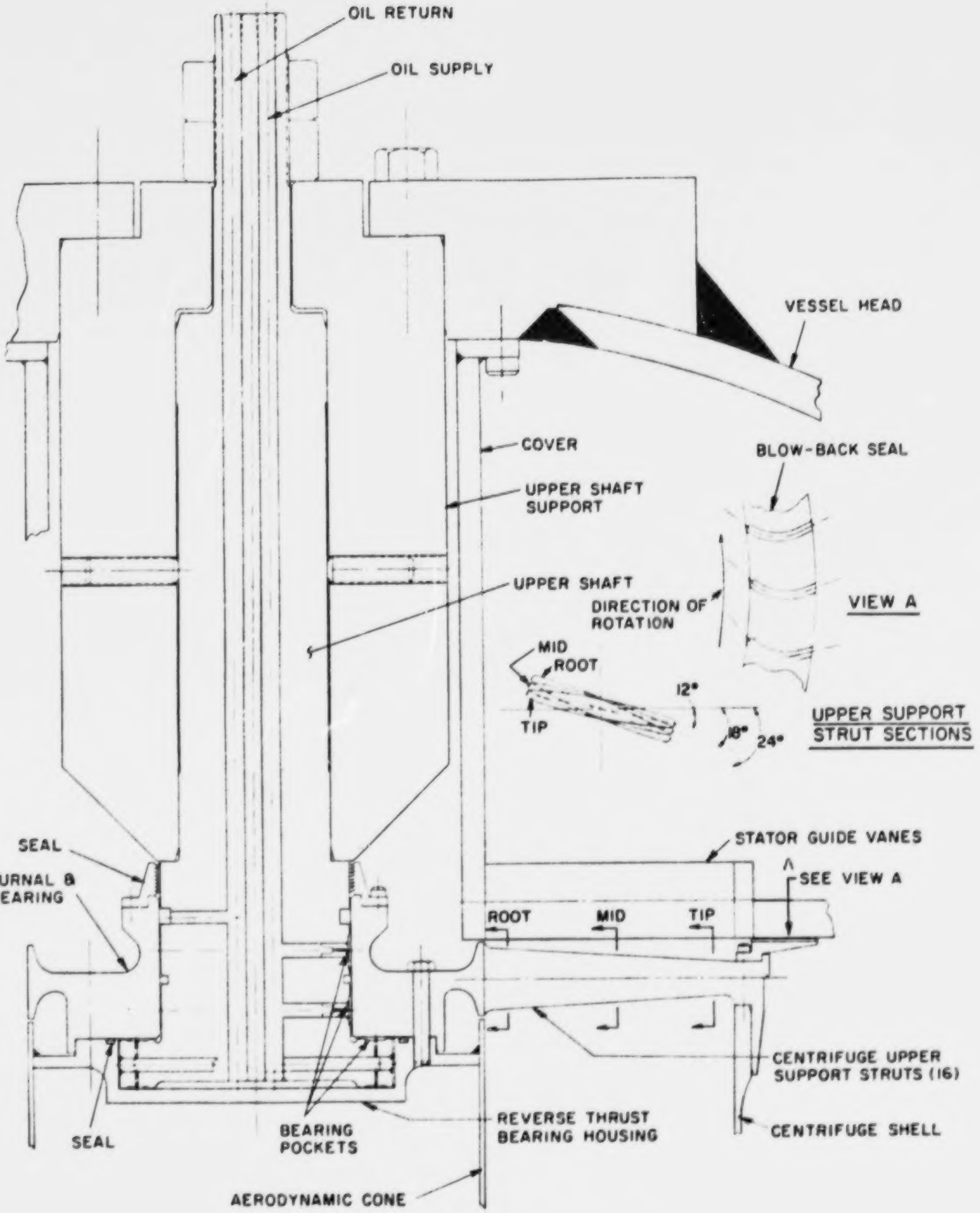
OIL RETURN
OIL SUPPLY
VESSEL HEAD
COVER
BLOW-BACK SEAL
UPPER SHAFT SUPPORT
UPPER SHAFT
DIRECTION OF ROTATION
VIEW A
MID
ROOT
TIP
12°
18°
24°
UPPER SUPPORT STRUT SECTIONS
STATOR GUIDE VANES
SEAL
UPPER JOURNAL & THRUST BEARING HOUSING
SEE VIEW A
ROOT
MID
TIP
CENTRIFUGE UPPER SUPPORT STRUTS (16)
SEAL
BEARING POCKETS
REVERSE THRUST BEARING HOUSING
CENTRIFUGE SHELL
AERODYNAMIC CONE

Fig. 4 Upper Bearing and Shaft Assembly - Cyclocentrifuge

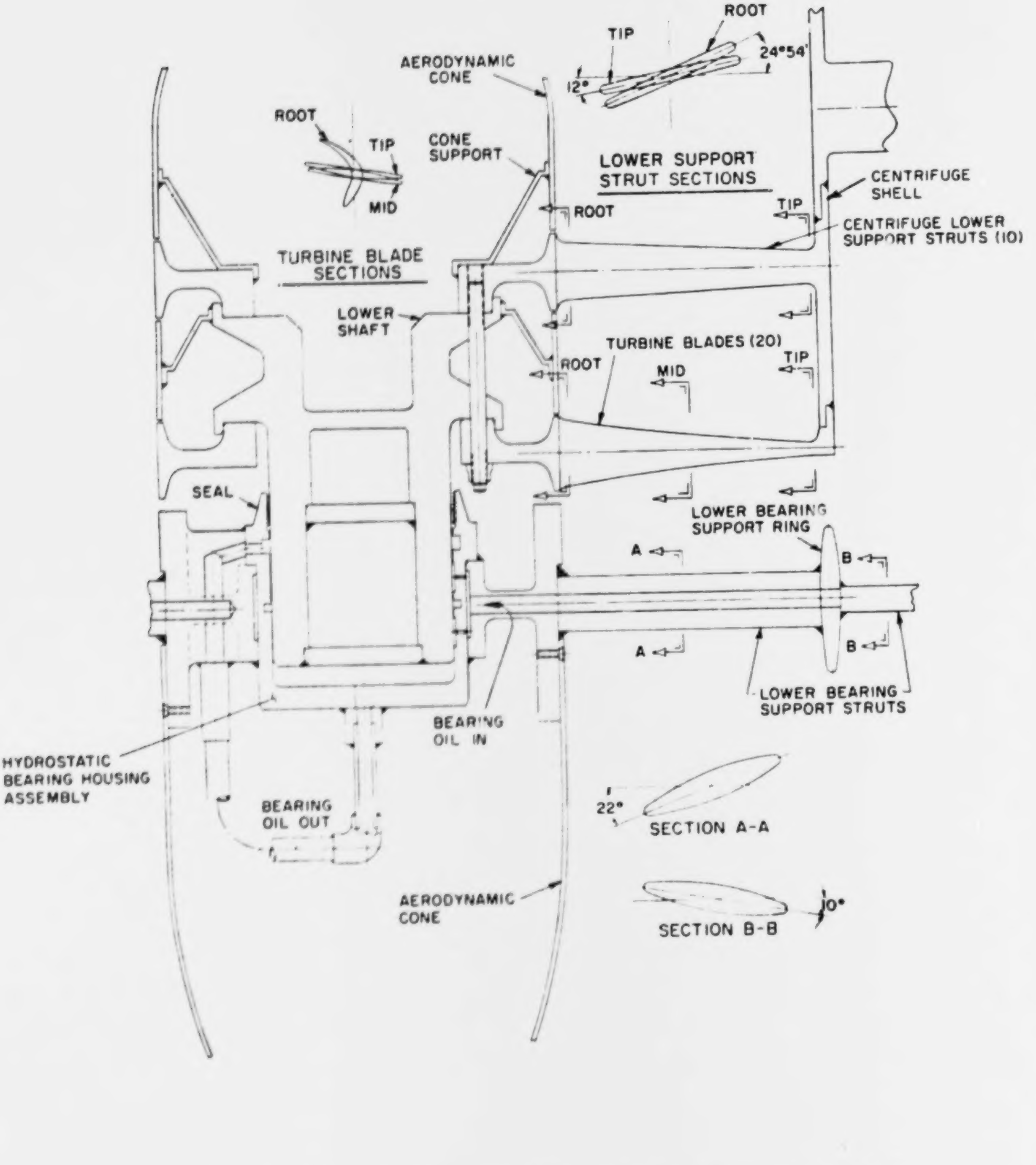
ROOT
TIP
24°54'
12°
AERODYNAMIC CONE
ROOT
TIP
MID
CONE SUPPORT
LOWER SUPPORT STRUT SECTIONS
ROOT
TIP
CENTRIFUGE SHELL
CENTRIFUGE LOWER SUPPORT STRUTS (10)
TURBINE BLADE SECTIONS
LOWER SHAFT
TURBINE BLADES (20)
ROOT
MID
TIP
SEAL
LOWER BEARING SUPPORT RING
A
B
A
B
LOWER BEARING SUPPORT STRUTS
BEARING OIL IN
HYDROSTATIC BEARING HOUSING ASSEMBLY
BEARING OIL OUT
22°
SECTION A-A
AERODYNAMIC CONE
10°
SECTION B-B

Fig. 5 Lower Bearing and Shaft Assembly - Cyclocentrifuge

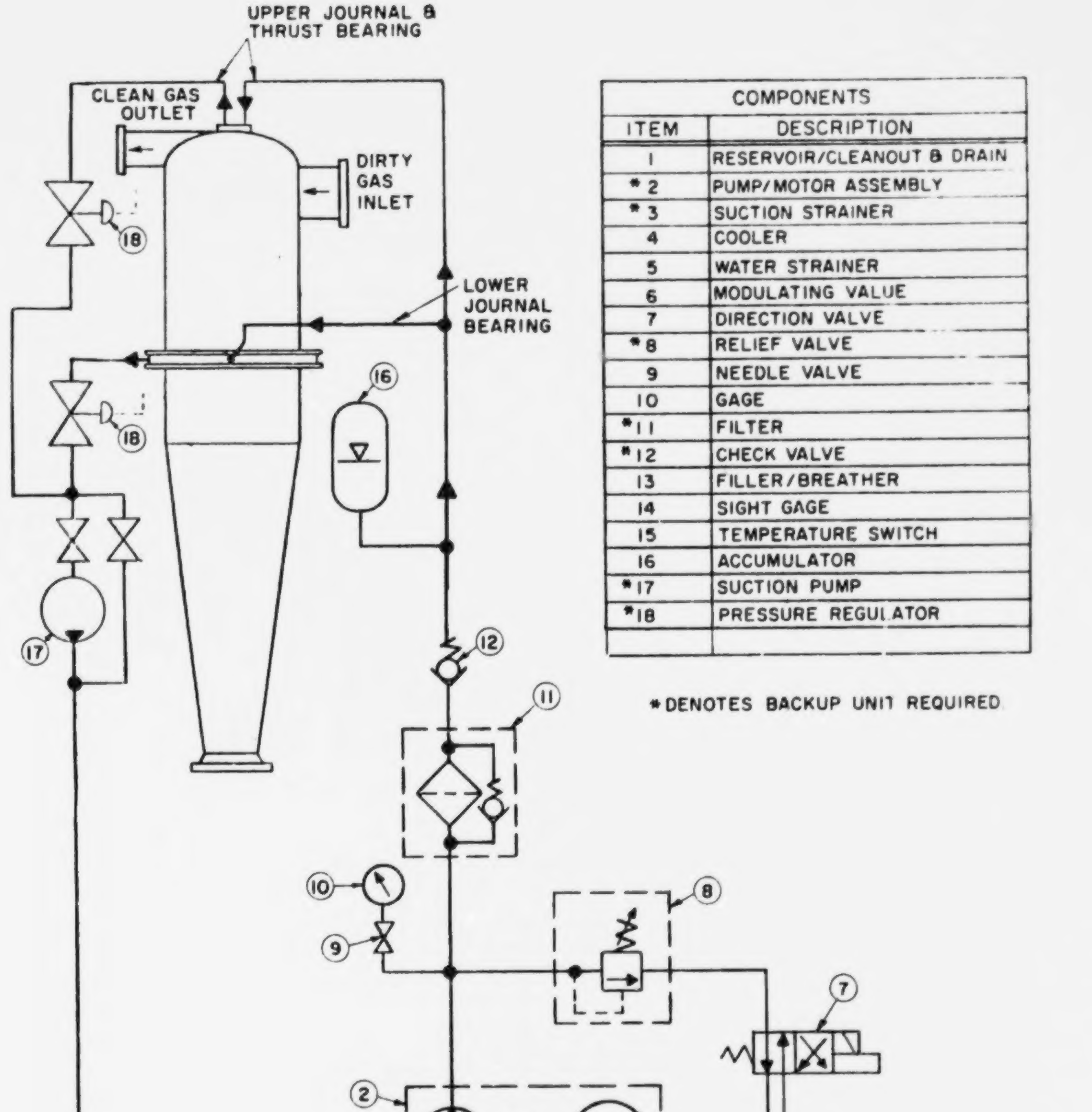
UPPER JOURNAL &
THRUST BEARING
CLEAN GAS
OUTLET
DIRTY
GAS
INLET
LOWER
JOURNAL
BEARING
H$_2$O COOLING
TS
1
2
3
4
5
6
7
8
9
10
11
12
13
14
15
16
17
18
18

| COMPONENTS | |
|---|---|
| ITEM | DESCRIPTION |
| 1 | RESERVOIR/CLEANOUT & DRAIN |
| *2 | PUMP/MOTOR ASSEMBLY |
| *3 | SUCTION STRAINER |
| 4 | COOLER |
| 5 | WATER STRAINER |
| 6 | MODULATING VALUE |
| 7 | DIRECTION VALVE |
| *8 | RELIEF VALVE |
| 9 | NEEDLE VALVE |
| 10 | GAGE |
| *11 | FILTER |
| *12 | CHECK VALVE |
| 13 | FILLER/BREATHER |
| 14 | SIGHT GAGE |
| 15 | TEMPERATURE SWITCH |
| 16 | ACCUMULATOR |
| *17 | SUCTION PUMP |
| *18 | PRESSURE REGULATOR |
| | |

*DENOTES BACKUP UNIT REQUIRED

Fig. 6 Lubrication System Schematic - Cyclocentrifuge

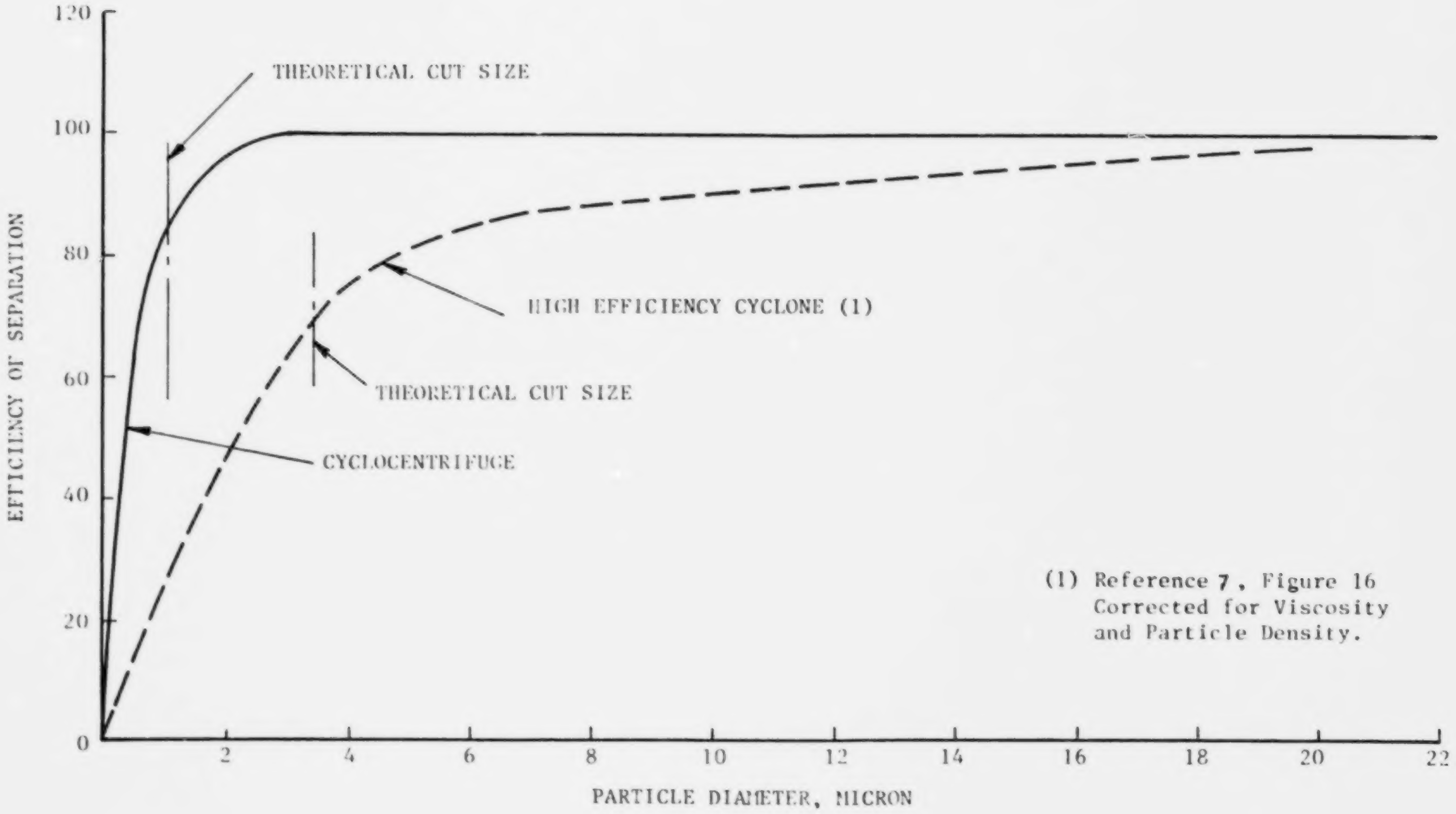

(1) Reference 7, Figure 16
Corrected for Viscosity
and Particle Density.

Fig. 7 Cyclocentrifuge Grade Efficiency

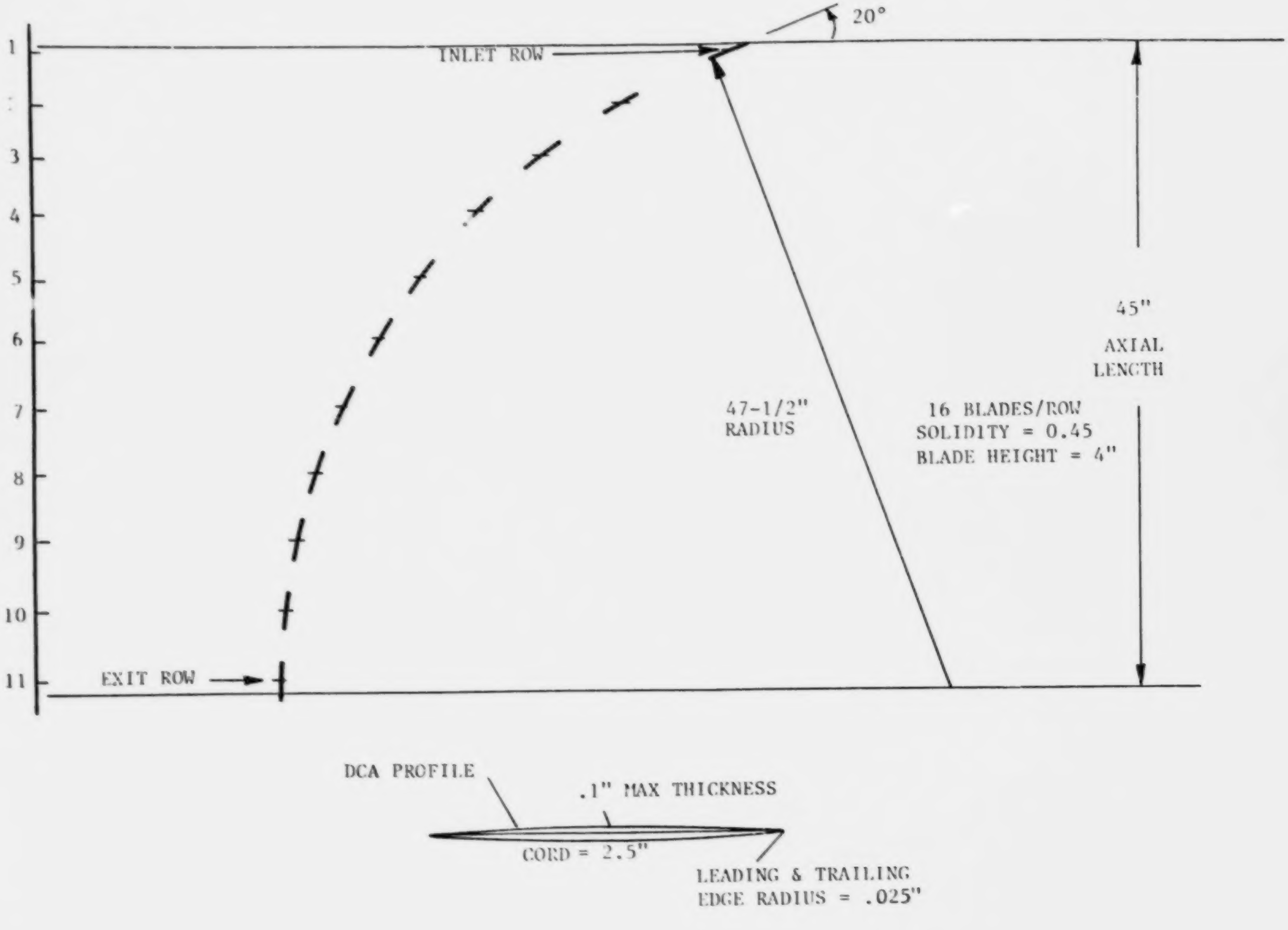
20°
1
3
4
5
6
7
8
9
10
11
INLET ROW
EXIT ROW
47-1/2"
RADIUS
45"
AXIAL
LENGTH
16 BLADES/ROW
SOLIDITY = 0.45
BLADE HEIGHT = 4"
DCA PROFILE
.1" MAX THICKNESS
CORD = 2.5"
LEADING & TRAILING
EDGE RADIUS = .025"

Fig. 8 Cascade Arrangement of Swirl Augmentation Blades

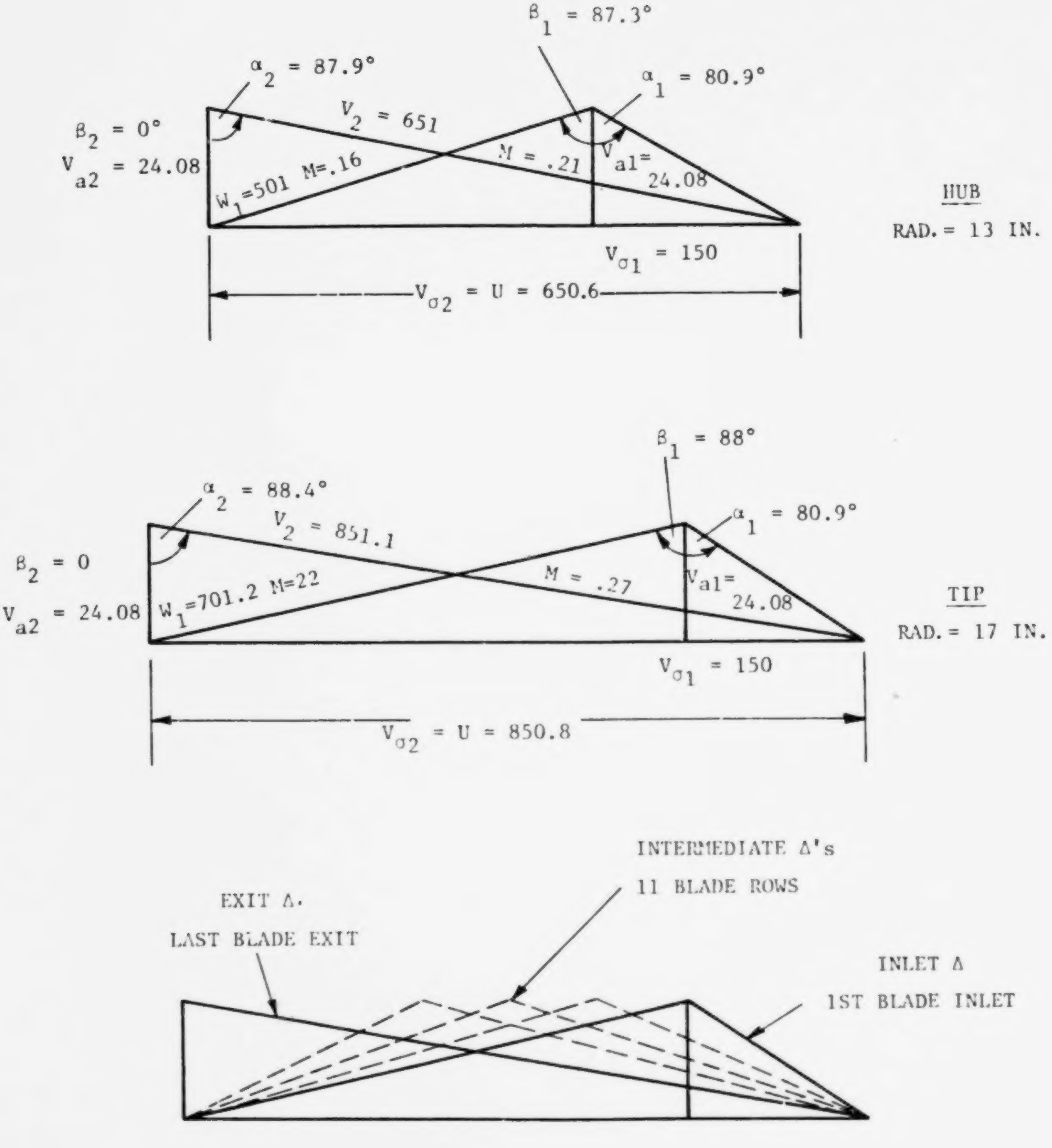
β1 = 87.3°
α2 = 87.9°
α1 = 80.9°
β2 = 0°
Va2 = 24.08
V2 = 651
W1 =501 M=.16
M = .21
Va1= 24.08
HUB
RAD. = 13 IN.
Vσ1 = 150
Vσ2 = U = 650.6
β1 = 88°
α2 = 88.4°
α1 = 80.9°
V2 = 851.1
β2 = 0
Va2 = 24.08
W1=701.2 M=22
M = .27
Va1= 24.08
TIP
RAD. = 17 IN.
Vσ1 = 150
Vσ2 = U = 850.8
INTERMEDIATE Δ's
11 BLADE ROWS
EXIT Δ.
LAST BLADE EXIT
INLET Δ
1ST BLADE INLET

Fig. 9 Velocity Triangles for Swirl Augmentation Blades

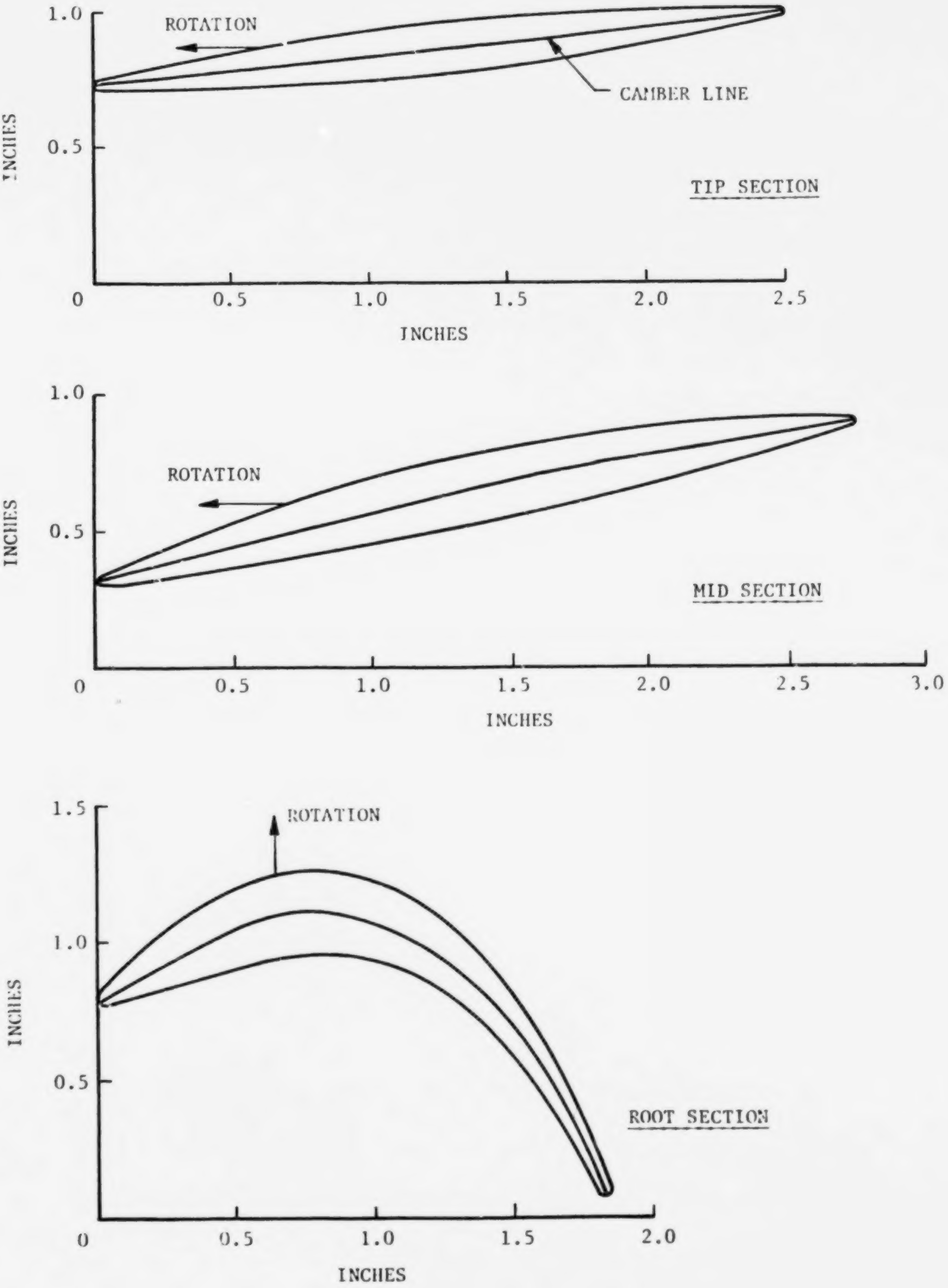
1.0
ROTATION
CAMBER LINE
0.5
INCHES
TIP SECTION
0
0.5
1.0
1.5
2.0
2.5
INCHES
1.0
ROTATION
0.5
INCHES
MID SECTION
0
0.5
1.0
1.5
2.0
2.5
3.0
INCHES
1.5
ROTATION
1.0
INCHES
0.5
ROOT SECTION
0
0.5
1.0
1.5
2.0
INCHES

Fig. 10 Drive Turbine Blade Sections

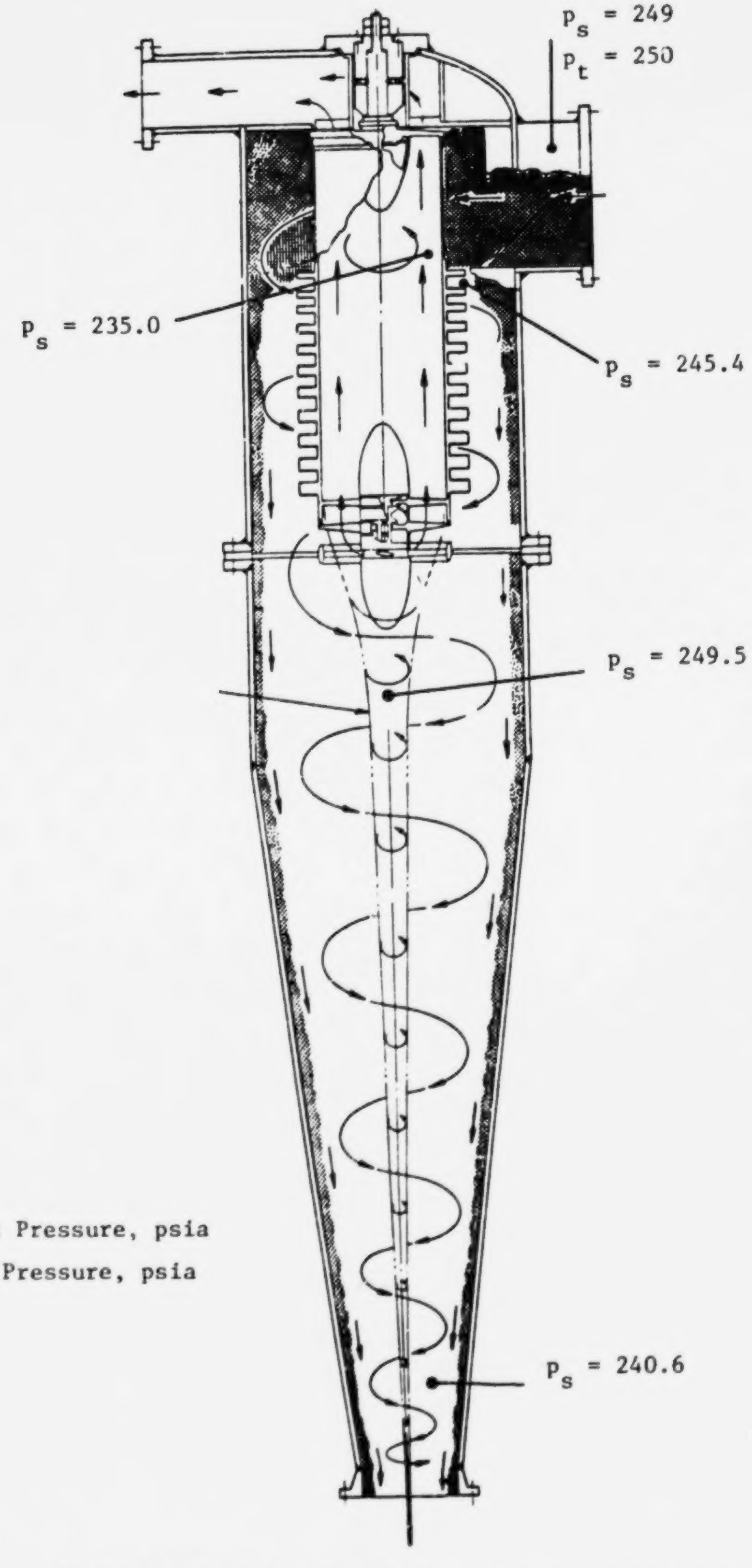
$p_s$ = 249
$p_t$ = 250
$p_s$ = 235.0
$p_s$ = 245.4
$p_s$ = 249.5
$p_s$ = 240.6

$p_s$ = Static Pressure, psia
$p_t$ = Total Pressure, psia

Fig. 11 Static Pressure at Selected Points in Cyclocentrifuge

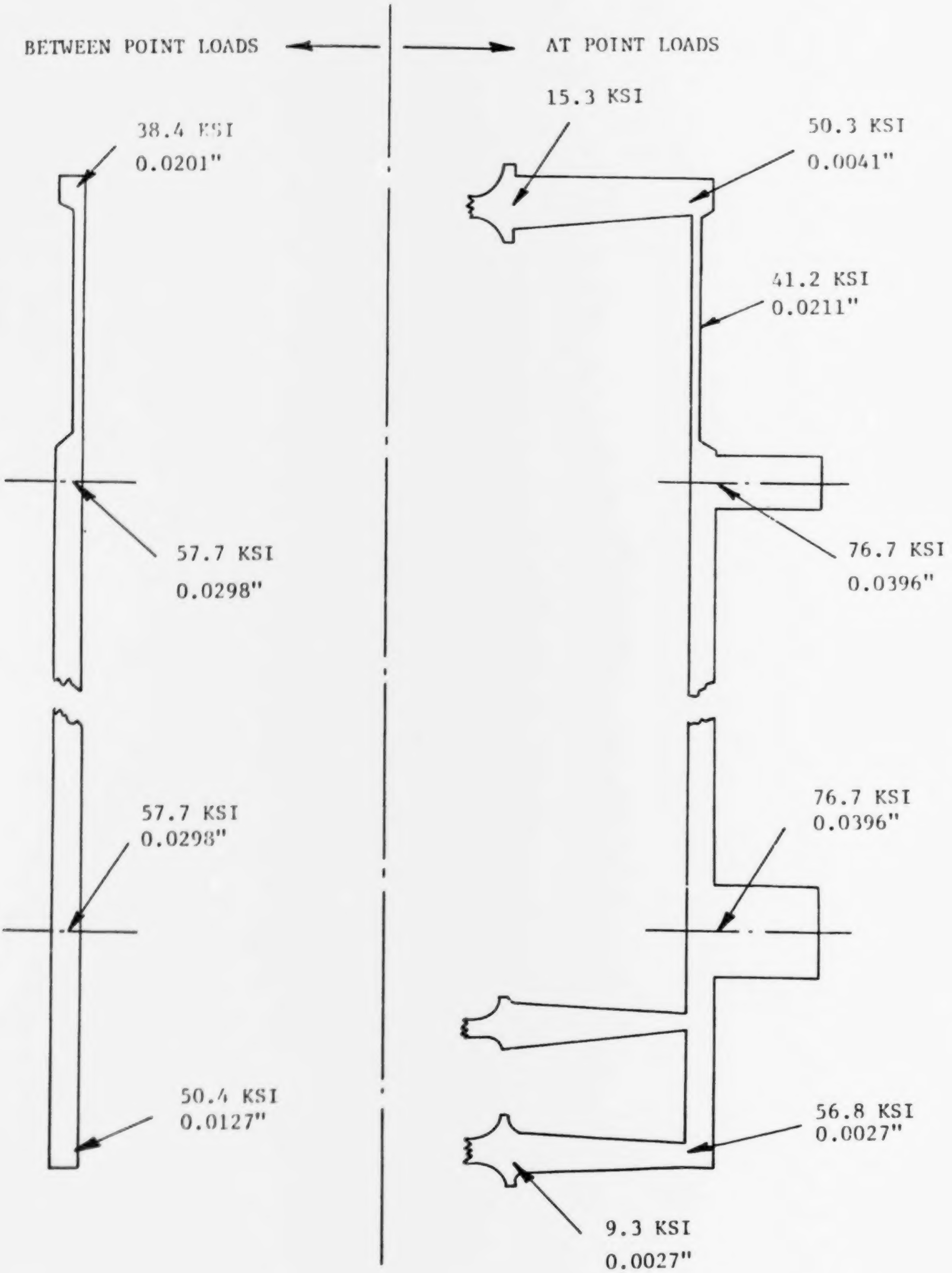
BETWEEN POINT LOADS
AT POINT LOADS
15.3 KSI
38.4 KSI
0.0201"
50.3 KSI
0.0041"
41.2 KSI
0.0211"
57.7 KSI
0.0298"
76.7 KSI
0.0396"
57.7 KSI
0.0298"
76.7 KSI
0.0396"
50.4 KSI
0.0127"
56.8 KSI
0.0027"
9.3 KSI
0.0027"

Fig. 12 Maximum Stress and Deflection at Selected Points in Centrifuge

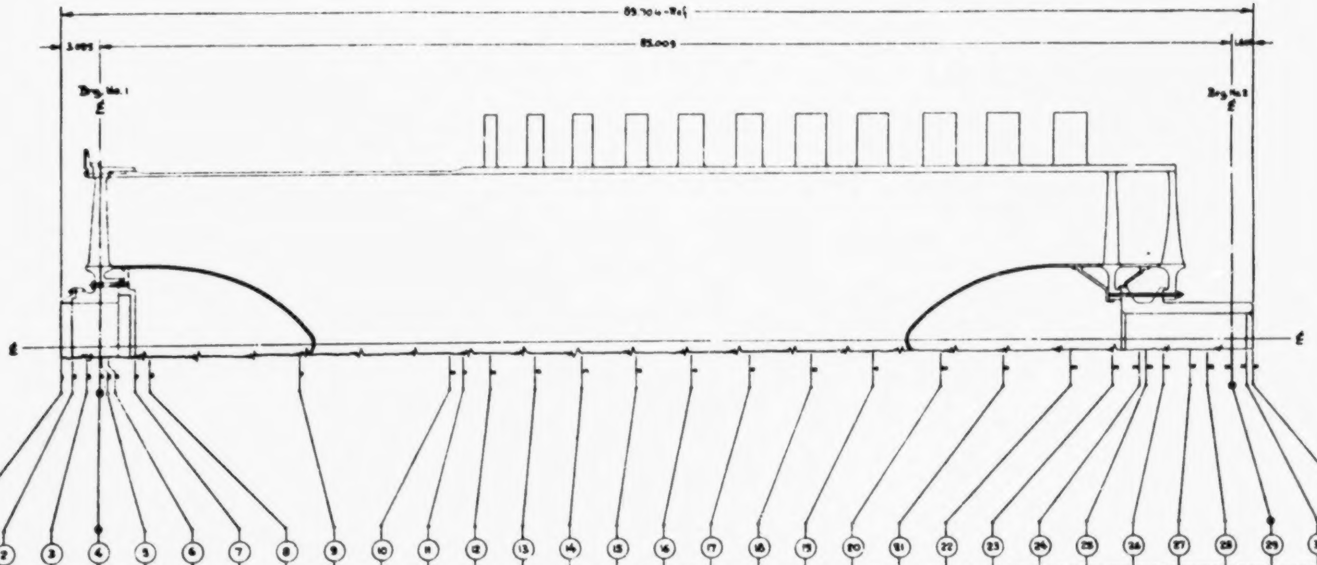

MTI
0242 - 46072 - 301

Mathematical Model of the
Cyclocentrifuge Rotor Assembly

No Scale

Feb. 15, 1977

| 1 | 2 | 3 | 4 | 5 | 6 | 7 | 8 | 9 | 10 | 11 | 12 | 13 | 14 | 15 | 16 | 17 | 18 | 19 | 20 | 21 | 22 | 23 | 24 | 25 | 26 | 27 | 28 | 29 | 30 | 31 | |
|---|---|---|---|---|---|---|---|---|---|---|---|---|---|---|---|---|---|---|---|---|---|---|---|---|---|---|---|---|---|---|---|
| — | — | — | 102.2 | 53.3 | — | — | — | — | — | — | 3.73 | 3.73 | 3.73 | 3.73 | 3.73 | 3.73 | 3.73 | 3.73 | 3.73 | 3.73 | 3.73 | 24.30 | 113.78 | — | 35.96 | — | — | — | 0.73 | — | Concentrated W – lbs. |
| — | — | — | 3114.3 | 8184.0 | — | — | — | — | — | — | 854.2 | 854.2 | 854.2 | 854.2 | 854.2 | 854.2 | 854.2 | 854.2 | 854.2 | 854.2 | 854.2 | 2922.0 | 7839.0 | — | 977.0 | — | — | — | 0.60 | — | Concentrated $I_p$ – lbs in$^2$ |
| — | — | — | 2953.1 | 4098.0 | — | — | — | — | — | — | 427.3 | 427.5 | 427.7 | 427.9 | 428.2 | 428.4 | 428.6 | 428.8 | 428.9 | 429.0 | 429.0 | 1463.0 | 4351.0 | — | 494.3 | — | — | — | 0.30 | — | Concentrated $I_T$ – lbs in$^2$ |
| 0.928 | 1.030 | 1.080 | 0.000 | 0.733 | 2.000 | 1.000 | 10.499 | 10.499 | 1.000 | 2.442 | 3.407 | 3.678 | 3.931 | 4.161 | 4.365 | 4.540 | 4.683 | 4.792 | 4.866 | 4.903 | 4.375 | 2.250 | 0.800 | 1.250 | 2.000 | 1.250 | 1.876 | 1.100 | 0.900 | — | Distance between Stations – in. |
| 5.040 | 6.000 | 6.000 | 1.128 | 26.000 | 26.000 | 25.740 | 25.559 | 25.559 | 25.740 | 26.000 | 26.000 | 26.000 | 26.000 | 26.000 | 26.000 | 26.000 | 26.000 | 26.000 | 26.000 | 26.000 | 26.000 | 26.000 | 4.786 | 5.000 | 5.000 | 5.000 | 5.000 | 5.000 | 5.000 | — | O.D. for Stiffness – in. |
| 8.040 | 7.000 | 6.000 | — | 26.306 | 26.280 | 25.740 | 25.559 | 25.559 | 25.740 | 26.000 | 26.000 | 26.000 | 26.000 | 26.000 | 26.000 | 26.000 | 26.000 | 26.000 | 26.000 | 26.000 | 26.000 | 26.000 | 3.000 | 5.000 | 5.000 | 5.000 | 5.000 | 8.000 | 5.000 | — | O.D. for Weight – in. |
| 5.000 | 5.000 | 5.000 | — | 25.262 | 25.262 | 25.262 | 25.262 | 25.262 | 25.262 | 25.262 | 25.262 | 25.262 | 25.262 | 25.262 | 25.262 | 25.262 | 25.262 | 25.262 | 25.262 | 25.262 | 25.262 | 25.262 | 3.000 | 3.000 | 3.000 | 3.000 | 3.000 | 3.000 | 2.500 | — | I.D. for both Stiffness and Weight – in. |
| 1 | 1 | 1 | 2 | 1 | 1 | 1 | 1 | 1 | 1 | 1 | 1 | 1 | 1 | 1 | 1 | 1 | 1 | 1 | 1 | 1 | 1 | 1 | 3 | 1 | 1 | 1 | 1 | 1 | 1 | 1 | Material No. (Ref. to Computer Input) |
| 1000 | | | | | | | | | | | | | | | | | | | | | | | | | | | | | | | Temperature of the Shaft – °F |
| Inconel 718 | | | | | | | | | | | | | | | | | | | | | | | | | | | | | | | Material of the Shaft |
| 24.8 | | | | | | | | | | | | | | | | | | | | | | | | | | | | | | | E – $(10)^6$ psi |
| 0.296 | | | | | | | | | | | | | | | | | | | | | | | | | | | | | | | $\rho$ – lbs/in$^3$ |
| 7.28 | | | 0.384 | 7.28 | | | | | | | | | | | | | | | | | | | 2.29 | 7.28 | | | | | | | $G \times \alpha$ – $(10)^6$ psi |

Fig. 13 Rotor Dynamic Model

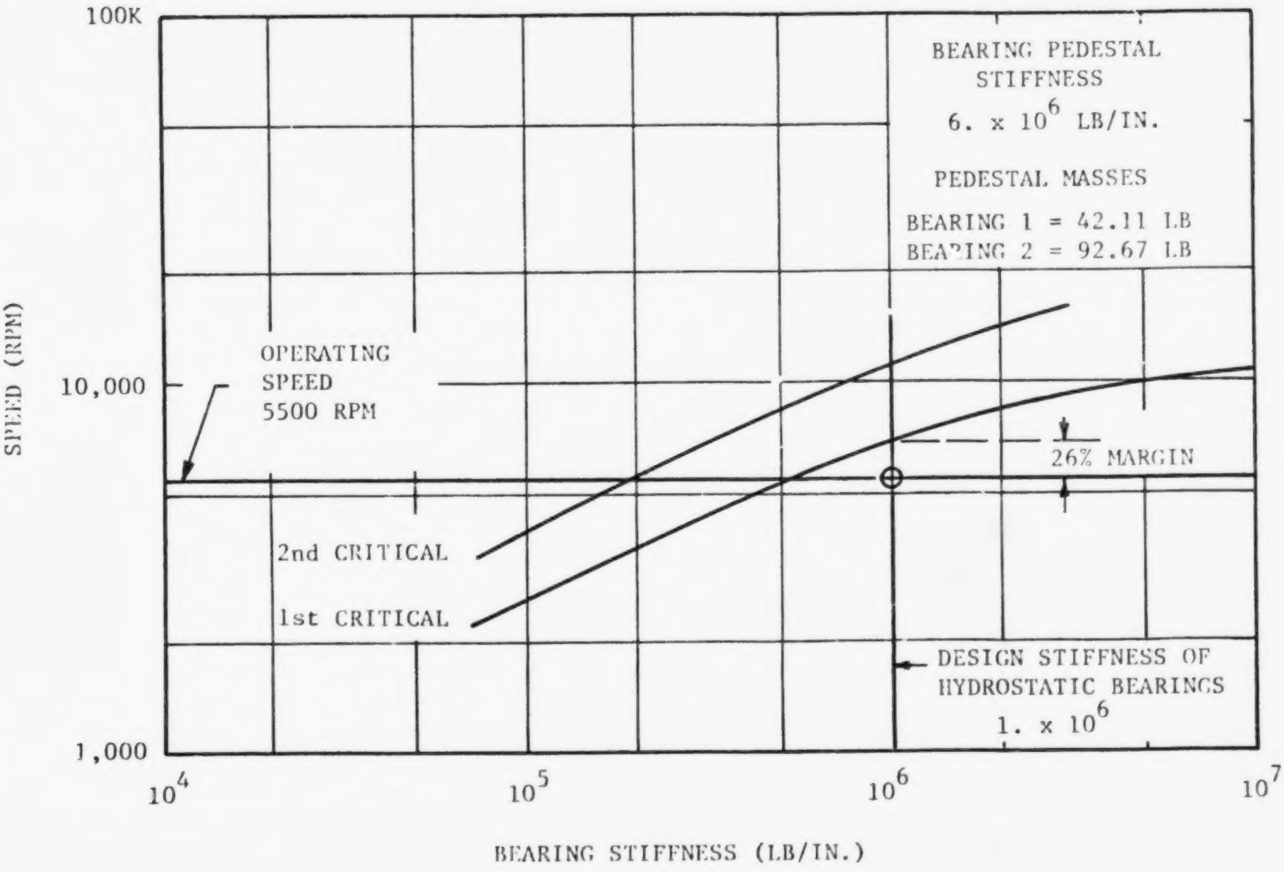

Fig. 14 Undamped Lateral Critical Speed Map for Cyclocentrifuge Rotor

```
CRITICAL SPEED         FREQUENCY          FREQ.RATIO
     6936.1 RPM        115.601 CPS
STATION  LENGTH     AMPLITUDE
   1       0.000     .58238E+00
   2        .925     .59125E+00
   3       2.015     .60170E+00
   4       3.095     .61198E+00
   5       3.105     .61207E+00
   6       3.838     .61918E+00
   7       5.838     .64101E+00
   8       6.938     .65068E+00
   9      17.337     .78701E+00
  10      27.936     .89679E+00
  11      28.936     .90222E+00
  12      31.274     .91769E+00
  13      34.685     .93725E+00
  14      38.363     .95559E+00
  15      42.294     .97185E+00


  16      46.455     .98515E+00
  17      50.820     .99469E+00
  18      55.360     .99980E+00
  19      60.043     .10000E+01
  20      64.835     .99505E+00
  21      69.701     .98504E+00
  22      74.604     .97030E+00
  23      78.979     .95368E+00
  24      81.229     .94373E+00
  25      81.729     .94147E+00
  26      82.979     .92105E+00
  27      84.979     .87191E+00
  28      86.229     .83443E+00
  29      89.104     .77331E+00
  30      89.204     .74471E+00
  31      89.704     .73169E+00

RELATIVE NORMALIZED PEDESTAL DEFLECTION

     STA  AMPLITUDE
      4    .8815E-01
     27    .1125E+00
```

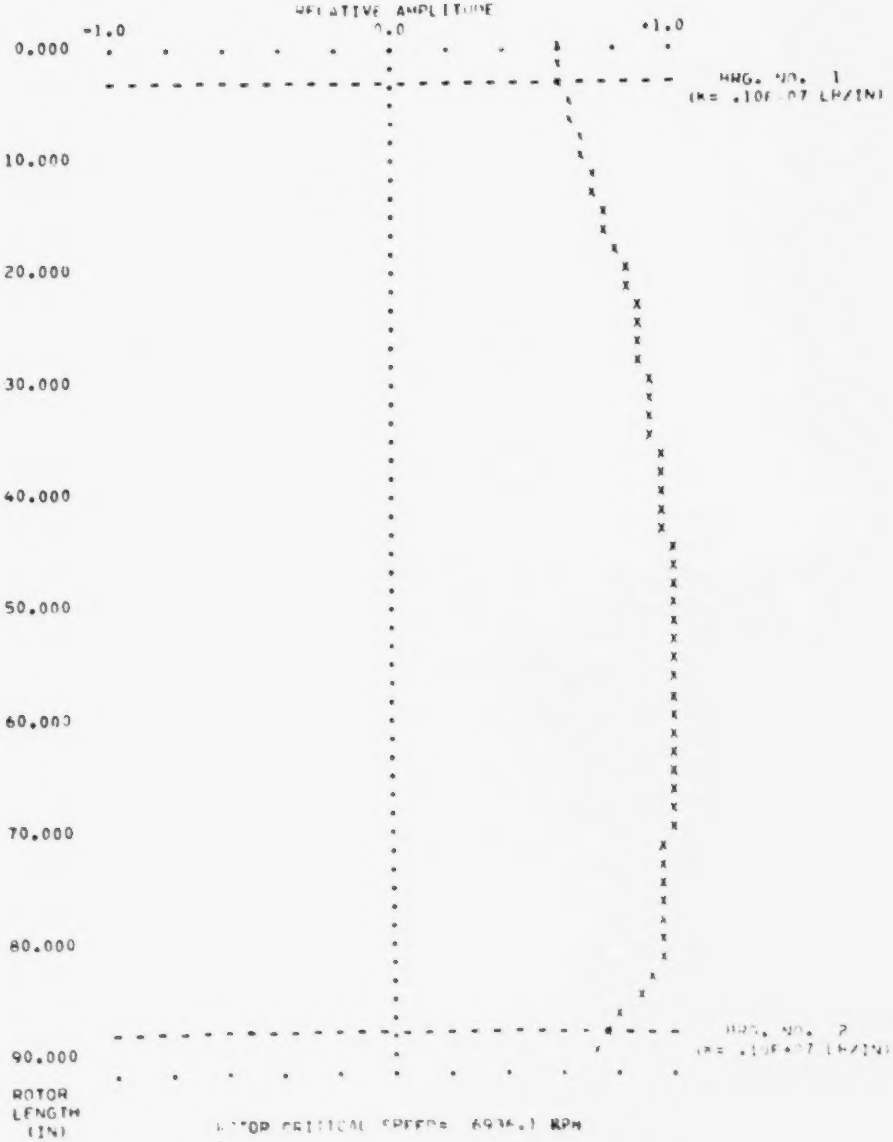

Fig. 15 Mode Shape for First Critical Speed

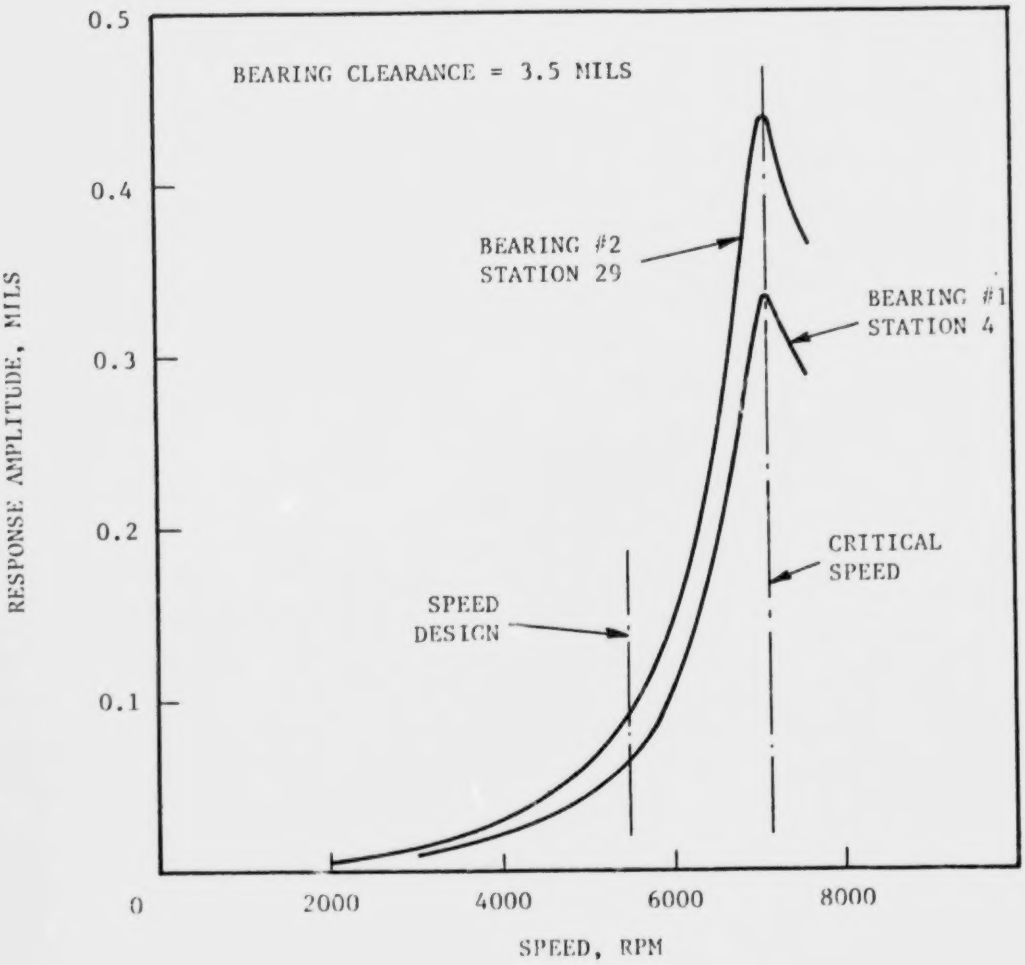

Fig. 16 Response Amplitude per In.-Oz of Unbalance at Station 18

```
1   CYCLOCENTRIFUGE - CONFIGURATION D - SINGLE LEVEL ROTOR - STABILITY
```

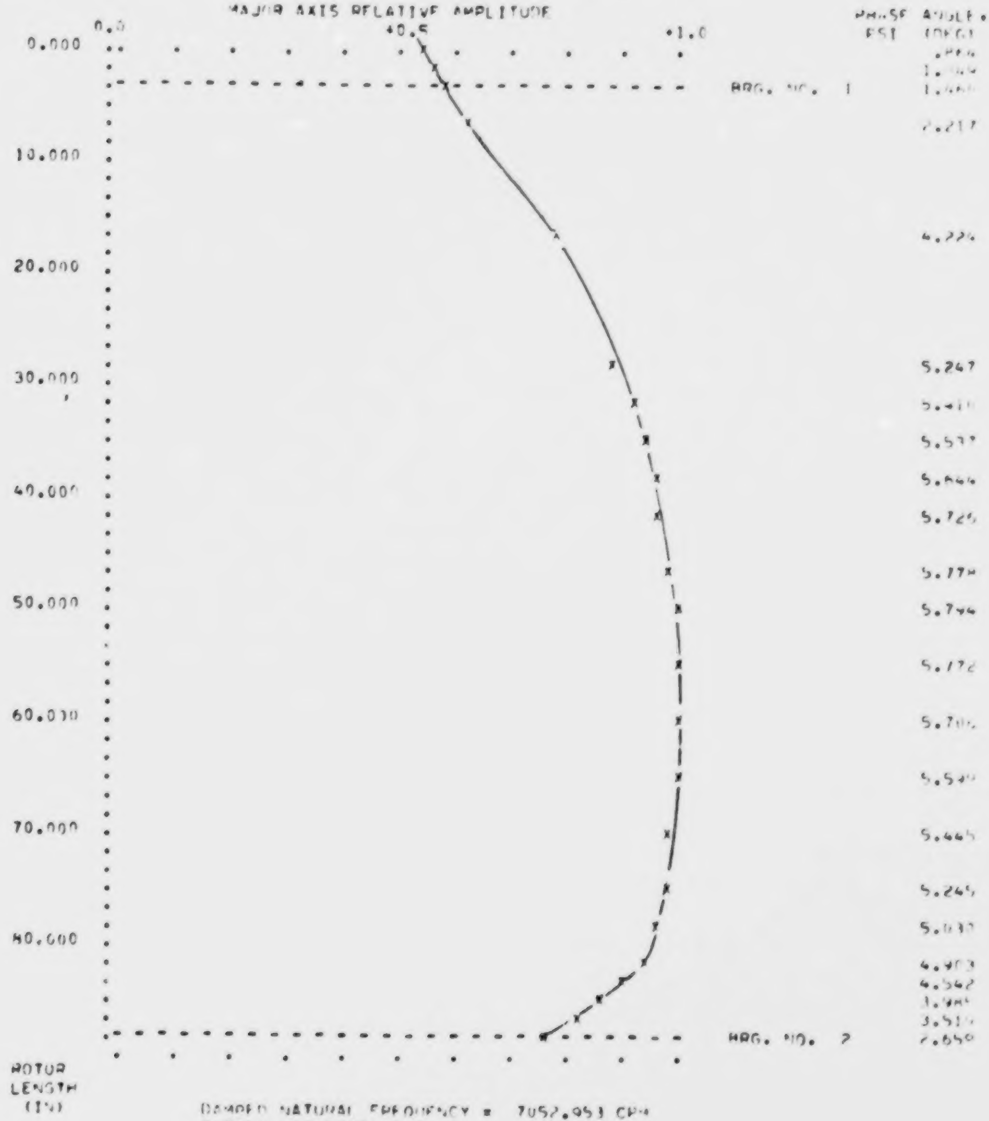

```
                 DAMPED NATURAL FREQUENCY =  7052.953 CPM
                 SYSTEM LOG DECREMENT =        .4415


IF X REPRESENTS THE ROTOR AMPLITUDE, A FREE VIBRATION MAY BE EXPRESSED AS -
         X   = ABS(X) * E**(LAMBDA*T) * COS(OMEG *T + PSI )
      ABS(X) = THE INITIAL AMPLITUDE
        T    = TIME (SECONDS)
       PSI   = PHASE ANGLE
      LAMBDA = DAMPING EXPONENT  (1/SEC)   = -51.9 (1/sec)
       OMEG  = DAMPED NATURAL FREQUENCY (RADIANS/SEC)
```

Fig. 17 Mode Shape and Stability for First Natural Frequency

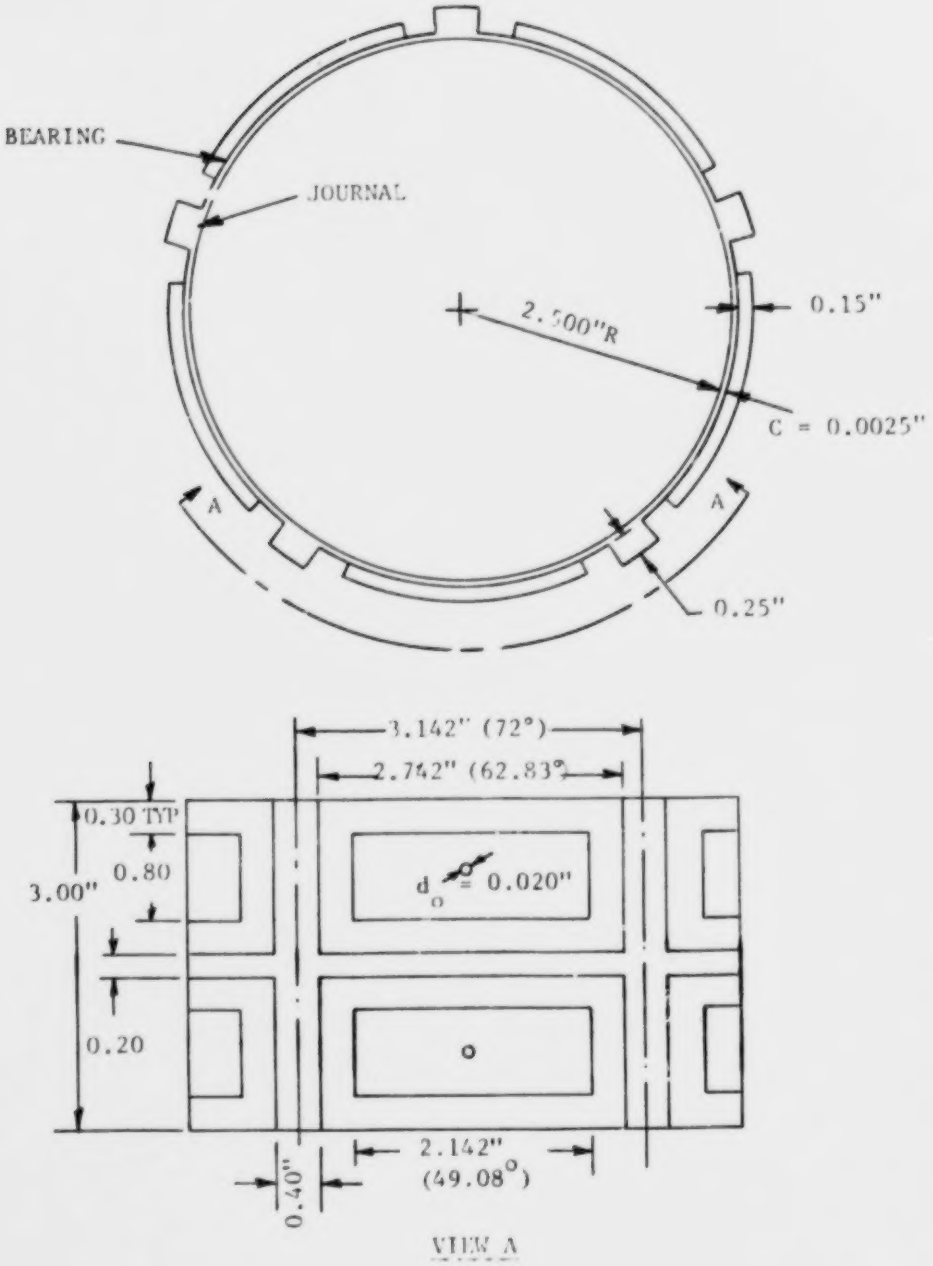
BEARING
JOURNAL
0.15"
2.500"R
C = 0.0025"
A
A
0.25"
3.142" (72°)
2.742" (62.83°)
0.30 TYP
0.80
3.00"
0.20
d_o = 0.020"
2.142" (49.08°)
0.40"
VIEW A

Fig. 18 Journal Bearing Geometry

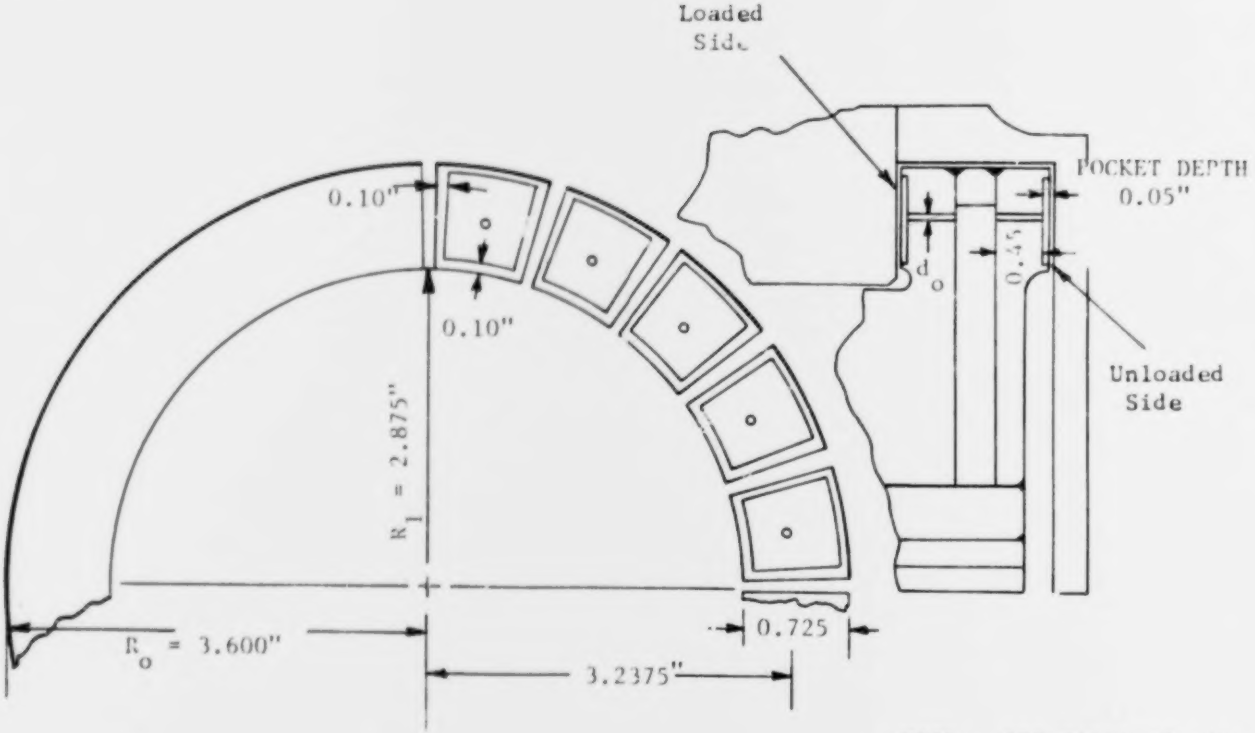
Loaded Side
POCKET DEPTH 0.05"
0.10"
0.10"
$d_o$
0.45
Unloaded Side
$R_I$ = 2.875"
$R_o$ = 3.600"
0.725
3.2375"

NOTE: SEE TABLE 10 FOR OTHER DESIGN PARAMETERS

Fig. 19 Thrust Bearing Geometry

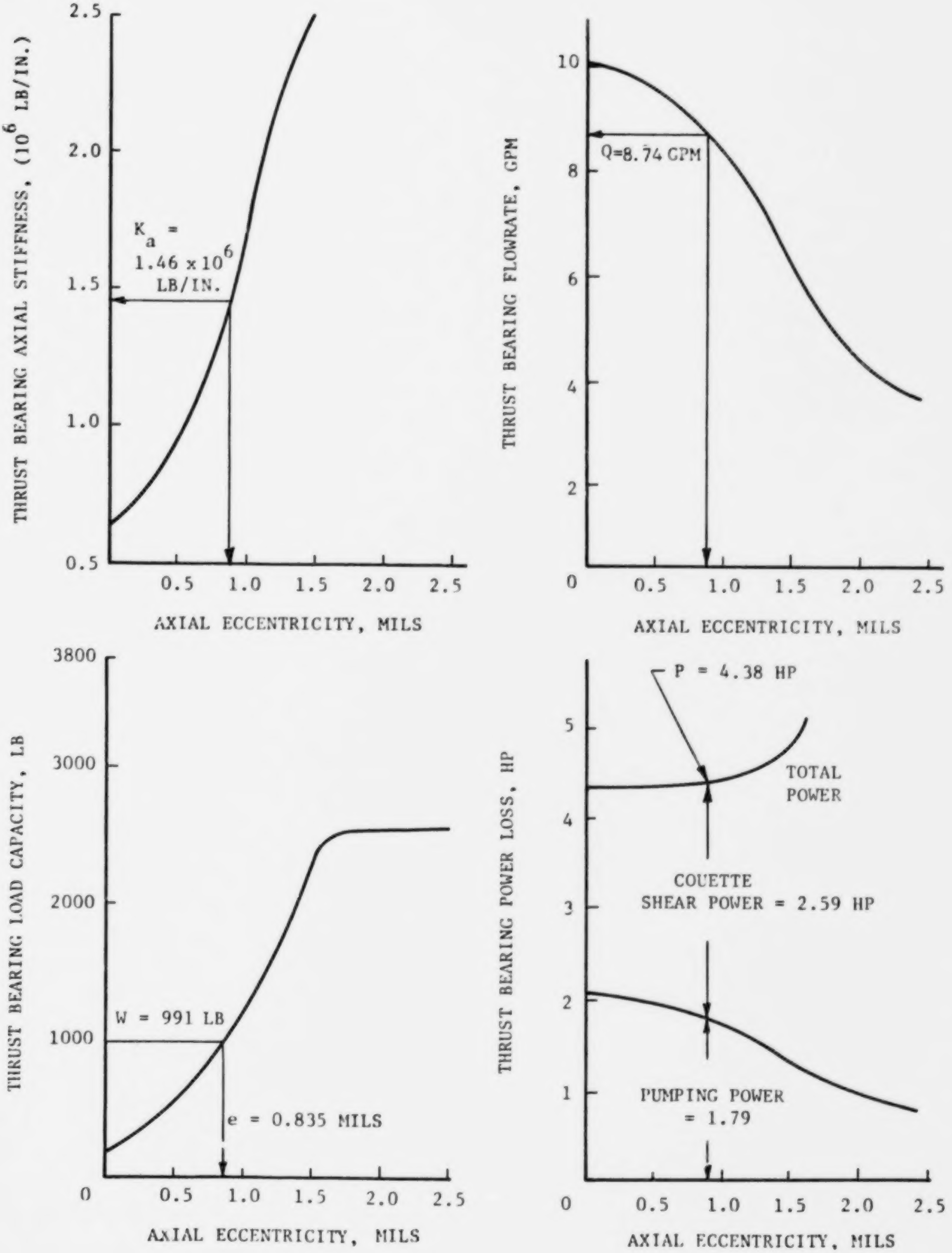

Fig. 20 Thrust Bearing Performance Characteristics

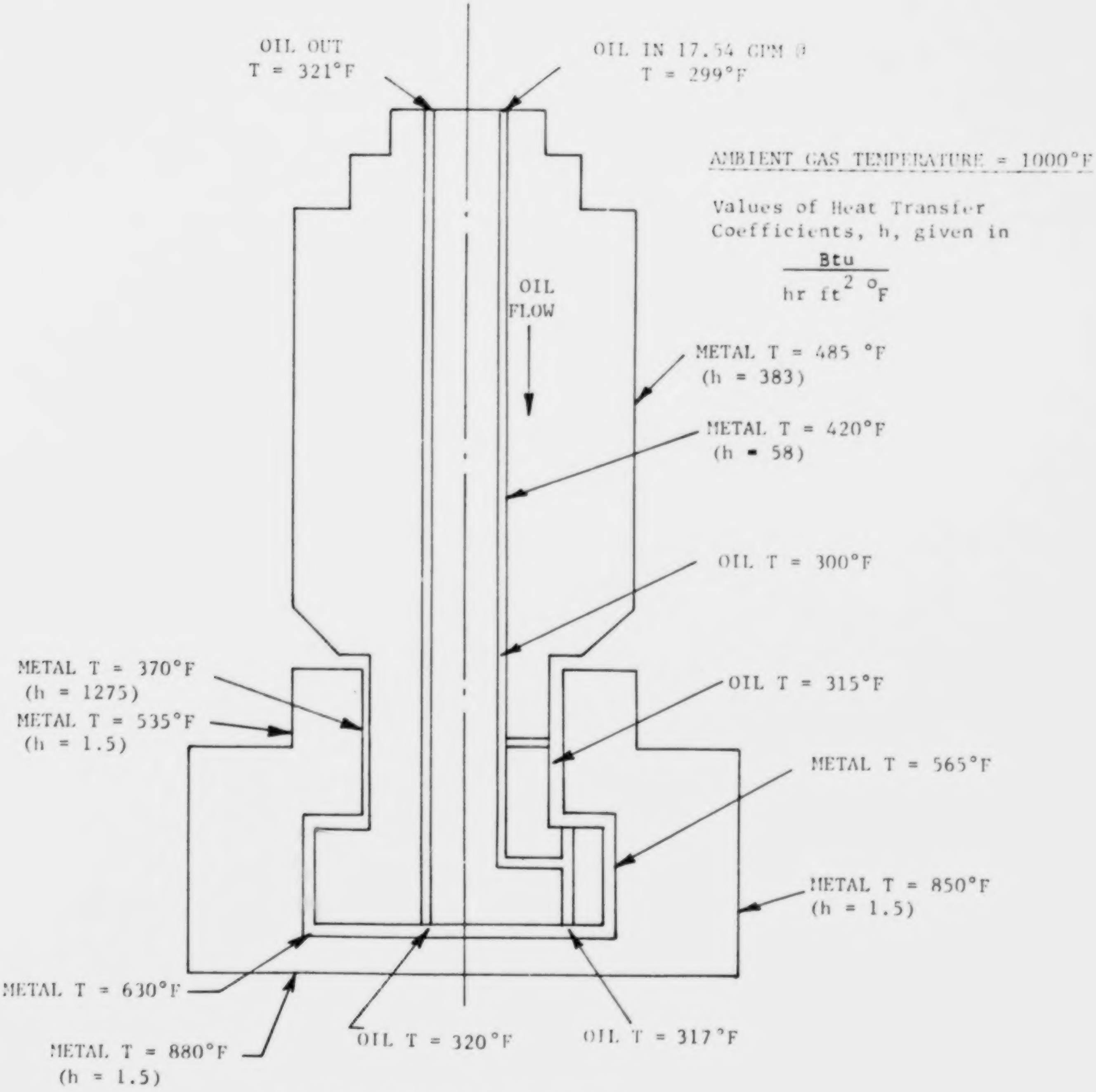
OIL OUT
T = 321°F
OIL IN 17.54 GPM @
T = 299°F
OIL
FLOW
METAL T = 485 °F
(h = 383)
METAL T = 420°F
(h = 58)
OIL T = 300°F
METAL T = 370°F
(h = 1275)
METAL T = 535°F
(h = 1.5)
OIL T = 315°F
METAL T = 565°F
METAL T = 850°F
(h = 1.5)
METAL T = 630°F
METAL T = 880°F
(h = 1.5)
OIL T = 320°F
OIL T = 317°F

AMBIENT GAS TEMPERATURE = 1000°F

Values of Heat Transfer Coefficients, h, given in $\frac{\text{Btu}}{\text{hr ft}^2\ {}^{\circ}\text{F}}$

Q (GAS → OIL) = 48,000 BTU/HR
Q J. BEARING = 10,700 BTU/HR
Q THR. BEARING = 11,200 BTU/HR

Fig. 21 Temperature Distribution at Upper Bearing

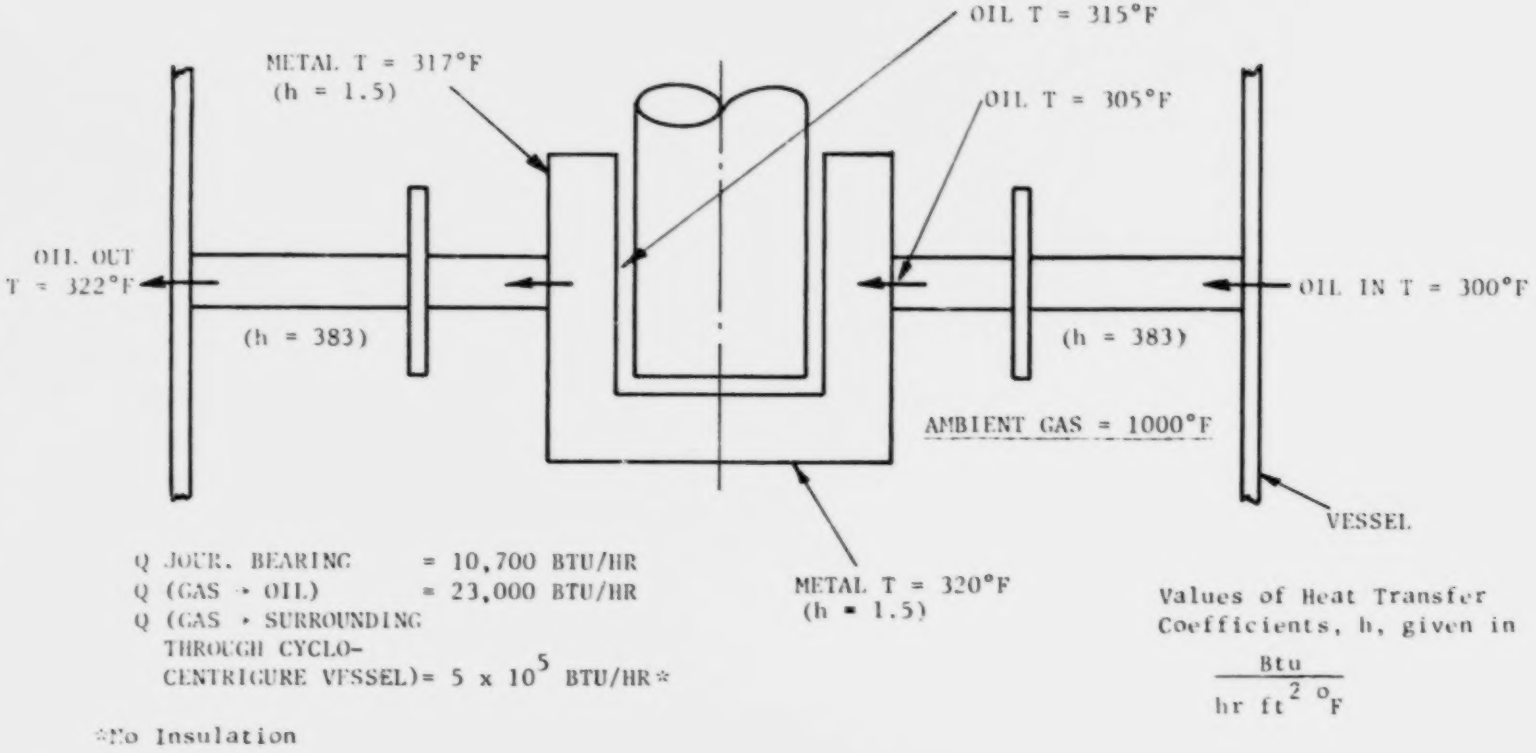
METAL T = 317°F
(h = 1.5)
OIL T = 315°F
OIL T = 305°F
OIL OUT
T = 322°F
(h = 383)
(h = 383)
OIL IN T = 300°F
AMBIENT GAS = 1000°F
VESSEL
METAL T = 320°F
(h = 1.5)
Q JOUR. BEARING = 10,700 BTU/HR
Q (GAS → OIL) = 23,000 BTU/HR
Q (GAS → SURROUNDING THROUGH CYCLO-CENTRIGURE VESSEL)= 5 x 10^5 BTU/HR*
*No Insulation
Values of Heat Transfer Coefficients, h, given in Btu / hr ft^2 °F

Fig. 22 Temperature Distribution at Lower Bearing

# FINE PARTICLE COLLECTION EFFICIENCY IN THE A.P.T. DRY SCRUBBER

By:

S. Calvert, R. G. Patterson
Air Pollution Technology, Inc.
San Diego, CA 92117

D. C. Drehmel
Environmental Protection Agency
Industrial Environmental Research Laboratory-RTP
Research Triangle Park, NC 27711

# FINE PARTICLE COLLECTION EFFICIENCY
# IN THE A.P.T. DRY SCRUBBER

By

Dr. Seymour Calvert
Dr. Ronald G. Patterson

Air Pollution Technology, Inc.
4901 Morena Blvd., Suite 402
San Diego, California 92117

and

Dr. Dennis C. Drehmel
Particulate Technology Branch
Utilities and Industrial Power Division
Industrial Environmental Research Laboratory
U.S. Environmental Protection Agency
Research Triangle Park, NC 27711

The Particle-by-Particle (PxP) scrubber is a device which can be used at high temperature and pressure for the collection of fine particles on larger particles, which can be cleaned and recycled. Particle collection is mainly by inertial impaction and to some extent by diffusion for smaller particles. Experimental data on particle collection are in agreement with a mathematical model.

# FINE PARTICLE COLLECTION EFFICIENCY
# IN THE A.P.T. DRY SCRUBBER

The development of advanced energy sources such as coal and shale oil gasification results in high temperature and pressure (HTP) process gas streams which require removal of particulates before utilization. For example, the ultimate use of such a process gas could be combustion and expansion in a gas turbine for generation of electric power. Turbo-machine experience indicates that potential erosion and/or corrosion of machine components are due in part to the particles in the gas stream.

Fine particle removal from gases at the high temperatures and pressures encountered in fluidized bed combustors and various fuel conversion processes places severe requirements on the gas cleaning system. The environment of reactive gas mixtures of temperatures up to 1,100°C and pressures up to 15 atmospheres can be withstood by only a few structural materials. Particle collection efficiency must be high; perhaps 90% for 1.0 μm diameter particles and 99.5% overall.

The elevated temperature and pressure conditions suggest that new devices for removal of fine particles may be necessary. Typical particle collectors used in fossil-fuel-fired power plants (electrostatic precipitators, scrubbers, fabric filters) generally operate at temperatures below 260°C and at low pressures. The suitability of these components at elevated temperatures and pressures may be limited. The A.P.T. dry scrubbing system, which we call the "PxP" system (for "particle collection by particles"), is compatible with the special demands of HTP gas cleaning.

## PxP SYSTEM

The PxP system for fine particle control utilizes relatively large particles as collection centers for the fine particles in the gas stream. The relatively large particles (collector particles) introduced to the gas stream can collect fine particles by mechanisms such as diffusion, inertial impaction, interception and electrophoresis. The larger size of the collector particles allows easy separation from the gas stream by methods such as cyclones, and gravitational settling.

Figure 1 is a functional diagram of the process steps for a representative PxP system. The functional phenomena represented on this diagram could occur concurrently or separately in several types of equipment.

The first step involves introducing the collectors to the gas stream. This process can involve pneumatic or mechanical injection into the gas stream. The second stage involves contacting the collectors with the gas in order to encourage the movement of the fine particles to the collectors. A venturi device can be used for the contactor which would be analogous to a venturi scrubber except that solid collectors are used instead of liquid drops. Alternative contactors such as a centrifugal scrubber could be used.

The next process step is to remove the collector particles after sufficient exposure in the contactor to cause capture of the initial fine particles present in the gas. At this stage the large size and mass of the collector particles is utilized to separate them from the gas. A cyclone separator could be used for this step. Two streams are shown leaving the separator: the cleaned gas leaves the process at this point and the second stream represents the flow of collector particles to the next step. The final process involves either discarding the collector particles or cleaning them for recycle and disposing of the material collected from the gas stream.

## Performance Prediction

The particle collection efficiency and pressure drop for an A.P.T. dry scrubber with cocurrent flow can be predicted with the same relationships that define cocurrent wet scrubber performance. The theoretical performance of the PxP scrubber has been determined based on the venturi scrubber model of Yung et al. (1977). For particle collection in the venturi throat, the penetration for a given particle size is:

$$Pt = \exp\left[\left[\frac{B}{K_{po}\left(1-u_d^*\right) + 0.7}\right]\left[4\ K_{po}\ \left(1-u_d^*\right)^{1.5} + 4.2\left(1-u_d^*\right)^{0.5} - 5.02\ K_{po}^{0.5}\left(\left(1-u_d^*\right) + \frac{0.7}{K_{po}}\right)\tan^{-1}\left(\frac{\left(1-u_d^*\right)K_{po}}{0.7}\right)^{0.5}\right]\right.$$

$$\left. - \frac{B}{K_{po}\left(1 + \frac{0.7}{K_{po}}\right)}\left[4\ K_{po} + 4.2 - 5.02\ K_{po}^{0.5}\left(1 + \frac{0.7}{K_{po}}\right)\tan^{-1}\left(\frac{K_{po}}{0.7}\right)^{0.5}\right]\right] \qquad (1)$$

$$\text{where } K_{po} = \frac{d_{pa}^{\ 2}\ u_{Gt}}{9\ \mu_G\ d_c} \qquad (2)$$

$$u_d^* = 2\left|1 - x^2 + \left(x^4 - x^2\right)^{0.5}\right| \qquad (3)$$

$$x = \frac{3\ \ell_t\ C_{Do}\ \rho_G}{16\ d_c\ \rho_c} + 1 \qquad (4)$$

$$\text{and } B = \left(\frac{Q_c}{Q_G}\right)\left(\frac{\rho_c}{\rho_G}\right)\frac{1}{C_{Do}} \qquad (5)$$

where $d_{pa}$ = aerodynamic particle size cm
$u_{Gt}$ = gas velocity at throat, cm/s
$\mu_G$ = gas viscosity, g/cm-s (poise)
$d_c$ = collector diameter, cm
$\ell_t$ = throat length, cm
$\rho_G$ = gas density, g/cm$^3$
$\rho_c$ = collector density, g/cm$^3$
$Q_G$ = gas volumetric flow, m$^3$/s
$Q_c$ = collector volumetric flow, m$^3$/s
$C_{Do}$ = drag coefficient for drops at the venturi throat inlet, dimensionless

Particle collection efficiency was predicted for several values of parameters in a cocurrent PxP scrubber using 100 μm diameter collectors and a gas velocity of 57 m/s. Figure 2 is a plot of particle penetration against particle size with collector/gas flow rate ratio as a parameter and with a 20°C gas temperature. Figure 3 is a similar plot with an 820°C gas temperature. To show the effect of temperature on penetration, the curves for a ratio of 0.002 and temperatures of 20°C and 820°C are plotted on Figure 4.

The predicted penetration curves have the following characteristics:

1. For a given set of operating conditions, the penetration decreases with increasing size of fine particles. This is expected since the collection mechanism is inertial impaction of the fine particles upon the collectors.

2. For a given size of collector particle and aerodynamic diameter of fine particle, the penetration decreases with increasing value of $(Q_c \rho_c / Q_G)$.

3. A similar dependence upon the gas velocity is apparent from equation (1).

4. For the 100 μm collectors and a given fine particle aerodynamic diameter, the penetration increases with increasing gas temperature. This is the result of an increase in gas viscosity with temperature which reduces the effective inertia of the fine particles.

It can also be shown that collector particle diameter affects collection efficiency when other factors are held constant. The cut diameter (i.e., the diameter of the particle which is collected at 50% efficiency) decreases as collector diameter decreases. Collection efficiency for particles larger than several microns diameter varies in a more complex way, depending on flow and geometric parameter combinations.

## Experimental Program

Experimental work has been done by A.P.T. to determine fine particle collection efficiency in a PxP scrubber in order to confirm the predictions obtained from available mathematical models. A dibutylphthalate (DBP) aerosol was used in collection efficiency experiments with 125 μm mean diameter nickel beads and with 100 μm mean diameter sand as collector particles. The DBP aerosol had a mass median aerodynamic diameter of

1.3 μmA and standard deviation, $\sigma_g = 2.0$

The collectors entered the T-shaped contactor through the branch leg and were entrained by air entering through one of the "run" legs. The length of the 1.1-cm diameter throat varied from 2.5 to 5.1 cm. The throat velocity was 57 m/s and $(Q_c \rho_c/Q_G)$ was around 0.005 g/cm$^3$ for the nickel beads and 0.0017 g/cm$^3$ for the sand.

The gravity separator used in these experiments is shown in Figures 5 and 6. The system gas flowed either horizontally or vertically downward flow into the separator. Cleaned gas flowed out of the branch of the separator Tee.

Test aerosol particle cumulative concentration was measured for each of several diameter increments by means of a Climet light scattering particle analyzer for the experiments with nickel collectors. Cascade impactors were used with the sand collectors. Inlet and outlet cumulative mass distributions were plotted and the particle collection efficiency was computed from the ratio of the curve slopes at several particle diameters.

The resulting penetration data are shown in Figure 7 for DBP collection on sand. The cascade impactor data led to the penetration relationship labeled "experimental curve." The prediction for $(Q_c \rho_c/Q_G) = 0.002$ is also shown in Figure 7 and compares well with the experimental curve.

Particle penetration data for all runs with nickel and sand collectors are represented in Figure 8, a "cut power plot." The cut diameter is plotted against gas pressure drop in Figure 8. The line represents the relationship which is predicted and which has been confirmed by a number of field tests on large wet scrubbers. Agreement between the data points and the line is good.

## CONCLUSIONS

The experimental data on the primary collection efficiency of the PxP system agree well with predictions based on a mathematical model which was first developed for wet scrubbers. Since the model was derived for the mechanism of particle collection by inertial impaction on spheres in a cocurrent scrubber, it is reasonable to expect it to fit the data. The PxP A.P.T. dry scrubber system has the same primary collection efficiency/

power relationship as a venturi type wet scrubber.

The overall efficiency of the PxP system will depend on the re-entrainment characteristics of the specific system in addition to the primary efficiency. Particle and collector properties, system geometry, flow rates, and other parameters will influence re-entrainment.

Research is continuing on the experimental evaluation of the PxP system for HTP application. The work upon which this paper is based is supported by the U.S. Environmental Protection Agency.

## REFERENCE

Yung, S.C., S. Calvert, and H.F. Barbarika, "Venturi Scrubber Performance Model", EPA-600/2-77-172, NTIS PB 271515/AS, August 1977.

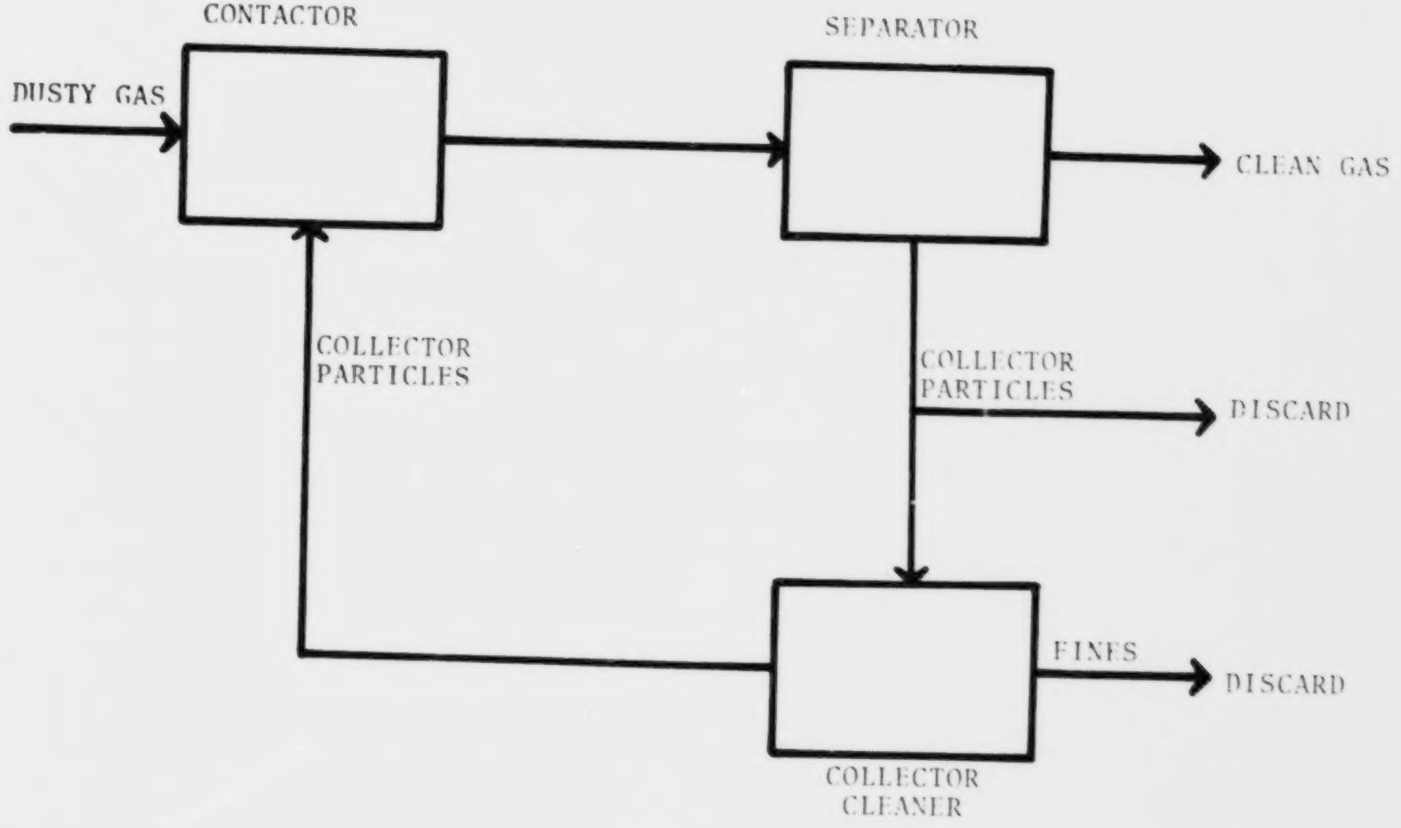
CONTACTOR
SEPARATOR
DUSTY GAS
CLEAN GAS
COLLECTOR PARTICLES
COLLECTOR PARTICLES
DISCARD
FINES
DISCARD
COLLECTOR CLEANER

Figure 1. Schematic diagram of A.P.T. dry scrubber system.

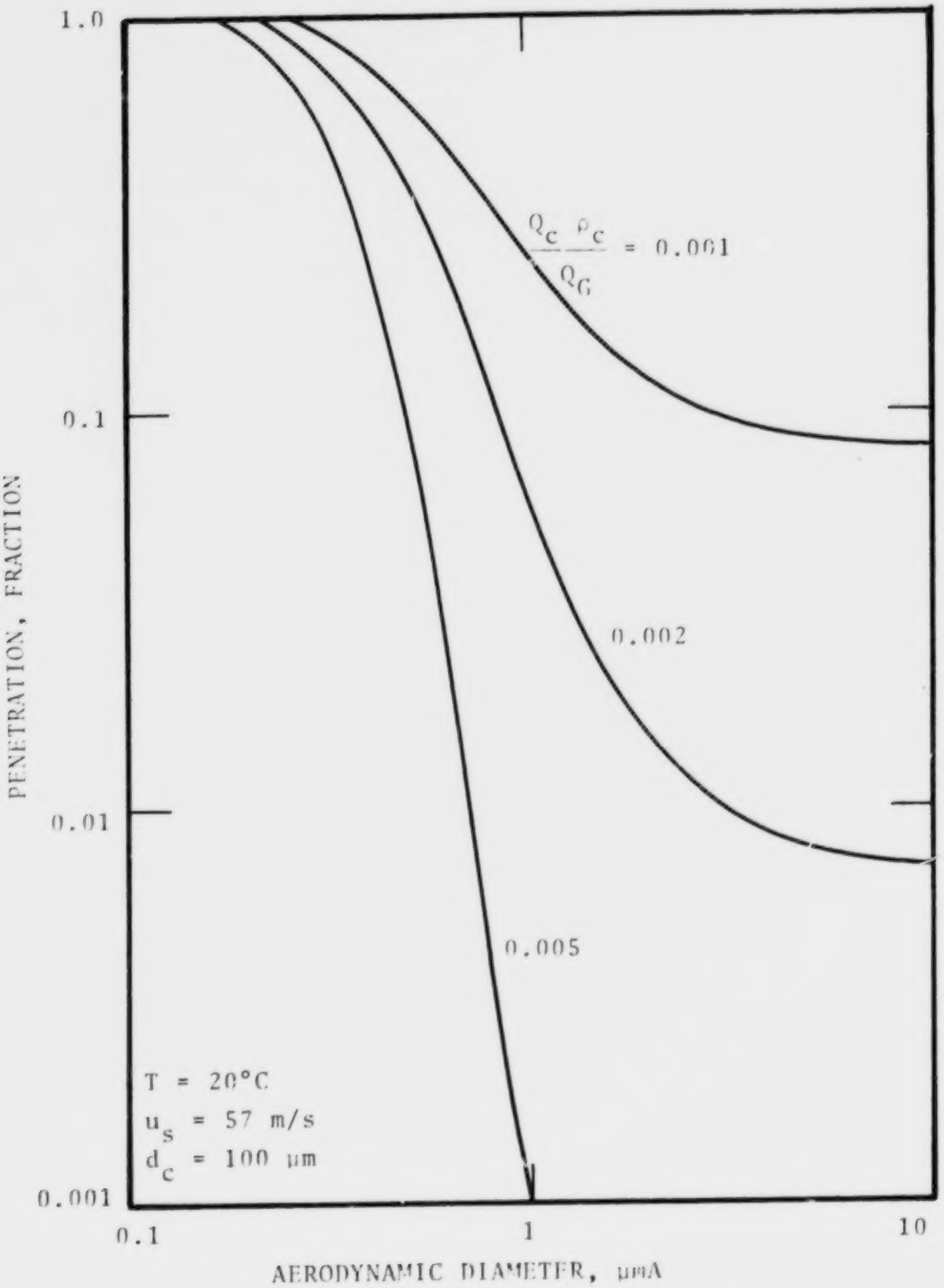

Figure 2. Theoretical particle collection characteristics of the A.P.T. dry scrubber.

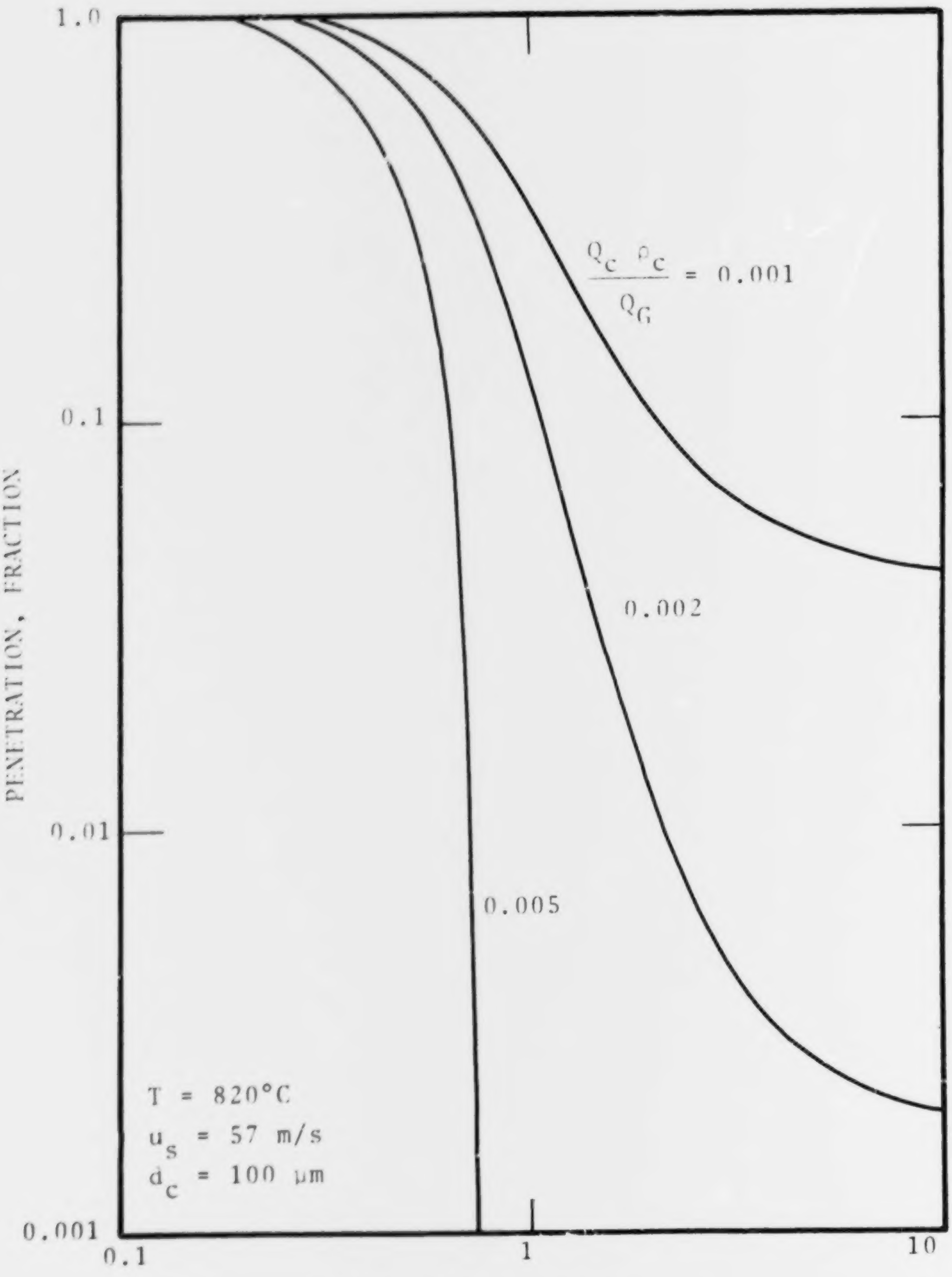

Figure 3. Comparison of the particle collection characteristics of the A.P.T. dry scrubber at 20°C and 820°C.

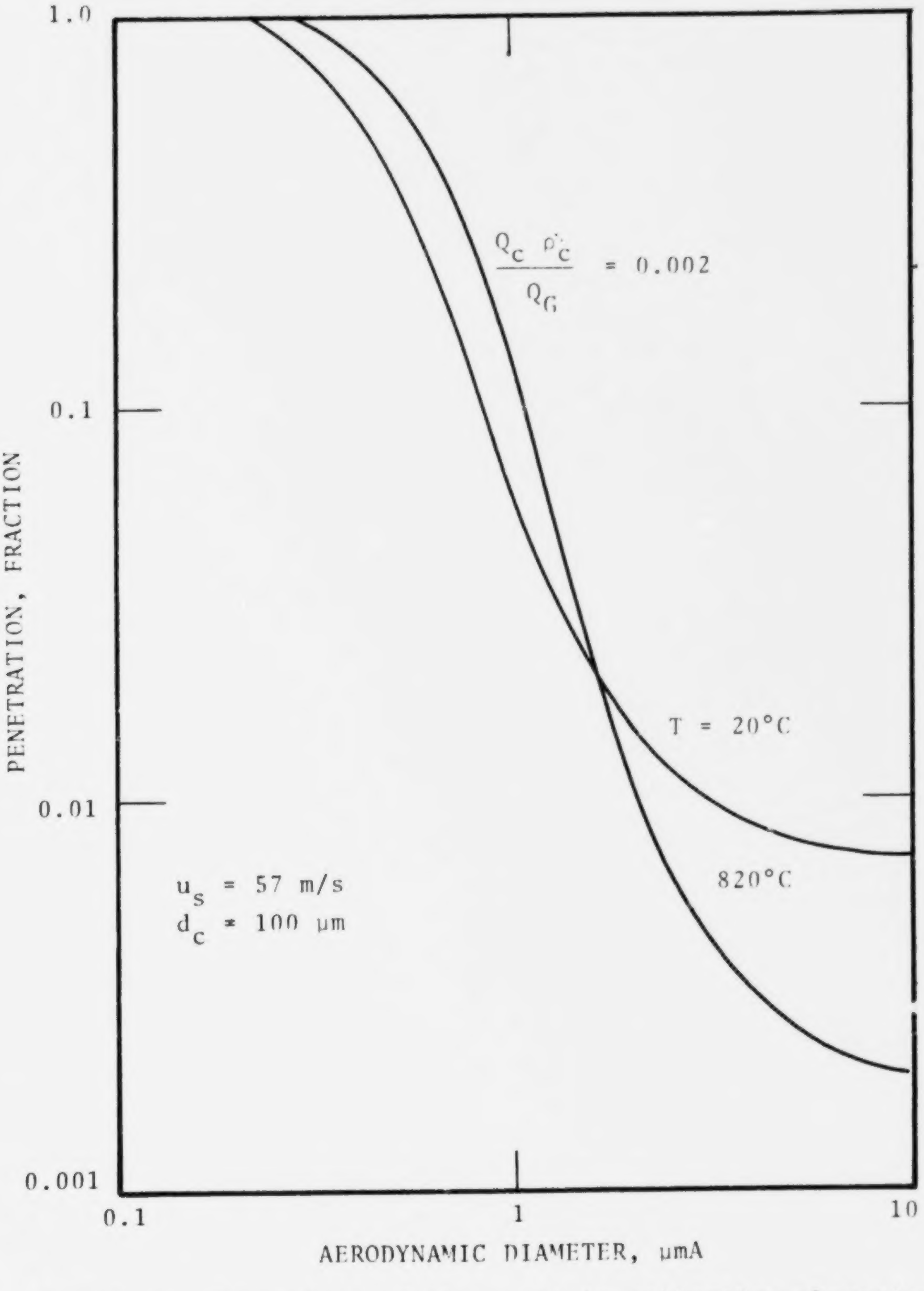

Figure 4. Comparison of the particle collection characteristics of the A.P.T. dry scrubber at 20°C and 820°C.

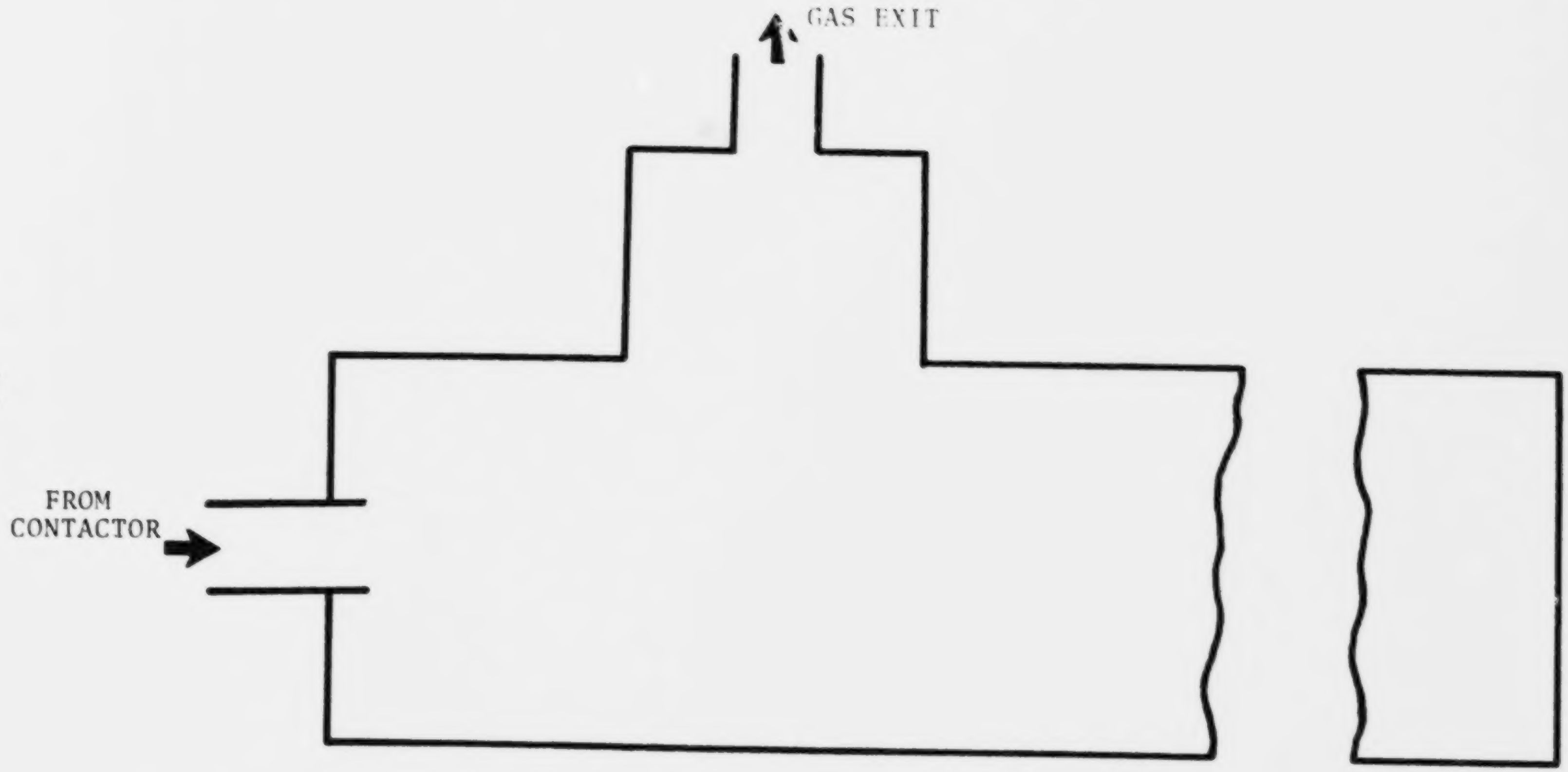
GAS EXIT
FROM
CONTACTOR

Figure 5. Horizontal flow separator.

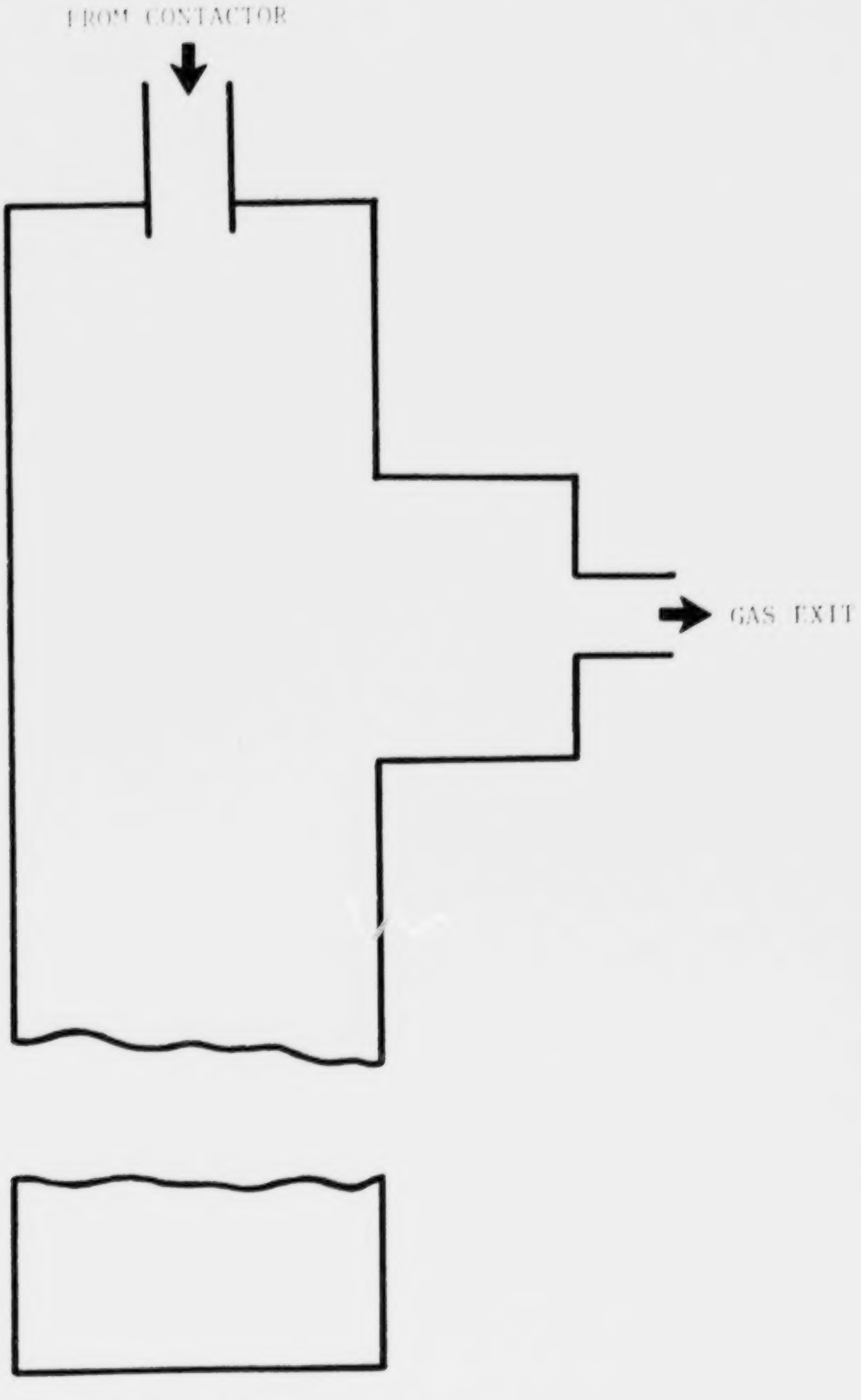
FROM CONTACTOR
GAS EXIT

Figure 6. Vertical flow separator.

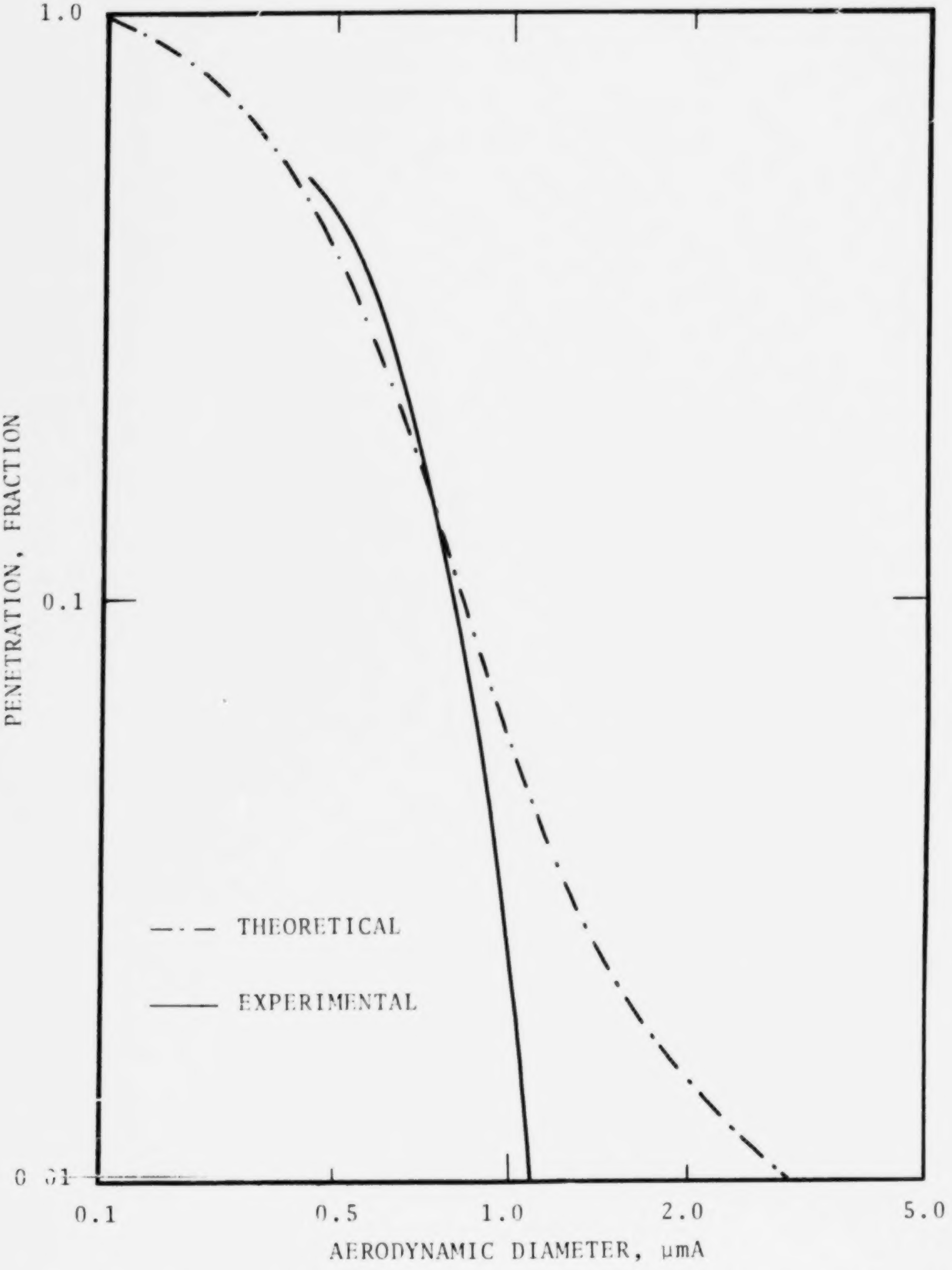

Figure 7. Comparison of experimental with theoretical particle collection characteristics of the A.P.T. dry scrubber.

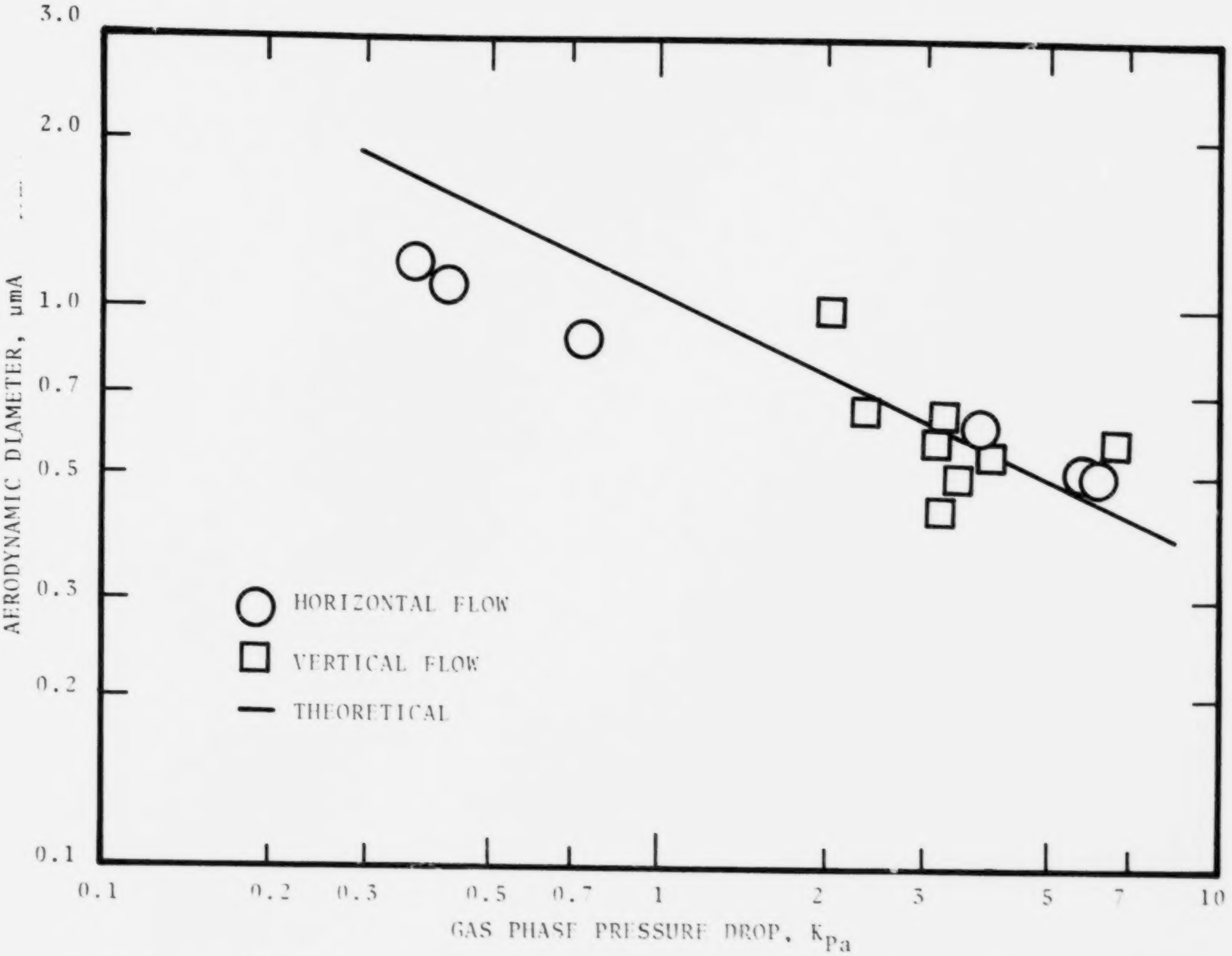

Figure 8. Comparison of particle collection characteristics of the A.P.T. dry scrubber with the A.P.T. cut/power relationship.

# HOT GAS CLEAN-UP BY PARTICLE ENTRAINMENT IN COAL SLAG~~E~~ BASED GLASSES

By:

L. R. McCreight, A. Gatti, H. W. Rauch, M. J. Noone
General Electric Company
Philadelphia, PA 19101

# HOT GAS CLEAN-UP BY PARTICLE ENTRAINMENT IN COAL SLAG BASED GLASSES

Louis R. McCreight - Arno Gatti - Harry W. Rauch - Michael J. Noone
Space Sciences Laboratory
General Electric Company
Valley Forge Space Center
P. O. Box 8555
Philadelphia, Pennsylvania 19101

An important problem in the utilization of gases from coal combustors to fuel gas turbines is the need to remove harmful particulates. For efficiency this must be done without appreciable cooling of the gases. Coal slag based glasses are being considered in an analogous manner to water scrubbers at normal ambient conditions for this purpose. Control of the viscosity by the use of both chemical and electrical energy additions is also included in the study to potentially permit operation over a temperature range of about 1000 to 1600°C. In this initial feasibility demonstration program, viscosity studies on various glasses including those made from fly ash and some model air cleaning studies are being performed in a clear plastic labyrinth unit using glycerine at room and low temperatures to simulate glasses. Later work will include high temperature studies and conceptual designs for a full sized system.

# HOT GAS CLEAN-UP BY PARTICLE ENTRAINMENT IN COAL SLAG BASED GLASSES

## INTRODUCTION

The objective of this study program is to demonstrate the technical and economic feasibility of utilizing coal slag based glasses as a fluid to entrain particulate matter at high temperatures without significant carry-over. This will permit the direct utilization of the effluent from a coal combustor without cooling the gases to effect the clean-up. The emphasis shall be on providing gas sufficiently free of particulates to permit turbine operation without undue corrosion or erosion. The primary benefit from the use of glass coated surfaces to trap particles is due to the viscosity or stickiness of the glass which will minimize richochet and fracture of the particles as apparently often happens in other apparatus. Then since the particles are often of a siliceous nature they should dissolve in the glass and thereby be less volatile or likely to carry over into the turbine. Thus in this approach to hot gas clean up the stickiness of the particles is a virtue rather than a problem as it is in some other processes.

In addition to this primary benefit, successful accomplishment of this program objective would provide more compact, easily handled waste products, since the solid glassy form of the fly ash occupied only about 20-25% of the volume of the powdered fly ash and may therefore have considerable utility as an aggregate etc. in building materials. These aspects are being considered but not extensively explored at this time.

Instead the primary effort is aimed at demonstrating both qualitatively and eventually quantitatively the practicality of the idea.

The work is currently being done under two principal tasks. I - "Fly Ash Melt Studies", and II - "Particle Collection Studies". The results of these two tasks will then be factored into a third task toward the end of the program titled "Total Power Generation Cycle Efficiency Study". Since the program is less than five months old. emphasis in this paper will be on the primarily qualitative demonstrations of feasibility being performed under the first two tasks.

## FLY ASH MELT STUDIES

Several widely used coals were considered as sources of typical fly ash for this program. These included Montana Rosebud, Pittsburgh No. 8 and Illinois No. 6, plus a standard soda lime silica and an amber container glass for model studies at elevated temperatures. Glycerine at various low temperatures is also used in the particle collection studies to be discussed. The compositions of these materials is shown in Table I and the viscosity versus temperature curves for synthetic versions of some of these materials are shown in Figures 1a and 1b along with the curve for an average synthetic slag prepared by the National Bureau of Standards which is designated as K-884 and is based on an average of Montana Rosebud and Illinois No. 6.

Flow studies on both the synthetic slags and samples of actual fly ash using a modification of the standard flow buttom test used for porcelain enamels have been carried out while work in a model duct using glycerine has been initiated under Task II, described later.

The flow button test has been used throughout the porcelain enamel industry for many years. It is a commonly used practical. quality control technique for checking the fluidity and fusibility of enamel frits. The test is considerably less expensive and simpler than high temperature viscometry while producing reliable practical data. However, Dekker (1) has shown that viscosity-temperature relationship can be determined but with a somewhat more elaborate procedure than the conventional flow button test.

Several factors must be controlled for reproducibility. These include particle size of the materials, forming pressure, height and weight of the pellets, composition of the materials and the temperature. However, Plankenhorn (2) concludes that the predominant factors are the temperature and the material composition. Our limited study supports that conclusion.

Fluidity studies are being conducted on the following materials:

Montana Rosebud fly ash

Pittsburgh #8 fly ash

An intermediate Montana Rosebud/Illinois #6
synthetic slag (NBS, K-884)

A standard soda lime silica glass

Amber container glass.

The Montana Rosebud fly ash was obtained from the Montana Power Company, Billings, Montana; the Philadelphia Electric Company supplied the Pittsburgh #8 fly ash; and, we synthesized the intermediate Montana Rosebud/ Illinois #6 slag from a composition derived by Capps and Kaufman of NBS and designated as K-884. The soda lime silica standard glass (Standard Reference Material-SRM 710) was purchased from the National Bureau of Standards. The amber container glass was obtained locally and ground in our laboratory.

Both of the fly ash materials were of sufficiently small particle size to readily pass through a 100 mesh sieve thus no further particle size reduction was required. Both the K-884 synthetic slag and the SRM-710 glass were ball milled until the particles passed through a 100 mesh screen.

Pellets were formed by mixing 25 grams of each material with 2.5 grams of 3.0% PVA solution, placing 1.5 grams of the mixture in a steel die and pressing at 15,000 psi. Specimens resulting from this treatment are cylinders 3/8" diameter and 3/8" high.

The fluidity runs were conducted by placing the pellets on tiles mounted at $30^o$ to the horizontal in a furnace preheated to the desired temperatures, leaving them for the predetermined time, and then removing them. Various refractory materials as tiles have been used including mullite, alumina coated mullite, and dense magnesia-alumina spinel. The latter has proven to be the most useful because of the lack of porosity which obscured the results with the other materials.

As a result of a number of trials, it was found that the amber container glass offered the most potential for operation at about $1000^oC$ where the current efforts on advanced gasifiers and combustors is focussed. Figure 2 illustrates the behavior of this glass and various mixtures of it with the K-884 synthesized coal slag in the flow button tests at temperatures from 1000 to $1250^oC$.

Some further tests utilizing this same container glass with admixtures of Montana Rosebud fly ash in the range of 2-10% indicates that small amounts (2-5%) of this fly ash noticeably lowers the viscosity of the glass. This is a very important finding in that it portends that an even broader range of fluidity may be achieveable.

## PARTICLE COLLECTION STUDIES

Early feasibility studies of this idea for collecting particulates were made with glazed wall tiles mounted in a manner to provide a labyrinth flow path for the gases from a gas burner into which silicon carbide particles could be entrained. These tests indeed showed the validity of the idea but were not easily quantified nor modified to test a wide variety of parameters.

Under this program a general purpose test duct was therefore designed, built, operated, and modified for gaining design ideas and data to be used in building a hot gas duct later in the program. The current test duct is built of clear plastic as shown in Figure 3a and b. It has 10 square feet of collection area, 0.1 sq. ft. inlet and exit ducts, and an internal cross-sectional area of 0.05 sq. ft. to give a two fold increase in pressure and flow. It is operated on a house air line at up to 100 cu. ft. per minute.

Collection of the fly ash particles in this duct is by means of glycerine which can be cooled to yield viscosities which corresponds to temperatures of 1000 to 1600°C in various glasses. The glycerine flows through 1/4" diameter holes in the bottom of the supply tank, down over the plates in the duct and initially into a common dump, however, this was later revised to provide 14 separate compartments so that the results from each collector section could be kept separate. Any particles which are not caught on the glycerine coated walls are finally trapped in a vacuum cleaner filter bag at the exit duct.

The duct has been operated several times with a manually operated syringe for injecting the fly ash, but is now equipped with a vibrator feeder on the Metco flame spray gun used to inject the fly ash. Another aspect of the operation that should be mentioned is that the flow of glycerine into the chamber is controlled by a slide valve that is manually opened to any desired setting at the beginning of the run. For high viscosity runs, the valve can be fully opened and still permit a several minute run on a tank of glycerine. A low viscosity run however will be quite short if the slide valve is completely opened but if it is only partially opened the glycerine flows in streams over only a portion of the plastic plates in the duct.

Two further variations of these tests are also underway. One is to coat the plates with a very viscous hydrocarbon to study the longer time operation of the duct under conditions in which there would not be a flow of glycerine (or glass). Another variation is to mount several plastic plates at a 45° angle to the gas flow such that glycerine flowing over and through the large number of small holes in the plates would serve as either or both a bubbler and/or a curtain to perhaps more completely trap the particles.

Test results in the duct to date have been very encouraging with 99% of the injected material trapped in the glycerine and usually mostly within the first third of the duct. The particles that reached the vacuum cleaner bag on the exhaust duct were generally less than 2 microns in diameter.

# TOTAL POWER GENERATION CYCLE EFFICIENCY STUDY

This aspect of the program is scheduled for later in the year when more quantitative information is available. However conceptual designs and operational scenarios are being developed against which to perform the previously described R & D work.

It is envisioned that the sequence of coal combustion or gasification to provide gas to drive a gas turbine may utilize a cyclone and this coal slag based glass process for cleaning the particles from the gas stream at temperatures of about 1000°C. The glass process is envisioned to consist of several vertical chambers (in order to provide standby reserve capacity each) of which would have the gas flow and the glass flow downward with the gas exiting on the side while the glass could be removed intermittently through a lock hopper. Means of combining it with the particulate effluent from the cyclone as well as recovering the sensible heat from these two sources is contemplated. The combined waste products from these two clean-up processes could then be either disposed of as a more compact fill than fly ash or perhaps used in building products as aggregate.

Start-up and operation of the unit are envisioned to be by coating a large number of square feet of ceramic plates with a fraction of an inch thick layer of powdered glass which would be fused in place and be continuously refurbished and replaced primarily by capturing and dissolving fly ash. If necessary some supplementary glass could be added in the gas stream or from a lock hopper. It is possible, if not probable, that some local control of the viscosity of the glass will also be necessary. It is especially likely that lowering of the viscosity will be needed. For this, two methods are possible, one is to add materials that will flux the glass/fly ash in the unit and the other will be to provide local heating (primarily electrical) much as is so widely done in the glass industry. The latter seems most desirable since presumably electrical energy is being generated in these plants and any usage of energy for this purpose would be largely recovered in the gas stream. Also the use of electrical energy as opposed to adding chemicals or low melting glasses for viscosity control would seem preferable from the standpoint of the potential carry over of low melting materials into the turbine.

## ACKNOWLEDGEMENTS

The authors thank ERDA and especially Mr. William Fedarko who represents them as the program manager for supporting this work under contract EF-77-C-01-2608. In addition, Mr. William Laskow of our laboratory has provided invaluable assistance in preparing and performing the experimental work.

## REFERENCES

1. Dekker, P., "Calculation of Viscosity-Temperature Curves for Porcelain Enamels from the Flow-Button Test," J.Am.Ceram.Soc. 48 (6) 319-27 (1965).

2. Plankenhorn, W.J., "Factors Affecting Reproducibility of Flow-Button Test." J.Am.Ceram.Soc. 31 (12) 338-44 (1948).

## TABLE I. COMPOSITION IN OXIDE WEIGHT PERCENT OF MATERIALS EVALUATED FOR FLUIDITY TEMPERATURE RELATIONSHIP

| Oxide | SRM-710* | Amber Container Glass** | Montana*** Rosebud | Pittsburgh*** #8 | K-884**** |
|---|---|---|---|---|---|
| $Na_2O$ | 8.7 | 13.3 | 0.4 | 1.5 | -- |
| $K_2O$ | 7.7 | 1.8 | 0.4 |  | - |
| CaO | 11.6 | 9.8 | 14.9 | 3.3 | 10.06 |
| MgO | - |  | 4.7 | 0.7 | 3.3 |
| $Al_2O_3$ | 0.18 | 4.2 | 21.7 | 21.4 | 21.8 |
| $Fe_2O_3$ | 0.02 | 0.4 | 8.0 | 28.3 | 16.6 |
| $Sb_2O_3$ | 1.1 |  | - | - | - |
| $P_2O_5$ | - |  | 0.4 | - | - |
| $TiO_2$ | - |  | 0.008 | - | - |
| $SiO_2$ | 70.5 | 70.6 | 47.5 | 44.8 | 47.8 |
| $SO_3$ | 0.2 | 0.02 | - | - | - |
|  | 100.00 | 100.12 | 99.78 | 100.0 | 100.1 |

* Soda-lime-silica glass from NBS

** Typical amber container glass composition

*** Fly ash

**** Synthetic slag developed by NBS-glass Section to represent intermediate composition between Montana Rosebud and Illinois #6 fly ash materials.

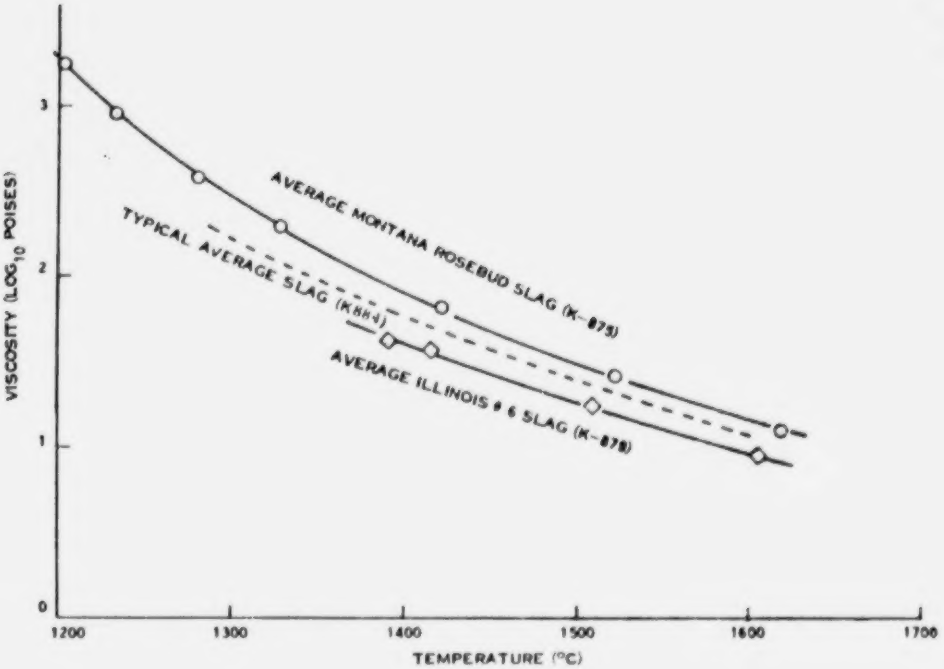

Figure 1A. Viscosity/Temperature Relationship Determined by NBS on Synthetic Slags Formulated to Represent the Average Compositions of Fly Ash from Montana Rosebud and Illinois No. 6 Coal Types. The Central Curve is an average of these Data and may be Considered to Represent "Typical" U.S. Coal Slag Behavior.

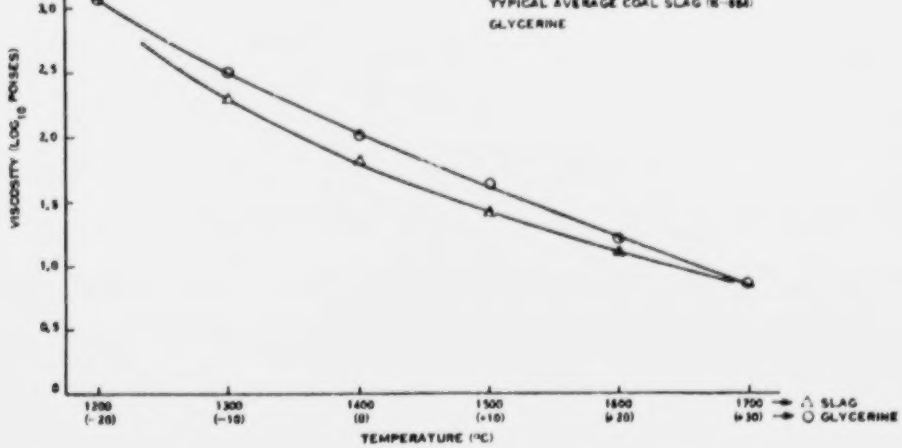

Figure 1B. Viscosity/Temperature Relationships for a Typical "Average" Coal Slag (NBS K-884) and Glycerine which will be Used as a Model System to Demonstrate Particulate Capture Mechanisms at Low Temperatures.

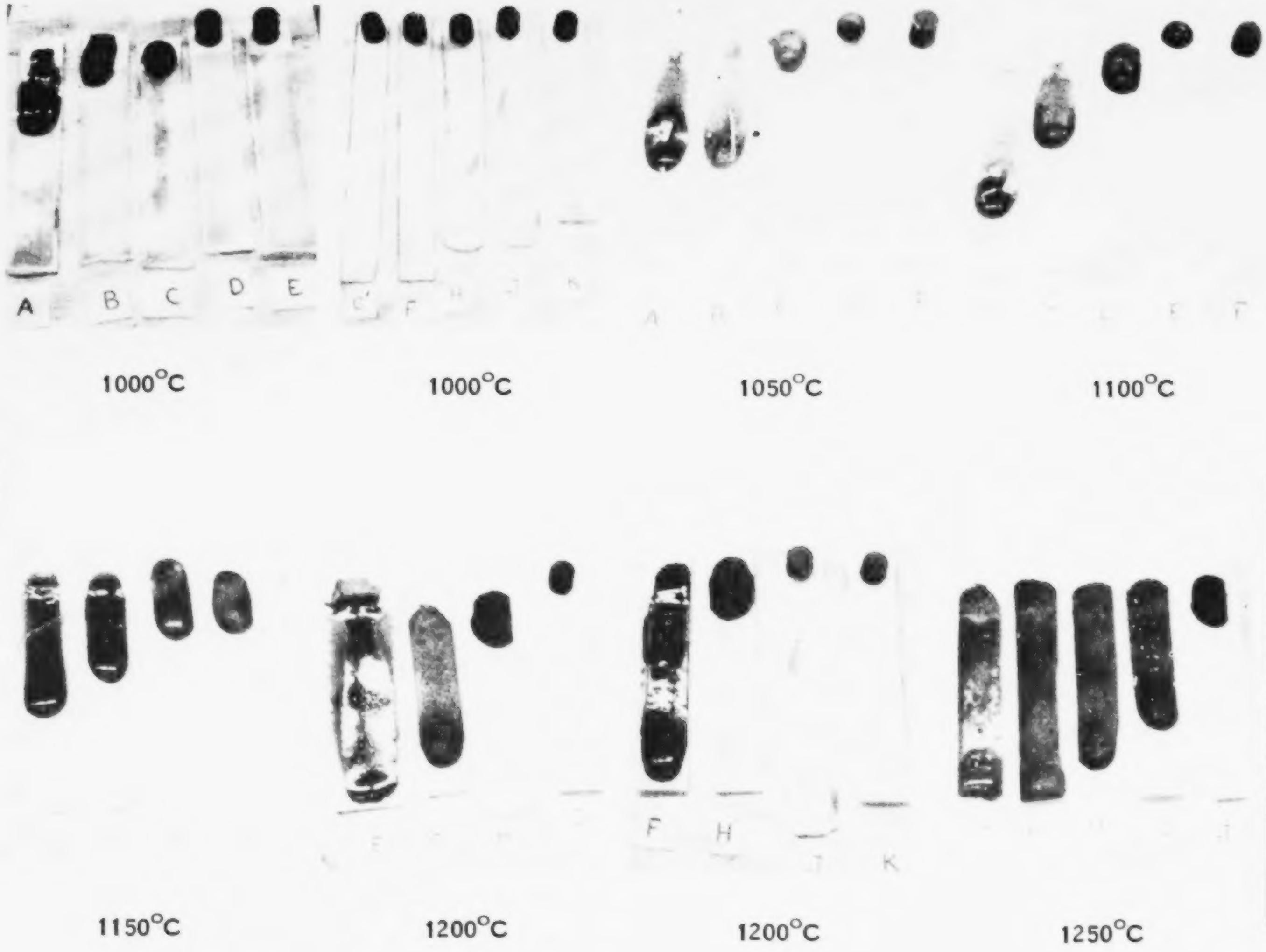
A
B
C
D
E
C'
F
1000°C
1000°C
1050°C
1100°C
1150°C
1200°C
F
H
K
1200°C
1250°C

LEGEND

| | WT. % | |
|---|---|---|
| | GLASS | K884 |
| A | 100 | – |
| B | 90 | 10 |
| C | 80 | 20 |
| C' | 75 | 25 |
| D | 70 | 30 |
| E | 60 | 40 |
| F | 50 | 50 |
| G | 40 | 60 |
| H | 30 | 70 |
| H' | 25 | 75 |
| I | 20 | 80 |
| J | 10 | 90 |
| K | – | 100 |

Figure 2. Flow Behavior of Amber Container Glass, Synthetic Slag K884, and Various Mixtures of These Two Materials after One Hour at Indicated Temperature

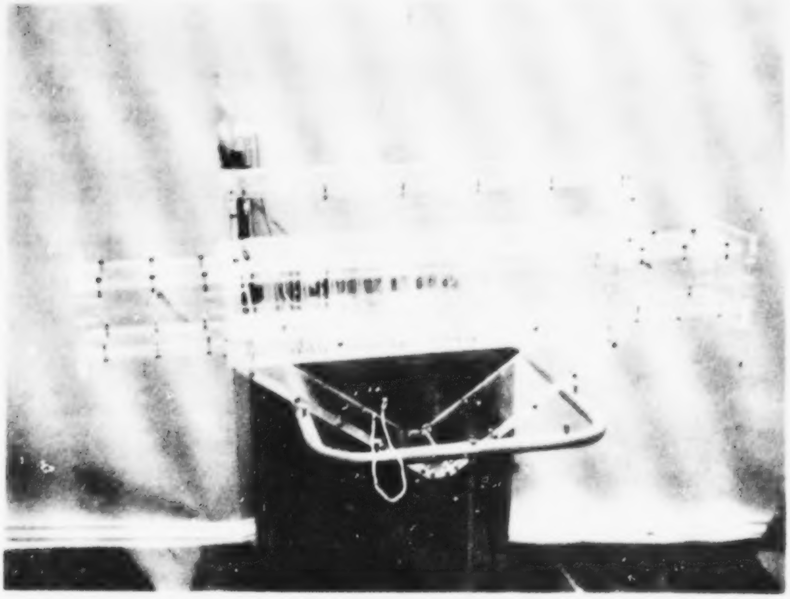

A

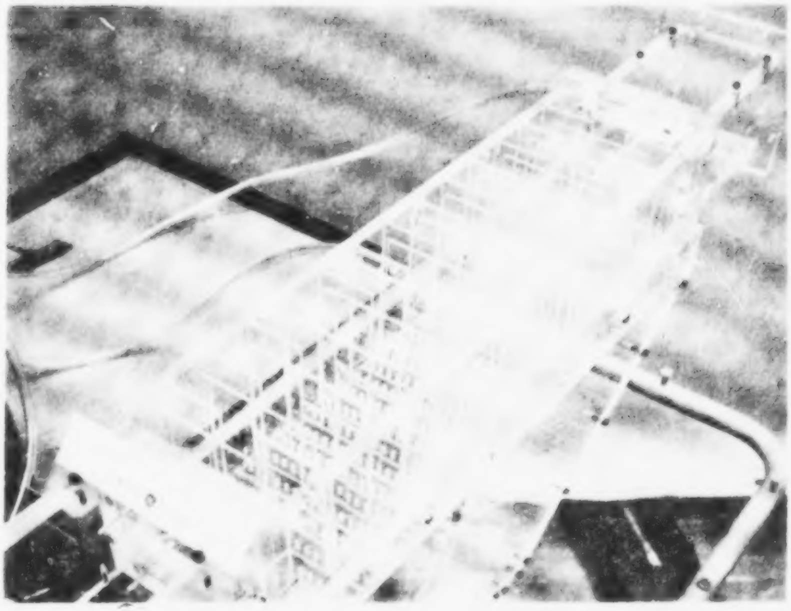

B

Figure 3. Photograph of a plexiglass model of a "sticky-wall" labyrinth gas scrubber (A) and (B) a close-up view of scrubber plate detail.

# MOLTEN SALT SCRUBBING FOR REMOVAL OF PARTICLES AND SULFUR FROM PRODUCER GAS

By:

R. H. Moore, G. F. Schiefelbein, G. E. Stegen, D. G. Ham
Battelle Memorial Institute
Richland, WA 99352

# MOLTEN SALT SCRUBBING FOR REMOVAL OF PARTICLES AND SULFUR FROM PRODUCER GAS

By.

R. H. Moore
G. F. Schiefelbein
G. E. Stegen
D. G. Ham

Battelle Memorial Institute
Pacific Northwest Laboratories Division
Richland, WA, 99352

Data are presented which shows 95 to 99% extraction of sulfur compounds from producer gas at 1250° to 1500°F has been achieved using a molten salt as the working fluid in a venturi scrubber. The salt was fully regenerable using excess steam + $CO_2$ to reverse the reaction. Efficient removal of particles was also achieved. Producer gas at a flow of 50 to 75 SCFM was generated in Battelle's fixed bed gasifier operating on metallurgical coke.

These data together with earlier laboratory data have enabled design of a Process Demonstration Unit for operation in fully continuous mode. This PDU is in final phases of construction. The design basis and a few details of equipment are presented here.

# MOLTEN SALT SCRUBBING FOR REMOVAL OF PARTICLES AND SULFUR FROM PRODUCER GAS

## INTRODUCTION

Reversible extraction of $H_2S$ from synthetic fuel gas by molten carbonates was demonstrated in laboratory scale bubble contactors early in 1973. These tests defined the equilibrium extraction of $H_2S$ as a function of temperature and provided data for subsequent Process Demonstration Unit design. Parallel corrosion tests disclosed that "alonized" 300 series stainless steels might be suitable for PDU construction.

On the basis of these experiments it was concluded that a process for hot fuel gas cleaning could be devised. It would have the following characteristics:

- The process would entail gas-liquid contacting at 500° to 750°C.
- Removal of sulfur compounds, particles, and low volatile tars would occur.
- The sulfur compound extraction capacity of the salt would be easily regenerated to yield a regenerator product gas sufficiently high in $H_2S$ to be a suitable Claus process feed gas.
- Numerous minor impurities (halogens, volatile metals and volatile non-metals) would be removed from the fuel gas. Ammonia removal, if it occurred, would occur only as a consequence of dissociation. Water vapor would not be removed.

Of course, there would be a few problems! Few molten salt processes with any degree of complexity have been operated. Serious problems have been encountered in the operation of mechanical pumps. This has forced adoption of processes so simple that no pumps are required. The Atomics International coal gasification process is an example. In consequence, the process capability becomes limited.

The hot fuel gas cleaning process employs a venturi scrubber--packed bed de-entrainer combination. The use of a mechanical pump can be avoided by operating the venturi in a vertical orientation. Salt fed to the venturi becomes totally entrained in the gas phase and is carried upward to a de-entrainer situated well above the level of the venturi feed tank. Upon de-entrainment the salt returns by gravity induced flow to the feed reservoir. It only remains to insert a salt regeneration step between the salt reservoir and the de-entrainer to achieve fully continuous operation in process mode. This is now being done, but initially, all effort was directed toward design, construction, and test of a venturi de-entrainer package operating on low Btu fuel gas produced by Battelle's fixed bed gasifier. Only the extraction portion of the process has been tested at PDU scale. These tests measured:

- the efficiency of $H_2S$ and COS removal
- the efficiency of particle removal
- the effectiveness of salt de-entrainment
- the behavior of materials
- the effectiveness of a vertical venturi scrubber for salt circulation.

To some it may appear the problem of particle removal has been complicated by introducing a salt dispersion. Certainly it is necessary to separate the ash-char particles from the salt. This will be done by treating a salt bleed in a separate aqueous process for salt recovery and recycle. So far as the gas is concerned, introduction of the salt may facilitate collection of particles. This is due to the tendency of a liquid to agglomerate and to occlude the particles in the agglomerating liquid droplets. On the other hand, specifications for alkali metals may be lower than for particles and this may further complicate the problem.

## THE VENTURI SCRUBBER-PACKED BED DE-ENTRAINER

The fuel gas will typically be used to fuel a gas turbine, and cleaning requirements were formulated on this basis. The venturi scrubber was designed with particle removal efficiency as the design basis. It was assumed that gas-salt dispersion and mass transfer efficiency would be such as to ensure a single equilibrium stage for $H_2S$ extraction.

The Battelle-Northwest gasifier shown in Figure 1 was originally designed for steam-air pyrolysis of carbonaceous wastes. It is a ceramic lined vessel 36 in. I.D. and 12 ft high with a lock hopper above for feed addition and a fixed grate through which air and steam may enter at its base. It operated well on coke and is expected to function equally well on non-caking coal. It will gasify such fuels at rates up to 150 lb/hr producing up to 150 SCFM of gas. At the modest rate of 50 to 75 SCFM the gasifier should operate continuously for 4 to 5 days before shutdown for ash removal becomes necessary.

At the time design of the venturi scrubber was initiated, nothing was known about the particle size distribution or particle loading in the gas produced from coke by this unit. A value of 0.1 lb/1000 SCF was assumed, a value which proved to be about twice the value measured. With coal, tars and oil will accompany the particles.

Particles which cause erosion of turbine blades must be larger than about 2.0 microns. This venturi scrubber was designed for 99% removal of particles 4.0 microns or larger. Calculations patterned after those of Seymour Calvert, et al(1) were used to establish the throat velocity sufficient to achieve this. The value turned out to be 200 ft/sec at a feed rate of 50 SCFM. For design conservatism this was increased by 20%.

Figure 2 shows a schematic of the venturi scrubber. The throat diameter is 1.5 in., the inlet angle is 25° and the exit angle 7°.

Considerable thought was given to the design of the salt inlet port. This venturi is so small no latitude exists to provide a distributor ring (the holes in the ring would be minute). There was concern about possible plugging of the inlet port and the decision was reached to provide a single inlet hole. A scrubber with an inlet of 3/16 in. diameter was used which allowed a maximum flow of 0.9 gal/min of molten salt under the available head.

The dispersion of salt generated by the atomizing action of the high velocity gas flowed upward through a heated pipe to a de-entrainer situated above the salt feed reservoir. The mean droplet size generated by the venturi at a gas flow of 50 SCFM was calculated from the equation of Nukiyama and Tanasawa given in Perry(2) and found to be 116 microns. It was easy to show that salt droplets of this size would be carried upward and into the de-entrainer. It was also necessary to show that transfer of momentum from the gas phase to the film of salt flowing along the pipe wall would be sufficient to ensure a climbing film. Measurements by Sutey and Knudsen(3) on aqueous solutions permitted calculation of the shear stress in the salt film assuming a simple linear proportionality between the shear stresses and density for various liquids. The gas velocity required to produce the calculated shear stress turned out to be 39 ft/sec. For higher velocities upward flow of the liquid film would occur. For conservatism and for more economical construction costs (smaller pipe) a design velocity of 100 ft/sec was selected. This led to a required pipe diameter of 2.4 in.

To recover the entrained salt a packed bed de-entrainer was selected. Jackson and Calvert(4) have demonstrated >99% collection of 4 micron oil mist droplets with such beds. A de-entrainer was designed initially for use with 1.5 in. Raschig rings. These proved unobtainable in alumina refractories and 1 in. mullite grinding balls were substituted. These were placed in a bed 12.5 in. in diameter and 25 in. deep. This bed was calculated to have a flooding velocity of ∿1200 ft/min and at 50% of this velocity should have a removal efficiency of 90% for 3.5 micron particles.

A demister was fabricated from stainless steel screen rolled into coils about 3/4 in. diameter by 3 in. long. Screen of 50 mesh and 20 mesh was used.

A 10 in. deep layer of the rolls of 20 mesh screen was placed above the 1 in. ceramic balls and covered with a 4 in. deep layer of the 50 mesh rolls. This arrangement was used during only one run. At other times no demister was used.

All equipment and pipe must be heated to the operating temperature. Trace heating and furnaces were used as shown in Figure 3. This large pot furnace heated a 30 gal salt pot from which salt was fed to the venturi. The packed bed de-entrainer was situated just above this pot and the replacement furnace elements used for heating are clearly visible.

Figure 4 shows trace heating in the form of tube furnace heating elements on lines leading to the venturi. The large pot furnace below contains a 30 gal pot to which the salt can flow in the event gas flow should be interrupted. This pot can be pressurized to transfer salt back to the upper pot. The completed PDU configured for extraction in batch mode is shown in Figure 5. Here insulation is in place and the plant is ready for operation. The gasifier is at the right, the venturi and de-entrainer at center, and a burner for gas disposal is at the left. Auxilliaries for gas preheating, aqueous carbonate scrubbing, and coal conveying are also visible.

## EXTRACTION OF SULFUR COMPOUNDS FROM LOW BTU FUEL GAS AT VARIOUS TEMPERATURES

The extraction section consisting of the venturi scrubber and packed bed de-entrainer was operated in a series of short runs which confirmed the laboratory data. Figure 6 shows the chemical reactions of interest here. In these runs a four component salt mixture was used which was of the composition shown in Table I. In this salt mixture, $CaCO_3$ is so much more reactive than any of the accompanying alkali metal carbonates that reaction to form CaS is almost the sole reaction until most of the $CaCO_3$ is consumed. This is illustrated by laboratory data which discloses the temperature dependence of the reactions of $H_2S$ with various molten and solid carbonates (Figure 7). Clearly $CaCO_3$(s) is much more reactive than $Na_2CO_3$(s) or mixtures of molten alkali carbonates. Its addition to the latter in amounts of from 15 to 20 mole % $CaCO_3$ substantially increases the reactivity of the mixture.

The schematic flow diagram for operation of the venturi scrubber-packed bed de-entrainer is illustrated in Figure 8. Hot fuel gas entered the venturi scrubber where it atomized and dispersed the entering flow of salt and carried the dispersed salt into the head space of the salt feed tank and into the packed bed de-entrainer. This was packed to a depth of about 24 in. with 1 in. balls, but most of the de-entrainment effect achieved occurred in the lower 3 to 4 in. The de-entrained salt returned to the venturi feed tank and the cleaned gas leaving the top of the de-entrainer passed to a burner for disposal.

Clearly the process operated in batch mode because the extraction of $H_2S$ would cease when the extraction capacity of the available salt was exceeded. When this occurred the salt would either have to be regenerated or replaced. The salt could be regenerated by allowing it to flow into a second pot furnace containing a 30 gal salt pot. Here it could be cooled to, e.g., 600°C, and treated with a steam-$CO_2$ mixture introduced via a distributor ring. The reaction with steam + $CO_2$ is a reversal of the extraction reaction and was shown in laboratory experiments to proceed readily to 96 to 98% completion. Here the reaction proceeded at a rate proportional to the rate of steam addition because the salt containing CaS was in large excess. Time was taken to regenerate no more than 80% of the theoretical maximum, but there is no reason to conclude that complete regeneration would not occur. An aqueous carbonate scrub was used to capture regenerated $H_2S$. The resulting NaHS solution was sewered for disposal.

Three runs of short duration were made using the venturi de-entrainer extraction section. In the first run (Table II) at 700°C, troubles were encountered adjusting liquid and gas flows and for a brief period operation of the venturi was accompanied by flooding. This resulted in loss of about half of the circulating salt inventory to the lower (regeneration) pot furnace. At the time, this was not obvious, and it appeared instead that the extraction capacity of the salt was much less than expected for reasons unknown. The data in Table II clearly shows the decay in recovery efficiency as the salt became saturated with sulfide. The unexpected path taken by the salt was discovered following termination of the run.

In a second run, this time at 750°C (Table III), operation was normal with excellent sulfur recovery. During the period from 1600 hours to 1855 hours, $CaCO_3$ utilization ranged from 16.7 to 29.5%. The recovery of 94 to 97% of the sulfur is in agreement with predictions from laboratory data.

In a run at still higher temperature (Table IV) difficulty was experienced in establishing salt flow during the early part of the run. At such high temperatures, the extraction efficiency of the alkali metal carbonates is fairly high and the addition of $CaCO_3$ may offer no advantage. $CaCO_3$ tends to dissociate as the temperature is increased forming CaO which has only limited solubility in the melt. When this solubility is exceeded, precipitation of CaO occurs accompanied by a marked increase in viscosity of the melt. The natural tendency to apply heat to lower the viscosity is the wrong thing to do in this case. Addition of $CO_2$ is effective. With full salt flow (evidenced by pressure drop) recovery of sulfur jumped to very high efficiency. The feed gas sulfur concentration was varied by addition of $H_2S$ cylinder gas and the high $H_2S$ concentration near the end of the run made it easy to demonstrate 99% $H_2S$ recovery.

The addition of supplemental $H_2S$ is considered to be responsible for the anomalous COS behavior. Reaction of added $H_2S$ with CO is believed to be the principal reaction which produces COS. The inlet feed sample is taken just downstream and around a bend from the point of $H_2S$ addition. Even here the increase in COS is evident in consequence of the variation of its formation rate with temperature (Table V). Even after entering the venturi scrubber reaction to form COS continues but as the $H_2S$ is extracted COS formation slows and may even reverse. The product sample analysis shows that the final COS concentration is above the equilibrium value predicted in terms of the final $H_2S$ concentration, but is below the equilibrium value for the inlet $H_2S$ concentration. This requires that the reaction rate be fast but not so fast that the reaction rate keeps up with the rate of $H_2S$ extraction. It is also required that the rate of direct COS extraction be less than the rate of $H_2S$ extraction. The data indicate that presence of COS in the product gas limits overall sulfur removal. The solution would appear to be to provide additional residence time in the extraction section (or additional extraction stages).

# BEHVAIOR OF PARTICLES AND EFFICIENCY OF SALT DISPERSION DE-ENTRAINMENT

Two isokinetic samplers were used to sample inlet and outlet gases for particles. The inlet sample was collected on a filter, so only total particle burden was obtained. The gas was also dried by passage through a silica gel absorption bulb. When this was weighed, the average moisture content of the gas could be calculated.

The outlet sample was passed through an Anderson-2000 Impinger, so in addition to total particle burden, the particle size distribution was obtained. Salt losses could be estimated from analysis of deposits on the plates.

Data obtained from runs at 750°C and >800°C are shown in Tables VI and VII. For the case shown in Table VI, the PDU was operating with no demister. For the data shown in Table VII, the wire screen demister described earlier was in place. The demister appears to have reduced the particle burden in the product gas by approximately a factor of three.

The data of Table VII show a total weight gain of 0.0301 g which corresponds to 0.0245 grains/SCF or about 40 ppm (by weight) in the product gas. The appearance of the deposits on the plates of the Anderson head is most informative. The deposits on plates 2, 3, and 4 are very thin and cast no shadow when viewed at moderate magnification, e.g., 80 x. On plates 5 through 8, however. the deposits are piled up in little mounds. These may have been formed by salt droplets which solidify as they hit. The deposit on plate 8, shown in Figure 9, is typical. The flat deposit on plate 4 is shown in Figure 10 for comparison.

When viewed at 2000 x under the scanning electron microscope (Figure 11), the deposit on plate 4 appears as round spherical particles of 4.5 microns diameter. This confirms the calculated cut-off diameter for this plate, but the point of major interest is the uniformly spherical nature of these particles. These must surely have been formed by solidification of a liquid.

Portions of the candle-shaped mound from plate 8 were transferred to sticky tape and viewed at 20,000 x under the scanning electron microscope. Again spherical particles are observed (Figure 12). These are 0.3 to 0.4 microns in diameter, slightly smaller than the calculated cut-off diameter for this plate.

The scanning electron microscope excites an x-ray fluorescence spectrum of the elements present in the sample. Figure 13 shows the spectrum of the deposit on plate number 4. Na is not efficiently detected and elements lighter in mass than Na are not observed. K and Ca, which are major salt components, are noted as well as S, which the salt has extracted. In addition Al, P, Si, Fe, and Zn, which are coke derived, were observed. Some Na, K, and Ca may also be coke derived. The deposit on plate 8 yields the spectrum shown in Figure 14. Here Ca, a major salt component is barely detected. Na and K and some S are evident. A major constituent is P. Si, Cl, Fe, Zn, and Ga are also present. Comparison of these and other measurements with spectra of the pure starting salt indicates that on average these deposits are about one third salt with the balance being material derived from coke. This means the product gases from this run contained approximately 12 ppm salt. This is slightly more than an order of magnitude too high to be of acceptable quality for turbine fuel; however, there are steps which can be taken to reduce salt and particle levels still further so continued development of this process seems warranted.

## DEVELOPMENT OF FULLY CONTINUOUS PROCESS

Operation of the venturi scrubber-packed bed de-entrainer disclosed some critically important information. It disclosed some severe operating problems (due to salt freeze-ups with salts high in $CaCO_3$. These would become serious at temperatures above 750°C. No serious corrosion of the alonized steel occurred, though the exposure history was short (at most 150 hours at temperatures >700°C). Some erosion occurred in the throat of the venturi scrubber and in the future, the shape of the venturi scrubber will be defined by a ceramic liner (high purity, high density $Al_2O_3$) which will fit inside an alonized steel shell. Finally, the data disclosed that regeneration of salts containing $CaCO_3$-CaS might require high steam consumption and might lead to a regenerant gas too lean in $H_2S$ for efficient conversion to S in a Claus process. Processes other than the Claus could, of course, be used.

These considerations led to design of a process which utilized the alkali carbonate eutectic with no deliberate $CaCO_3$ additions. Small amounts of $CaCO_3$ which enter from coal ash will cause no problem. A vertically oriented venturi scrubber is again to be used to circulate the salt. As shown in Figure 15, the salt dispersion will be carried upward to a de-entrainer where the flow of salt is split. Most of the salt recycles to the venturi feed tank. A smaller amount containing sulfur in an amount roughly equivalent to that in the feed gas is cooled and passed through a regeneration column countercurrent to a flow of steam + $CO_2$. The regenerator is a 6 in. diameter column containing eight bubble cap trays with two caps per tray. It will operate at 500° to 600°C. It is designed to produce a $CO_2$-$H_2S$ mixture, following steam removal, containing 30% $H_2S$ (from fuel gas of 1.3 v/o $H_2S$).

Salt fed to the regeneration column is so rich in sulfur (in order to meet the requirements of the Claus process) that it is not possible to produce a fuel gas adequately low in sulfur in a single equilibrium extraction stage. The regenerated salt will flow to the salt make-up tank, here it will mix with fresh salt entering sporadically as bleed make-up, and then flow to the top tray of a two tray, 10 in. diameter bubble cap column. (The trays in this column contain 4 bubble caps.) On this top tray, the sulfur in the salt and in the product gas are in equilibrium. The level to which sulfur can be reduced by these additional extraction stages will be determined by the efficiency of regeneration. Removal efficiencies exceeding 95% with a maximum of 98% are anticipated.

The packed bed de-entrainer is situated above the top tray of the 10 in. extraction column. It is packed with one layer of 1 in. balls and 15 in. of $Al_2O_3$ catalyst support cylinders 5/8 in. in diameter by 5/8 in. long containing a central 1/4 in. diameter hole. Above this packing, there is a volume 12.5 in. in diameter by 25 in. high for which the following is planned:

1) A thin bed, 2 to 3 in. in thickness, of -4 +8 mesh activated carbon will be placed above the $Al_2O_3$ cylinders. This bed will partly fludize and will both absorb submicron salt droplets and will trap them by wake effects and/or inertial impaction. Other absorbants such as $Al_2O_3$ and $SiO_2$ may be tried.

2) Alternatively, this space will be filled with a wire demister of fine copper wire. Wires of other material may also be tried.

3) An experimental material has been furnished by 3M Company from which a filter of ceramic felt can be fabricated. Other filter materials such as graphite felt and cloth may also be tried. Quartz wool may be feasible.

Figure 16 shows a view of the supporting structure for the new PDU. The gasifier with its drag chain conveyor and lock hopper appears at the right. The burner and stack are visible at left-center. The storm cap on the stack is 50 ft above the concrete pad.

Figure 17 is a view showing the 10 in. extraction column and packed bed de-entrainer assembly. Also visible are the 2.5 in. venturi off-gas line and the 4 in. recycle line. The coarse de-entrainer is barely visible. The upper level grating is 31 ft above grade.

It is planned to have the remodeled PDU operating by October 1, 1977. It is the intention to demonstrate continuous operation over a period of 5 to 6 weeks. This will provide data necessary for economic and engineering evaluation of this process and for a management decision to proceed with its future development.

## ACKNOWLEDGEMENTS

The authors recognize a debt of gratitude for major assistance in early design phases involving the efforts of C. H. Allen and Dr. Arlin Postma. Additionally, the contributions of R. F. Maness in selection of materials and corrosion testing is gratefully acknowledged. More recently D. H. Mitchell and Dr. R. J. Robertus have played major roles in remodeled PDU design and construction and in process modeling.

This work was initiated with support from the Office of Coal Research under Contract 14-32-0001-1519. Continuing support by ERDA Fossil Energy's Division of Coal Conversion and Utilization and particularly the support of E. (Zeke) Clark and Dr. Michael Gurevich is gratefully acknowledged.

## REFERENCES

1. S. Calvert, et al., "Scrubber Handbook," Report for EPA Contract CPA-70-95, July 1972, A.P.T. Inc., Riverside, CA, 92502.
2. J. H. Perry, Chemical Engineers Handbook, 4th Edition, Chapter 20, McGraw-Hill Book Company, New York, NY, 1963.
3. A. M. Sutey and J. G. Knudsen, "Mass Transfer at the Solid-Liquid Interface for Climbing Film Flow in an Annular Duct," AICHE Journal, 15:719-726, 1969.
4. S. Jackson and S. Clavert, "Entrained Particle Collection in Packed Beds," AICHE Journal, 12:1075-1078, 1966.

TABLE I. Salt Composition Used in PDU Demonstration Runs

| Component | Mole % | Weight % |
|---|---|---|
| $Li_2CO_3$ | 18.0 | 13.0 |
| $Na_2CO_3$ | 37.3 | 36.0 |
| $K_2CO_3$ | 29.6 | 37.3 |
| $CaCO_3$ | 15.1 | 13.8 |

TABLE II. Data Summary Molten Salt Pilot Plant Run Number 2*

| Time | Gas Flow SCFM | Salt Temp. °C | Gas Temp. °C | Gas Press. psig | v/o $H_2S$ (in) | ppm $H_2S$ (out) | v/o COS (in) | v/o COS (out) | % Rec. S |
|---|---|---|---|---|---|---|---|---|---|
| 1533 | 48 | 700 | 675 | 0.9 | 0.84 | 5 | 0.021 | 0.016 | 98.9 |
| 1551 | 55 | 700 | 525 | 1.0 | 0.84 | 5 | 0.021 | 0.1 | 93.3 |
| 1640 | 60 | 700 | 525 | 1.0 | 0.84 | 5 | 0.021 | 0.049 | 96.7 |
| 1720 | 48 | 700 | 500 | 1.0 | 0.84 | 840 | 0.021 | 0.136 | 83.4 |
| 1755 | 50 | 700 | 500 | 0.9 | 0.84 | 0.57% | 0.021 | 0.104 | 25.9 |

---

* Nominal gas flow 50 SCFM; nominal salt flow 0.9 gal/min. During this run partial loss of salt to the lower tank and to piping up stream of this lower tank occurred which reduced the circulating salt inventory. This caused breakthrough of sulfur compounds earlier than anticipated.

TABLE III. Data Summary Molten Salt Pilot Plant Run Number 3

| Time | Gas Flow SCFM | Salt Temp. °C | Gas Temp. °C | Gas Press. psig | v/o $H_2S$ (in) | ppm $H_2S$ (out) | v/o COS (in) | v/o COS (out) | % Rec. S |
|---|---|---|---|---|---|---|---|---|---|
| 1552* | 71 | 750 | 750 | 0.5 | 0.35 | 101 | 0.026 | 0.068 | 86.6* |
| 1605* | 68 | 750 | 750 | 0.5 | 0.35 | 103 | 0.026 | 0.08 | 84.7* |
| 1617 | 68 | 750 | 750 | 0.5 | 0.35 | 25 | 0.026 | 0.04 | 93.1 |
| 1650 | 67 | 750 | 750 | 1.8 | 0.38 | 11 | 0.026 | 0.016 | 97.3 |
| 1715 | 67 | 750 | 750 | 2.3 | 0.38 | 10.5 | 0.023 | 0.018 | 97.1 |
| 1740 | 70 | 750 | 750 | 2.3 | 0.45 | 11 | 0.023 | 0.024 | 96.8 |
| 1805 | 67 | 750 | 750 | 3.05 | 0.40 | 13.5 | 0.026 | 0.0285 | 95.8 |
| 1835* | 67 | 750 | 750 | 2.3 | 0.41 | 63.5 | 0.026 | 0.05 | 91.8* |

---

* Nupro valve open only 2 turns. All other times valve was fully open. At fully open position, salt flow may be as much as 0.9 gal/min. At 2 turns, salt flow is estimated to be <0.5 gal/min.

TABLE IV. Data Summary Molten Salt Pilot Plant Run Number 6*

| Time | Gas Flow SCFM | Salt Temp. °C | Gas Temp. °C | Gas Press. psig | v/o $H_2S$ (in) | v/o $H_2S$ (out) | v/o COS (in) | v/o COS (out) | % Rec. S |
|---|---|---|---|---|---|---|---|---|---|
| 1527 | 70 | 813 | 750 | 0.6 | 0.425 | 0.060 | 0.040 | 0.094 | 74.3 |
| 1542 | 70 | 823 | 750 | 0.6 | 0.425 | 0.060 | 0.040 | 0.092 | 74.9 |
| 1612 | 74 | 860 | 750 | 0.4 | 0.530 | 0.275 | 0.054 | 0.125 | 38.3 |
| 1625 | 74 | 840 | 750 | 0.4 | 0.530 | 0.270 | 0.054 | 0.117 | 40.0 |
| 1635 | 74 | 830 | 750 | 0.4 | 0.530 | 0.285 | 0.054 | 0.120 | 37.1 |
| 1708 | 74 | 816 | 750 | 1.6 | 0.530 | 0.00595 | 0.054 | 0.0395 | 94.9 |
| 1730 | 75 | 816 | 750 | 1.8 | 0.685 | 0.0145 | 0.038 | 0.0085 | 97.4 |
| 1745 | 60 | 816 | 750 | 1.5 | 1.30 | 0.0136 | 0.061 | 0.0075 | 98.7 |
| 1820 | 55 | 816 | 750 | 1.4 | 1.38 | 0.0029 | 0.019 | 0.0125 | 99.3 |

---

* From 1445 until 1708 attempts were being made to establish salt flow. Apparently a very slight, perhaps sporadic flow existed from 1527 to 1700 hours, but at 1700 hours, a marked increase in pressure accompanied by increased recovery efficiency gave definite evidence of flow at near minimum rate ∿0.9 gal/min.

TABLE V. Variation of Inlet COS Contentration with Temperature Due to the Reaction: $H_2S + CO \rightleftharpoons COS + H_2$

| Temp. °C | Inlet COS % |
|---|---|
| 700 | 0.021 |
| 750 | 0.026 |
| 816 | 0.043 |
| 840 | 0.054 |

TABLE VI. Particle Behavior; Molten Salt Pilot Plant Run Number 3

Inlet Gas; Total Particle Burden = 0.109 Grains/SCF, % $H_2O$ = 9.1

Outlet Gas; Total Particle Burden = 0.0772 Grains/SCF,* % $H_2O$ = 4.5

Anderson Head Particle Size Distribution

| Plate No. | Wt. Gain g | Calculated Effective Cut-off Dia, μ | % | Concentration in Gas Grains/SCF | Westinghouse Spec. |
|---|---|---|---|---|---|
| 1 | 0.0048 | 17.6 | 1.5 | 0.00114 | 0 |
| 2 | 0.0042 | 11.2 | 1.3 | 0.00099 | 0 |
| 3 | 0.0327 | 7.5 | 10.1 | 0.00774 | 0.001 |
| 4 | 0.0498 | 5.3 | 15.3 | 0.0118 | |
| 5 | 0.0405 | 3.5 | 12.5 | 0.0096 | |
| 6 | 0.0381 | 1.7 | 11.7 | 0.0091 | 0.75 |
| 7 | 0.0289 | 1.0 | 8.9 | 0.0069 | |
| 8 | 0.0314 | 0.7 | 9.7 | 0.0075 | |
| Filter | 0.0948 | 0.15 EST | 29.2 | 0.0224 | |
| Total | 0.3253 | | | | |

---

* Appearance of deposits on the plates of the Anderson head is indicative of substantial salt contamination (especially on plates 5, 6, 7 and 8).

TABLE VII. Particle Behavior; Molten Salt Pilot Plant Run Number 6

Inlet Gas; Total Particle Burden = 0.074 Grains/SCF, % $H_2O$ = 11.2

Outlet Gas; Total Particle Burden = 0.0245 Grains/SCF, % $H_2O$ = 3.3

Anderson Head Particle Size Distribution

| Plate No. | Wt. Gain g | Calculated Effective Cut-off Dia, μ | % | Concentration in Gas Grains/SCF | Westinghouse Spec. |
|---|---|---|---|---|---|
| 1 | 0.0015 | 20.1 | 5.0 | 0.0012 | 0 |
| 2 | 0.0013 | 10.5 | 4.3 | 0.0011 | 0 |
| 3 | 0.0016 | 7.0 | 5.3 | 0.0013 | 0 |
| 4 | 0.0019 | 5.0 | 6.3 | 0.0015 | 0.001 |
| 5 | 0.0026 | 3.1 | 8.6 | 0.0021 | |
| 6 | 0.0029 | 1.6 | 9.6 | 0.0021 | 0.75 |
| 7 | 0.0030 | 1.0 | 10.0 | 0.0024 | |
| 8 | 0.0047 | 0.6 | 15.6 | 0.0038 | |
| Filter | 0.0106 | 0.15 EST | 35.2 | 0.0086 | |
| Total | 0.0301 | | | | |

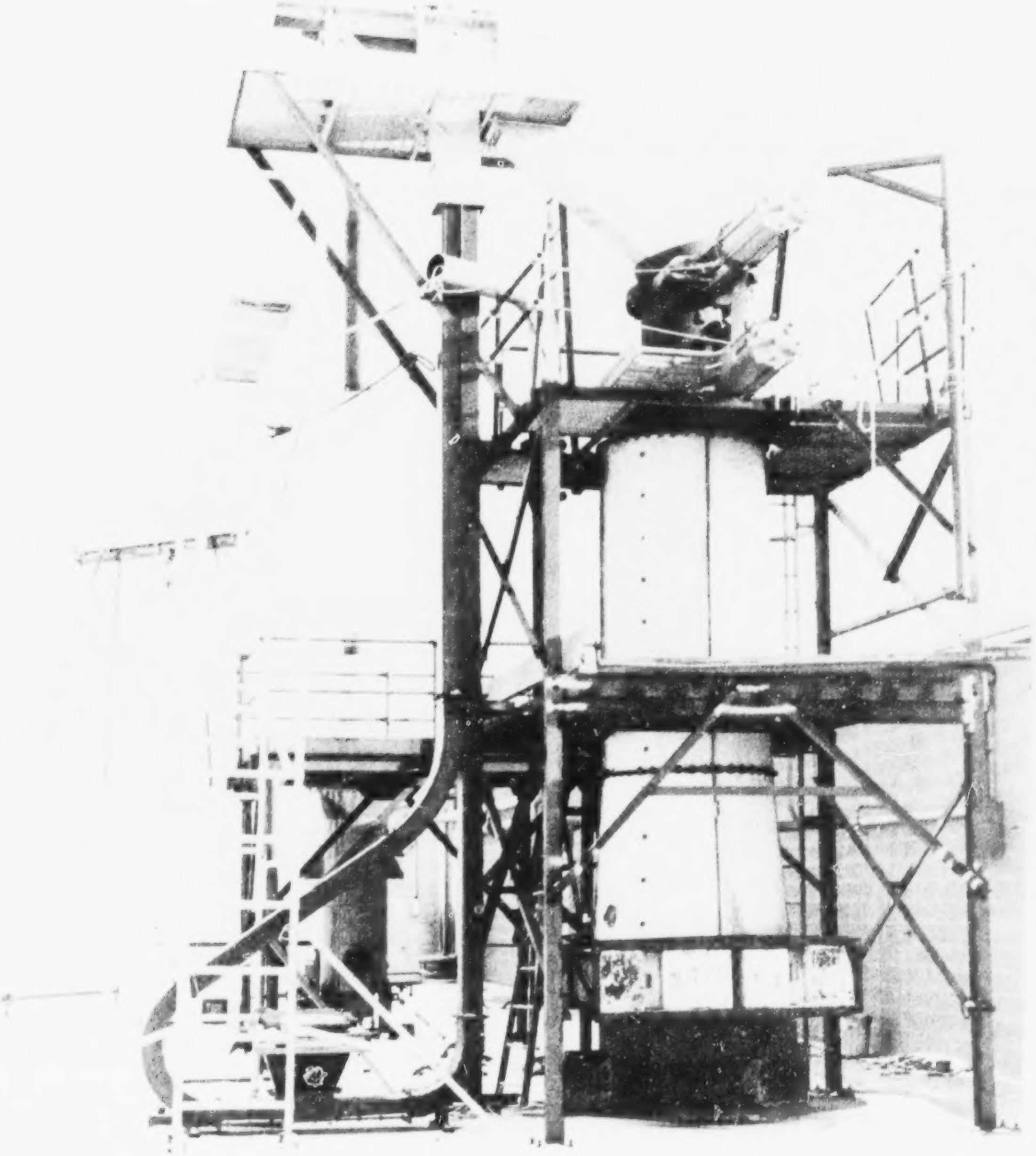

Figure 1. The Battelle Fixed Bed Gasifier During Early Construction of the PDU

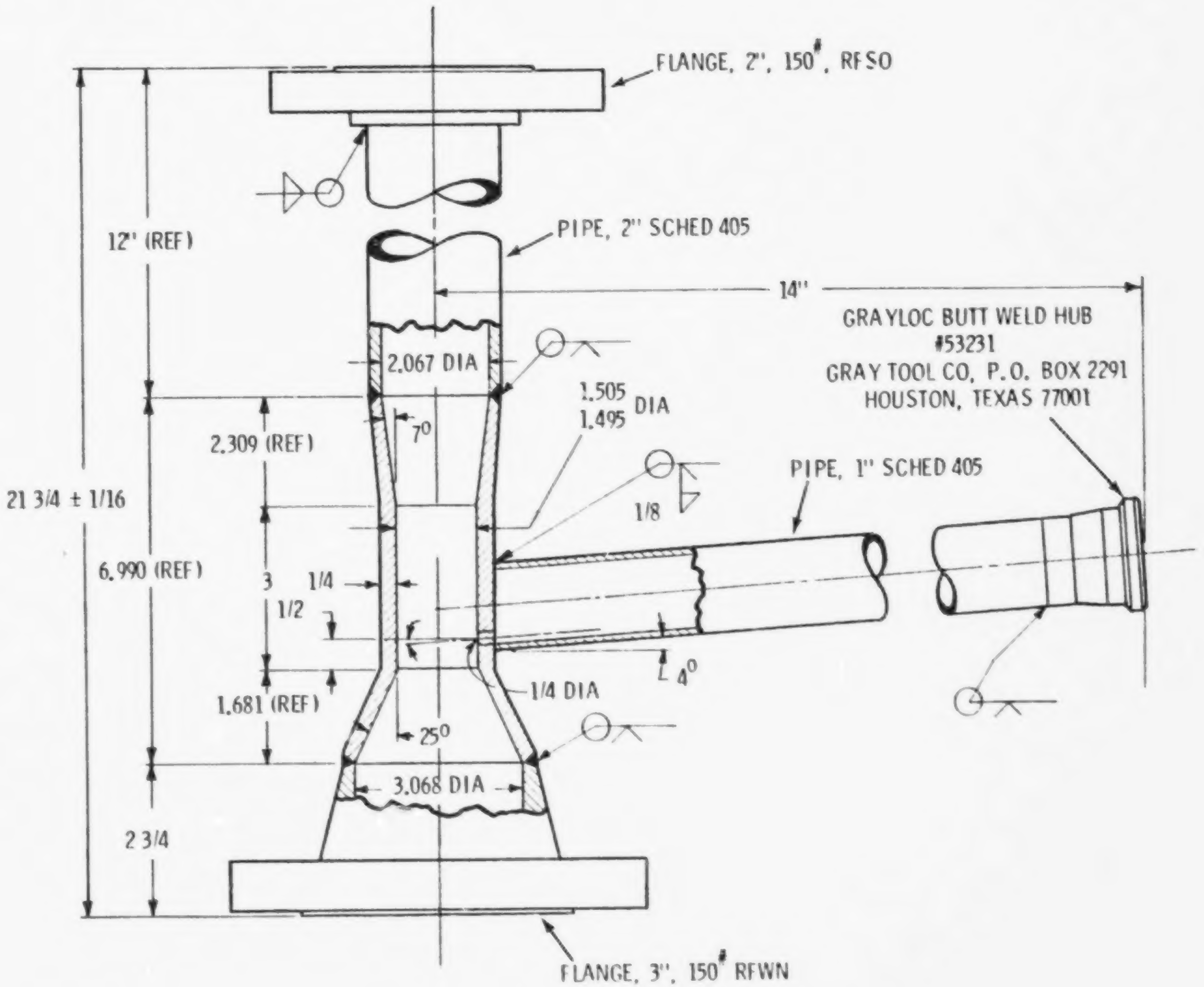
FLANGE, 2", 150#, RFSO
PIPE, 2" SCHED 405
12" (REF)
14"
GRAYLOC BUTT WELD HUB
#53231
GRAY TOOL CO, P.O. BOX 2291
HOUSTON, TEXAS 77001
2.067 DIA
1.505
1.495 DIA
7°
2.309 (REF)
PIPE, 1" SCHED 405
1/8
21 3/4 ± 1/16
6.990 (REF)
3
1/4
1/2
4°
1/4 DIA
1.681 (REF)
25°
3.068 DIA
2 3/4
FLANGE, 3", 150# RFWN

Figure 2. Schematic of Venturi Scrubber

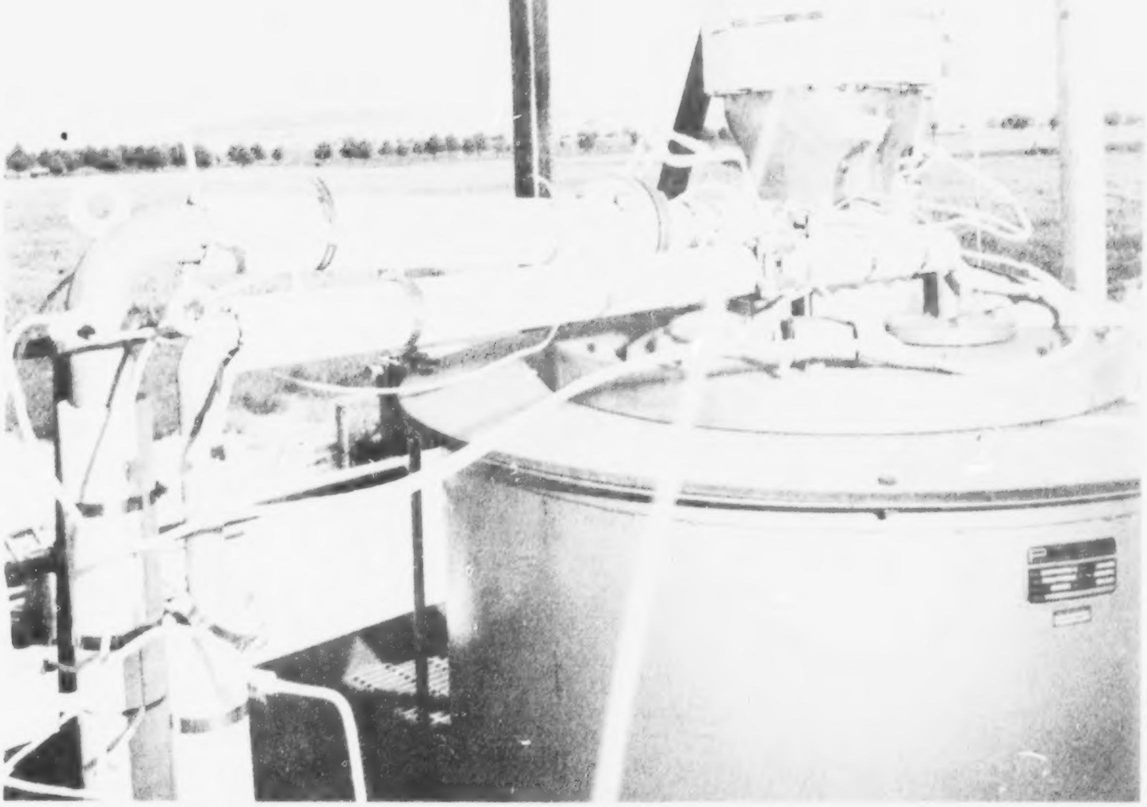

Figure 3. Packed Bed De-entrainer Assembly Showing Installation of Trace Heaters

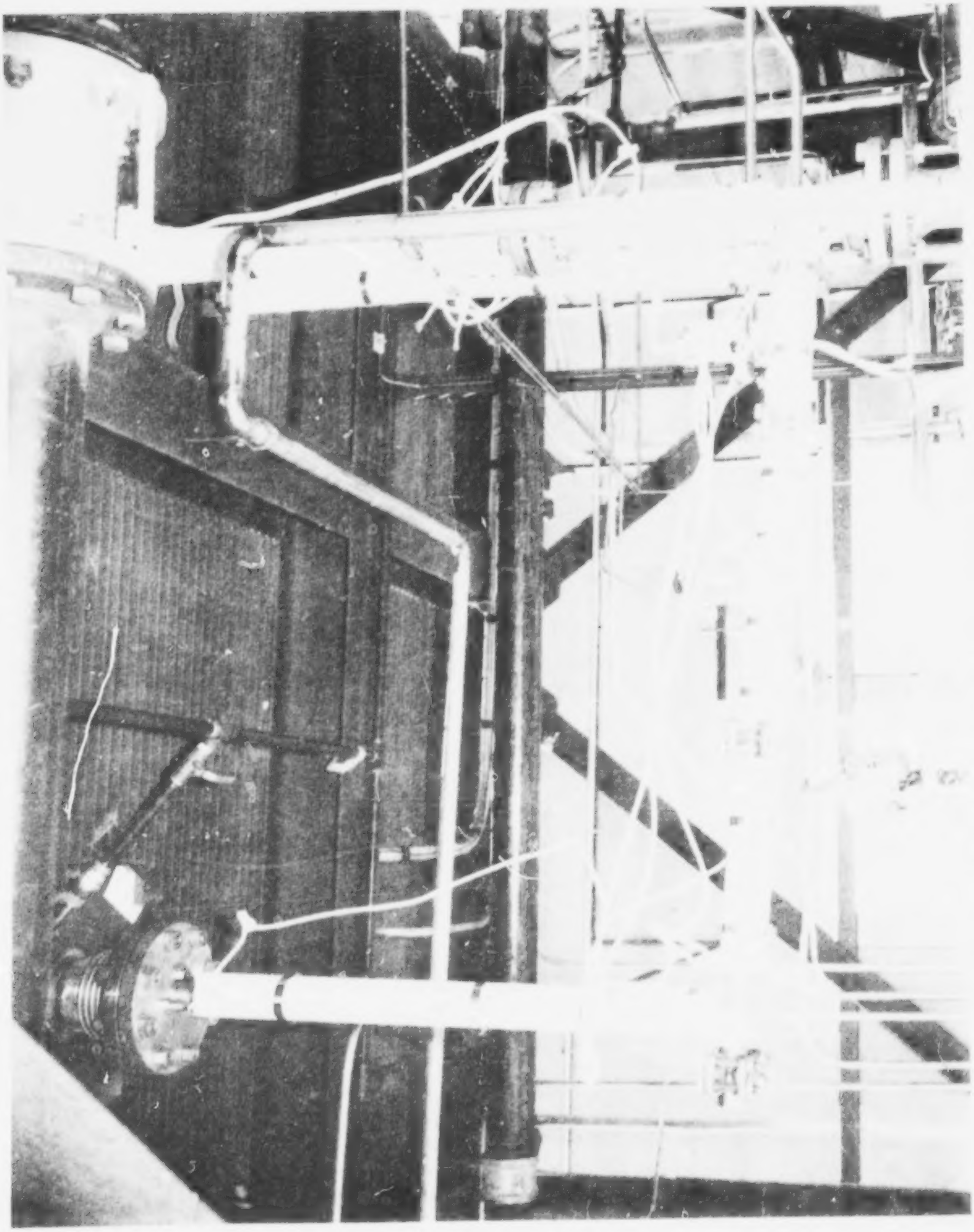

Figure 4. Installation of Trace Heaters on the Venturi Inlet Line

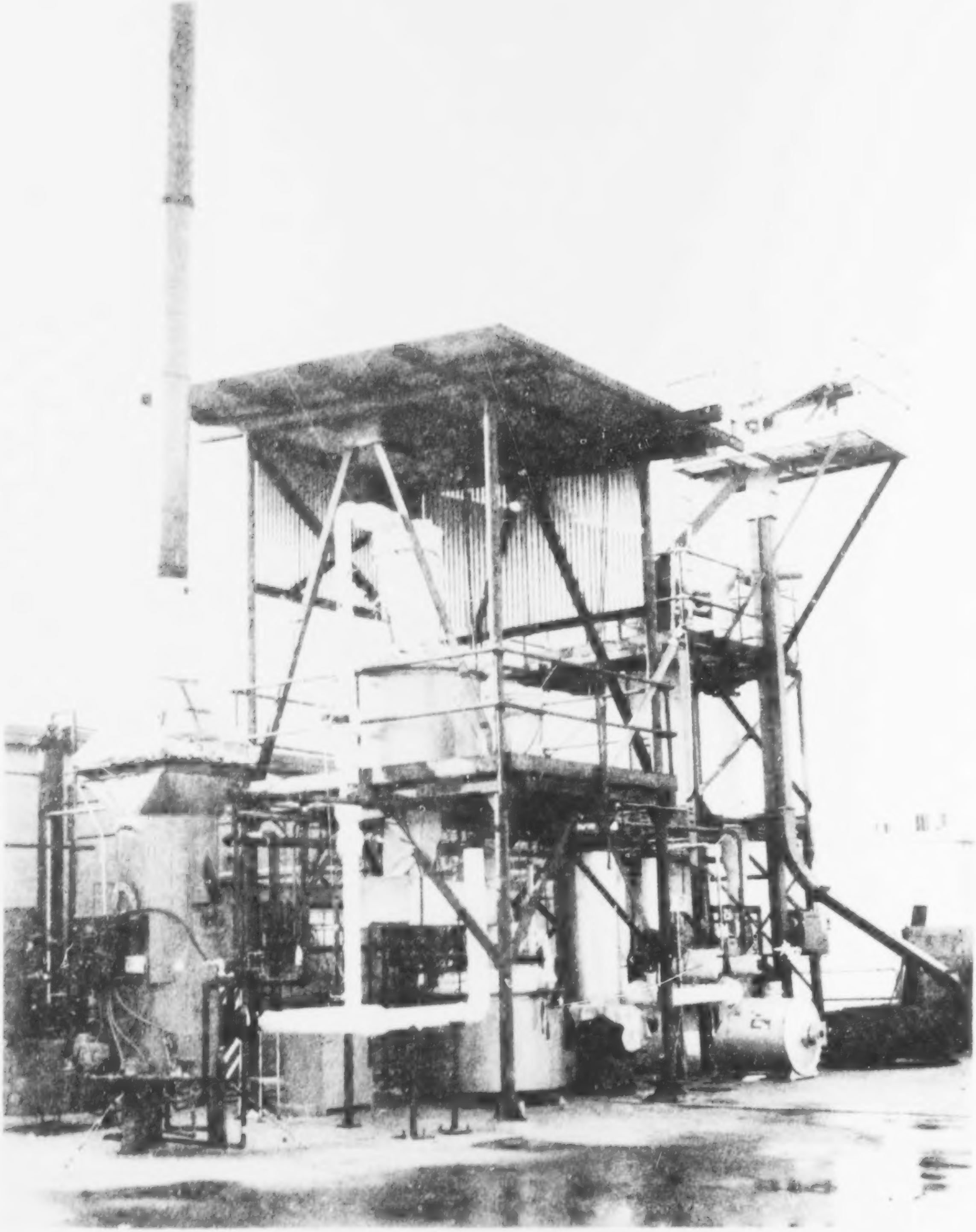

Figure 5. Completed Process Demonstration Unit
(Configured in Batch Operating Mode)

$$CaCO_3\,(\ell) + H_2S\,(g) \rightleftharpoons CaS\,(\ell) + CO_2\,(g) + H_2O\,(g) \qquad (1)$$

$$CaCO_3\,(\ell) + COS\,(g) \rightleftharpoons CaS\,(\ell) + 2\,CO_2\,(g) \qquad (2)$$

Figure 6. Reactions of $CaCO_3$ with $H_2S$ and with COS

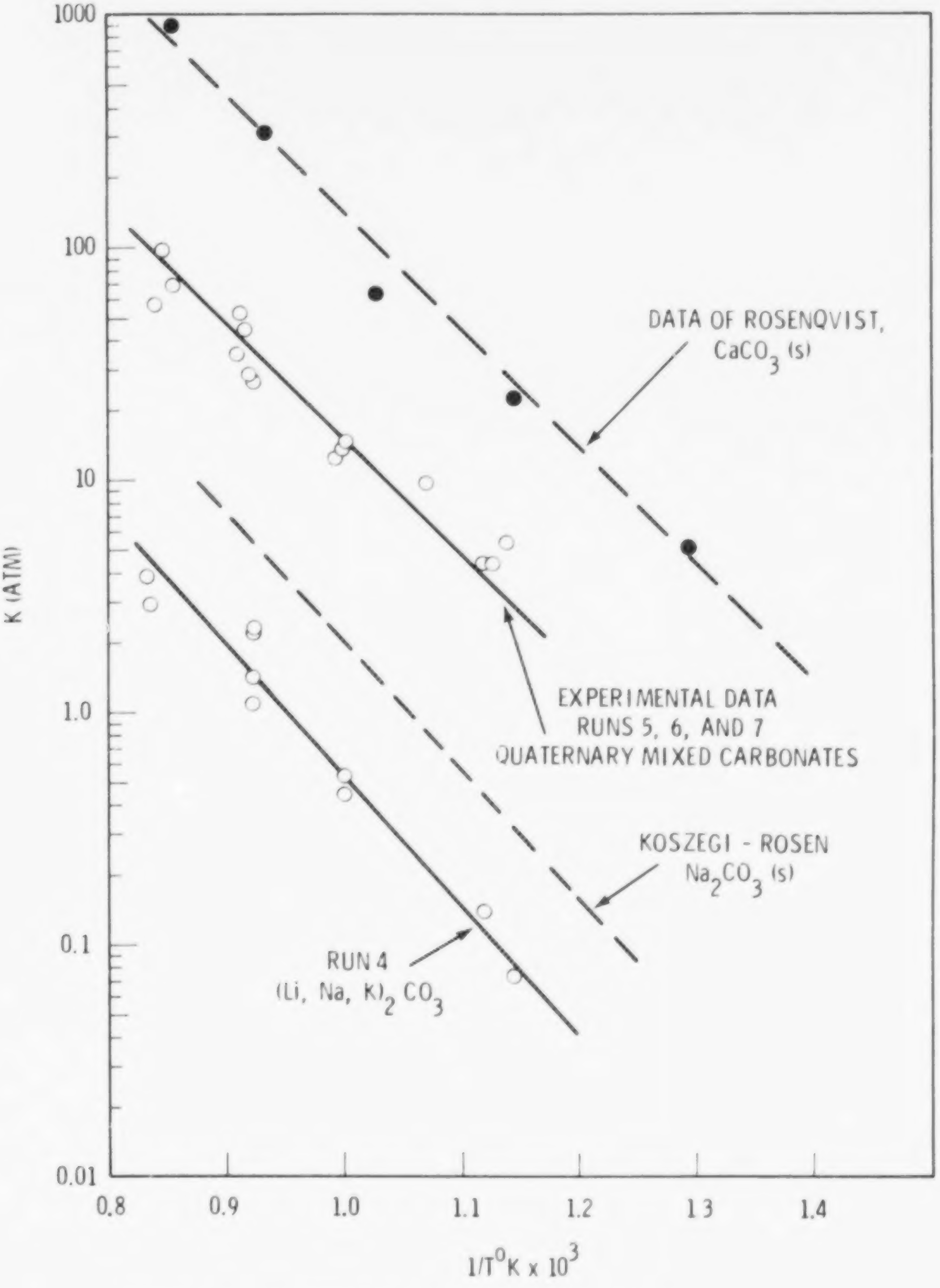

Figure 7. Temperature Dependence of the Equilibrium Constants for Reaction with $H_2S$

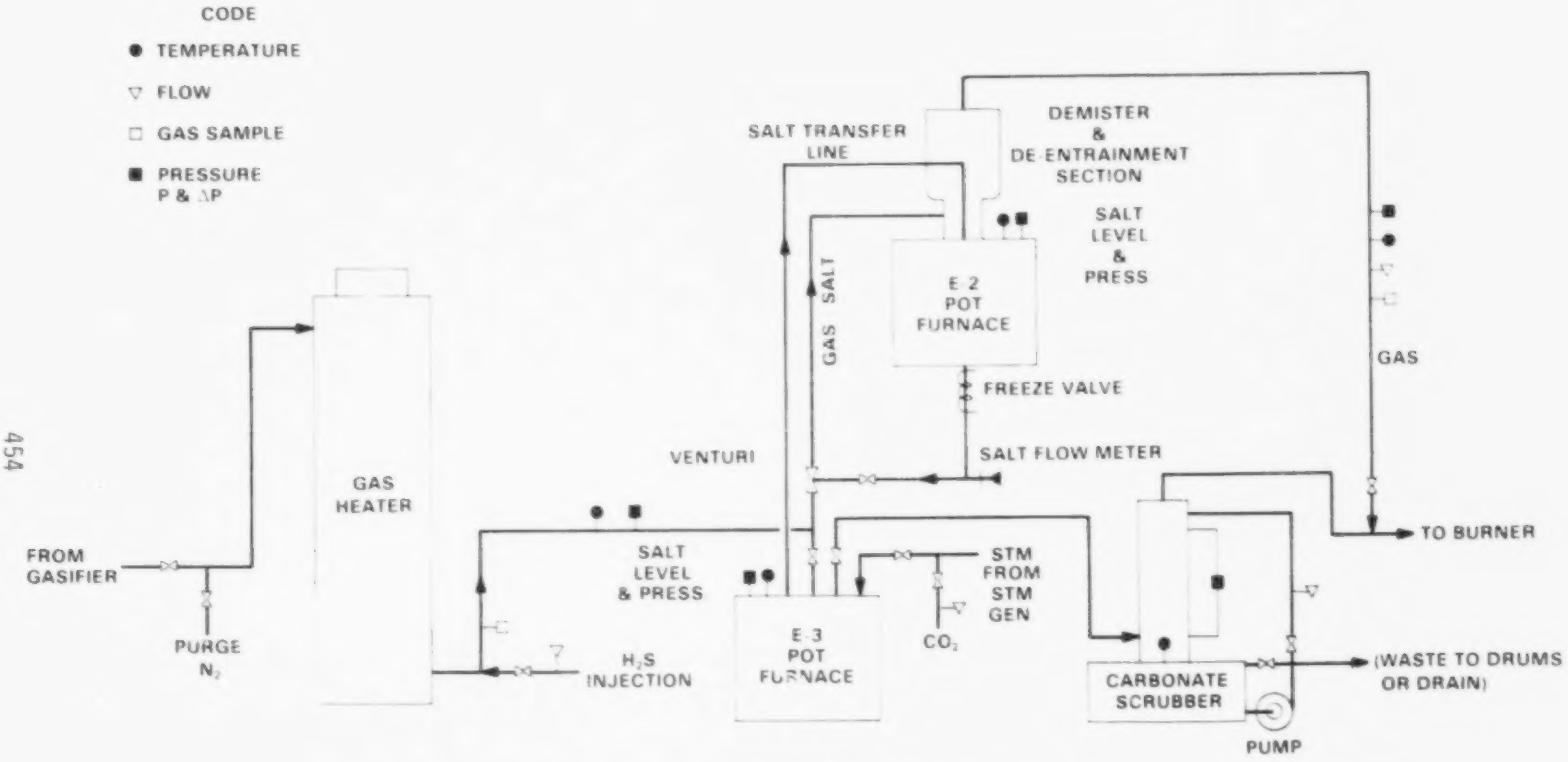
CODE
● TEMPERATURE
▽ FLOW
☐ GAS SAMPLE
■ PRESSURE P & ΔP
FROM GASIFIER
PURGE $N_2$
GAS HEATER
$H_2S$ INJECTION
SALT LEVEL & PRESS
VENTURI
SALT TRANSFER LINE
GAS SALT
E-3 POT FURNACE
E-2 POT FURNACE
DEMISTER & DE-ENTRAINMENT SECTION
SALT LEVEL & PRESS
FREEZE VALVE
SALT FLOW METER
STM FROM STM GEN
$CO_2$
GAS
TO BURNER
CARBONATE SCRUBBER
PUMP
(WASTE TO DRUMS OR DRAIN)

Figure 8. Sulfur Gas Removal System

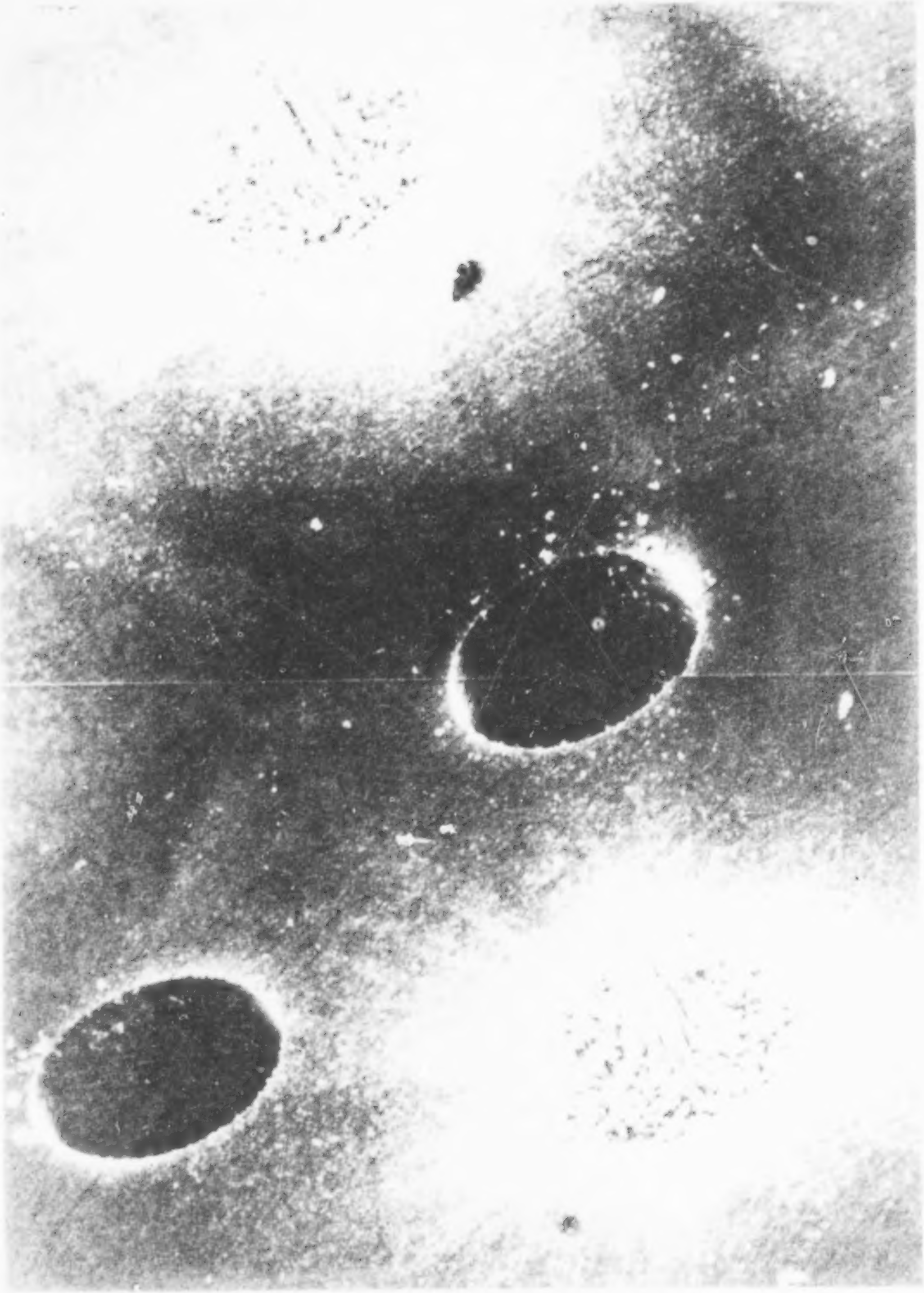

Figure 9. Deposit on Plate Number 8 at 80 X Magnification

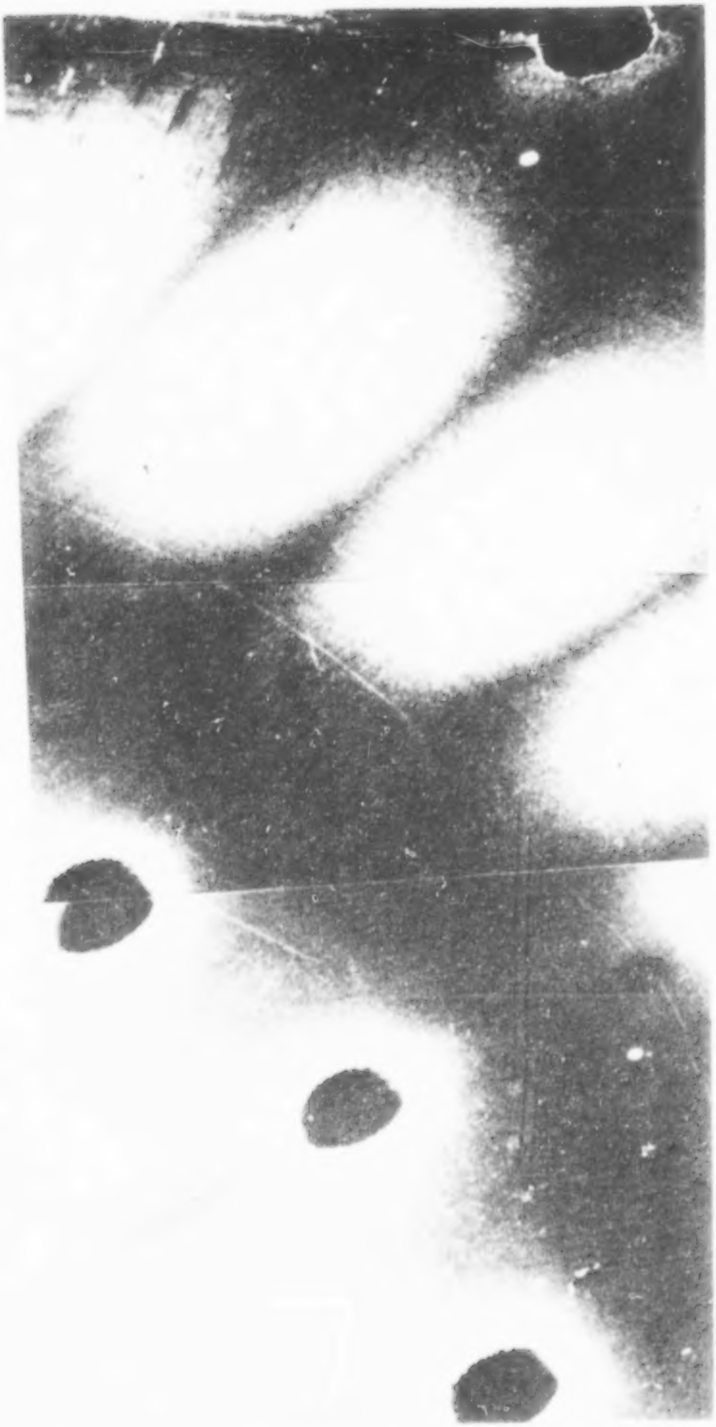

Figure 10. Composite Photo Showing Deposit on Plate Number 4 at 80 X Magnification

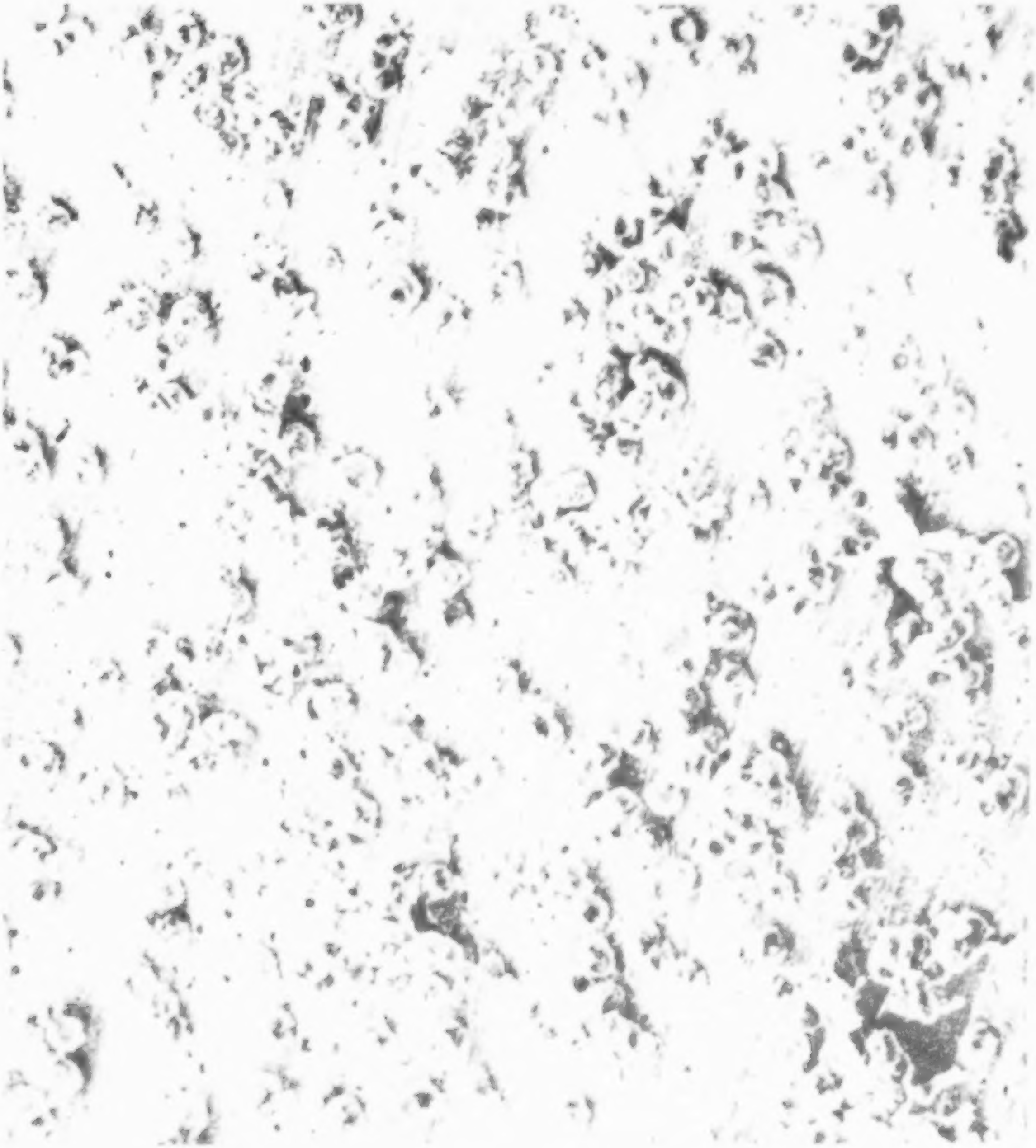

Figure 11. Scanning Electron Microscope Photo of Deposit on Plate Number 4 (2000 X)

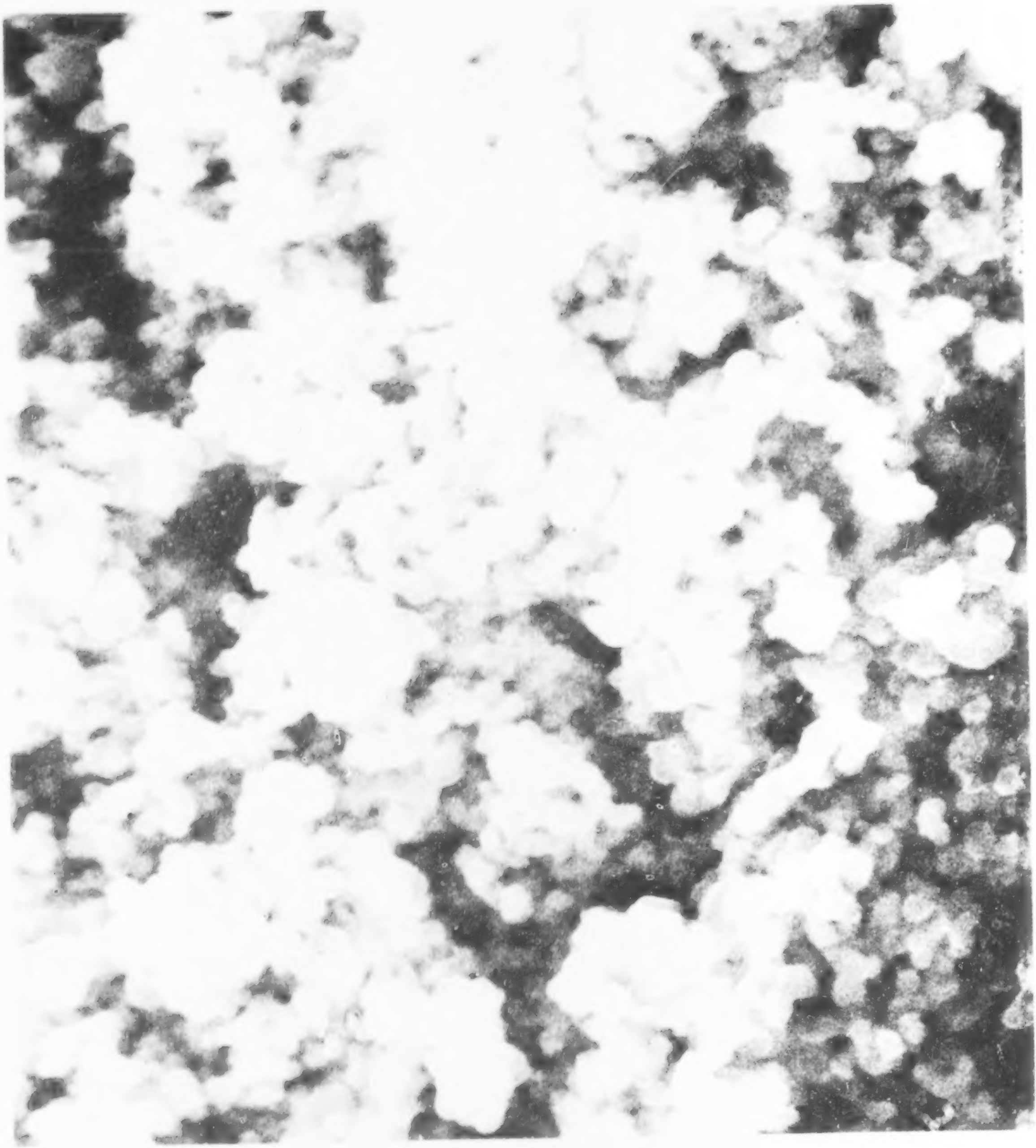

Figure 12. Scanning Electron Microscope Image of Deposit Lifted from Plate Number 8 Using Sticky Tape (20,000 X)

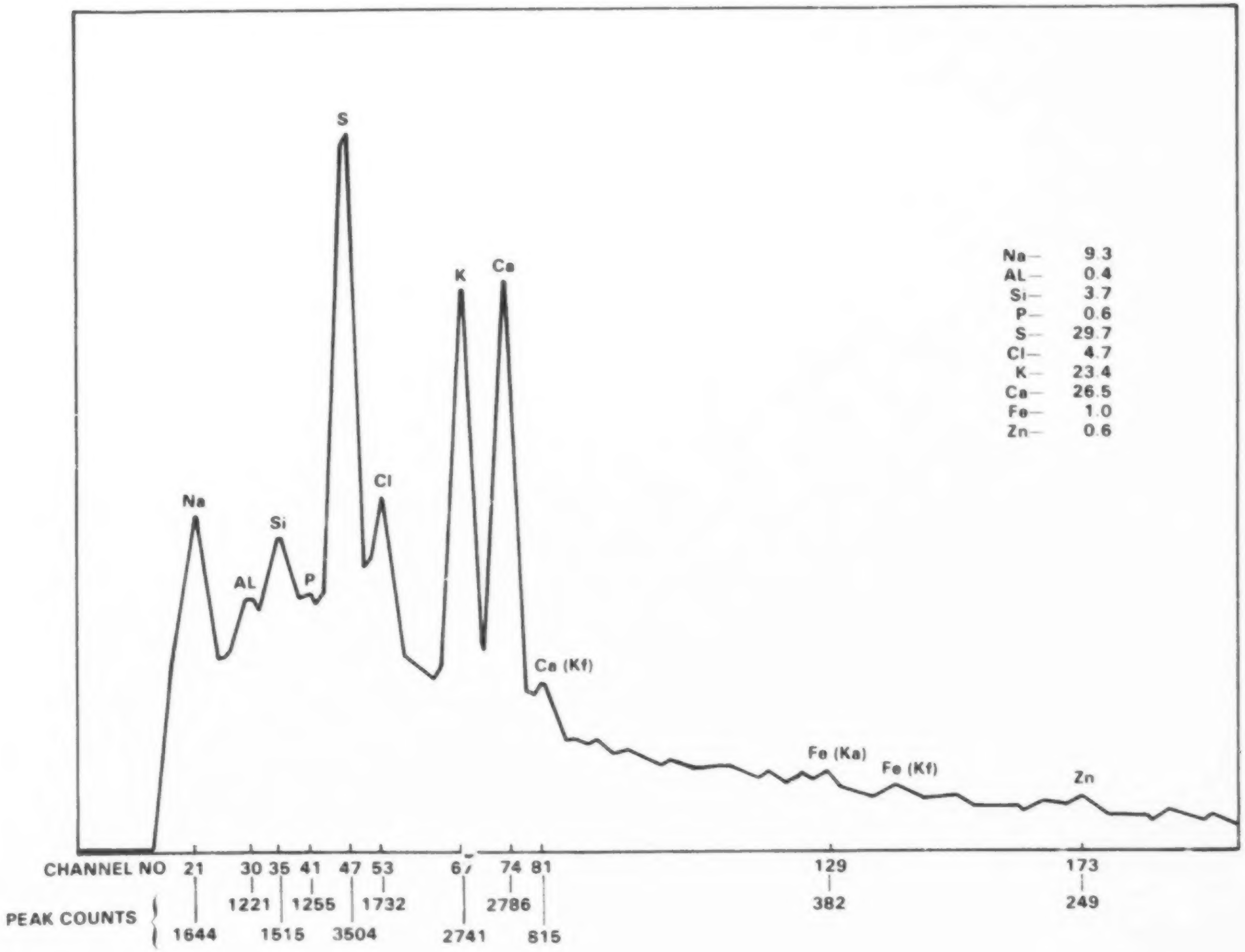

Figure 13. X-Ray Fluorescence Spectrum of Deposit on Plate 4

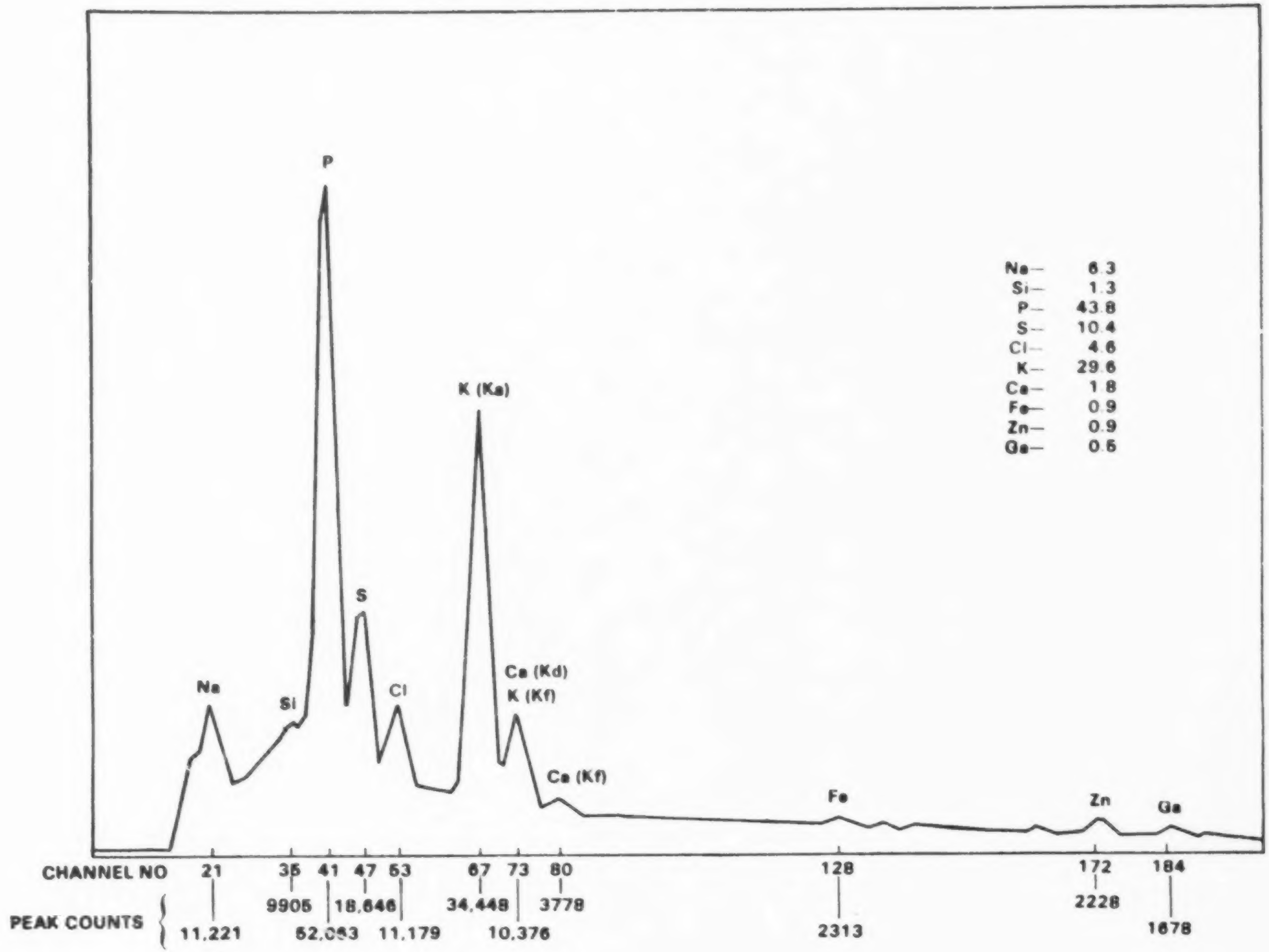

Figure 14. X-Ray Fluorescence Spectrum of Deposit on Plate 8

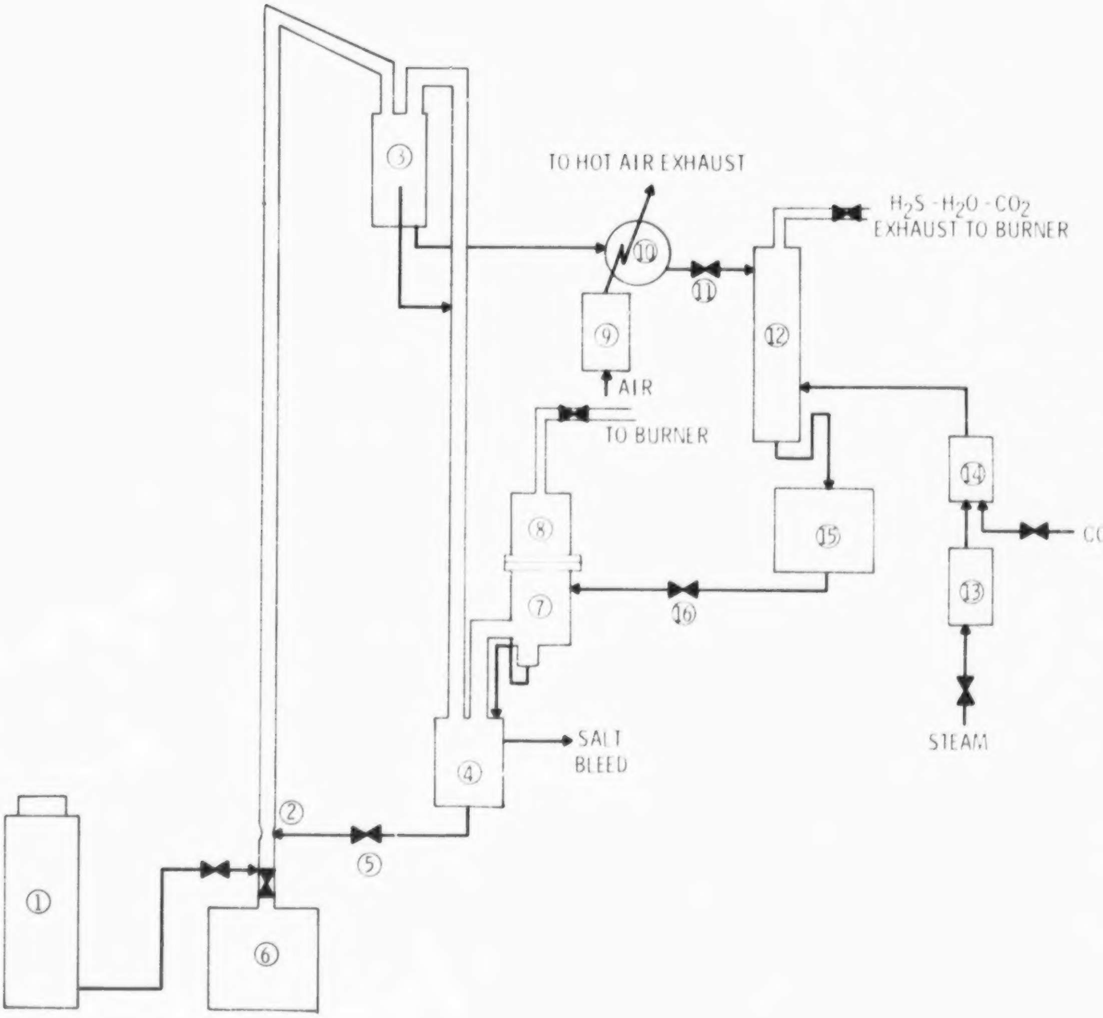
①
②
③
④
⑤
⑥
⑦
⑧
⑨
⑩
⑪
⑫
⑬
⑭
⑮
⑯
TO HOT AIR EXHAUST
$H_2S - H_2O - CO_2$ EXHAUST TO BURNER
AIR
TO BURNER
$CO_2$
STEAM
SALT BLEED

Figure 15. Process Flow Diagram

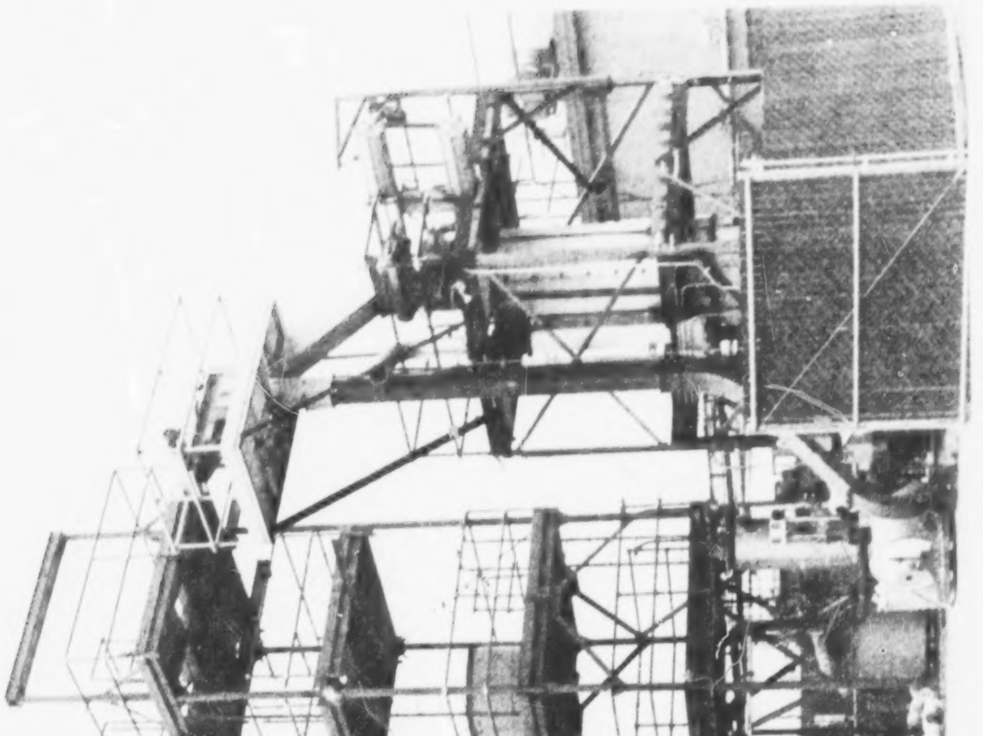

Figure 16. Support Structure (center) for Remodeled PDU

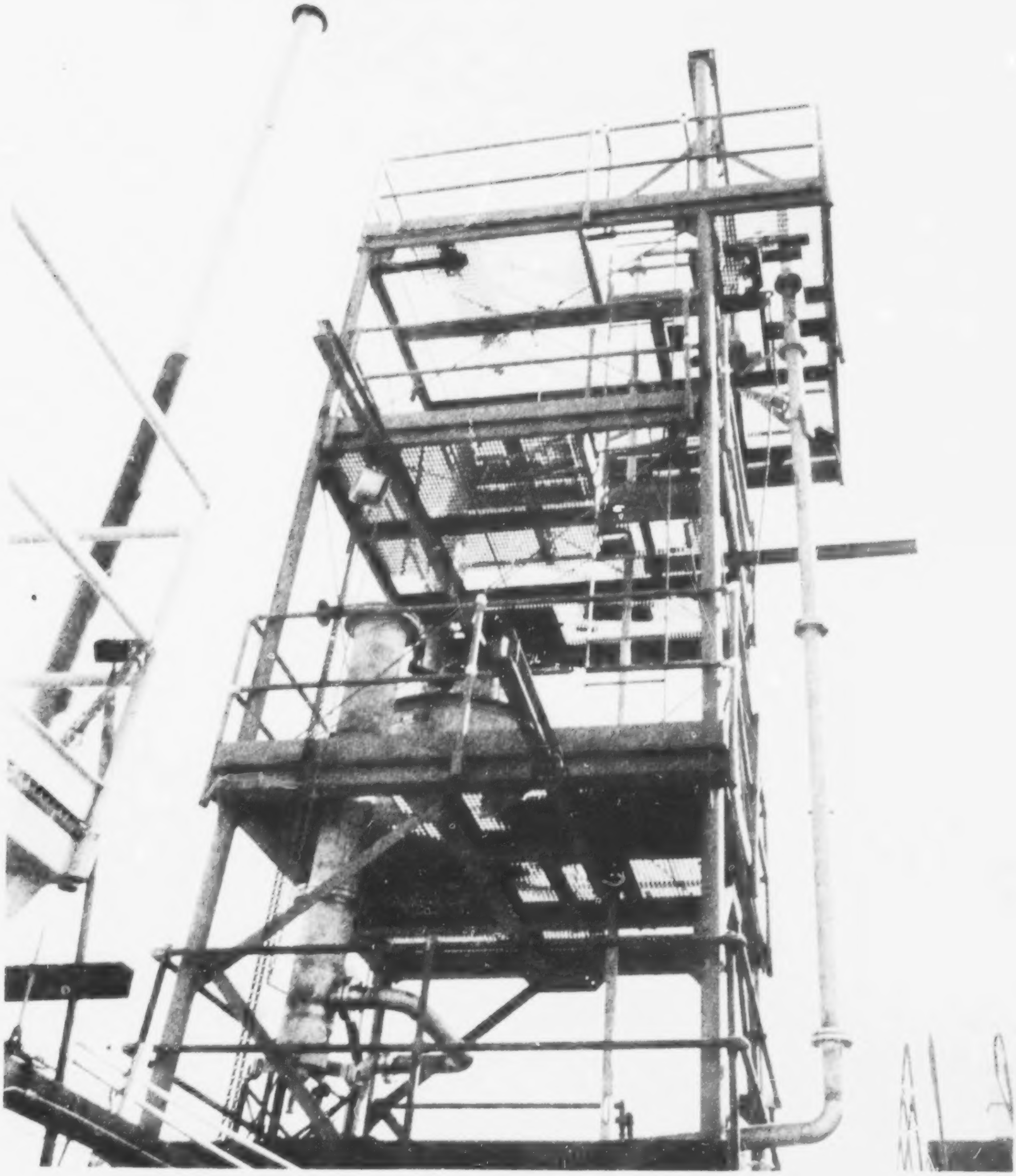

Figure 17. Support Structure Showing Preliminary Equipment Installation

# SESSION IV:

# PARTICLE SAMPLING AND MEASUREMENT

JOHN GEFFKIN
CHAIRMAN

CONF-791170--1

# PARTICULATE SIZING IN HIGH-TEMPERATURE HIGH-PRESSURE COMBUSTION SYSTEMS

By:

H. W. Coleman
Sandia Laboratories
Livermore, CA 94550

# PARTICULATE SIZING IN HIGH-TEMPERATURE, HIGH-PRESSURE COMBUSTION SYSTEMS

By:

Hugh W. Coleman
Combustion Sciences Department
Sandia Laboratories, Livermore, CA 94550

The results of a review of particulate sizing techniques for application to turbine inlet flows in advanced, open-cycle gas turbine systems fired with pulverized coal, liquid and gaseous fuels derived from coal, and heavy residual fuels are discussed. Emphasis of the study was on optical techniques, which provide nonperturbing, *in situ* measurements. It was concluded that there are presently no commercially available instruments for reliable measurement of particulate sizes in high-temperature, high-pressure flows containing a polydisperse system of particles of unknown shape, index of refraction and composition. For particulate size distribution measurement, the visibility, diffraction, intensity ratio and photography techniques were identified as the most promising for further development. Since some of the particulates in the combustor exit flow will be porous or hollow and agglomerates may contain voids, there is no reliable method for converting optically-determined number density and size distribution measurements into mass loading density values. Consequently, there appears to be no alternative to probe sampling and subsequent weighing of the particulate matter for the determination of spatial distributions of mass loading density.

# PARTICULATE SIZING IN HIGH-TEMPERATURE, HIGH-PRESSURE COMBUSTION SYSTEMS

## SECTION 1

## INTRODUCTION

A review[1] of diagnostic techniques for application to turbine inlet flows in advanced, open-cycle gas turbine systems fired with pulverized coal, liquid and gaseous fuels derived from coal, and heavy residual fuels was recently completed. This review was part of the initial phase of the Diagnostics Assessment Program conducted by the Combustion Sciences Department at Sandia Laboratories and sponsored by the Advanced Power Systems Branch of ERDA/Fossil Energy. The Interim Report[1] discussed the diagnostic requirements for advanced, open-cycle gas turbine systems and presented an assessment of current techniques for measurement of particulate size distributions and loading densities, velocity, temperature, and species concentrations in "dirty" flows. Emphasis of the study was on optical techniques, which provide nonperturbing, *in situ* measurements. The present paper discusses the results of the study which pertain to measurement of particulate size distributions and mass loading densities.

Diagnostic needs and constraints on the measurement systems will vary as the combustor/turbine program progresses. During component development, reasonable spatial resolution and accuracy are required, but rapid time response is not necessarily essential. During prototype evaluation, spatial and temporal resolution, accuracy, reliability and long lifetimes are necessary. Measurements required later for on-line system monitoring and control are not yet defined. During this phase, one would expect that less complex diagnostic systems than those required for prototype evaluation will be sufficient; but reliability, long lifetimes, and rapid time response will be required.

In the past, most particulate sizing research programs have been aimed primarily at characterization of atmospheric aerosols, sprays from nozzles (droplets in the 10 to 100 microns range), and particulates in various exhausts in the size range to be respirable health hazards (submicron to five microns). In general, the environments of interest in these programs are much less hostile than the high-temperature, high-pressure combustion systems being considered here.

The particulate sizes of interest in combustor exhausts (immediately upstream of the turbine inlet) will range from submicron to a maximum of 5 to 50 microns. The smaller particles are of interest from a health hazard standpoint, while the upper limit on size will be determined by blade erosion and impaction considerations. This upper size limit, together with permissible loading densities, will be dictated by the turbine design.

## SECTION 2

## MEASUREMENT OF PARTICULATE SIZE DISTRIBUTION

Conventional techniques (and the commercial instruments utilizing them)[2,3] as a general rule require sample withdrawal by a physical probe with subsequent dilution and/or cooling of the sample prior to sample introduction into the particulate sizing instrument. Insertion of the probe into the flow may have significant effects on the flow field in the vicinity of the probe. (For the high-temperature, particulate-laden and highly oxidative flows expected in advanced gas turbine/combustor systems, water-cooling of the probe is required --which leads to a fairly bulky sampling system.) Furthermore, dilution and/or cooling of the sample may induce substantial particle size changes in the sample due to agglomeration and condensation of gaseous species, in particular, water. Cold traps may reduce the magnitude of such errors, but particle size distribution estimates from cooled samples are not expected to be representative of the hot gas flow. It was concluded[1] that there are presently no commercially available instruments for reliable measurement of particulate sizes in high-temperature, high-pressure flows containing a polydisperse system of particles of unknown shape, index of refraction and composition.

There is, however, a sizable amount of research underway on various laser-based optical techniques for particulate sizing, and several of these appear promising for application to the present problem. These techniques are nonperturbing in that no physical probe is inserted into the flow; however, they do require optical access to the flow. The problems associated with providing adequate optical access are not explicitly considered in the following discussion.

The optical particulate sizing methods can be broadly categorized into imaging (photography, holography) and scattered light techniques. The range of applicability of the second category of techniques considered is related directly to the physics of light scattering processes. In order to discuss these range limitations it is useful to briefly consider the Mie theory of light scattering from spherical particles. Then various optical techniques for particle sizing and their application to the present problem will be examined.

## MIE THEORY

Descriptions of the Mie theory of light scattering are given in the books by van de Hulst[4] and Kerker.[5] Mie theory is an exact solution of Maxwell's equations for the scattering of electromagnetic radiation. In the discussion below, which will be restricted to spherical particles, the following definitions will be required:

$\lambda$ = wavelength of incident light

$m = n - ik$ = complex refractive index of the scatterer

$d$ = diameter of scatterer

$\alpha = \pi d/\lambda$ = optical size of scatterer

$I$ = intensity of light

$r$ = distance from scatterer to detector

The geometry to be used for the discussion of light scattering is shown in Figure 1. The linearly polarized incident light wave propagates along the z axis in the positive direction with its electric vector, $\overline{E}$, parallel to the x axis and its magnetic vector, $\overline{H}$, parallel to the y axis. The plane of polarization of the incident light is designated as the plane containing the electric vector and the propagation vector (the xz plane). The scattering direction, defined by $\overline{r}$ in the figure, is taken from the origin of the scatterer to the point of observation. The angle $\theta$ is measured from the forward direction (direction of propagation) to the direction of observation (defined by $\overline{r}$), and the angle $\phi$ is measured from the plane of polarization to the scattering plane, defined by the propagation vector and vector $\overline{r}$.

For unit incident light intensity, the expressions for the scattered light intensity polarized in the directions perpendicular and parallel to the scattering plane are, respectively:

$$I_{\perp} = I_0 \lambda^2 / 4\pi^2 r^2 \, |S_1(\theta, m, \alpha)|^2 \sin^2\phi \qquad (1)$$

$$I_{||} = I_0 \lambda^2 / 4\pi^2 r^2 \, |S_2(\theta, m, \alpha)|^2 \cos^2\phi \qquad (2)$$

The $S_1$ and $S_2$ functions are the complex amplitude functions calculable using Mie theory. Particles of general shape require calculation of two additional amplitude functions.

If an experiment is arranged such that $\phi = 90°$, where the plane of observation is perpendicular to the polarization vector of the incoming beam, then Equations 1 and 2 give $I_{||} = 0$ and $I_{\perp}$ equals some non-zero value. Thus, for a spherical particle, the scattered light is polarized in the same plane as the illuminating radiation. This is not true in general for a nonspherical particle, and this fact can be used as a qualitative indication of the deviation of a particle's shape from spherical. Jones and Wong,[7] for instance, used shape and polarization characteristics as an indicator that soot particles form elongated agglomerates in flames.

For scattering from small particles, Mie theory reduces to Rayleigh scattering in the lower optical size limit ($\alpha < 0.3$ or $d < 1/10$ the incident wavelength). In the larger optical size limit (exact $\alpha$ of this limit is dependent on m), the forward scattering pattern calculated from Mie theory corresponds closely to Fraunhofer diffraction, with the forward lobe intensity increasing in amplitude and decreasing in angular spread as particle size increases. In the Rayleigh range, scattered intensity increases as the sixth power of the particle diameter and the inverse fourth power of $\lambda$. With increasing $\alpha$, the scattered intensity increases less rapidly with diameter and becomes increasingly forward-directed. An array of lesser maxima and minima in intensity develops in addition to the large forward maximum. For nonabsorbing particles (when $k = 0$, so that m is real), the number of maxima between $\theta = 0°$ and $180°$ is $\approx \alpha$. Absorbing particles ($k > 0$, so that m is complex) exhibit less intensity oscillation with $\theta$, so that the curve of intensity versus $\theta$ is smoother. The variations of $I_{\perp}$ and $I_{||}$ with $\theta$ and $\alpha$ for a nonabsorbing sphere[8] are shown in Figure 2 as an example of scattered light patterns.

For the case of multiple scatterers in a region, the scattered intensities from each of the particles add in the scalar sense to give the total observed scattering if the effects of multiple scattering (secondary scattering of the originally scattered light) are small. As particle loading densities increase, multiple scattering effects cause increasing deviation from the summation of individual scattered intensities.

Shape effects on the scattering from nonspherical particles are minimized if the resultant scattering is from a large number of particles with random orientation. For example, the Fraunhofer diffraction patterns from individual nonspherical particles (with $\alpha$ large) vary significantly with shape, but the resulting forward diffraction lobe for a collection of nonspherical, randomly oriented particles does not differ greatly from that for a collection of spheres equal in projected area to the collection of irregular particles.[7]

## DISCUSSION OF TECHNIQUES

The discussion of individual techniques based on various characteristics of light scattering will not cover all the methods of this class which have been proposed. A comprehensive discussion of all such work reported in the literature would fill a volume by itself. The emphasis in this discussion will be on the methods which have potential application to a high-temperature, high-pressure flow containing particulates of unknown refractive indices and which have a polydisperse distribution.

Several techniques should be mentioned in addition to those to be discussed in detail. The first of these is the light extinction (or transmittance) technique, which is reviewed in detail by Hodkinson.[7] The basis of the method is to measure the percent of the incident light scattered and absorbed or, equivalently, the percent of the incident light transmitted through a volume containing scatterers. According to Hodkinson, for a polydisperse system with particle sizes larger than ∿ 1 micron (for visible light) the total area projected by the particles can usually be determined without prior knowledge of size, shape or refractive index. The mean particle size (but not size distribution) can be calculated if particle number density or mass concentration is known. If the refractive index of the particles is known, both mean particle size and number density can be determined from transmittance measurements at several wavelengths.

Another approach for large particles ($d > 2$-$5\ \mu$) is relating the amplitude of the scattered signal to particle size. Yule, et al.,[9] relate particle diameter to forward-scattered signal amplitude from a particle traversing the measuring volume of a crossed-beam laser Doppler anemometer as a function of collection angle (aperture size). This method requires knowledge of refractive index. Durst and Umhauer[10] use a white light source and 90° collection in a method relating signal amplitude to particle diameter. They report excellent comparison of measured size distributions of particles of known refractive index using the optical method and electron microscope measurements. Their results extended down to the submicron diameter range.

Penner, et al.,[11,12] have reported results from recent work, both theoretical and experimental, relating the frequency distribution of measured photocurrent power spectra to particle size. This approach, with further development, may have potential over a fairly wide range of particle sizes.

Specific classes of methods discussed in more detail below are photography, holography, visibility, ratios of angular intensities, and diffraction.

### Photography

This is a fairly standard technique using either a spark or pulsed laser beam to illuminate the system of interest, as in Figure 3. The collection system can be designed to magnify the particle images if necessary before transmission to the recording device. Images may be recorded on film or by a television-type camera with a videotape recorder. Commercial instruments are available for semi-automatic or automatic analysis of particle sizes from recorded images. Cadle[3] provides a description of several of these systems.

An indication of the lower size resolution limit for photographic systems can be obtained from the Rayleigh criterion

$$d_{min} = (1.22\ \lambda\ f)/D \qquad (3)$$

where f and D are the focal length and diameter of the collecting lens, respectively. For an f/2 lens and taking $\lambda = 0.5\ \mu$, $d_{min} = 1.22\ \mu$. This value is for an ideal optical system. It is generally agreed that the lower limit on resolution using visible light is in the $d \gtrsim 2\text{-}5\ \mu$ range.

The maximum illumination pulse width for a particle of known size and velocity can be determined as follows: if a permissible movement of the particle is taken as, say, 10% of its diameter during the pulse duration, then a 10 μ diameter particle moving at 50 m/s would require a pulse of maximum duration equal 20 ns. The energy per pulse required is determined by the optical arrangement and the sensitivity of the recording system.

Disadvantages of the photography approach for the present application are its limited sensitivity to small particles, the low f/D collecting lenses required, and the narrow depth-of-field when large magnifications are used. Advantages are its insensitivity to refractive index, applicability to relatively heavy particle-loading densities, relative simplicity of the optical arrangement, and relatively unambiguous determination of size and shape for large particles. This technique can be applied in a "real time" mode by use of a TV-type camera, subsequent digitization of the output signal, and interfacing with a properly programmed minicomputer.

### Holography

A description of laser holography applied to particle size measurement is contained in the recent review article by McCreath and Beer.[14] A schematic of a holography system is shown in Figure 4. A hologram is formed by splitting a laser beam into a beam which illuminates the object and a reference beam which is reflected with phase unchanged. Both beams fall on the holographic emulsion, with the phase difference between them (caused by the object) forming an interference pattern on the emulsion. The image is reconstructed by illuminating the hologram. A wave pattern formed behind the hologram appears as an image of the original object.

Advantages of holography in particle-sizing[14] are that there is little depth-of-field restriction and that upon projection of a hologram the magnification of particles separated along the original optical axis is uniform. Holography has been used to measure particle sizes down to the 5-10 μ diameter range. The pulse width requirement for moving particles is the same as that presented earlier in the photography discussion.

Disadvantages of the holography technique are its complexity (as compared with photography), the time required to obtain size information (as compared with potential real-time operation of the photography method), and the limitation to large particles.

### Visibility

The visibility method relates particle diameter to the degree of modulation of the Doppler-shifted signal from the particle as it traverses a measurement volume formed by two laser beams which intersect with a small angle between them. The frequency information in the signal used to determine visibility can be processed by the electronics of a laser Doppler velocimeter (LDV) system to determine particle velocity.

The system used to provide visibility information is shown schematically in Figure 5. A laser beam of wavelength $\lambda$ is split into two equal intensity beams, which are focused and intersect at angle $\psi$ to form a measurement volume. Interference of the two coherent beams forms a fringe pattern in the volume with fringe spacing $\delta$ given by

$$\delta = \lambda/(2 \sin \psi/2) \tag{4}$$

As the particle moves through the fringe pattern, a modulated signal results as illustrated in Figure 5. The visibility of the signal is defined as

$$V = \frac{I_{max} - I_{min}}{I_{max} + I_{min}} \tag{5}$$

As the technique was originally formulated by Farmer,[15] the intersection angle $\psi$ was small (1-2°) and the scattered light collected either by on-axis backscatter or forward scatter. By assuming the particle was spherical, located at the center of the measurement volume, and using approximations accurate for $d/\delta \leq 2$, Farmer obtained a closed-form solution for the visibility as

$$V = 2J_1(\pi\ d/\delta)/(\pi\ d/\delta) \tag{6}$$

where $J_1(\pi\ d/\delta)$ is a first-order Bessel function. This solution is plotted in Figure 6. As represented by Equation 6, the visibility is independent of index of refraction. It is also evident from Figure 6 that particle diameter is an unambiguous (single-valued) function of visibility only for $V \gtrsim 0.2$.

Since Farmer's original proposal, there has been much additional research, both experimental and analytical, on the technique. Orloff, et al.,[16] and Yule, et al.,[9] have experimentally observed much higher values of visibility for $d/\delta > 1$ than Equation 6 would predict. Durst and Eliasson[8] have published theoretical calculations which show the same result. Both Robinson and Chu[17] and Hong and Jones[18] have published analytical results showing visibility to be a function of aperture size. In addition, it was shown[18] that visibility also has a strong dependence on refractive index under certain conditions.

In a recent paper, Roberds[19] reported both analytical and experimental results based on the visibility technique. For large spherical particles ($d \gg \lambda$) and carefully designed collection optics geometry, he concluded that the visibility method used in the forward scatter configuration could be used to reliably size single particles. He also concluded that backscattered light was unreliable for sizing by this method.

A particulate sizing system based on the visibility technique and designed by Spectron Development Laboratories was recently used to determine particulate sizes in the flue gas from a fluidized bed combustor at Argonne National Laboratory. This work is discussed in another paper at this symposium.

The visibility technique is dependent on having only one particle in the measuring volume at any one time. For measuring volumes with dimensions typical of most LDV systems, this translates to particle loading densities of the order of $10^4$-$10^5$ particles/cm$^3$. However, one must be careful in using particle loading density figures without considering the corresponding distribution of sizes. In combustion systems where small particles ($d <$ .1-.2 μ) are present in addition to larger particles ($d >$ 1-2 μ), signals from the smaller particles in the measuring volume will contribute to the background noise when compared with the Doppler signals from the large particles. The effect of this background can be eliminated or minimized in many cases by careful signal analysis and system design.

## Ratios of Forward-Scattered Intensities

This method, first proposed by Hodkinson,[21] uses the ratio of the intensities of light scattered at different angles from the forward direction to determine particle size. A laser beam is focused into the flow system, and the scattered light is collected at desired angles from the forward direction by use of apertures and light pipes, lens and mirror arrangements, or an array of photodetectors.

In further developing this technique, Gravatt[22] presented results of Mie calculations for spherical particles over a refractive index range of 1.33 to 2.0 for the real component and 0.0 to 4.0 for the imaginary component. Figure 7 shows results he obtained for $I_{10°}/I_{5°}$ (where $I_\theta$ is the intensity of light scattered at angle $\theta$ from the incident beam), with unpolarized incident radiation and no detector aperture assumed. The error envelope includes all ranges of refractive indices used in the calculations. Gravatt suggested a cut-off based on intensity at $\alpha = 19$ for $I_{10°}/I_{5°}$ measurements to avoid the multiple-valued function problem at larger $\alpha$ shown in the figure. Based on his calibrations and experimental results with a variety of particulate materials, he concluded the technique was relatively insensitive to particle shape and that within the range of applicability of the method the total sizing error was no greater than 20%.

Hirleman, et al.,[23] extended the ratio technique by using two ratios, $I_{12°}/I_{6°}$ and $I_{6°}/I_{3°}$, in order to avoid the ambiguity caused by the increase in ratio as $\alpha$ becomes large. They developed a data acquisition scheme which allowed real-time particle size analysis in automobile exhausts.

Results of Mie theory calculations by the author for spheres with a refractive index typical of soot ($m = 1.57 - 0.56\ i$) are shown in Figure 8. These calculations assume no collection aperture and incident radiation linearly polarized perpendicular to the scattering plane. The smoothness of the curves is characteristic of absorbing particles. If incident radiation with $\lambda = 0.488\ \mu$ is assumed, an $\alpha$ of 30 corresponds to a particle diameter of 4.7 $\mu$. Figure 8 shows that by measuring intensity ratios between $I_{4°}/I_{2°}$ and $I_{12°}/I_{6°}$, particles with diameters between approximately 0.6 $\mu$ and 4.7 $\mu$ could be sized.

Hirleman[24] pointed out a significant source of error which affects the ratio technique and possibly other light scattering methods as well. The sensitive volume from which valid signals are obtained is a function of both particle size and index of refraction. Calculations[24] of the ratio of the sensitive area $A_s$ at the beam focal point to the $1/e^2$ area are shown in Figure 9 versus particle diameter for two values of index of refraction assuming 12° scattering. If this effect is not considered carefully in both system design and data reduction, the resulting uncertainties can easily render the data worthless.

Advantages of the ratio technique are its relative insensitivity to index of refraction (see preceding paragraph, however), its apparent low sensitivity to particle shape (though this aspect needs more definition), and the acquisition of real-time information. A disadvantage is its limitation to loading densities low enough for acquisition of single-particle signals, though the comments made in this respect about the visibility method also apply to the ratio technique.

## Diffraction

This technique determines the size distribution of particles within the cylindrical volume formed by a laser beam passing through a flow system from the total Fraunhofer diffraction pattern from the particles within the volume. The size distribution can be calculated by matrix inversion or a least squares determination of parameters in an assumed size distribution law. The method is described in the review by McCreath and Beer,[14] and results using the technique were reported by Swithenbank, et al.[25] An instrument based on this principle and built by Leeds and Northrup was described by Wertheimer.[26] Application of this instrument to the fluidized bed combustor at Argonne National Laboratory is reported in other papers at this symposium.

Using visible laser light, the method is applicable for particles of diameter greater than about 2 μ. Movement of the particles does not alter the diffraction pattern, since the collection lens focuses parallel (undiffracted) light on the axis and a given diffraction angle results in a constant radial displacement in the focal plane. Size determination in real time is possible by using an array of photo-detectors in the focal plane to measure the diffracted light energy distribution. Signals from the detector array can be processed by a minicomputer to provide size distributions.

Advantages of the method are its relatively simple optical arrangement, real-time operation, insensitivity to particle shape if the particles are randomly oriented, independence of refractive index and applicability to relatively high loading densities. Disadvantages are the limitation to particles greater than about 2 μ in diameter and the large measurement volume--it is a line-of-sight rather than point measurement technique.

Self, et al.,[27] have reported on a sizing system under development using the diffraction pattern from single particles. The system uses an expanded, truncated laser beam and cylindrical lenses to provide an almost uniform intensity in the measurement volume. Collection of scattered light at 90° in a gating-discrimination channel assures a well-defined measurement volume size. The system has been calibrated with pinholes and polystyrene spheres. This method appears very promising for single-particle measurements for diameters greater than approximately 2 μ.

## SECTION 3

## MEASUREMENT OF PARTICULATE MASS LOADING DENSITY

As discussed by Coleman, et al.,[1] both the absolute value of mass loading density and its spatial distribution at the turbine inlet are critical factors in the operation of a coal combustor/gas turbine system.

It seems practical to use optical techniques to measure particulate number density in given size ranges. Number densities could be determined by using, say, the single-particle measurements of particle size distribution and the velocity measurements from an LDV system. By knowing the volumetric gas flow rate through the measurement volume and the number of single-particle signals per unit time, the number density within a given size range could be calculated. The variation of true measurement volume size with particle size[23,24] would have to be taken into account in this procedure.

However, the conversion of number density and size distribution measurements into mass loading density values is of questionable validity in the type of flow systems under consideration. Fly ash and soot particles may be porous or hollow, and agglomerates will usually contain voids. The photographs[28] in Figure 10 are a vivid demonstration of the physical characteristics one may observe in fly ash samples. Similar micrographs have been reported by Fisher, et al.[29] Therefore, a knowledge of the material density and composition of the particles is insufficient in general for an accurate conversion to mass loading density.

It appears that the only presently available method of determining mass loading density for these systems is collection of a sample of the flow with subsequent determination of the mass of particulates present. The collection may be with an isokinetic probe used also for species concentration sampling or with a probe designed especially for collection of particulate matter.

# SECTION 4

# SUMMARY

No technique or instrument is currently available which will meet all the requirements for measurement of particulate size distribution and/or mass loading density in the systems under discussion. The photography, holography, visibility and diffraction techniques show promise for particulate size measurements over a fairly wide range of flow conditions and for particulate diameters of 2-5 microns or greater. The intensity ratios technique has potential, with further research, for measurement of particulate sizes in the 0.2-5 micron range in certain flow conditions of interest. A probe sampling system appears to be necessary for determination of particulate mass loading density and its distribution in the flow system.

# REFERENCES

1. H. W. Coleman, et al., "Interim Report: Diagnostics Assessment for Advanced Power Systems," Sandia Laboratories, Livermore, Report SAND77-8216, March 1977.

2. D. A. Lundgren, "Aerosol Measurement Methods," Paper No. TUA1 in NASA CP-2004, 1976.

3. R. D. Cadle, The Measurement of Airborne Particles, John Wiley and Sons, 1975.

4. H. C. van de Hulst, Light Scattering by Small Particles, John Wiley and Sons, 1957.

5. M. Kerker, The Scattering of Light and Other Electromagnetic Radiation, Academic Press, 1969.

6. A. R. Jones and W. Wong, "Direct Optical Evidence for the Presence of Sooty Agglomerates in Flames," Combustion and Flame 24, p. 139-140, 1975.

7. J. R. Hodkinson, "The Optical Measurement of Aerosols," Aerosol Science, C. N. Davies, editor, Academic Press, 1966.

8. F. Durst and B. Eliasson, "Properties of Laser Doppler Signals and Their Exploitation for Particle Size Measurements," Proceedings of the LDA-Symposium Copenhagen 1975, 1976.

9. A. J. Yule, N. A. Chigier, S. Atakan and A. Ungut, "Particle Size and Velocity Measurement by Laser Anemometry," AIAA Paper No. 77-214, 1977.

10. F. Durst and H. Umhauer, "Local Measurements of Particle Velocity, Size Distribution and Concentration with a Combined Laser Doppler Particle Sizing System," Proceedings of the LDA-Symposium Copenhagen 1975, 1976.

11. S. S. Penner, J. M. Bernard and T. Jerskey, "Power Spectra Observed in Laser Scattering from Moving, Polydisperse Particle Systems in Flames--I. Theory," Acta Astronautica 3, p. 69-91, 1976.

12. S. S. Penner, J. M. Bernard and T. Jerskey, "Laser Scattering from Moving Polydisperse Particles in Flames--II. Preliminary Experiments," Acta Astronautica 3, p. 93-105, 1976.

13. C. S. Williams and O. A. Becklund, *Optics*, Wiley-Interscience, p. 198ff, 1972.

14. C. G. McCreath and J. M. Beer, "A Review of Drop Size Measurement in Fuel Sprays," *Applied Energy 2*, p. 3-15, 1976.

15. W. M. Farmer, "Measurement of Particle Size, Number Density and Velocity Using a Laser Interferometer," *Applied Optics 11*, p. 2603-2612, 1972.

16. K. L. Orloff, F. C. Myer, M. F. Mikasa and J. R. Phillips, "Limitations On the Use of Laser Velocimeter Signals for Particle Sizing," *Proceedings Minnesota Symposium on Laser Anemometry (1975)*, p. 359-370, 1976.

17. D. M. Robinson and W. P. Chu, "Diffraction Analysis of Doppler Signal Characteristics for a Cross-Beam Laser Doppler Velocimeter," *Applied Optics 14*, p. 2177-2183, 1975.

18. N. S. Hong and A. R. Jones, "Light Scattering by Particles in Laser Doppler Velocimeters Using Mie Theory," *Applied Optics 15*, p. 2951-2953, 1976.

19. D. Roberds, "Particle Sizing Using Laser Interferometry," *Applied Optics 16*, p. 1861-1868, 1977.

20. Spectron Development Laboratories Report 77-6171, April 1977.

21. J. R. Hodkinson, "Particle Sizing by Means of the Forward Scattering Lobe," *Applied Optics 5*, p. 839-844, 1966.

22. C. C. Gravatt, "Light Scattering Methods for the Characterization of Particulate Matter in Real Time," *Aerosol Measurements*, NBS Special Publication 412, p. 21-32, 1974.

23. E. D. Hirleman, S. L. K. Wittig and J. V. Christiansen, "Development and Application of an Optical Exhaust Gas Particulate Analyzer," Laboratoriet for Energiteknik Report RE76-4, Technical University of Denmark, 1976.

24. E. D. Hirleman, "Optical Technique for Particulate Characterization in Combustion Environments: The Multiple Ratio Single Particle Counter," Ph.D. Thesis, Purdue University, August 1977.

25. J. Swithenbank, J. M. Beer, D. S. Taylor, D. Abbot and G. C. McCreath, "A Laser Diagnostic Technique for the Measurement of Droplet and Particle Size Distribution," AIAA Paper No. 76-69. 1976.

26. Alan Wertheimer, "Optical Methods for Real Time Particulate Measurements," paper presented at Air Pollution Control Association (Ontario Section) Symposium, April 27, 1977, Toronto, Ontario, Canada.

27. S. A. Self, et al., "Investigation of Novel Laser Anemometer and Particle Sizing Instrument," Project SQUID Semi-Annual Progress Reports, October 1, 1976, and April 1, 1977.

28. Photographs from research performed at MIT under the direction of Professor A. F. Sarofim of the Chemical Engineering Department.

29. G. L. Fisher, et al., "Fly Ash Collected from Electrostatic Precipitators: Microcrystalline Structures and the Mystery of the Spheres," *Science* *192*, May 7, 1976.

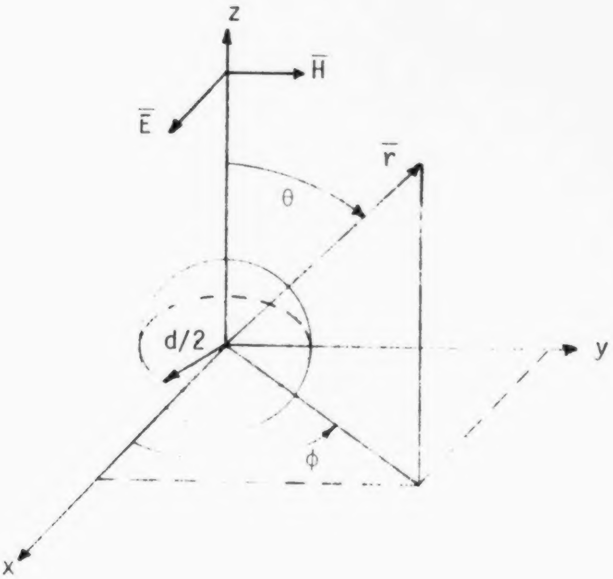

Figure 1. Geometry for Light Scattering Analysis

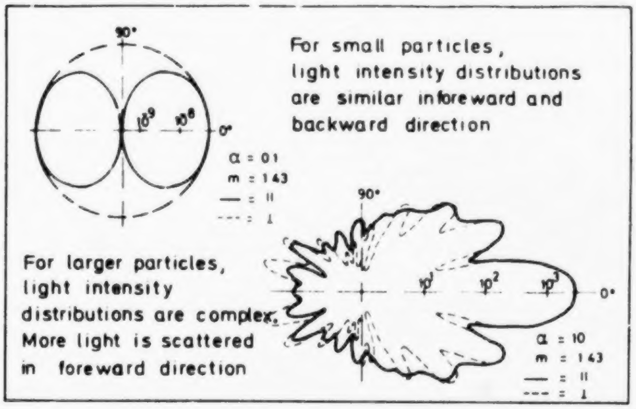

For small particles, light intensity distributions are similar inforeward and backward direction

For larger particles, light intensity distributions are complex. More light is scattered in foreward direction

Figure 2. Mie Theory Results: Variation of Scattered Intensity with θ for Two Sphere Sizes (Figure from Reference 8)

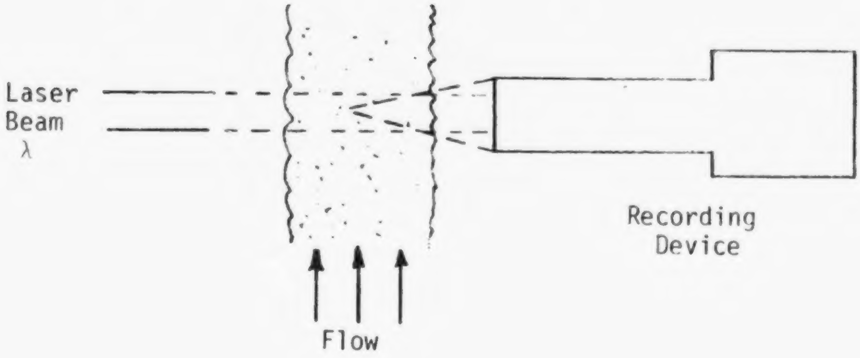
Laser
Beam
λ
Recording
Device
Flow

Figure 3. Schematic of Photography System for Particle Sizing

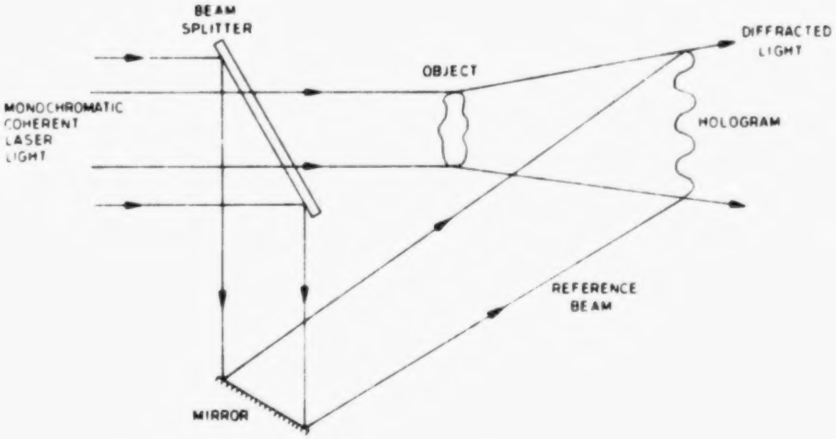
BEAM
SPLITTER
OBJECT
DIFFRACTED
LIGHT
MONOCHROMATIC
COHERENT
LASER
LIGHT
HOLOGRAM
REFERENCE
BEAM
MIRROR

Figure 4. Schematic of Holography System
(Figure from Reference 14)

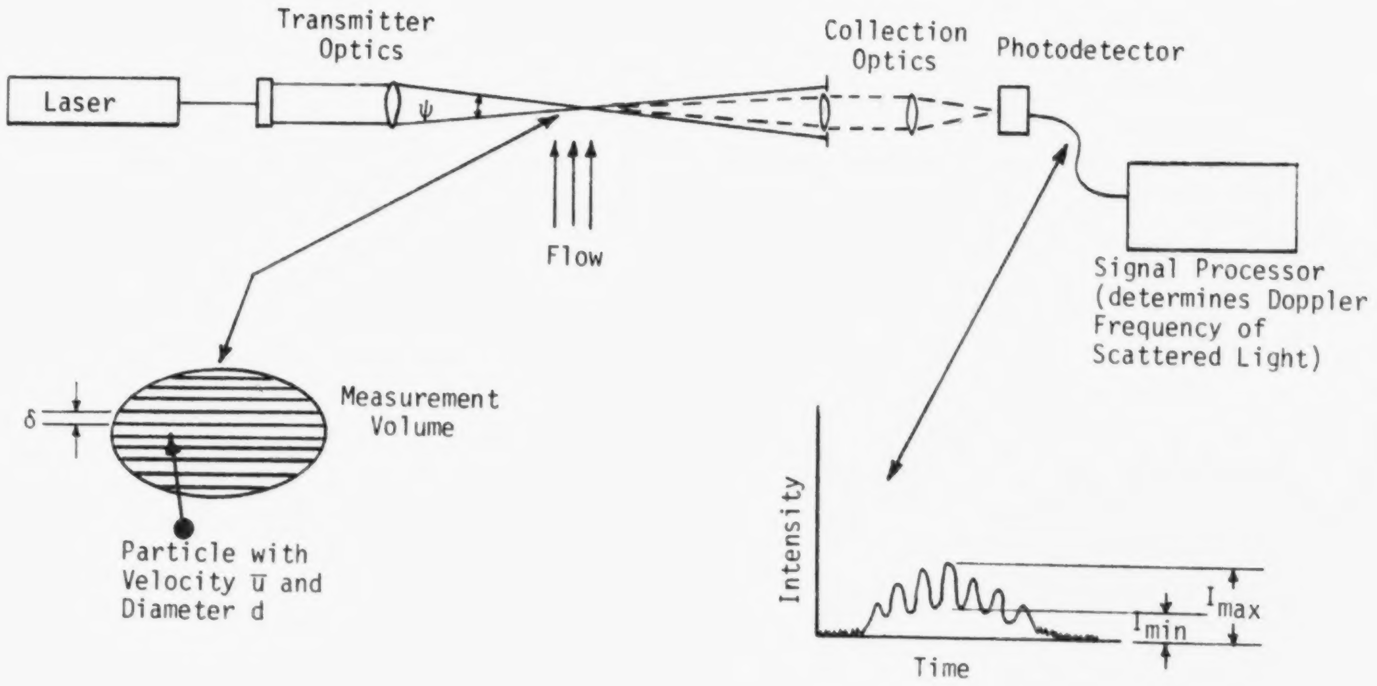
Transmitter Optics
Laser
$\psi$
Flow
Collection Optics
Photodetector
Signal Processor (determines Doppler Frequency of Scattered Light)
$\delta$
Measurement Volume
Particle with Velocity $\overline{u}$ and Diameter d
Intensity
Time
$I_{max}$
$I_{min}$

Figure 5. Laser Doppler Velocimeter (LDV) System Used to Size Particles by the Visibility Technique

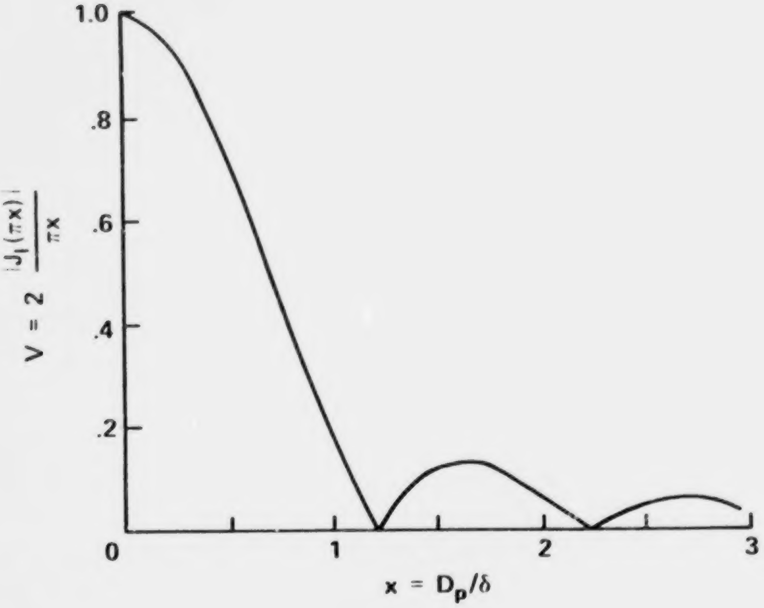

Figure 6. Visibility Function for Spherical Particles as Determined by Farmer (Reference 15)

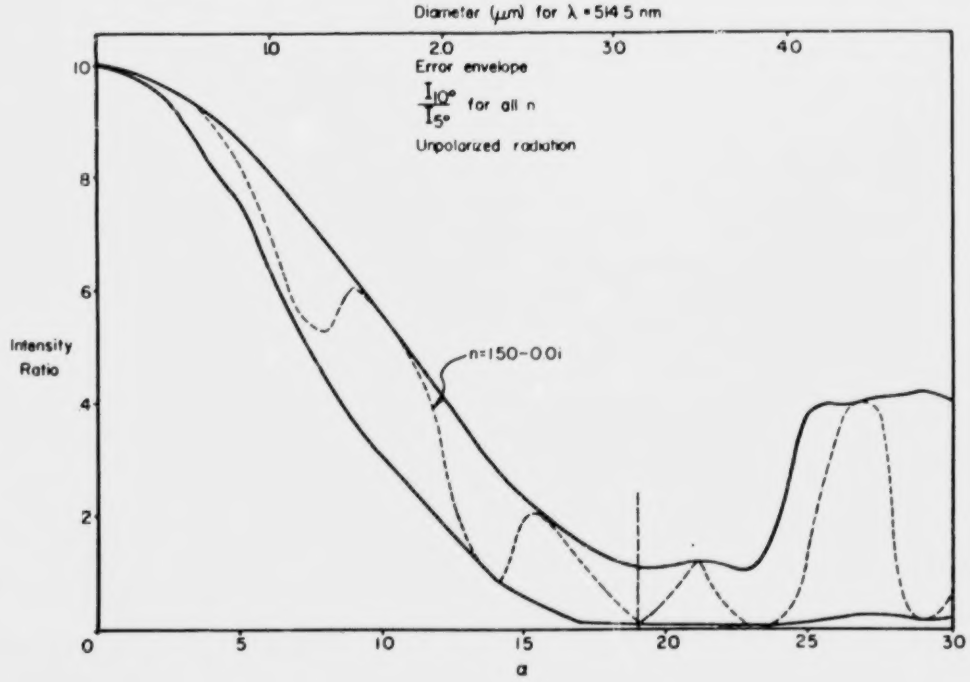

Figure 7. Intensity Ratio (10°/5°) for a Wide Range of Indices of Refraction as Calculated by Gravatt (Reference 22)

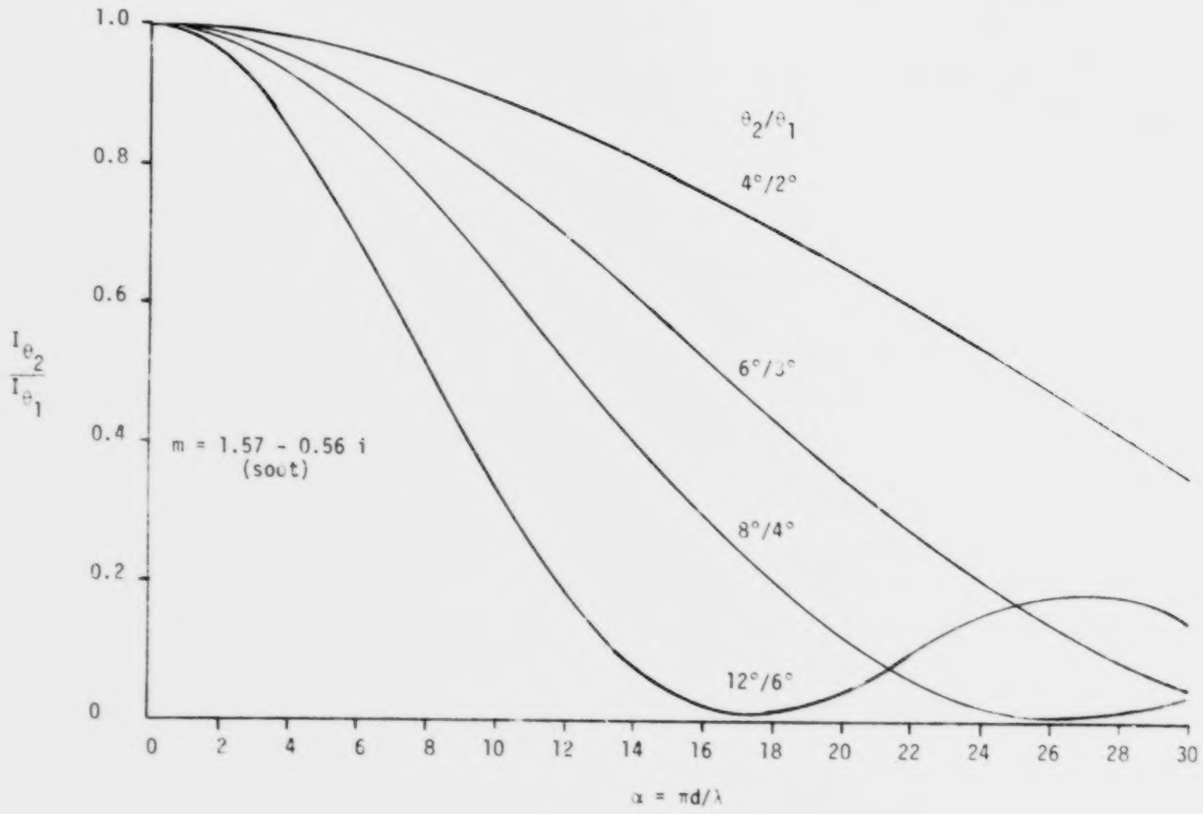

Figure 8. Intensity Ratios as a Function of Particle Size Using the Index of Refraction for Soot

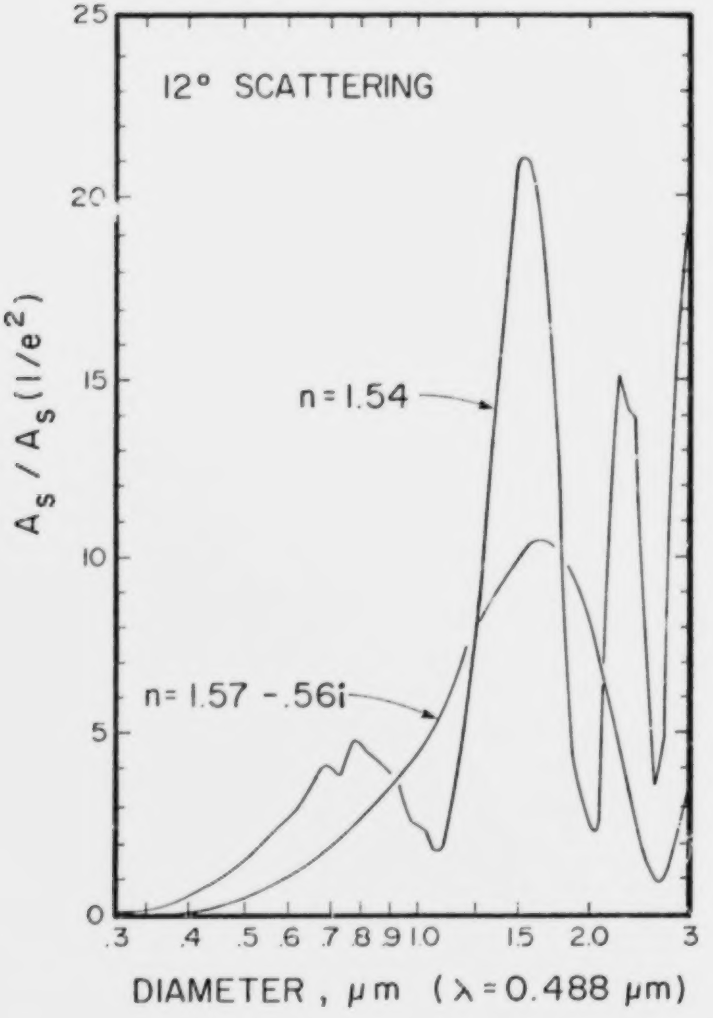

Figure 9. Sensitive Area $A_s$ vs Particle Size for Two Indices of Refraction, Accounting Only for Intensity Effects (from Hirleman, Reference 24)

Lignite (75-90) Coal, Complete Combustion

(Photograph shows a big ash cenosphere containing many smaller spheres)

B

Lignite (75-90) Coal, Complete Combustion

(Photograph shows a big broken cenosphere of ash)

Figure 10. Scanning Electron Micrographs of Fly Ash (Reference 28)

# PARTICULATE SAMPLING AT HIGH-TEMPERATURE AND HIGH-PRESSURE – THE EXTRACTIVE APPROACH

By:

W. Z. Masters
Acurex Corporation/Aerotherm Division
Mountain View, CA 94042

BLANK PAGE

# PARTICULATE SAMPLING AT HIGH-TEMPERATURE AND HIGH-PRESSURE -- THE EXTRACTIVE APPROACH

By:
William Masters
Acurex/Aerotherm
Mountain View, California 94042

## ABSTRACT

A particulate sampler for high-temperature, high-pressure processes has been developed and successfully demonstrated. The system uses an extractive approach, removing samples from the process stream for complete analysis of particulate size distribution, morphology, and chemical composition. System capabilities have been demonstrated by sampling a pressurized fluidized bed combustor. This paper describes the extractive sampling approach, the HTHP sampler design, and the data obtained from sampling operations.

# PARTICULATE SAMPLING AT HIGH-TEMPERATURE AND HIGH-PRESSURE -- THE EXTRACTIVE APPROACH

## INTRODUCTION

Advanced coal conversion processes present new problems in particulate sampling, including severe environments beyond the capabilities of conventional equipment. This paper describes a newly developed sampling system, specifically designed for the high temperatures and pressures found in pressurized fluidized bed combustors. The system uses an extractive sampling approach, withdrawing samples from the process stream for complete analysis of particulate concentration, shape, size, and chemical composition. The capabilities of the new system have been demonstrated in sampling operations at a pilot-scale fluidized bed combustor. The system performed successfully in a variety of operating modes, producing sample data.

Acurex/Aerotherm has developed the HTHP sampler for the Industrial Environmental Research Laboratory of the Environmental Protection Agency. The work is part of a broad program investigating new sampling technology for advanced coal conversion processes (Contract 68-02-2153). The EPA Project Officer for the contract is William Kuykendal.

The following sections of this paper discuss the extractive sampling concept, the HTHP sampler design, and sampling operations that have been performed with the new system.

### Extractive Sampling

In extractive sampling, a quantity of particle-laden product gas is drawn out of the process for analysis. Once extracted, the sample can be thoroughly examined by conventional methods. If proper care is taken to obtain and maintain a representative sample, the extractive approach will provide complete, accurate information on process constituents.

The sample is typically extracted through a probe inserted into the process duct. The sample withdrawal rate at the probe nozzle must be matched to the duct velocity to avoid biasing particle size distribution measurements (isokinetic sampling).

The error in measured particle content as a function of anisokinetic velocity mismatch can be estimated analytically (see Figure 1). For fine particles at low velocities the error is negligible, but for larger particles or high velocities, serious errors result.

Sample temperature is also a consideration in the extractive approach. Ideally, the temperature would be maintained at process conditions during particulate separation and analysis. In practice, however, the sample is usually cooled to temperatures compatible with analysis equipment.

The major advantage of the extractive method is that the sample can be analyzed by conventional techniques. For example, particulate removal and size classification devices, trace element collectors, and chemical analysis techniques are all highly developed (References 1 to 5). Extractive sampling is commonly used in emissions measurement and combustion studies.

Access to the pressurized duct is the main difficulty in extending extractive sampling technology to high-pressure, high-temperature processes. The hardware requirements for entering a pressurized process are much more complex than for ambient pressure applications. The selected design for the HTHP sampler is described in the following section.

## HTHP SAMPLER DESIGN

The new sampler design adapts conventional sampling technology to high-temperature, high-pressure environments. Key system components are:

- A traversing sample probe that can be inserted or withdrawn during process operation
- A probe housing that contains process pressure during sampling
- A cascade impactor to both collect and size particulate
- Conventional trace element collectors (organics trap and impingers)
- Measurement and control instrumentation to assure isokinetic conditions

A schematic diagram of the sampler is shown in Figure 2. The sample probe is mounted within a pressure-containment housing. The probe can be inserted into stream through valves that connect the housing assembly to the process duct. Sample flow in the probe passes through a cooler and particulate collector (cascade impactor). Flowrate is controlled by a throttle valve at the probe exit. After leaving the probe, sample gases are conducted through the trace element collectors, and vented.

The sampling system is shown in Figure 3. In addition to the probe and housing assembly, controls, and sample collectors, the system includes a portable hydraulic pump.

One of the basic decisions in designing the sampler was the choice between fixed and translating probe configurations. A translating probe (one that is insertable and removable during process operation) is more complex than a stationary probe, but offers several operating advantages:

- Particulate deposition losses in the probe can be recovered
- Nozzles can be changed to maintain isokinetic conditions
- The probe can traverse the duct to measure flow variations
- Probe exposure to erosive/corrosive conditions is minimized
- Inspection and maintenance are possible during process operations.

Based on these advantages, the translating probe design was selected for the HTHP sampler. The sample probe and particle collector are shown in Figure 4.

Selecting the particulate collection temperature was a second major design decision. A number of well-characterized devices are available for use below 500°F, but, high-temperature particulate collectors are in an early stage of development. Based on this practical limitation, a collection temperature of 450°F was selected with the awareness that possible changes in particulate composition would have to be considered. Major changes in composition are not likely above the sulfuric acid dewpoint. However, changes in trace element concentration are a potential concern. The HTHP sampler has been used in an experiment investigating the effect of collection temperature on particulate composition, as described in a later section of this paper. The impactor used with the HTHP sampler is a Mark III, University of Washington Source Test Cascade Impactor, Model D.

The cascade impactor has several advantages over other particle collectors. The device provides many stages of size classification in a small volume. Also, impactors classify particle size based on inertial and aerodynamic properties that relate directly to the performance of particulate removal devices. Impactor performance is well characterized for moderate temperature, ambient pressure operation. The effect of high pressure on sizing performance can be estimated using theoretical correction factors. For fine particles at moderate temperatures, even large pressure increases have little effect on impactor performance. Collection temperature, however, can affect measurements more significantly. Variations in cut size with temperatures have been calculated by the impactor supplier for temperatures up to 500°F.

In the selected sampler design, the sample probe enters the pressurized process through 4-inch diameter full-opening valves while process pressure is contained by a surrounding housing assembly. The housing, shown in Figure 5, consists of two telescoping cylinders which move the probe into and out of the process. Hydraulic cylinders connect the two parts of the housing. Their function is to accurately position the probe, and withstand the large forces from process pressure. Sealing at the joint between the housing cylinders is critical, so redundant seals are used. The telescoping housing is the most complex part of the sampling system and consequently required the most design and development effort.

The HTHP sampling system also includes the instruments and controls necessary for accurate sampling. Sample flowrate is one of the important parameters that is monitored and controlled. Flow must be both isokinetic at the probe nozzle and within the operating limits of the particle collector. For proper control, flow conditions in both the process steam and sample probe must be measured. A pitot tube and thermocouple are mounted on the probe to measure process stream conditions, and a calibrated orifice and thermocouple check the sample flow. The flowrate is adjusted to particle collector requirements by a valve near the probe exit. Nozzle entrance velocity is varied by selecting larger or smaller nozzles. The sampling system includes other controls for sample temperature, probe traverse, trace element collector flow, and other key operating parameters. System controls are housed in two portable enclosures, shown in Figure 6.

The trace element collection equipment included in the sampling system consists of an organics module and impinger train (see Figure 7). Both units are identical to those used in the Source Assessment Sampling System that is commercially available from Acurex/Aerotherm. The organic module cools the sample gas to 70°F and traps organic vapors in a porous polymer granular bed. The polymer used in this test series is Rohm & Haas XAD-2 gas chromatographic packing material. The impinger train has four high-volume glass impingers, three filled with collector and one with silica gel moisture absorbant. The oxidizing reagents in the impingers collect volatile trace elements by oxidative dissolution. The reagents are:

| Impinger | Solution |
|---|---|
| No. 1 | 6M $H_2O_2$ |
| No. 2 | 0.2M $(HN_4)_2S_2O_8$ + 0.02M $AgNO_3$ |
| No. 3 | 0.2M $(NH_4)_2S_2O_8$ + 0.02M $AgNO_3$ |
| No. 4 | Silica gel |

The peroxide solution in Impinger No. 1 collects reducing gases such as sulfur dioxide which would lessen the oxidative capability of Impingers Nos. 2 and 3. The ammonium sulfate and silver nitrate solutions serve as the trace element collectors in the impinger train (Reference 3).

## PFBC Facility

The new HTHP sampler has been demonstrated in operations at the Exxon Miniplant PFBC. The PFBC facility is described in this section.

The Miniplant is a pilot-scale pressurized fluidized bed combustor operated for the EPA by the Exxon Research and Engineering Company in Linden, New Jersey. The PFBC process, shown in Figure 8, is a combined-cycle coal combustion process. Combustion occurs under pressure in a limestone bed that is fluidized by incoming air. Fluidization gives good mixing for efficient combustion, and the limestone bed removes much of the sulfur released during the combustion process. Added useful energy can be produced by expanding high-pressure flue gases in a gas turbine, if particulate loading can be reduced to the levels (0.0002 to 0.002 gr/scf) required to protect turbine blades. The Exxon Miniplant facility is being used to investigate fluidized bed combustion, gas cleanup devices, and particulate effects on turbine components. At the time of sampling, the facility did not include a gas turbine or final cleanup device.

For the sampler demonstration tests, the sampling location is downstream of the primary cyclone as indicated in Figure 8. At this location, there is a specially constructed duct section with a sampling port (4-inch, 300-pound pipe flange) which interfaces with the sampling system access valves. Measured process conditions were 1350°F and 118 psig.

The Miniplant facility is a four-story structure, with platforms at each level (see Figure 9). The sampling location is physically located at the top of the combustor tower. When installed, the probe assembly is horizontal, about 4 feet above the platform (see Figure 10). The coolant console and hydraulic pump are also placed on the top platform, near the probe assembly. The control consoles and gas train equipment are set up one floor below, where a partial enclosure gives some weather protection.

## Systems Operations and Test Data

The new HTHP sampler has been used in two series of operations at the Miniplant PFBC. One series was a field test of system capabilities, the other an investigation of the effect of collection temperature on particulate compensation. The sampler operated successfully in both test series. These operations and some of their results are described in this section.

The first series of sampling operations investigated system performance under field conditions. These operations successfully demonstrated a variety of system capabilities. Three sampling runs were made: one using a filter to collect total particulate, and two using a cascade impactor. Trace element collection equipment was operated during the filter run. The tests produced the following data:

- Particulate size distribution
- Particulate chemical composition
- Particulate shape
- Particulate concentration

- Process temperature and pressure
- Moisture content
- Structure temperatures (valves and probe housing)
- Trace element samples (not yet analyzed)

Particle size distributions from cascade impactor data are plotted in Figure 11. The effect of pressure and temperature on impactor size cuts was estimated using Reference 5. At the relatively low collection temperatures used, increased pressure had little effect on impactor performance for particles larger than 1 micrometer.

The impactor substrates are shown in Figure 12. Generally, the patterns are regular indicating normal impactor operation. Stage 7, however, shows evidence of several plugged jets. The substrates from Run 2 are lightly loaded. Those from Run 3 show heavier, three-dimensional deposits.

Examples of particulate photomicrographs, showing particle size and shape, are shown in Figures 13 and 14. These plots were made by a scanning electron microscope. The irregular appearance is typical of flyash from lower temperature combustion processes (Reference 8). The plots show the trend of decreasing physical size from Stage 1 to State 6, although irregular shape and possible agglomeration make visual interpretation of particle size very difficult.

The chemical composition of the collected particulate was analyzed by dispersive X-ray fluorescence. Spectra of X-ray emissions from impactor Stage 1 and Stage 6 are shown in Figure 15. The peaks in the spectra correspond to the number of emissions detected at characteristic wavelengths of various elements. Results show the presence of a aluminum, silicon, sulfur, potassium, calcium, titanium, iron and copper.

Comparing the relative height of the peaks in two spectra can give a rough indication of the relative quantities of elements present in two samples. The comparison of Stage 1 and Stage 6 spectra shows no apparent difference in bulk composition between the coarse particles collected ($D_{50}$ of about 30 microns) and the finer particles ($D_{50}$ of about 0.6 micron).

Data from the system demonstration tests are discussed more extensively in a test report submitted to EPA IERL (Reference 9).

Following the system demonstration tests, a second series of sampling operations was conducted at the Exxon Miniplant. The purpose of these tests was to investigate the effect of sample cooling on measured particulate composition. We were specifically concerned that trace elements might condense between process temperature and conventional particulate collection temperature (about 450°F). For these tests, the sampler was setup to collect particulate at process temperature, so trace element condensation could be investigated in two ways. First, the trace element content of particulate collected at 450°F (from the demonstration test series) could be compared with the content of particulate collected at duct temperature to see if any significant differences result. Second, after the particulate was removed at process temperature, the sample gasses could be cooled and filtered to collect condensation products.

The probe configuration for the condensation tests is shown in Figure 16. A scalping cyclone and filter are mounted at the front of the probe to remove particulate at process temperature, a series of orifices gradually reduce sample gas pressure, and a final filter collects condensation products. The cyclone used is a Southern Research Institute model, designed for much less severe operating temperature. This cyclone was readily available, was small enough for insertion into the duct, and had a very efficient 0.6-micron cut-point. During the tests, however, the cyclone's protective gold plating blistered and fell off, leaving titanium surfaces exposed to heavy oxidation. The chemical analyses of particulate samples may show some debris from the plating failure.

The high-temperature filter following the scalping cyclone is made of saffil alumina, a material that Acurex is currently testing for high-temperature baghouse filters. This material seems to offer excellent temperature resistance and effective filtration, but its performance hasn't yet been fully characterized. Its performance in the condensation tests was quite good. The estimated filter efficiency was well over 90 percent of the fine particulate passed by the scalping cyclone.

The final filter at the sample probe exit is a standard Gelman "microquartz" type with high efficiency and low trace element content. It is possible to use conventional filter materials at this location because sample gas temperatures are substantially reduced by the probe cooler section.

In the condensation test series, we completed four sampling runs. Analysis of the samples is still in progress, so no conclusions on trace element condensation have been reached. Some sample data is available, however. The particulate collected at process temperature has been analyzed by spark source mass spectrometer. The results are presented in Table 1. The measured trace element content is similar to common flyash. A better evaluation will be possible when spark source mass spectrometer analysis of particulate samples from the demonstration test series is completed. The comparison will show if the different collection temperatures result in different chemical composition measurements.

The material collected on the final filter has been analyzed in detail by the Arthur D. Little Company. The goal of this analysis was to find what materials were collected on the filter at the probe exit, and determine if they would have resulted from condensation processes. The analysis showed that the material collected is partly particulate which penetrated the hot filter, partly contaminants from a Grafoil packing in a value at the probe exit, and partly sulfuric acid residue. The acid residue is a condensation product caused by inadequate heat tracing in the probe valve area. A thermocouple in this area measured sample gas temperatures as low as 200°F during the condensation tests. This is well below the 450°F target for proper sample conditioning. At this point, it appears that more meaningful information on trace element condensation will come from the comparison of the hot particulate catch and demonstration test particulate catch than from further examination of the materials collected on the final filter. However, further analysis of the final filter is planned.

Photomicrographs of the particulate samples from the condensation tests are shown in Figures 17 and 18. The particulate is similar in appearance, supporting the conclusion that part of the material on the final filter carried through the hot filter. Dispersive fluorescent X-ray spectra in Figure 19 show a similarity in composition between the filter catches, except for the increased sulfur contents of the rear filter.

Further data will be available when the analyses of condensation tests samples are completed.

## Conclusions

The sampling system described in this paper demonstrates that extractive sampling is a feasible approach for sampling high-temperature, high-pressure processes. Technology for sampling pressurized fluidized bed combustors is now developed and available. Future development also will be required, however, to make useful application of this technology and extend it to other advanced coal conversion processes.

For FBC sampling, remaining issues include collection temperature selection and system cost/performance trade-offs. The collection temperature issue will be resolved by further condensation tests or by the development of high-temperature particulate collectors. Process developers seem to be interested in both upgraded and downgraded versions of the sampling system. Upgraded versions offer longer sampling durations, quicker turnaround and better operating convenience. Downgraded versions, such as fixed-probe designs, are cheaper, but give less information.

The next objective for extractive sampling is to develop technology for coal gasifiers. Particulate measurement is also important for developing these processes, and environmental difficulities are even more severe than for PFBC's.

# REFERENCES

1. Lundgren and Calvert, "Aerosol Sampling with a Side Port Probe," Amer. Ind. Hyg. Ass. J., 28:213 (1967).

2. Calvert and Parker, "Collection Mechanisms at High Temperature and Pressure," *Symposium on Particulate Control in Energy Process*, EPA-600/7-76-010, Sept. 1976.

3. Homersma, et al., *IERL-RTP Procedures Manual: Level 1 Environmental Assessment*, EPA-600/2-76-106a, June 1976.

4. Blake, D. E., *Operating and Service Manual – Source Assessment Sampling System*, Aerotherm Report UM-77-80, March 1977.

5. Gooding, C. H., *Wind Tunnel Evaluation of Particle Sizing Instruments*, EPA-600/2-76-073, March 1976.

6. ________, *Operation Manual, Mark III University of Washington Source Test Cascade Impactor (Model D)*, Pollution Control Systems Corporation, Renten Washington, March 1974.

7. Hoke, R. C., "FBC Particulate Control Practice and Future Needs: Exxon Miniplant," *Symposium on Particulate Control in Energy Processes*, EPA-600/7-76-010, September, 1976.

8. Hoke, R. C., Exxon Research and Engineering Company, Linden, New Jersey, Personal Communication.

9. Masters, W. Z., "Field Testing of a Sampling System for High-Temperature/High-Pressure Processes," *Annual Report, Measurements of High Temperature, High Pressure Processes*, Aerotherm Report TR-77-55, July 1977.

10. Lee and Lehmden, "Trace Metal Pollution in the Environment," *Journal of the Air Pollution Control Association*, Vol. 23, No. 10, October 1973.

## TABLE I. CONCENTRATIONS OF METALS IN FLYASH – SSMS DATA

From Condensation Test Samples:

| Element | Cyclone (PPM) | Hot Filter (PPM) |
|---|---|---|
| K | 8200 | 8850 |
| Na | 1310 | 2500 |
| V | 185 | 135 |
| Dℓ | 16400 | 9400 |
| Si | 94000 | 82600 |
| Fe | 30000 | 13000 |
| Ca | 20000 | 19000 |
| Mg | 11400 | 17800 |
| Ti | 2430 | 1950 |
| Cu | 248 | 165 |
| Ni | 120 | 100 |
| Mn | 59 | 49 |
| Zn | < 13 | < 80 |
| Tℓ | 6 | 1950 |

TABLE II. TRACE METALS IN FLYASH AS A FUNCTION OF PARTICLE SIZE.[10]

| | Concentration, ppm | | | | |
|---|---|---|---|---|---|
| Element[a] | 25 µm | 12.5 µm | 10 µm | 3.5 µm | 1.5 µm |
| Al | 67,000 | 54,300 | 57,300 | 63,600 | 59,300 |
| B | 300 | 500 | 500 | 500 | 500 |
| Be | 2 | 1 | 2 | 2 | 2 |
| Cd | ≤ 5 | ≤ 5 | ≤ 5 | ≤ 5 | 100 |
| Cr | 130 | 130 | 130 | 300 | 300 |
| Cu | 150 | 150 | 200 | 200 | 200 |
| Fe | 40,000 | 59,000 | 43,500 | 35,500 | 32,300 |
| Mn | 200 | 240 | 290 | 390 | 500 |
| Ni | 300 | 200 | 200 | 300 | 300 |
| Pb | 300 | 200 | 300 | 300 | 500 |
| V | 200 | 200 | 200 | 200 | 200 |

[a] Sample collected from a coal-fired steam power plant and analyzed by neutron activation and spark source mass spectrometry.

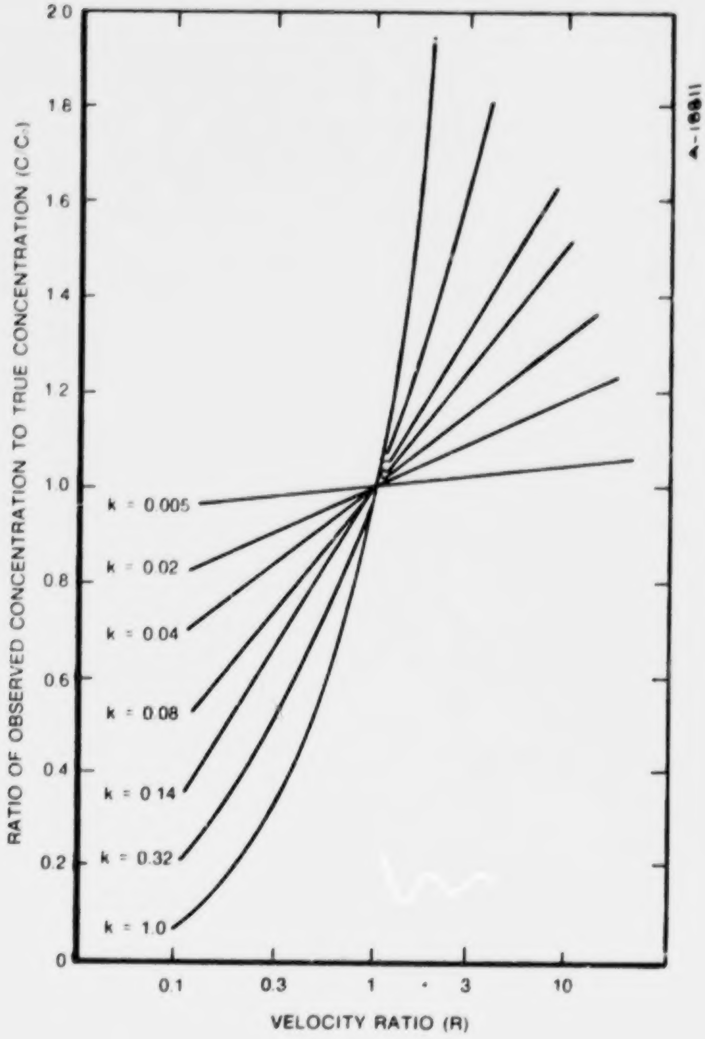

Figure 1. Probe inlet bias (from reference 1).

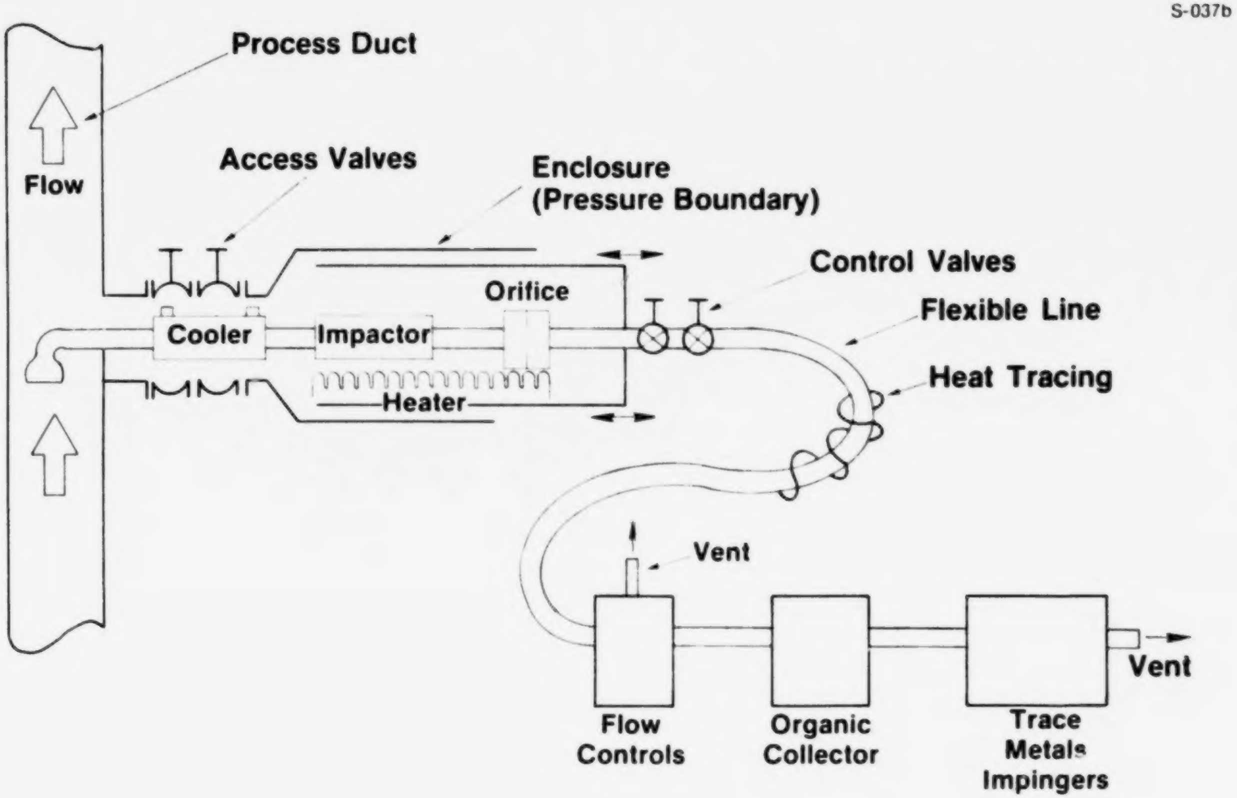
S-037b
Process Duct
Flow
Access Valves
Enclosure
(Pressure Boundary)
Control Valves
Orifice
Cooler
Impactor
Heater
Flexible Line
Heat Tracing
Vent
Flow
Controls
Organic
Collector
Trace
Metals
Impingers
Vent

Figure 2. System schematic.

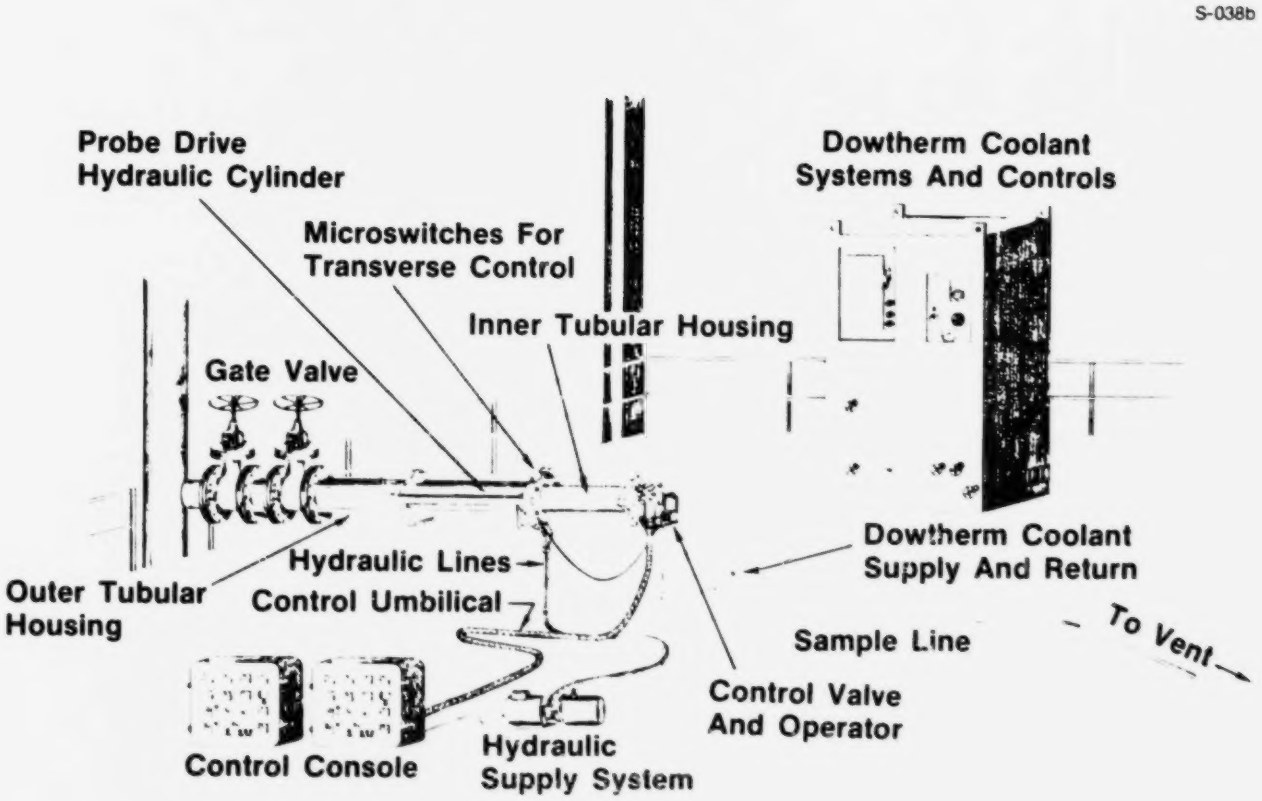
S-038b
Probe Drive
Hydraulic Cylinder
Microswitches For
Transverse Control
Inner Tubular Housing
Dowtherm Coolant
Systems And Controls
Gate Valve
Dowtherm Coolant
Supply And Return
Hydraulic Lines
Outer Tubular
Housing
Control Umbilical
Sample Line
To Vent
Control Valve
And Operator
Hydraulic
Supply System
Control Console

Figure 3. High-temperature, high-pressure sampling system.

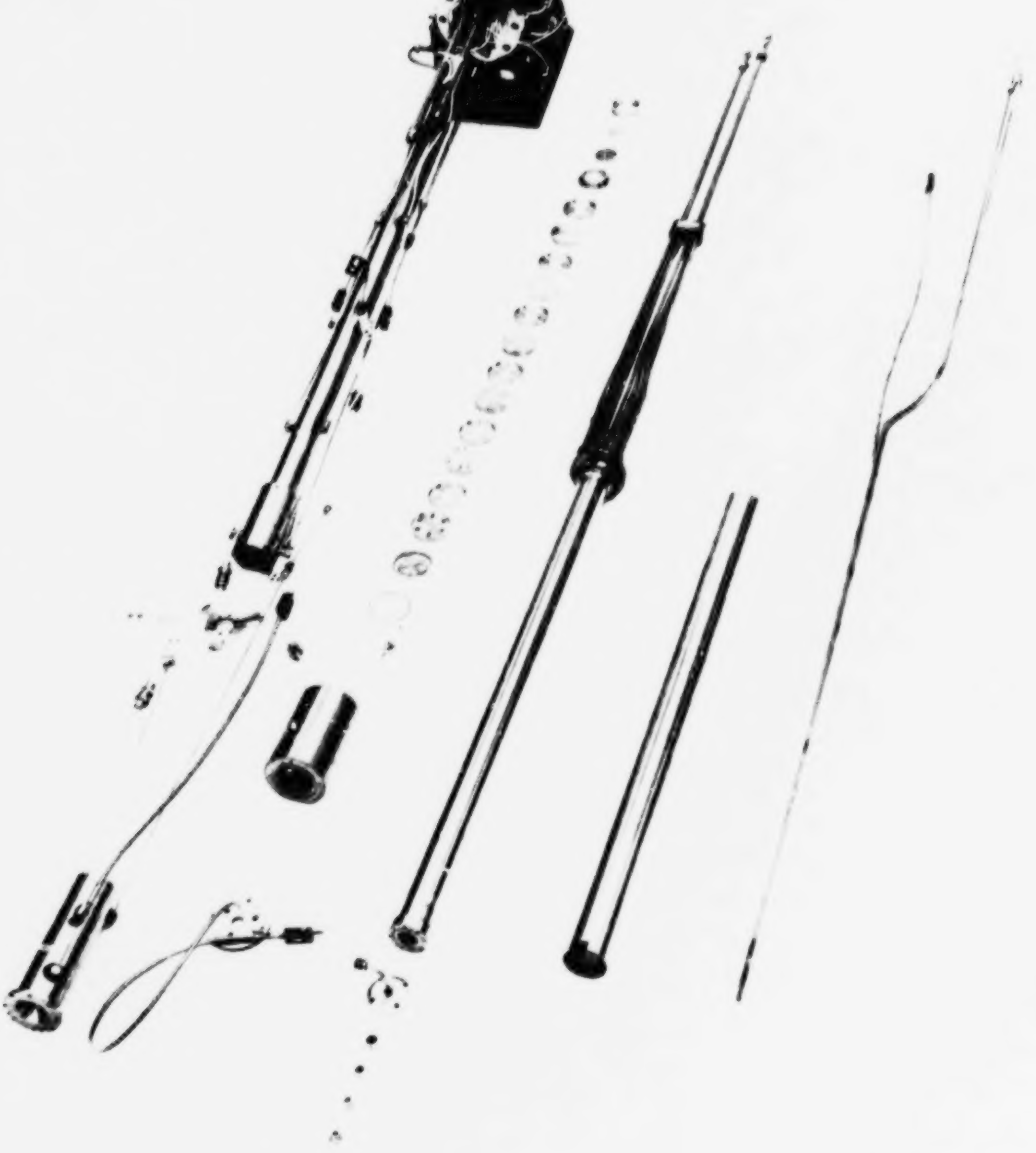

Figure 4. Exploded view of HTHP probe.

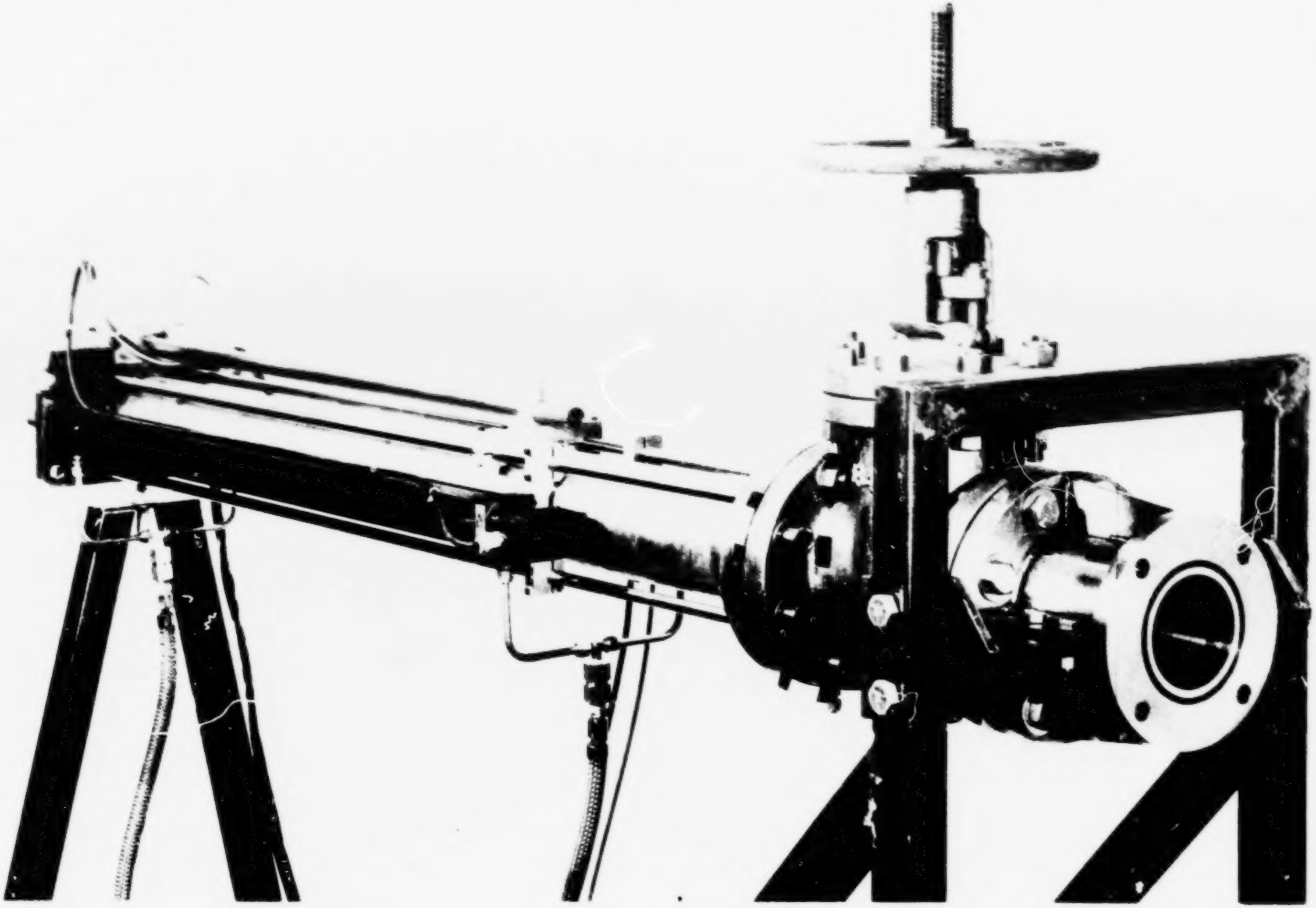

Figure 5. Aerotherm HTHP sampling probe and duct interface valve.

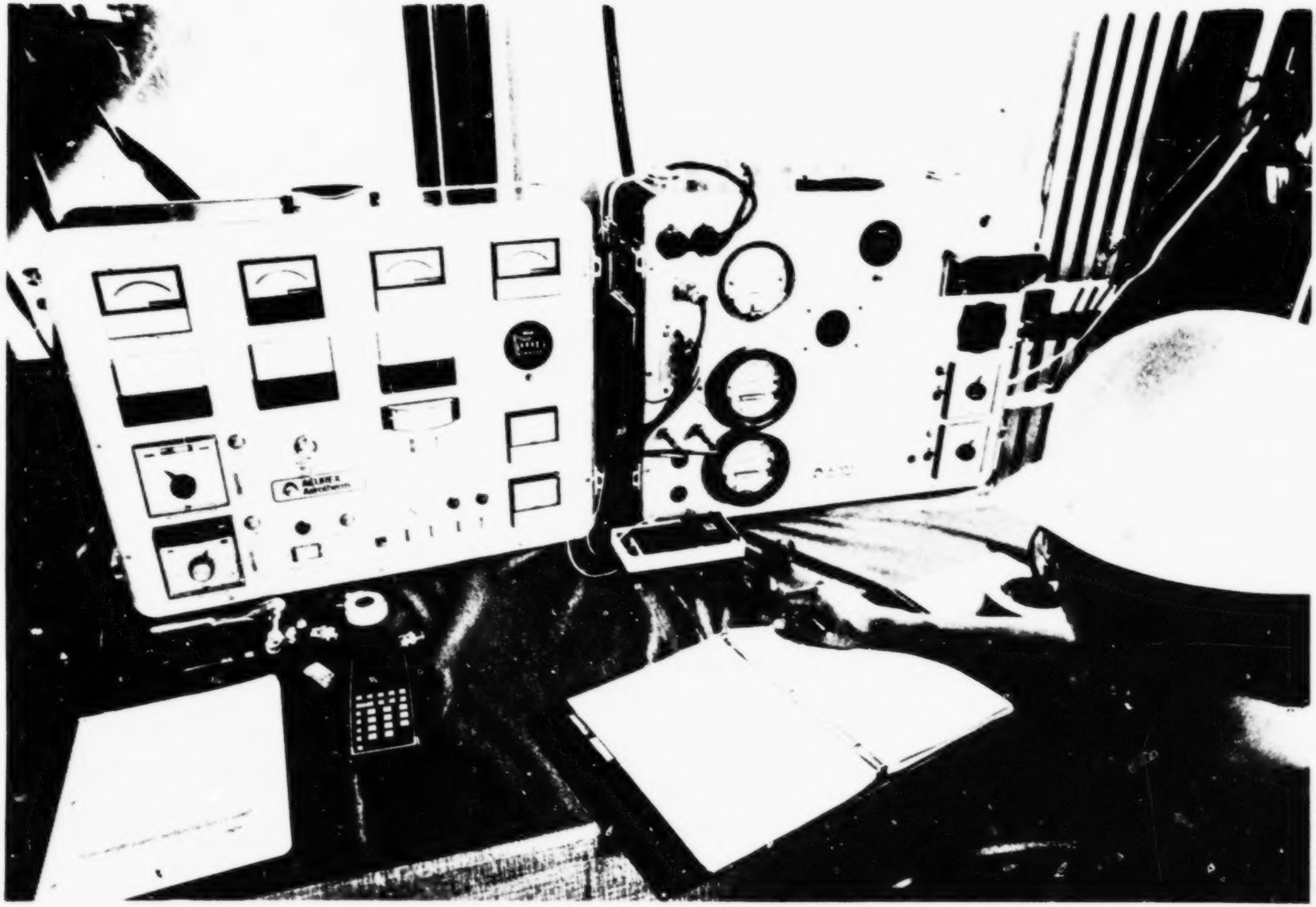

Figure 6. Control consoles.

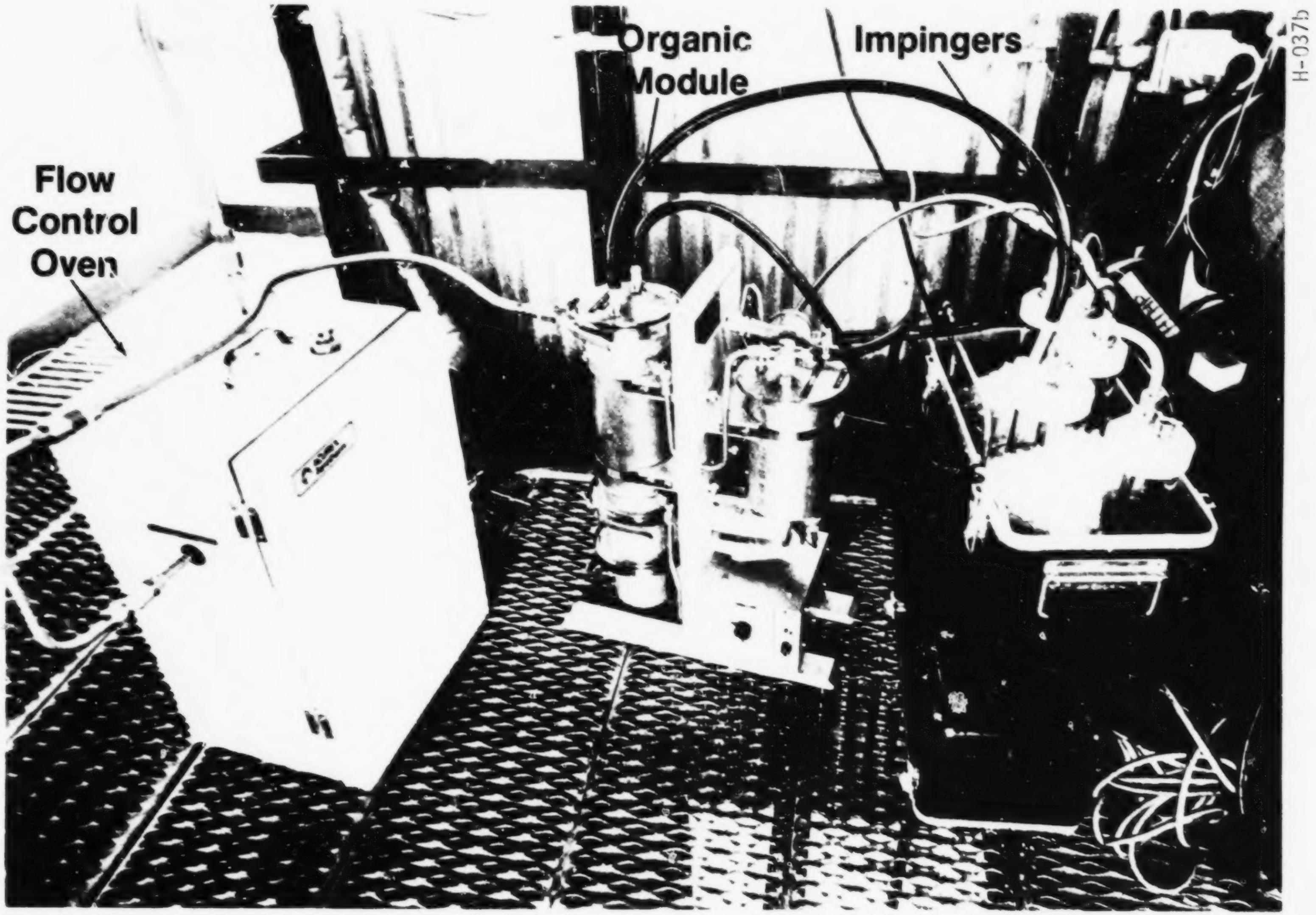
Flow Control Oven
Organic Module
Impingers
H-0375

Figure 7. Flow control oven and gast train.

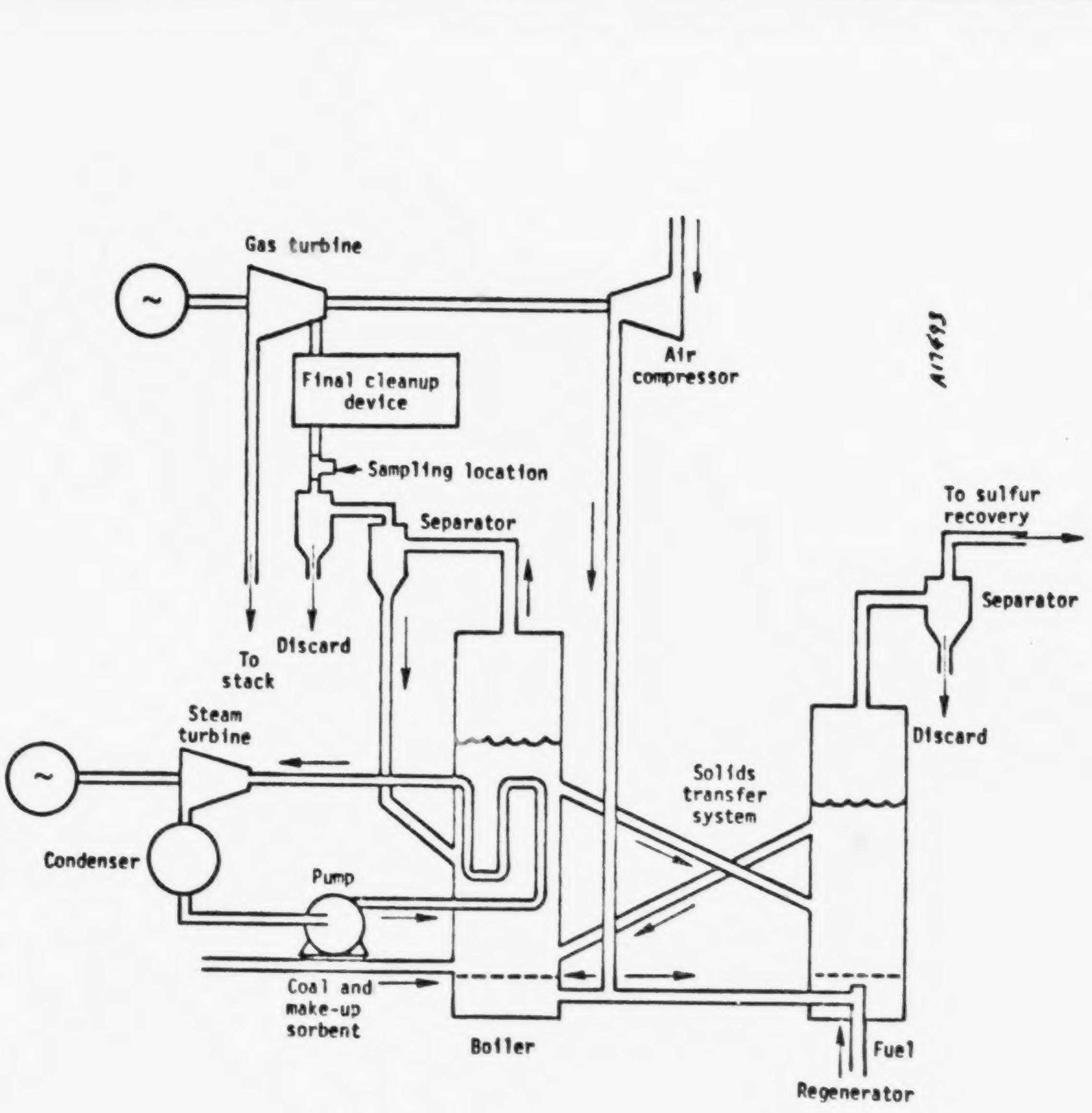
Gas turbine
~
Final cleanup device
Sampling location
Separator
Discard
To stack
Air compressor
A17495
To sulfur recovery
Separator
Discard
Steam turbine
~
Condenser
Pump
Solids transfer system
Coal and make-up sorbent
Boiler
Fuel
Regenerator

Figure 8. Pressurized fluidized bed coal combustor system.

4-0346

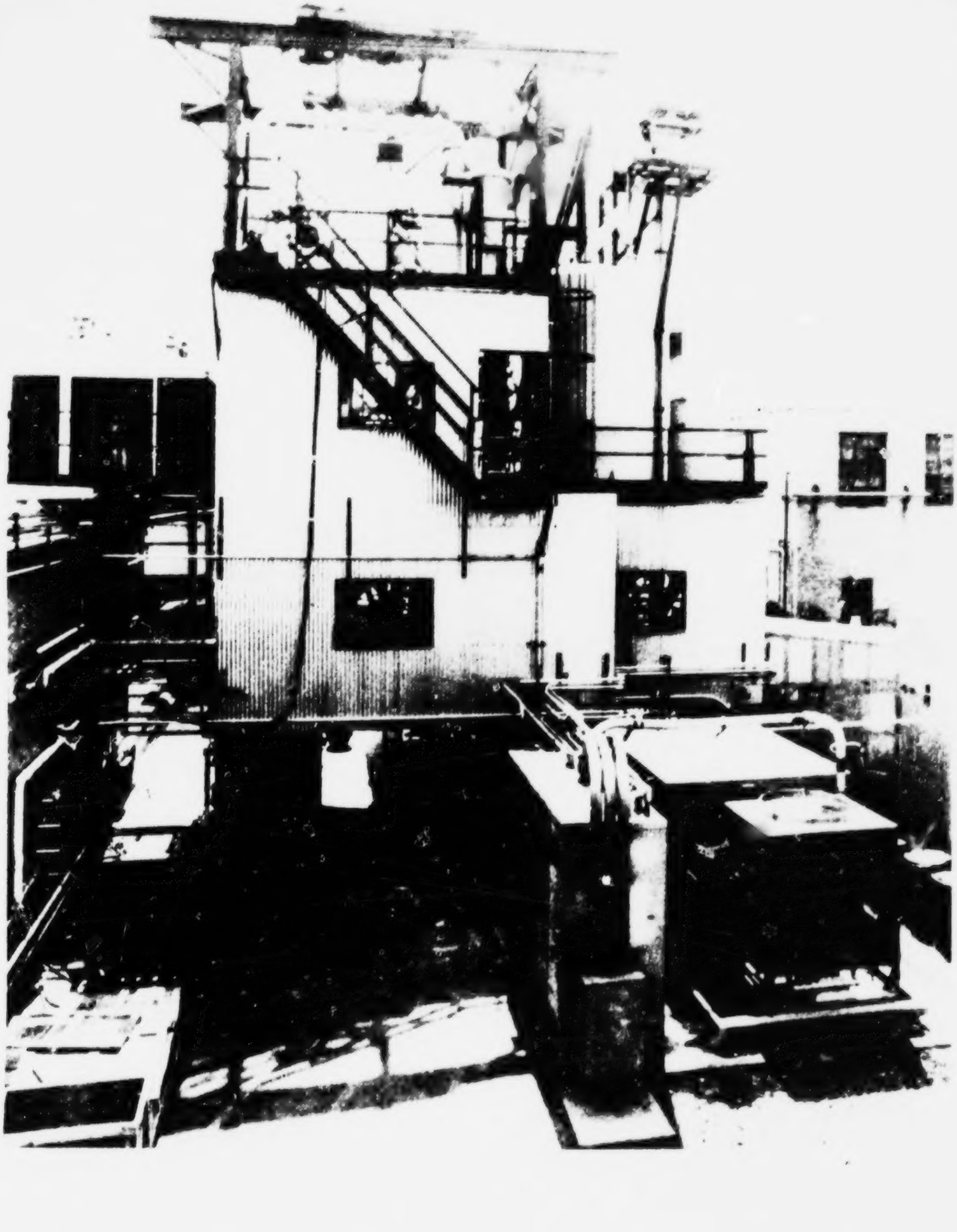

Figure 9. Miniplant PFBC.

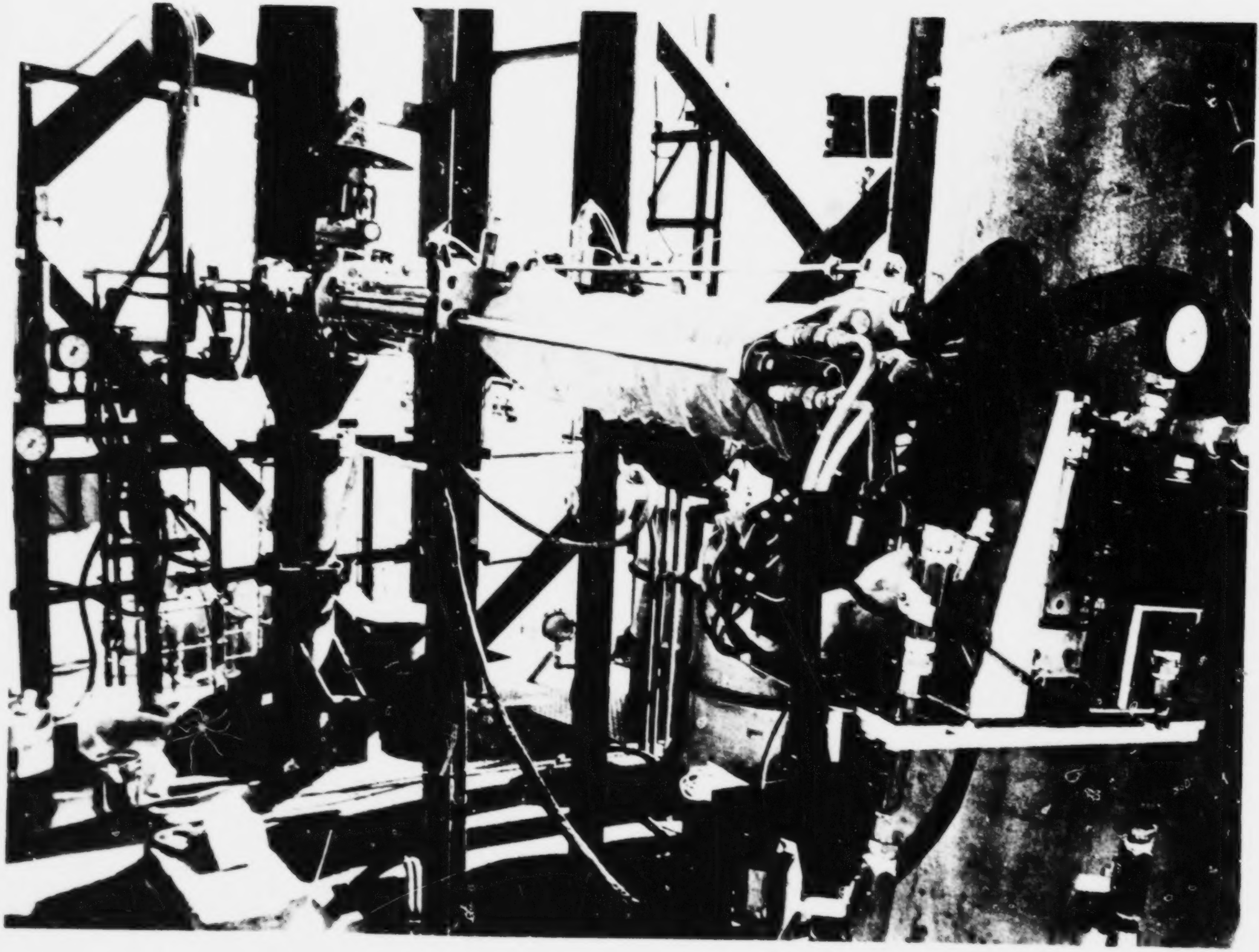

Figure 10. HTHP probe assembly installed at Exxon miniplant.

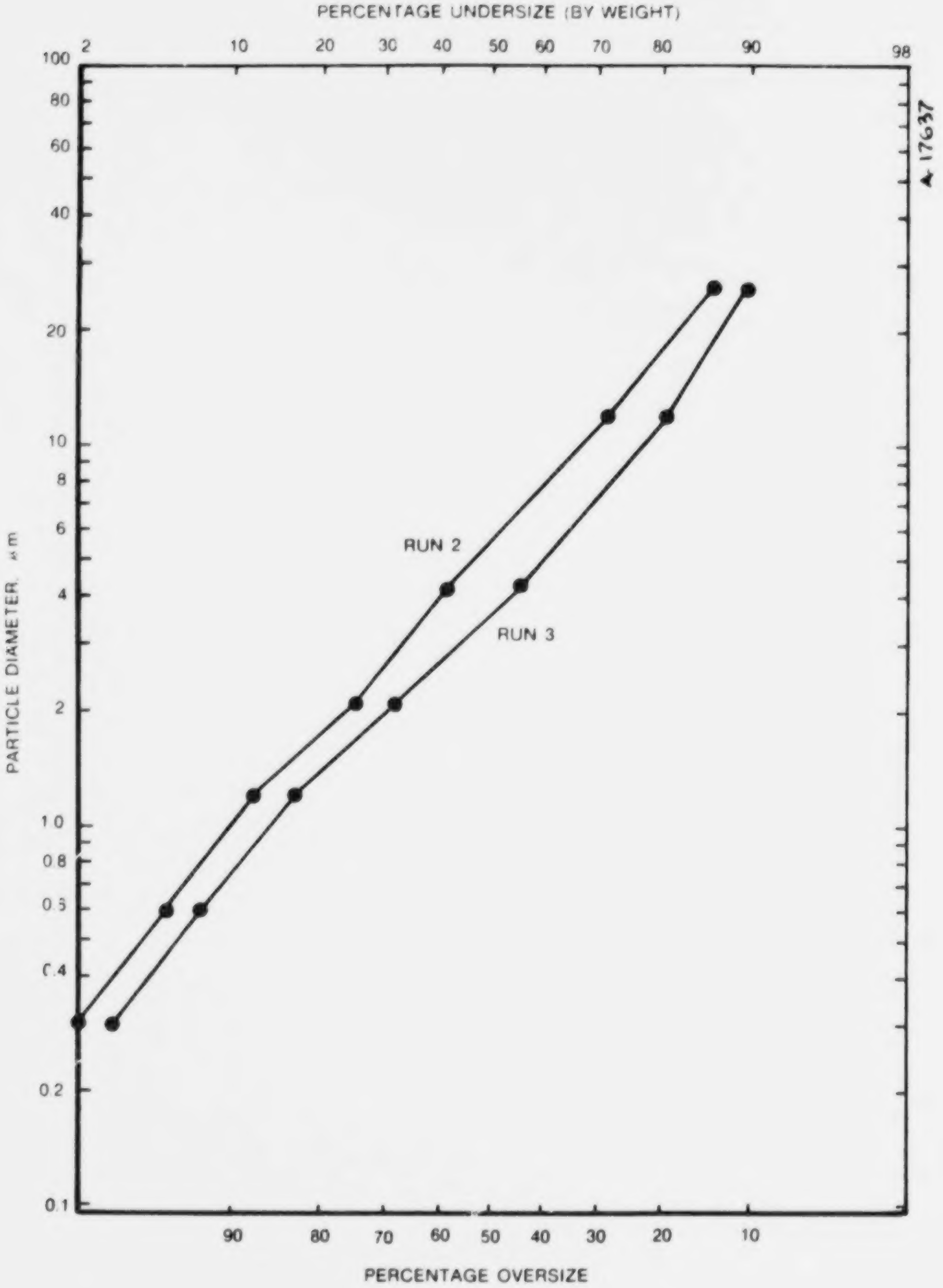

Figure 11. Particle size distribution.

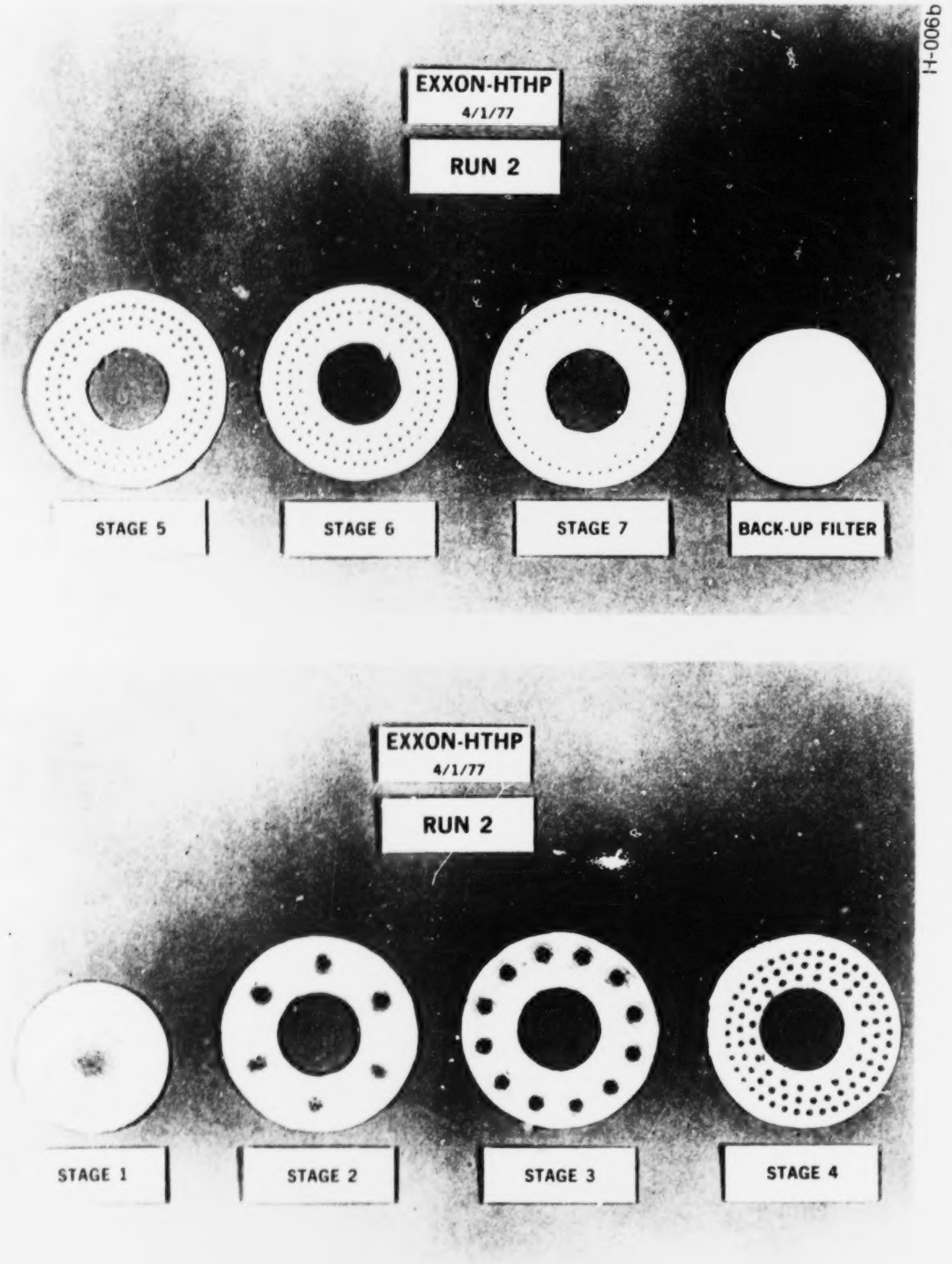
H-006b
EXXON-HTHP
4/1/77
RUN 2
STAGE 5
STAGE 6
STAGE 7
BACK-UP FILTER
EXXON-HTHP
4/1/77
RUN 2
STAGE 1
STAGE 2
STAGE 3
STAGE 4

Figure 12. Impactor substrates.

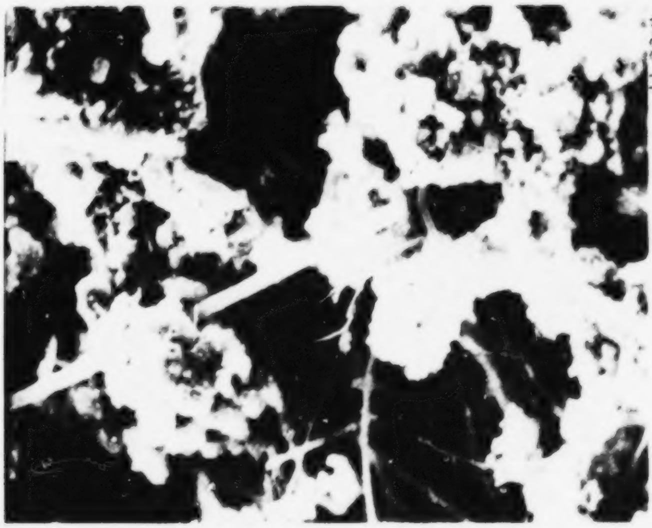

1000X

10 Microns

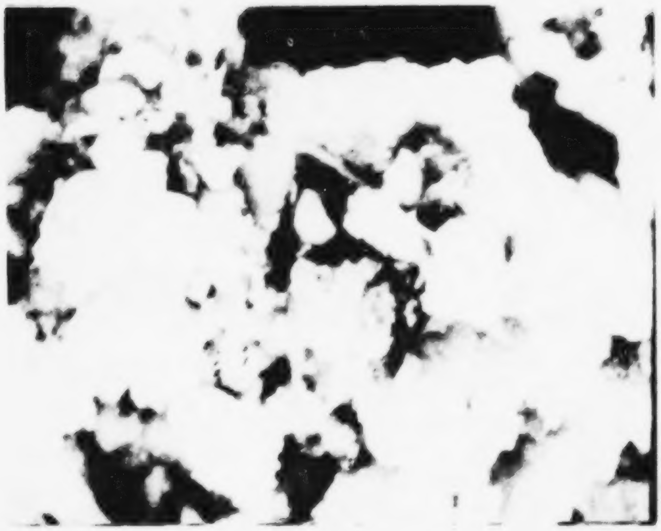

3000X

3 microns

Figure 13. Particle photomicrographs impactor Stage 1.

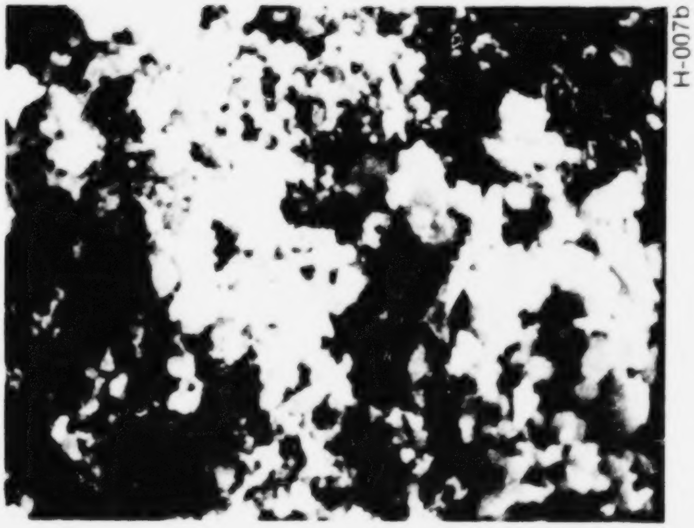

3000X

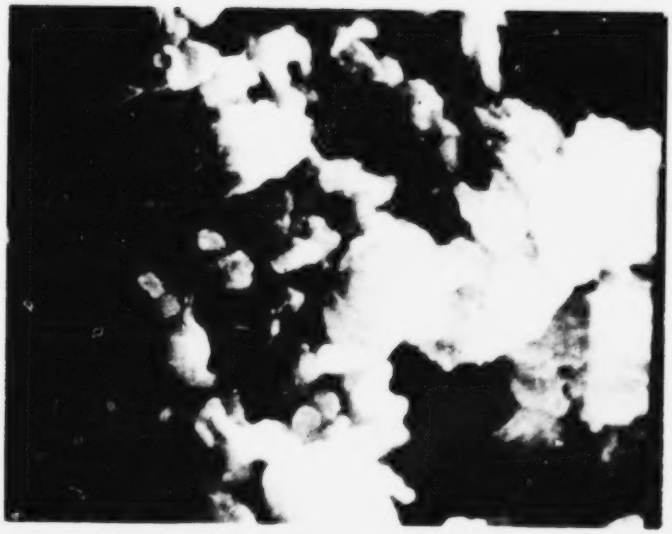

10000X

⊢⟶⊣ 1 micron

Figure 14. Particle photomicrographs impactor Stage 6.

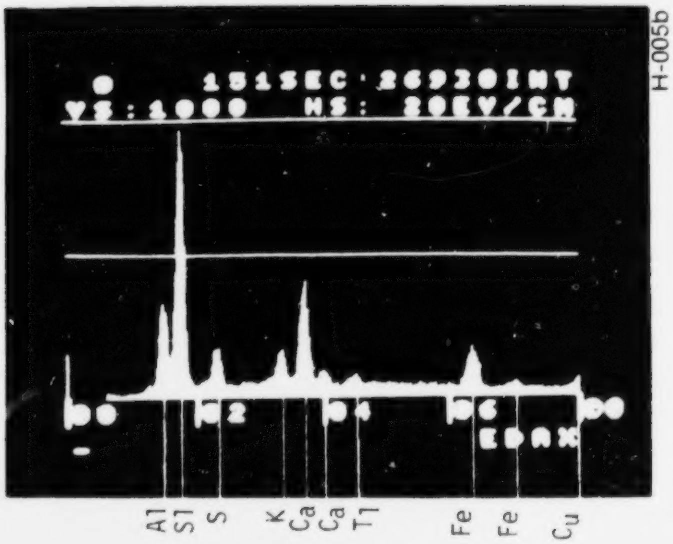

Impactor Stage 1, Run 2

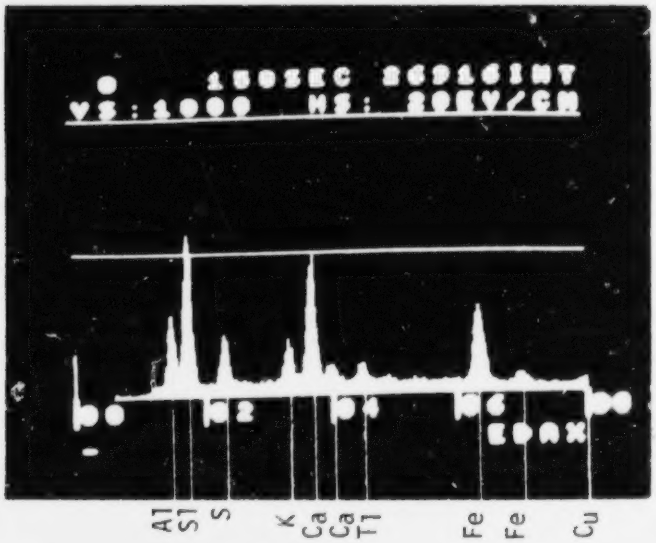

Impactor Stage 6, Run 2

Figure 15. Particle chemical composition - demonstration tests.

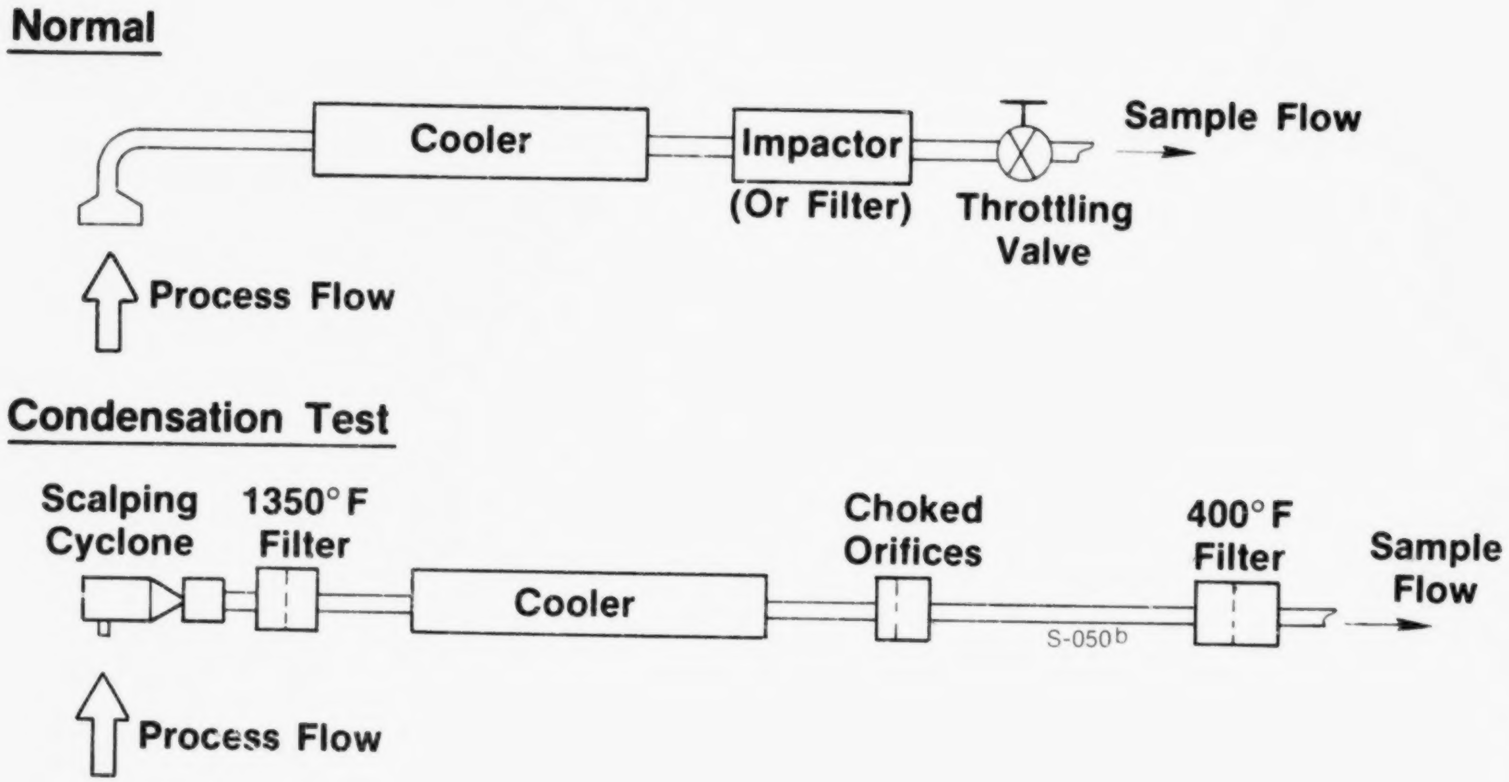
Normal
Cooler
Impactor
(Or Filter)
Throttling
Valve
Sample Flow
Process Flow
Condensation Test
Scalping
Cyclone
1350° F
Filter
Cooler
Choked
Orifices
400° F
Filter
Sample
Flow
S-050b
Process Flow

Figure 16. Probe configurations.

# PARTICLE FIELD DIAGNOSTIC SYSTEMS FOR HIGH TEMPERATURE/PRESSURE ENVIRONMENTS

By:

J. D. Trolinger, W. D. Bachalo
Spectron Development Laboratories, Inc.
Costa Mesa, CA 92626

BLANK PAGE

# PARTICLE FIELD DIAGNOSTIC SYSTEMS
# FOR HIGH TEMPERATURE/PRESSURE ENVIRONMENTS

By:

J. D. Trolinger and W. D. Bachalo
Spectron Development Laboratories, Inc.
3303 Harbor Boulevard, Suite G-3
Costa Mesa, California 92626

Particle diagnostic techniques and instrumentation are reviewed and their relative operational characteristics are discussed. A brief appraisal of optics techniques based on imaging and on light scattering methods has been given. The description of the principles of operation, applicability, and measuring characteristics of the instrumentation being developed by Spectron Development Laboratories (SDL) has been reviewed. These laser-based light scatter detection instruments are based on the predictable angular scattering characteristics of small particles and the interference of coherent light. Angular scattering intensity ratios are used for sizing particles in the range of 0.5 - 10 μm and particle sizing interferometry (visibility) is used in the range 2 - 100 μm.

# PARTICLE FIELD DIAGNOSTIC SYSTEMS
# FOR HIGH TEMPERATURE/PRESSURE ENVIRONMENTS

## SECTION 1

## INTRODUCTION

In view of the shift of emphasis to coal combustion as an energy source, the monitoring of particulates associated with the utilization of coal has become a very important area for technological development. Of the particle sizing systems available, few can withstand the high temperature and high pressure environments of the power plants. However, monitoring the particle flux in such systems is imperative to both the design and operation of the facility. As an example, in fluidized bed combustion (FBC) systems there are a number of areas in which the knowledge of the particle size and morphology would be valuable.

In the bed area, the coal particles under combustion could be monitored for temporal size variation as they pass through the combustion process and for formation of soot and fly ash. Dense spheres of fly ash formed in a stoichiometric combustion are borne in the hot gases. These particles, if not removed by the cyclone separators, can cause excessive erosion (and corrosion) of the gas turbine blades. Efficient removal of particles in the size range of 2 to 10 μm in diameter from the flue gas is especially difficult. Reliable measurements in this size range are required to evaluate the effectiveness of particulate removal systems. Only sparse data now exists on particle loading in this area.[1]

In combined cycle systems where gas and steam turbines are used, water droplets in the steam system may form at lower superheat temperatures. An undetected excess of such droplets will cause greatly accelerated erosive damage to the steam turbine. Reliable droplet detection instrumentation would allow closer control of the steam turbine cycle efficiency.

Environmental concerns require that the levels of emissions from a FBC plant be acceptable or at least tolerable. Of the particulates released into the atmosphere, those in the range of about 0.2 to 3.0 μm are perhaps most damaging to the human respiratory track. Monitoring of these small particulates in a polydisperse effluent in the presence of larger particles is a challenging problem. Typically, particle collection systems can remove most of the larger particles from the effluents. It is a reasonable assumption that the submicron particulates are, to date, escaping undetected.

At Spectron Development Laboratories we have been involved in extensive particle diagnostics research in a broad area of applications including all of the areas mentioned above. For example, holographic particle field diagnostic instrumentation is being tested for its feasibility in monitoring the combustion of coal particles in a laboratory FBC system. Information regarding the particle distribution, size, morphology, and the dynamics of the process are possible with this instrument. Furthermore, there is a possibility of obtaining some information about the flame structure engulfing individual particles. We are refining our particle interferometer and scattering intensity ratioing systems for application in FBC plants. These systems will soon be tested in the ANL Solids/Gas Flow Test Facility. The instrument provides non-intrusive on-line monitoring of flow velocity and particulate content (hence, particle flux). Design of the latest instruments has been directed toward making them operable in the FBC plant environments shown by flags on Figure 1.

In the spirit of the goals of the meeting, our paper will review some of the general principles and techniques available that may be applicable in high temperature/pressure environments as particle diagnostics instruments. The laser-based light scattering optical systems developed by SDL will be discussed in detail with emphasis on the systems' performance and range of application.

## SECTION 2

## A REVIEW OF PARTICLE DIAGNOSTIC TECHNIQUES

In previous research and development of particle diagnostic methods, we compiled and studied more than 500 research publications dealing with this subject. These reports dealt with a wide variety of techniques. To select the instrument concepts that are satisfactory for the application, careful consideration must be given to what characteristics constitute a viable instrument. Some of the criteria to be considered are the following: The instrument must be reliable. In the early stages of development, reliability may mean that the instrument works or does not. The physics concept or concepts involved must be shown to be applicable in the expected particle size range; that is, the system must be suited to the specific application.

As in most situations, the simplest device that performs the desired task is usually the best. This is particularly true where the user of the device sees it as a tool to attain his goals and does not care to or have time to fully understand the details of its operation. In this vain, ease of operation of the instrument must be a fundamental concern. How well the instrument performs may be as dependent on its proper utilization as it is on its conceptual and design integrity. A field-ready instrument must be as rugged as possible and portable, preferably one-man portable. Data retrieval should be straightforward and conveniently formatted. Modern microprocessor technology provides the medium to reduce most instrument information with usable data.

The selection of a particle diagnostics concept from which an instrument may be developed includes four major problem areas: (a) the choice and development of the probing head, (2) calibration and verification of the technique, (3) information processing, and (4) packaging. The instrument development should follow this same order.

The probing element produces the measured parameters for the individual or a collection of particles passing through the sample volume. Selection of this element of the system is critical and hence, the previously mentioned criteria must be fully considered at this stage. In situ instruments typically have even more stringent requirements as they are subjected to the process environment. Once selected, the concept must undergo an exacting verification and calibration with standardized particle fields. Not only does this require verification of the sizing capabilities but also of the operational limitations such as particle loading limitations, rejection of spurious signal, and the system's dynamic range. The system's information storage, retrieval, and display can be as sophisticated as is necessary in light of the advanced electronics technology available in minicomputers and microprocessors. The output may entail doing some statistical analysis on the data, it may be simple mean quantities, or it could be a warning signal transmitted to the plant operator or directly to the plant electronic controls.

There are many methods currently available for measuring size distributions of particulates in gaseous streams, each with their advantages and disadvantages. In this report we review only those techniques that have a possibility of being applied in high temperatures (1000-2000°F) and high pressure (1-10 atms) plants. Some of the techniques require withdrawal of a sample from the stream and the sample then must be analyzed in the laboratory. Others are in situ devices which eliminate some of the uncertainties due to the handling of the sample. However, data quality from such devices is often questionable. Most of the techniques are limited to a definite particle size range. For real particle field measurements, two or more techniques may be required to cover the range of sizes.

Particle sizing techniques fall into one of the following categories:

- Optical
  - Imaging
  - Light Scattering
- Aerodynamic
  - Impaction
  - Centrifugation
  - Sedimentation (Gravitational)

- Filtration
    - Barrier
    - Sieving
- Electrostatic
- Condensation
- Diffusion
- Acoustic

## NON-OPTICAL TECHNIQUES

### Aerodynamic

Particle impactors are currently the standard means of obtaining size distribution measurements under field conditions. Particle laden air is extracted by means of a sampling probe and passed through a series of orifices or slits arranged in order of decreasing size (increasing velocity) and directed against impaction plates. Particles are thus collected on the plates in proportion to their size and information can be gained by counting, weighing or other analytical techniques. Unfortunately, several drawbacks exist which have prompted the need for other methods. Sampling by means of a probe has inherent problems and inaccuracies. Great care must be taken to insure that the sample is extracted isokinetically and that the diameter of the probe and extraction velocities are chosen correctly (to avoid particle deposition). Analyzing the impactor stages after a sample has been taken is also very time consuming. Impactors must be disassembled and careful weighing of samples must occur under laboratory conditions. Weight gain of or loss from the collection substrates is caused by the presence of some gasses and can be a serious problem in data analysis.

Centrifugal devices such as cyclones are also used routinely for particle size determination. Cyclones operate by injecting a particle laden stream tangentially into a tapered conical enclosure. Centrifugal acceleration afforded by the spiral motion determines whether the particle is collected by the cyclone or remains suspended and continues out the exhaust.

Cyclones can be cascaded like impactors to provide a range of particle cut points. Their advantages are that they adapt easily to sampling apparatus and they provide a large collection capacity. Unfortunately, they have the same disadvantages common to impactors.

Centrifugal elutriation devices are also available and this method is the accepted ASME means for fly ash classification. Disadvantages of this device, like impactors and cyclones, are the lack of in situ measuring and the time required for sizing analysis. Other disadvantages are that the sample must be collected and then redispersed into the instrument, classification is highly dependent on flow conditions and inlet geometry, and these devices are generally more expensive than impactors and cyclones.

Gravitational devices depend on particle weight to determine a settling velocity and trajectory causing a distribution by size on the bottom of a settling chamber. This method requires the minimization of convective thermal currents and very long periods of time (several hours) to resolve fine particles which makes it an unattractive means to size particles.

## Filtration

Particles drawn into a sampling probe can be collected by barrier filtration. The barrier filter can be designed to collect essentially 100 percent of the particles present in the stream. This technique is often used as the final collection stage of an inertial impactor train or series of cyclones. This method can also be used as the only collection device. While it is not an in situ method, it does have the advantage that essentially all the particulates are collected in one place. As with several of the other techniques, it has the disadvantage that size distribution is done by time-consuming laboratory techniques such as Coulter counter analysis, optical or SEM microscopy. Accuracy is dependent upon the ability to redisperse the particles. As a rule, this is increasingly difficult as particle size is reduced.

The size distribution of particles in bulk form can be obtained down to about 2 μm by sieving. Sieves for fine particle analysis are pans with bottoms of electroformed grids. Particles are separated into size fractions by means of a series of sieves and the particle mass retained on each sieve is usually determined by weighing.

## Acoustic

A relatively large airborne particle, e.g., 15 μm, passing rapidly through a gradually tapering tube that expands rapidly after a small throat, produces an audible click that can be counted or recorded electronically. The click originates near the end of the throat as a shock wave due to boundary-layer disturbance in the throat created by the particle. The device is simple, but no embodiment yet designed responds to small particles, and the response that is given is only a rough indication of particle size.

Particle size can be deduced from the sinusoidal paths particles follow if a slowly rising aerosol stream is dark-field illuminated and exposed to low-power sound waves. The method is obviously tedious and is to be recommended only if special circumstances dictate its use.

A measure of the particle size and concentration of aerosol can also be deduced from the extinction of ultrasonic sound waves passing through an aerosol and through the same gas without particles. Conditions are most favorable for the application of sound-attenuation techniques with aerosols of high concentrations. This makes such techniques of dubious practical value in most instances.

## Vibrating Crystals

Piezoelectric crystal mass monitors in combination with an impactor train would appear to hold some promise for an in situ particle size distribution and concentration device. The piezoelectric mass monitors are intriguing because of their extreme sensitivity. However, such a device can be expected to be subject to several sources of error: linearity problems could require short sampling periods especially in high concentrations, errors could result from temperature or humidity fluctuations, non-uniform particle density could be interpreted as changes in concentration and the devices would require a crystal cleaning device for subsequent readings.

## Filter Tape with Beta Absorption Mass Monitor

A device of this type has been sued to measure the mass of atmospheric fine particle aerosol. Since it is basically a mass measurement device, it is probably not easily adapted to in situ measurements. Particle sizing would depend upon impactors and the mechanism required for moving the filter tape would be prone to problems in the severe environment contemplated for the in situ fine particle analyzer.

### Contact Electrification Devices

This is a class of instruments which provides an electrical current proportional to the particle mass concentration in a gas stream. They work by transfer of charge from the particulate to the instrument probe through particulate probe collisions. The sensitivity of the devices depend on the electrical resistivity of the particulate as well as upon the condition of the surface of the probe. The theory for operation of these devices is poorly understood. They can be expected to suffer from the effects of sticky particles and from particulate streams of varying composition. Furthermore, the device does not seem well suited to measurement of particle size distribution.

## OPTICAL TECHNIQUES

### Imaging Methods

A number of considerations and definitions apply in general to imaging techniques. The most fundamental is the degree of resolution attainable with the system. For a perfect imaging system, a point source of light will be imaged to a finite sized spot (impulse response, point spread function, blur circle) limited in size by the laws of diffraction. This image size represents the smallest object which can be resolved in the image or the smallest spot to which a light beam may be focused. The diffraction limited resolution is given approximately by

$$R_D = 1.22 \lambda S/D \tag{1}$$

where S is the lens to object distance, D is the effective diameter of the collecting system (lens or limiting aperture) and $\lambda$ is the wavelength of the light. Smaller objects than this can be detected in the image if the signal-to-noise ratio is sufficient, but the dimensions of smaller particle images can be no smaller than the resolution limit. Except for very limited cases, resolution is worse than that given by the above relationship because geometrical aberration terms must be added.

Another important consideration is optical noise or system signal-to-noise ratio. Every optical system scatters useless light into the vicinity of the image being analyzed to the extent that this usually limits the utility of the imaging technique. In particle field diagnostics, the situation is amplified by the fact that all particles besides the one being imaged at a given time are potential sources of optical noise. This means that not only the optical system but the particle field itself must be considered in evaluating ultimate system capability. Ambient light usually represents a noise source, but methods are now available to effectively eliminate this as a problem.

## Holography

Holography or wavefront reconstruction allows the reproduction of the scattered light field in the laboratory. With this technique, holograms are made of the particle field (Figure 2); and after processing, the image is reconstructed and scanned with the aid of microscopy and video techniques.[2] The narrow depth of field is given approximately by

$$S = \frac{R^2}{\lambda} \tag{2}$$

which is a problem in photography but is relaxed with holography. The reconstructed image can be scanned in depth with a microscope. Thus, for a given resolution, holography expands the image storage capability by three or four orders of magnitude.

Holography has been shown capable of resolving particle sizes as small as 1 micron in diameter. The advantage of this technique is that a global view of the particle field is available. Spatial and temporal variations in the field may be detected and evaluated as they relate to the process at hand. This is a particularly useful capability when investigating processes such as the ignition and combustion of coal in a fluidized bed. Shape variations as well as size change can be observed with this technique. Double pulse holography poses the possibility of investigating the local temperature field simultaneously.

The processing of holograms requires a period of time for recovering the information making real time diagnostics impossible with the materials currently available. Holography related technology is almost certain to produce real time recording and reduction materials. When combined with rapid electronic image analysis, holography would qualify as a valid method for a much greater range of high temperature/pressure applications.

## Scattering Instruments

Instruments based on light scattering can measure particle sizes to at least an order of magnitude smaller than the resolution limit of the system's transmitting lenses. This can be done without high quality scattered light collecting systems. However, the transmitting optics must be of a high quality.

Particles illuminated by a high intensity light beam will scatter light by an amount and in a spatial distribution that depends on several factors. Careful optical selection of conditions can reduce the number of parameters or provide for factoring out such parameters. When the particle diameter is greater than the light wavelength and when only forward scattered light is considered, the Fresnel-Kirkhoff approximations may be used to predict the diffracted light intensity distributions. The intensity of forward scattered light is given for a circular disk by:

$$I(a) = I_0 k^2 a^4 \left[\frac{J_1(Ka\omega)}{Ka\omega}\right]^2 \qquad (3)$$

where $I_0$ = the incident flux per unit area

$k = 2\pi/\lambda$

$\omega = \sin\theta$ where $\theta$ is the angle relative to the incident beam

$a$ = particle radius.

An instrument that collects the scattered light making a single measurement per particle collects the integrated intensity over the collecting angle. When the collecting angle is small enough such that $J_1(ka\omega)/(ka\omega)$ is constant, the intensity is approximately:

$$I_t^0 \cong \frac{\pi}{4} I_0 k^2 \omega_0^2 a^4 \qquad (4)$$

Thus, a particle sizing instrument could be based on the collection of forward scattered light yielding a signal proportional to $a^4$. It is important to note that since the scattering is based upon diffraction theory, the scattered light is not dependent on refractive index.

If light collection is taken over a large scattering angle, the collected intensity is approximated by

$$I_t^{\angle} = \int_0^{\infty} I(\omega) 2\pi\omega d\omega \approx \pi I_0 a^2 \quad . \qquad (5)$$

The important result being that when all the scattered light is collected, a signal proportional to $a^2$ results.

Scattering Ratio Measurements

In order to overcome the sensitivity of a scatter-based instrument to refractive index and to incident intensity variation, the ratio of the scattered light intensity at two angles may be measured. In polydisperse particle fields of unknown materials or with several known materials of different index of refraction, insensitivity to this parameter is important. Furthermore, the light intensity incident on the particle in a laser-based system will show large intensity variation (at least an order of magnitude) depending on where the particle crosses the focal volume. Ratioing of the light scattered at two angles eliminates the uncertainty due to the variations in incident light intensity.

Figure 3 shows a polar plot of angular scattering intensity for representative particle sizes. These scattering relationships are based on Mie scattering theory. Because the forward scatter lobes become very narrow for larger particles, this technique is limited to particle diameters between about 0.5 and 5 μm for an incident light wavelength of 0.633 μm (Figure 4). For smaller particle diameters, ratioing of the forward and backscatter intensities may be used. This reintroduces at least a weak dependence on index of refraction due to the backscatter measurement. However, particles in the range of 0.1 to 1.0 μm in diameter have been measured using this principle.

Because this type of measurement does not require single particle scattering to provide useful information, the device is well-suited for making measurements in the small size range with a relatively high number of particles. When an ensemble of particles is illuminated, it can be shown that measurements of intensity ratio of light scattered at two angles can produce the mean diameter of the sample.

We are currently actively involved in developing this technique into a workable instrument. Incorporation of this system into our particle sizing interferometer will enhance the accuracy of our small particle measurements and alleviate the difficulties with multiple particles being in the probe volume simultaneously.

## Particle Sizing Interferometry

When a laser beam is split into two equal intensity beams and the beams are focused to a crossover, fringes formed of spatially varying light intensity occur (Figure 5). The fringes fill the small ellipsoidal space that constitutes the focal volume. These fringes are parallel (if the system is properly designed) and equally spaced a distance $\delta$ apart, given by

$$\delta = \frac{\lambda}{2 \sin \theta/2} \tag{6}$$

where $\theta$ is the beam intersection angle (Figure 6).

Particles moving through the focal volume will scatter light in proportion to the encountered spatially varying light intensity. The scattered light signal is a type of convolution of the particle geometry with the probe volume intensity distribution. As the particle size with respect to the fringe spacing increases, the scattered light signal increases in strength but decreases in modulation percentage. The measure of the ratio of the minimum to maximum signal modulation has been termed the visibility (Figure 7).

This technique possesses the desired features of the best scattering methods; a well-defined and controlled sample volume; a measurement of ratios of intensity as opposed to absolute magnitude; and perhaps most important, an independence from refractive index of the particle. Because the optics arrangement is identical to that of the well-known and powerful laser velocimeter technique, the velocity of the particles is simultaneously available. Hence, particle flux and concentration can be evaluated with this device.

The technique has been demonstrated by several researchers$^{3-6}$ to be exceptionally reliable when operated in the forward scatter mode of light collection. Particle sizes in the range from 5 - 100 μm have been measured accurately. Smaller sizes may be measured[6] but care must be taken in properly designing the collection system. At one fringe setting, a decade in particle size range can be measured. A simple adjustment is required to change the probe size and fringe spacing to cover a larger range in decade steps. We are presently engaged in designing a system to cover two decades in particle size without any manipulations required by the operator.

Considerable effort has been devoted in the development of the signal processing electronics (Figure 8). Good accuracy has been achieved with our visibility processor. The instrument's noise rejection logic has been further refined to decrease the possibility of spurious signal acceptance.

We are also concentrating on developing a more rugged and compact packaging arrangement (Figures 9 and 10). The package is being planned such that little or no operator adjustments need be made after the system has been established. Furthermore, the enclosure for the instrument will protect the optics and laser from damage or contamination when in the hazardous plant environment.

Particle sizing interferometer instruments have been developed by Spectron Development Laboratories and applied in the field to a wide range of situations. The following is a list of such applications demonstrating the instrument's versatility:

1. Pollution monitoring from a helicopter platform.
2. Cloud diagnostics from a high altitude aircraft.
3. Particle diagnostics in simulated erosion facilities.
4. Diagnostics of fuel droplet sizes from nozzles.
5. Metrologic measurements in cloud chambers.
6. Analysis of medical nebulizers.
7. Rocket exhaust diagnostics.
8. Fog diagnostics.

# SECTION 3

# CONCLUSIONS

Although a number of techniques may be devised for application to high temperature/pressure environments, we believe the optical methods will produce the most desirable instruments. Optical particle sizing instruments are non-intrusive and hence do not disturb the flow field. Only a window access to the test region is required. In situ measurements have been made with acceptable reliability. The data retrieval systems can be automated and measurements can be made in almost real time. Sampling techniques invariably require significant time periods in handling the sample and recovering the desired information.

A disadvantage in using light scattering techniques is the inability to determine the particle shape. Analysis and calibrations are based on spherical particles. In flow fields where particle shapes may deviate from spherical errors in the size determination will occur. We are investigating certain possibilities that may allow the determination of at least gross shape information from additional scattering information.

In the future, we anticipate that longer range operations (1 - 2 meters) of our scattering instruments will be required. Research is being carried out on photon correlation processors for our particle sizing interferometer. That would allow processing of signals wherein only a slightly greater number of photons reach the detector when the particle is in a bright fringe than when it is in the dark region (Figure 11). Such techniques have the advantage of utilizing low-power lightweight lasers for long range measurements.

The data storage and processing systems we have available will be updated with programmed microprocessors. We expect to have a broad range of data management formats to supply the user's special requirements. In addition, we have the capability of interfacing our systems to minicomputers and providing the software for more elaborate data analysis and systems automation.

## SECTION 4

## REFERENCES

1. Brooks, Robert D., "Coal Fired Combined Cycle Development Programs," Proceedings of the Fluidized Bed Combustion Technology Exchange Workshop, April 1977, pp 109-124.

2. Trolinger, J. D., "Particle Field Holography," Optical Engineering, Vol. 14, No. 5, p 383 (1975).

3. Farmer, W. M., "Measurement of Particle Size, Number Density, and Velocity Using a Laser Interferometer," Applied Optics, 11, 2603 (1972).

4. Adrian, R. J. and Orloff, K. L., "Laser Anemometer Signals: Visibility Characteristics and Application to Particle Size," Applied Optics, 16, No. 3, 677 (1977).

5. Robinson, D. M. and Chu, W. P., "Diffraction Analysis of Doppler Signal Characteristics for a Cross-Beam Laser Doppler Velocimeter," Applied Optics, 14, No. 9, 2177 (1972).

6. Chu, W. P. and Robinson, D. M., "Scattering from a Moving Spherical Particle by Two Crossed Coherent Plane Waves," Applied Optics, 16, No. 3, 619 (1977).

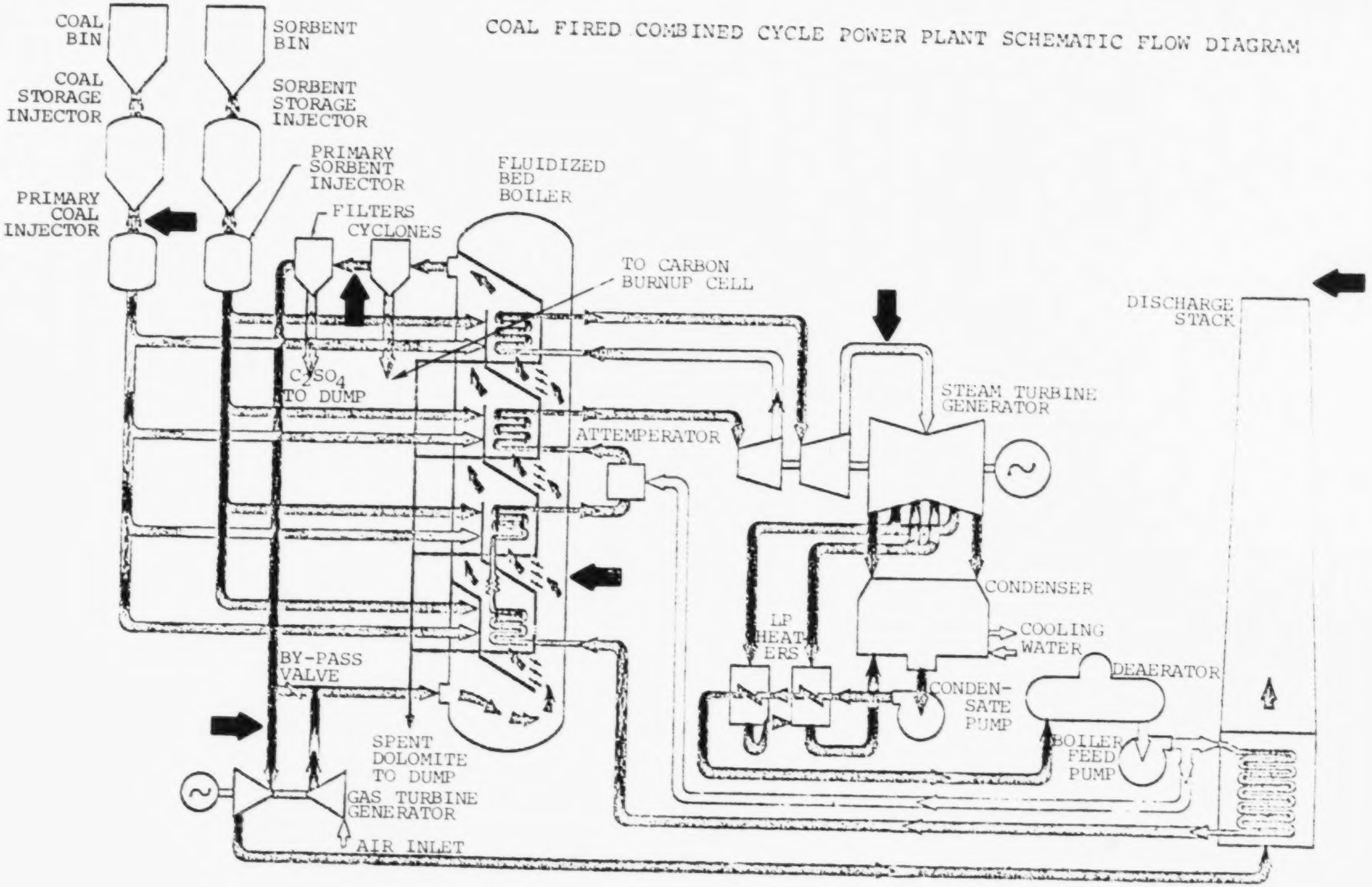
COAL FIRED COMBINED CYCLE POWER PLANT SCHEMATIC FLOW DIAGRAM
COAL BIN
COAL STORAGE INJECTOR
PRIMARY COAL INJECTOR
SORBENT BIN
SORBENT STORAGE INJECTOR
PRIMARY SORBENT INJECTOR
FILTERS
CYCLONES
FLUIDIZED BED BOILER
TO CARBON BURNUP CELL
$C_2SO_4$ TO DUMP
ATTEMPERATOR
STEAM TURBINE GENERATOR
DISCHARGE STACK
CONDENSER
COOLING WATER
LP HEATERS
CONDENSATE PUMP
DEAERATOR
BOILER FEED PUMP
BY-PASS VALVE
SPENT DOLOMITE TO DUMP
GAS TURBINE GENERATOR
AIR INLET

Figure 1. Fluidized Bed Combustion Plant with Particle Monitoring System Locations Indicated by Arrows.

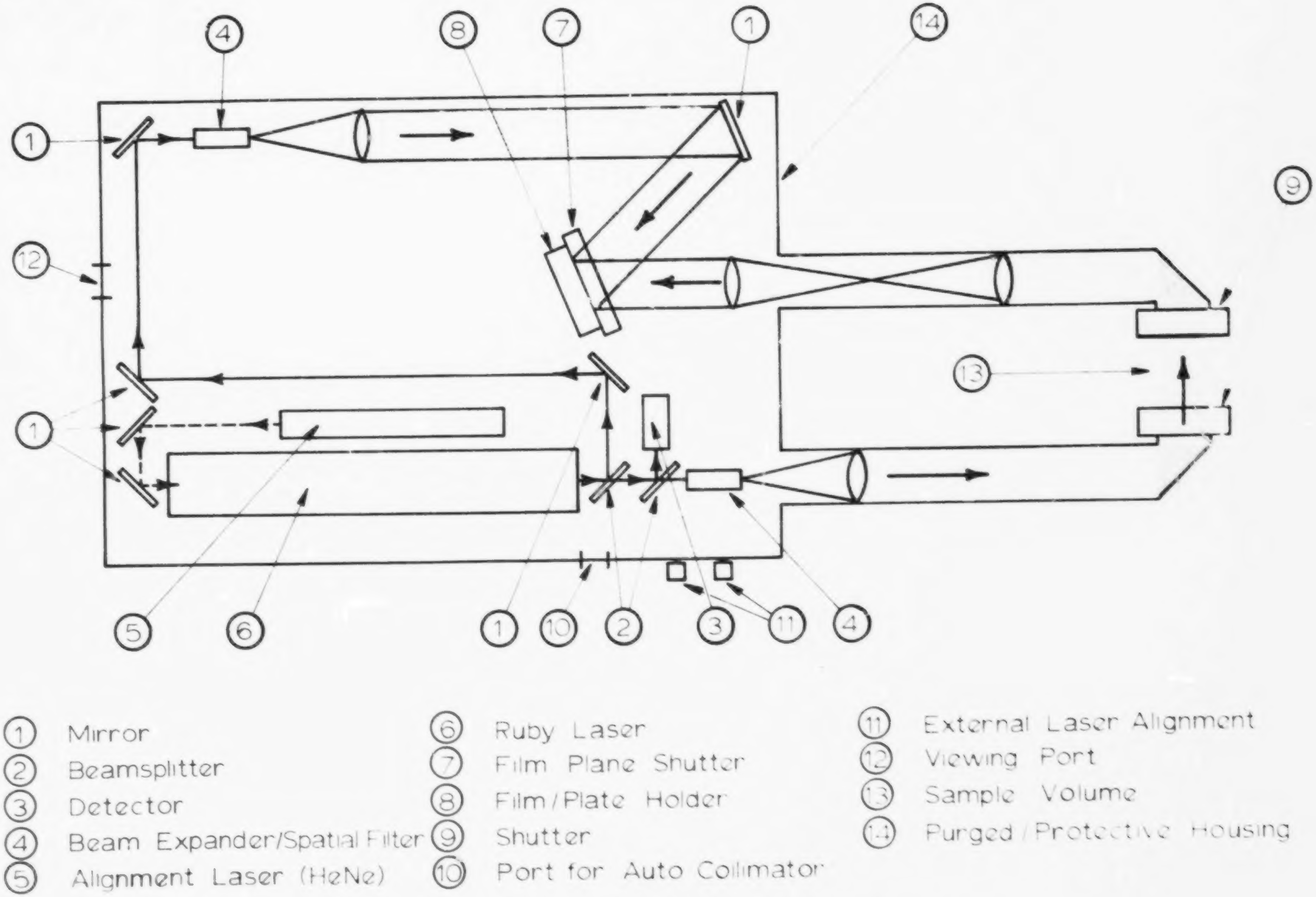
① Mirror
② Beamsplitter
③ Detector
④ Beam Expander/Spatial Filter
⑤ Alignment Laser (HeNe)
⑥ Ruby Laser
⑦ Film Plane Shutter
⑧ Film/Plate Holder
⑨ Shutter
⑩ Port for Auto Collimator
⑪ External Laser Alignment
⑫ Viewing Port
⑬ Sample Volume
⑭ Purged/Protective Housing

Figure 2. Field Portable Particle Holocamera.

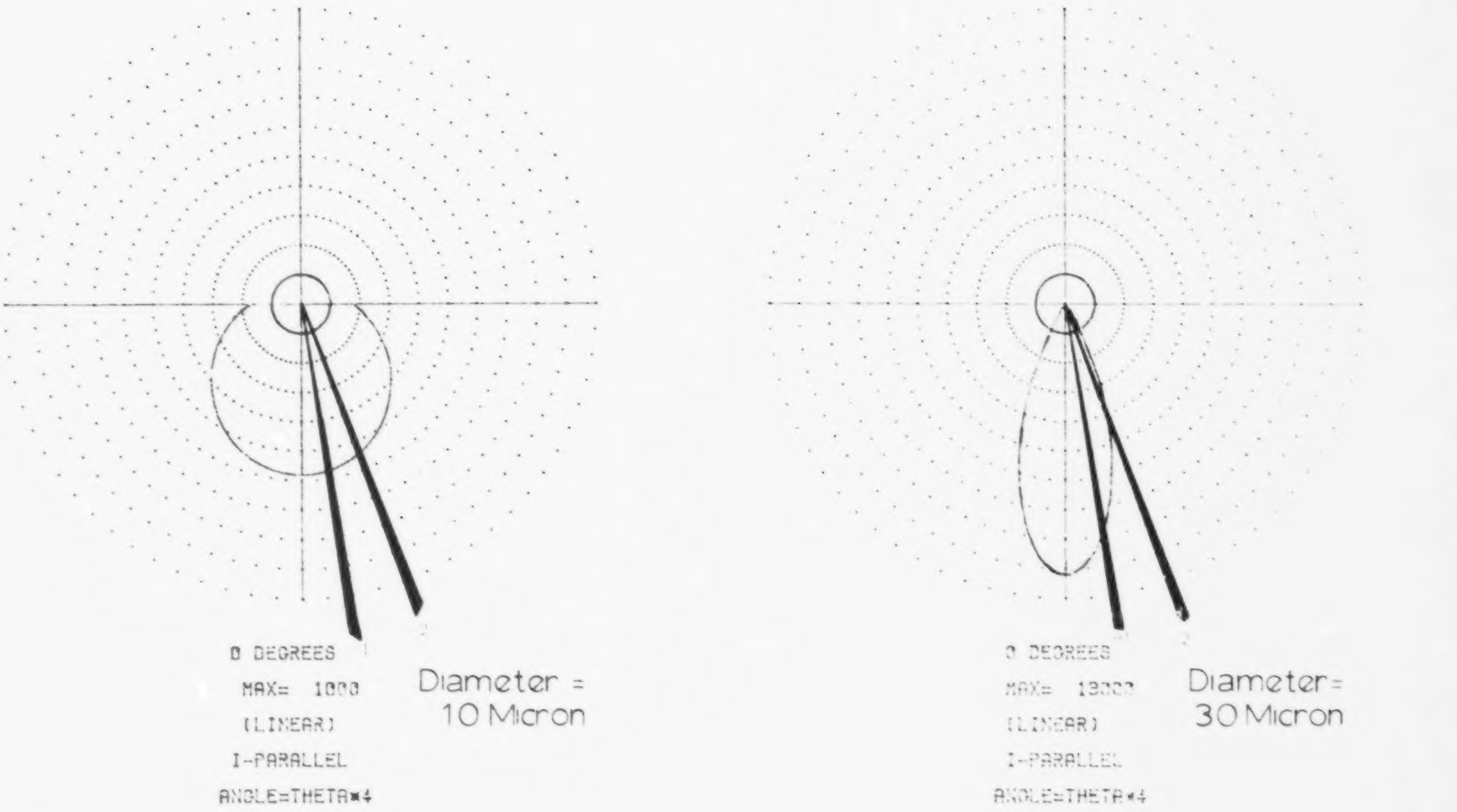

Figure 3. Polar Diagrams for the Scattering of Linearly Polarized Light.

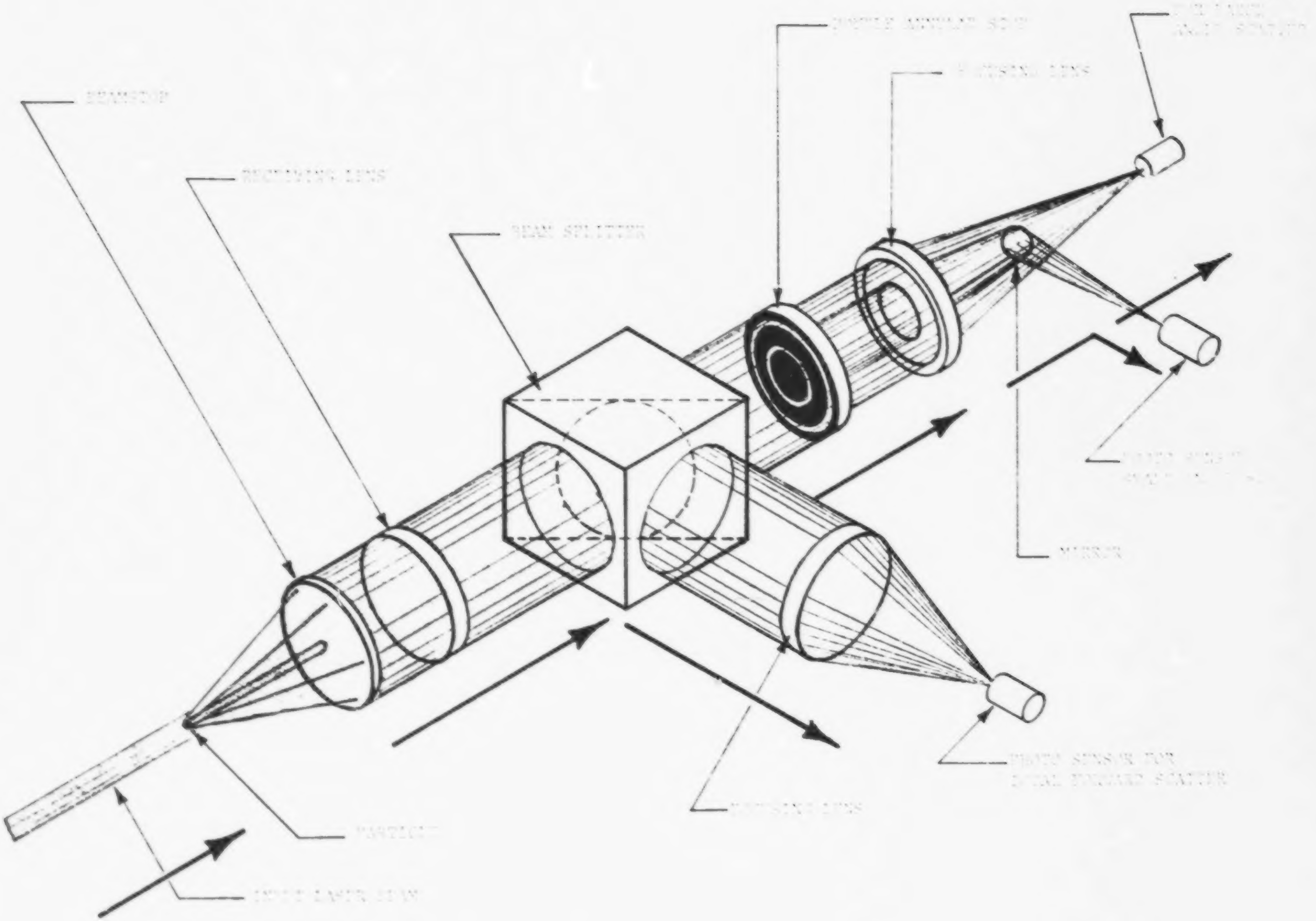
BEAMSTOP
RECEIVING LENS
BEAM SPLITTER
DOUBLE ANNULAR STOP
FOCUSING LENS
MIRROR
PHOTO SENSOR FOR
TOTAL FORWARD SCATTER
FOCUSING LENS
PARTICLE
INPUT LASER BEAM

Figure 4a. Optical Layout for Angular Scattering Intensity Ratioing.

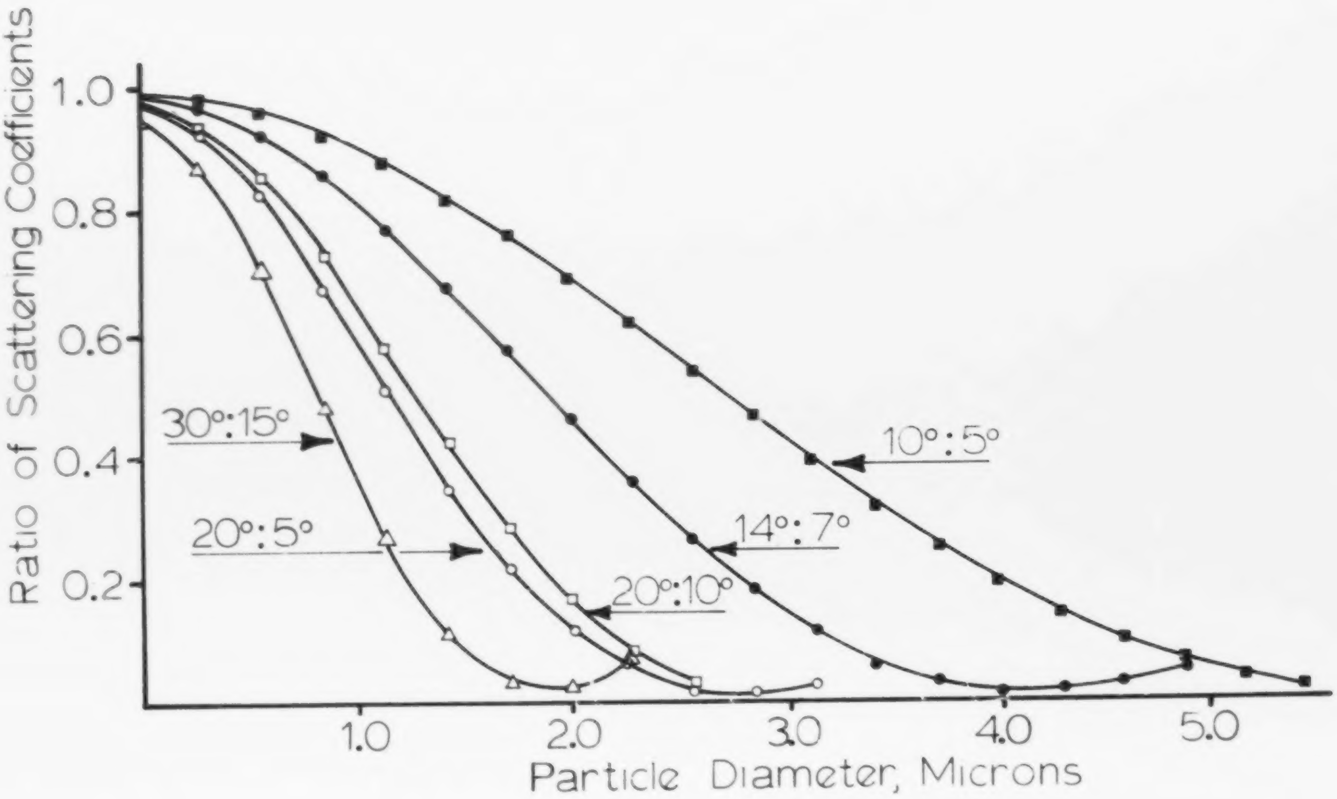

Figure 4b. Scattering Coefficients Vs. Particle Diameter at Various Angle Pairs.

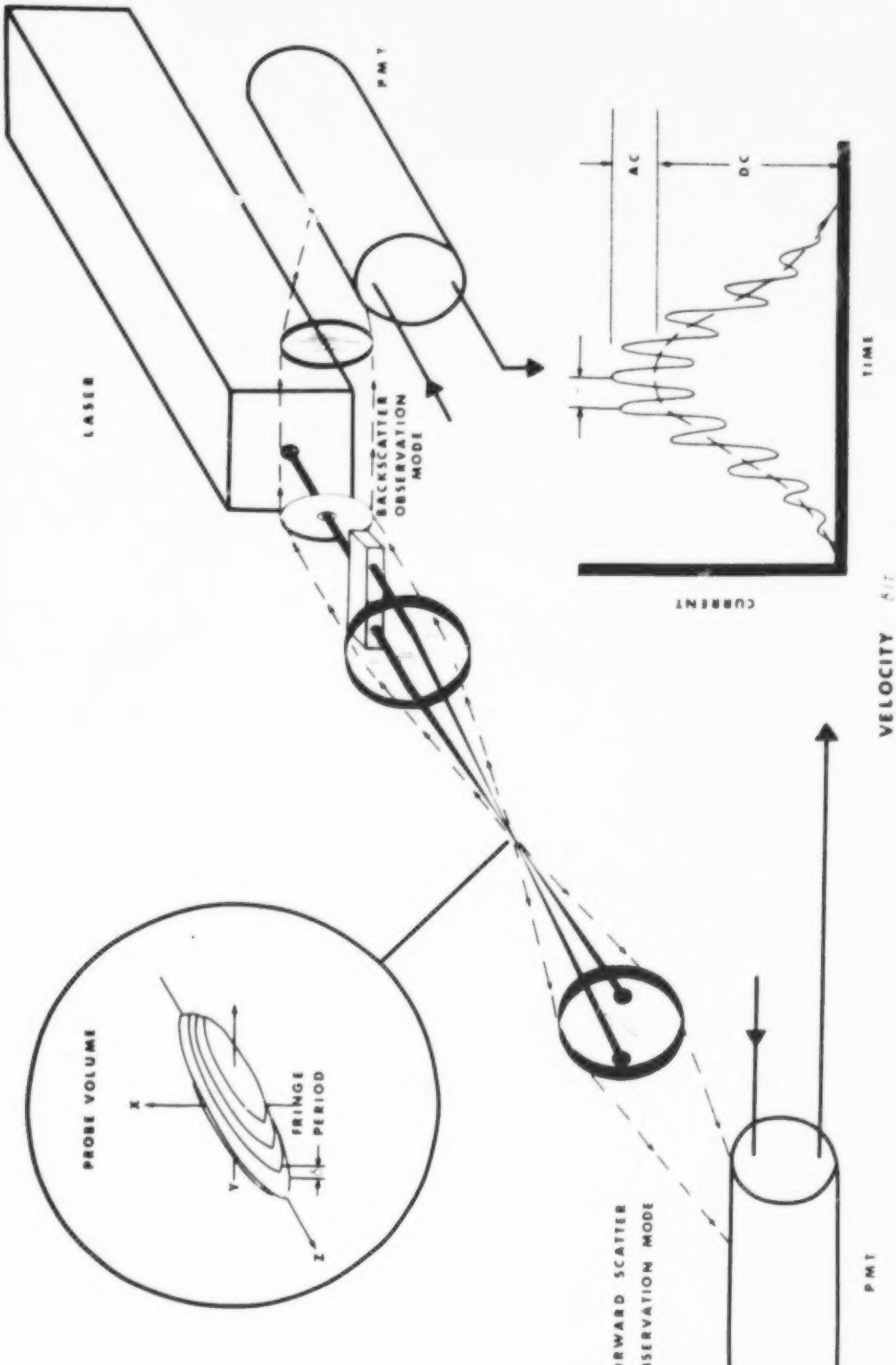
LASER
PMT
BACKSCATTER OBSERVATION MODE
AC
DC
CURRENT
TIME
VELOCITY
PARTICLE SIZE - AC DC
PROBE VOLUME
X
Y
Z
FRINGE PERIOD
FORWARD SCATTER OBSERVATION MODE
PMT

Figure 5. Particle Sizing Interferometer Schematic.

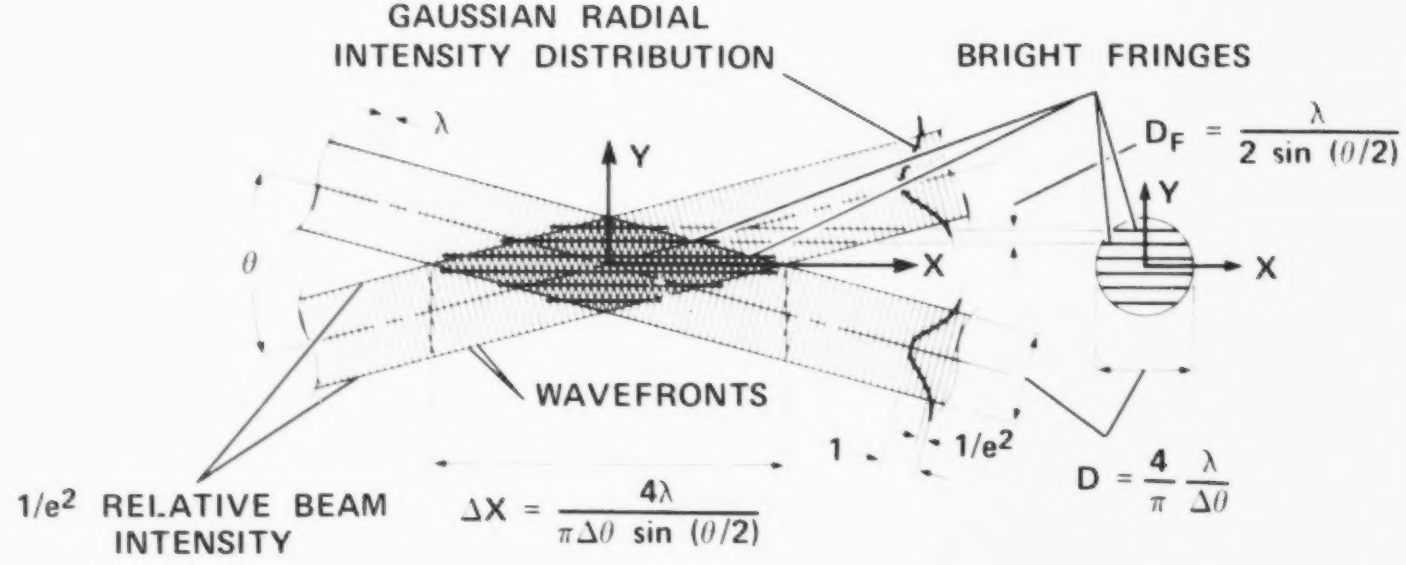
GAUSSIAN RADIAL INTENSITY DISTRIBUTION
BRIGHT FRINGES
$\lambda$
$D_F = \frac{\lambda}{2 \sin (\theta/2)}$
Y
X
Y
X
$\theta$
WAVEFRONTS
1
$1/e^2$
$1/e^2$ RELATIVE BEAM INTENSITY
$\Delta X = \frac{4\lambda}{\pi \Delta\theta \sin (\theta/2)}$
$D = \frac{4}{\pi} \frac{\lambda}{\Delta\theta}$

Figure 6. Enlarged Cross-Sectional Views of the Beam Crossover Region.

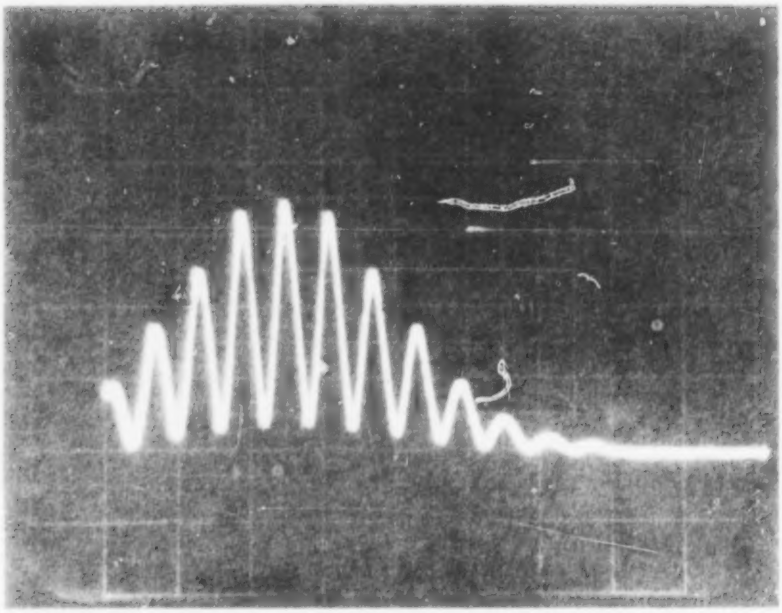

(a) $V = \frac{v_{max} - v_{min}}{v_{max} + v_{min}} = 0.84$

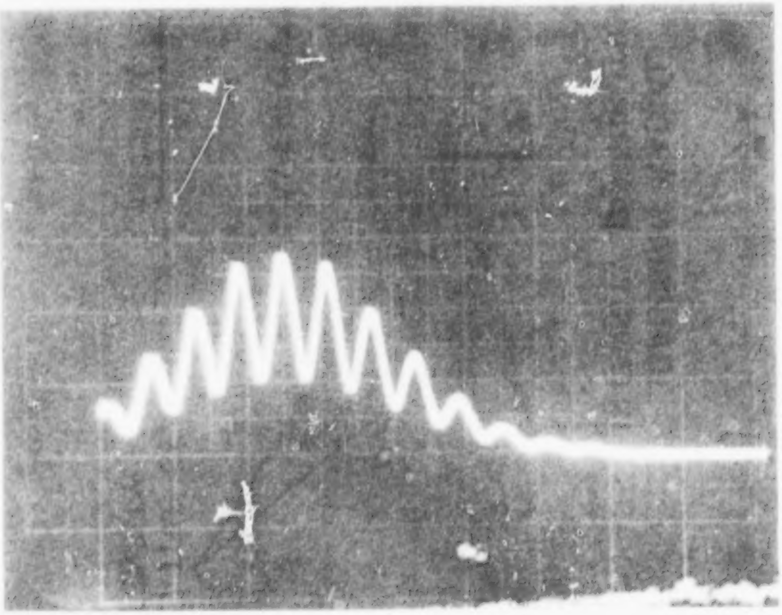

(b) V = 0.47

Figure 7. Oscilloscope Traces of Visibility Signals from the Particle Sizing Interferometer.

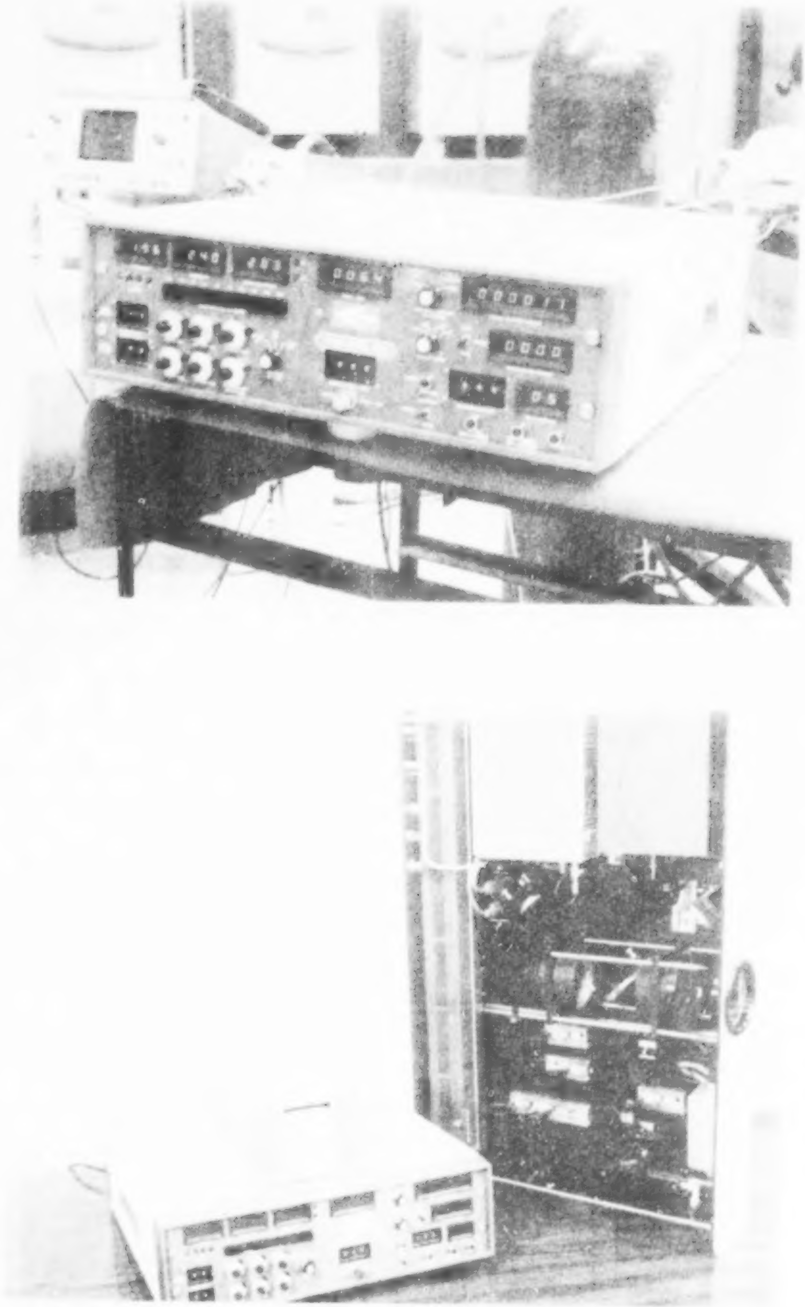

Figure 8. Particle Sizing Interferometer System.

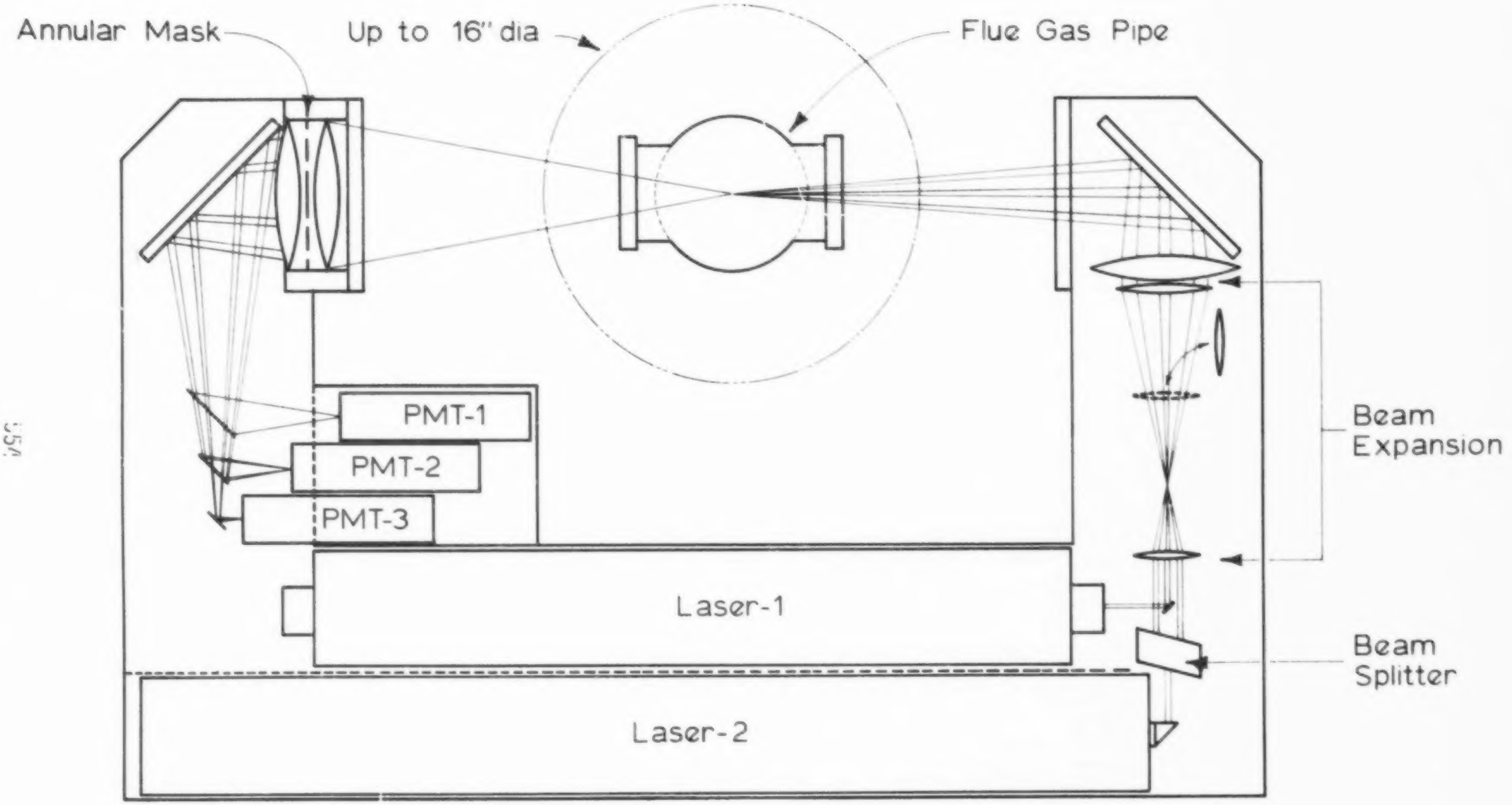
Annular Mask
Up to 16" dia
Flue Gas Pipe
PMT-1
PMT-2
PMT-3
Beam
Expansion
Laser-1
Beam
Splitter
Laser-2

Figure 9. Two-Color Laser-Based Particle Analyzer for High Temperature/Pressure Applications.

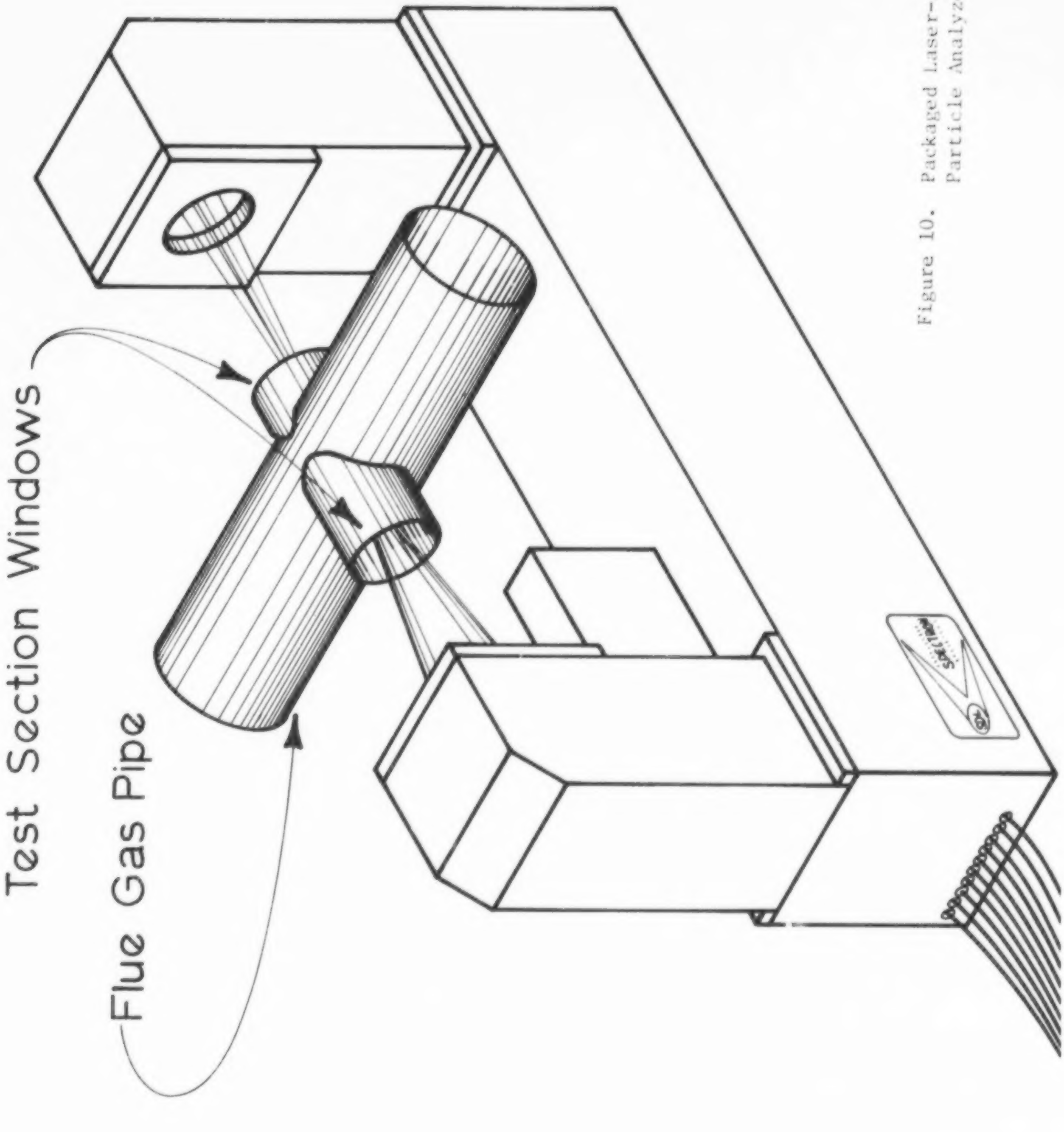
Test Section Windows
Flue Gas Pipe

Figure 10. Packaged Laser-Based Particle Analyzer.

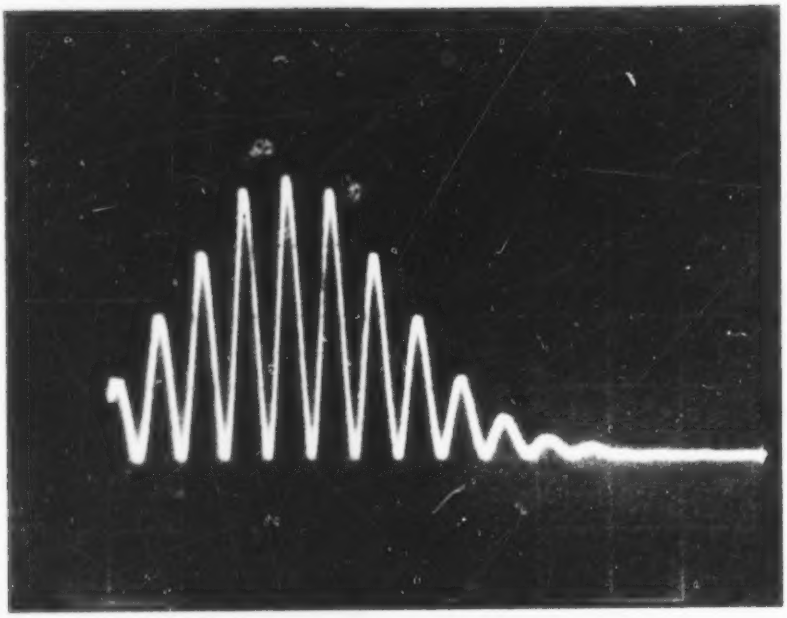

(a) Classical Signal, 100% Visibility

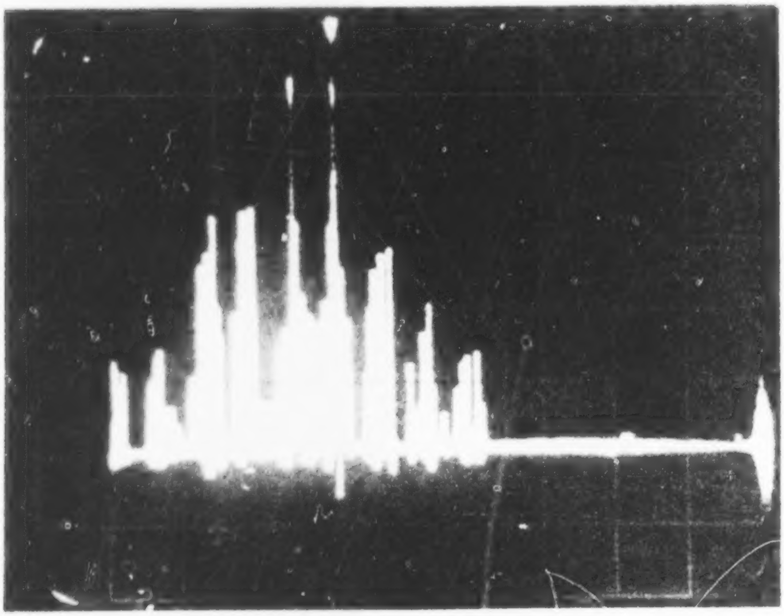

(b) Signal Composed of Individual Photon Bursts

Figure 11. Classical Versus Photon Limited Visibility Signals.

# ON LINE PARTICULATE ANALYSIS ON A FLUIDIZED-BED COMBUSTOR

By:

E. S. VanValkenburg, H. N. Frock
Leeds & Northrup Company
North Wales, PA 19454

# ON LINE PARTICULATE ANALYSIS ON A FLUIDIZED-BED COMBUSTOR

By:

E. S. VanValkenburg
H. N. Frock

Leeds & Northrup Company
North Wales, Pa. 19454

## ABSTRACT

An on-line particulate analysis instrument has been developed by Leeds & Northrup Company under ERDA sponsorship for monitoring particle loadings in the gas clean up stages of advanced combustion systems. This instrument utilizes low angle forward scattering of optically illuminated particles by across-the-duct measurements to determine their size and concentration.

A prototype instrument has been designed and constructed to evaluate this means of measuring particles on fluidized bed combustion systems and field tests have been completed on this unit at the Argonne National Laboratory. This paper presents a brief description of the instrument and discusses results obtained from the Argonne tests.

# ON-LINE PARTICULATE ANALYSIS ON A FLUIDIZED-BED COMBUSTOR

## SECTION 1

## INTRODUCTION

An on-line particulate analysis instrument has been developed by Leeds & Northrup Company under ERDA sponsorship for in situ measurement of particle loading and size in the product gas streams of advanced combustion systems. A prototype instrument has been designed and constructed to evaluate this means of measuring particles on fluidized bed combustion systems and field tests have been completed on this unit at the Argonne National Laboratory. This paper presents a brief description of the instrument and discusses results obtained from the Argonne tests.

This particulate instrumentation is based on Leeds & Northrup's prior research in low-angle forward scattering of light by micron size particles suspended in fluid streams. When such particles are optically illuminated, the scattered light intensity at any given angle is a function of the size, shape and index of refraction of the particles. In the case where the wavelength is small in comparison to the size of the particles, the spatial distribution of the scattered light in the far field is dominated by the volume and size characteristics of the particles. The design of the ERDA instrument is based on utilization of simple diffraction theory to convert measurements of the composite Fraunhofer diffraction pattern for a large number of particles into meaningful particle data which characterizes the size distribution and concentration.

This type of instrumentation will be used later to evaluate the performance of secondary particle clean up and to measure the size distribution and concentration of particles at the inlet to gas turbines in direct combustion coal-fired systems. The latter application requires instrumentation amenable to measurement of particles in high temperature (1500-2000F) pressurized (up to 10 atmospheres) gas streams and be adaptable to rather large diameter gas ducts. The prototype instrument will accommodate gas ducts up to one foot internal diameter.

Field tests were completed at ANL on August 19, 1977 and the prototype instrument is now at Leeds & Northrup Company for calibration recheck. It will be delivered to Curtiss Wright Corporation soon where it will be installed on the Small Gas Turbine fluidized bed combustion system. This installation will enable testing the instrument performance for in situ measurements at seven atmospheres pressure and 1600F range.

I will first describe the particulate analysis instrument and then present some of the results from the tests at Argonne National Laboratory.

## SECTION 2

## INSTRUMENT DESCRIPTION

A schematic diagram of the optical train of the ERDA instrument is shown in Figure 1. This instrument consists of optical elements mounted to an optical bench which extends under a horizontal run of the combustion system duct. (The duct is not shown in the schematic, only its vertical center line). The illumination source is a helium cadmium laser mounted to the underside of the optical bench. Folding optics, attached to the left end of the optical bench, direct the laser beam across the duct where particles in the gas stream, which are illuminated by the beam, scatter the light. The scattered flux is collected by a lens and focused on a set of function masks. The portions of flux, which are transmitted through the function masks, are focused by a second lens on to the photomultiplier detector.

The output power of the laser is measured by a silicon photodiode which detects radiation from the rear Brewster window of the laser. This signal is displayed on a meter for ease of adjusting the laser alignment to maintain peak power output (10 to 20 mW).

A photograph of the prototype instrument is shown in Figure 2. This instrument consists of the optical subsystem assembly, an electronics package, laser power supply, and a digital line printer. All units, except the printer, are contained in NEMA 12 class enclosures to meet industrial environmental requirements. The laser and receiving optics units contain thermostat controlled heaters so that the optical subsystem may be installed on a gas duct which is located outside of a building.

The electronics package includes a microcomputer, visual display and all the operating controls. This unit can be located up to 200 feet from the optical subsystem. The digital data printer is used to log the output measurements and can be located remotely from the electronics package, if desired.

The opening on the optical subassembly from the folding optics on the left to the collection lens bezel is 30 inches. The vertical clearance above the optical bench to the laser beam center line is 9-1/2 inches. These dimensions were chosen to accommodate a 12-inch I.D. duct with a tee section viewing port extending on each side of the duct.

Mechanical adjustments are provided on the folding optics for alignment of the optical train to the duct windows after the instrument is installed. The instrument can be mechanically mounted to the duct through the load carrying base structure.

Without going into detail on the theory of optically scattering measurements, I will describe the basic fundamentals to enable those who may not be familiar with our instrument to understand the nature of its data outputs.

All particles illuminated by the collimated laser beam as it traverses across the gas duct scatter flux off the beam axis. For particles in the size range 1-100 microns most of the scattered flux is in the near forward direction. We collect that flux and through an optical process convert that data into information concerning the particle size distribution and the particle loading. The particle loading output is calibrated to be direct reading in parts per million by volume, i.e., ratio of total volume of particles per unit volume of gas.

A common means of presenting size distribution is to plot the population of particles as a function of their size as shown in Figure 3A. In order to obtain data more useful for control purposes, it is possible to describe size distributions in ways other than number density. Three means of presenting the same particle distribution are shown in Figure 3. The area distribution $D_A(a)da$ is the fraction of the total surface area of the particles within the range a to a + da. This is shown in Figure 3B. Similarly, Figure 3C shows the distribution by volume of particles. This cubic response biases the distribution towards the larger size particles. Thus, the mean volume size $\bar{a}_V$ is always larger than $\bar{a}_A$ and it can be shown that the width of the area distribution is

$$\sigma_A = [\bar{a}_A(\bar{a}_V - \bar{a}_A)]^{1/2} \qquad (1)$$

The Leeds & Northrup particle instrument provides the following data outputs:

dV = volume of particles in ppm
MV = mean volume diameter in microns ($2\bar{a}_V$)
MA = mean area diameter in microns ($2\bar{a}_A$)
WA = width of area distribution in microns ($2\sigma$)

## SECTION 3

## PARTICLE INSTRUMENT TESTS AT ANL

Photographs of the prototype instrument installed on a one inch i.d. pipe at the Argonne facility are shown in Figures 4-6. Figure 4 shows the optical assembly mounted to the gas duct sample cell. After initial alignment, the laser beam is enclosed with a rubber boot from the instrument to the ports. There is no laser radiation danger to personnel as long as the equipment is maintained in this buttoned up state. No realignment of the optics was required during the two month test period.

The data processor and cortrol console are located in the enclosure shown in Figure 5. The data logging printer is shown on the shelf above the enclosure. There were no electronic malfunctions during the course of the tests. The only problem encountered was an unexpected reduction in laser power. However, this didn't inhibit operation of the instrument even though the power dropped over a period of a few weeks from 20 to 8 mW.

A close-up of the ANL sample cell is shown in Figure 6. Two sets of air purge lines were provided by ANL to generate air curtains across each of the viewing port quartz windows. These optical quality windows were coated to eliminate reflection at the laser wavelength (442 nm). The windows were cleaned weekly but daily background measurements with clean air flowing in the duct show insignificant particle deposits between cleanings.

The Leeds & Northrup instrument was operated solo by ANL personnel for the evaluation tests after a one week break-in and training period.

The piping arrangement at Argonne permitted measurement of particles after the secondary cyclone and after the metal filter which is downstream from the cyclones. Flue gas flow was directed to the particle instrumentation by valves to enable measurement of particles at either the input to or output from the metal filter.

Argonne provided an extractive port upstream of the optical windows that allowed particle size analysis on sampled material with cascade impactors. In addition, steady state grab particle samples were obtained with membrane filters.

The results of three combustion test runs utilizing Sewickley coal and Greer limestone are presented in Table I and Figures 7-9. Table I gives a comparison of size measurements made with the Leeds & Northrup instrument, called MICROTRAC, with the reduced data from the Anderson Cascade Impactor samples.

The average mean volume diameters, MV, for the impactor samples were calculated from truncated log normal distributions obtained via the Anderson Impactor. Since the MICROTRAC has a linear size response for particles one micron in diameter and larger, and a highly attenuated response to submicron size particles, the lowest channel (submicron region) data points from the impactor were not used. This provides directly comparable data over the size range 1-20 microns. The average mean area diameters, MA, were similarly calculated from the Anderson Impactor data. The differences between the direct reading, on-line observations via MICROTRAC and the impactor data are tabulated.

The median diameter, 50th percentile for log normal distributions can be expressed as Median Diameter = $\sqrt{MV \times MA}$. The results of this computation are shown in the bottom three rows of Table I.

These results indicate good agreement between optical scattering and cascade impactor methods for particle sizing. In all but one case, the difference is less than one micron.

Two interesting characteristics are observed, however. The MICROTRAC size measurement tends to indicate slightly smaller size for the median diameter and the MICROTRAC consistently shows the size of particles coming out of the final filter to be larger than at the input. In one of the three tests, the impactor data also shows the output particle size to be greater than the input. Further studies are needed to determine whether these are real characteristics of the particle dynamics, characteristics of the experimental method or a function of the instrument. It will be interesting to make similar measurements on a broader distribution of particle sizes and on a different type of particle separator to ascertain whether these observations are unique to the Argonne tests.

The loading data as functions of time are shown in Figures 7-9 for the three operating tests. The in situ volumetric loadings, as outputted by the MICROTRAC instrument, are converted to standard pressure/temperature conditions by the following equation:

$$I\ (\text{Grains/scf}) = \frac{D(1 + 0.00367T)dV}{2.29P} \qquad (2)$$

where D = density of particulate (gm/cc)

T = gas temperature, nominally 160C

P = gas pressure, nominally 3 atms.

dV = instrument output in ppm.

The density of the material samples in these tests was 1.2 gm/cc.

The data from MICROTRAC are shown as dots for unit intervals of time. The loading is always high at the beginning of each run due to material loosened in setting the duct valves. It takes about 15 to 20 minutes for this to be purged out and reach a steady state.

The MICROTRAC data shows a slow oscillatory characteristic. Its means of measuring particle size is independent of laser power whereas the indicated loading is directly proportional to laser beam intensity. Similar variations in the dV output were observed when clean air was directed through the gas duct -- when a steady state zero was expected. Therefore, it is most likely that the oscillations were caused by laser instability. This condition is now being investigated by us to identify cause and determine means of eliminating this condition.

Smooth lines are drawn through the MICROTRAC data points to show the loading trends. In addition, the loading values obtained by the cascade impactor and the membrane filter samples are shown. The horizontal location and length of lines for the extracted sample loadings indicate approximate time and duration for collection of each of those samples. The vertical location of each line designates its loading measurement.

A significant part of the variance between MICROTRAC and extracted samples may be due to non-uniformity of loading across the pipe or, probably more likely, due to problems of achieving isokenetic sampling with the extractive probe. A particular advantage of the MICROTRAC type of instrument is that it measures all particles passing through the laser beam and the gas flow is not influenced in any way by this method of measurement.

For installations on larger ducts, such as on the 10 inch i.d. duct at Curtiss Wright, the scattered flux from some particles 1 to 3 microns in size will be vignetted due to the limited size of the collecting optics. The scatter angle $\theta_{min}$, to the first minimum in the diffraction pattern is a function of wavelength ($\lambda$) and particle diameter (d) as shown in Figure 1. Thus, very small particles at long distance from the collector lens scatter flux outside this lens. To compensate for this factor (vignetting), we assume that the smallest particles are either uniformily distributed or distributed concentrically about the center of the line of the gas stream. The data processing routine provides a weighting factor for particles producing vignetting, to compensate for their lost flux.

In such installations, the MICROTRAC will detect and measure all particles traversing across the laser beam which are larger than a specified size (e.g., 3 microns). The amount of scatter flux collected from particles smaller than that size is determined by the distance of the collecting lens from the center line of the duct and the size and quantity of these particles. Thus, once the installation geometry is specified, the appropriate weighting factors are determined for compensating that flux which is lost. These constants are then inserted into the microcomputer program to correct the size distribution and loading data and provide a uniform response over the total range of particle size (1 to 20 microns).

The effectiveness of this method for compensating micron size particles in large ducts will be evaluated in the next few months at the Curtiss Wright facility. The instrument will be installed first on a 4 inch duct just upstream of the turbine. The receiving optics can be moved on its optical bench to vary the distance of the collector lens from the duct and thus compare data output for various distances.

This evaluation will complete our work on the existing ERDA contract and we will be ready to investigate its application to demonstration and commercial size combustion system installations.

TABLE I: Particle Sizing in Microns

| Measurement | In | Out | In | Out | In | Out |
|---|---|---|---|---|---|---|
| Calculated MV Anderson Impactor Sample | 5.77 | 4.64 | 5.39 | 7.44 | 5.33 | 4.74 |
| MICROTRAC MV | 2.92 | 5.13 | 3.91 | 5.45 | 3.62 | 4.39 |
| Difference ΔMV | +2.85 | -0.49 | +1.48 | +1.99 | +1.71 | +0.35 |
| Calculated MA Anderson Impactor Sample | 2.98 | 2.34 | 2.08 | 3.04 | 2.20 | 2.58 |
| MICROTRAC MA | 2.15 | 2.39 | 2.26 | 2.64 | 2.19 | 2.71 |
| Difference ΔMA | +0.83 | -0.05 | -0.18 | +0.40 | +0.01 | -0.13 |
| 50 Percentile Anderson Impactor Sample | 4.15 | 3.29 | 3.35 | 4.75 | 3.42 | 3.50 |
| 50 Percentile MICROTRAC | 2.50 | 3.50 | 2.97 | 3.79 | 2.82 | 3.45 |
| Difference | +1.65 | -0.21 | +0.38 | +0.96 | +0.60 | +0.05 |

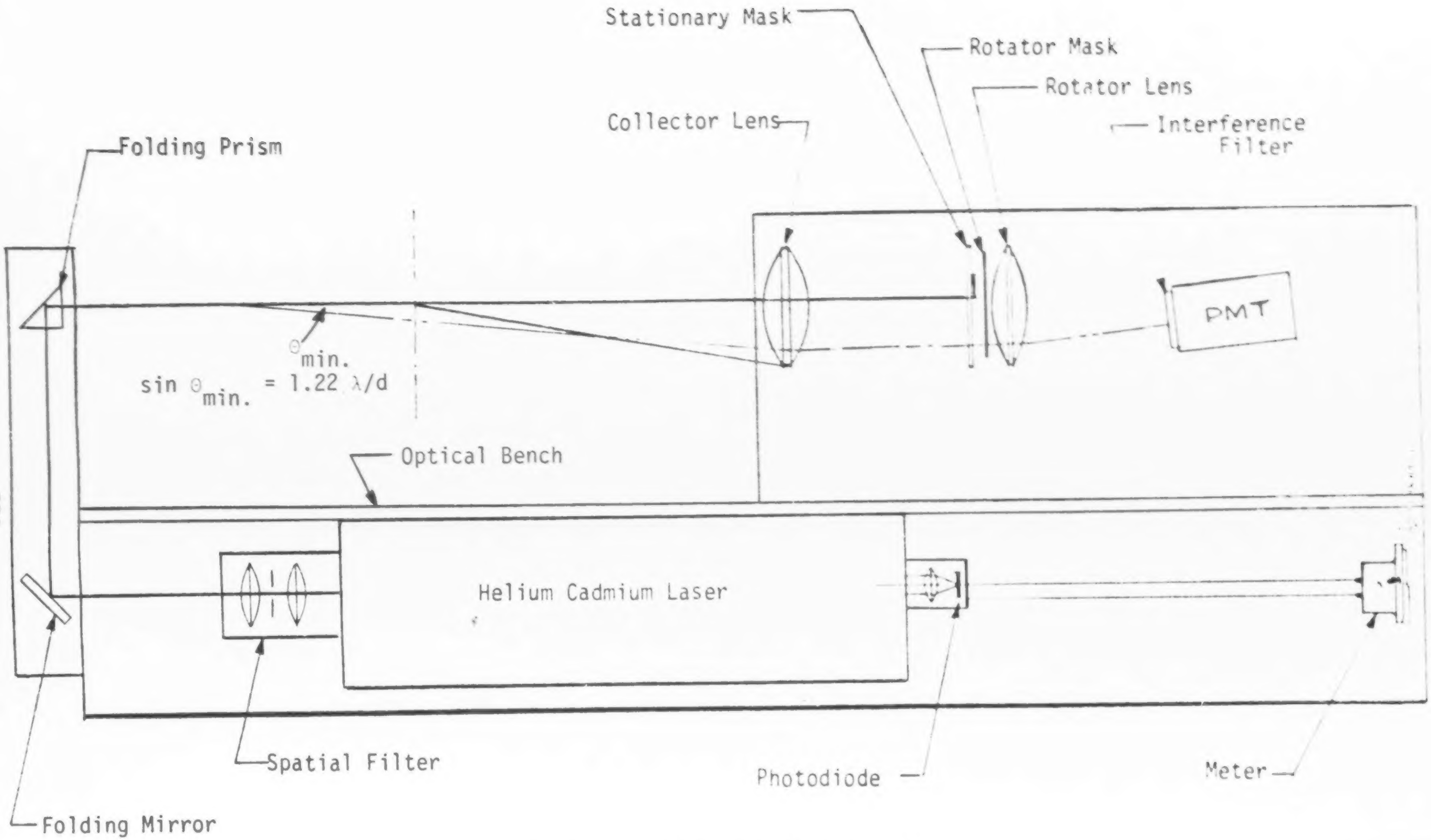
Stationary Mask
Rotator Mask
Rotator Lens
Collector Lens
Interference Filter
Folding Prism
PMT
$\Theta_{min.}$
$\sin \Theta_{min.} = 1.22 \lambda/d$
Optical Bench
Helium Cadmium Laser
Spatial Filter
Photodiode
Meter
Folding Mirror

Figure 1: Particulate Instrument Schematic

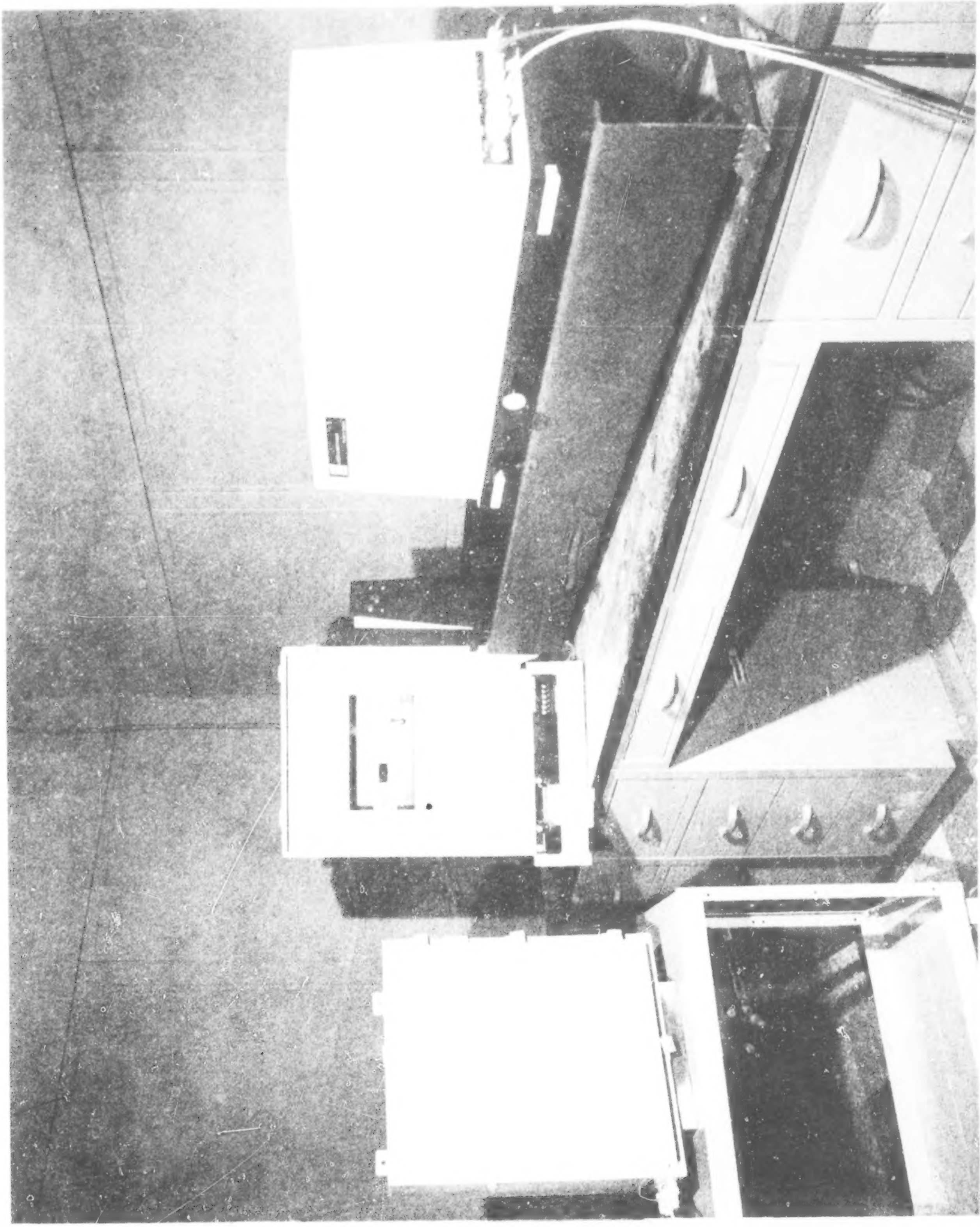

Figure 2: Prototype Particulate
Instrument

Figure 3

Three Methods of Defining a Particle Distribution

(A) by number,
(B) by area, and
(C) by volume

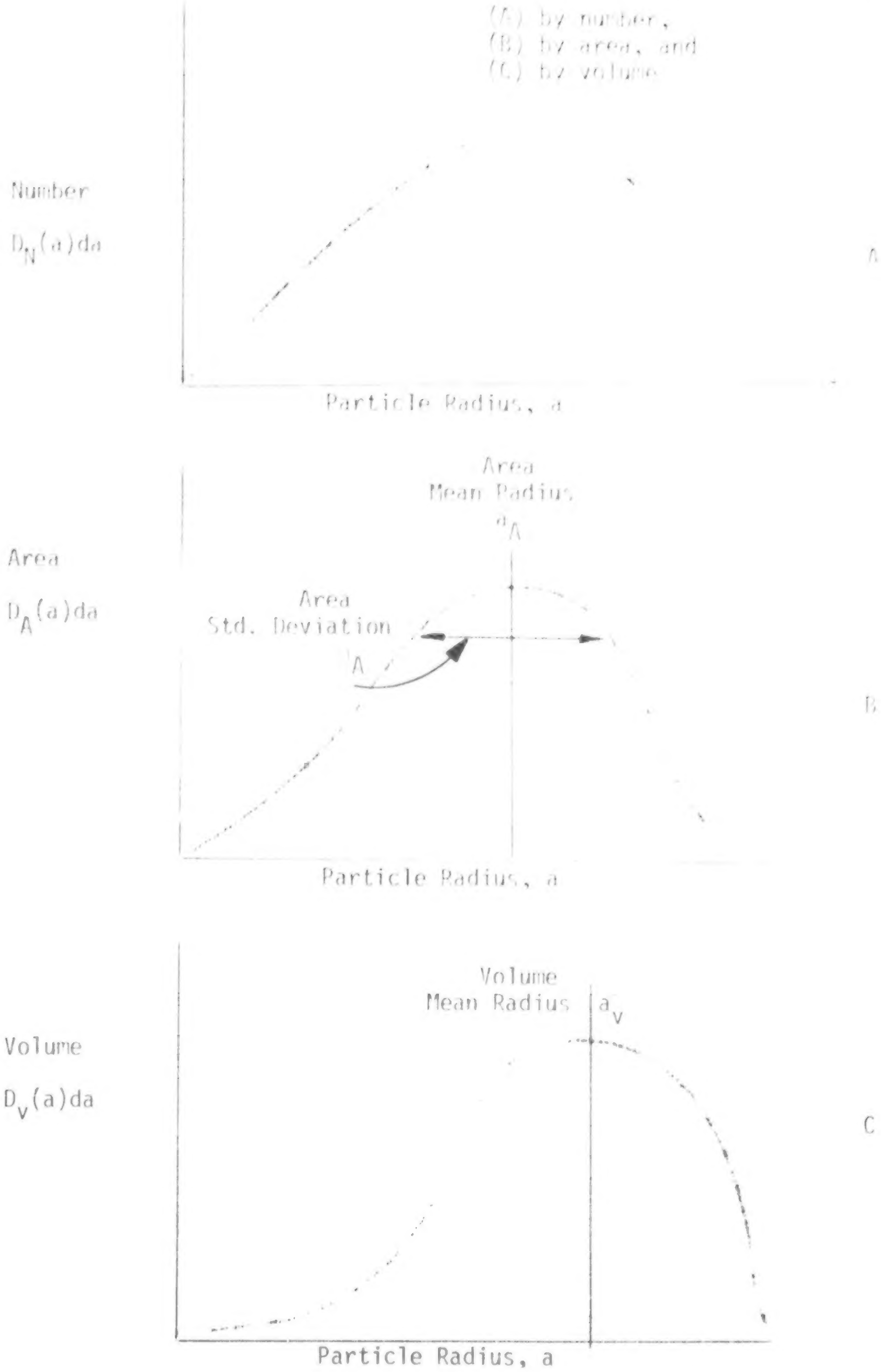

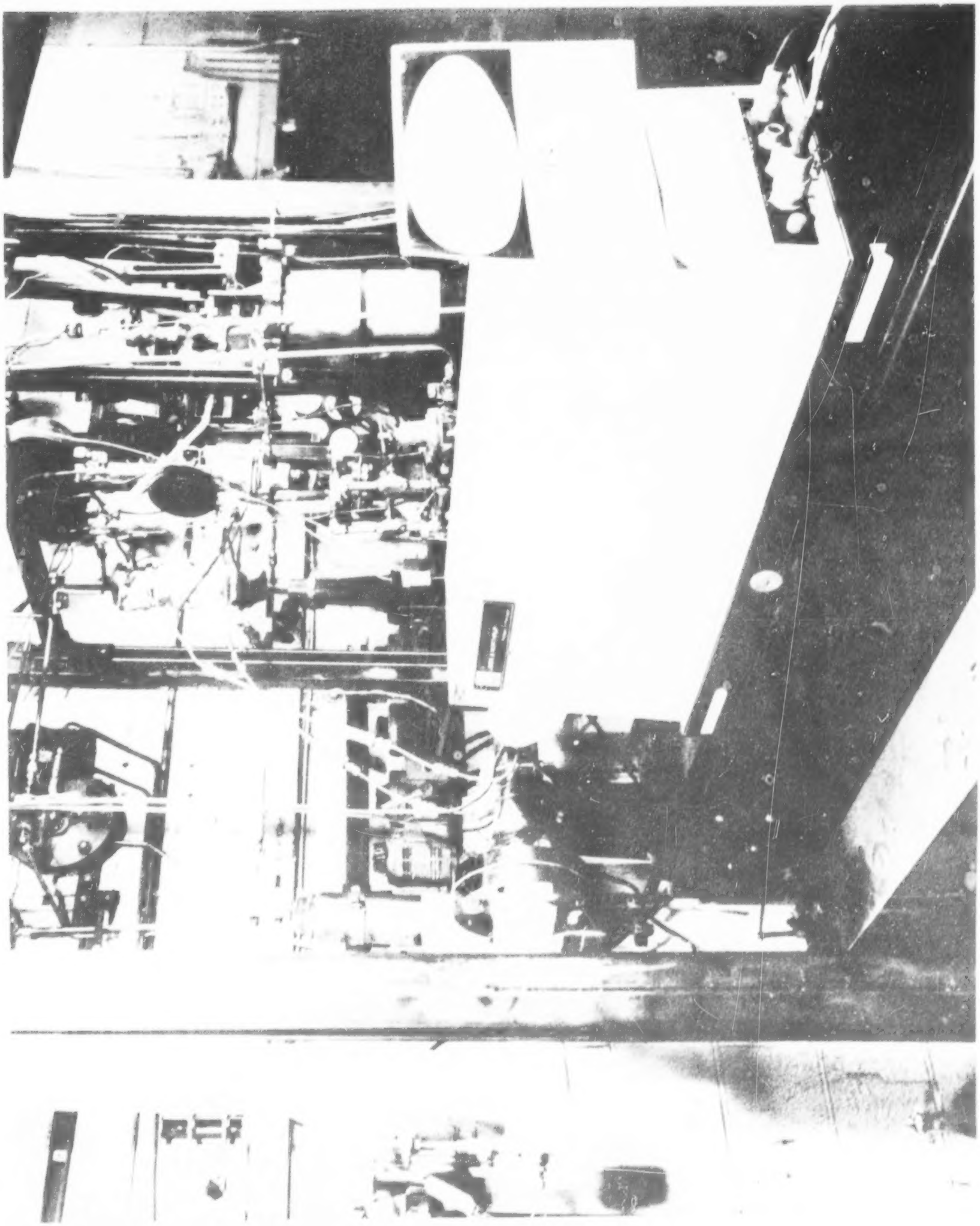

Figure 4: Optical Assembly
Installation at ANL

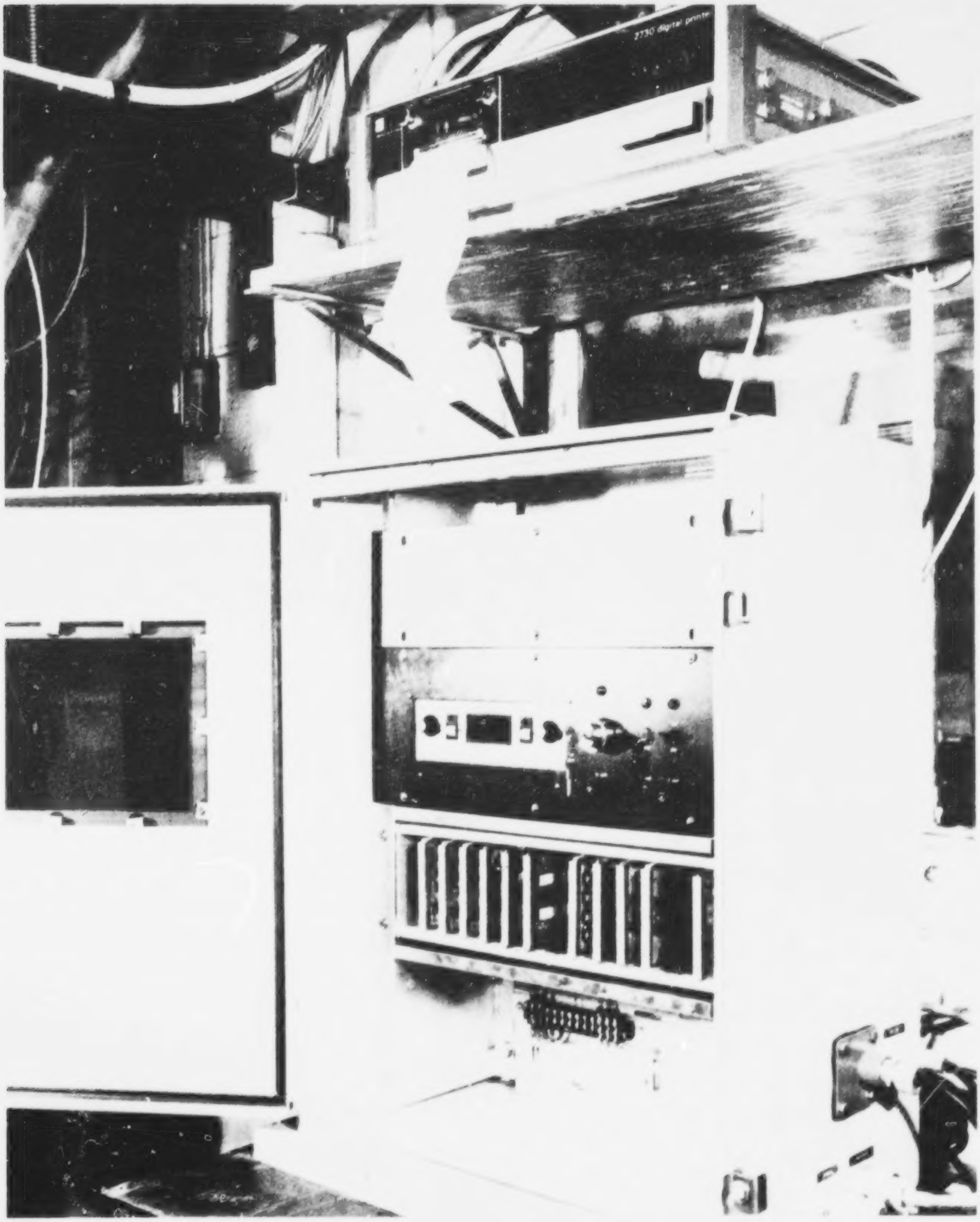
2730 digital printe

Figure 5: Electronics Unit
Installation at ANL

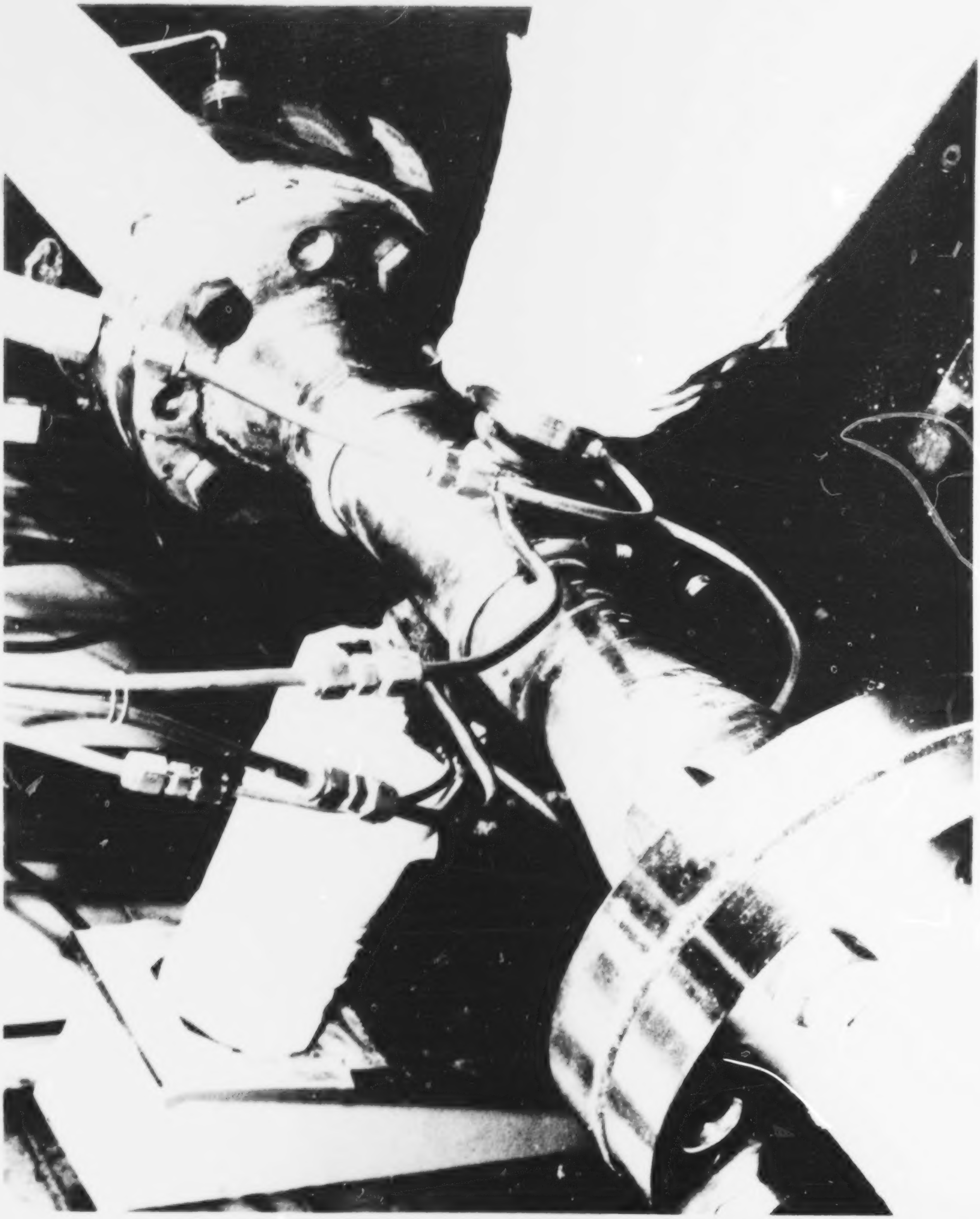

Figure 6: Close-up View of ANL
Sample Cell

Figure 7: EXPERIMENT L&N - 4

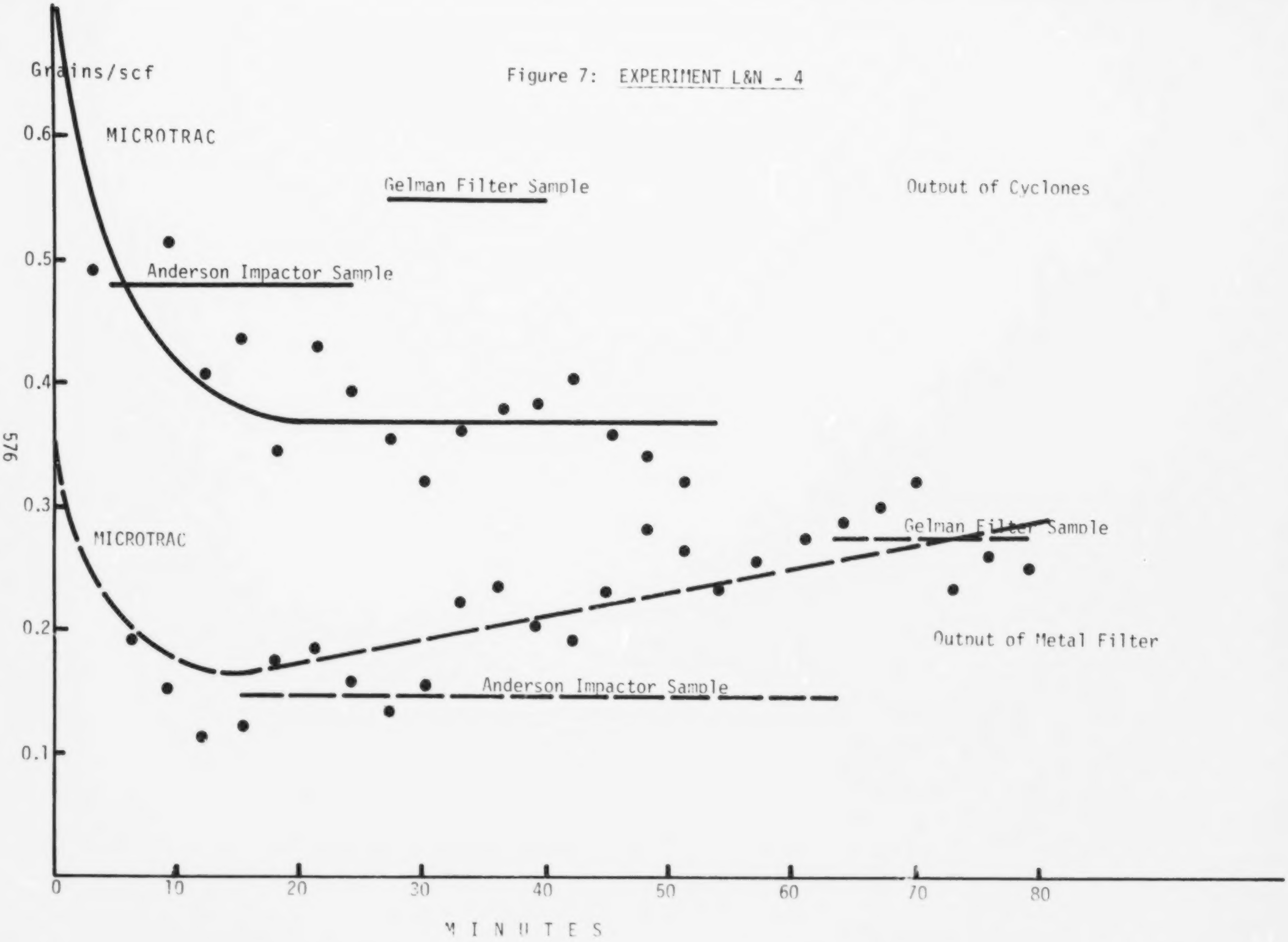

Figure 8: EXPERIMENT L&N - 5

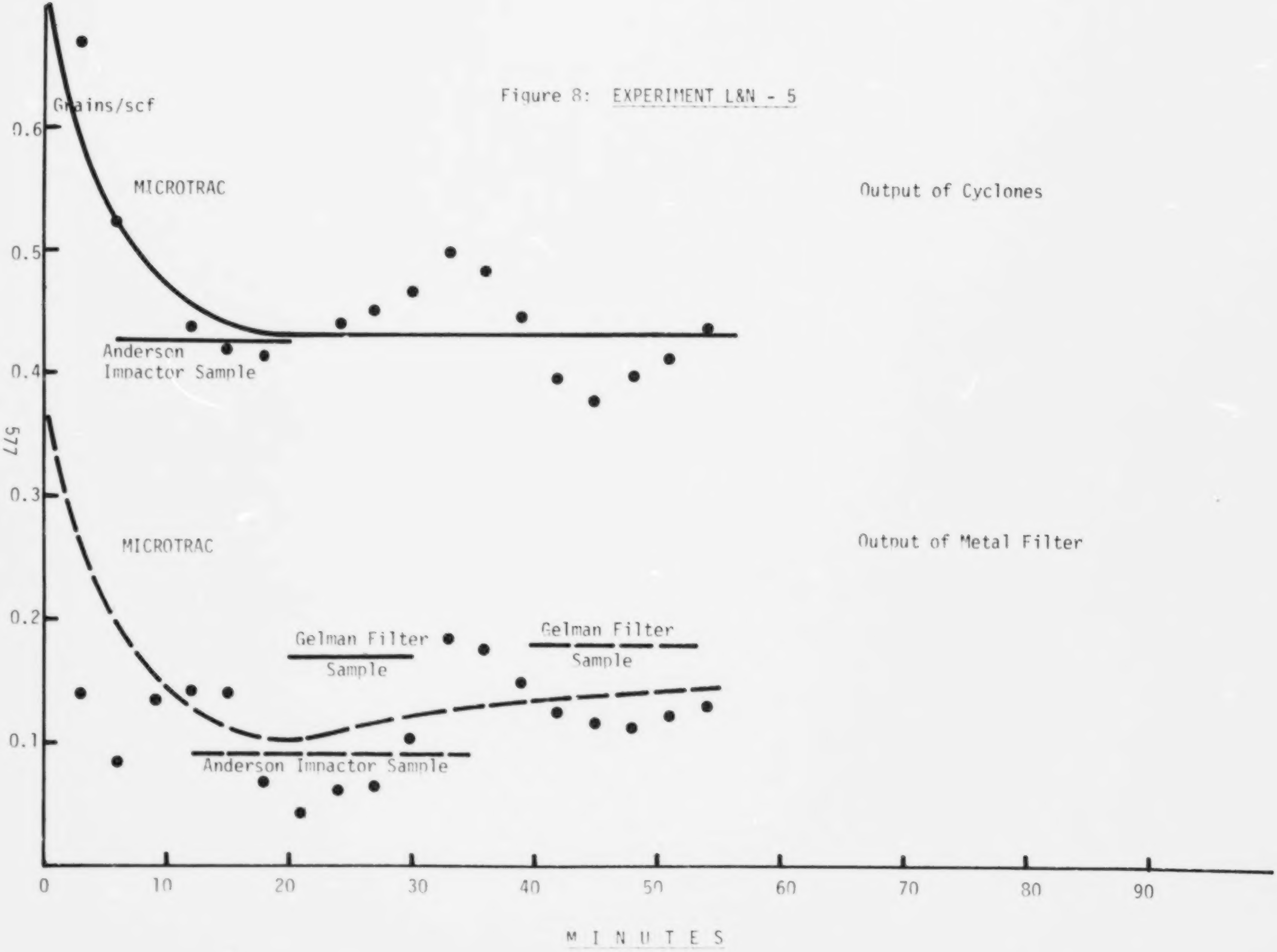

Figure 9: EXPERIMENT L&N - 6

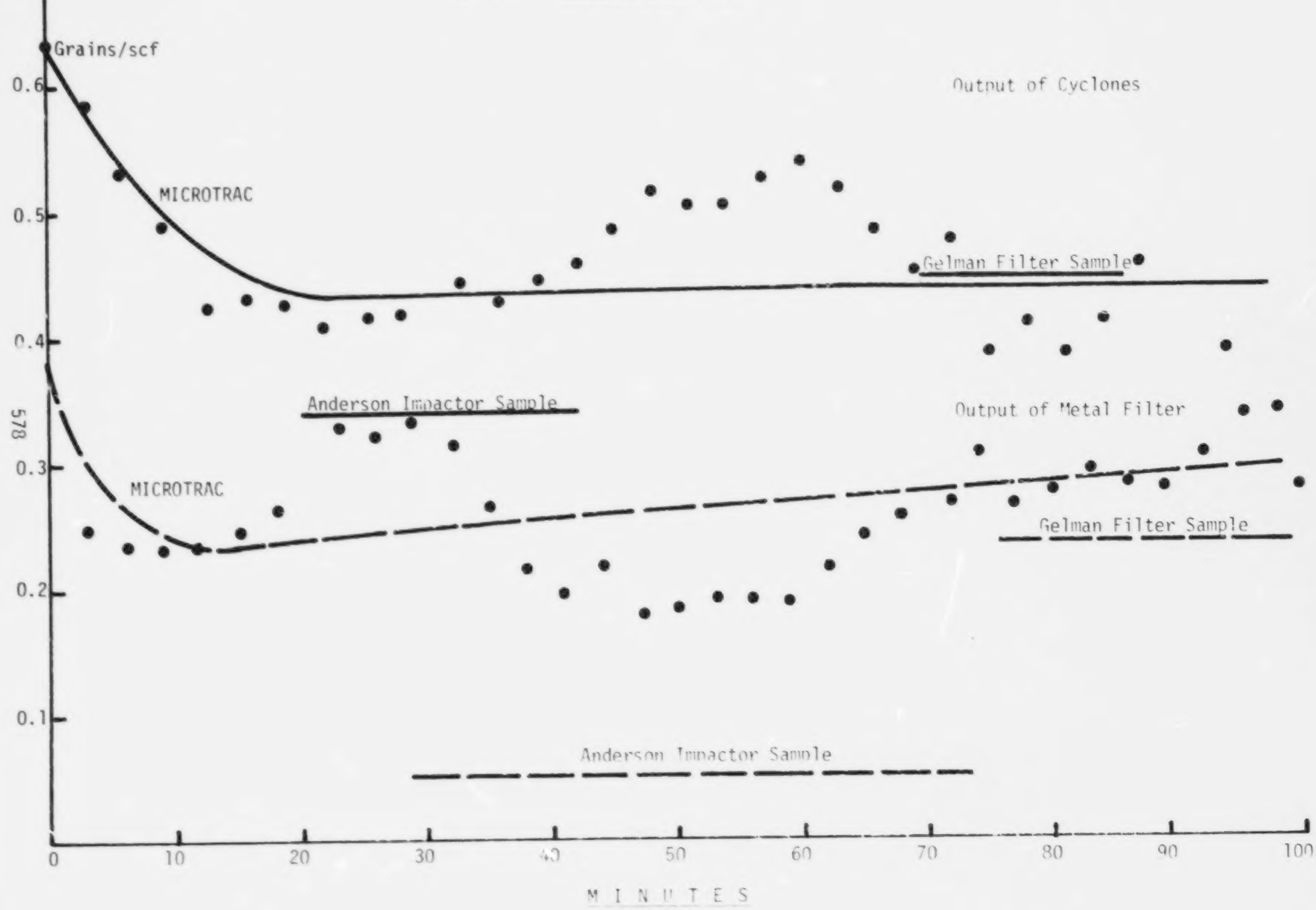

CONF-770970--2

By acceptance of this article, the publisher or recipient acknowledges the U.S. Government's right to retain a nonexclusive, royalty-free license in and to any copyright covering the article.

# CHARACTERIZATION OF SUSPENDED FLUE GAS PARTICLE SYSTEMS WITH ON-LINE LIGHT SCATTERING PARTICLE ANALYZERS

By:

J. C. Montagna, G. W. Smith, G. G. Teats
G. J. Vogel, A. A. Jonke
Argonne National Laboratory
Argonne, IL 60439

# CHARACTERIZATION OF SUSPENDED FLUE GAS PARTICLE SYSTEMS WITH ON-LINE LIGHT SCATTERING PARTICLE ANALYZERS

by

John C. Montagna, Gregory W. Smith, F. Gale Teats,
G. John Vogel, and Albert A. Jonke

Argonne National Laboratory
Argonne, Illinois 60439

## ABSTRACT

Two light-scattering particle size analyzers have been tested at ANL in the process development unit (PDU) fluidized-bed combustion system. The analyzers are (1) a single-particle analyzer developed by Spectron Development Laboratory and (2) a multiparticle analyzer developed by Leeds and Northrup. Particle size distributions and mass loadings determined at different flue gas duct locations with the Spectron and the Leeds and Northrup instruments have been compared with those obtained with (1) an Andersen cascade impactor, (2) a Coulter counter, and (3) positive filters. These comparison were used to evaluate the two instruments at their present state of development.

# CHARACTERIZATION OF SUSPENDED FLUE GAS PARTICLE SYSTEMS WITH ON-LINE LIGHT SCATTERING PARTICLE ANALYZERS

## INTRODUCTION

In the development of pressurized fluidized-bed combustion (PFBC) systems, an on-line particle analyzer for the flue gas could provide continuous particle size and loading analysis without disturbing the off-gas stream. These measurements will be used (1) in measuring the efficiency of upstream particulate-removing devices (cyclones and filters), (2) establish gas turbine performance at different particulate loadings, and (3) to protect turbines or a test cascade in the event of sudden system upsets. In a pressurized FBC system, the flue gas will be at $\sim$900°C and $\sim$1000 kPa ($\sim$10 atm) between the boiler and the turbine. In the absence of an on-line particle analyzer, routine batch sampling of the hot off-gas using inertial impactors will be necessary. Batch sampling from a pressurized hot off-gas environment (described in a following section) is difficult, and the long time lag between sampling and analysis of samples by the latter technique is also a disadvantage.

Two types of optical analyzers which have not yet been proven for fluidized-bed application were evaluated. Both instruments use laser light beams. One is a single-particle analyzer (a particle morphokinetometer, developed by Spectron Development Laboratory) which characterizes the scattered light from each particle (laser interferometer method), and the other is a Microtrac multiparticle analyzer developed by Leeds and Northrup, which characterizes the entire particle distribution in its optical path.

### Single-Particle Analyzer

The single-particle analyzer measures the sizes of particles and their velocities by measuring the light scattered from each particle as it crosses an interference pattern generated by the intersection of two laser beams. A schematic drawing of a typical single-particle analyzer is given in Fig. 1. The laser beams are directed radially into the flue-gas duct of the ANL PDU combustion system through specially designed windows. The region of measurement of this instrument, called the probe volume or sample space, is at the center of the duct where the two coherent beams intersect and generate the interference pattern. The scattered light signal from each particle in the sample sapce is detected and is changed to an electric signal shown in Fig. 1. The light may be detected in either a forward or backward observation mode. In the ANL evaluation, forward-scattered light was detected. Particle size has been shown to be a function of (1) the ratio of the AC to DC amplitude of this signal and (2) the shape of the particle.[1] (Farmer, 1972) The particle sizes that can be measured depend on the interference fringe spacing ($\delta$) in the sample space. The interference fringe periods and the corresponding detectable spherical particle size ranges used in this evaluation are given in Table I. The fringe periods were set by adjusting the angle ($\alpha$) at which the two laser beams intersected.

A more detailed description of the principles of the single-particle analyzer is available in the literature.[1] (Farmer, 1972)

## Multiparticle Analyzer

In the more conventional light-scattering technique used in multiparticle analyzers, a single laser beam is directed into the off-gas duct. The particle size distribution is obtained by examining the Mie scattered light from particle-laser beam interaction. All of the particles in the beam's path (off-gas duct cross section) simultaneously scatter incident light. As a result, the size of an individual particle cannot be determined. The particle size distribution can be obtained by examining the total scattering intensity as a function of angle and laser beam polarization and by comparing the experimental data with theoretical calculations for assumed size distributions.[2] (Weiss and Frock, 1976)

The multiparticle analyzer used in this work utilizes a new measurement technique in which three measurements of the scattered light are made. These measurements are accomplished by means of a uniquely shaped spatial filter which, when placed in the Fraunhofer diffraction plane, transmits the proper amount of light as a function of scattering angle to give the desired responses. These measurements may be used to determine the mean diameter and variance of the distribution for particles in the 1-50 μm range. Also, one measured signal is proportional to the volume of the particles illuminated, and this can be used to calculate the concentration of particles (loading) in the fluid stream.

If the type of distribution is known (*i.e.*, normal or log-normal) and if the distribution is unimodal, the information on mean diameter and variance is sufficient to completely describe the distribution of the suspended particles. The distribution of the particles leaving the combustor is multimodal (see next section) and cannot be characterized with this instrument. The distribution of the particles leaving the cyclones is unimodal and very nearly log-normal; it is expected that a multiparticle analyzer is capable of characterizing the suspended particles in the flue gas on either side of the filter upstream from the turbines. The primary objective in this work was to evaluate these instruments for gas-particle streams that would be expected on either side of such a filter.

## SYSTEM AND PROCEDURE FOR FLUE-GAS PARTICLE MEASUREMENTS

The flue gas system of the ANL fluidized-bed combustion system (PDU) has been modified for these evaluations, as shown in Fig. 2. Windows for particle analyzers have been installed in two locations; one pair is upstream from the primary cyclone. The other windows are near the system outlet with the capability of routing the flue gas past these windows, either upstream or downstream from the sintered metal filters (S4 and S5, Fig. 2). With this arrange, it is possible to size (1) the coarse entrained particles from the combustor, (2) the smaller particles escaping the two cyclones, and (3) the smallest particles passing through the sintered metal filters (representative of particles that might enter turbines). The coarse particles leaving the combustor were not sized with the multiparticle analyzer. Downstream from each window location, sampling ports have been installed that allow (1) particle size analysis of representative grab samples with cascade impactors and (2) measurement of particle loading with membrane filters. Also, steady state particle samples were obtained from the cyclones and test filter.

The particle size measurements were obtained (1) with on-line particle analyzers, (2) using an Andersen cascade impactor (described below), and (3) from steady state samples obtained from the cyclones and/or the test filter. The steady state samples were analyzed by sieve analysis and with a Coulter counter.

Coulter counter analyses are performed by suspending the particles in an electrolyte (2 wt % NaCl in $H_2O$); surfactants are used to enhance dispersion. In the Coulter counter, the suspension is passed through an orifice which isolates two electrodes. As a particle passes through the orifice, it generates a resistance pulse; the size of the pulse is proportional to the volume of the particle or the electrolyte that is displaced by the particle. The measurable size range of particles is limited by the size of the orifice (~2-50% of the orifice diameter). A distribution is calculated by assuming that the particles are all spherical. This instrument was calibrated with standard particles (Dow polystyrene latex particles, pollen, and National Bureau of Standards glass beads).

Particle size distributions on a weight basis were obtained by assuming that all observed particles were spheres of equal density and that the particles observed with the on-line instruments (single-particle and multiparticle analyzers) were identical to those that were mechanically removed from the system and later analyzed. Since density is assumed to be constant for all particle diameters, the fractional volume distribution and fractional mass distribution are equivalent.

Cascade impactors are the devices used most often for obtained size distributions of airborne particles in process or ambient air in the size range 0.3-20 μm. In this study, an Adersen cascade impactor was used to obtain combustor flue gas particle size distribution data for flue gas grab samples. Each stage of the impactor consists of equidiameter orifices followed by a target plate for collecting the particles. Smaller orifices are used in successive stages, and thus smaller particles are collected in successive stages. The particle size distributions are calculated from experimental data by relating the mass that is collected on each stage to the corresponding stage diameter. Impactor designs (including the design of the impactor used) are based on the theoretical development of Ranz and Wong.[3] (Ranz and Wong, 1952) The size measurements obtained with the cascade impactors are aerodyanmic diameters (based on aerodynamic behavior of spherical unit-density particles). This particle measurements should be most appropriate in characterizing airborne particles in relation to turbine erosion, which is an aerodynamic process. Previous FBC studies have shown that measurements of combustion particles with cascade impactors, Coulter counters, and microscopes are in good agreement.[4,5] (Vogel *et al.*, 1974) (Hoke *et al.*, 1977) Because of previously found agreement between the different measuring techniques and of the scope of this evaluation, no direct microscopic comparisons have been made in this evaluation. However, it is planned to perform such a comparison during the on-going work on the evaluation of particulate clean-up components at ANL, which is a much more extensive task.

The total cumulative mass distributions obtained with the impactor in two consecutive measurements of suspended particles leaving the secondary cyclone (SGL-2C) are given in Fig. 3. Aerodynamic mass diameters of 2.7 μm and 3.0 μm were obtained, it being assumed that the apparent density of all particles was 1.0 g/cm$^3$. The sampling conditions for the impactor samples are given in Table II. The total cumulative mass distribution obtained with the Coulter counter is also given in Fig. 3. The log-mean diameter was found to be 3.5 μm, which compares favorably with the distribution means obtained with the cascade impactor. Because the Coulter counter was calibrated with standard particles and its measurements of combustion particles agreed well with cascade impactor measurements, it was assumed that these comparative measurements were representative of the true particle distributions. The evaluation of the multiparticle analyzer was performed only with cascade impactor comparative measurements.

The sampling system in the FBC system for the cascade impactor is illustrated in Fig. 4; for some samples, a glass fiber membrane filter was substituted for the impactor. The particle laden-flue gas flowed by the optical windows (located in the line downstream from the cyclones or metal filter), where the particles were sized with a light-scattering particle analyzer. Next, the off-gas line was expanded to reduce the velocity to that compatible to isokinetic sampling with the cascade impactor and membrane filters. The tip of the sampling probe (0.78-cm ID for single-partcile analyzer evaluation and 1.33-cm ID for the multiparticle analyzer evaluation) was machined to enhance aerodynamic stability near the probe entrance. The sample line was electrically heated to maintain the temperature of the gas sample above its water dew point. The cascade impactor and the membrane filter holders was contained in a heated pressure shell to permit sampling from the pressurized (3 to 8 atm) combustion system. Gas velocities were calculated from measured gas flows and local temperatures.

# CHARACTERISTICS OF SUSPENDED PARTICLE DISTRIBUTIONS AT DIFFERENT FLUE-GAS CLEANUP STAGES

The total size distribution of particles elutriated in the combustor during a coal combustion experiment (SGL-1) was obtained by combining Coulter counter measurements with sieve analyses of samples collected in the cyclones and metal filter. The particles passing through the metal filter were justifiably assumed not to contribute significantly to the total mass size distribution. The fractional mass distribution in sucessive half-volume intervals of all particles between 2 μm and 1000 μm is given in Fig. 5. (The loading in the flue gas leaving the combustor is $\sim$14 grains/scf or $\sim$20 grains/acf which is quite high.) This distribution consists of elutriated partially sulfated limestone (apparent density; $\rho_a = 1.9$ g/cm$^3$), unburned coal ($\rho_a \simeq 1.0$ g/cm$^3$), and coal ash ($\rho_a \simeq 0.6$ g/cm$^3$). Since these materials could not be separated, the distribution could only be obtained by assuming a uniform density; thus, the smaller-diameter fractions, which contain more of the lighter ash and carbon, are probably biased high.

Since the distribution of particles leaving the combustor is multimodal, the detailed characteristics of the distribution can only be obtained with a single-particle analyzer such as was used in this work. However, because the distribution extended from 2 μm to 1000 μm, only that part of the distribution below $\sim$70 μm could be sized with the single-particle analyzer.

The distribution of the particles escaping from the cyclones during a different coal combustion experiment (SGL-2C) is given in Fig. 6. The mass loading at this flue gas location is $\sim$0.2-0.5 grain/scf, and the mass contribution by particles larger than 10 μm is small. The largest mass fraction consisted of 3.0 to 3.8 μm particles, which contained 22.5 wt % of the total loading. This distribution can be characterized as a log-normal distribution and it is expected that particles escaping from the filter have the same type of distribution. Thus, because the type of particle distribution that a gas turbine will see is expected to be log-normal, both single-particle analyzers and multiparticle analyzers can be used in the hot flue gas of a PFBC system.

Because the flue-gas particle distributions are not homogeneous (carbon, fly ash, and unburned coal), the extent to which particle shapes, apparent densities, refractive indices, *etc.* affected the differences between measurements obtained by different measuring principles (techniques) was evaluated with experiments in which only virgin limestone particles were suspended and measured in the flue gas. This was accomplished by continually feeding virgin limestone into the cold combustor, thereby maintaining a steady state fluid bed of virgin limestone. The particles that elutriated were generated by attrition and had basically homogeneous properties. The fractional mass distribution of virgin limestone leaving the cyclones of the PDU system was determined with the Coulter counter and is given in Fig. 5 (LASER-1B). It was also log-normal in nature and the log-mean diameter was approximately equal to that obtained for the combustion experiment measurement (SGL-2C). Thus, this distribution can also be characterized by use of both single-particle and multiparticle light-scattering analyzers.

## EXPERIMENTAL EVALUATION OF THE SINGLE-PARTICLE ANALYZER

Some results of particle size measurements obtained with the single-particle analyzer for several combustion experiments have been compared with size distributions determined by Coulter counter for steady state particle samples and cascade impactor measurements. In addition to size measurements, particulate loading measurements were compared. The measurements with this laser instrument were made in the PDU combustion system's off-gas duct between the combustor and the primary cyclone, where all particles elutriated in the combustor were observed. Also, particle size measurements between the secondary cyclone and the metal filters are reported.

### Measurements of Particle Size Distribution

The conditions for the combustion experiments in this evaluation are given in Table II. In the first experiment (SGL-1), the distribution of particles leaving the combustor was measured. Two fringe periods, see Table I, were used on the single-particle analyzer, 71.4 μm and 22.3 μm. The measured particles consisted of limestone fragments, coal ash, and unburned coal.

In the comparison, only the mass distributions in the measurable particle size ranges (1.5-23 μm and 5-74 μm) of the single-particle analyzer were compared with the corresponding distributions obtained with the Coulter counter. The small (1.5-23 μm) and the large (5-74 μm) particle measurement comparisons are given in Figs. 7 and 8, respectively. For the small-particle size range (Fig. 7), the mass log-mean particle diameters obtained were 8.5 μm with the Coulter counter and 20 μm with the single-particle analyzer. For the large-particle size range, the mass log-means of the partial distributions were found to be 26 μm with the Coulter counter and 70 μm with the single-particle analyzer (Fig. 8). The difference between the two measurements is greater for larger particles.

The conditions for combustion experiments SGL-2C and SGL-1C, in which the sizes of suspended particles between the secondary cyclone and the metal filters of the PDU combustion system were measured, are given in Table II. Particles with diameters of 0.2 to 3.1 μm, and 1.5 to 23 μm were sized with the single-particle analyzer. The resulting partial (1.5-2.3 μm) mass distributions are given in Fig. 9. The mass log-means of these distributions are 3.5 μm (Coulter counter) and 17 μm (Curve A, single-particle analyzer). In the distribution obtained with the single-particle analyzer, the mass particule population increased sharply for particles larger than 15 μm. Since at this point the flue gas had passed through two cyclones, most particles larger than 10 μm should have been removed, as found with the Coulter counter measurements.

The submicron particles were measured with the single-particle analyzer in experiment SGL-1C (see Table II), using a fringe period of 2.94 μm. To achieve the recommended velocity of ∼3.0 m/s or less (necessary due to response of electronics), the flue stream was split downstream from the cyclones and only a metered portion was allowed through the sampling system. Because the Coulter counter at ANL is not capable of measuring particles smaller than 1.5 μm, the small particle measurements made with the single-particle analyzer were compared with the partial mass cumulative distribution obtained with the cascade impactor (Fig. 10). The mass log-means obtained were 0.72 μm (single-particle analyzer) and 1.6 μm (impactor). The agreement obtained is considered to be as good as might be expected for the small particle measurements.

Because of the low loadings (∼0.05 grain/scf) downstream from the metal filter, no size measurements could be made with the single-particle analyzer. Not enough measurable (1.5-23.9 μm) particles passed through the sample space. However, the present state of the art on turbine technology suggests that this particle size range will be significant at loadings of ∼0.05 grain/scf in causing turbine damage.

On-line particle analyzers will be most useful downstream from FBC particle-removal devices to monitor particle distributions and loadings in the flue gas that enters gas turbines. Particles <10 μm and >1 μm are expected to erode the turbines. It is encouraging that the characteristics of the fractional distributions obtained by the two different methods (single-particle analyzer *vs* Coulter counter) were the same and that the discrepancy between the two measurements became smaller for smaller particles (<20 μm). However, a significant difference remained between the comparative measurements for 1.5 to 23.9 μm particles (the mass log-means obtained with the single-particle analyzer were a factor of at least 3 larger). Possible reasons for the difference are given below:

a. The mass loading downstream from the combustor was ~14 grains/scf (~20 grains/acf), which is quite high. Thus, for the measurements upstream from the cyclone, the chance that there would be more than one particle in the sample space of the single-particle analyzer was high. Over 98% of the signals were rejected by the single-particle analyzer because of particle coincidence interference. (Signal rejection rates between 97% and 90% are considered acceptable by the manufacturer.)

b. The original calibration for spherical particles, which was obtained with low number densities of mists and aerosols by microscopic measurements, is greatly influenced by particle shape and orientation in the sample space. The bias becomes more pronounced for larger particles via visibility function.[1] (Farmer, 1972).

c. Fragile particles might have broken up as the particle samples were collected in the cascade impactor or in the cyclones and test filter or as they were prepared for Coulter counter analysis (dispersed in an electrolyte). This effect could impose a bias towards small diameters in Coulter counter and impactor measurement.

The agreement in the cold experiments between the single particle analyzer and impactor was better for the measurements with the lower loading (downstream from the cyclones). However, because the suspended virgin limestone particles were relatively homogeneous, similar in shape (not dependent on diameter), and consistent in scattering properties (refractive indices), a better than the found agreement was expected between the single-particle analyzer measurements, the measurements with the cascade impactor (seen in Fig. 11), and the Coulter counter.

Because of difficulties in evaluating the causes for discrepancies between the single-particle analyzer and comparative measurements, an empirical correlation of the experimental data was used to obtain a best fit for the calibration curve. In this analysis, it was assumed that the Coulter counter and inertial impaction measurements were correct. The particle distribution measurements obtained with the Coulter counter and cascade impactor were expressed as histograms, with intervals equivalent to the single-particle analyzer increments. The diameter-dependent factor necessary to force the fractional contributions of the histogram intervals from the single-particle analyzer into agreement with those from the Coulter counter and impactor measurements was obtained. The ratios of the fractional contributions obtained from the Coulter counter and impactor measurements to those obtained from the single-particle analyzer for a considerable number of measurements were correlated with the reduced diameter of the interval, $D/\delta$. ($D$ is the particle diameter and $\delta$ is the fringe period of the laser probe volume.) By use of least squares techniques, the following correlation was obtained:

$$\ln (K) = -4.91 \ln(\frac{D}{\delta}) - 2.5 [\ln(\frac{D}{\delta})]^2 \qquad (1)$$

where $K$ is the ratio of the expected mass concentration in the diameter interval to the measured number of particles within the analyzer interval. This correlation gives a fair fit (the correlation coefficient is $\sim$0.88).

The above discussed experiments were reanalyzed using this empirical calibration and the measurements in these experiments were adjusted using the calibration function (Eq. 1). The results for SGL-2C, in which the particle measurements were performed on suspended particles downstream from the cyclones, are given in Fig. 9 (Curve B). This figure also contains the distribution which is based on the calibration function originally supplied by the manufacturer (Curve A):

$$K \propto 1/D \qquad (2)$$

The mass log-mean diameters for SGL-2C (Fig. 9) were: 3.5 μm (Coulter counter), 8.8 μm (Eq. 1 calibration), and 18 μm (supplied analyzer calibration). Although the adjusted (by Eq. 1) analyzer measurements still deviate from the Coulter counter measurements, agreement of the measurements improved significantly.

## Measurement of Particulate Loadings

Loading measurements cannot be made with the single-particle analyzer in its present state of development because the appropriate volume of the sample space is not readily attainable without a comparison measurement. Comparative loading measurements by gravimetric means were used to predict the probe volumes, and it was estimated that at best, the loadings could be estimated within one order of magnitude with the single-particle analyzer for high loading conditions ($>0.1$ g/m$^3$).[6] (Montagna *et al.*, 1977) No particle measurements were made with the analyzer under low loading conditions because too few particles passed through the probe volume.

## EXPERIMENTAL EVALUATION OF THE MULTIPARTICLE ANALYZER

Windows for the multiparticle analyzer were installed near the system outlet with the capability of routing the flue gas past these windows, either upstream or downstream from the metal filters. The sampling port for representative grab samples was installed upstream from the window location. Steady-state grab particle samples were obtained with: the cascade impactors, membrane filters, and a total flue gas test filter. (The test filter replaced the metal filter during sampling periods, but loadings obtained with this filter are not reported in this paper.)

### Measurement of Log-Mean Particle Size

The log-mean aerodynamic particle diameter ($\bar{D}_{AE}$) measurements obtained with the impactor may be compared with the "projected" particle area mean diameter ($\bar{D}_A$) obtained with the multiparticle analyzer. The volume mean diameter $\bar{D}_V$, also obtained with the multiparticle analyzer, is larger by definition:

$$\ln \bar{D}_V = \ln \bar{D}_A + 0.5 \ln^2 \sigma_n \qquad (3)$$

where $\sigma_n$ is the geometric standard deviation on a number basis;[7] (Irani and Callis, 1963) $\bar{D}_V$ is more sensitive to changes in the distribution. $\bar{D}_A$ corresponds more closely than does $\bar{D}_V$ to impactor diameter measurements, $\bar{D}_{AE}$, which are dependent on the particle's aerodynamic drag and inertia.[8] (Orr and Dalla Valle, 1960) The multiparticle analyzer also measured the arithmetic deviation of the distribution. The geometric standard deviation, $\sigma_n$, can be calculated from Eq. 1 and the measurements $\bar{D}_A$ and $\bar{D}_V$. The calculated value of $\sigma_n$ and $\bar{D}_A$ were used to characterize the log-normal distribution of suspended flue gas particles.[6] (Montagna *et al.*, 1977) The resulting distributions from the multiparticle analyzer are slightly narrower (less variance) than the distribution from the cascade impactor.

The conditions for the combustion experiments and some cold experiments are given in Table III together with the measured diameters and loadings. Because the contribution of particles smaller than 1 μm was less than 10%, mass basis, the impactor distributions were not truncated to accommodate the range of the multiparticle analyzer (1-20 μm-dia). In coal combustion experiments, the aerodynamic log-mean diameter ($\overline{D}_{AE}$) ranged from 2 to 3.5 μm and the projected area mean diameter ($\overline{D}_A$) ranged from 2.2 to 3.4 μm for all suspended particle measurements when the loading (gravimetrically obtained) was relatively high ($>0.1$ g/m$^3$ or $>0.044$ grain/scf). The volume mean diameters ($\overline{D}_V$) ranged from 2.9 to 5.5 μm for the same measurements.

In "cold" experiment LN-9-5, only virgin limestone particles were measured. The loading was also relatively high ($>0.1$ g/m$^3$); $\overline{D}_A$ was 2.7 μm, in comparison with 1.5 μm for $\overline{D}_{AE}$. It had been expected that the measurements made on the suspended virgin limestone would have agreed better than those made on the mixture of particles during combustion experiments. However, the ($\overline{D}_{AE}$ and $\overline{D}_A$) agreement for suspended combustion particles was slightly better than for the above measurements under high loading ($>0.1$ g/m$^3$) conditions. In comparison with the multiparticle analyzer, the mass log-mean diameters of particles leaving the cyclones (loadings $\geq 0.1$ g/m$^3$) measured with the single-particle analyzer (only particles between 1.5 and 23.9 μm were compared) were at best a factor of three greater than those obtained by the Coulter counter and impactor measurements.

The agreement of $\overline{D}_{AE}$ with $\overline{D}_A$ was poorer for measurements made at lower loading conditions ($\leq 0.01$ g/m$^3$) in experiments LN-9 and LN-11. $\overline{D}_{AE}$ ranged from 0.63 to 1.9 μm and $\overline{D}_A$ ranged from 2.0 to 5.5 μm. The loading of $\sim 0.05$ g/m$^3$ for particle diameters of 1-10 μm is presently being proposed as the approximate maximum tolerable loading for turbines. Because the particulate loading tolerances on turbines remain uncertain, it is desirable to have optical instruments capable of measuring particle loadings $<0.05$ g/m$^3$. In these low loading measurements, $\overline{D}_A$ was approximately three times larger than $\overline{D}_{AE}$. Considering the difficulty of obtaining accurate impactor measurements for the comparison, this agreement can be considered fair at this stage. In comparison, no particle measurements could be made with the single-particle analyzer at these low loadings because not enough particles passed through the sample space of the instrument.

## Measurement of Particulate Loadings

In these experiments, particulate loadings were measured in addition to mean particle sizes. Values for comparison were obtained by three backup methods. The amount of particulate collected on a total flue gas metal filter located downstream from the multiparticle analyzer windows and sampling port provided one backup measurement. The other backup measurements were grab samples, and each consisted of (1) the particulate collected in the impactor including a backup filter to the impactor and (2) the material collected on a membrane filter.

For the measurements during the combustion experiments in which the loadings were high (>0.1 $g/m^3$, gravimetric), the gravimetric loadings were a factor of four or less smaller than the optical loading measurements made with the multiparticle analyzer, see Table III. (The loadings from the multiparticle analyzer are proportional to the particulate density assumed; 1.0 $g/cm^3$.) For many high loading measurements, such as LN-4-2, the gravimetric and multiparticle analyzer loadings were very close. The gravimetric loadings under low loading conditions (<0.01 $g/m^3$) were one order of magnitude less than the optical multiparticle analyzer loadings. The semicontinuous background loading signal is compared with the background plus sample loading signal in Fig. 12 for low loading ($\leq$0.01 $g/m^3$) measurements. The loading measurements signal is only 4% greater than the background; this can account for the order of magnitude difference between the multiparticle analyzer measurements and the gravimetric loading measurements. These low loading measurements were made on suspended particles that had escaped through the metal filter.

In the cold experiment (LN-9), loadings determined gravimetrically were one order of magnitude smaller than those obtained in the hot experiments for the high loading measurements; they were about two orders of magnitude smaller for the low loading experiments. This large difference may be due to an increase (over the period of an hour) in the multiparticle analyzer background signal during these cold experiments (see Fig. 13). The average gas linear velocity in the flue gas duct near the optical windows was ∿30 m/s during the cold experiments; during the hot combustion experiments, the linear gas velocity was only ∿3 m/s. A higher gas velocity creates more turbulence and a greater chance for particles to build up in the free space between the windows and

and the flue gas flow stream. The background was observed to decay to normal after flow of limestone-laden air was turnded off.

# CONCLUSIONS

The single-particle analyzer is capable of characterizing a suspended-particle distribution as a histogram. Thus, the actual shape of the size distribution can be obtained. The multiparticle analyzer can characterize a distribution by giving the mean and a nongeomtric variance of the distribution. Unless the type of distribution is known and it is unimodal, the latter instrument cannot describe the distribution of the particles. The distribution downstream from the cyclones of a PFBC system is expected to be log-normal, based on measurements in this and other studies. Therefore, the distribution can also be obtained with multiparticle analyzer measurements. However, the single-particle analyzer has a greater capability to characterize particle distributions.

For high-loading ($>0.1$ g/m$^3$) measurements, the projected particle area mean diameters obtained with the multiparticle analyzer were generally $<25\%$ smaller than the aerodynamic mass log-mean particle diameters determined with the impactor. In comparison, for the same loading conditions, the mass log-mean particle diameters obtained with the single-particle analyzer were a factor of three (or more) greater than those obtained by Coulter counter and impactor measurements. For low loading conditions ($<0.01$ g/m$^3$), the mean diameters obtained with the multiparticle analyzer were approximately three times larger than log-mean diameters obtained with the impactor. No particle size measurements could be made at these low loadings with the single-particle analyzer.

For high loadings, the gravimetric loadings were a factor of four or less smaller than the optical loading measurements made with the multiparticle analyzer. However, many measurements made at these relatively high loadings by the two techniques were very close. Under low loading conditions ($\leq 0.01$ g/m$^3$), the gravimetric loadings were one order of magnitude less than the optical measurements with the multiparticle analyzer. For these low loads, the loading measurement signal is only 4% greater than the background; this is a potential source of error. If the background can be reduced electronically or via cleaner windows and/or optical path, this instrument would be very promising for on-line PFBC measurements to protect the gas turbines.

For the single-particle analyzer, loading measurements cannot be made at its present state of development because the appropriate volume of sample space is not readily calculable. Based on comparative measurements by gravimetric means, it was estimated that at best, loadings could be estimated within one order of magntidue with the single-particle analyzer for high loads. No low loading ($<0.01$ g/m$^3$) measurements have been made with the single-particle analyzer.

The multiparticle analyzer is a state of development allowing it to be used with little operator training. Operation of the single-particle analyzer requires much more care, and data reduction is presently very time-consuming. The single-particle analyzer is a first-generation instrument and has much potential. On the other hand, the multiparticle analyzer is a more advanced instrument and with some r[illegible] t can be useful now in the development of PFBC technology.

# ACKNOWLEDGMENTS

The support of this program by the Energy Research and Development Agency and the Environmental Protection Agency is gratefully acknowledged. This study was made under the direction of Messrs. A. A. Jonke, D. Webster, and L. Burris of the Chemical Engineering Division. Experimental data were obtained by Messrs. H. Lautermilch, S. Smith, J. Stockbar, and A. Ziegler.

## REFERENCES

1. W. M. Farmer, *Measurements of Particle Size, Number Density, and Velocity Using a Laser Interferometer*, Applied Optics 10, 2603 (1972).

2. E. L. Weiss and H. N. Frock, *Rapid Analysis of Particle Size Distribution by Laser Light Scattering*, Power Technology 14, 287 (1976).

3. W. E. Ranz and J. B. Wong, *Impaction of Dust and Smoke Particles*, Ind. Eng. Chem. 44(6), 1371 (1952).

4. G. J. Vogel, W. M. Swift, J. F. Lenc, P. T. Cunningham, W. I. Wilson, A. F. Panek, F. G. Teats, and A. A. Jonke, *Reduction of Atmospheric Pollution by the Application of Fluidized-Bed Combustion and Regeneration of Sulfur-Containing Additives*, Annual Report, July 1973-June 1974, ANL/ES-CEN-1007 (1974).

5. R. C. Hoke, *et al.*, *A Regenerative Limestone Process for Fluidized Bed Coal Combustion and Desulfurization*, Monthly progress Report No. 77, July 1977.

6. J. C. Montagna, G. W. Smith, F. G. Teats, G. J. Vogel, and A. A. Jonke, *Evaluation of On-Line Light-Scattering Particle Size Analyzers for Measurements at High Temperature and Pressure*, ANL/CEN/FE-77-7 (in preparation).

7. Riyad R. Irani and Clayton F. Callis, *Particle Size: Measurement, Interpretation, and Application*, p. 43, John Wiley & Son, Inc., New York, 1963.

8. C. Orr and J. M. Dalla Valle, *Fine Particle Measurement, Size, Surface and Pore Volume*, pp 83-91, McMillan, New York, 1960.

TABLE I. SELECTED INTERFERENCE FRINGE SPACINGS AND THE CORRESPONDING MEASURABLE SPHERICAL PARTICLE SIZE RANGES

| Fringe Period, μm | Min. Particle Diameter, μm | Max. Particle Diameter, μm |
|---|---|---|
| 71.4 | 4.9 | 74 |
| 22.3 | 1.5 | 23 |
| 2.94 | 0.2 | 3.1 |

TABLE II. EXPERIMENTAL CONDITIONS FOR A COMBUSTION EXPERIMENT IN THE EVALUATION OF THE SINGLE-PARTICLE ANALYZER

Location of PM Windows: Between PDU combustor and cyclones, SGL-1.
Between second cyclone and filter, SGL-2C.
Sorbent: Greer Limestone
Coal: Sewickley
System Pressure, kPa: 308 (3 atm)
Fluidizing Gas Velocity, m/s: 1.0

| Exp. | Combustor Temp, °C | Conditions at PM Windows Gas Velocity, m/s | Conditions at PM Windows Temp, °C | Conditions Near Probe at Sampling Duct Gas Velocity $V_{fg}$, m/s | Conditions Near Probe at Sampling Duct Temp, °C | Conditions Near Probe at Sampling Duct Ratio of Duct Velocity to Probe Gas Velocity $V_{fg}/V_s$ |
|---|---|---|---|---|---|---|
| SGL-1 | 850 | 5.2 | 350 | - | - | - |
| SGL-2C | 855 | 11.8 | 123 | 3.26 | 110 | 1.16 |
| SGL-1C | 855 | 2.6 | 90 | 0.91 | 60 | 1.15 |

TABLE III. COMPARISON OF PARTICLE SIZES AND LOADINGS OBTAINED WITH THE MULTIPARTICLE ANALYZER, THE ANDERSEN IMPACTOR, AND MEMBRANE FILTER

FBC Combustor Conditions:

| | |
|---|---|
| Pressure | 308 kPa (3 atm) |
| Temperature | 855°C |
| Fluidizing Velocity | 1 m/sec |
| Sorbent | Greer Limestone |
| Coal | Sewickley |

| | MICROTRAC | | | Andersen Impactor | | Membrane Filter |
|---|---|---|---|---|---|---|
| Exp. | $\bar{D}_V$[c] (μm) | $\bar{D}_A$[d] (μm) | Loading (g/m$^3$)[α] | $\bar{D}_{AE}$[e] (μm) | L (g/m$^3$) | Loading (g/m$^3$) |
| LN-4-1-a | 5.1 | 2.8 | 0.43 | 2.2 | 0.33 | 0.64 |
| LN-4-1-b | 2.9 | 2.2 | 0.83 | 3.5 | 1.1 | 1.3 |
| LN-5-1-a | 5.5 | 3.4 | 0.18 | 6.0[f] | 0.21 | 0.41 |
| LN-5-2-b | 3.9 | 2.3 | 1.0 | 3.2 | 0.98 | 0.40 |
| LN-6-1-a | 4.4 | 2.8 | 0.46 | 3.0 | 0.12 | 0.54 |
| LN-6-2-b | 3.6 | 2.2 | 0.64 | 3.5 | 1.1 | 1.0 |
| LN-10-3-b | 3.8 | 2.2 | 1.5 | 2.0 | 0.56 | - |
| LN-10-4-b | - | - | 0.37 | - | - | 0.63 |
| LN-11-1-a | 11.9 ±.3 | 5.5 ±.11 | 0.12±.01 | 1.9 | 0.01 | |
| LN-11-2-a | - | - | 0.13±.01 | - | - | 0.009 |
| LN-11-3-a | 10.5 ±.2 | 4.97±.12 | 0.11±.02 | 1.8 | 0.01 | |
| LN-9-3-a[g] | 2.24±.36 | 2.01±.06 | 0.21±.04 | 0.63 | 0.001 | |
| LN-9-2-a[g] | - | - | 0.10±.02 | - | - | 0.003 |
| LN-9-5-b[g] | 3.77±.23 | 2.72±.07 | 1.20±.06 | 1.5 | 0.115 | |
| LN-9-4-b[g] | - | - | 0.52±.17 | - | - | 0.110 |

[α] 1 g/m$^3$ = 0.437 grain/scf

[a] After filter.

[b] Between secondary cyclone and filter.

[c] Volume mean diameter.

[d] Projected area mean diameter.

[e] Aerodynamic mean diameter.

[f] Suspect, possibly due to unexpected flue gas re-entrainment.

[g] Cold elutriation experiments - only virgin limestone particles measured.

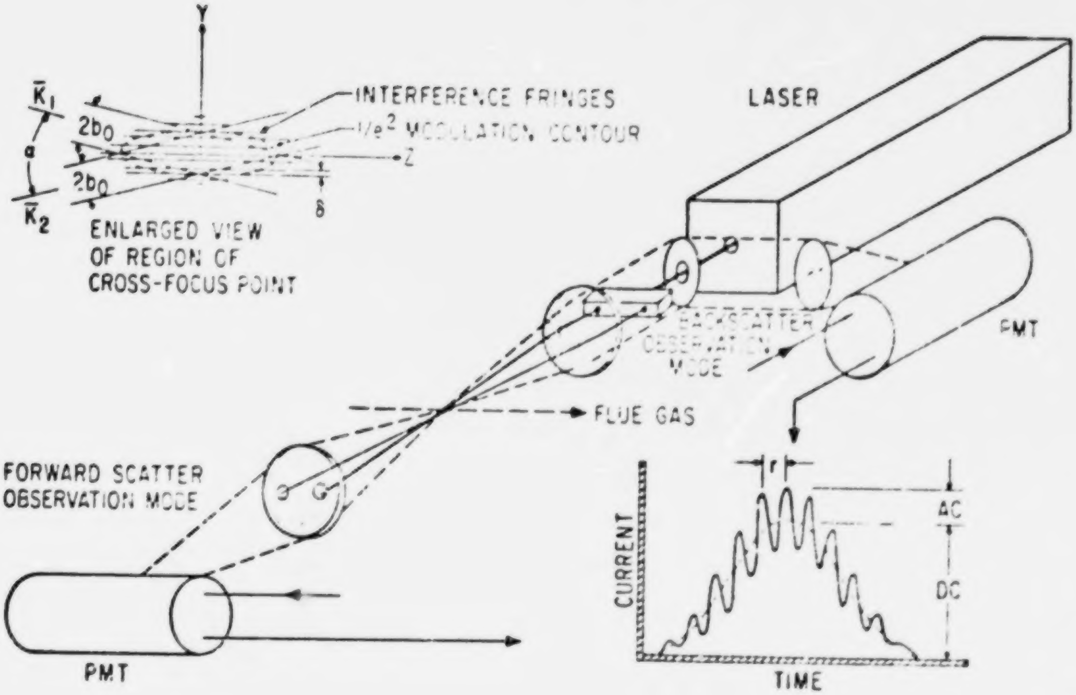
Y
$\bar{K}_1$
$2b_0$
$\alpha$
$2b_0$
$\bar{K}_2$
INTERFERENCE FRINGES
$1/e^2$ MODULATION CONTOUR
Z
$\delta$
ENLARGED VIEW OF REGION OF CROSS-FOCUS POINT
LASER
BACKSCATTER OBSERVATION MODE
PMT
FLUE GAS
FORWARD SCATTER OBSERVATION MODE
PMT
$\tau$
AC
DC
CURRENT
TIME

Fig. 1. Spectron Development Laboratory's PM Analyzer System for Velocity and Particle Measurement

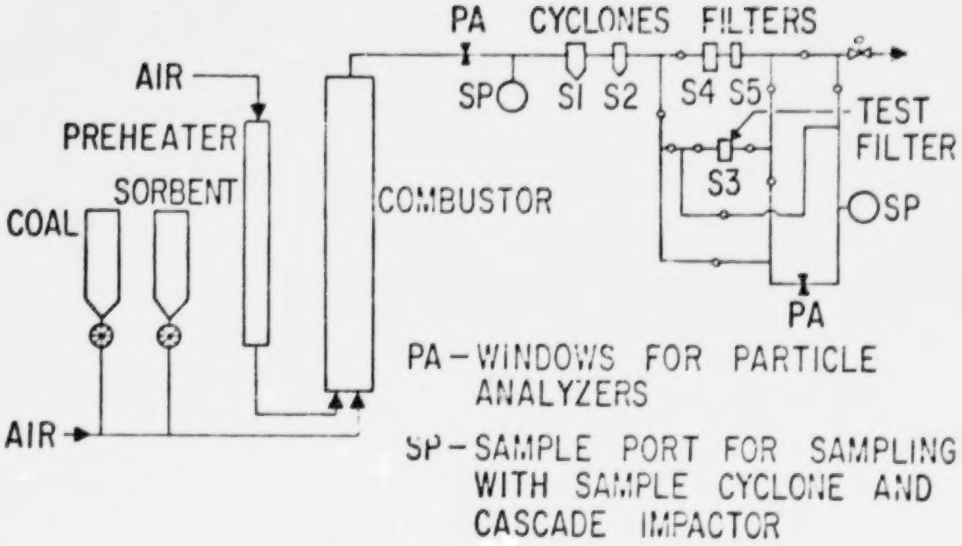
PA
CYCLONES
FILTERS
AIR
PREHEATER
SORBENT
COAL
COMBUSTOR
SP
S1
S2
S4
S5
S3
TEST FILTER
SP
PA
AIR
PA – WINDOWS FOR PARTICLE ANALYZERS
SP – SAMPLE PORT FOR SAMPLING WITH SAMPLE CYCLONE AND CASCADE IMPACTOR

Fig. 2. Schematic of FBC System with Modified Flue-Gas System

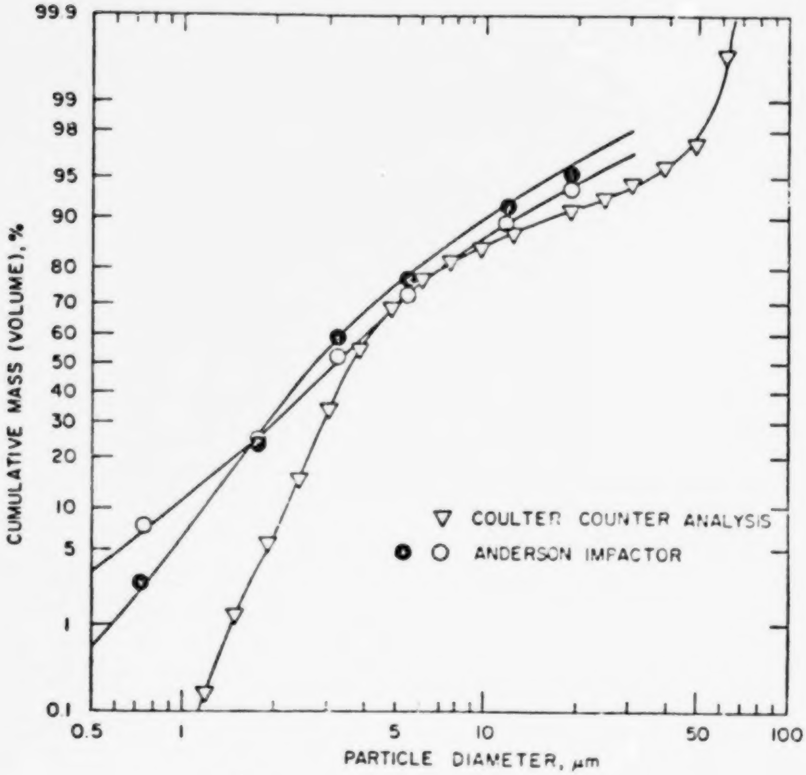

Fig. 3. Cumulative Mass Distribution of Particles in the Flue Gas Between the Secondary Cyclone and the Metal Filter (SGL-2C)

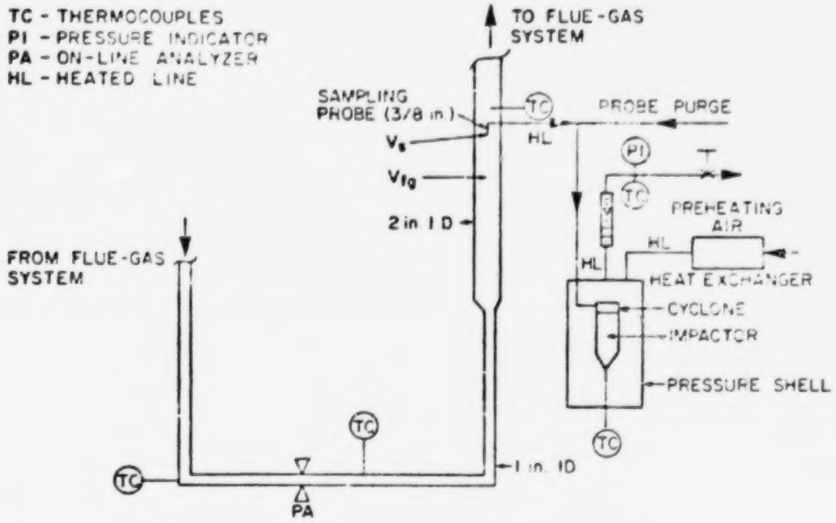
TC - THERMOCOUPLES
PI - PRESSURE INDICATOR
PA - ON-LINE ANALYZER
HL - HEATED LINE
TO FLUE-GAS SYSTEM
SAMPLING PROBE (3/8 in.)
TC
PROBE PURGE
HL
$V_s$
PI
$V_{fg}$
TC
PREHEATING AIR
2 in I D
HL
FROM FLUE-GAS SYSTEM
HL
HEAT EXCHANGER
CYCLONE
IMPACTOR
PRESSURE SHELL
TC
TC
TC
1 in. ID
PA

Fig. 4. Flue Gas Particle Sampling System

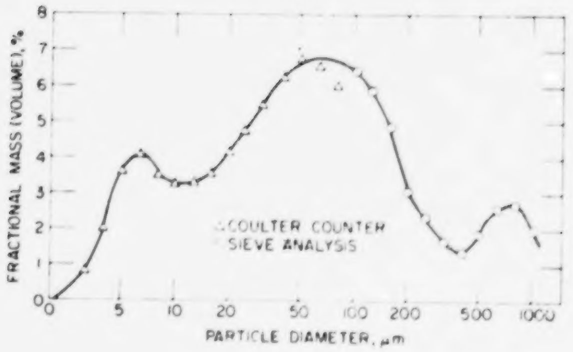

Fig. 5. Fractional Mass Distribution of All Elutriated Particles during a Combustion Experiment (SGL-1) from the ANL FBC Combustor

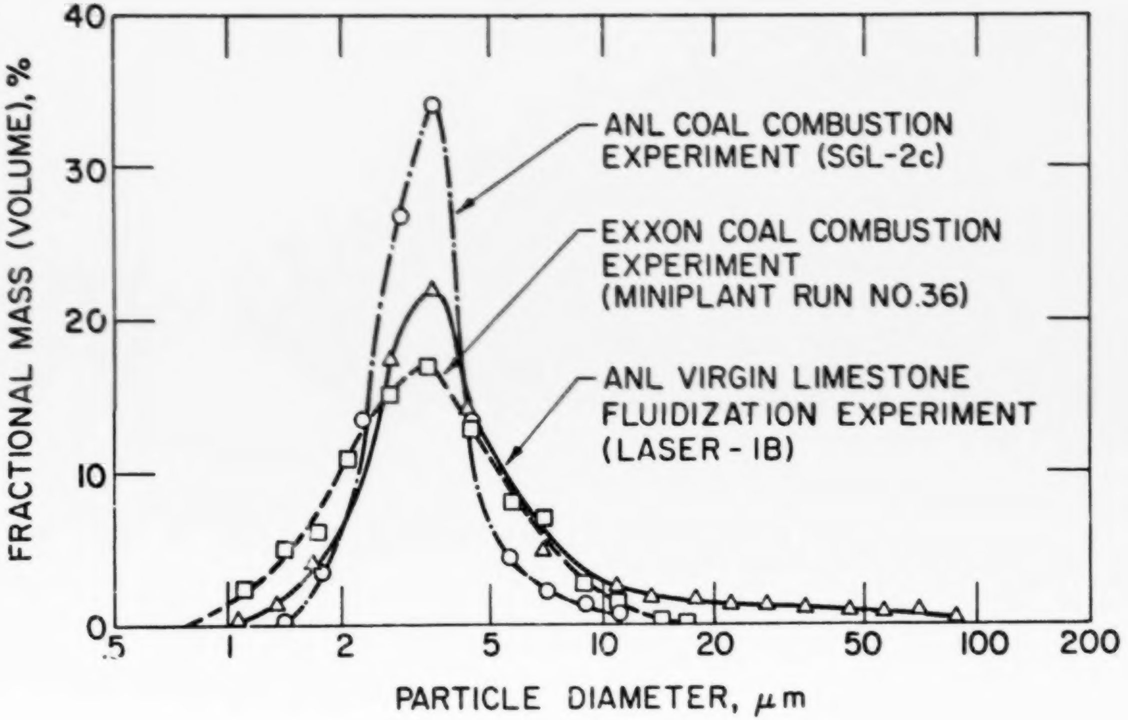

Fig. 6. Fractional Mass Distribution of Particles Escaping FBC Flue Gas System's Cyclones

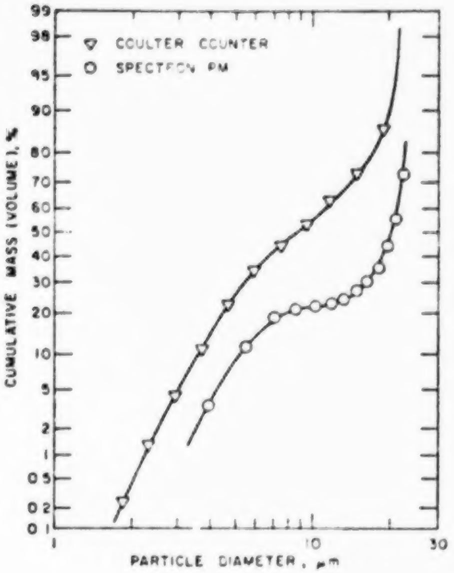

Fig. 7. Comparison of the Partial (1.5-23 µm) Cumulative Mass Distribution of Particles Leaving the Combustor (SGL-1)

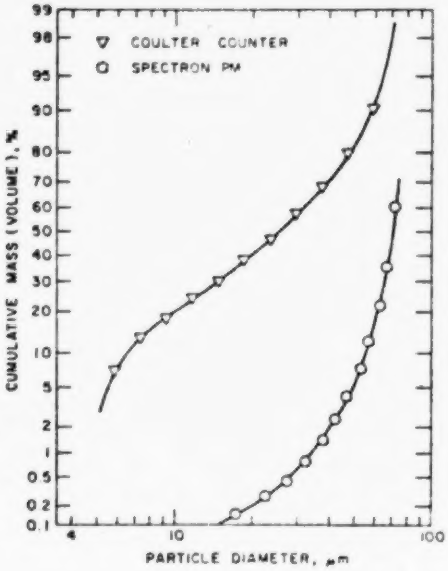

Fig. 8. Comparision of the Partial (5-74 μm) Cumulative Mass Distribution of Particles Leaving the Combustor (SGL-1)

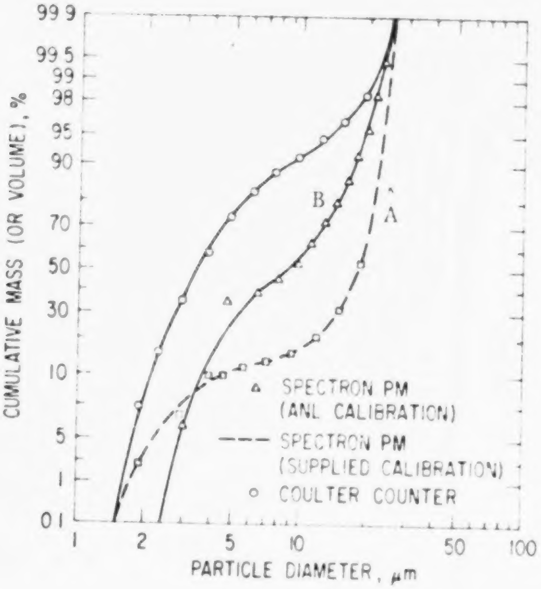

Fig. 9. Comparison of the Partial (1.5-23.8 μm) Cumulative Mass Distribution of Particles Leaving the Secondary Cyclone (SGL-2C)

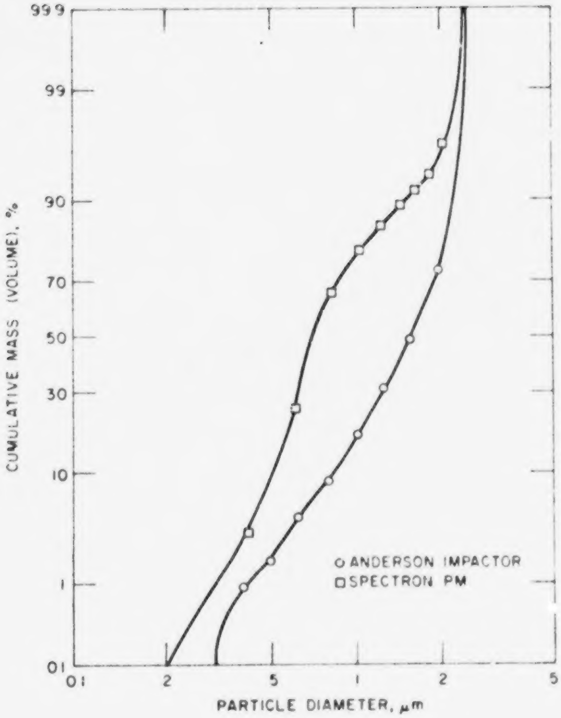

Fig. 10. Comparison of the Partial (0.2-3.1 μm) Cumulative Distribution of Particles Leaving the Secondary Cyclone (SGL-1C)

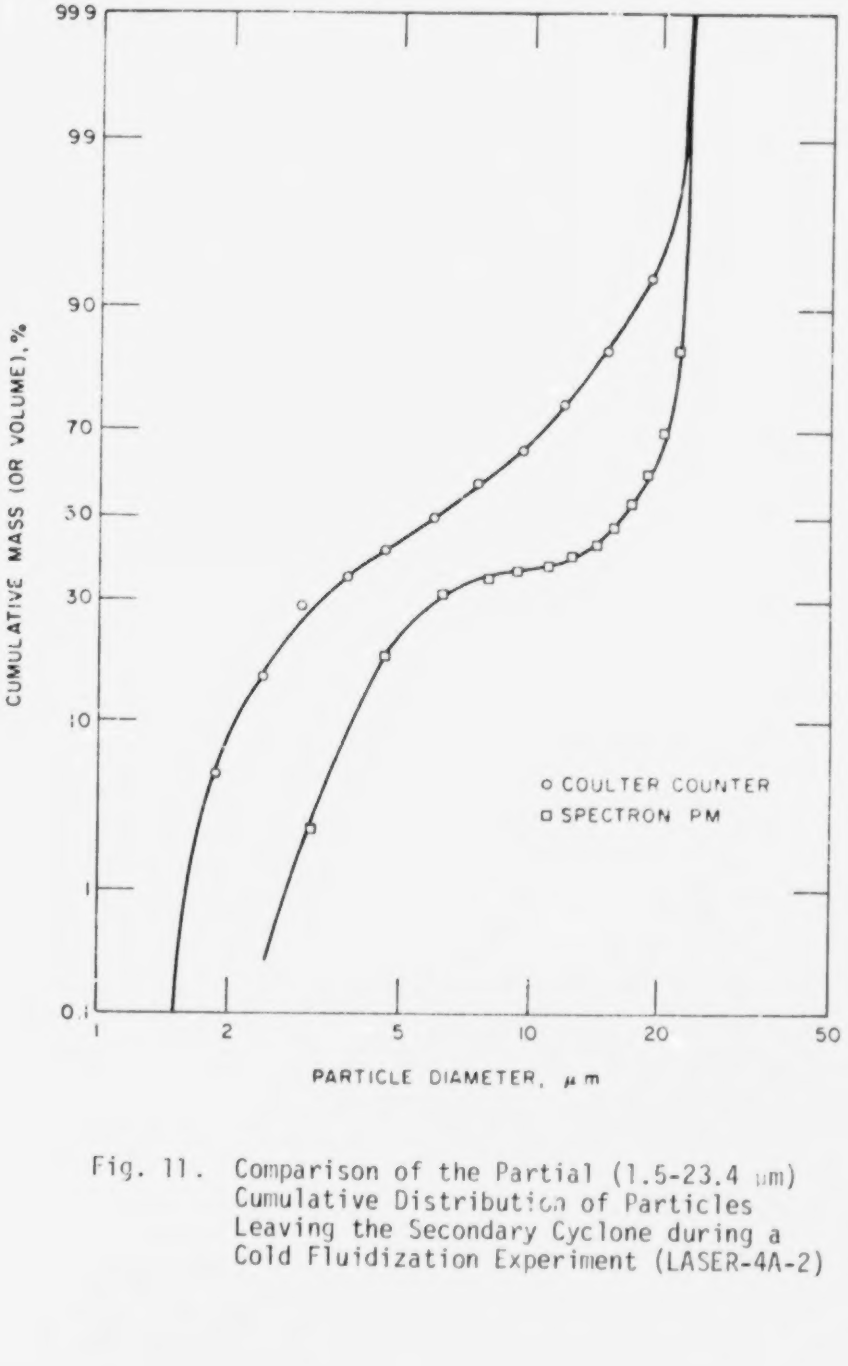

Fig. 11. Comparison of the Partial (1.5-23.4 μm) Cumulative Distribution of Particles Leaving the Secondary Cyclone during a Cold Fluidization Experiment (LASER-4A-2)

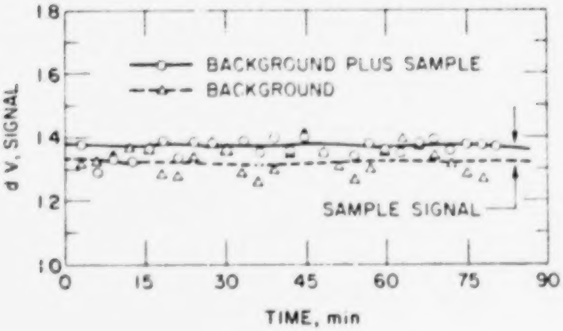

Fig. 12. A Comparison of the Semi-continuous Background Signal with the Background plus Sample Signal from MICROTRAC, Experiment LN-11

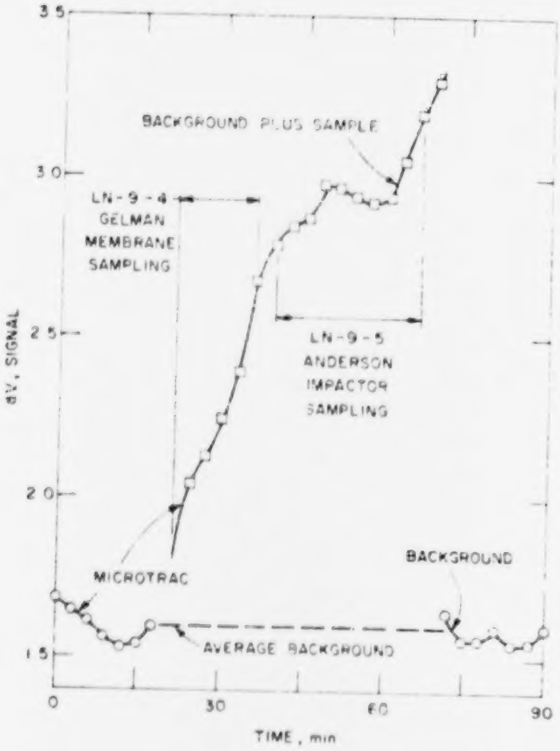

Fig. 13. The Semi-continuous Particulate Lading Signal from the MICROTRAC Particle Size Analyzer for Measurements LN-9-4 and -5

## LIST OF PROCEEDINGS RECIPIENTS

EPA/ERDA SYMPOSIUM ON HIGH
TEMPERATURE/PRESSURE PARTICULATE
CONTROL
SEPTEMBER 20-21, 1977

Jim Abbott
EPA
IERL-RTP
Research Triangle Park
North Carolina 27711

N. Abuaf
Brookhaven National Laboratory
Upton Long Island
New York 11973

Richard L. Adams
Wheelabrator-Frye Inc.
600 Grant Street
Pittsburgh PA 15219

Jeffery C. Alexander
M.I.T.
Room 36-323
Cambridge, MA 02139

Francis M. Alpiser
Chemical Environmental Engineering
EPA III--AHMD-SIP
Sixth and Walnut
Curtis Building Ms-3A-H11
Philadelphia, PA 19106

Gerald L. Anderson
Institute of Gas Technology
3424 South State Street
Chicago, IL 60616

Herman B. Anderson, Jr.
General Services Administration
Region 3, PBS
Technical Field Office
7th & D Sts., SW
Washington, DC 20407

Dr. John W. Anderson
Rexnord, Inc.
1914 Albert Street
Racine, WI 53404

Larry W. Anderson
Acurex/Aerotherm
485 Clyde Avenue
Mountain View, CA 94042

Stig Andersson
STAL Laval
S-61320 Finspong
Sweden

D. H. Archer
Westinghouse
Beulah Road
Pittsburgh, PA 15235

Ted Atwood
Process Engineering
Department of Energy
Room 504
20 Massachusetts Avenue
Washington, DC 20545

-B-

Dr. Suresh P. Babu
Institute Gas Technology
3424 South State Street
Chicago, IL 60616

W. D. Bachalo
Spectron Development Labs.
3303 Harbor Blvd.
Costa Mesa, CA 92626

E. T. Barrow
Ministry of the Environment
Air Resources Branch
44880 Bay Street
Toronto, Ontario MS5 128
Canada

Walter A. Baxter
Environmental Elements Corp.
P.O. Box 1318
Baltimore, MD 21230

Roland Beck
Department of Energy
7374 S. Forest
Whittier, CA 90602

Robert W. Bee
Consultant
126 Hopeland Lane
Sterling, VA 21170

K. Bekofske
General Electric Co.
CR&D
P.O. Box 8
Schnectady, NY 12301

Michael Beltran
Beltran Assoc., Inc.
1133 E. 35th Street
Brooklyn, NY 11210

Dr. Michael Benarie
Chef Du Services Pollution
Stmospherique
Institute National De Recherche
Chimique Applique I.R.Ch.A.
Centre De Recherche
91710-Vert-Le-Petit, France

Paul A. Berman
Westinghouse Electric Corp.
P.O. Box 9175, Lester Branch
Philadelphia, PA 19113

Dr. Samuel Bernstein
Flow Research Co.
P.O. Box 5040
Kent, WA 98031

Albert J. Bevolc
Associate Physicist
US Department of Energy
Ames Laboratory
A205 Physics
Ames, IA 50011

Prem Sagar Bhardwaja, PhD
Lawrence Berkeley Laboratory
Univ. of California
Berkeley, CA 94720

Charles E. Billings
Environmental Engineering Science
740 Boylston Street
Chestnut, MA 02167

Samuel J. Biondo
Federal Power Commission
825 N Capitol Street, NE
Room 5008
Washington, DC 20426

David Blake
Acurex/Aerotherm
485 Clyde Avenue
Mountain View, CA 94042

Dale Blann
Acurex/Aerotherm
3301 Woman's Club Drive
Raleigh, NC 27611

Frederick L. Blum
Research-Cottrell Inc.
P.O. Box 750
Bound Brook, NJ 08805

B. H. Bochenek
U.S. EPA
401 M Street, SW (A-134)
Washington, DC 20460

Dr. R. Boericke
General Electric Co.
Building 2, Room 712
One River Road
Schnectady, NY 12345

Bruce Boggs
Amax
5020 S Atlanta Rd, SE
Smyra, GA 30080

Dr. R. H. Boll
Babcock and Wilcox
Research Center
P.O. Box 835
Alliance, OH 44601

J. Bormans
General Secretary Ecochem
FICB-ECOCHEM
Square Marie-Louise 49
1040 Brussels, Belgium

Jeffery Bradley
Research Associate
University of Wisconsin
at Milwaukee
3200 N Cramer Street
Milwaukee, WI 53201

William L. Brangers
U.S. Army Environmental
Hygiene Agency
Abeerdeen Proving Grounds
MD 21010

Ed Brooks
TRW
One Space Park Drive
Redondo Beach, CA 90278

Beth A. Brown
Aspen Systems Corporation
20010 Century Blvd.
Germantown, MD 20767

Robert F. Brown
Research-Cottrell
P.O. Box 750
Bound Brook, NJ 08805

Warren L. Buck
Argonne National Lab.
9700 S Cass Avenue, Bldg. 308
Argonne, IL 60439

Charles L. Burton
Combustion Engineering
1000 Prospect Hill Road
Windsor, CT 06095

Chris Busch, President
Spectron Dev. Lab.
3303 Harbor Blvd.
Costa Mesa, CA 92606

John R. Bush
Research-Cottrell
P.O. Box 750
Bound Brook, NJ 08805

-C-

Captain Jesse B. Cabellon
US Army Environmental
Hygiene Agency
Abeerdeen Proving Grounds, MD 21010

Dr. Seymour Calvert
Air Pollution Technology, Inc.
4901 Morena Blvd., Suite 402
San Diego, CA 92117

Robert Carlson
Acurex/Aerotherm
485 Clyde Avenue
Mountain View, CA 94042

Dr. R. L. Carpenter
Lovelace Biomedical and
Environmental Research Institute
P.O. Box 5890
Albuquerque, NM 87115

Captain James W. Carroll
US Army Environmental Hygiene Agency
Abeerdeen Proving Grounds, MD 21010

John J. Casey
Sr. Marketing Engineering
Fluidyne Engineering Corp.
5900 Olson Memorial Highway
Minneapolis, MN 55422

Gilbert K. C. Chen
Monsanto
800 N Lindbergh Blvd.
St. Louis, MO 63166

Gregory H.S. Cheng
Environeering, Inc.
4233 N United Parkway
Schiller Park, IL 60176

C.K.H. Choi
TRW Energy Systems Group
Bldg. R4/Room 2136
One Space Park Drive
Redondo Beach, CA 90278

Robert A. Chronowski
MITRE Corporation
Westgate Research Park
McLean, VA 22101

Dr. David F. Ciliberti
Westinghous R&D Center
Beulah Rd, Bldg. 501-3E29

Neil H. Coates
MITRE Corp./Metrek Div.
1820 Dolly Madison Blvd.
McLean, VA 22101

John F. Cobianchi
J.P. Stevens & Company, Inc.
1185 Avenue of the Americas
New York, NY 10036

Dr. Hugh Coleman
Sandia Laboratories
P.O. Box 5800
Albuquerque, NM 87115

Leland Collins
Mech. Eng. Dept.
Stanford University
Stanford, CA 94305

Steven D. Colome
Harvard School of Public Health
665 Huntington Avenue
Boston, MA 02115

John Colton
TRW
7600 Colshire Drive
McLean, VA 22101

James Colyar
Process Engineering
Cogas Development Company
P.O. Box 8
Princeton, NJ 08540

Peter Costanza
Staff Scientist
Textile Research Inst.
P.O. Box 65
Princeton, NJ 08540

Glenn Coury
Coury & Associates, Inc.
7400 W. 14th Avenue
Lakewood, CO 80214

Fred Cox
Menardi Southern
1201 W. Francisco Blvd.
Torrance, CA 90502

Rufus Crawford
Stearns-Roger Eng. Co.
P.O. Box 5888
Denver, CO 80217

Steven R. Cross
Buell-Envirotech
253 N. Fourth Street
Lebanon, PA 17042

T. E. Ctrvtnicek
Monsanto-Dayton Labs
1515 Nicholas Road
Dayton, OH 45407

John S. Cvicker
Foster-Wheeler Energy Corp.
110 S. Orange Avenue
Livingston, NJ 07039

-D-

Alberta M. Dawson
Sala Magnetics, Inc.
247 Third Street
Cambridge, MA 02142

John C. Dempsey
Program Manager
US Department of Energy

Mark N. Director
Head, Gas Physics Section
Atlantic Research Corp.
5390 Cherokee Avenue
Alexandria, VA 22314

Thomas Donnelly
Donaldson Company, Inc.
P.O. Box 1299
Minneapolis, MN 55440

John M. Ducan
Shell Development
P.O. Box 2463--One Shell Plaza
Houston, TX 77001

Frederick J. Dudek
UOP, Inc. Air Correction Div.
P.O. Box 1107, Tokeneke Road
Darien, CT 06820

-E-

Sally Edler
Bendix Environmental & Process
  Instruments Div.
1400 Taylor Avenue
Baltimore, MD 21204

Heinz L. Engelbrecht
Wheelabrator-Frye Inc.
600 Grant Street
Pittsburgh, PA 15219

Harold M. Englund
Editor, APCA Journal
Air Pollution Control Association
P.O. Box 2861
Pittsburgh, PA 15230

Joseph Epstein
MHD Division
US Department of Energy
20 Massachusetts Avenue, NW
Washington, DC 20545

George Erskine
MITRE Corp./Metrek Div.
1820 Dolly Madison Blvd.
McLean, VA 22101

-F-

James Facet
Facet Enterprises
434 W. 12 Mile Road
Madison Hts., MI 48071

B. P. Faulkner
Allis-Chalmers Corp.
P.O. Box 512
Milwaukee, WI 53201

William Fedarko
US Department of Energy
20 Massachusetts Avenue, NW
Washington, DC 20545

Paul L. Feldman
Research-Cottrell
P.O. Box 750
Bound Brook, NJ 08805

Lewis K. Felleisen
EPA, Region III
Curtis Building
Sixth and Walnut Streets
Philadelphia, PA 19106

Oliver Foo
MITRE/Metrek Div.
Westgage Research Park
McLean, VA 22101

Paul E. Fredette
Midland-Ross Technical Center
P.O. Box 907
Toledo, OH 43691

Max Friedman
Chemico Air Pollution Control Co.
One Penn Plaza
New York, NY 11801

H. N. Frock
Leeds & Northrup
Dickerson Road
North Wales, PA 19454

Robert Frumerman
Frumerman Associates
5423 Darlington Road
Pittsburgh, PA 15217

Dale Furlong
Buell Emission Control Div.
Envirotech Corp.
200 N. Seventh Street
Lebanon, PA 17042

-G-

John A. Garbak
Montgomery County
Dept. of Environmental Protection
6110 Executive Blvd., Room 340
Rockville, MD 20852

John A. Garbak
Environmental Engineering
Montgomery County
1909 Hyannis Ct. #202
McLean, VA 22101

Betty Gaskins
Library Services
Pollution Abstracts
Data Courier Inc.
620 South 5th Street
Louisville, KY 40202

John Gefkin
Department of Energy
Fossil Energy/Advanced Power Systems
20 Massachusetts Avenue, NW
Washington, DC 20545

Peter Gelfand
Buell Emission Control Div.
Envirotech Corp.
200 N. Seventh Street
Lebanon, PA 17042

Masood Ghassemi
TRW, Bldg. R4/Room 1128
One Space Park Drive
Redondo Beach, CA 90278

James A. Gieseke
Batelle-Columbus Labs.
505 King Avenue
Columbus, OH 43201

W. Giles
General Electric Co.
Corporate R&D
P.O. Box 8
Schenectady, NY 12301

Gerald M. Goblirsch
Mechanical Engineering
Department of Energy
Grand Forks Energy Research Ctr
Box 8213 University Station
Grand Forks, ND 58202

John C. Gordon
TRW
Energy Systems Planning Div.
7600 Colshire Drive
McLean, VA 22101

Dr. Simon L. Goren
National Science Foundation
Engineering Divsion
Washington, DC 20550

Eugene Grassel
Donaldson Company
P.O. Box 1299
Minneapolis, MN 55440

Michael W. Gregory
Exxon Res. & Dev.
1600 Linden Avenue
Linden, NJ 07036

Ulrich Grimm
MERC
US Department of Energy
P.O. Box 880
Morgantown, WV 26537

Stanley S. Grossel
Process Design Section
Hoffman-LaRoche, Inc.
Nutley, NJ 07110

Robert Gugger
Curtiss-Wright Corporation
One Passaic Street
Wood Ridge, NJ 07075

Nigel Guilford
Ontario Res. Foundation
Sheridan Park
Mississauga, Ontario L5K 1B3
Canada

Michael Gurevick
US Department of Energy
1900 S. Eads Street
Arlington, VA 22202

Karl-Axel Gustavsson
Bahco Ventilation
Bahco Systems, Inc.
P.O. Box 48116
Atlanta, GA 30362

Adi R. Guzdar
Foster-Miller Association
135 Second Avenue
Waltham, MA 02176

-H-

Francine Hakimian
Librarian
McIlvaine Co.
2970 Maria Avenue
Northbrook, IL 60062

H. J. Hall
H. J. Hall Associates
Cherry Valley Road
Princeton, NJ 08540

D. G. Ham
Battelle-Northwest
Battelle Blvd.
Richland, WA 99352

C. Frederick Hansen
Ames Research Center
NASA, Div. 229-3
Moffet Fi ld, CA 94033

Mark S. Hanson
Battelle-Northwest
P.O. Box 999
Richland, WA 99352

Michael J. Hargrove
C-E Power Systems
1000 Prospect Hill Road
Windsor, CT 06095

G. O. Haroldsen
Allied Chemical Corporation
550 Second Street
Idaho Falls, ID 83401

Andrew Harvey
Foster-Miller Associates
135 Second Avenue
Waltham, MA 02154

William J. Havener
Waltz Mill Site Box 158
Westinghouse Madison, PA 15663

J. H. Hedberg
Aeroject Energy Conversion Co.
P.O. Box 13222
Sacramento, CA 95813

K. H. Hemsath
Surface Division
Midland-Ross Corp.
P.O. Box 907
Toledo, OH 43691

Howard E. Hesketh
Southern Illinois University
School of Eng.
Carbondale, IL 62901

Graham Hilder
BP North America
620 - 5th Avenue
New York, NY 10020

R. C. Hoke
Exxon Research and Engineering
P.O. Box 8
Linden, NJ 07036

John D. Holmgren
Westinghouse
Waltz Mill Site Box 158
Madison, PA 15663

Dr. Donald J. Holve
Stanford University
Mechanical Engineering
Stanford, CA 94305

Robert Hoseman
PG&E
77 Beale Street
San Francisco, CA 94106

Dr. Chao-Ming Huang
TVA Energy Research
1320 Commerce Union Bank Bldg.
Chattanooga, TN 37401

Gordon Huddleston
Montana Energy and MHD
Research and Development Inst.,Inc.
P.O. Box 3809
Butte, MT 59701

Jacques Hull
Acurex/Aerotherm
485 Clyde Avenue
Mountain View, CA 94042

-J-

I. L. Jashnani
Arthur D. Little, Inc.
One Acorn Park
Cambridge, MA 02140

Albert A. Jonke
Argonne National Lab.
9700 S Cass Avenue
Argonne, IL 60439

-K-

Yale G. Kardish
Peabody Air Resources Equip. Co.
P.O. Box 5202
Princeton, NJ 08540

Harry F. Keller
Carrier Corporation/Research Div.
Carrier Parkway
Syracuse, NY 13201

William M. Kelly
Environmental Elements Corp.
P.O. Box 1318
Baltimore, MD 21203

Richard A. Kennedy
MITRE/Metrek Division
1820 Dolly Madison Blvd.
McLean, VA 22101

Frank J. Kiernan
Aerojet Energy Conversion Co.
99 Clinch Avenue
Garden City, NY11530

Mike Klett
Process Engineering
Gilbert Associates
P.O. Box 1498
Reading, PA 19603

Richard N. Kniseley
Department of Energy
Ames Laboratory, DOE
Iowa State University
Ames, IA 50011

Dr. Charles E. Knox
Uniglass Industries
1440 Broadway
New York, NY 10018

Arthur L. Kohl
Rockwell International/
Atomics International Div.
8900 DeSoto Avenue
Canoga Park, CA 91304

John J. Kovach
MERC
Department of Energy
P.O. Box 880
Morgantown, WV 26505

Dr. A. Krishan Rao
Monsanto Enviro-Chem
P.O. Box 14547
St. Louis, MO 63178

William Krisko
Donaldson Co., Inc.
P.O. Box 1299
Minneapolis, MN 55440

Harry Krokta
The Ducon Company, Inc.
147 E. Second Street
Mineola, NY 11501

Andres Kullendorff
Atal-Laval Turbin AB
S-61220 Finspong, Sweden

T. Kumar
Occidental Research Corporation
1855 Carrion Road
LaVerne, CA 91750

William B. Kuykendal
IERL-RTP
Environmental Protection Agency
Research Triangle Park, NC 27711

-L-

Norman R. LaMarche
General Electric
1 River Road
Bldg. 23, Room 355
Schenectady, NY 12345

George Lamb
Textile Research Institute
P.O. Box 625
Princeton, NJ 08540

William T. Langan
Buell Emission Control Div.
Envirotech Corporation
200 N. Seventh Street
Lebanon, PA 17042

Robert Langley
Inex Resources, Inc.
7475 W. Fifth Avenue
Lakewood, CO 80226

C. E. Lapple
Chemical Engineering Department
SRI International
333 Ravenswood Avenue
Menlo Park, CA 94025

Benjamin Linsky
A Different Air -- Skyline
1360 Anderson
Morgantown, WV 26505

C. E. Lombardi
Teller Environmental Systems, Inc.
10 Faraday Street
Worcester, MA 01605

Bruno Loran
Ralph M. Parsons Co.
100 W Walnut Street
Pasadena, CA 91124

E. T. Losin
Allis-Chalmers Corporation
Milwaukee, WI 53201

F. E. Lukens
Western Arcadia
4115 W. Ogden Avenue
Chicago, IL 60623

-M-

M. MacCafferty
IEA Coal Research
Technical Information Service
14/15 Lower Grosvenor Place
London SWIW OEX, England

Andrej Macek
Department of Energy
Fossil Energy/Advanced Power Systems
20 Massachusetts Avenue, NW
Washington, DC 20545

Dr. Ray F. Maddalone
TRW Defense and Space Systems
Group
Bldg. 01/2020
One Space Park Drive
Redondo Beach, CA 90278

Capt. Joseph A. Martone
USAF, BSC
DET 1, HC ADTC
Tyndall AFB, FL 32403

Dr. Lidia Manson
TRW
Bldg. 01/2161
One Space Park Drive
Redondo Beach, CA 90278

William Masters
Acurex/Aerotherm
485 Clyde Avenue
Mountain View, CA 94042

Sigvard Mats
Flakt Inc.
1500 E Putnam Avenue
Old Greenwich, CT 06870

I. Matsunga
Mitsubishi Heavy Industries
875 North Michigan Avenue
Suite 2100
Chicago, IL 60611

Mike May
Babcock and Wilcox Company
20 S VanBuren
Barberton, OH 44203

J. T. McCabe
Mechanical Technology
968 Albany-Shaker Road
Latham, NY 12110

J. D. McCain
Southern Research Institute
2000 9th Avenue
Birmingham, AL 35205

William McCarthy
Chemical Engineering
US/EPA -- OEMI
Waterside Mall
Washington, DC 20460

Joseph E. McGreal
United States Steel Research
"B" Street
Penn Hills, PA 15235

James R. Melcher
MIT
Room 36-313, 50 Vassar Street
Boston, MA 02139

Dr. Arthur G. Metcalfe
Solar Turbines International
Mail Zone R-1, Box 80966
San Diego, CA 92138

Dr. Jim Meyer
Research Engineering
Oak Ridge National Lab.
P.O. Box "X"
Oak Ridge, TN 37830

Larry Michalec
Code 64270 NARF
NAS North Island
San Diego, CA 92135

M. Miller
Fluidyne Engineering Corporation
5240 Port Royal Road
Springfield, VA 22151

Ron Miller
PSM Sales -- Rexnord
7675 Maple Avenue
Pennsauken, NJ 08109

Richard Mitchell
Inex Resources, Inc.
7475 W. Fifth Avenue
Lakewood, CO 80226

Henry Modetz
EPA, Region IV
230 S. Dearborn
Chicago, Il 60604

John C. Montagna
Argonne National Lab.
9700 S. Cass Avenue
Argonne, IL 60439

R. H. Moore
Battelle-Northwest
Battelle Boulevard
Richland, WA 99352

Samuel J. Moore
Carrier Corp/Research Div.
Carrier Parkway
Syracuse, NY 13201

William E. Moore
Fossil Energy/Adv. Power Systems
Department of Energy
20 Massachusetts Avenue
Washington, DC 20545

John A. Morris
Air Pollution Div.
Rexnord Inc.
P.O. Box 13226
Louisville, KY 40213

Tom Mosure
US/EPA
Environmental Research Inf. Ctr
26 W. St. Clair
Cincinnati, OH 45268

Andy Murphy
Acurex/Aerotherm
3301 Woman's Club Drive
Raleigh, NC 27611

Keshava S. Murthy
Battelle-Columbus Labs.
505 King Avenue
Columbus, OH 43201

-N-

Leonard M. Naphtali
Department of Energy
Fossil Energy/CCN
20 Massachusetts Avenue
Washington, DC 20545

James C. Napier
Solar Turbines International
P.O. Box 80966
2200 Pacific Hwy
San Diego, CA 92138

Charles K. Neulander
General Electric Company
P.O. Box 8, Bldg. K-1
Schnectady, NY 12301

G. S. Newton
Lovelace Biomedical
Environmental Research Institute
P.O. Box 5890
Albuquerque, NM 87115

-O-

Thomas O'Hare
Brookhaven National Laboratory
Upton, Long Island, NW 11973

Dr. Morris S. Ojalvo
National Science Foundation
Engineering Division
Washington, D.C. 20550

John M. Ondov
Lawrence Livermore Lab.
P.O. Box 808
Livermore, CA 94550

Dr. H. H Osborn
C-E Air Preheater Co.
P.O. Box 372
Wellsville, NY 14895

-P-

James B. Padden
Facet Filters
434 W. 12 Mile Road
Madison Heights, MI 48071

Dr. Richard D. Parker
Air Pollution Technology, Inc.
4901 Morena Blvd., Suite 402
San Diego, CA 92117

Subhash S. Patel
Hittman Associates, Inc.
9151 Rumsey Road Bldg.
Columbia, MD 21045

Dr. Ronald G. Patterson
Air Pollution Technology, Inc.
4901 Morena Blvd., Suite 402
San Diego, CA 92117

Walter Podolski
Argonne National Lab.
9700 S. Cass Avenue
Argonne, IL 60439

Jospeh R. Polek
Catalytic, Inc.
1500 Market Street, CSW-10
Philadelphia, PA 19102

Duane H. Pondius
Southern Research Inst.
2000 9th Avenue S.
Birmingham, AL 35205

-Q-

Sandra Quinlivan
TRW
Bldg. R4/Room 1120
One Space Park Drive
Redondo Beach, CA 90278

-R-

E. Radhakrishnan
Battelle-Columbus Labs.
505 King Avenue
Columbus, Ohio 43201

Madhav B. Ranade
Research Triangle Inst.
P.O. Box 12194
Research Triangle Park
NC 27709

David L. Raring
Sonic Development Corporation
3 Industrial Avenue
Upper Saddle River, NJ 07458

Dr. Richard Razgaitis
Ohio State University
206 W. 18th Avenue
Columbus, Ohio 43221

D. L. Reid
Battelle-Northwest
P.O. Box 999
Richland, WA 99352

R. B. Reif
Battelle-Columbus Labs.
505 King Avenue
Columbus, OH 43201

Jean V. Remillieux
Air Industrie
19, Avenue DuBonnet
92401 Courbevoie
France

Ronald Renko
Development Engineering
C-E Air Preheater
Wellsville, NY 14895

George Rey
Office of R&D (RD-681)
EPA
Washington, DC 20460

George Rinard
Research Engineer
Denver Research Inst.
Denver, CO 80208

Frank G. Rinker
Midland-Ross
P.O. Box 907
Toledo, OH 43691

Thomas J. Robertazzi
Facet Enterprises
6521 Arlington Blvd.
Falls Church, VA 22042

George L. Roberts
Vice-President
Universal Transport Systems, Inc.
2665 Marine Way
Mountain View, CA 94040

David R. Rubin
USDA, Rural Electrification Admin.
Agriculture South Bldg.
14th & Independence Ave., SW
Washington, DC 20250

Stephen N. Rudnick
Harvard School of Public Health
665 Huntington Avenue
Boston, MA 02115

## -S-

Gene Schaltenbrand
C-E Preheater Company
P.O. Box 387
Wellsville, NY 14895

Robert K. Schaplowsky
Chemist
Aerojet
7767 LaRivera Drive #219
Sacramento, CA 95826

Robert Scheck
Stearns-Roger
P.O. Box 5888
Denver, CO 80217

G. F. Schiefelbein
Battelle-Northwest
Battelle Blvd.
Richland, WA 99352

Martin Schiller
CSI Engineering
P.O. Box 1515
Fairfield, CT 06430

J.W. Schindeler
John Zink Company
P.O. Box 7388
Tulda, OK 74105

Dr. Schnittgrunt
Consolidated Aluminum
2302 Weldon Way
St. Louis, MO 63178

H. F. Schulte
Rexnord, Inc.
1914 Albert Street
Racine, WI 53404

Richard A. Schwartz
Koch Engineering Co., Inc.
161 East 42nd Street
New York, NY 10017

Gernot Mayer Schwinning
Lurgi Apparate-Technik GmbH
Postfash 1, Gwinner Street
6000 Frankfort am Main-2
West Germany

Dr. David S. Scott
Dept. of Mech Engineering
Univ. of Toronto
Toronto, Ontario M5S 1A4
Canada

Stanley J. Selle
Grand Forks Energy Res. Ctr.
Department of Energy
P.O. Box 8213, University Station
Grand Forks, ND 58202

Michael Shackleton
Acurex/Aerotherm
485 Clyde Avenue
Mountain View, CA 94042

J. K. Shah
Surface Div.
Midland-Ross Corporation
P.O. Box 907
Toledo, OH 43691

Jer-Yu Shang, PhD
MITRE Corp./Metrek Div.
Westgate Research Park
McLean, VA 22101

Jer-Yu Shang
Professional Engineering
4524 Andes Drive
Fairfax, VA 22030

David Shaw, Professor
State University of NY/Buffalo
4232 Ridge Lea Road
Buffalo, NY 14226

W. J. Sheeran
General Electric Company
Corporate R&D
P.O. Box 43
Schenectady, NY 12301

Dr. Thomas S. Shevlin
3M Company
3M Center, P.O. Box 33221, Bldg. 230
St. Paul, MN 55138

Kevin Shields
Hittinaw Associates, Inc.
9190 Red Branch Road
Columbia, MD 21045

Dr. Gajendra H. Shroff
Bechtel Power Corporation
15740 Shady Grove Road
Gaithersburg, MD 20760

Jack Siegel
Department of Energy
Fossil Energy/Advanced Power
Systems
20 Massachusetts Avenue
Washington, DC 20545

Dr. A. P. Sikri
US Department of Energy
Gas & Shale Technology
20 Massachusetts Avenue
Washington, DC 20545

Dean Simeroth
California Air Resources Board
P.O. Box 2815
Sacramento, CA 95812

Theodore B. Simpson
Department of Energy
Fossil Energy/Advanced Power S
Systems
20 Massachusetts Avenue
Washington, DC 20545

A. V. Slack
SAS Corporation
Wilson Lake Shores
Sheffield, AL 35660

A. A. Smith
Babcock and Wilcox Ltd.
Woodall-Duckham House
Crawley, Sussex,
United Kingdom

Dr. Donald W. Smith
HAVEG Industries
900 Greenbank Road
Wilmington, DE 19808

Gregory W. Smith
Argonne National Lab.
9700 S. Cass Avenue
Argonne, IL 60439

Wallace B. Smith
Southern Research Inst.
2000 9th Avenue
Birmingham, AL 35205

John H. Smithson
Department of Energy
20 Massachusetts Avenue
Washington, DC 20545

Herbert W.Spencer, III
Western Precipitation Division
Joy Manufacturing
4565 Colorado Blvd.
Los Angeles, CA 90039

John Spriggs
Donaldson Company, Inc.
P.O. Box 1299
Minneapolis, MN 55440

Dr. C. J. Stairmand
Babcock and Wilcox Ltd.
Woodall-Duckham House
Crawley, Susses, United Kingdom

William A. Sandstrom
Institute of Gas Technology
3424 South State Street
Chicago, IL 60616

Walter Steen
Chemical Engineering
US EPA IER
IERL-RTP
Research Triangle Park
NC 27711

G. E. Stegen
Battelle-Northwest
Battelle Blvd.
Richland, WA 99352

David Stelman
Rockwell/Atomics Int. Div.
8900 DeSoto Avenue
Canoga Park, CA 91304

Ed Stenby
Project Engineering
Stearns-Roger
P.O. Box 5888
Denver, CO 80217

Richard C. Stone
Stone & Webster Engineering Co.
P.O. Box 2325
Boston, MA 02107

E. F.Sverdrup
Westinghouse
Beulah Road
Pittsburgh, PA 15235

William M. Swift
Argonne National Laboratory
9700 S. Cass Avenue, Bldg. 205
Argonne, IL 60439

Ronald D. Snyder
Buell Emission Control Division
Envirotech Corporation
200 N. Seventh Street
Lebanon, PA 17042

-T-

S. I. Taub
IU Conversion Systems, Inc.
Joshua Rd & Stenton Ave.
P.O. Box 331
Plymouth Meeting, PA 19462

F. Gale Teats
Argonne National Lab.
9700 S. Cass Avenue
Argonne, IL 60439

Suresh P. Tendulkar
Westinghouse
Waltz Mill Site, Box 158
Madison, PA 15663

C. M. Thoennes
General Electric Company
Bldg. 2, Room 712
One River Road
Schnectady, NY 12345

Yung Kwang Ti
Research Associates
Univ. of Wisconsin at Milwaukee
3200 N Cramer Street
Milwaukee, WI 53201

C. Tien
Syracuse University
Syracuse, NY 13210

R. F. Toro
Recon Systems, Inc.
Cherry Valley Road
Princeton, NJ 08540

Richard H. To  in
NY State Energy Research
and Development Authority
230 Park Avenue
New York, NY 10017

Dr. Jim Trolinger
Spectron Development Labs
3303 Harbor Blvd.
Costa Mesa, CA 92626

Norman P. Troxel
Research-Cottrell, Inc.
P.O. Box 750
Bound Brook, NJ 08805

Keh C. Tsao
Univ. of Wisconsin at Milwaukee
College of Engineering
3200 N. Cramer Street
Milwaukee, WI 53211

Alex Turchine
Proctor and Gamble
7162 Reading Road
Cincinnati, OH 45222

-U-

V. S. Underkoffler
Manager, Combustion & Advanced Power
Gilber Associates, Inc.
525 Lancaster Avenue
Reading, PA 19603

-V-

E. S. Van Valkenburg
Leeds and Northrup Company
Dickerson Road
North Wales, PA 19454

V. A. Varady
UOP Process Division
UOP Plaza
Des Plaines, IL

F. Munro Veazie
Owens-Corning Fiberglass Corp.
Technical Center
Granville, OH 43023

John A. Verrant
Donaldson Company, Inc.
P.O. Box 1299
Minneapolis, MN 55440

S. N. Vines
University of VA, Chemical
Eng. Dept.
Thornton Hall
Charlottesville, VA 22901

G. J. Vogel
Argonne National Lab.
9700 S. Cass Avenue
Argonne, IL 60439

D. V. Vukovic
Faculty of Technology and
Metallurgy
Belgrade University
1100 Beogard, Karnegijeva 4,
P.O.B. 494
Yugoslavia

-W-

Gordon L. Wade
Combustion Power Company
1346 Willow Road
Menlo Park, CA 94025

Peter Waldstew
Physical Chemist
RDR
P.O. Box 33128
District Heights, MD 20028

Andrew Wallo
Env. Scientist
1605 Craig Street
Sterling, VA 22170

Walter Wolowodivk
Foster-Wheeler Dev. Corp.
12 Peach Tree Hill Road
Livingston, NJ 07039

Donald E. Wambsgans, II
District of Columbia
Dept. of Environmental Services
Room LL-3
614 "H" Street, NW
Washington, DC 20001

Stephen Wander
Dept. of Energy
400 First Street, NW
Washington, DC 20545

Frank Weiskopf
Environmental Elements Corp.
P.O. Box 1318
Baltimore, MD 21203

Phillip C. White
Dept. of Energy
Fossil Energy/Advanced Power
Systems
20 Massachusetts Avenue
Washington, DC 20545

Clyde L. Witham
SRI International
333 Ravenswood
Menlo Park, CA 94025

-Y-

Dr. H. C. Yeh
Lovelace Biomedical and Environmental
Research Institute
P.O. Box 5890
Albuquerque, NM 87115

-Z-

Dr. Karim Zahedi
President
EFB, Inc.
94 Francis Street
Brookline, MA 02146

John H. Zarnitz
NYC Dept. of Air Resources
7044 Manse Street
Forest Hills, NY 11375

Dr. F. A. Zenz
The Ducon Company
147 East Second Street
Mineola, LI, NY 11501

August H. Zoll
Curtiss-Wright Corporation
Power Systems
Wood Ridge, NJ 07075

[illegible]na M. Zuk
Interdevelopment, Inc.
Rutherford B. Hayes Bldg.,Suite 104
2361 South Jefferson Davis Hwy
Arlington, VA 22202

Stephen H. Zukor
Department of Energy
OGST
20 Massachusetts Avenue
Washington, DC 20545

## TECHNICAL REPORT DATA

*(Please read Instructions on the reverse before completing)*

| | | |
|---|---|---|
| 1. REPORT NO.<br>EPA-600/9-78-004 | 2. | 3. RECIPIENT'S ACCESSION NO. |
| 4. TITLE AND SUBTITLE<br>EPA/DOE Symposium on High Temperature/Pressure Particulate Control | | 5. REPORT DATE<br>March 1978 |
| | | 6. PERFORMING ORGANIZATION CODE |
| 7. AUTHOR(S)<br>Mike Shackleton (Compiler) | | 8. PERFORMING ORGANIZATION REPORT NO. |
| 9. PERFORMING ORGANIZATION NAME AND ADDRESS<br>Acurex Corporation/Aerotherm Division<br>485 Clyde Avenue<br>Mountain View, California 94042 | | 10. PROGRAM ELEMENT NO.<br>EHE623 |
| | | 11. CONTRACT/GRANT NO.<br>68-02-2611, Task 2 |
| 12. SPONSORING AGENCY NAME AND ADDRESS<br>EPA, Office of Research and Development*<br>Industrial Environmental Research Laboratory<br>Research Triangle Park, NC 27711 | | 13. TYPE OF REPORT AND PERIOD COVERED<br>Proceedings; 6-12/77 |
| | | 14. SPONSORING AGENCY CODE<br>EPA/600/13 |

15. SUPPLEMENTARY NOTES (*) The U.S. Department of Energy (formerly ERDA) cosponsored the symposium. IERL-RTP project officer is D.C. Drehmel, Mail Drop 61, 919/541-2925.

16. ABSTRACT The proceedings are a compilation of papers presented at the EPA/ERDA (now DOE) Symposium on High Pressure/Temperature Particulate Control, in Washington, DC September 20-21, 1977. The symposium was sponsored jointly by EPA's Industrial Environmental Research Laboratory (Research Triangle Park) and ERDA's (now DOE's) Fossil Energy Division. Session I, on Fundamentals, included turbine erosion/corrosion effects, materials, and the theory of HT/P particulate control. Session II, on Filtration, included granular bed filter test results, tests of ceramic fiber filtration, tests of rigid ceramic filters, and a summary from the Federal Republic of Germany. Session III, on Other Collection Devices, included HT/P electrostatic precipitation, sonic agglomeration, a cyclocentrifuge device, and scrubbing with dry particles, molten glasses, and molten salts. Session IV, on Particle Sampling and Measurement, included optical and extractive sampling for HT/P particulate analysis.

17. KEY WORDS AND DOCUMENT ANALYSIS

| a. DESCRIPTORS | b. IDENTIFIERS/OPEN ENDED TERMS | c. COSATI Field/Group |
|---|---|---|
| Air Pollution, Dust Control, Turbines | Air Pollution Control | 13B, --, -- |
| High Temperature Tests, Erosion | Stationary Sources | 14B, -- |
| High Pressure Tests, Corrosion | Particulate | --, -- |
| Sampling, Optics, Extraction | Sonic Agglomeration | --, 20F, 07A |
| Measurement, Filtration, Ceramics | Cyclocentrifuge | --, 07D, 11B |
| Electrostatic Precipitation, Acoustics | Molten Glass | 13H, 20A |
| Agglomeration, Centrifuges, Fused Salts | | --, --, -- |

| | | |
|---|---|---|
| 18. DISTRIBUTION STATEMENT<br>Unlimited | 19. SECURITY CLASS *(This Report)*<br>Unclassified | 21. NO. OF PAGES |
| | 20. SECURITY CLASS *(This page)*<br>Unclassified | 22. PRICE |

EPA Form 2220-1 (9-73)